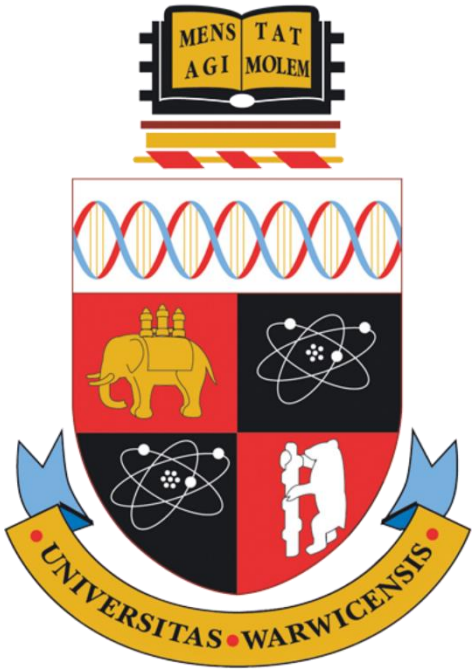

Analysis of biocompatible polymers and cyclic peptide-polymer conjugates by one- and two-dimensional Fourier transform ion cyclotron resonance mass spectrometry

Tomos Morgan

A thesis submitted for the degree of

Doctor of Philosophy

Department of Chemistry

University of Warwick

March 2020

Acknowledgements

It's often said it takes a village to raise a child, similar things could be said of a scientist but the village spans multiple countries, backgrounds, and scientific disciplines… and they're all a bit crazy.

First and foremost, thanks are extended to my supervisors the professors Peter O'Connor, Sebastien Perrier, and Tony Bristow. To say that you've all been great would be an understatement. Peter O'Connor for his extensive knowledge and the highest standard of science: pushing for the correct answer over anything else is a characteristic I will keep with me. The opportunities Pete has offered me throughout the PhD has been well above my expectations and it's been an honour to work under him. Sébastien, for putting up with a student who gate crashed his lab, I cannot stress how important it has been to my development to be involved with such high quality science as part of this PhD work, his "this could be interesting" comments produced most of the direction of this thesis. And finally Tony Bristow, for believing in the science, and putting the science first, the light touch and knowledge produced much of the success in this project. Overall, the thesis presented is a joining together all these visions which, hopefully, offers a coherent scientific contribution.

Spanning across different groups has been a key feature of this project. The contribution of my peers towards this work has been massive and cannot be understated. First, the contribution from Dr. Chris Wootton cannot be understated, from teaching me almost everything I know of FT-ICR to then guiding the individual projects later in my PhD as well as offering a bed when I ran out of housemates. Dr. Mark Barrow, for checking through all my work at some point, as well as looking after the SolariX, this thesis literally wouldn't exist without that contribution. Dr. Alina Thiesen who joined later in the PhD offered extensive knowledge in a technique I knew nothing about as well as keeping me company on some cripplingly boring UVPD experiment days. Dr. Yuko Lam who offered knowledge on the SolariX and guidance. Dr. Maartje van Agthoven, the queen of 2D, who was vital at the start of my PhD. Cookson and Meng who put up with me when I was an annoying starter student and offered so much help in my first years. Sam, sorry for stealing all your cutlery. Mary,

for taking the PhD road together. Anisha, Bryan, and Johanna, you all owe me one, but I've had so much fun working with you all, and I certainly learnt as much from each of you as you learnt from me, you're all fantastic scientists and I better get a shout out in the scientific awards you'll surely win.

From Sebastien's group, past and present, Dr. Andrew Kerr, Dr. Julia Rho, Sean Ellacott, and Thomas Flloyd, your support with samples and often crazy asks for various polymeric species was incredibly useful. I can't thank Seb's group enough for all their input.

Finally, from a professional point of view, the ones that allowed me to get to this position. Prof. Manfred Bochmann, my MChem supervisor, gave my arse a serious kicking that turned me into the scientist willing to work hard, and learn harder. Dr. Stephen Ashworth, for pushing me to carry on along the path of a chemist. Dr James and Dr. Julio, for giving a timid Master's student the self-belief to actually put book smarts into some sort of use. And Dr. Tony New, Dillan, and Dr. Ian Davison, who all gave a chance to a student that was passionate in science, but ultimately clueless. I certainly wasn't the perfect candidate, and I hope I can offer much the same back to the scientific community that they all offered me.

Non-professionally, the various brass bands deserve a mention, the ability to leave the lab and office for 8 hours a week to play an instrument was always a welcome relief. Greeno, Ginge, and Josie, thank you all so much for putting up with a friend who lives two and a half hours away, is terrible at organising anything, would call up regularly to vent about things you couldn't care less about and was generally quite cantankerous during the PhD process. My girlfriend, Connie, for putting up with me when my "lines" weren't working, your support has been vital to my success. My brother and his fiancé Hana, I hope you're not married by the time you read this because that means I've had more corrections than planned, you've both been amazing throughout. My parents and their partners, thank you so much for all the amazing support.

Thank you, everyone!

Also, thanks to whoever reads this, I know, I know, could you imagine writing it!

Author page

Education

[redacted]

Work Experience

[redacted]

Volunteering and personal interests

Publications

Accepted

Tomos E. Morgan, Sean H. Ellacott, Christopher A. Wootton, Mark P. Barrow, Anthony W. T. Bristow, Sébastien Perrier, Peter B. O'Connor, *Coupling Electron Capture Dissociation and the modified Kendrick mass defect for sequencing of a poly(2-ethyl-2-oxazoline) polymer.*, Anal. Chem., 2018, 90 (19) 11710-11715.

Bryan P. Marzullo, **Tomos E. Morgan,** Christopher A. Wootton, Meng Li, Simon J. Perry, Mansoor Saeed, Mark P. Barrow, Peter B. O'Connor, *Comparison of Fragmentation Techniques (CAD and EID) for the structural characterisation of singly charged agrochemicals*, Analytical Chemistry, Just accepted manuscript.

Maria A. van Agthoven, Alice M. Lynch, **Tomos E. Morgan,** Christopher A. Wootton, Yuko P. Y. Lam, Lionel Chiron, Mark P. Barrow, Marc-Andre Delsuc, Peter B. O'Connor, *Can Two-Dimensional IR-ECD Mass Spectrometry Improve Peptide de Novo Sequencing?, Anal. Chem.*, 2018, 90, 3496.

Maria A van Agthoven, David PA Kilgour, Alice M Lynch, Mark P Barrow, **Tomos E Morgan**, Christopher A Wootton, Lionel Chiron, Marc-André Delsuc, Peter B O'Connor, *J. Am. Soc. Mass Spec.*, 2019, 30, 12, 2594

Submitted/in preparation

Tomos E. Morgan, Andrew Kerr, Christopher A. Wootton, Mark P. Barrow, Anthony W. T. Bristow, Sébastien Perrier, Peter B. O'Connor, *Radical depolymerisation: electron capture dissociation of RAFT acrylamide homo- and co- polymers*, Article submitted.

Tomos E. Morgan, Thomas Floyd, Bryan P. Marzullo, Christopher A. Wootton, Mark P. Barrow, Anthony W. T. Bristow, Sébastien Perrier, Peter B. O'Connor, *Understanding poly(2-ethyl-2-oxazoline) hydrolysis using tandem mass spectrometry methods*, Article submitted.

Tomos E. Morgan, Thomas Floyd, Bryan P. Marzullo, Christopher A. Wootton, Mark P. Barrow, Anthony W. T. Bristow, Sébastien Perrier, Peter B. O'Connor, *2DMS analysis of acrylamide homo- and co-polymers – understanding a polymeric dispersity by tandem mass spectrometry*, Article in preparation.

Johanna Paris, **Tomos E. Morgan,** Christopher A. Wootton, Mark P. Barrow, John O'Hara, Peter B. O'Connor, *Facile determination of phosphorylation sites in peptides using (2DMS),* Article submitted.

Tomos E. Morgan, Andrew Kerr, Alina Theisen, Sean Ellacott, Anisha Haris, Christopher A. Wootton, Mark P. Barrow, Anthony W. T. Bristow, Sébastien Perrier, Peter B. O'Connor, *UVPD of biologically compatible copolymers*, Article in preparation.

Presentations

Modifying the Kendrick Mass Defect for polymer analysis, (oral, **EFTMS: Young speaker prize winner)** *Tomos E. Morgan, Christopher A. Wootton, Andrew Kerr, Sean Ellacott, Rémy Gavard, Diana Catalina Palacio, Maria A. van Agthoven, Mark P. Barrow, Anthony W. T. Bristow, Sebastien Perrier, Peter B. O'Connor*

Advancing biocompatible synthetic polymer mass spectrometry into the second dimension, (oral, **Warwick postgraduate symposium: best analytical talk prize winner**) *Tomos E. Morgan, Christopher A. Wootton, Andrew Kerr, Sean Ellacott, Rémy Gavard, Diana Catalina Palacio, Maria A. van Agthoven, Mark P. Barrow, Anthony W. T. Bristow, Sebastien Perrier, Peter B. O'Connor*

2D-MS ECD of polyoxazolines, (oral, **UPCONN**) *Tomos E. Morgan, Christopher A. Wootton, Sean* Ellacott, *Maria A. van Agthoven, Mark P. Barrow, Anthony W. T. Bristow, Sebastien Perrier, Peter B. O'Connor*

Analysis of polyoxazolines by 2D-MS, (Poster, **BMSS 2018)** *Tomos E. Morgan, Christopher A. Wootton, Sean Ellacott, Maria A. van Agthoven, Mark P. Barrow, Anthony W. T. Bristow, Sebastien Perrier, Peter B. O'Connor*

Cyclic peptide-polymer conjugate characterisation using SNAP algorithm and Fourier Transform Ion Cyclotron Resonance Mass Spectrometry, (Poster, **BMSS 2017**) *Tomos E. Morgan*, Christopher A. Wootton, Sebastien Perrier, Anthony W. T. Bristow, Mark P. Barrow and Peter B. O'Connor*

Analysis of polymers by ultra-high resolution FT-ICR MS, *(o*ral, **Polymer club**) *Tomos E. Morgan*, Christopher A. Wootton, Sebastien Perrier, Anthony W. T. Bristow, Mark P. Barrow and Peter B. O'Connor*

Declaration

I hereby declare that, except for where specifically stated/references are made to other sources. The thesis titled “Analysis of biocompatible polymers and cyclic peptide-polymer conjugates by one- and two-dimensional Fourier transform ion cyclotron resonance mass spectrometry” is the original work of the named author. The work has been composed by myself and co-authors where stated and has not been submitted as whole or in part for any other diploma, degree, or qualification.

Tomos Morgan

Abstract

The work presented in this thesis focusses on the analysis of biocompatible polymers and cyclic peptide-polymer conjugates with the use of Fourier transform ion cyclotron resonance mass spectrometry. The analysis of these polymeric species is carried out extensively by their fragmentation to understand copolymer sequences and end groups.

The thesis contributes a significant number of novel methods and observations relating to the mass spectrometry analysis of polymers. Modified Kendrick mass defect analysis (chapter 2) is used extensively in all of the chapters as a method to simplify the data *de novo*. Electron capture dissociation methods are shown to be able to characterise polyacrylamides and polyoxazolines. The corresponding studies shows a novel dissociation mechanism for polyacrylamides (chapter 4) and previously unseen hydrolysis properties of polyoxazolines (chapter 5).

Novel ultraviolet dissociation methods produced complete coverage of the polyoxazoline and polyacrylamide polymers used (chapter 6). All of this culminates in the analysis of complex cyclic peptide-polymer conjugates (chapter 7) shows how a suite of mass spectrometry methods can be bought together to further the analysis of these complex polymeric species.

Finally, the final chapter is based on the analysis of polymeric species using two-dimensional mass spectrometry. The ability to analyse multiple polymer species by tandem mass spectrometry, in one experiment, without the need to isolate precursor species, is an incredibly powerful tool within polymer analysis.

Table of contents

Figure List

Abbreviations

MS	Mass Spectrometry
FT-ICR	Fourier-transform ion cyclotron resonance
FT-ICR MS	Fourier-transform ion cyclotron resonance Mass Spectrometry
ESI	Electrospray ionisation
nESI	Nano-electrospray ionisation
MALDI	Matrix assisted laser desorption ionisation
EI	Electron impact ionisation
eV	Electron volt
IEM	Ion ejection model
CRM	Charge residue model
CEM	Chain ejection model.
TOF	Time of flight
UV	Ultraviolet
UVPD	Ultraviolet photodissociation
IR	Infrared
IRMPD	Infrared multiphoton absorption dissociation
CAD/CID	Collision activated/induced dissocaition
SORI-CAD	Sustained off resonance irradiation collision activated dissociation
NMR	Nuclear magnetic resonance
NOESY NMR	Nuclear Overhauser effect spectroscopy
2D	Two-dimensional
2DMS	Two-dimensional mass spectrometry
PEG	Poly(ethylene glycol)
PPG	Poly(propylene glycol)
PS	Poly(styrene)
GPC	Gel permeation chromatography

DLS	Dynamic light scattering
SNAP	Sophisticated numerical annotation procedure.
P(Ox)	Polyoxazoline
P(EI)	Poly(ethylenimine)
P(NAM)	Poly(n-acryloylmorpholine)
P(DMA)	Poly(dimethylamine)
KMD	Kendrick mass defect
HRMKMD	High resolution modified Kendrick mass defect
MKMD	Modified Kendrick mass defect
fKM	Fractional Kendrick mass
S/N	Signal to noise ratio
ppm	Parts per million
CP	Cyclic peptide

1. Introduction to mass spectrometry and polymers

1.1. Introduction and history of Mass Spectrometry

Mass spectrometry is an analytical method that manipulates and differentiates ions to measure the mass to charge ratio of ions of interest. Mass spectrometry is split into three distinct steps: ionisation, separation, and detection of ions in the gas phase. As there are multiple steps in the analytical process various instrumentation has been developed with differences in the analytical process but still based on the fundamental ionisation, separation, and detection process.

Historically, a majority of the improvements in mass spectrometry were tied to the technical advancements of the vacuum pump. Thomson studied ion rays and their manipulation in electric fields produced by heated cathodes. He often noticed that pumping for several days as well as running currents through the cathodes to heat the instrument greatly improved results, something now recognised as an early form of bake out! Thomson developed the first mass spectrographs discovering the two major isotopes of neon ^{20}Ne and ^{22}Ne, importantly a measurement at mass-to-charge ratio eleven was seen, which Thomson correctly identified as a doubly charged neon isotope. The observation of a doubly charged species showed not only the mass, but the mass to charge ratio was measured and this could be utilised for the analysis of particles. Thomson's spectrographs, Figure 1.1, show the photographic means in which he detected ions as they were manipulated.[1]

Francis Aston made significant contributions to the development of the "whole number rule" which suggested that the subatomic build-up of all atoms were the same, he then developed this further suggesting that slight differences between element mass could be a difference in sub-atomic energy.[2]

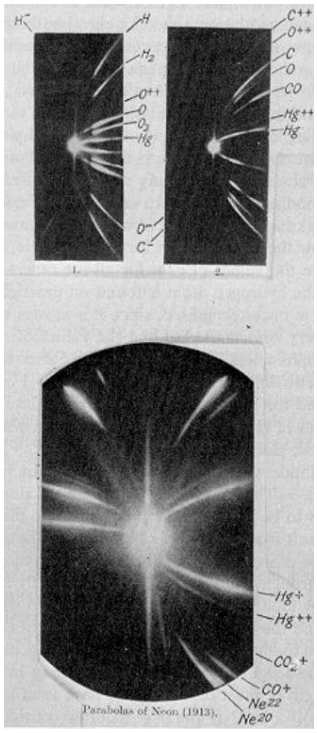

Figure 1.1: Thomson's experiment showing the presence of ions deflected depending on their mass to charge ratios. Thomson produced many of these through his studies showing the presence of many of the low molecular weight isotopes. Reproduced from the Proceedings of the Royal Society.[1]

Most of Aston's work focussed on the ability to analyse a large range of masses, Dempster developed velocity focussing mass spectrometry devices which would now be recognised as the first magnetic sector instruments.[3] These principles have been developed into isotopic determination and fine structure analysis which are both actively used today.

The continued development of mass spectrometry has occurred, but all mass spectrometers are based on the same principles developed by these first practitioners.

1.2. Ionisation methods

The ionisation of molecules and analytes is one of the most important aspects of mass spectrometry. The transport and detection of ions is not possible if the ions have not been produced in the first place!

The major differences between ionisation methods are:

1. The state that the analyte needs to be present in during ionisation: some ionisation methods are only possible in the gas phase requiring volatile analytes whereas others are possible from the liquid and solid states.

2. The internal energy transfer during the ionisation event. Higher energy ionisation methods are known as "hard" ionisation methods. Hard ionisation methods transfer large amounts of energy to analytes often resulting in fragmentation. The opposite, "soft" ionisation methods transfer less energy during ionisation. The energy transferred in soft ionisation methods may be sufficient to cause fragmentation or tertiary structure change but significantly less than harder methods.

1.2.1. Electron Ionisation (Electron impact ionisation)

Electron ionisation (EI), originally termed Electron impact ionisation, is the process in which analyte ionisation occurs via bombardment of high energy electrons. The electron ionisation process was first discussed by Dempster in his paper "*positive ray analysis"* where "positive ions from electron bombardment"[6] is discussed. Interestingly, even in the first electron impact experiments carried out by Dempster it is noted that significant complexity is added due to the break up of ions and the presence of numerous other species from a heated Wehnelt cathode.[4,5]

The ionisation process in EI requires removal of an electron from the analyte with bombardment of the analyte with high energy electrons. The positively charged radical ion formed can be observed as a molecular ion of the analyte or as fragments generated during radical dissociation.[6]

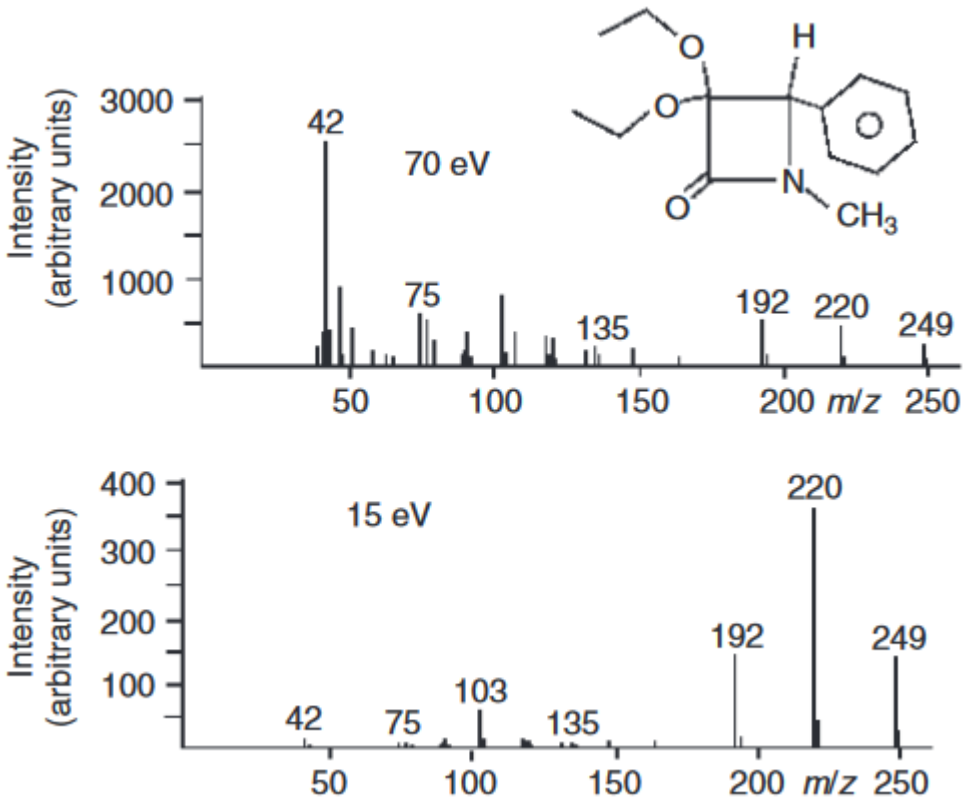

Figure 1.2: Fragmentation of β-lactam showing the relative intensity of fragments being much higher at higher electron impact energies. The experiment also shows significantly higher ionisation efficiency overall at higher electron impact values. Figure reproduced from Hoffmann et al. Figure 1.3.[7] Copyright 2008 John Wiley and Sons.

The radical formation process requires little tuning, often due to the excess energies used, often upwards of 65 eV. The formation of the high energy radical during the EI process does limit EI's usefulness. Radical formation on larger molecules almost always results in rapid radical dissociation and breakdown of the molecule. For small species, the high energy radical dissociation can often produce structural information through expected fragmentation pathways.[6] The radical dissociation pathways are often much more complex with larger species and are therefore not well predicted, meaning EI cannot be used for large species and still retain structural information.

1.2.2. Electrospray ionisation

Electrospray ionisation (ESI) is one of the most common ionisation sources used in mass spectrometry analysis of large or fragile molecules.[8] The ESI process can be carried out on analytes in solution meaning non-volatile molecules can be ionised.

Ionisation occurs when a solution containing the analyte is pushed through a capillary or needle with an applied potential difference. The potential difference applied causes an electrophoretic charge separation of ions within the solution generating a Taylor cone.[9] The Taylor cone emits droplets, which consist of the solvent and any analytes present. The evaporation of solvent from the droplet increases the total charge density of the droplet. The charge density will increase until the droplet reaches its Rayleigh limit, a limit where the charge of the droplet becomes greater than the stabilisation of the surface tension.[10] The destabilisation produces droplet fission that then undergoes evaporation in a series of evaporation/fission cycles.[11,12]

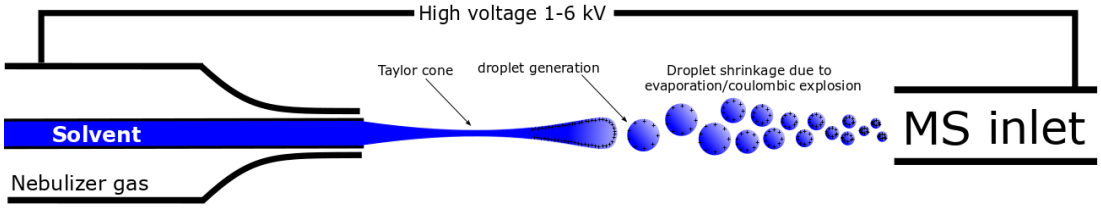

Figure 1.3: Schematic of the electrospray process with a liquid flow, the droplets are generated by the Taylor cone and the droplets become smaller on evaporation.[13] As droplet size becomes smaller the charge density of each droplet increases causing ionisation of the analyte.

After each of these evaporation/fission events the charge concentration of the droplet remains the same but the overall volume decreases. Beauchamp found that the fission events themselves don't decrease charge density.[13] The final charge concentration is higher than the charge concentration in solution as a large amount of solvent has been lost as neutral species, although it's important to recognise that some charge is lost as part of the fission/evaporation process.

The formation of the ions themselves can occur in numerous ways. Smaller ions are thought to be produced by the ion ejection model (IEM). The IEM is the evaporation of a charged ion from the droplet surface and occurs where, by size, the analyte ion

is significantly smaller than the droplet so will be removed in continuous evaporation and emission events.

The charge residue model (CRM) is suggested to occur when there is the loss of solvent building up charge density on the remaining droplet but the analyte, by size, makes up a significant amount of the droplet. The CRM may be affected by tertiary structure of the analyte but is simply solvent evaporation until only the analyte is remaining. Importantly, this process allows the formation of gaseous species of very high molecular weight, by removing the solvent around the species and then suspending the remaining charged analyte in electric/magnetic fields, proteins, polymer conjugates, and large dendrimer complexes can be manipulated in the gaseous phase. The CRM is one of the key reasons that electrospray ionisation is ubiquitous. The formation of large, multiply charged species, is a huge advantage to the analytical chemist.

The final model, the chain ejection model (CEM) is an explanation to the formation of higher charged species that will have an open tertiary structure. A good example of this is the ionisation of branched polymers which tend to be very linear. The CEM is based on a charge equilibrium with the charge density of the analyte species and the droplet's surface. As the chain begins to eject charge moves from the droplets surface onto the chain, this process continues pushing the chain further out until the chain is ejected. When work with denatured proteins or polymers is carried out ionisation is mostly through both the CRM and CEM processes, as, even though denatured, as the solvent evaporates it is possible for the protein to become globular in structure again depending on the re-folding energies and therefore times involved.

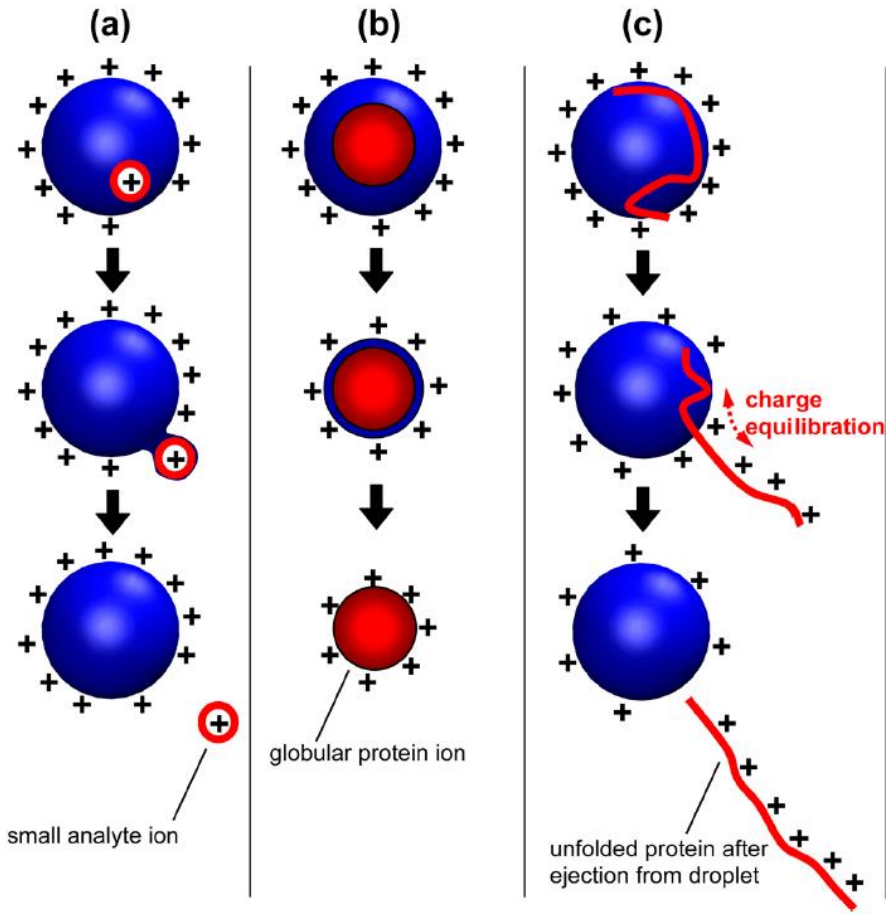

Figure 1.4: (a) Ion Ejection Model (IEM) small ion ejection from a droplet. (b) Charge residue model (CRM) larger species are not ejected but remain after solvent evaporation and (c) Chain ejection model where a chain is ejected through a charge equilibrated chain method. Figure reproduced with permission from Konermann et al. Figure 5.[14] Copyright 2013 American Chemical Society.

An advantage afforded by these ionisation processes is that there is very little energy transferred into the molecule. Often external heating is used to assist with solvent evaporation from the droplet surface, but this is not always necessary, and even under quite aggressive solvent evaporation conditions (heat, or buffer gas) the energy transferred is still significantly lower than electron ionisation techniques. The reduction in energy transfer means that the analysis of very large and fragile species can be carried out by electrospray which would otherwise fragment before analysis can take place. Finally, the ability for electrospray to produce multiply charged species comes with many distinct advantages to many mass spectrometry processes.

Multiple charge states allow the use of electron capture fragmentation methods, as well as increased opportunities of fragmentation due to the increased free energy of an analyte with a higher charge density. Figure 1.5 shows the ESI of myoglobin generating multiply charged states.

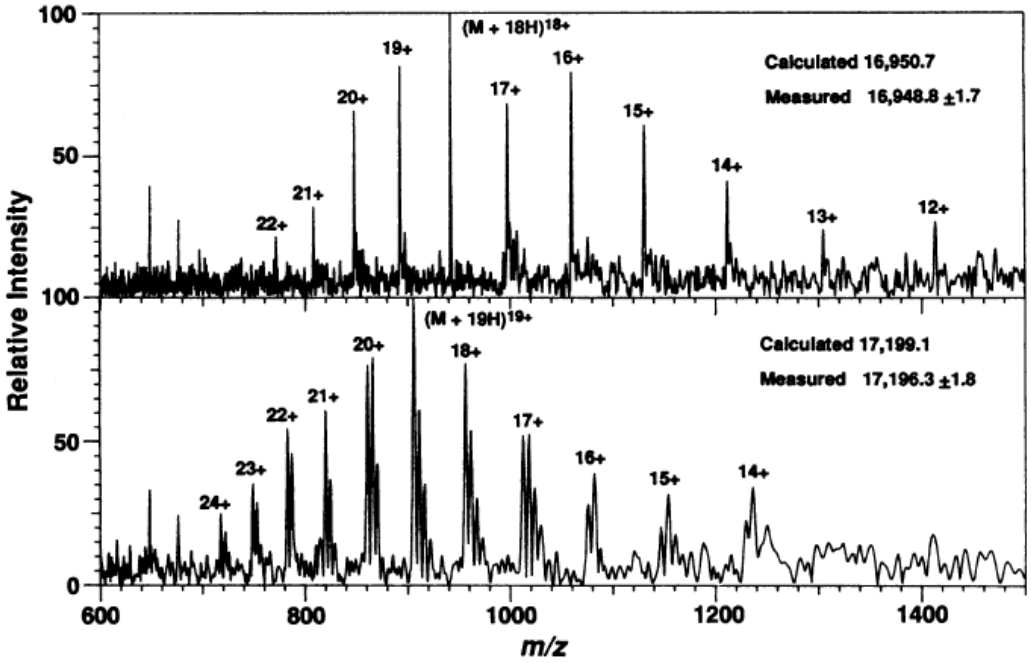

Figure 1.5: Example of one of the first electrospray ionisation spectra of large molecules, myoglobin was analysed by FT-ICR by Mclafferty and coworkers, the charge states are an obvious distribution of multiply charged ions. Figure reproduced with permission from Henry et al. Figure 3.[15]

Multiple charging, and low energy ionisation allows analysis of some of the largest molecules possible in mass spectrometry by electrospray ionisation has meant that different ways of generating electrospray signals have also been investigated.

1.2.2.1. Nano-electrospray ionisation (nESI)

Nano-electrospray ionisation (nESI) is simply electrospray carried out at a much lower flow rate and initial droplet sizes. Slower flow rates are achieved by greatly reducing the electrospray exit orifice size, thus reducing the overall size of the Taylor cone. With a smaller overall volume of droplets being produced, the ionisation process is more efficient a more sensitive measurement.[16]

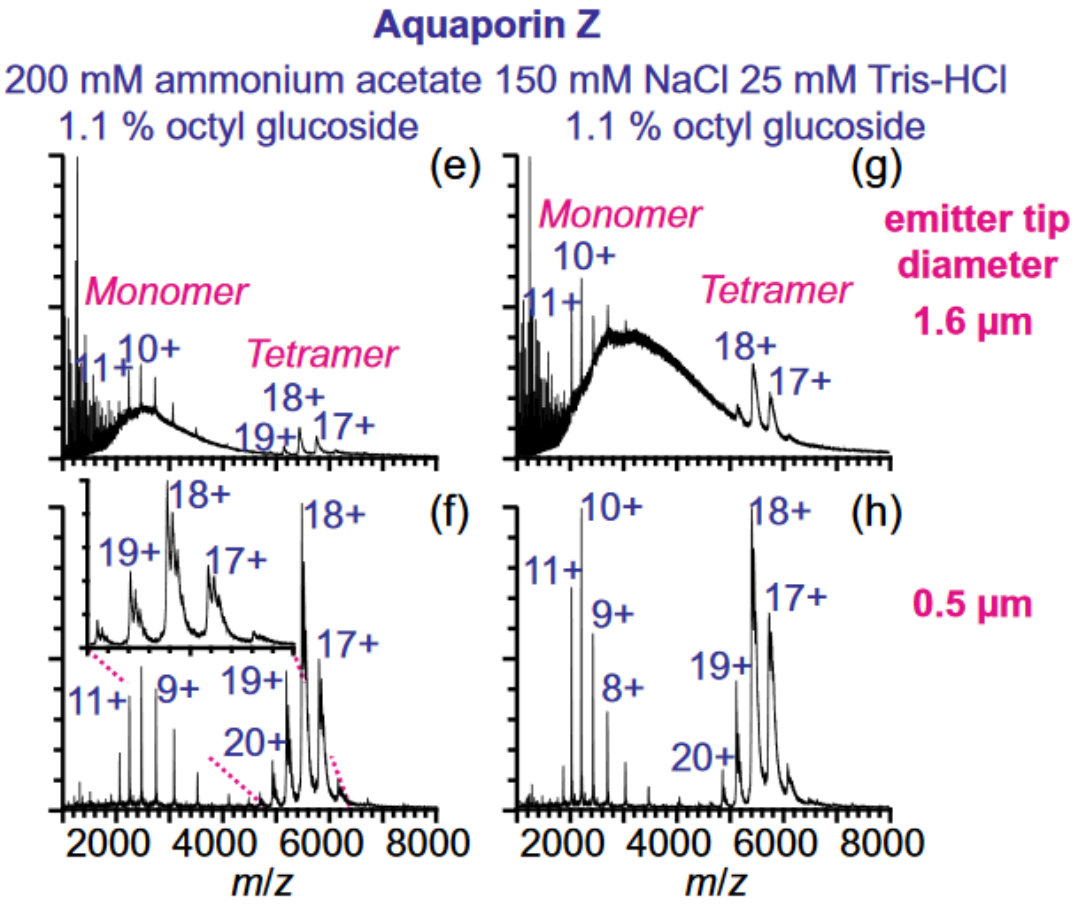

Figure 1.6: Aquaporin Z in various salt solutions sprayed with different sized nESI emitters. Reproduced from Susa *et al.* Figure 1.[17] Copyright 2018 American Chemical Society.

The use of nESI sources has become much more common for use in research purposes as the added complexity of sample handling is more than offset by the allowance for significantly less sample usage with increased sensitivity.

1.2.3. Matrix Assisted Laser Desorption Ionisation

Matrix assisted laser desorption ionisation (MALDI) is another commonly used technique for the analysis of high mass species. MALDI relies on the presence of a matrix mixed with an analyte, that is able to absorb radiation and often to act as an adduct donator. The first publications of MALDI work comes from the parallel work of Karas and Hillenkamp[18,19], and separately Tanaka.[20] Both works showed the ionisation of large molecular ions with the presence of a matrix, Figure 1.7.

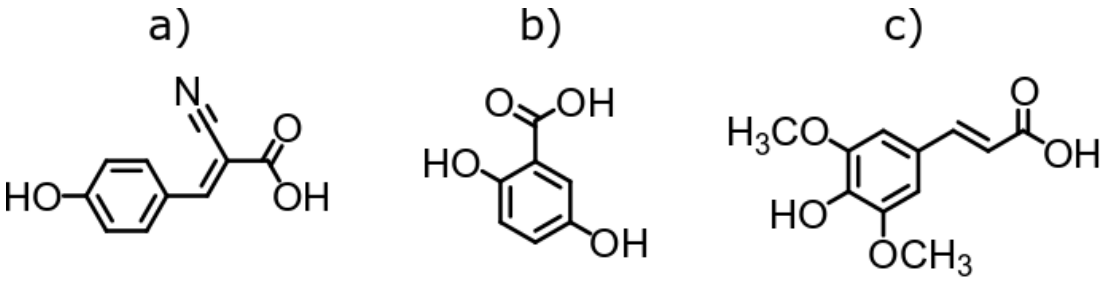

Figure 1.7: Common MALDI matricies, a) α-cyano-4-hydroxycinnamic acid (CHCA) b) dihydroxy-benzoic acid (DHB), both often used for peptides and proteins, and c) sinapinic acid, often used for RNA/DNA analysis.

MALDI analysis uses a laser, often UV, to ablate the matrix and sample from the surface of a target plate. The matrix must contain a chromophore that can absorb UV radiation and is often zwitterionic or an organic acid to encourage the formation of crystals, the importance in crystal formation is that crystals will absorb UV radiation much more uniformly in a solid state. The process of laser absorption in a matrix causes a 'super heating' effect of the solid. During super heating there is a build-up of pressure within the solid which causes ablation from the surface.

The charge formation mechanism is complex and not well understood. It is often best to describe the formation of ions as a series of observations common for MALDI analysis and then fit a model to this. The currently accepted MALDI ionisation process is based on the Karas 'lucky survivor model'.[21] The model explains that the formation of ions in MALDI are often singly charged, even in the presence of multiply charged salts. As ions become larger it is possible to see higher charge states but still much less large than the equivalent ESI data.

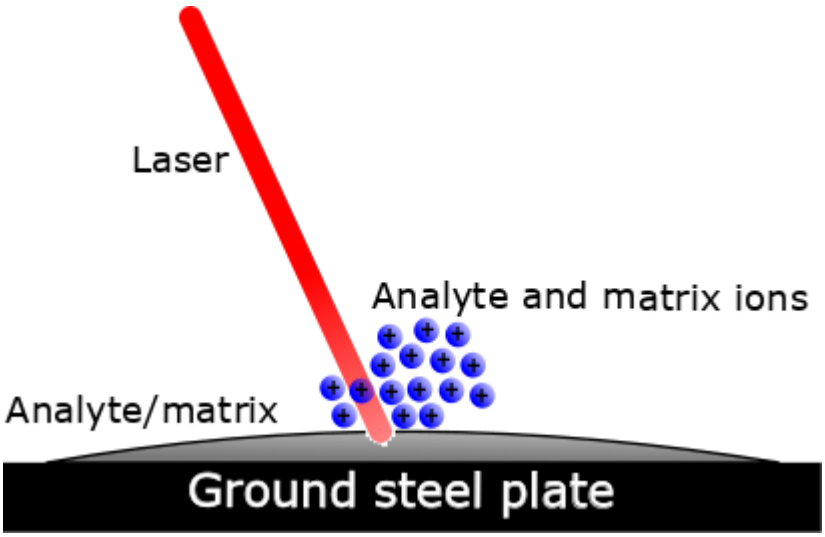

Figure 1.8: Schematic of laser induced ablation from a surface for MALDI analysis.

The model is based on ionisation occurring after an initial laser ablation event, which causes clusters of uneven ion charges and then electron capture occurring until formation of singly charged ions. Rapid charge capture of this type presents a lucky survivor principle where the ions observed are the ions that avoided neutralisation by the electron capture process.

There are many different MALDI preparation techniques, the use of solid crystal MALDI matrices has historically been the most common method of analysis varying from multiple layers of liquid matrix and liquid analyte allowed to evaporate down into a 'sandwich' like sample all the way to crushed crystal methods where solid sample and matrix are mixed together to form a sample for analysis. With various matrices and techniques a large variation of samples can be analysed.[22,23]

Significant development into the matrices used has greatly increased the variation in species that can be analysed and at increasingly sensitive levels. Viscous liquids of CHCA and 3-aminoquinoline were shown to increase the sensitive of the MALDI of glycans by multiple orders of magnitude.[24] The use of liquid matrices is becoming increasingly common due to advantages in consistent distribution of the analyte within the matrix, and therefore more consistent response. Often, similar matrix molecules are used and there is the addition of support liquid (often glycol based)[25,26] or the use of liquid salts which can absorb UV radiation.[27-29] The use of different ionic

liquid matrices has allowed the analysis of species that are incredibly difficult to carry out through electrospray processes.[30-33]

Further development of MALDI has involved the development of further ionisation with a second laser pulse of laser onto the plume formed after the initial ablation/desorption process. The second laser pulse works to further breakdown matrix/analyte clusters to increase the total material ionised and detected, potentially increasing signal by two orders of magnitude.[34-36]

1.3. Tandem mass spectrometry and fragmentation methods

The ability for mass spectrometry to elucidate molecular information, such as amino acid or base pair sequence in biomolecules, polymer end groups, and structural information of small molecules, greatly increases its analytical usefulness. From the initial experiments using EI to ionise molecules the fragmentation of molecules was clearly observed and over time techniques were developed to better understand how the fragmentation could be related back to the initial molecules that were present, the precursors. With improvement in ionisation techniques to facilitate ionisation of larger molecules and mass spectrometers to more accurate analysis the development of fragmentation techniques was close to follow.

1.3.1. Tandem mass spectrometry

Tandem mass spectrometry is a mass spectrometry process aiding the analysis of sequence and structural information of the analyte by activation of the ions causing intramolecular dissociation.

A standard tandem mass spectrometry experiment, Figure 1.9, must have a separation or isolation step so only one ion is being fragmented at a time. The simplest example of this is by carrying out an external separation technique, such as liquid chromatography, gas chromatography, or ion mobility mass spectrometry. Separation can also be carried out with the use of selective ion optics, this is most obvious in triple quadrupole instruments, although it is now common for almost all instrument designs to come with a quadrupole housed within the front end to facilitate some form of isolation allowing tandem mass spectrometry to be carried out.

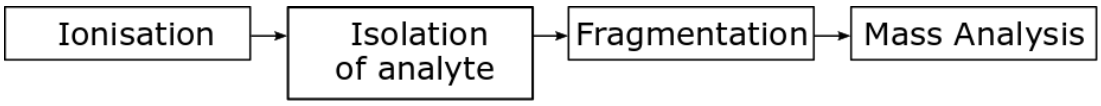

Figure 1.9: Outline of tandem mass spectrometry experiment.

Fragmentation of ions during tandem mass spectrometry can follow many reaction paths depending on the chemistry of the species being fragmented. These various fragmentation pathways will occur with different probabilities from and ensemble of ions, and so some pathways will appear more represented and some may not appear above the measurable threshold in a spectrum created from a finite number of precursor ions. Taking many ensembles of ions (also known as averaging spectra) allows better sampling of these pathways. The averaging principle is especially important in the event that unlikely fragmentation events may still be observed, even if their intensity is much lower than other more energy favourable pathways.

1.3.1.1. Nomenclature of fragmentation

The success of tandem mass spectrometry experiments is often discussed within the terms of sequence or fragmentation coverage. The basis of this measure is best described with the tandem mass spectrometry of poly-peptides. In protein systems amino acids are bound together by the presence of amide bonds. To discern the primary sequence, in which order the amino acids are present in within the protein or peptide, the molecule is fragmented in such a way that produces a 'ladder' of fragments. As the chain fragments the amino acid losses form a mass spectra where the spacing between fragment ions represent the sequence structure. Further, the agreement between researchers in the use of the Roepstorff and Fohlman nomenclature makes peptide and protein fragmentation straightforward to contextualise.[37]

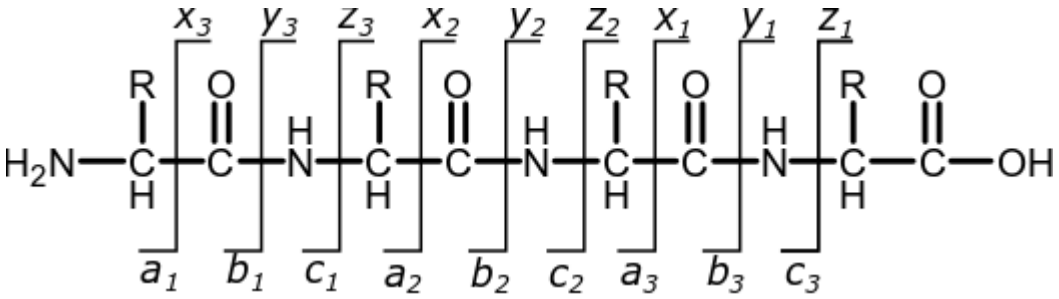

Figure 1.10: Fragmentation map proposed by Roepstorff and Fohlman, the peptide fragmentation nomenclature was an important step in the discussion of fragmentation between mass spectrometrists. The only change since has been the use of lower case lettering for fragmentation assignment. The simplicity in assignment of a, b, and c, fragmentation to the N-terminus and x, y, and z, to the acidic terminus allows easy communication of fragmentation types.[37]

The principles of sequence coverage and fragment assignment can be extended to other molecules which may not have obvious amino acid sequences but structural information like small molecules, polymers, and glycans. Fragmentation coverage can also be specified to further functionality, such as functional group coverage of rings.

Although fragmentation coverage quantitates the number of successful cleavages it does not always quantify true analytical utility. Glycans, for example, rely on extensive cross ring cleavages to fully characterise primary structure. Complete characterisation requires not only extensive cleavage of the ether linkages but also cross ring cleavages to identify positioning of modifications and branching. [38]

Different fragmentation methods have different fragmentation pathways which can greatly increase the variety and coverage of fragmentation. Using different fragmentation methods coupled together also means that two different types of bond cleavage may be obtained therefore producing complementary fragmentation coverage leading to further information for subsequent structure elucidation.

1.3.1.2. Secondary and tertiary structure considerations

The secondary and tertiary structure of analytes needs to be considered at the fragmentation stage of the analysis. All fragmentation relies on the molecule interacting with an external fragmentation source. Put simply, if the analyte in question is significantly contracted or constricted so that external fragmentation sources cannot interact with all the bonds present the amount of fragmentation coverage will be reduced.

1.3.2. Collision activated/induced dissociation (CAD/CID)

Collision activated/induced dissociation (CAD/CID) is one of the most common fragmentation techniques, it is often the 'default' fragmentation method when discussing MS/MS capability on instrumentation.

Collision induced fragmentation was introduced by Jennings in the late '60s as a way to fragment ions by a method other than high energy electrons.[39] CAD/CID is simply activation of ions using collision gas, repeated collisions cause an increase in the internal energy of the precursor ions causing bond breakage. The uses of CAD/CID are numerous as fragmentation may occur without a specific acceptor group, such as a chromophore. Fragmentation itself is controlled by the excitation of the ions into the collision gas. At higher excitation energies stable structures can be broken down.

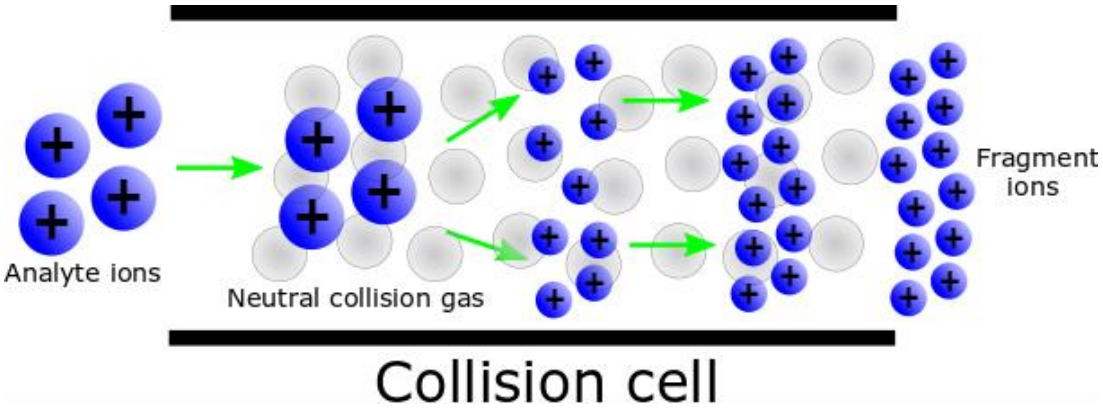

Figure 1.11: CAD fragmentation by collisions of parent ions with a neutral bath gas. Formation of smaller ions occurs over time due to multiple collisions.

A draw back of the CAD/CID fragmentation technique is that the internal energy is spread across the precursor analyte through vibrational and rotational energy modes, so bond fragmentation is often selective to the weakest bond in the molecule or the lowest energy rearrangement pathway. In the presence of a single weak bond, say a tagging agent or drug interaction, this bond may be broken first and the energy lost on fragmentation of this bond causes a distinct lack of information as most of the fragmentation events will occur through the lower energy fragmentation

pathway. In the event of many identical bonds, such as polymers, it is often seen that there is little fragmentation until there is over fragmentation of the species.[40]

Fragmentation of the weakest bonds is often useful for the analysis of biological structures as the amide bond that holds these structures together is weaker than carbon-carbon bonds in amino acid side chains. Fragmentation along the amide bond gives good structural information and therefore CAD/CID is used to a great extent in the fragments of biological molecules. The fragmentation by CAD/CID of peptides and proteins generate a large amount of *b* and *y* fragmentation as these are the weakest bonds as part of the protein backbone, the amide bond itself.

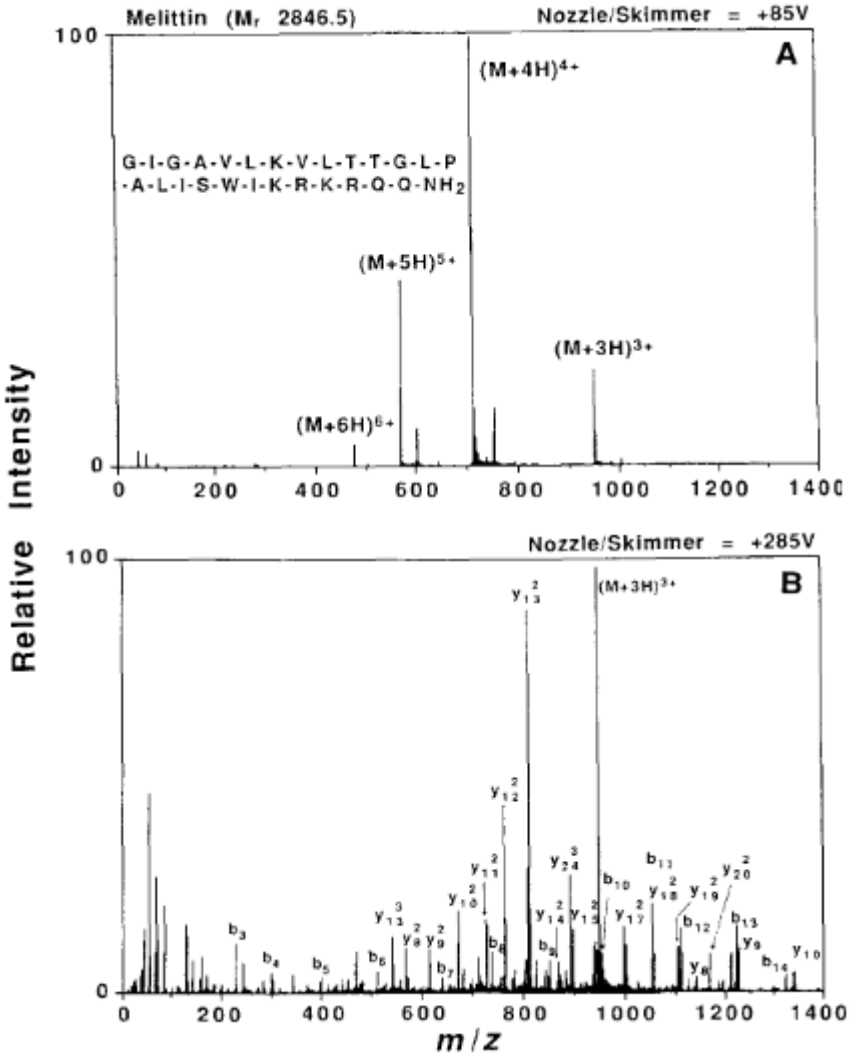

Figure 1.12: Fragmentation of melittin, a 26 amino acid polypeptide, showing the increase in Nozzle/Skimmer voltage which in this case was the

excitation voltage into the collision gas (argon). Reproduced with permission from Smith et al. Figure 4.[41] Copyright Elsevier 1990.

It is important to also note, that higher energy CAD/CID methods are regular CAD/CID methods carried out at higher energies. Any fragmentation differences seen are due to different bonds being able to fragment at these higher energies, not due to a different form of fragmentation occurring.

Another variation on the use of CAD/CID is the use of sustained off resonance irradiation collision induced excitation (SORI-CID)[42] in Fourier transform ion cyclotron resonance cells. The ions to be fragmented are excited inside the ion trapping cell once the pressure has been raised the ions collide with the collision gas and fragment. The collision gas is then pumped out and analysis occurs. SORI-CID is not commonly used in current studies due to high cycle time between pump stages, as well as reduced accuracy of analysis at higher pressures.

1.3.3. Infrared multiphoton absorption dissociation (IRMPD)

Infrared absorption is well characterised within organic chemistry and the use of infrared radiation to stimulate reactions has also been heavily explored.[43] By selecting wavelengths targeting a chromophore different rotational and vibrational energy levels can be stimulated. Initial work of spectroscopy carried out in ion traps was developed to small molecule species showing that excitation could lead to fragmentation. Further work by Eyler and co-workers[44] showed that small molecule losses from organic species could be achieved with IRMPD.

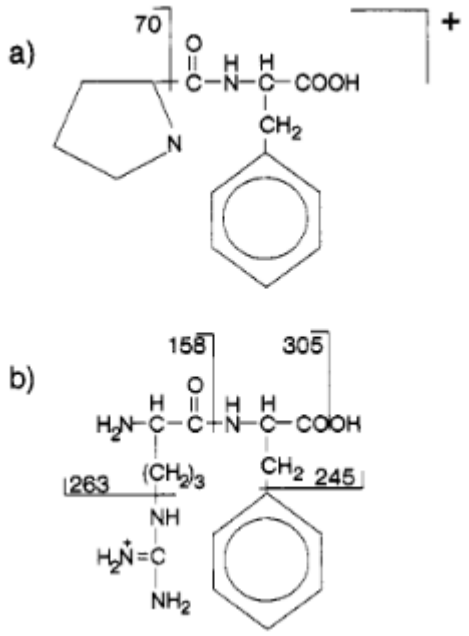

Figure 1.13: Ions formed by IRMPD of dipeptides. One of the first examples of a molecule with biological bases being fragmented by IRMPD. Reproduced with permission from Zimmerman *et al*. Figure 9.[44] Copyright 1991 American Chemical Society.

Infrared multiphoton absorption dissociation fragments ions by exciting bond vibrational modes until bond breakage. Much like CID/CAD the breaking of bonds by this method is a 'slow heating' process caused by repeated absorption of energy into the molecules vibrational or rotational energy modes. The fragmentation of amide bonds with the use of IRMPD was used for large biological molecules by McLafferty and co-workers,[45] with the analysis of the protein Ubiquitin and other larger peptides. The fragmentation of these groups by IRMPD offered good sequence coverage of these larger peptide species.

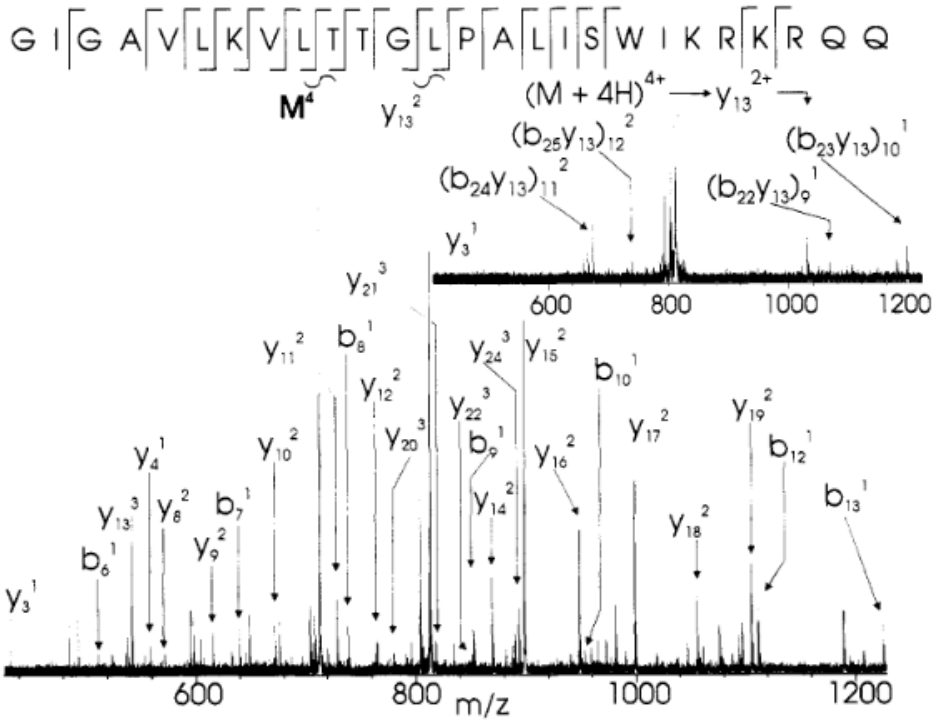

Figure 1.14: Bee venom melittin analysis with a 200 ms IR pulse. Top is the tandem MS of the initial precursor ion, bottom is further fragmentation of the y132+ fragment ion in an MS^3 experiment. Reproduced with permission from Little *et al.* Figure 5.[45] Copyright 1994 American Chemical Society.

IRMPD does have an advantage of being an easily controllable slow heating process, slow heating allows molecules with tighter tertiary structure to be activated by IRMPD unfolding the protein, allowing greater fragmentation as more of the structure is accessible for fragmentation.

1.3.4. Electron Capture Dissociation (ECD)

Electron capture dissociation (ECD) is less ubiquitous than CAD/CID but still a common fragmentation technique. Fragmentation differs from CAD/CID and IRMPD in that it is much more bond selective as the dissociation pathways are based on radical chemistry rather than accumulation of internal energy.[46] ECD involves the capture of a low energy electron onto the molecule, forming an odd electron radical species, the molecule then dissociates via radical pathway forming fragments. Bond selectivity comes from the necessity for the acceptance of an electron and then radical dissociation to occur, selectivity is based on where the electron was captured

and dissociation from that point. ECD has an advantage in the analysis of certain molecules since weaker bonds, which are preferentially fragmented in slow heating processes like IRMPD and CID/CAD, may not be favoured by ECD fragmentation meaning ECD can achieve more complete fragmentation coverage.

Many fragmentation mechanisms have been put forward for the dissociation of amide bonds by electron capture dissociation but the most accepted reaction mechanism is that presented by the Utah-Washington mechanism, Simons and Tureček group's respectively.[47,48]

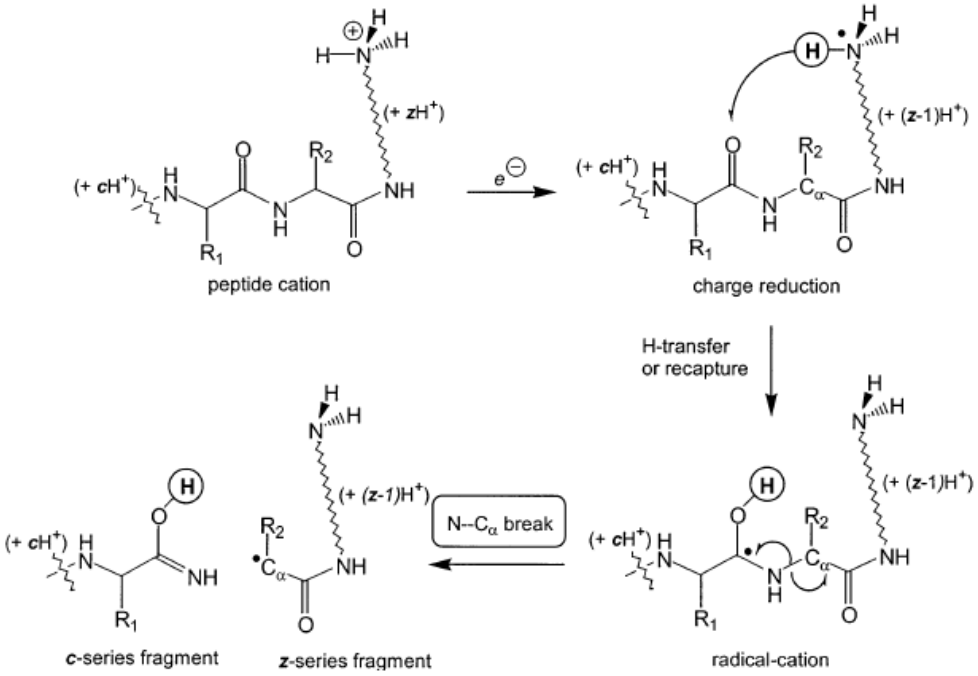

Figure 1.15: Utah-Washington dissociation mechanism of amides by ECD. Reproduced from with permission Tureček et al. Scheme 1.[48] Copyright 2003 American Chemical Society.

The Utah-Washington mechanism specifies that capture of an electron occurs at a positively charged position by capture into a high level Rydburg orbital, relaxation occurs and H-transfer occurs with formation of a radical. The radical will likely be generated with the electron occupying the amide π* orbital, or σ* orbitals in disulphide bonds, which then undergo dissociation with the formation of *c* and *z* fragments.

ECD uses a cathode to release low energy electrons into an ion trap to allow for electron capture. Fragmentation that occurs via the Utah-Washington mechanism forming *c* and *z* fragmentation via an ECD process is most commonly seen at lower electron energies (<1 eV) although the actual electron energies are hard to predict and dependent on the instrument parameters being used. Viable ECD energies are often judged sufficient via the presence of *c* and *z* fragments but the lack of other higher energy fragment pathways.

The capture of electrons by a cationic species causes a decrease in charge that needs to be accounted for, if singly charged analytes are exposed to low energy electrons the charge capture will neutralise the molecule, which will then no longer be trapped inside the MS instrument and simply pumped away, meaning no analytical result can be obtained. The capture of electrons is also greatly favoured by higher charged species. Meaning that the irradiation time of the analyte to the electrons needs to be tuned depending on the total charge of the analyte. Highly charged analytes will accept electrons, both due to their higher positive charge but also by the likely increase in size that comes with a more highly charged species. Small molecules which may only be doubly charged will require much higher irradiation times than highly charged species such as proteins/polymers.

At higher electron energies the fragment intensities change as well as a significant change in the types of fragments generated.[49,50] Higher energy electron capture can produce significant secondary and alternative fragmentation.[51] Importantly, the relationship between the fragments observed and the energy of the electrons allows predictions to be made on the fragmentation efficiency of the analyte.

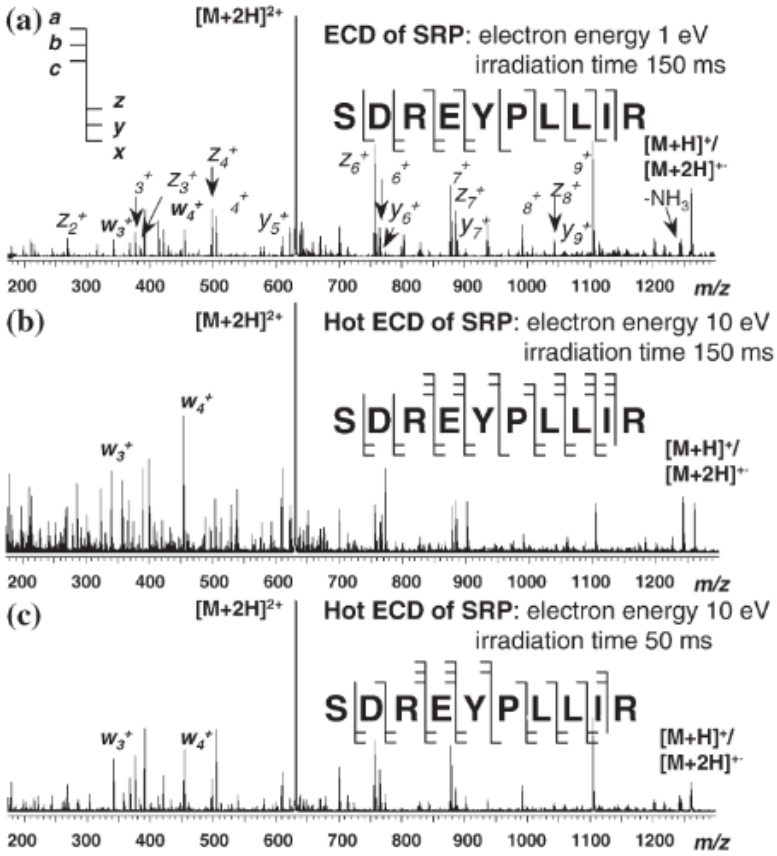

Figure 1.16: Difference in dissociation as electron energy in increased. The top spectrum shows the presence of sequence fragments with little internal fragmentation. There is increased secondary fragmentation present at higher electron energies and irradiation times in the bottom two spectra. Reproduced from with permission Tsybin et al. Figure 6.[51] Copyright 2004 John Wiley and Sons.

1.3.5. Ultraviolet photodissociation (UVPD)

The use of Ultraviolet radiation as a means to analyse molecules through absorption and fluorescence studies is very common, and the knowledge that UV radiation can cause degradation in species is also well established.

Ultraviolet photodissocaition (UVPD) involves the interaction of trapped ions with ultraviolet light.[52] The excitation of electrons within molecular orbitals allows the dissociation of molecules due to electrons being excited into antibonding or higher energy molecular orbitals that cause fragmentation. Recently there have been significant advances in the instrumentation and analysis of analytes by the use of ultraviolet photodissociation (UVPD).[52,53] Proteins and peptides have been

fragmented by UVPD.[54-58] Even a single UVPD pulse can cause dissociation allowing a very rapid fragmentation event.[59]

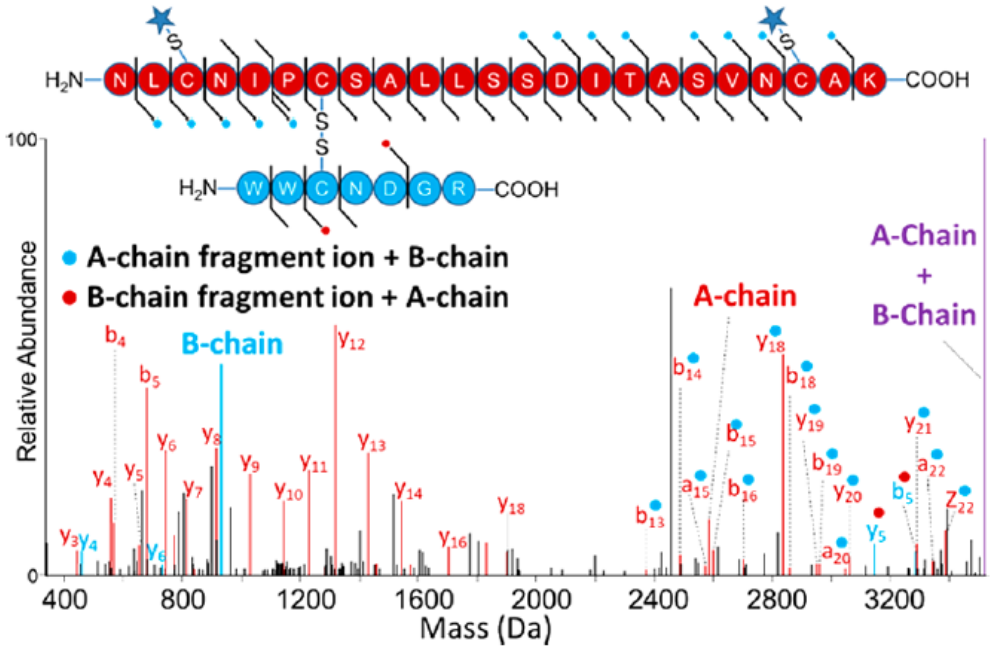

Figure 1.17: Dissociation of lysozyme digest showing the localisation of the disulphide bond with the use of UVPD. Reproduced with permission from Quick et al. Figure 3.[60] Copyright 2018 American Chemical Society.

UVPD has been used for the study of proteins in their native states, showing extensive fragmentation.[61,62] UVPD provides a robust fragmentation method for the analysis of many biological molecules for example UVPD has been used for lipid analysis in which fragmentation of the acyl chain enabled localisation of the double bond position.[63-65] Other studies by UVPD investigated cross ring fragmentation with oligosaccharides[66] , and nucleic acids.[67]

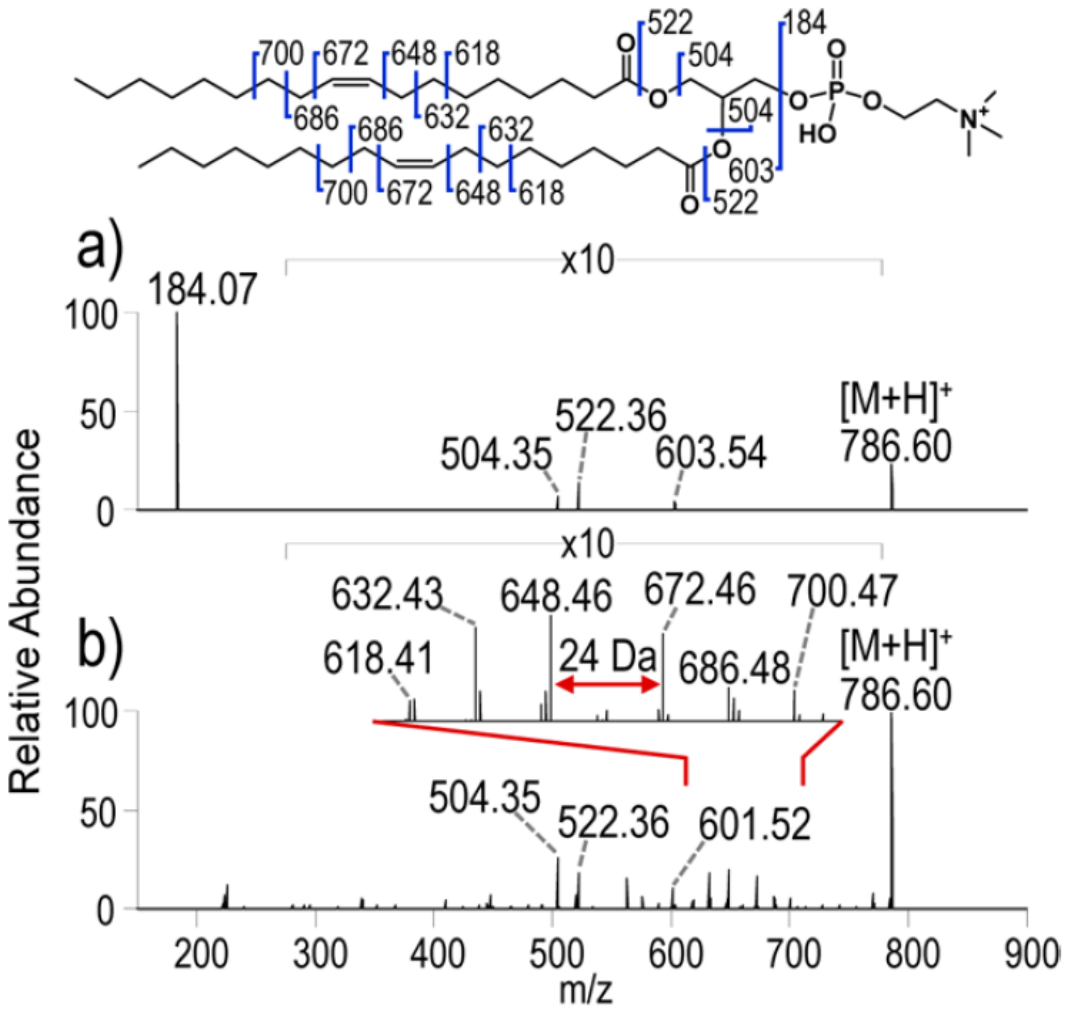

Figure 1.18: Comparison of a) CAD/CID and b) UVPD of phosphatidylcholine. Importantly showing the large increase in fragmentation with the use of UVPD compared to CAD/CID. Reproduced with permission from Klein et al. Figure 1.[65] Copyright 2017 American Chemical Society.

The UVPD dissociation event can be used for directed dissociation to control fragmentation or introduce chromophores to molecules, inducing fragmentation.[68-70] Fragmentation by 193 nm wavelength radiation produces all *a/x*, *b/y*, and *c/z* fragmentation events in peptide species through mechanisms that are still being investigated.[71]

1.4. Fourier Transform Ion Cyclotron Resonance Mass Spectrometry FT-ICR MS

FT-ICR was the first example of a Fourier transformed mass spectrometry technique. Based on fundamental interactions between ions and electromagnetic fields ion cyclotron resonance was developed by Lawrence and Edlefsen in the 1930s studying how ions could be accelerated in magnetic fields and how fundamental properties could be measured from this interaction (such as cyclotron frequency, charge, and mass). The first example of what could be described as an ICR MS was developed by Hipple to accurately measure the charge on a proton. The measurement was carried out by exciting a select mass with the use of a RF wave. The excited ions would increase in excitation radius until the ions contacted a detector which measured the current produced.[72]

Marshall and Comisarow[73,74] developed what can now be recognised as the first FT-ICR MS. Knowing the cyclotron resonance of every ion is different and related to the mass of the ion the relation between the cyclotron frequency and the mass to charge ratio can be measured of all the ions present in a mixture if all the ions are excited in radius. After excitation the frequency of the ions can be measured by their induced current producing a complex waveform. Fourier transforming the waveform generated can then produce a frequency measurement which can be converted to a *m/z* measurement through calibration.[75]

Over the years magnet strength has increased and overall front end instrument design has changed, although the measurements are still based on the same principles developed by Marshall and Comisarow initially.

The main principle of FT-ICR mass spectrometry is the use of both an electric field and magnetic field to trap ions within an ion trap (known as a cell), in the presence of a magnetic field the ions will precess normal to the plane of the magnetic field at their cyclotron frequency. The ions are excited using an excitation frequency which increases each ions radius, excitation can be carried out in a number of different ways explained below. After excitation the now coherent ions are present at a higher

radius within the ICR cell where their individual cyclotron frequencies can be measured.

1.4.1. Cyclotron frequency

The cyclotron frequency of an ion is a unique frequency based on the *m/z* ratio of the ion. The cyclotron frequency is a circular motion which occurs in the plane perpendicular to the direction of the magnetic field. The cyclotron frequency is based on the motion of an ion after excitation in a circular motion at a set frequency.

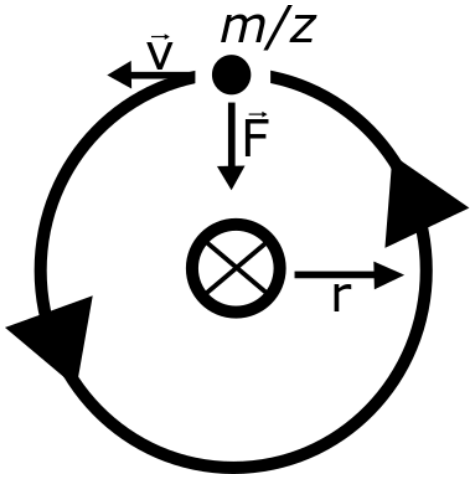

Figure 1.19: Cyclotron resonance of a particle when the magnetic field is going into the plane of view. The frequency that the ion spins is only dependent on the mass to charge ratio and the strength of the magnetic field.

The generation of the cyclotron motion of an ion is based on force exerted by the magnetic field when an ion is in motion within it and since motion is always circular:

$$F = m \times a = m\frac{dv}{dt} = \frac{mv^2}{r} = qvB$$

Equation 1.1: Relationship between the force and the charge (q), velocity (v), mass (m), radius (r), and magnetic field strength (B).

The angular speed of rotation is the velocity divided by the radius the angular speed can be calculated as:

$$\omega = \frac{v}{r} \quad and \quad r = \frac{mv^2}{qBv} \qquad \therefore \qquad \omega = \frac{qB}{m}$$

Equation 1.2: Calculation of angular velocity

The cyclotron frequency ω_c can then be calculated by:

$$f_c = \frac{qB_0}{2\pi m}$$

Equation 1.3: Cyclotron frequency of an ion in radial motion

The cyclotron frequency is, importantly, only dependent on the charge, mass, and magnetic strength.

The final frequency measured takes into account the cyclotron frequency and a further magnetron frequency. The magnetron frequency is further explained below but the frequency measured is now the "reduced cyclotron frequency" taking into account both frequencies.

$$\omega_{-} = \frac{\omega_c}{2} \pm \sqrt{\left(\frac{\omega_c}{2}\right)^2 - \frac{\omega_z^2}{2}} \qquad \omega_z = \sqrt{\frac{2qV_{trap}\alpha}{ma^2}}$$

Equation 1.4: Reduced frequency (ω_{-}) dependent on the cyclotron frequency ω_c and the magnetron motion ω_z.

When an ion is excited it is absorbing energy as a function of the electric field used for excitation and the velocity of the ion. As the energy of the ion increases; the radius of the ion increases as the mass, charge, and exerted field remain equal.

$$r = \frac{E_0 T_{excite}}{2B_0}$$

Equation 1.5: The radius of the ion increases with the energy exerted in excitation and the length of time that energy is exerted for.

$$K.E = \frac{m\omega_2^c r^2}{2} = \frac{q^2 E_0^2 (T_{excite})^2}{8m}$$

Equation 1.6: The kinetic energy is raised as a function of the energy and excite time, as all of these are constants the radius of the ion must increase with kinetic energy.

The properties of an ion in cyclotron motion can give guidance to the design of the magnets and cells used for FT-ICR MS.

1.4.2. Magnetron motion

Magnetron motion is a slower frequency motion in the plane of the trapping magnetic field, much like the cyclotron frequency. The magnetron frequency is detrimental to the analysis of the ions by FT-ICR as the relationship between magnetron motion and cyclotron motion is not the same reducing the relationship between the *m/z* ratio and the cyclotron frequency.[75]

The magnetron motion of an ion in the cell is caused by the electric fields of the trapping plates causing an outward radial force, away from the centre of the cell. The magnetron motion is therefore caused by a force in direct opposition to the trapping Lorentz force. The magnetron motion is not possible to remove due to the fundamental relationship between the motion and the trapping potential. The magnetron motion can be reduced though initially by reducing the initial displacement of the ions when they are introduced to the cell. If the ions start the excite/detect motion offset from the centre of the cell the magnetron motion is greatly increased, the lowering of the potentials of the trap plates also reduces the magnetron motion as the overall opposing force is reduced allowing the ions to remain in the centre of the cell. Unlike the cyclotron frequency the magnetron motion is also not damped by collisions like the cyclotron frequency. The cyclotron frequency damps quickly as energy is transferred to the colliding molecules causing a reduction in energy and therefore radius of the ion. As the magnetron motion is caused by a static trapping potential collisions with neutral species does not cause a reduction in this frequency, but may often increase it as the ion is pushed through the electric field non-uniformly.

The magnetron motion, although detrimental, occurs at a much lower frequency that than of the cyclotron frequency. Often the effect is low when trapping plates are held at low electronic potentials and a good vacuum is maintained.[76]

1.4.3. Magnetic field in FT-ICR

The presence of the magnetic field trapping the ions in the *x*-*y* plane is due to the bending of the path around the axis of the magnetic field. Modern FT-ICR mass spectrometers use super conducting solenoidal magnets which are shaped around the trapping cell meaning the magnetic field moves in the *z*-axis of the cell plane.

The ions are trapped in the *x*-*y* plane by the presence of the magnetic field, trapping plates or potentials are used at either end of the cell to trap the ions in the *z*-axis. Figure 1.20 shows how an ICR-cell is set within the magnet. The magnetic field lines have been reduced for ease of viewing, but essentially the super conducting coil that is present the entire length of the ICR-cell, and often longer to generate a true homogenous magnetic region within the ICR-cell space, the magnetic field will be present in the *z*-axis and therefore trap ions in the *x*-*y* plane.

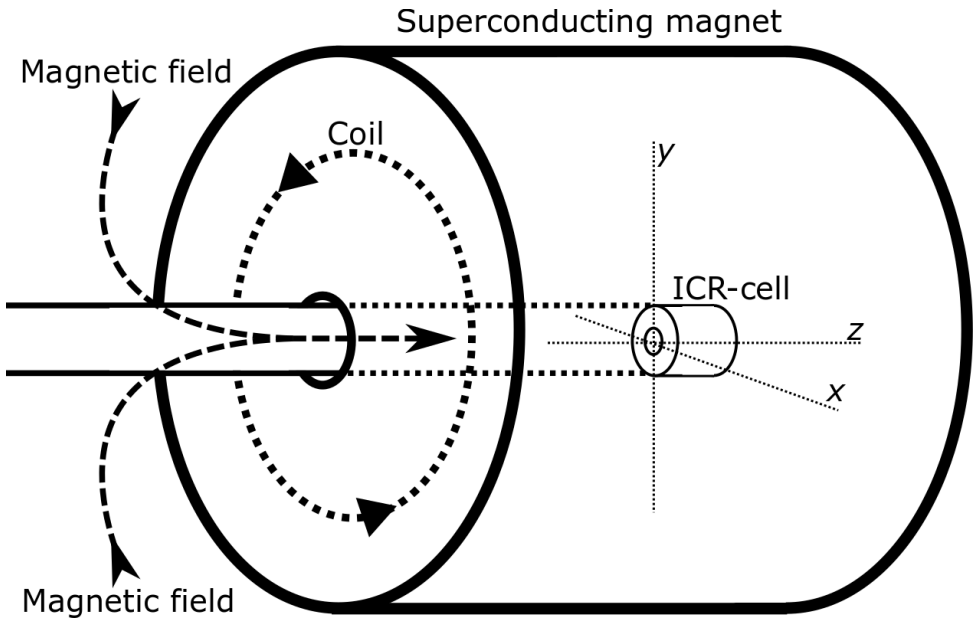

Figure 1.20: Simplified outline of a FT-ICR magnet showing the position of the ICR-cell, the superconducting coils which generate the magnetic field will cover the entirety of the ICR-cell to generate a homogenous magnetic field region. The magnetic field generated is present in the z-direction within the ICR-cell region trapping ions in the x-y plane.

At higher magnetic field strengths the kinetic energy of the ions can be greatly increased and still contained within small ion radii causing a significant decrease in the ion radius at higher kinetic energies. Another feature is higher masses can be

stored within a tighter space with an increase in magnetic field strength, shown in Figure 1.21.

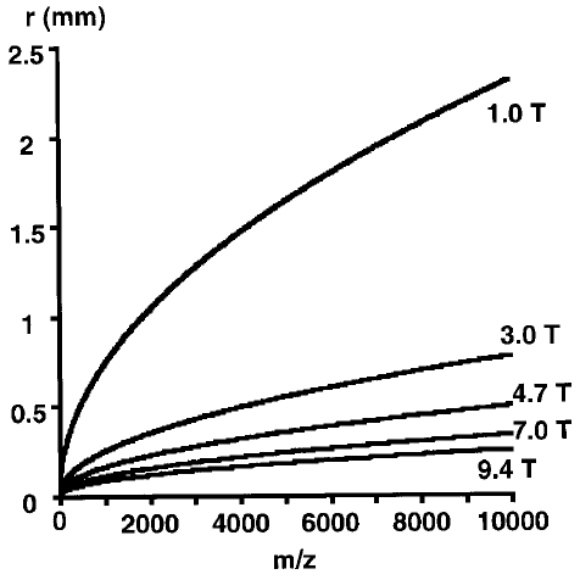

Figure 1.21: ICR orbital radius of various ions in different strengths of magnetic fields. Reproduced with permission from Marshall *et al.* Figure 3.[75] Copyright 1998 John Wiley and Sons.

An increased magnetic field also gives a significant advantage to the mass accuracy of the instrument. Also higher magnetic fields reduces the mass domain peak width. Taking the first derivative of Equation 1.2 shows how an increasing magnetic field strength must be met with a decreasing peak width.

$$\omega_c = \frac{qB}{m} \qquad \frac{\delta\omega_c}{\delta m} = -\frac{qB}{m^2} \qquad \left|\frac{m}{\Delta m}\right| = \left|\frac{qB}{m\Delta\omega_c}\right|$$

Equation 1.7: The variation in cyclotron motion of a particle is directly related to the magnetic field meaning higher accuracy mass measurements can be made with higher magnetic field strengths.

The relationship between magnetic field strength and circular ion velocity also means that the resolving power increases linearly with magnetic field strength. The increased velocity of the ions means that for a given mass resolving power the time taken to acquire a mass spectrum can be reduced inversely proportional to the magnetic field strength. Likewise for the same experiment time higher resolving power can readily be obtained.

$$\frac{m}{\Delta m} \alpha \frac{qBT}{m}$$

Equation 1.8: Relationship between the magnetic field strength and the time needed, T, to acquire a spectrum with a set resolving power (m/Δm). At higher magnetic field strengths a shorter time may be used.

The maximum number of ions that may be trapped is based on complex relationships regarding, charge concentration, total ion charge, and ion temperature, but the contraction effect of larger magnets generally means more ions may be stored in the same sized trap before significant space charge limitations occur. There are also other advantages based on the reduced amount of peak coalescence that occurs at higher magnetic field strengths.

Peak coalescence is not a feature of space charge effects but much more to do with the relationship between ions that have a very similar cyclotron motion, each of these exert an electric field repulsing one another generating their own magnetic fields. The generation of magnetic fields between the ions causes further motion outside of the cyclotron motion, a form of magnetron motion, and the ion clouds no longer travel at the expected (accurate) cyclotron motion but begin to 'lock' into one another. The locking effect is reduced by higher external magnetic fields as this decreases the spread of discrete ion packets, more effectively separating cyclotron motion of nearby ions, therefore reducing ion coalescence.

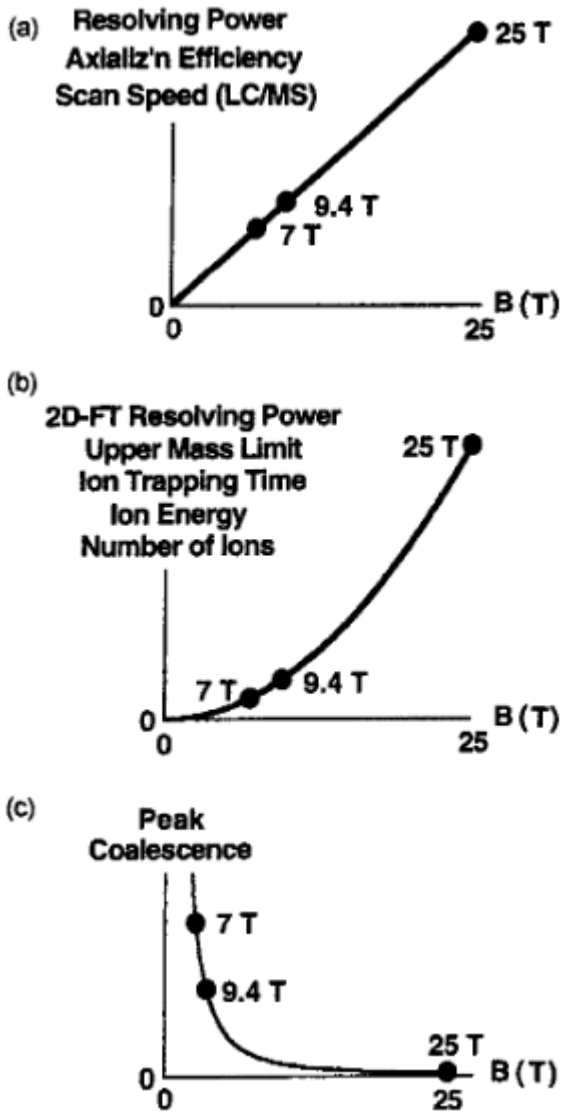

Figure 1.22: Magnet strength effects on (a) Resolving power, caused by increased rotational speed for a given time. b) Resolving power in the second dimension. c) Reduction in peak coalescence at higher magnetic fields caused by an increase in the difference between ion cyclotron resonances. Reproduced with permission from Marshall et al. Figure 1.[77] Copyright 1998 John Wiley and Sons.

1.4.4. Calibration in FT-ICR MS

The ability to achieve very high mass accuracy with FT-ICR MS instruments is a significant analytical advantage with the use of FT-ICR methods. High mass accuracy measurements can be used for the analysis of complex mixtures of species confirming chemical composition.

Production of accurate mass measurements requires extensive calibration. Theoretically, there is a direct conversion between the cyclotron frequency and the *m/z* of the ions, **Error! Reference source not found.** above. In practice the r elationship isn't that simple, the magnetron motion and space charge of other ions within the analytical cell changes the electro-magnetic profile each ion experiences and therefore there is a shift in the cyclotron frequency.[78-80]

The first steps towards taking into account the various charge effects were carried out by Jeffries in which the trap electrodes were accounted for by assuming a "perfect" electronic effect across the cell.[81,82] Further work showed how increasing the space charge effects could be mapped within ICR cells but the variation was based on the amount of space charge present, but the relationships were far from random, and linear within certain ranges, allowing calibration to be carried out.[83]

By adjusting the mass-to-charge ratios by a set calibration function, which was experimentally determined based on the observed frequencies.

$$\frac{\mathrm{m}}{\mathrm{z}} = \frac{a}{f} + \frac{b}{f^2}$$

Equation 1.9: Frequency calibration taking a constant magnetic and static electric fields caused by ion space charge and trapping voltages, the differences between the effective frequencies measured by be used to determine the effective difference between known frequencies f.

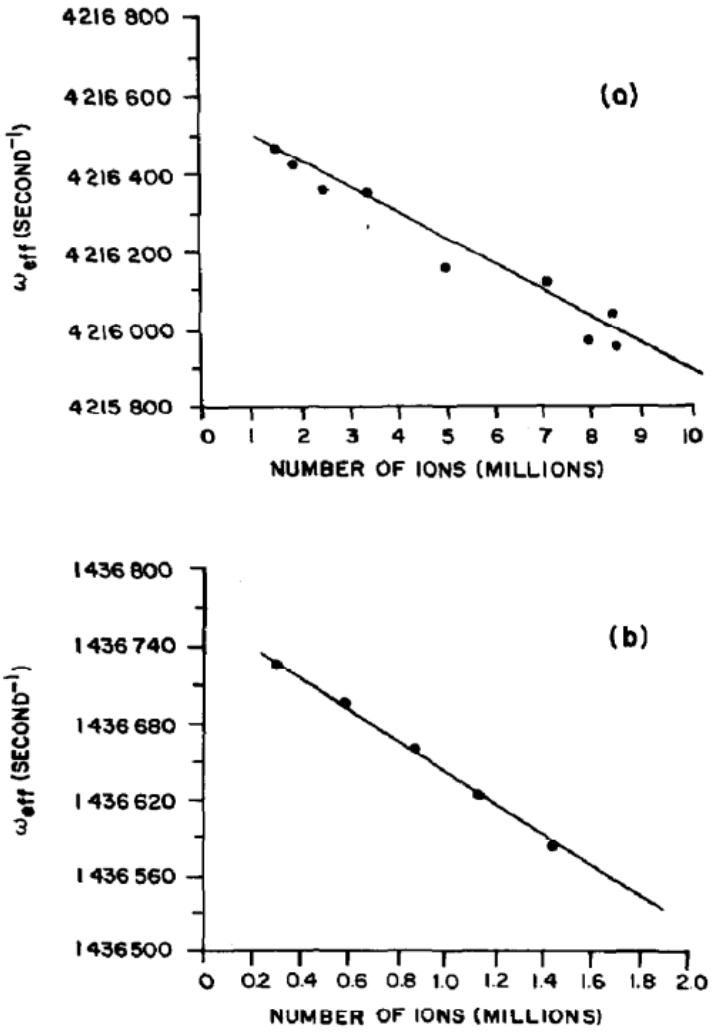

Figure 1.23: **Change in the effective frequency with the addition of more ions and therefore an increased in the space charge of two different ICR cell sizes (a) 3.18 cm x 3.18 cm x 15.34 cm and b) 5.5 cm x 5.5 cm x 5.5 cm cell. Reproduced with permission from Francl *et al* Figure 4.[82] Copyright 1983 Elsevier.**

Further developments from these equations have occurred taking into account more variables and generally working towards better fitting of the parameters within the FT-ICR cell.

Increasing the number of factors (a, b, c) in the calibration equation serves the purpose of providing a better fit but with the disadvantage of significantly less external calibration accuracy, to put simply a, b, and c hold best for the space charge that the values were calculated from.

$$\frac{\mathrm{m}}{\mathrm{z}} = \frac{a}{f} + \frac{b}{f^2} + \frac{c}{f^3}$$

Equation 1.10: Frequency calibration taking a constant magnetic and static electric fields caused by ion space charge and trapping voltages, addition of a third variable allows further accuracy to significantly below ppm orders of error.

The ability to use the calibration function as an external calibration function can be extended by the correction for intensity, which is a reasonable prediction of space charge field effects. [78]

$$f_{estimated} = f_{measured} + c(I_{calibrant} - I_{analyte})$$

Equation 1.11: Correction function to allow calibration to be adjusted for an unknown peak at a higher accuracy.

The following functions have been modified and changed for various different tasks[84] [85-87]but the core calibration functions and the principals behind them have stayed the same. The table below shows different calibration functions discussed in Gross and coworkers review on calibration functions giving a good idea of the development of calibration methods in FT-ICR.[88] Further adjustments to calibration equations may be carried out by changing the values within the calibration equation based on the space charge found within a *m/z* region within the spectrum.

Table 1.1 Different calibration equations used for the analysis of FT-ICR data and the development process, from [88] used with permission.

$f = \frac{a}{m}$	basic law of ions in a B field
$f^2 = \frac{a}{m^2} + \frac{b}{m}$	(Beauchamp-Armstrong et al., 1969)
$f^2 = \frac{a}{m^2} + \frac{b}{m} + c$	(Ledford et al., 1980)
$f_{sideband} = \frac{a}{m}$	(Allemann et al., 1981)
$f = \frac{a}{m} + c$	(Francl et al., 1983)
$\left(\frac{M}{Z}\right) = \frac{a}{f_{obsd}} + \frac{b}{f_{obsd}^2}$	(Ledford et al., 1984b)
$f_{estimated} = f_{measured} + c(I_{calibrant} - I_{analyte})$ $\frac{m}{z} = \frac{A}{f_{estimated}} + \frac{B}{f_{estimated}^2} + \frac{C}{f_{estimated}^3}$	(Easterling et al., 1999)
$M = (\frac{kB}{f_n + \Delta f})n - n(M_c)$	(Bruce et al., 2000)
$\left(\frac{M}{Z}\right)_i = \frac{a}{f_{obsd}} + \frac{b}{f_{obsd}^2} + \frac{CI_i}{f_{obsd}^2}$	(Masselon et al., 2002)
$\frac{m}{z} = \frac{A}{v} + \frac{B}{v^2} + \frac{C}{v^3} + \frac{BC}{Av^4}$	(Wang et al., 1988)

1.4.5. Cell design

The main features of FT-ICR MS cell design are that the ions are trapped axially by trapping voltages and can be excited into a higher energy state and therefore a higher radius. Once the ions have entered the higher radius the excitation frequency can be removed and the current induced by the rotating ions can be measured.

The presence of the magnetic field produces a trapping force within the plane of the trapping cell, meaning electronic voltages only need to be present to trap the ions axially. Trapping plates are used within the *z* axis of the cell, the trapping plates will be adjusted with the front trapping plate held at a lower voltage to allow ions to enter the cell. The potential with the cell will be lower than this and trap the ions within the cell, there may be the addition of side kick potentials to adjust the initial position of the ions as they enter the cell. Finer controls, such as side kick, are

important for the highest resolution experiments to minimise potential effects of the ions been excited off-centre.

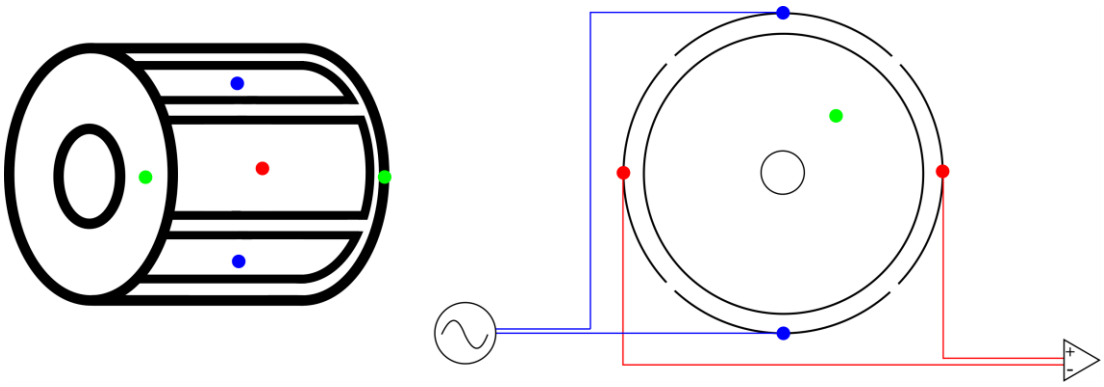

Figure 1.24: Excitation plates (blue) are used to drive the ions to a higher radius which can then be measured by the detection plates (red) the two end plates are the trapping plates which trap the ions axially.

z-axis ejection was the most common issue affected ICR cells historically, the presence of significant *z*-axis electric fields within the centre of the cell increases magnetron motion and destabilises ions within the cell. TO minimise the effects of these *z*-axis fields the trapping voltage can be varied along the back-trapping plates of the cell.

By varying the voltage from high to low on the front and back trap plate by using a series of resistivity coupled plates, the electric field within the *z*-axis can be minimised and provide better results. The "infinity cell" is designed in such a way that the reduction of the voltage across the trap means the ions experience an electric field of "infinite" length.[89]

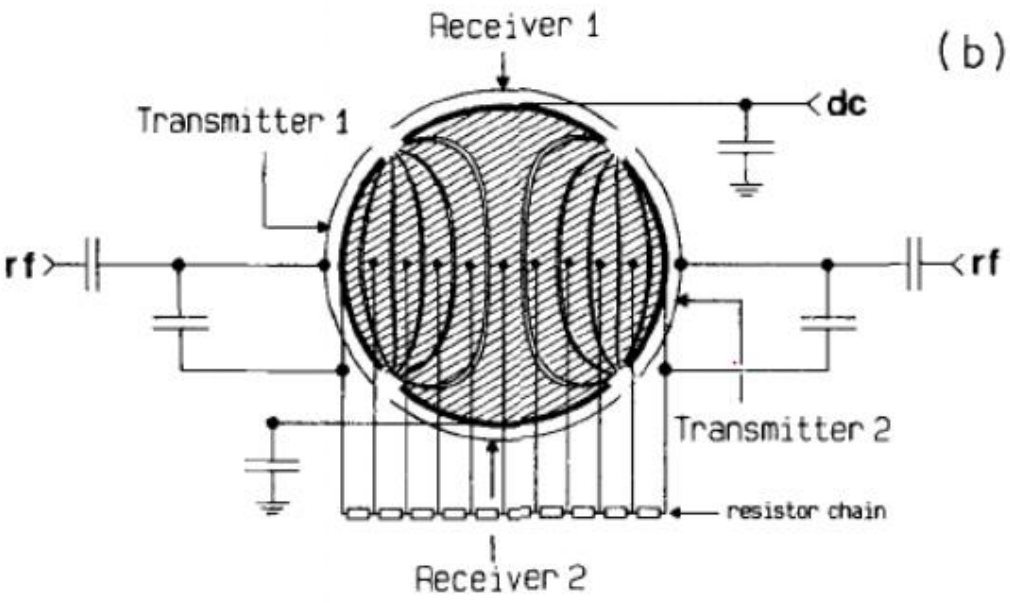

Figure 1.25: Infinity cell diagram showing the separation of a resistively coupled trapping electrodes which allows a more uniform electric potential within the cell increasing the mass accuracy measurements from the cell. Reproduced with permission from Caravatti and Allemann, Figure 2[89] reproduced with permission. Copyright Wiley and Sons 1991.

Further improvements have also been found with the use of dynamically harmonised cells. The idea behind the cells present here is the *z*-axis trapping motion is on a much longer time scale than the cyclotron frequency and the *z*-axis electric field may be able to be changed in such a way that over the course of the cyclotron motion the *z*-axis electric field stays constant. [90]

The use of curved electrodes as part of the excite and detect plates allow a continuous change in the electric field of the ion as it completes its cyclotron motion meaning, overall, the electric field experienced by the ion stays the same. The cell achieves the dynamic electric field effects by having convex and concave plates. The convex electrode plates act as trapping plates by having the maximum size at the ends of the ICR cell and their smallest width in the middle. The excite and detect plates are largest within the middle of the cell.[91]

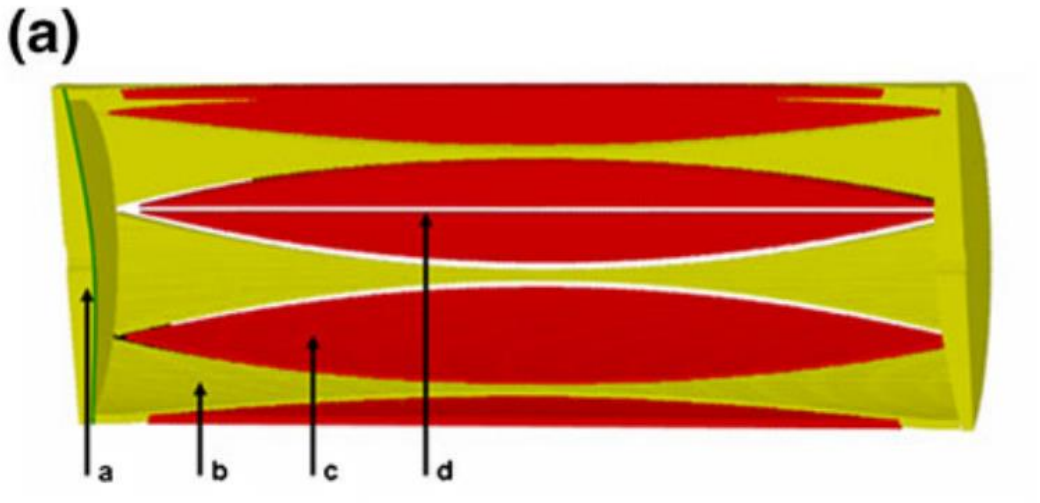

Figure 1.26: The dynamically harmonized cell, a) trapping electrodes with circular geometry, b) electrostatic field harmonization electrodes with set voltage, c) segments that produce excite/detect separated by d) grounded line that separates excite/detect regions of the ICR cell. Reproduced with permission from Kostyukevich *et al.* Figure 1 from [92] Copyright Springer 2012.

The increased mass accuracy afforded by the use of more accurate control of the electric fields within cell designs has meant there has been a significant increase resolving power and mass accuracy of analysis carried out on the new cells.[93]

Overall, the motion and understanding of how ion excitation occurs within a cell is incredibly important to achieving accurate analysis within FT-ICR mass spectrometers.

1.5. Two-Dimensional mass spectrometry

Two-dimensional mass spectrometry (2D MS) is an analysis technique that has had a basis of understanding now for approximately thirty years.[94-96] Initial work by Gaumann showed that precursors and fragments could be correlated in much the same way that 2D NMR can utilise a pulse sequence, to change electromagnetic states of species and then correlate coupling between them.

The most obvious technique that holds similarity is the NOESY NMR type experiment. The bases of the NOESY experiment is two pulses which consist of delays: evolution time and mixing time. The delays present in the pulse sequence are important as they allow a change in electromagnetic state to develop and therefore interactions between these states to be quantified.

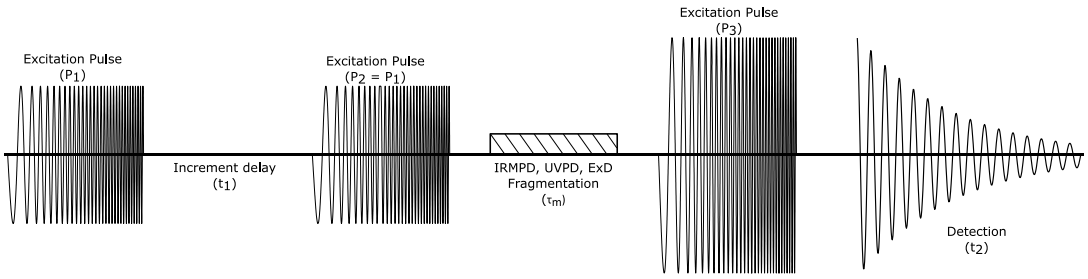

Figure 1.27: 2D MS pulse sequence. The t_{mix} that is present in a NOESY experiment is now replaced by a fragmentation event. P_1 and P_2 are importantly identical chirp pulses the phase of the ions dictates whether the ions are excited or relaxed

The Marshall group published a seminal paper in the use of pulses to move ions within an ICR cell using low energy frequency pulses. An interesting result from these experiments was the ability to excite the ions partially, increasing their radius, and then pulsing another identical energy pulse once the ions phase had inversed as the ions travelled across the cell. The second pulse caused the ions to reduce in energy, as they're now being excited in the opposite direction, and therefore reduce in radius back into the centre of the cell. The movement of ions inside and FT-ICR cell is essential to the use of 2DMS.[97]

2DMS is based on a series of excite and delays that allow ions to separate spatially. A fragmentation method is then used which has spatial resolution meaning ions are

fragmented depending on their *m/z* ratio caused by the delays in the pulse sequence. The intensity variation as precursors are fragmented and fragments are generated allows the coupling of precursors and their respective fragments.

Uptake of 2D techniques though has been limited due to hardware and software shortcomings on data file handling and acquisition of data for the 2D technique. Recently there has been a push in 2DMS development due to the increase computing capacity and power.

1.5.1. The 2D process

2DMS is a technique in which analytes are modulated within a fragmentation region. The modulation of the ions allows the phase of the fragments to be assigned to their respective precursors.

2DMS can be incorporated in any ion trapping mass spectrometer where manipulation of ion radii is possible and a radius dependent fragmentation process is. This rest of this section will focus on the use of 2D in a FT-ICR cell but the principles are applicable to any 2D MS process.

P1 - A low energy excitation pulse excites ions partially out from the centre of the ICR cell.

T1 - The pulse delay, this allows **spatial resolution** of the ions to occur within the cell as they will all move around the cell at different frequencies. The delay is incremented over the course of the experiment so every scan allows the ions to precess around the cell for a different amount of time. The reason that the delay stops at a value of 2^n allows the fast Fourier Transform to be used.

P2 - An identical excitation pulse to **P1**; now that the ions have been spatially resolved the excitation pulse will cause ions to de-excite back into the centre of the cell or be further excited out depending on the ion's phase.

Fragmentation - fragmentation is carried out using a **radius dependent** fragmentation method. The ions that have been de-excited back further into the fragmentation region fragment more than those less so, or excited outwards.

Excite - Detect - These steps measure the ions based on their ion cyclotron resonance as this is carried out in FT-ICR MS. The relative intensity of each response from precursors and fragments are measured together.

Overall, the ions will **modulate** in intensity depending on if they are excited/de-excited within the fragmentation region. The ion response of the fragments and precursors will be inverse to one another. Using a Fourier Transform the fragments can now be linked to their precursors.

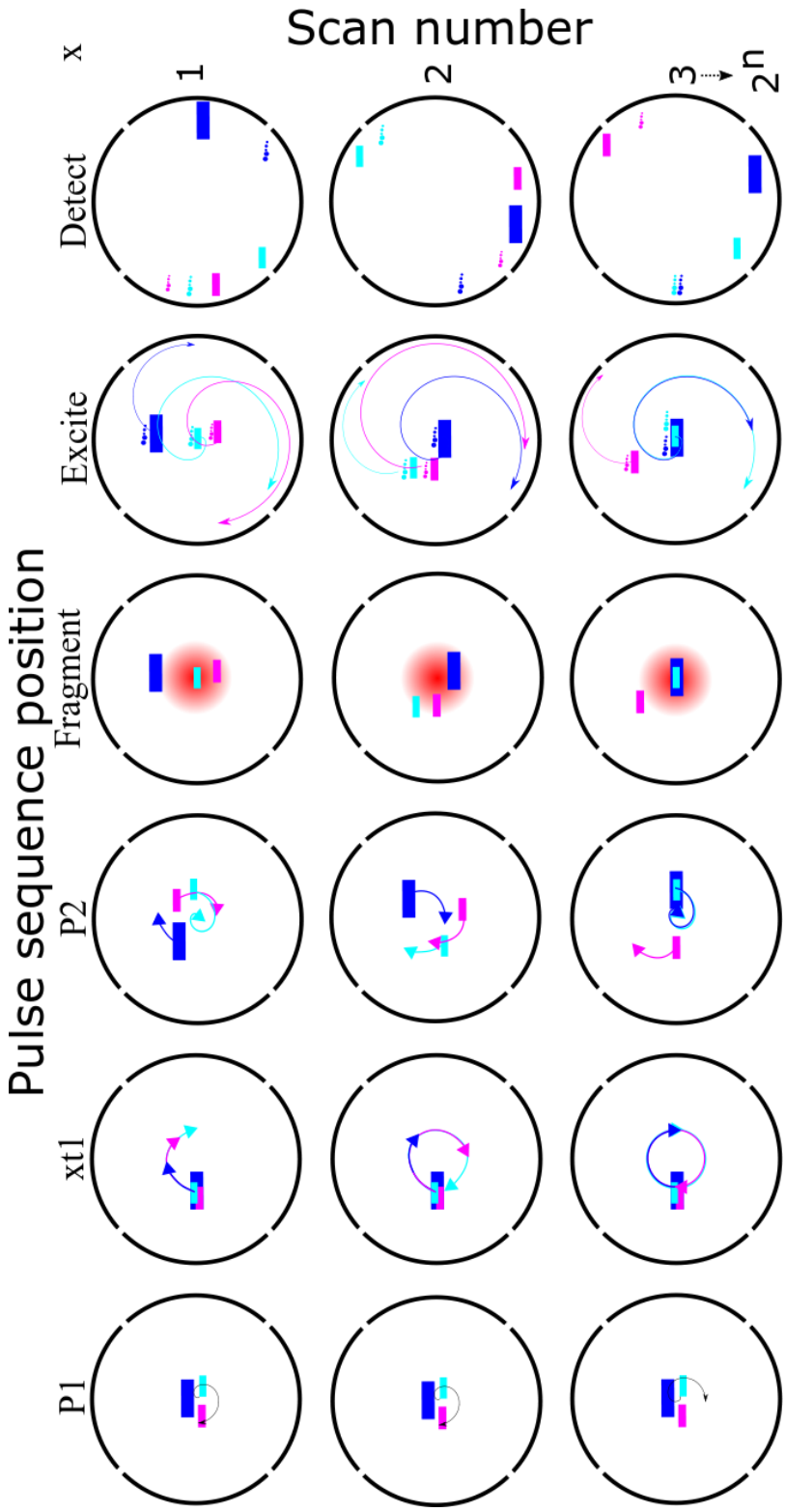

Figure 1.28: Diagram which shows the first ion motion for the first 3 scans as part of a 2D experiment. The P1 and P2 are identical pulses that cause ions to excite or de-excite out of/into the fragmentation region. The delay t1 is the basis of a 2D-MS experiment. Importantly, this delay changes causing the ions to modulate in intensity with each scan.

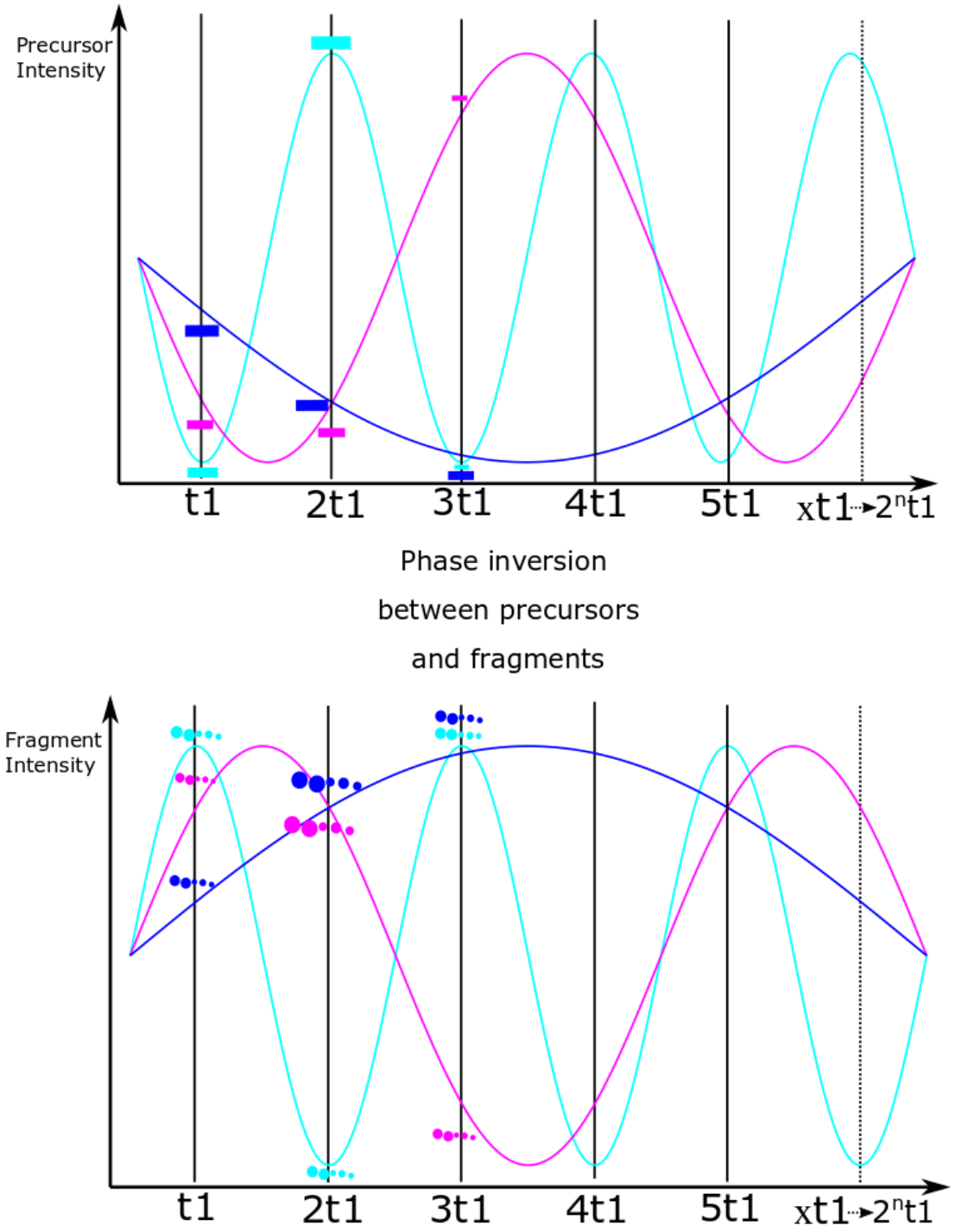

Figure 1.29: Diagram which shows the variation in precursor ion intensity with the scan. The fragment ion intensities will vary with an inverted phase to the precursors. If multiple precursors generate the same fragment the relationship will still be seen due to the sine wave formation allowing Fourier transform of both dimensions.

An issue that is formed with this experimentation is that any consistent modulation will be measured as part of the 2D FT and will, therefore, affect the results. The effect of inconsistent ion intensities from scan to scan was shown to add scintillation noise by Marshall *et al*,[98] scintillation noise is a presence of streaks in the *y*-dimension. The presence of streaks in the *y*-dimension are also present in 2D NMR but are often caused by inconsistencies with excitation pulse power, variations in the phase of pulse used, and significant issues in the first NMR instruments to accurately convert between analogue and digital signals in pulse measurement and generation. With better technology the issues in 2D NMR have been fixed allowing clearer NMR spectra to be produced.[98,99]

The spectra generated by 2D MS experiments are often complex, but information dense. The 2D MS spectrum represents the overall response from both the first and second dimension results. While the 2D MS representing the overall relationship may seem like an obvious factor it is easy to treat the axis as completely separate and miss represent the data produced.

1.5.2. 2D MS research

A significant advantage offered by 2D MS is the redundancy of an external separation method. The separation of ions occurs within the mass spectrometer itself. Without the need for external separation a much greater number of species that may be analysed become available.

The focus on 2D MS experimentation has been on the analysis of biological molecules as method development for the analysis of more complex biological systems. Research has focussed on the use of IRMPD or ECD fragmentation within an ICR cell to achieve modulated fragmentation resulting in 2D experiments. Work carried out by Agthoven *et al.* showed that ECD can be used in a 2D MS setup for the analysis of peptides and glycopeptides.[100]

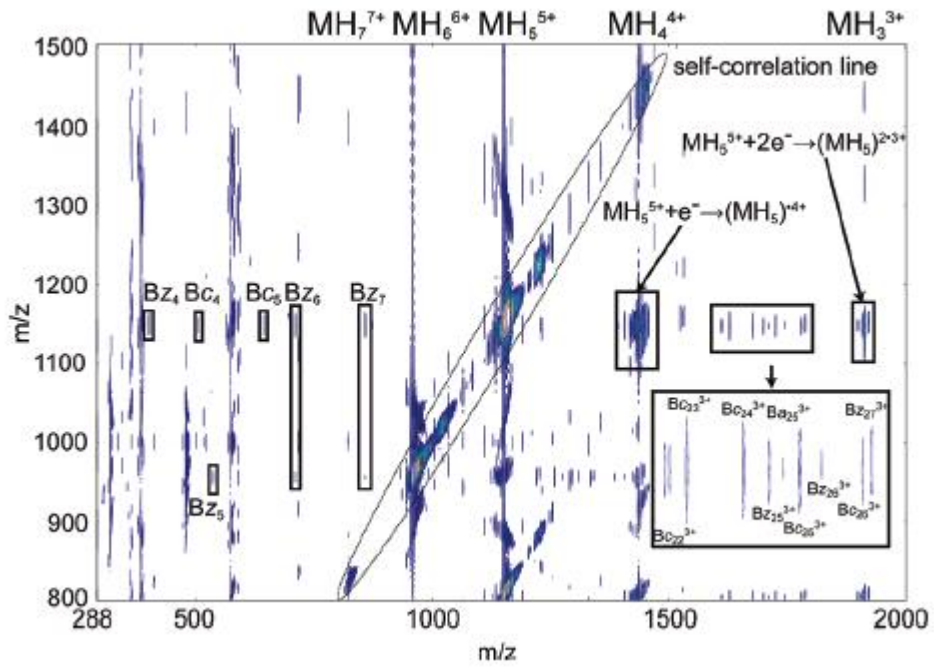

Figure 1.30: 2D MS of bovine pancreatic insulin using ECD as the fragmentation technique. The large intensity ions in the centre are the precursor ions marked at the top, the c and z fragment ions can be seen in the same fragment ion m/z as the same precursors produce the same fragments. Reproduced from Agthoven et al. Figure 5.[100] Copyright 2012 American Chemical Society.

An obvious issue with 2D MS work could be seen from the presence of t_1 or scintillation noise. Persuing this work a series of papers have been published on the use of different denoising algorithms for 2D MS data sets. The main focus of denoising 2D MS is the reduction of noise by removing peaks that are seen consistently in the t_1 dimension, the equivalent of a fragment peak being present at every precursor *m/z*.[101,102]

Further work into more complex biological species was carried out by bottom-up analysis of collagen samples.[103] Bottom-up analysis of biological samples was well suited to 2D MS due to the formation of many species after digestion, 2D MS allowed the analysis of many individual peptide species without the need for a pre-MS separation method. Individual peptide lines were extracted and analysed showing good cleavage coverage.

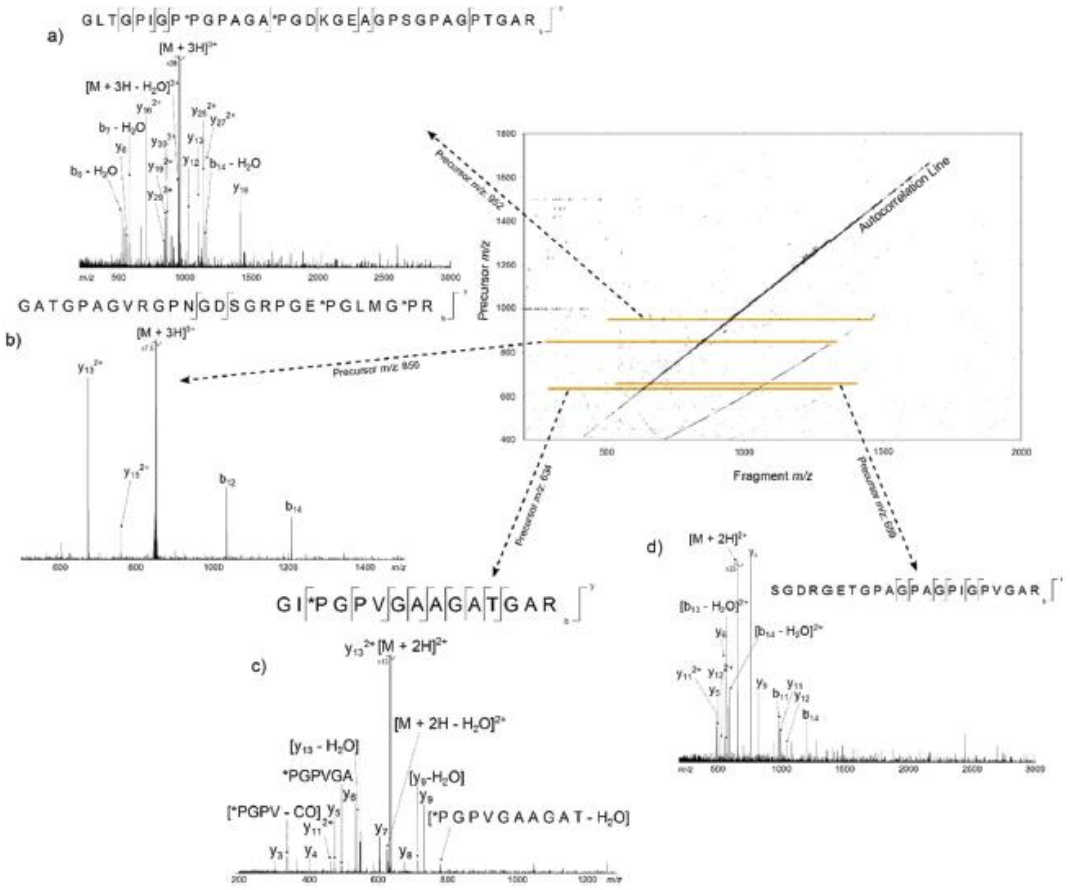

Figure 1.31: 2D MS of a digested collagen mixture. Orange lines represent extracted precursor lines showing the fragments that each precursor generated. Reproduced from Simon et al. Figure 2.[103] Published by the Royal Society of Chemistry.

Calmodulin was analysed by both top-down and bottom-up analysis in a 2D MS exepriment.[104] The analysis was carried out by IRMPD on both a digested sample and a un-digested sample to act as a comparison of the fragmentation methods. The use of 2D MS again showed significantly lower coverage compared to one dimentional methods. For data storage reasons the top down and bottom up experiments were carried out by either significuntly cutting the number of vertical or horizontal scan transient lengths. In terms of data points, the top-down 2D MS was carried out using 4 M data points in the *x* dimension and 512 scans in the *y* dimension. The bottom up 2D MS used 4096 scans at 512 k points.

The two experiments achieved similar fragmentation coverage but showed that the successful analysis of intact proteins was possible by 2D MS opening up the potential for use on more complex biological matricies.

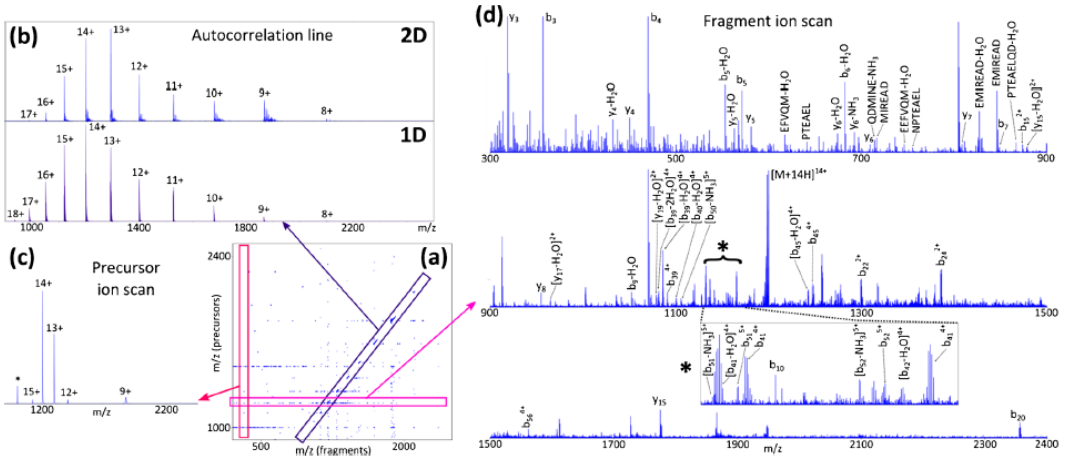

Figure 1.32: 2D MS of calmodulin in a top-down format. Each charge state is analysed for fragment coverage in one experiment. The autocorrelation line shows the different precursor charge states that are present and precursor ion scans can show which fragments are generated by which precursors. The extracted fragment ion scans show the coverage at each precursor. Reproduced with permission from Floris et al. Figure 3.[105] Copyright 2018 American Chemical Society.

Proof of concept of 2D MS analysis of polymers has been carried out with the analysis of TPGS, and polysorbate 80 (a PEG based polymer) using IRMPD fragmentation methods. The analysis of the different molecules showed that multiple oligomer unit values of the polymers could be analysed at one time without the need for separation of each oligomer unit. Suprisingly, the study did not find significant fragmentation along the polymer backbone with the use of IRMPD, likely due to the fragmentation of the weakly bound end groups before fragmentation of the PEG chain.

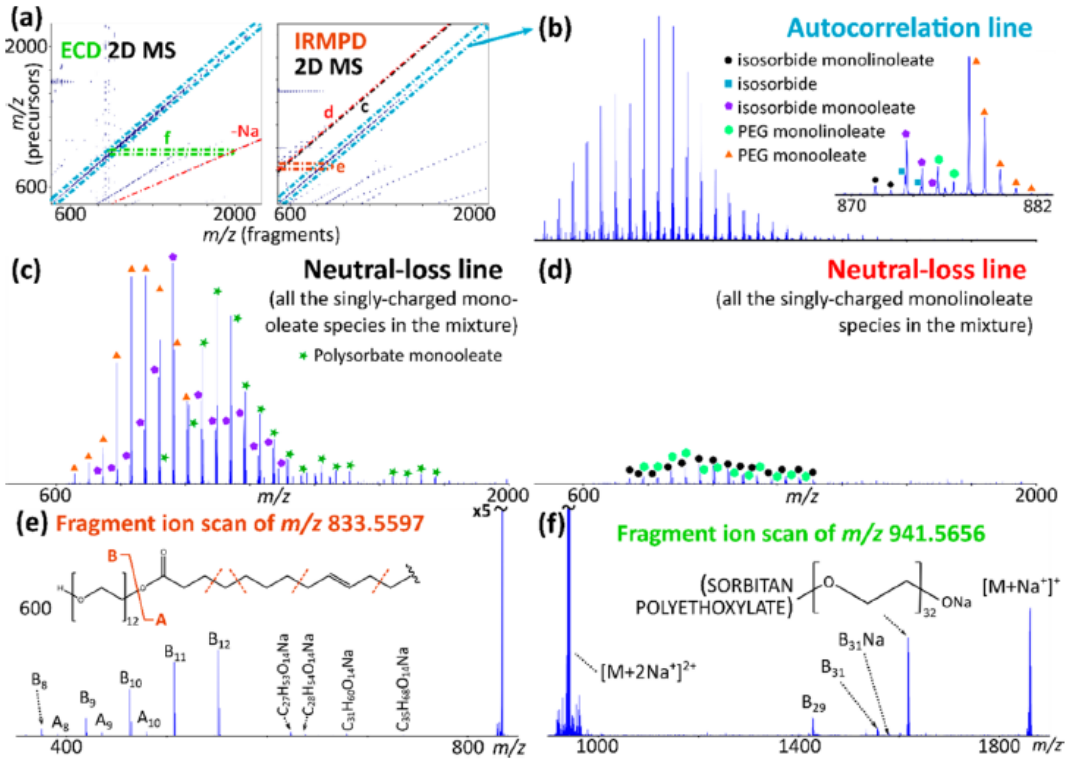

Figure 1.33: 2D MS analysis of polysorbates by 2D MS the analysis of these species shows fragmentation along the end group and that the fragment lines can be extracted and end group fragments identified. Reproduced with permission from Floris et al. Figure 2.[106] Copyright 2017 American Chemical Society.

2D MS analysis so far has been mostly focussed on the proof on concept of a variety of materials. Improvements to the fragmentation optimisation as well as the resolving power in both axes would increase the reliability and accuracy of the method allowing a greater variety of species to be analysed.

1.6. Polymers, peptide-polymer conjugates, and polymer analysis

Polymers are macromolecules that can be identified as being made up of shorter groups, called monomers, covalently bonded together. The polymerisation process is useful due to the ability of making large structures in relatively simple synthetic processes. Polymers produced can cover a wide range of complexity and the classification of polymers is important in the understanding of their analysis, especially to an unfamiliar mass spectrometry specialist.

The synthetic process of all polymers involves the initiation of monomer species in a way that they polymerise together. The nature of the initiation and corresponding monomer chain reaction cause a statistical increase in polymer size. The resulting polymer is therefore a mixture of species within the statistical distribution of chain lengths/sizes that are produced.

1.6.1. Polymer classification

Historically, polymers have been classified based on the synthetic steps that were taken to produce the polymer.[107,108] Separating polymer classification based on addition, such as polystyrene, or condensation, such as polyesters, was simple but ineffective at separating similar polymers made through different synthetic routes such as nylon formation through condensation of an amine and carboxylic acid, or ring opening of caprolactam.

As synthetic methods have been developed the idea of classifying the polymer itself based on its synthetic route has stopped being used. Polymers are now classified by their monomer make up, side chain variation, cross linking and tacticity.

1.6.2. Homo- and co-polymers

The monomer, expectedly, has a large effect on polymer properties. The monomer will dictate the hydrophilicity, reactivity, and many of the physical properties of the final polymer.[109] A homopolymer is a polymer made from a single type of monomer unit. An advantage in producing homopolymers is a reduced product complexity due to further considerations of monomer reaction rates not needing to be taken into account.

Copolymers allow variation of a polymer's properties by changing the monomer within the chain. There are several different types of copolymer described by the International union of Pure and Applied Chemistry (IUPAC) polymer division.

The type of copolymer produced can depend on the synthetic conditions, such as reducing concentrations of a monomer at a certain time point, or by taking advantage of the reactivity's between different monomers.

Figure **1.34** gives an example of a selection of linear copolymer types. Random copolymers are ones in which the monomer order is truly statistically random, although true randomness is rarely the case due to differences in favourability of reaction of differing monomers due to the polymerisation methods used.

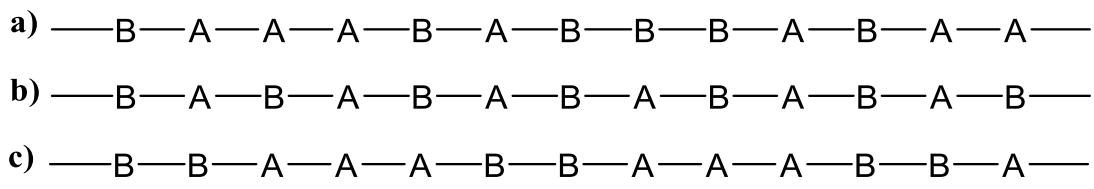

Figure 1.34: In this example a copolymer of monomers A and B are used to represent different copolymer structures. (a) An example of a random or statistical copolymer. (b) An example of an alternating polymer and (c) a periodic polymer.

1.6.3. Branched polymers

Linear polymers consist of one major polymer chain, the groups that are part of the monomer can be reasonably large and the polymer still considered linear and have properties expected of linear polymers. A branched polymer is one that has groups protruding from the main polymer backbone to create new chain directions/growth. Depending on how these branches are arranged then there can be significant differences in polymer properties. Graft polymers are an example of polymers that have multiple branches of an identical polymer off a different polymer backbone, Figure 1.35.

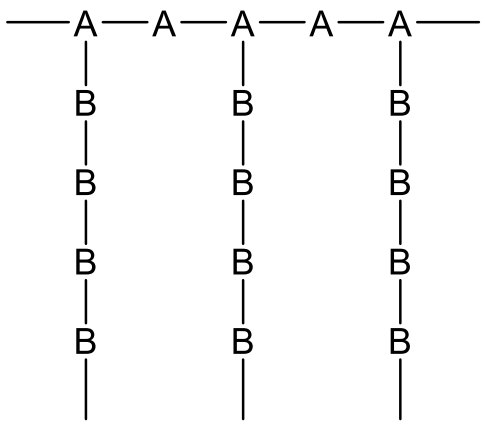

Figure 1.35: An example of a graft polymer with backbone monomer A and branching chains of monomer B.

Depending on the arrangement of the branches, as well as further branching from the branches themselves, the properties of the polymer can be varied. Hyper-branched and dendritic polymers are key examples of these which lead onto greater macromolecular chemistry.[110]

1.7. Polymer characterisation

There are various analytical methods used for polymer analysis and characterisation. As polymers are macroscopic molecules there is a significant amount of variation in the use of bulk analysis type methods as well as molecular characterisation methods. It is common for the analysis used to vary depending on the expected usage of the polymer. Recently, polymers have seen much more use as medicinal excipients increasing the need for accurate and in-depth characterisation.[111]

1.7.1. The molecular weight of a polymer

A polymer's properties are dependent on the number of chains that are present and the length of those respective chains. The most obvious calculation is the "number-average" molecular weight $\overline{M}_n$ of a polymer, Equation 1.12.

$$\overline{M}_n = \frac{\sum M_x}{\sum N_x}$$

Equation 1.12: The "number-average" molecular weight of a polymer. Where the total mass of all the polymer chains are summed and then divided by the total number of polymer chains. This gives an average mass of each polymer chain.

The $\bar{M}_n$ of a polymer is not the most affective descriptive tool since unreacted monomer and smaller chain lengths can rapidly lower this value even when the bulk of the material is of a longer chain length which will have the greatest effect on a polymer's properties.

One way in which this is overcome is using a "weight-average" molecular weight $\bar{M}_w$, this is a weighted average that considers the mass of each polymer chain to a much greater extend. This gives a better representation of the overall polymer size, Equation 1.13:

$$\bar{M}_w = \frac{\sum M_x^2 N_x}{\sum N_x M_x}$$

Equation 1.13: The "weight-average" molecular weight of a polymer. This averages polymer mass, meaning that the value is less effected by shorter polymer lengths.

The difference between The difference between the $\bar{M}_n$ and $\bar{M}_w$ of a polymer is known as the dispersity Đ, Equation 1.14. A value of one for the dispersity means that all the polymer chains are the same length, and therefore mass in a homopolymer. It is often favourable to have a dispersity value as close to one as possible as this shows that the polymerisation isn't being terminated before completion or that there is a lack of initiation forming active sites for polymerisation to occur.

$$Đ = \frac{\bar{M}_n}{\bar{M}_w}$$

Equation 1.14: The dispersity of a polymer. This considers the difference between the two molecular masses averages. A large value of Đ means that there is a large molecular weight distribution across the polymer chains.

The use of the two averages and the dispersity is a good example of the technicalities of measuring a polymer as both many individual polymer chains and the bulk combination and those properties.

1.8. Polymers: poly(2-oxazoline)s and polyacrylamides

Drug-polymer conjugation is a common usage for polymers in biomedical applications. Polymers offer a framework in which an active drug molecule can be modified while retaining activity of the active species. Depending on the polymer properties a drug may be conjugated onto to increase stability, hydrophobicity, or transport properties as well as blocking opsonisation. Poly(ethylene glycol) is the most commonly used drug conjugation agent, but may different species are being investigated as different conjugation species. Poly(2-oxazoline)s are being investigated as an alternative to PEG due to similar hydrophilic properties, and poly(acrylamides) are highly modifiable giving another potential conjugation agent.

A common polymer system used in biomedical applications is poly(ethylene glycol) (PEG).[112,113] PEG is water soluble and non-toxic, and when conjugated to proteins forms drug species with improved activity, circulation time, and cell interactions.[114] A disadvantage of the use of PEG is the observation of the accelerated blood clearance (ABC) phenomenon.[112] The ABC phenomenon is understood to be an immune response to the continued use of PEG as an excipient in drug formulations culminating in a much reduced drug lifetime within the body.[115]

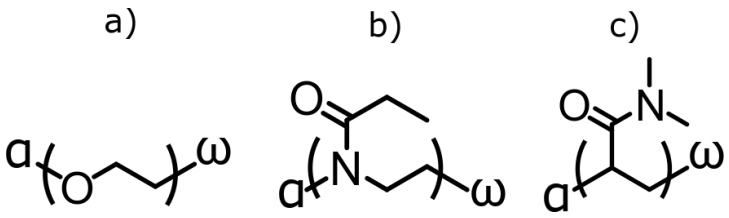

Figure 1.36: a) poly(ethylene glycol) b) poly(2-oxazoline), and c) polyacrylamide polymer species.

Poly(2-oxazoline)s consist of a carbon – nitrogen backbone, the amide is offset as part of the side chain making short carbon side chain poly(2-oxazoline)s water soluble below masses of 50 kDa.[116,117] Biological applications of poly(2-oxazoline)s and modified poly(2-oxazolines) has also been investigated[118,119] showing low toxicity and the ability to excrete poly(2-oxazoline)s below 40 kDa.

Polyacrylamides have shown significant increase in use with the development of well controlled synthetic methods.[120] The resulting polyacrylamides are biocompatible,

easily functional, and biologically and hydrolytically stable.[120,121] The use of copolymers for fine tuning chemical properties has also been extensively investigated.[122,123]

Cyclic peptide polymer conjugation is carried out for the same reasons as conjugation of a polymer to any biological species. Cyclic peptides are well characterised to be highly active biological species.[124-126] Cyclic peptides, due to their constrained structure, can also form large tertiary structures based on intermolecular interactions between amino acids in each end group.[127,128] The formation of higher order structures with the cyclic peptide species is reliant on thermodynamic processes that lack control within pharmaceutical use.[129]

By conjugating polymers onto cyclic peptide species the cyclic peptide structures may be stabilised and controlled self-assembly may occur with an external trigger.[128,130-132] The control of the cyclic peptide stacking can form Janus nanotubes and even hydrogel structures.[133-135] The nanotube structures can be used as drug delivery vectors for many different complexes. [136,137]

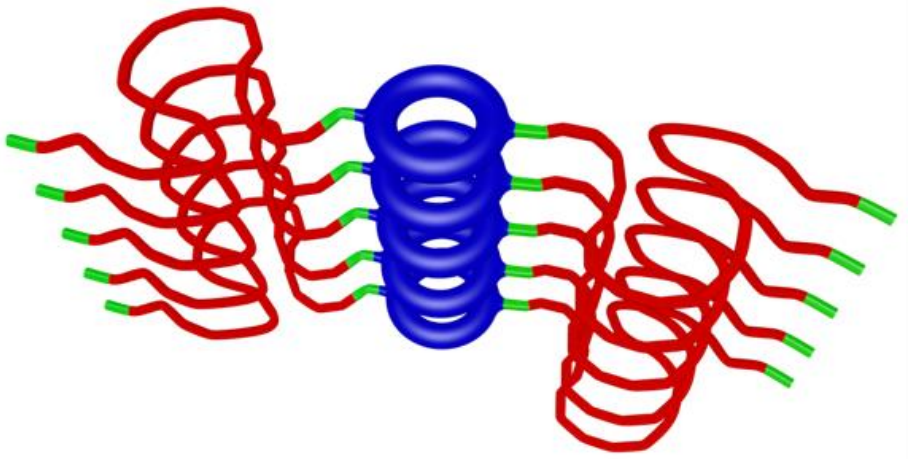

Figure 1.37: Stacking of a cyclic peptide-polymer conjugates. The cyclic peptides are thermodynamically favoured in a stacked formation and the polymer steric bulk allow control of the stacking number.

1.9. Polymer Analysis

The dispersity of polymers offers a unique analytical challenge in that a polymer is a mixture of species even in a “pure” form. Accurate chemical determination of all the size, chemical, end group, and further tertiary structures, is highly challenging. The discussion of polymer analysis is wide reaching, although mentions of numerous polymer species will be discussed the focus will be on poly(oxazolines), poly(acrylamides), and peptide-polymer conjugates. Importantly, some species will behave similarly analytically to other polymer species and their challenges may be similar but to treat all polymeric species the same is an oversimplification of the chemistry which critically affects all analysis of these species and is unique to each polymer.

1.9.1. Size characterisation analysis

Size characterisation analysis of polymer structures can be indirectly carried out using gel permeation chromatography (GPC). GPC as a technique separates molecules based on their hydrodynamic volume due to how polymers interact with porous column. A polymer with a smaller volume will spend longer within the column as there is a highly probability it will interact with a pore space. A larger polymer will not enter the same pore volume and remain mobile through the column.

A disadvantage with GPC analysis is that the analysis is predominantly based on an external calibration of the GPC instrument based on a more tightly controlled standard calibrant. The two most common calibrants used are poly(styrene) and poly(methyl methacrylate), which unfortunately only provides a relative relationship for any polymer analysed which is not the exact same chemical makeup as the calibrant used.

1.9.2. Tertiary structure analysis

In comparison to similarly sized protein complexes the lack of ability to crystallise many polymers leads to significant difficulties in understanding potential polymer structures. Broad structural characterisation can be made using imaging or scattering techniques such as dynamic light scattering (DLS), but these do have size limitations.[138]

1.10. Polymer analysis by mass spectrometry

Mass spectrometry analysis of polymers is extensive: a review published by Montaudo in 2006 presents over 60 referenced works focused only on analysis of polystyrene species by MALDI-TOF mass spectrometry.[139] Importantly, mass spectrometry offers a tool that the direct analysis of polymer mass can be carried out without calibration to other species or without needing to take into account solvent or matrix effects.

Mass spectrometry also allows the chemical analysis of polymers by the coupling of fragmentation methods to the mass spectrometry analysis allowing the analysis of more complex species.

1.10.1. Mass spectrometry analysis

Mass spectrometry of polymers allows the characterisation of the polymer by accurate mass determination. The size of polymer species may also be calculated from the mass spectrometry measurement, although the ionisation differences between different sized species may have an effect on the measurement. Depending on the detection method used there may also be a bias towards one species over another.

Accurate mass determination of polymers allows calculation of the polymer end groups by removal of monomer units. Although calculating the end group by deduction is possible and useful to the polymer chemist with increasing complexity of end groups, and especially in the event of unexpected side reactions or subsequent reactions such as conjugation to proteins or peptides. In the case of conjugation calculation of the end groups by monomer can be difficult due to the monomer unit being much smaller than the end group. Taking PEG as an example with a molar mass of 44 g mol^{-1} a peptide conjugation with a molar mass of greater than 1000 g mol^{-1} leaves much room for error as a small modification to the peptide could account for multiple PEG units.

$$m_{total} = m_{end\ group\ a} + m_{end\ group\ b} + (n \times m_{monomer})$$

Equation 1.15: the total mass of the polymer is the end groups multiplied by the number (n) of monomer units present making up the polymer chain.

$$m_{total} - (n \times m_{monomer}) = m_{end\ group\ a} + m_{end\ group\ b}$$

Equation 1.16: Calculation of the end group mass by deduction of monomer units. Although the deduction method is effective in calculating known end group masses its analytical power is limited as end groups can't be separated and the monomer number (n) maybe unknown. [140]

Accurate mass determination of polymers was some of the first work every carried out with the use of MALDI, carried out by Tanaka *et al.*[20] Initial studies of polymers mostly consisted of glycol based species such as poly(ethylene glycol) (PEG) and poly(propylene glycol) (PPG) on TOF instruments[141,142] and on FT-ICR instruments.[140] ESI analysis of PEG up to 24 kDa was carried out and showed the increased complexity caused by the multiply charged species formed by ESI analysis.[143]

ESI studies of the larger polymer species required increased instrument resolving power due to the closely spaced *m/z* ratio's produced within the charge distributions due to the different oligomer units and charge states. Polymers offer a clear example of the stacking of charge onto species during the ESI process. As the polymer grows the number of charges the polymer is able to pick up increases, meaning that a polymer with a large mass range may take up a small *m/z* range, increasing the analytical demand on instruments to effectively analyse these species.

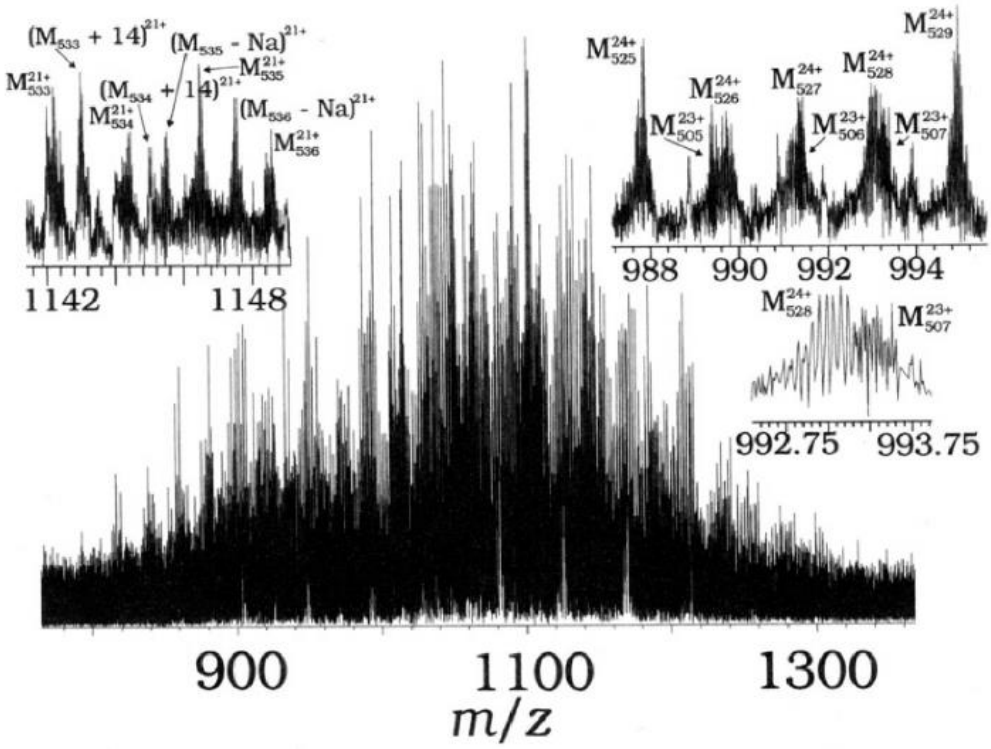

Figure 1.38: ESI-FT-ICR MS spectrum showing the complexity of a PEG 20,000 species although individual PEG species could be resolved isotopically the quality of the spectrum is degraded due to charge and oligomer overlap in m/z space. Reproduced with permission from O'Connor et al. Figure 3.[143] Copyright 1995 American Chemical Society.

Analysis of complex polymeric species even lacking resolving power can still be analytically useful by looking at direct mass determinations. An example shown by Gallet *et al.* shows the complexity of analysing polymer species at higher orders of complexity. A triblock polymer of PEG-*b*-PPG-*b*-PEG analysed by MALDI-TOF shows lack of resolution of any unique species, but simply mass unresolved "humps" in the mass spectrum. Although analytically useful for some cases this shows the complexity of accurately assigning polymer species at higher orders of complexity. Figure 1.39 shows the complex MALDI-TOF spectrum of Gallet's study. Higher orders of complexity have been analysed by MALDI-FT-ICR, Rooij *et al.* showed that well resolved copolymer distributions could be plotted as a heat map and the relative monomer amounts compared to one another.[140] Low mass errors were shown to be easily achievable with longer transient times.[144] Similar analytical work on PEGs was

also carried out with the use of ESI-FT-ICR showing that low mass errors could be achieved from PEG 3000 species up to 7+ charges.[145]

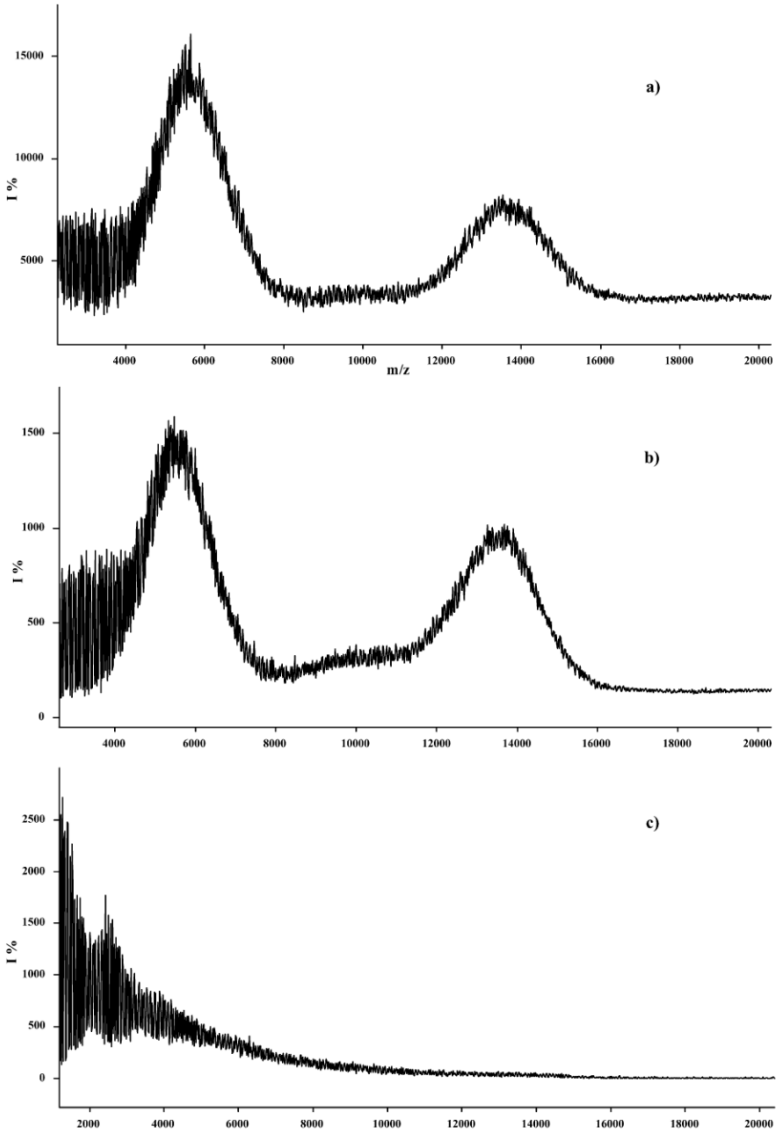

Figure 1.39: MALDI-TOF analysis of thermally degraded (PEG-b-PPG-b-PEG) copolymers showing the change in polymer size as thermal degradation occurred over a) initial sample b) thermoxidised over 21 days and c) 24 days. The lack of resolving power shows the complexity of these samples by mass analysis. Reproduced with permission from Gallet et al. Figure 6.[146] Copyright 2002 Elsevier.

Multiple branched polymer species have been analysed by high resolution mass spectrometry. Sorbitan polyethoxylates underwent ESI FT-ICR MS analysis producing

high resolution analysis of multiple polymeric species present within a single sample.[147]

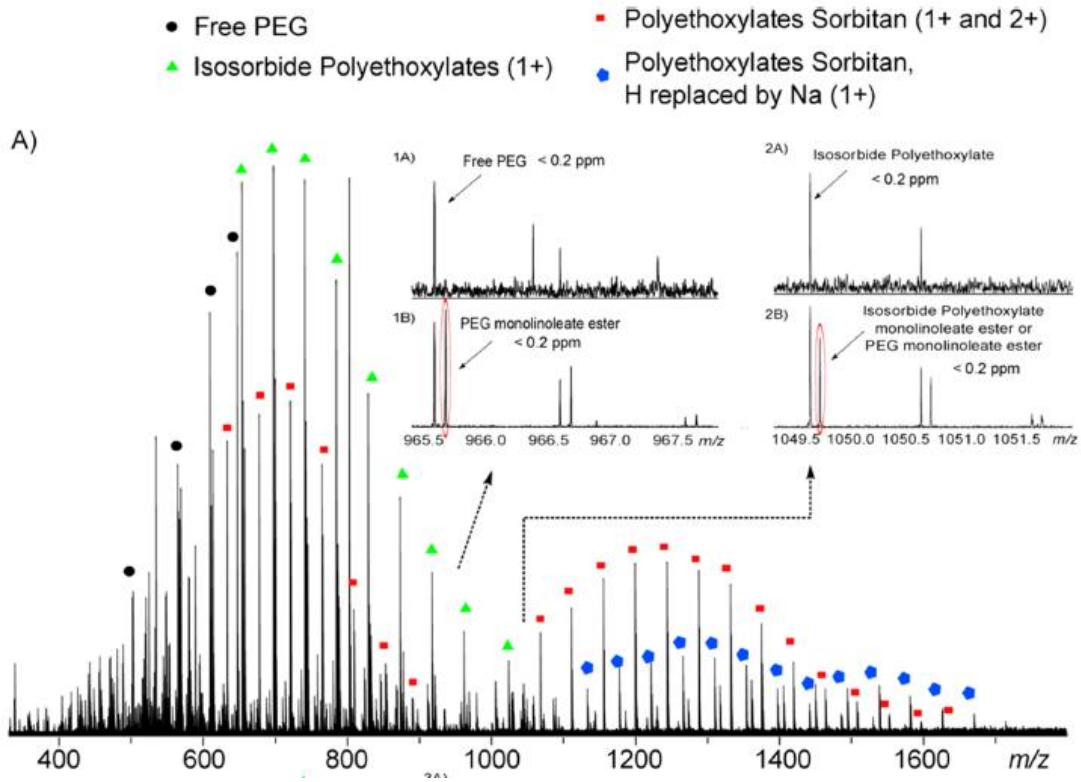

Figure 1.40: ESI FT-ICR analysis of sorbitan polyethoxylate mixtures, showing both multiple charge states as well as different polymeric species. Reproduced with permission from Perez-Hurtado et al. Figure 6.[147] Copyright 2012 American Chemical Society.

Recent studies have shown the analysis of poly(oxazolines) by ESI and MALDI.[148,149] Accurate determination of the mass of polyoxazoline species by both ionisation methods. The ESI process produced multiply charged species across the dispersity of the polymer increasing spectral complexity but having the advantage of removing the need for MALDI sample preparation. Poly(2-ethyl-oxazoline) which are commonly used polyoxazoline backbones are water soluble providing a significant advantage to their ionisation under ESI conditions. Hydrolysis of poly(oxazolines) to poly(ethyleneimines) has also been carried out and analysed by mass spectrometry using both MALDI and ESI processes.[150]

Polyacrylamide analysis by mass spectrometry has been explored to a much smaller degreed.[40] Although analysis has been carried out by MALDI-TOF[151] and by ESI[152] the polymers used in these experiments were of a very short chain length, n<10.

1.10.2.Tandem mass spectrometry analysis of polymers

Fragmentation of polymers provides the potential to increase the characterisation of the polymer by breaking down the backbone sequenceable fragments. The analytical power of tandem mass spectrometry affords the analysis of numerous polymeric properties:

End group analysis – the ability to analyse end groups is much improved by fragmenting the polymer, with direct analysis of the end group itself being possible, or in the event that the end group is removed the calculation of the end group by monomer deduction is made possible as mass differences between the ultimate fragment and precursor.

Copolymer architecture – The copolymer architecture can be directly observed via fragmentation, as the oligomer units produced will form either randomly distributed monomer chains within oligomer units or distinct blocks containing one monomer unit and then the other. Synthesis routes can also be determined after the synthesis has taken place by analysing which block is directly bound to each end group.

Conjugation groups or linkers – similar to the use of tandem mass spectrometry in proteomics but the ability to analyse conjugation species or linkers directly rather than inference through a mass increase is critical when exploring new chemistries or when requiring exact chemical identification for medicinal use etc.

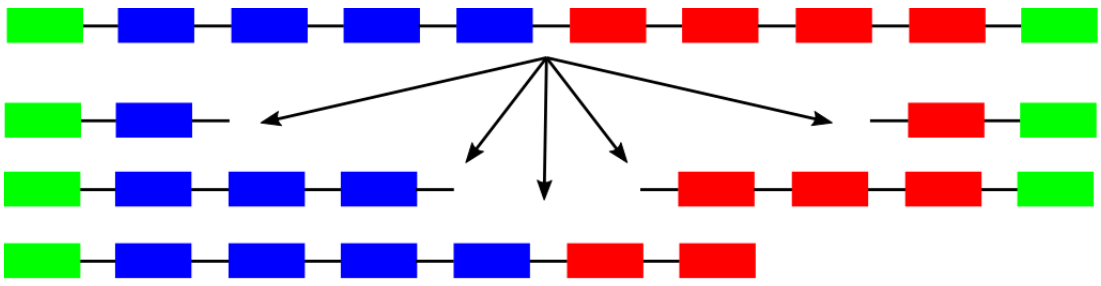

Figure 1.41: The tandem mass spectrometry process explained graphically, by breaking down a single polymer chain end group, block size, and modifications can be much more effectively characterised.

Post source decay (PSD) of polymers was often used for the analysis of end group structures.[139,153] PSD is naturally low intensity due to the reliance of energy transfer due to the ionisation process. The addition of CAD/CID based systems to MALDI mass spectrometers allowed the increased control of the fragmentation events.[154]

MALDI SORI-CID analysis of PEG was carried out by Wilkins and coworkers,[155] showing the loss of PEG monomer units from the isolated precursor. The fragmentation occurred along the least stable carbon oxygen bond in the PEG backbone.

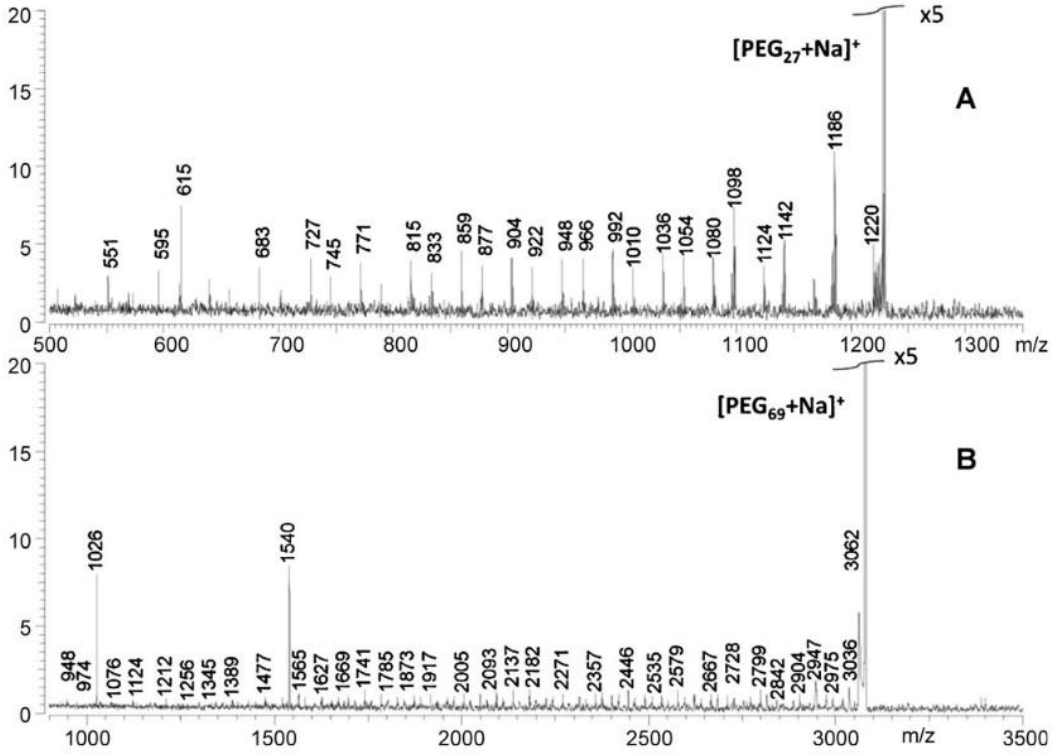

Figure 1.42: SORI-CID spectrum of sodiated PEG showing the fragmentation of monomer units being removed. Reproduced with permission from Miladinović *et al.* Figure 6.[155].Copyright 2008 Springer Nature.

The use of MALDI-SID analysis of polymers showed that fragmentation of carbon-backbone polymers results can be carried out. The polymer must contain a bond in the backbone that can undergo a homolytic cleavage causing radical formation on the backbone of the polymer species.[156]

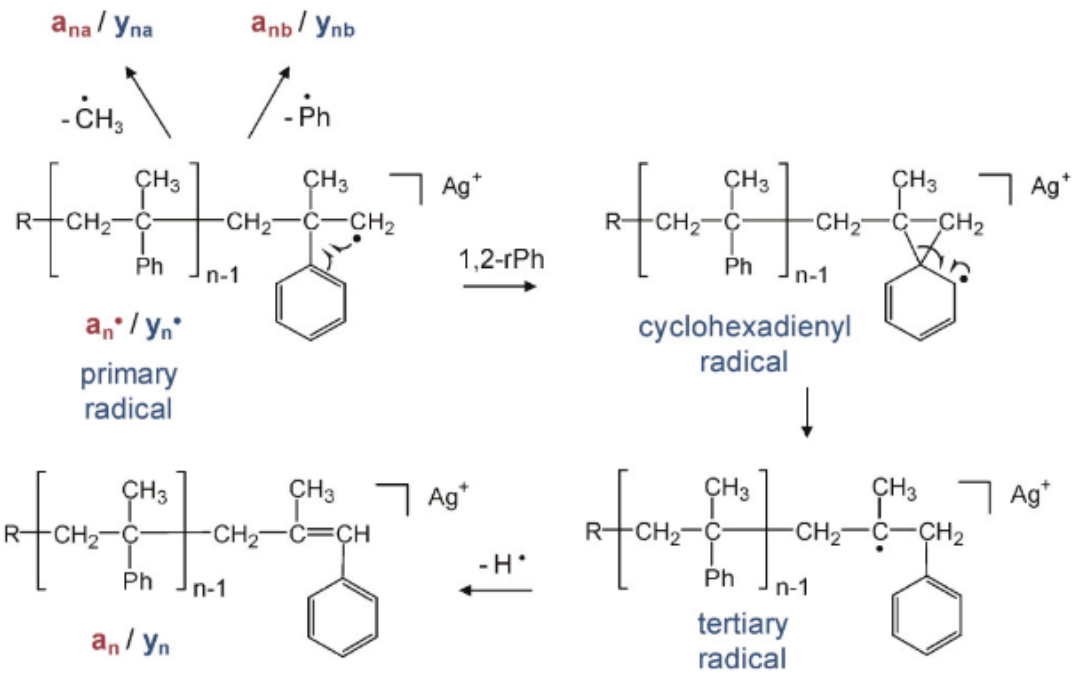

Figure 1.43: poly(styrene) fragmentation pathways, the initial radical is formed with the homolytic cleavage of weaker bond, often an alkene or silane end group. Reproduced with permission from Polce *et al.* Scheme 2.[157] Copyright 2008 American Chemical Society.

The fragmentation of poly(styrenes) was used successfully in the analysis of different cyclic and linear poly(styrene) structures.[156,157] The fragmentation ladder forms between the cyclic and linear structures show significant differences in fragmentation characteristics. One of the biggest differences between the linear and cyclic fragmentation pathways was the trapping of an electron on the structure after the first dissociation due to the cyclic structure. The trapped radical produces multiple side reactions greatly increasing the complexity the corresponding tandem mass spectrum due to side chain migrations.[158] The side chain fragmentation caused by the free radical present on the polymer may cause issues with understanding more complex structures and produces challenging data analysis demands.

Fragmentation of styreneic copolymers was also carried out by Wesdemiotis and co-workers looking at characterising modified styreneic positions throughout the copolymers.[159] The work was mostly successful but at high levels of copolymerisation the complexity of the fragmentation spectrum created difficulty in the accurate analysis of the copolymers being analysed.[160]

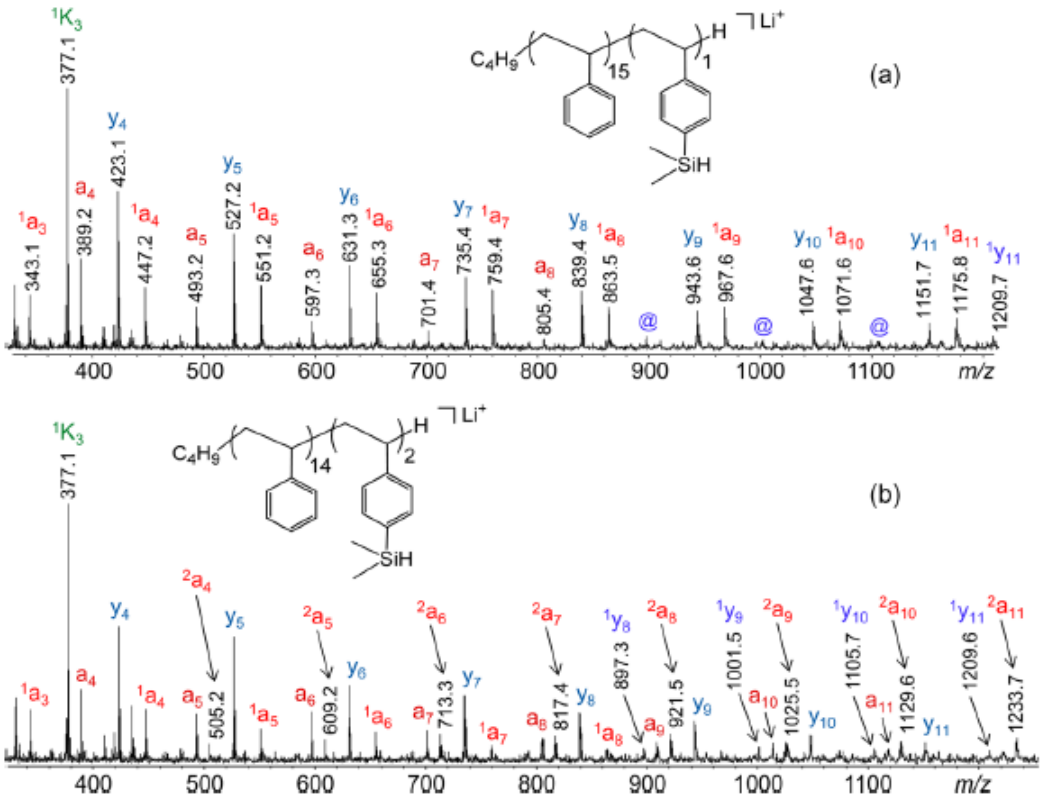

Figure 1.44: Fragmentation of a copolymeric styrene molecule. The fragmentation seen here is the same as other styreneic fragmentation, the complication increase with increased copolymeric character is seen clearly comparing the a) and b) spectra. Reproduced with permission from Yol *et al.* Figure 5.[160] Copyright 2014 American Chemical Society.

The MALDI-CAD spectrum of acrylates carried out by Wesdemiotis and coworkers characterised linear and branched polyacrylates[161] interestingly the work presented shows the formation of radicals and radical backbiting, the formation of the different fragmentation pathways due to the radical dissociation process produced a complex mass spectrum with multiple fragment pathways present for each monomer unit. Figure 1.45 shows the dissociation of a poly(methacrylate) the *a* and *y* fragmentations formed the majority of the observable fragment ladders, the "*b*" mark on a fragment relates to the loss of the acrylate ester group and the formation of an alkene end group.

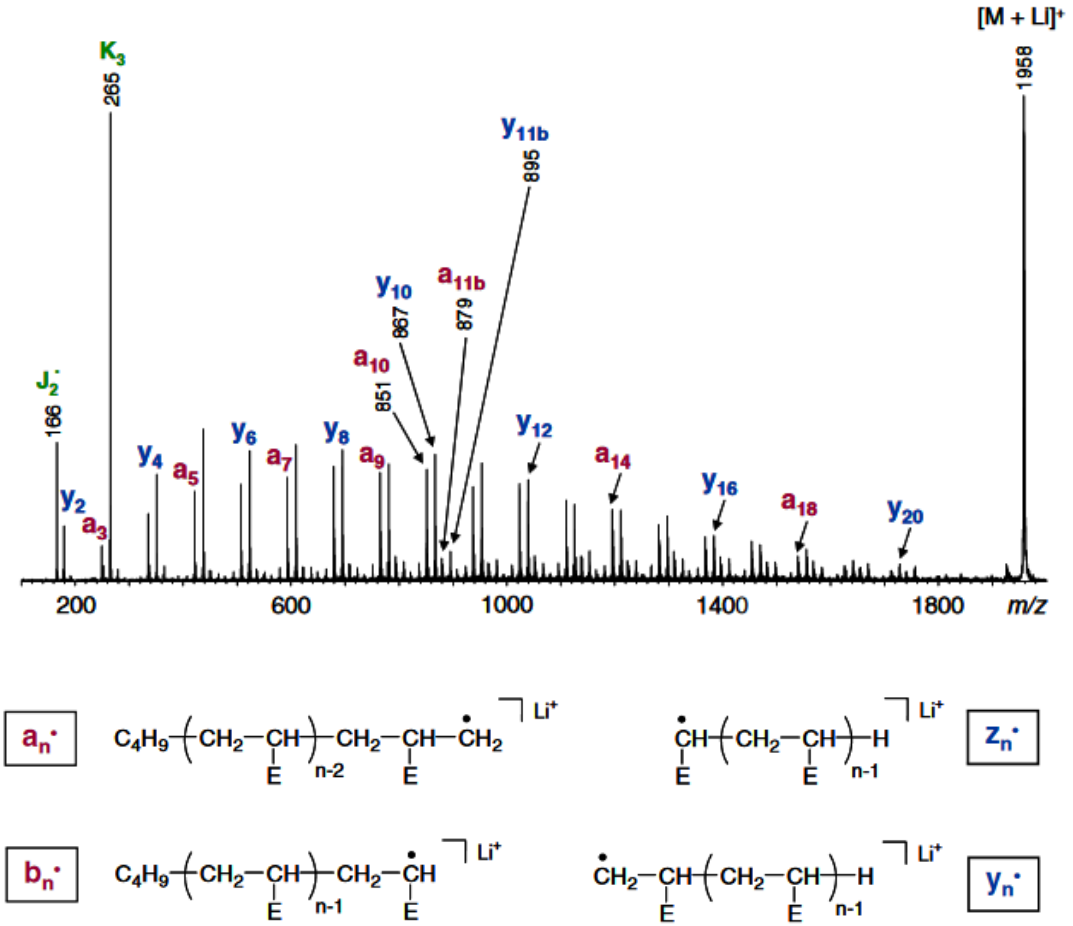

Figure 1.45: poly(methylacrylate) fragmentation showing the multiple radical products formed during the dissociation. The ladder of fragments formed by the dissociation of these polymers is based on primary radical dissociation as well as further secondary dissociations. Reproduced with permission from Chaicharoen *et al.* Modified Figure 3.[161] Copyright 2008 Springer Nature.

Tandem mass analysis of poly(oxazolines) showed fragmentation of the carbon-nitrogen bonds along the polymer backbone. Fragmentation using CAD/CID showed good sequence coverage of the polyoxazoline was achievable but highly dependent on the strength of bonds within the polyoxazoline. In the present of a particularly weak end group bond the loss of the end group was the much favoured fragmentation pathway.[149,162]

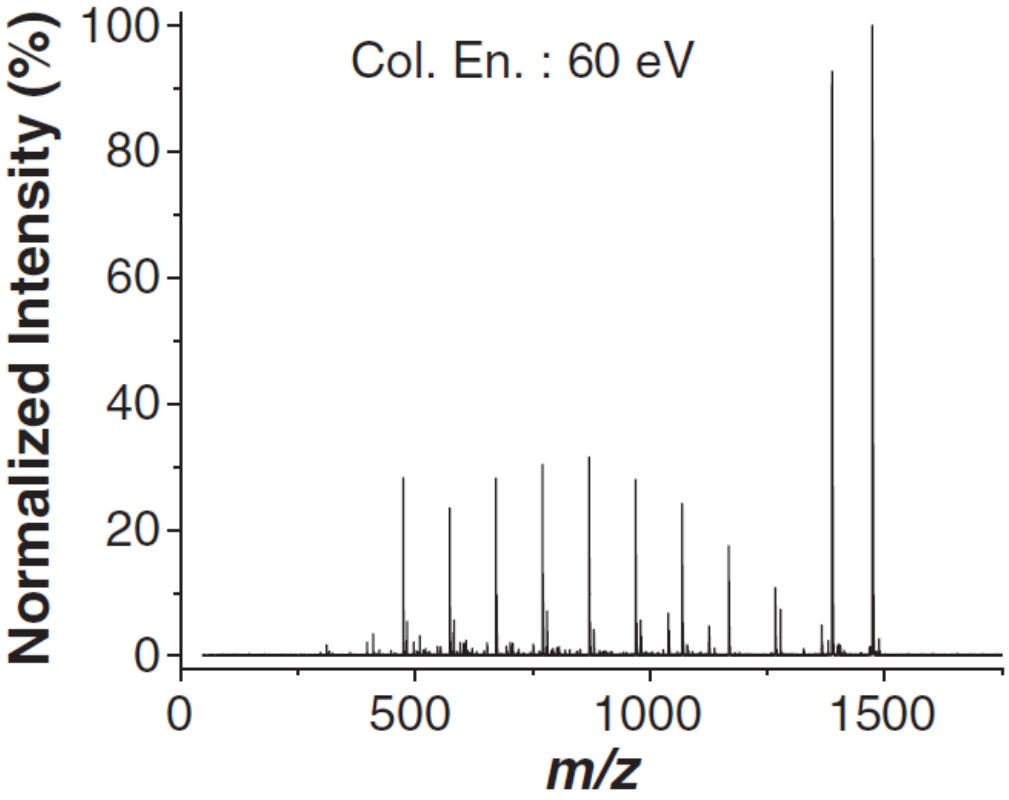

Figure 1.46: Fragmentation of a polyoxazoline showing the fragmentation ladder caused by CID. The differences in sequence coverage at different fragmentation energies can be used as a rough prediction of end group characteristics. Reproduced with permission from Altuntaş *et al.* Figure 1(g).[149] Copyright 2013 John Wiley and Sons.

MALDI-LID-ToF/ToF analysis of copolymers can be carried out by taking advantage of new technologies of laser dissociation with the MALDI system. The analysis carried out by Haddleton and co-workers on the sequencing of poly(acrylates) involved the breaking of a weaker bond (a carbon halide bond) forming a radical. After radical formation a hydrogen transfer could occur between the terminal where the radical was formed and a point on the carbon backbone. After hydrogen transfer has occurred homolytic dissociation of the backbone could occur at any transfer point. The ability to fragment molecules via a radical dissociation process is highly advantageous, allowing carbon-carbon backbones to be significantly fragmented and sequenced.[163] Figure 1.47 shows the high level of sequence coverage achieved of a poly(acrylate) using the radical dissociation methods described.

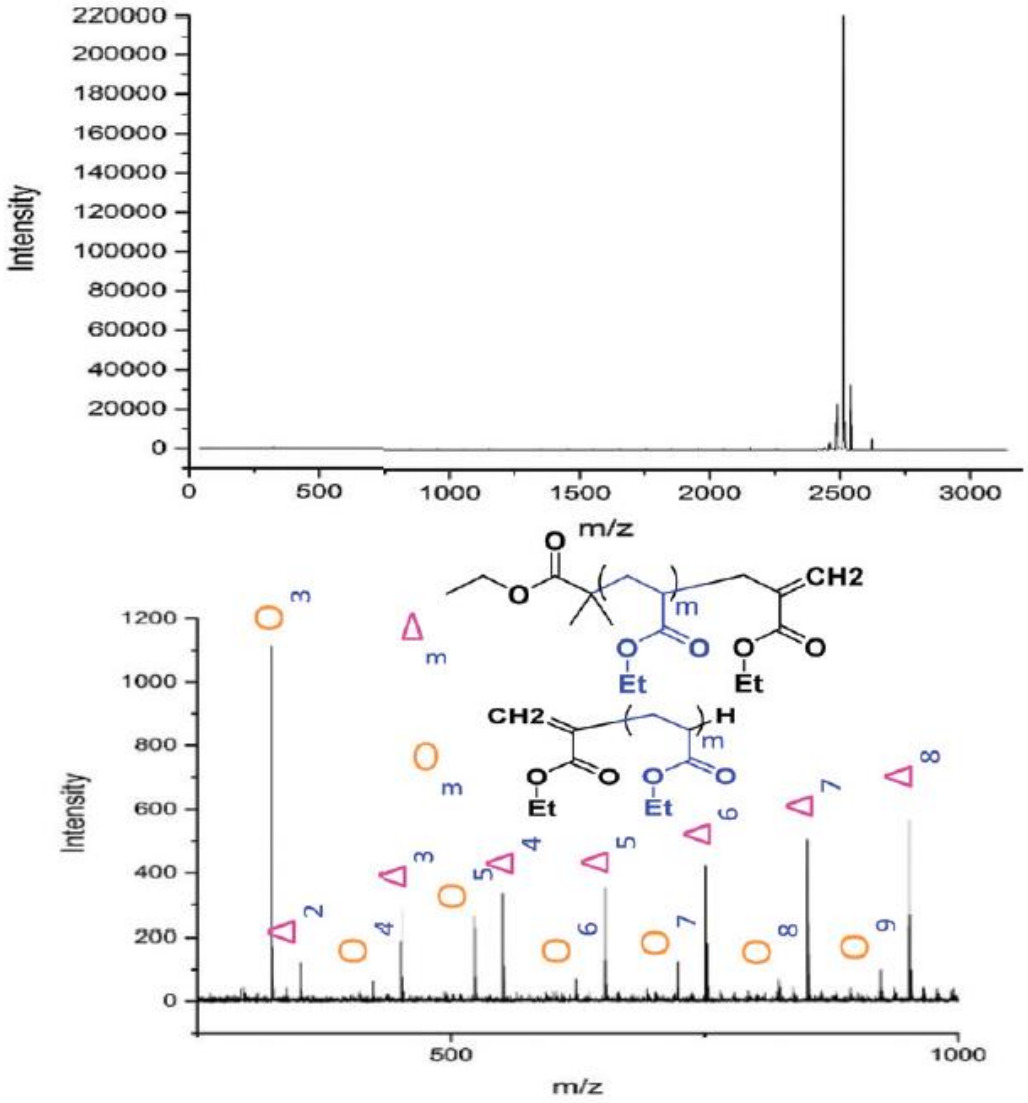

Figure 1.47: Fragmentation of a poly(methyacrylate) by MALDI-LID showing fragmentation the Δ and O fragmentation is equivalent to *k* and *j* fragmentation from the Wesdemiotis papers. Reproduced with permission from Town *et al.* Figure 5.[163] Published by Royal Society of Chemistry.

Fragmentation of random copolymers was also carried out by Haddleton and coworkers resulting in the sequencing and characterisation of a poly(methyl acrylate-b-ethyl acrylate) copolymer showing mixing in the synthesis of block copolymers at the boundary region. The findings showed a significant advantage that mass spectrometry can offer in the analysis of complex polymeric systems. The mixing region present in block copolymers is very difficult to analyse through other analytical

methods as the amount of mixing is low and the chemical change is small, often the switching of a few monomer units.[163,164]

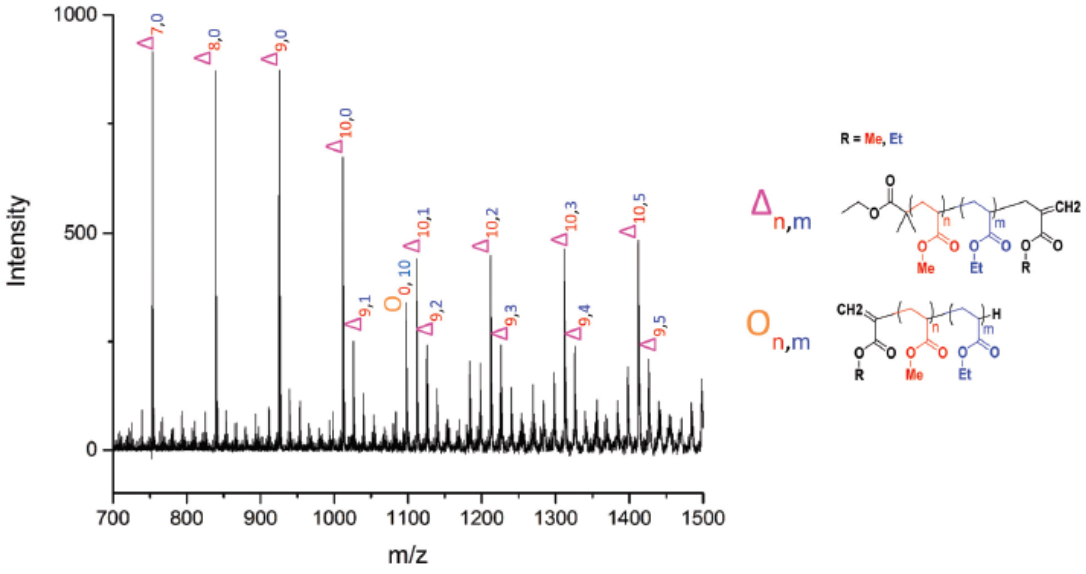

Figure 1.48: Fragmentation of a poly(methyl acrylate-b-ethyl acrylate) by MALDI-LID. The overlapping region caused by the mixing of the two block copolymers giving the polymer random character. Reproduced with permission from Town *et al.* Figure 9.[163] Published by Royal Society of Chemistry.

MALDI-LID was also used in the analysis of styrenes and polyoxazolines, the analysis showed the formation of PSD decay and CID fragmentation within the LID experimentation. CID analysis produced fewer sequence fragments compared to LID and was therefore less favoured.[164]

Electron dissociation fragmentation of polymers has not been well explored[165] although electron based fragmentation methods can offer compelling complimentary fragmentation compared to CAD/CID. Importantly, issues with end group, or side chain, bond strength becomes much less of an issue. Very labile groups can be maintained in electron dissociation studies as the fragmentation is radical directed, rather than a slow heating process.[46]

Wesdemiotis and co-workers published work on the ETD of polyesters and concluded that the fragmentation gave good complimentary data to the CAD/CID without causing excessive secondary fragmentation of the structure.[166] Fragmentation of the

D-α-tocopheryl polyethylene glycol 1000 succinate was carried out by O'Connor and co-workers comparing CAD/CID fragmentation with electron capture methods of fragmentation.[167] The study also goes into detail of how ionisation can change the fragments observed during the dissociation. The addition of silver adducts allow the cationisation of the aromatic end group, with ionisation of the aromatic end group many more fragments are observed which contain the end group, rather than the polymer chain.

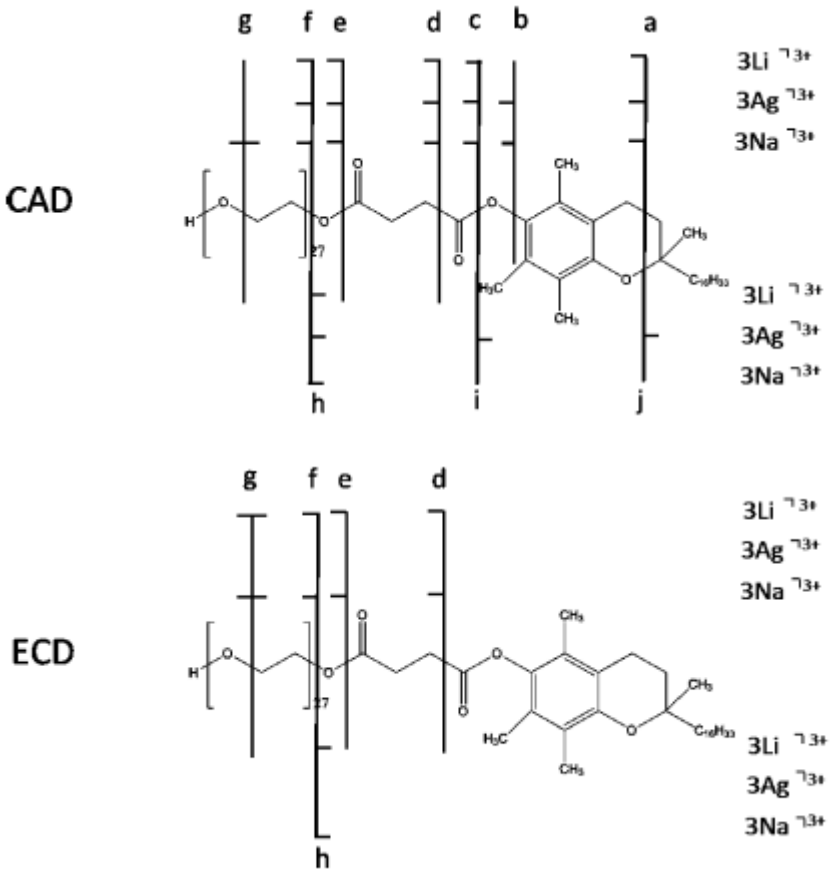

Figure 1.49: Fragmentation of a polymer conjugated drug excipient. The difference in fragmentation between both methods and due to the presence of different adducts is well observed. Reproduced with permission from Wei *et al.* Scheme 2.[167] Copyright 2014 American Chemical Society.

To conclude, there is a large amount of mass spectrometry literature focussed on the analysis of polymeric species. An often overlooked aspect of polymer mass spectrometry is that there is much variation in polymer species which has a large

effect on the mass spectrometry methods available to be used, mainly ionisation and fragmentation methods.

1.11. References

(1) Thomson, J. J. Rays of positive electricity for chemical analysis *Proc. R. Soc. Lond. A* **1913**, *89*, 1-20.
(2) Aston, F. W. Isotopes and Atomic weights *Nature* **1920**, *105*, 617-619.
(3) Dempster, A. J. A new method of positive ray analysis *Phys. Rev.* **1918**, *11*, 316-324.
(4) Dempster, A. J. A new Method of Positive Ray Analysis *Physical Review* **1918**, *11*, 316-325.
(5) Aston, F. W. LXXIV. A positive ray spectrograph *The London, Edinburgh, and Dublin Philosophical Magazine and Journal of Science* **1919**, *38*, 707-714.
(6) McLafferty, F. W.; Tureček, F. *Interpretation of mass spectra 4th ed*; University Science Books: Mill Valley, California, 1993.
(7) Hoffmann, E. d.; Vincent, S. *Mass Spectrometry: Principles and Applications 3rd edition*, 3rd ed.; John Wiley & Sons Ltd: London, 2007.
(8) Yamashita, M.; Fenn, J. B. ELectrospray Ion Source. Another Vairation on the Free-Jet Theme *J. Phys. Chem.* **1984**, *88*, 4451-4459.
(9) Taylor, G. Disintegration of water drops in an electric field *Proceedings of the Royal Society of London. Series A, Mathematical and Physical Sciences* **1964**, *280*, 383-397.
(10) Konermann, L. A simple model for the disintegration of highly charged solvent droplets during electrospray ionization *J. Am. Soc. Mass. Spectrom.* **2009**, *20*, 496-506.
(11) Konermann, L.; Elias, A. Surface Charge of Electrosprayed Water Nanodroplets: A Molecular Dynamics Study *J. Am. Chem. Soc.* **2010**, *132*, 11270-11277.
(12) Konermann, L.; Rodriguez, A. D.; Liu, J. On the formation of highly charged gaseous ions from unfolded proteins by electrospray ionization *Anal. Chem.* **2012**, *84*, 6798-6804.
(13) Smith, J. N.; Richard, C. F.; Beauchamp, J. L. Droplet Evaporation and discharge dynamics in Electrospray ionisation *J. Phys. Chem. A* **2002**, *106*, 9957-9967.
(14) Konermann, L.; Ahadi, E.; Rodriguez, A. D.; Vahidi, S. Unraveling the mechanism of electrospray ionization *Anal. Chem.* **2013**, *85*, 2-9.
(15) Henry, K. D.; Williams, E. R.; Wang, B. H.; McLafferty, F. W.; Shabanowitz, J.; Hunt, D. F. Fourier-transform of large molecules by electrospray ionisation *Proc. Natl. Acad. Sci. U.S.A* **1989**, *86*, 9075-9078.
(16) Karas, M.; Bahr, U.; Dülcks, T. Nano-electrospray ionization mass spectrometry: addressing analytical problems beyond routine *Anal. Chem.* **2000**, *366*, 669-676.
(17) Susa, A. C.; Lippens, J. L.; Xia, Z.; Loo, J. A.; Campuzano, I. D. G.; Williams, E. R. Submicrometer Emitter ESI Tips for Native Mass Spectrometry of Membrane Proteins in Ionic and Nonionic Detergents *J. Am. Soc. Mass. Spectrom.* **2018**, *29*, 203-206.
(18) Karas, M.; Bachmann, D.; Hillenkamp, F. Influence of the Wavelength in High-Irradiance Ultraviolet Laser Desorption Mass Spectrometry of Organic Molecules *Anal. Chem.* **1985**, *57*, 2935-2939.
(19) Karas, M.; Hillenkamp, F. Laser Desoprtion ionisation of Proteins with Molecular Masses Exceeding 10000 Daltons *Anal. Chem.* **1988**, *60*, 2301-2303.
(20) Tanaka, J.; Waki, H.; Ido, Y.; Akita, S.; Yoshida, Y.; Yoshida, T. Protein and Polymer analyses up to m/z 100000 by Laser Ionisation time of flight Mass Spectrometry *Rapid Commun. Mass Spectrom.* **1988**, *2*, 151-153.
(21) Karas, M.; Glückmann, M.; Schäfer, J. Ionization in matrix-assisted laser desorption/ionization: singly charged molecular ions are the lucky survivors *J. Mass Spectrom.* **2000**, *35*, 1-12.

(22) Teramoto, K.; Sato, H.; Sun, L.; Torimura, M.; Tao, H. Simple Intact Protein Analysis by MALDI-MS for Characterization of Ribosomal Proteins of Two Genome-Sequenced Lactic Acid Bacteria and Verification of Their Amino Acid Sequences *J. Prot. Res.* **2007**, *6*, 2899-1907.
(23) Kühn-Hölsken, E.; Lenz, C.; Sander, B.; Lührmann, R.; Urlaub, H. Complete MALDI-ToF MS analysis of cross-linked peptide–RNA oligonucleotides derived from nonlabeled UV-irradiated ribonucleoprotein particles *RNA* **2005**, *11*, 1915-1930.
(24) Kolli, K. V. S.; Orlando, R. A new matrix for matrix-assisted laser desorption/ionisation on magnetic sector instruments with point detectors *Rapid Commun. Mass Spectrom.* **1996**, *10*, 923-926.
(25) Ryumin, P.; Cramer, R. The composition of liquid atmospheric pressure matrix-assisted laser desorption/ionization matrices and its effect on ionization in mass spectrometry *Anal. Chim. Acta* **2018**, *103*, 43-45.
(26) Hale, O. J.; Ryumin, P.; Brown, J. M.; Morris, M.; Cramer, R. Production and analysis of multiply charged negative ions by liquid atmospheric pressure matrix-assisted laser desorption/ionization mass spectrometry *Rapid Commun. Mass Spectrom.* **2018**.
(27) Carda-Broch, S.; Berthod, A.; Armstrong, D. W. Ionic matrices for matrix-assisted laser desorption/ionization time-of-flight detection of DNA oligomers *Rapid Commun. Mass Spectrom.* **2003**, *17*, 553-560.
(28) Li, Y. L.; Gross, M. L. Ionic-liquid matrices for quantitative analysis by MALDI-TOF mass spectrometry *J. Am. Soc. Mass. Spectrom.* **2004**, *15*, 1833-1837.
(29) Armstrong, D. W.; Zhang, L.-K.; Lingfeng, H.; Gross, M. L. Ionic liquids as matrixes for matrix-assisted laser desporption/ionisation mass spectrometry *Anal. Chem.* **2001**, *73*, 3679-3686.
(30) Kosyakov, D. S.; Anikeenko, E. A.; Ul'yanovskii, N. V.; Khoroshev, O. Y.; Shavrina, I. S.; Gorbova, N. S. Ionic liquid matrices for MALDI mass spectrometry of lignin *Anal. Bioanal. Chem.* **2018**, *410*, 7429-7439.
(31) Beaufour, M.; Ginguene, D.; Le Meur, R.; Castaing, B.; Cadene, M. Liquid Native MALDI Mass Spectrometry for the Detection of Protein-Protein Complexes *J. Am. Soc. Mass. Spectrom.* **2018**, *29*, 1981-1994.
(32) Fukuyama, Y.; Nakaya, S.; Yamazaki, Y.; Tanaka, J. Ionic Liquid Matrixes Optimized for MALDI-MS of

Sulfated/Sialylated/Neutral Oligosaccharides and

Glycopeptides *Anal. Chem.* **2008**, *80*, 2171-2179.
(33) Meriaux, C.; Franck, J.; Wisztorski, M.; Salzet, M.; Fournier, I. Liquid ionic matrixes for MALDI mass spectrometry imaging of lipids *J Proteomics* **2010**, *73*, 1204-1218.
(34) Barre, F. P. Y.; Paine, M. R. L.; Flinders, B.; Trevitt, A. J.; Kelly, P. D.; Ait-Belkacem, R.; Garcia, J. P.; Creemers, L. B.; Stauber, J.; Vreeken, R. J.; Cillero-Pastor, B.; Ellis, S. R.; Heeren, R. M. A. Enhanced Sensitivity Using MALDI Imaging Coupled with Laser Postionization (MALDI-2) for Pharmaceutical Research *Anal. Chem.* **2019**, *91*, 10840-10848.
(35) Niehaus, M.; Soltwisch, J.; Belov, M. E.; Dreisewerd, K. Transmission-mode MALDI-2 mass spectrometry imaging of cells and tissues at subcellular resolution *Nat Methods* **2019**, *16*, 925-931.
(36) Spivey, E. C.; McMillen, J. C.; Ryan, D. J.; Spraggins, J. M.; Caprioli, R. M. Combining MALDI-2 and transmission geometry laser optics to achieve high sensitivity for ultra-high spatial resolution surface analysis *J. Mass Spectrom.* **2019**, *54*, 366-370.
(37) Roespstorff, P.; Fohlman, J. Proposal for a common nomenclature for sequence ions in mass spectra of peptides *Biomedical mass Spectrom.* **1984**, *11*, 601.

(38) Domon, B.; Costello, C. E. A systematic nomenclature for carbohydrate fragmentations in FAB-MS/MS spectra of glycoconjugates *Glycoconjugate J.* **1988**, *5*, 397-409.
(39) Jennings, K. R. Collision-induced decompositions of aromatic molecular ions *Int. Jour. Mass Spectrom. and Ion Phys.* **1968**, *1*, 227-235.
(40) Altuntaş, E.; Schubert, U. S. "Polymeromics": Mass spectrometry based strategies in polymer science toward complete sequencing approaches: a review *Anal. Chim. Acta* **2014**, *808*, 56-69.
(41) Smith, R. D.; Loo, J. A.; Barinaga, C. J.; Edmonds, C. G.; Udesth, H. R. Collisional Activation and Collision-Activated Dissociation of Large Multiply Charged Polypeptides and Proteins produced by Electrospray Ionization *J. Am. Chem. Soc.* **1989**, *1*, 53-65.
(42) Heck, A. J. R.; De Koning, L. J.; Pinkse, F. A.; Nibbering, N. M. M. Mass-specific Selection of Ions in Fourier-transform ion cyclotron resonance mass spectrometry *Rapid Commun. Mass Spectrom.* **1991**, *5*, 406-414.
(43) Basov, N. G.; Markin, E. P.; Oraevskii, A. N.; Pankratov, A. V.; Skachkov, A. N.; Lebedev, P. N. Stimulation of chemical processes by Infrared laser radiation *JETP Lett.* **1971**, *14*, 251-253.
(44) Zimmerman, J. A.; Watson, C. H.; Eyler, J. R. Multiphoton ionization of laser-desorbed neutral molecules in a Fourier transform ion cyclotron resonance mass spectrometer *Anal. Chem.* **1991**, *63*, 361-365.
(45) Little, D. P.; Spier, J. P.; Senko, M. W.; O'Connor, P. B.; McLafferty, F. W. Infrared multiphoton dissociation of large multiply charged ions for biomolecule sequencing *Anal. Chem.* **1994**, *66*, 2809-2815.
(46) Zubarev, R. A.; Kelleher, N. L.; McLafferty, F. W. Electron Capture Dissocaition of Multiply Charged Protein Cations. A nonergodic Process *J. Am. Chem. Soc.* **1998**, *120*, 3265-3266.
(47) Sawicka, A.; Skurski, P.; Hudgins, R. R.; Simons, J. Model calculations relevant to disulfide bond cleavage via Electron capture influenced by positively charged groups *J. Phys. Chem. B* **2003**, *107*, 13505-13511.
(48) Tureček, F. N-C alpha Bond Dissociation Energies and Kinetics in Amide and Peptide Radicals. Is the Dissociation a Non-ergodic Process? *J. Am. Chem. Soc.* **2003**, *125*, 5954-5963.
(49) Zubarev, R. A.; Horn, D. M.; Fridriksson, E. K.; Kelleher, N. L.; Kruger, N. A.; Lewis, M. A.; Carpenter, B. K.; McLafferty, F. W. Electron Capture Dissociation for structural characterization of multiply charged protein cations *Anal. Chem.* **2000**, *72*, 563-573.
(50) Kjeldsen, F.; Haselmann, K. F.; Budnik, B. A.; Jensen, F.; Zubarev, R. A. Dissociation capture of hot (3-13 eV) electrons by polypeptide polycations: an efficient process accompanied by secondary fragmentation *Chem. Phys. Lett.* **2002**, *356*, 201-206.
(51) Tsybin, Y. O.; Witt, M.; Baykut, G.; Hakansson, P. Electron capture dissociation Fourier transform ion cyclotron resonance mass spectrometry in the electron energy range 0-50 eV *Rapid Commun. Mass Spectrom.* **2004**, *18*, 1607-1613.
(52) Brodbelt, J. S. Photodissociation mass spectrometry: new tools for characterization of biological molecules *Chem. Soc. Rev.* **2014**, *43*, 2757-2783.
(53) Macias, L. A.; Santos, I. C.; Brodbelt, J. S. Ion Activation Methods for Peptides and Proteins *Anal. Chem.* **2019**.
(54) Moon, J. H.; Yoon, S. H.; Kim, M. S. Photodissociation of singly protonated peptides at 193 nm investigated with tandem time-of-flight mass spectrometry *Rapid Commun. Mass Spectrom.* **2005**, *19*, 3248-3252.
(55) Morgan, J. W.; Hettick, J. M.; Russell, D. H. In *Biological Mass Spectrometry*, 2005, pp 186-209.

(56) Shaw, J. B.; Li, W.; Holden, D. D.; Zhang, Y.; Griep-Raming, J.; Fellers, R. T.; Early, B. P.; Thomas, P. M.; Kelleher, N. L.; Brodbelt, J. S. Complete protein characterization using top-down mass spectrometry and ultraviolet photodissociation *J. Am. Chem. Soc.* **2013**, *135*, 12646-12651.
(57) Cannon, J. R.; Kluwe, C.; Ellington, A.; Brodbelt, J. S. Characterization of green fluorescent proteins by 193 nm ultraviolet photodissociation mass spectrometry *Proteomics* **2014**, *14*, 1165-1173.
(58) Mistarz, U. H.; Bellina, B.; Jensen, P. F.; Brown, J. M.; Barran, P. E.; Rand, K. D. UV Photodissociation Mass Spectrometry Accurately Localize Sites of Backbone Deuteration in Peptides *Anal. Chem.* **2018**, *90*, 1077-1080.
(59) Theisen, A.; Yan, B.; Brown, J. M.; Morris, M.; Bellina, B.; Barran, P. E. Use of Ultraviolet Photodissociation Coupled with Ion Mobility Mass Spectrometry To Determine Structure and Sequence from Drift Time Selected Peptides and Proteins *Anal. Chem.* **2016**, *88*, 9964-9971.
(60) Quick, M. M.; Crittenden, C. M.; Rosenberg, J. A.; Brodbelt, J. S. Characterization of Disulfide Linkages in Proteins by 193 nm Ultraviolet Photodissociation (UVPD) Mass Spectrometry *Anal. Chem.* **2018**, *90*, 8523-8530.
(61) Morrison, L. J.; Brodbelt, J. S. 193 nm Ultraviolet Photodissociation Mass Spectrometry of Tetrameric Protein Complexes Provides Insight into Quaternary and Secondary Protein Topology *J. Am. Chem. Soc.* **2016**, *138*, 10849-10859.
(62) Theisen, A.; Black, R.; Corinti, D.; Brown, J. M.; Bellina, B.; Barran, P. E. Initial Protein Unfolding Events in Ubiquitin, Cytochrome c and Myoglobin Are Revealed with the Use of 213 nm UVPD Coupled to IM-MS *J. Am. Soc. Mass. Spectrom.* **2019**, *30*, 24-33.
(63) O'Brien, J. P.; Needham, B. D.; Henderson, J. C.; Nowicki, E. M.; Trent, M. S.; Brodbelt, J. S. 193 nm Ultraviolet Photodissociation Mass Spectrometry for the Structural Elucidation of Lipid A Compounds in Complex Mixtures *Anal. Chem.* **2014**, *86*, 2138-2145.
(64) Morrison, L. J.; Parker, W. R.; Holden, D. D.; Henderson, J. C.; Boll, J. M.; Trent, M. S.; Brodbelt, J. S. UVliPiD: A UVPD-Based Hierarchical Approach for De Novo Characterization of Lipid A Structures *Anal. Chem.* **2016**, *88*, 1812-1820.
(65) Klein, D. R.; Brodbelt, J. S. Structural Characterization of Phosphatidylcholines Using 193 nm Ultraviolet Photodissociation Mass Spectrometry *Anal. Chem.* **2017**, *89*, 1516-1522.
(66) Ko, B. J.; Brodbelt, J. S. 193 nm Ultraviolet Photodissociation of Deprotonated Sialylated Oligosaccharides *Anal. Chem.* **2011**, *83*, 8192-8200.
(67) Smith, S. I.; Brodbelt, J. S. Hybrid activation methods for elucidating nucleic acid modifications *Anal. Chem.* **2010**, *83*, 303-310.
(68) Ly, T.; Julian, R. R. Residue-specific radical-directed dissociation of whole proteins in the gas phase *J. Am. Chem. Soc.* **2008**, *130*, 351-358.
(69) Ly, T.; Julian, R. R. Elucidating the Tertiary Structure of Protein ions in Vacuo with Site Specific Photoinitiated Radical Reactions *J. Am. Chem. Soc.* **2010**, *132*, 8602-8609.
(70) Talbert, L. E.; Julian, R. R. Directed-Backbone Dissociation Following Bond-Specific Carbon-Sulfur UVPD at 213 nm *J. Am. Soc. Mass. Spectrom.* **2018**, *29*, 1760-1767.
(71) Julian, R. R. The Mechanism Behind Top-Down UVPD Experiments: Making Sense of Apparent Contradictions *J. Am. Soc. Mass. Spectrom.* **2017**, *28*, 1823-1826.
(72) Hipple, J. A.; Sommer, H.; Thomas, H. A. A Precise Method of Determining the Faraday by Magnetic Resonance *Phy. Rev.* **1949**, *76*, 1877-1878.
(73) Comisarow, M. B.; Marshall, A. G. Fourier transform ion cyclotron resonance mass spectrometry *Chem. Phys. Lett.* **1973**, *25*, 282-283.
(74) Marshall, A. G.; Comisarow, M. B. Fourier transform ion cyclotron resonance mass spectrometry *Chem. Phys. Lett.* **1974**, *25*, 282-283.

(75) Marshall, A. G.; Hendrickson, C. L.; Jackson, G. S. Fourier transform ion cyclotron resonance mass spectrometry: A primer *Mass Spectrom. Rev.* **1998**, *17*, 1-35.
(76) Amster, I. J. Fourier Transform Mass Spectrometry *J. Mass Spectrom.* **1996**, *31*, 1325-1337.
(77) Marshall, A. G.; S., G. Advantages of High Magnetic Field for Fourier transform ion cyclotron resonance mass spectrometry *Rapid Commun. Mass Spectrom.* **1996**, *10*, 1819-1823.
(78) Easterling, M. L.; Mize, T. H.; Amster, I. J. Routine Part-per-Million Mass Accuracy for high mass Ions: Space-charge effects in MALDI FT-ICR *Anal. Chem.* **1999**, *7*, 624-632.
(79) Ledford, E. B.; Rempel, D. L.; Gross, J. H. Space charge effects in Fourier transform mass spectrometry mass calibration *Anal. Chem.* **1984**, *56*, 2744-2748.
(80) Wu, J.; Fannin, S. T.; Franklin, M. A.; Mollnski, T. F.; Lebrilla, C. B. Exact mass determination for elemental analysis of ions produced by matrix-assisted laser desorption *Anal. Chem.* **1995**, *67*, 3788 - 3792.
(81) Jeffries, J. B.; Barlow, S. E.; Dunn, G. H. Theory of space-charge shift of ion cyclotron resonance frequencies *Int. J. Mass Spectrom. Ion Processes* **1983**, *54*, 169-187.
(82) Han, S.-J.; Shin, S. K. Space-Charge effects on Fourier transform Ion Cyclotron resonance Signals: Experimental Observations and Three-Dimensional Trajectory Simulations *J. Am. Soc. Mass. Spectrom.* **1997**, *8*, 319-326.
(83) Mallelon, C.; Tolmachev, A. V.; Anderson, G. A.; Harkewicz, R.; Smith, R. D. Mass measurement errors caused by "local" frequency perturbations in FTICR mass spectrometry *American Society of Mass Spectrometry* **2002**, *13*, 99-106.
(84) Gross, J. H. Wide-range mass calibration for negative-ion DART mass spectrometry *Eur J Mass Spectrom (Chichester)* **2014**, *20*, 155-161.
(85) Savory, J. J.; Kaiser, N. K.; McKenna, A. M.; Xian, F.; Blakney, G. T.; Rodgers, R. P.; Hendrickson, C. L.; Marshall, A. G. Parts-per-billion Fourier transform ion cyclotron resonance mass measurement accuracy with a "walking" calibration equation *Anal. Chem.* **2011**, *83*, 1732-1736.
(86) Jing, L.; Amster, I. J. An improved calibration method for the matrix-assisted laser desorption/ionization-Fourier transform ion cyclotron resononance analysis of 15N-metabolically- labeled proteome digests using a mass difference approach *Eur J Mass Spectrom (Chichester)* **2012**, *18*, 269-277.
(87) Smith, D. F.; Kharchenko, A.; Konijnenburg, M.; Klinkert, I.; Pasa-Tolic, L.; Heeren, R. M. Advanced mass calibration and visualization for FT-ICR mass spectrometry imaging *J. Am. Soc. Mass. Spectrom.* **2012**, *23*, 1865-1872.
(88) Zhang, L.-K.; Rempel, D.; Pramanik, B. N.; Gross, M. L. Accurate mass measurements by Fourier transform mass spectrometry *Mass Spectrom. Rev.* **2005**, *24*, 286-309.
(89) Caravatti, P.; Allemann, M. The 'Infinity Cell': a New Trapped-ion Cell With Radiofrequency Covered Trapping Electrodes for Fourier Transform Ion Cyclotron Resonance Mass Spectrometry *Org. Mass Spectrom.* **1991**, *26*, 514-518.
(90) Boldin, I. A.; Nikolaev, E. N. Fourier transform ion cyclotron resonance cell with dynamic harmonization of the electric field in the whole volume by shaping of the excitation and detection electrode assembly *Rapid Commun. Mass Spectrom.* **2011**, *25*, 122-126.
(91) Lioznov, A.; Baykut, G.; Nikolaev, E. Analytical Solution for the Electric Field Inside Dynamically Harmonized FT-ICR Cell *J. Am. Soc. Mass. Spectrom.* **2019**, *30*, 778-786.
(92) Kostyukevich, Y. I.; Vladimirov, G. N.; Nikolaev, E. N. Dynamically harmonized FT-ICR cell with specially shaped electrodes for compensation of inhomogeneity of the magnetic field. Computer simulations of the electric field and ion motion dynamics *J. Am. Soc. Mass. Spectrom.* **2012**, *23*, 2198-2207.

(93) Popov, I. A.; Nagornov, K.; Vladimirov, G. N.; Kostyukevich, Y. I.; Nikolaev, E. N. Twelve million resolving power on 4.7 T Fourier transform ion cyclotron resonance instrument with dynamically harmonized cell--observation of fine structure in peptide mass spectra *J. Am. Soc. Mass. Spectrom.* **2014**, *25*, 790-799.
(94) Pfandler, P.; Bodenhausen, G.; Rapin, J.; Houriet, R.; Gaumann, T. Two-dimensional Fourier transform ion cyclotron resonance mass spectrometry *Chem. Phys. Lett.* **1987**, *138*, 195-200.
(95) Pfandler, P.; Bodenhausen, G.; Rapin, J.; Walser, M.; Gaumann, T. Broad-Band Two-Dimensional Fourier Transform Ion Cyclotron Resonance *J. Am. Chem. Soc.* **1988**, *110*, 5628-2633.
(96) Bodenhausen, G.; Pfandler, P.; Rapin, J.; Gaumann, T.; Houriet, R. U. S., 4855593.1989.Spectrospin, AG, Zurich, Switzerland
(97) Ross, C. W.; S., G.; Grosshans, P. B.; Ricca, T. L.; Marshall, A. G. Two-dimensional Fourier transform ion cyclotron resonance mass spectrometry with stored waveform ion radius modulation *J. Am. Chem. Soc.* **1993**, *115*, 7854-7861.
(98) Marshall, A. G.; Rest, G. v. d. Noise analysis for 2D tandem Fourier transform ion cyclotron resonance mass spectrometry *Int. J. Mass spectrom.* **2001**, *210*, 101-111.
(99) A. F. Mehlkopf, D. K., T. A. Tiggelman, R. Freeman. Sources of tI Noise in Two-Dimensional NMR *Journal of Magnetic Resonance* **1984**, *58*, 315-323.
(100) van Agthoven, M. A.; Chiron, L.; Coutouly, M. A.; Delsuc, M. A.; Rolando, C. Two-dimensional ECD FT-ICR mass spectrometry of peptides and glycopeptides *Anal. Chem.* **2012**, *84*, 5589-5595.
(101) van Agthoven, M. A.; Coutouly, M. A.; Rolando, C.; Delsuc, M. A. Two-dimensional Fourier transform ion cyclotron resonance mass spectrometry: reduction of scintillation noise using Cadzow data processing *Rapid Commun. Mass Spectrom.* **2011**, *25*, 1609-1616.
(102) Chiron, L.; van Agthoven, M. A.; Kieffer, B.; Rolando, C.; Delsuc, M. A. Efficient denoising algorithms for large experimental datasets and their applications in Fourier transform ion cyclotron resonance mass spectrometry *Proc Natl Acad Sci U S A* **2014**, *111*, 1385-1390.
(103) Simon, H. J.; van Agthoven, M. A.; Lam, P. Y.; Floris, F.; Chiron, L.; Delsuc, M. A.; Rolando, C.; Barrow, M. P.; O'Connor, P. B. Uncoiling collagen: a multidimensional mass spectrometry study *Analyst* **2016**, *141*, 157-165.
(104) Floris, F.; van Agthoven, M.; Chiron, L.; Soulby, A. J.; Wootton, C. A.; Lam, Y. P.; Barrow, M. P.; Delsuc, M. A.; O'Connor, P. B. 2D FT-ICR MS of Calmodulin: A Top-Down and Bottom-Up Approach *J. Am. Soc. Mass. Spectrom.* **2016**, *27*, 1531-1538.
(105) Floris, F.; Chiron, L.; Lynch, A. M.; Barrow, M. P.; Delsuc, M. A.; O'Connor, P. B. Top-Down Deep Sequencing of Ubiquitin Using Two-Dimensional Mass Spectrometry *Anal. Chem.* **2018**, *90*, 7302-7309.
(106) Floris, F.; Vallotto, C.; Chiron, L.; Lynch, A. M.; Barrow, M. P.; Delsuc, M. A.; O'Connor, P. B. Polymer Analysis in the Second Dimension: Preliminary Studies for the Characterization of Polymers with 2D MS *Anal. Chem.* **2017**, *89*, 9892-9899.
(107) Mayo, F. R. Chain Transfer in the polymerization of Styrene: The Reaction of Solvents with Free Radicals *J. Am. Chem. Soc.* **1943**, *65*, 2324-2329.
(108) Carothers, W. H.; Arvin, J. A. STUDIES ON POLYMERIZATION AND RING FORMATION POLY-ESTERS *J. Am. Chem. Soc.* **1919**, *51*, 2560-2570.
(109) Hamley, I. W. *Block copolymers in solution*; Wiley and Sons Ltd. : London, 2005.
(110) Caminade, A. M.; Yan, D.; Smith, D. K. Dendrimers and hyperbranched polymers *Chem. Soc. Rev.* **2015**, *44*, 3870-3873.
(111) Liechty, W. B.; Kryscio, D. R.; Slaughter, B. V.; Peppas, N. A. Polymers for drug delivery systems *Annual Review of Chemical and Biomolecular Engineering* **2010**, *1*, 149-173.

(112) Abu Lila, A. S.; Kiwada, H.; Ishida, T. The accelerated blood clearance (ABC) phenomenon: clinical challenge and approaches to manage *J. Controlled Release* **2013**, *172*, 38-47.
(113) Pelegri-O'Day, E. M.; Lin, E. W.; Maynard, H. D. Therapeutic protein-polymer conjugates: advancing beyond PEGylation *J. Am. Chem. Soc.* **2014**, *136*, 14323-14332.
(114) Ekladious, I.; Colson, Y. L.; Grinstaff, M. W. Polymer-drug conjugate therapeutics: advances, insights and prospects *Nat. Rev. Drug Discov.* **2019**, *18*, 273-294.
(115) Knop, K.; Hoogenboom, R.; Fischer, D.; Schubert, U. S. Poly(ethylene glycol) in drug delivery: pros and cons as well as potential alternatives *Angew. Chem. Int. Ed.* **2010**, *49*, 6288-6308.
(116) Legros, C.; Wirotius, A. L.; De Pauw-Gillet, M. C.; Tam, K. C.; Taton, D.; Lecommandoux, S. Poly(2-oxazoline)-based nanogels as biocompatible pseudopolypeptide nanoparticles *Biomacromolecules* **2015**, *16*, 183-191.
(117) Glassner, M.; Vergaelen, M.; Hoogenboom, R. Poly(2-oxazoline)s: A comprehensive overview of polymer structures and their physical properties *Polym. Int.* **2018**, *67*, 32-45.
(118) Lambermont-Thijs, H. M. L.; van der Woerdt, F. S.; Baumgaertel, A.; Bonami, L.; Du Prez, F. E.; Schubert, U. S.; Hoogenboom, R. Linear Poly(ethylene imine)s by Acidic Hydrolysis of Poly(2-oxazoline)s: Kinetic Screening, Thermal Properties, and Temperature-Induced Solubility Transitions *Macromolecules* **2010**, *43*, 927-933.
(119) Mees, M. A.; Hoogenboom, R. Full and partial hydrolysis of poly(2-oxazoline)s and the subsequent post-polymerization modification of the resulting polyethylenimine (co)polymers *Polymer Chemistry* **2018**, *9*, 4968-4978.
(120) Palivan, C. G.; Goers, R.; Najer, A.; Zhang, X.; Car, A.; Meier, W. Bioinspired polymer vesicles and membranes for biological and medical applications *Chem. Soc. Rev.* **2016**, *45*, 377-411.
(121) Hamidi, M.; Shahbazi, M. A.; Rostamizadeh, K. Copolymers: efficient carriers for intelligent nanoparticulate drug targeting and gene therapy *Macromolecular Bioscience* **2012**, *12*, 144-164.
(122) Obermeyer, A. C.; Olsen, B. D. Synthesis and Application of Protein-Containing Block Copolymers *ACS Macro Letters* **2015**, *4*, 101-110.
(123) Ghosh, S.; Basu, S.; Thayumanavan, S. Simultaneous and Reversible Functionalization of Copolymers for Biological Applications *Macromolecules* **2006**, *39*, 5595-5597.
(124) Qian, Z.; Dougherty, P. G.; Pei, D. Targeting intracellular protein-protein interactions with cell-permeable cyclic peptides *Curr. Opin. Chem. Biol.* **2017**, *38*, 80-86.
(125) Zorzi, A.; Deyle, K.; Heinis, C. Cyclic peptide therapeutics: past, present and future *Curr. Opin. Chem. Biol.* **2017**, *38*, 24-29.
(126) Dougherty, P. G.; Sahni, A.; Pei, D. Understanding Cell Penetration of Cyclic Peptides *Chem. Rev.* **2019**, *119*, 10241-10287.
(127) Khazanovich, N.; Granja, J. R.; McRee, D. E.; Milligan, R. A.; Ghadiri, M. R. Nanoscale Tubular Ensembles with Specified Internal Diameters. Design of a Self-Assembled Nanotube with a 13-A Pore *J. Am. Chem. Soc.* **1994**, *116*, 6011-6012.
(128) Chapman, R.; Danial, M.; Koh, M. L.; Jolliffe, K. A.; Perrier, S. Design and properties of functional nanotubes from the self-assembly of cyclic peptide templates *Chem. Soc. Rev.* **2012**, *41*, 6023-6041.
(129) Ghadiri, M. R.; Kobayashi, K.; Granja, J. R.; Chadha, R. J.; McRee, D. E. The Structural and Thermodynamic Basis for the Formation of Self-Assembled Peptide Nanotubes *Angew. Chem. Int. Ed.* **1995**, *34*, 93-96.

(130) Chapman, R.; Warr, G. G.; Perrier, S.; Jolliffe, K. A. Water-soluble and pH-responsive polymeric nanotubes from cyclic peptide templates *Chem. Eur. J.* **2013**, *19*, 1955-1961.
(131) Blunden, B. M.; Chapman, R.; Danial, M.; Lu, H.; Jolliffe, K. A.; Perrier, S.; Stenzel, M. H. Drug conjugation to cyclic peptide-polymer self-assembling nanotubes *Chem. Eur. J.* **2014**, *20*, 12745-12749.
(132) Méndez-Ardoy, A.; Granja, J. R.; Montenegro, J. pH-Triggered self-assembly and hydrogelation of cyclic peptide nanotubes confined in water micro-droplets *Nanoscale Horizons* **2018**, *3*, 391-396.
(133) Danial, M.; Tran, C. M.; Young, P. G.; Perrier, S.; Jolliffe, K. A. Janus cyclic peptide-polymer nanotubes *Nat Commun* **2013**, *4*, 2780.
(134) Shaikh, H.; Rho, J. Y.; Macdougall, L. J.; Gurnani, P.; Lunn, A. M.; Yang, J.; Huband, S.; Mansfield, E. D. H.; Peltier, R.; Perrier, S. Hydrogel and Organogel Formation by Hierarchical Self-Assembly of Cyclic Peptides Nanotubes *Chem. Eur. J.* **2018**, *24*, 19066-19074.
(135) Binfield, J. G.; Brendel, J. C.; Cameron, N. R.; Eissa, A. M.; Perrier, S. Imaging Proton Transport in Giant Vesicles through Cyclic Peptide-Polymer Conjugate Nanotube Transmembrane Ion Channels *Macromol. Rapid Commun.* **2018**, *39*.
(136) Larnaudie, S. C.; Sanchis, J.; Nguyen, T. H.; Peltier, R.; Catrouillet, S.; Brendel, J. C.; Porter, C. J. H.; Jolliffe, K. A.; Perrier, S. Cyclic peptide-poly(HPMA) nanotubes as drug delivery vectors: In vitro assessment, pharmacokinetics and biodistribution *Biomaterials* **2018**, *178*, 570-582.
(137) Larnaudie, S. C.; Brendel, J. C.; Romero-Canelon, I.; Sanchez-Cano, C.; Catrouillet, S.; Sanchis, J.; Coverdale, J. P. C.; Song, J. I.; Habtemariam, A.; Sadler, P. J.; Jolliffe, K. A.; Perrier, S. Cyclic Peptide-Polymer Nanotubes as Efficient and Highly Potent Drug Delivery Systems for Organometallic Anticancer Complexes *Biomacromolecules* **2018**, *19*, 239-247.
(138) Stetefeld, J.; McKenna, S. A.; Patel, T. R. Dynamic light scattering: a practical guide and applications in biomedical sciences *Biophys Rev* **2016**, *8*, 409-427.
(139) Montaudo, G.; Samperi, F.; Montaudo, M. S. Characterization of synthetic polymers by MALDI-MS *Prog. Polym. Sci.* **2006**, *31*, 277-357.
(140) Rooij, G. J. v.; Durrsma, M. C.; Heeren, R. M. A.; Boon, J. J.; de Koster, C. G. High Resolution End Group Determination of Low Molecular Weight Polymers by Matrix- Assisted Laser Desorption Ionization on an External Ion Source Fourier Transform Ion Cyclotron Resonance Mass Spectrometer *J. Am. Soc. Mass. Spectrom.* **1996**, *7*, 449-457.
(141) Danis, P. O. Analysis of Poly(styrenesulfonicacid) by Matrix-Assisted Laser Desorption/ionization Time-of-Flight Mass Spectrometry *Macromolecules* **1995**, *28*, 8548-8551.
(142) Schriemer, D. C.; Li, L. Detection of high molecular weight narrow polydisperse polymers up to 1.5 million daltons by MALDI mass spectrometry *Anal. Chem.* **1996**, *68*, 2721.
(143) O'Connor, P. B.; McLafferty, F. W. Oligomer Characterization of 4—23 kDa Polymers by Electrospray Fourier Transform Mass Spectrometry *J. Am. Chem. Soc.* **1995**, *117*, 12826-12831.
(144) Easterling, M. L.; Amster, I. J.; Rooij, G. J. v.; Heeren, R. M. A. Isotope beating effects in the analysis of polymer distributions by Fourier transform mass spectrometry *J. Am. Soc. Mass. Spectrom.* **1999**, *10*, 1074-1082.
(145) Koster, S.; Durrsma, M. C.; Boon, J. J.; Heeren, R. M. A. Endgroup Determination of Synthetic Polymers by Electrospray Ioniszation Fourier Transform Ion Cyclotron Resonance Mass Spectrometry *J. Am. Soc. Mass. Spectrom.* **2000**, *11*, 536-543.
(146) Gallet, G.; Carroccio, S.; Rizzarelli, P.; Karlsson, S. Thermal degradation of polyethylene oxide–propylene oxide–ethylene oxide) triblock copolymer: comparative

study by SEC/NMR, SEC/MALDI-TOF-MS and PME/GC-MS *Polymer* **2002**, *43*, 1081-1094.
(147) Perez Hurtado, P.; Lam, P. Y.; Kilgour, D.; Bristow, A.; McBride, E.; O'Connor, P. B. Use of high resolution mass spectrometry for analysis of polymeric excipients in drug delivery formulations *Anal. Chem.* **2012**, *84*, 8579-8586.
(148) Baumgaertel, A.; Scheubert, K.; Pietsch, B.; Kempe, K.; Crecelius, A. C.; Bocker, S.; Schubert, U. S. Analysis of different synthetic homopolymers by the use of a new calculation software for tandem mass spectra *Rapid Commun. Mass Spectrom.* **2011**, *25*, 1765-1778.
(149) Altuntaş, E.; Weber, C.; Schubert, U. S. Detailed characterization of poly(2-ethyl-2oxazoline)s by energy variable collision-induced dissociation study *Rapid Commun. Mass Spectrom.* **2013**, *27*, 1095-1100.
(150) Rivera-Tirado, E.; Wesdemiotis, C. Characterization of polyethylenimine by electrospray ionization and matrix-assisted laser desorption/ionization *J. Mass Spectrom.* **2011**, *46*, 876-883.
(151) Favier, A.; Ladaviere, C.; Charreyre, M.-T.; Pichot, C. MALDI-TOF MS Investigation of the RAFT polymerisation of water-soluble acrylamide derivative *Macromolecules* **2004**, *37*, 2026-2034.
(152) Haler, J. R. N.; Far, J.; Aqil, A.; Claereboudt, J.; Tomczyk, N.; Giles, K.; Jerome, C.; De Pauw, E. Multiple Gas-Phase Conformations of a Synthetic Linear Poly(acrylamide) Polymer Observed Using Ion Mobility-Mass Spectrometry *J. Am. Soc. Mass. Spectrom.* **2017**, *28*, 2492-2499.
(153) Goldschmidt, R. J.; Wetzel, S. J.; Blair, W. R.; Guttmann, C. M. Post-Source decay in the analysis of polystyrene by Matrix-Assisted Laser Desorption/Ionisation Time-of-flight Mass Spectrometry *J. Am. Soc. Mass. Spectrom.* **2000**, *11*, 1095-1106.
(154) Hoteling, A. J.; Kawaoka, K.; Goodberlet, M. C.; Yu, W. M.; Owens, K. G. Optimization of matrix-assisted laser desorption/ionization time-of-flight collision-induced dissociation using poly(ethylene glycol) *Rapid Commun. Mass Spectrom.* **2003**, *17*, 1671-1676.
(155) Miladinović, S. M.; Robotham, S. A.; Wilkins, C. L. Wide mass range trapping using a 7-T internal sourcematrix-assisted laser desorption/ionization Fourier transformmass spectrometer *Anal. Bioanal. Chem.* **2008**, *392*, 585-594.
(156) Polce, M. J.; Ocampo, M.; Quirk, R. P.; Wesdemiotis, C. Tandem Mass Spectrometry Characteristics of Silver-Cationized Polystyrenes: Backbone Degradation via Free Radical Chemistry *Anal. Chem.* **2008**, *2*, 347-354.
(157) Polce, M. J.; Ocampo, M.; Quirk, R. P.; Leigh, A. M.; Wesdemiotis, C. Tandem Mass Spectrometry Characteristics of Silver-Cationized Polystyrenes: Internal Energy, Size, and Chain End versus Backbone Substituent Effects *Anal. Chem.* **2008**, *80*, 355-362.
(158) Yol, A. M.; Dabney, D. E.; Wang, S. F.; Laurent, B. A.; Foster, M. D.; Quirk, R. P.; Grayson, S. M.; Wesdemiotis, C. Differentiation of linear and cyclic polymer architectures by MALDI tandem mass spectrometry (MALDI-MS2) *J. Am. Soc. Mass. Spectrom.* **2013**, *24*, 74-82.
(159) Wesdemiotis, C.; Solak, N.; Polce, M. J.; Dabney, D. E.; Chaicharoen, K.; Katzenmeyer, B. C. Fragmentation pathways of polymer ions *Mass Spectrom. Rev.* **2011**, *30*, 523-559.
(160) Yol, A. M.; Janoski, J.; Quirk, R. P.; Wesdemiotis, C. Sequence analysis of styrenic copolymers by tandem mass spectrometry *Anal. Chem.* **2014**, *86*, 9576-9582.
(161) Chaicharoen, K.; Polce, M. J.; Singh, A.; Pugh, C.; Wesdemiotis, C. Characterization of linear and branched polyacrylates by tandem mass spectrometry *Anal. Bioanal. Chem.* **2008**, *392*, 595-607.

(162) Altuntaş, E.; Weber, C.; Kempe, K.; Schubert, U. S. Comparison of ESI, APCI and MALDI for the (tandem) mass analysis of poly(2-ethyl-2-oxazoline)s with various end-groups *Eur. Polym. J.* **2013**, *49*, 2172-2185.
(163) Town, J. S.; Jones, G. R.; Haddleton, D. M. MALDI-LID-ToF/ToF analysis of statistical and diblock polyacrylate copolymers *Polymer Chemistry* **2018**, *9*, 4631-4641.
(164) Town, J. S.; Jones, G. R.; Hancox, E.; Shegiwal, A.; Haddleton, D. M. Tandem Mass Spectrometry for Polymeric Structure Analysis: A Comparison of Two Common MALDI-ToF/ToF Techniques *Macromol. Rapid Commun.* **2019**, 1900088-1900094.
(165) Hart-Smith, G. A review of electron-capture and electron-transfer dissociation tandem mass spectrometry in polymer chemistry *Anal. Chim. Acta* **2014**, *808*, 44-55.
(166) Scionti, V.; Wesdemiotis, C. Electron transfer dissociation versus collisionally activated dissociation of cationized biodegradable polyesters *J. Mass Spectrom.* **2012**, *47*, 1442-1449.
(167) Wei, J.; Bristow, A.; McBride, E.; Kilgour, D.; O'Connor, P. B. D-alpha-tocopheryl polyethylene glycol 1000 succinate: a view from FTICR MS and tandem MS *Anal. Chem.* **2014**, *86*, 1567-1574.

2. Introduction to modified Kendrick mass defect analysis

Tomos E. Morgan[1], Andrew Kerr[1], Remy Gavard[1], Christopher A. Wootton[1], Mark P. Barrow[1], Anthony W. T. Bristow[2], Sebastien Perrier[1], Peter B. O'Connor[1]*

[1]Department of Chemistry, University of Warwick, Coventry, Midlands, CV4 7AL, UK.

[2]Chemical Development, Pharmaceutical Technology & Development, Operations, AstraZeneca, Macclesfield, UK.

The results presented in this chapter are predominantly from the FT-ICR MS data acquired by the thesis author. Some parts of this work was carried out by collaborators: Polyacrylamide samples were synthesised and purified by Dr. Andrew Kerr, and code for the weighted fitting functions was coded by Dr. Remy Gavard.

2.1. Abstract

Natural variation in polymer length, termed dispersity, is an inherent property of polymers caused by the statistic nature of polymer synthesis. Most chemical variation of polymers comes from their end groups, backbone modifications, and molecular weight average. The molecular weight average can be elucidated from gel permeation methods, but variations in end group and backbone modifications are harder to analyse.

Polymeric species produce dense mass spectra due to their dispersity. Petroleomic samples are polymeric with a CH_2 repeating unit, analysts therefore try and group petroleum samples based on heteroatomic content as heteroatoms have a much greater chemical effect. The Kendrick mass defect is a way to normalise petroleomic samples based on the CH_2 series, and separates them based on their heteroatomic content.

This chapter focusses on the use of a modified Kendrick mass defect to analyse acrylamide homo- and co-polymers that will be met in further chapters. By changing the homologous series of a Kendrick analysis to one of the monomers present in the copolymer, the proportion of the other monomer can be predicted.

2.2. Introduction

Recent advances in the efficiency and control of various reversible addition-fragmentation chain transfer (RAFT) polymerisation techniques has means there's been a large increase in the variation and complexity of homo- can co-polymer structures that can be produced.[1,2] With alternatives to Poly(ethylene glycol) (PEG),[3,4] being sought due to accelerated blood clearance and lack of modification available to the PEG backbone. Well controlled acrylamide polymer architectures present a possible alternative as a drug carrier or conjugation species. As these polymers find an increased use in biological[5] and medicinal applications[6] there has been an increased interest in the accurate chemical analysis of these polymeric species.[7]

Kendrick mass defect analysis is ubiquitous within the petroleomic industry,[8,9] this method of analysis assigns a homologous series in analysis which normalises the most common elemental composition present. This is carried out in petroleomics by assigning the CH_2 alkyl repeat unit to a mass of integer 14. Differences in mass defect are produced by elements different to the CH_2 repeat unit. Any variation in the mass defect, therefore, groups heteroatoms together, regardless of overall size of alkyl chain. The different heteroatoms are designated "classes" which characterise the chemical composition of the petroleum sample. Class based analysis has become a staple form of petroleum analysis made possible by the use of these Kendrick mass defect techniques.

Recent improvements of homo- and co- polymer analysis have been reported with the use of modified Kendrick Mass Defect techniques.[10-14] Modified Kendrick mass defect analysis can be used to characterise any polymer much like the petroleum samples but by using the monomer of the polymer to renormalize as an integer, instead of the CH_2 repeat unit. The use of a modified Kendrick mass defect therefore causes heteroatoms to become anything different to the monomer unit composition, allowing a grouping of different polymer end groups, adducts, backbone modifications, and copolymer content.

Polyacrylamide analysis by mass spectrometry has been limited to short chained acrylamides and is coupled to liquid chromatography or ion mobility systems.[15,16] ESI

is effective for the ionisation of polyacrylamide species for MS analysis. The increased complexity of the polymer mass spectra benefit from the usage of more accurate peak picking algorithms. The use of the Bruker sophisticated number annotation procedure (SNAP) algorithm which takes isotopes and charge state into account for monoisotopic assignment.[17-19]

This chapter outlines how the mass defect can be used to group polymers as well as give insight into the copolymer chemical composition without extensive *de novo* assignment.

2.3. Methods

2.3.1. Synthesis

N-*N*-dimethylacrylamide (DMA, Sigma Aldrich, 99%), and *N*-*a*cryloylmorpoline (NAM, Sigma Aldrich,97%) homo- and co-polymers were synthesized by RAFT polymerization. 2,2'-azobis[2-(2-imidazolin-2-yl)propane]dihydrochloride (VA-044, >98%, Wako) was used as the initiator and 2-(((butylthio)carbonothioyl)thio) propanoic acid (PABTC) as the RAFT reagent. Synthetic procedures were followed according to previous literature.[20]

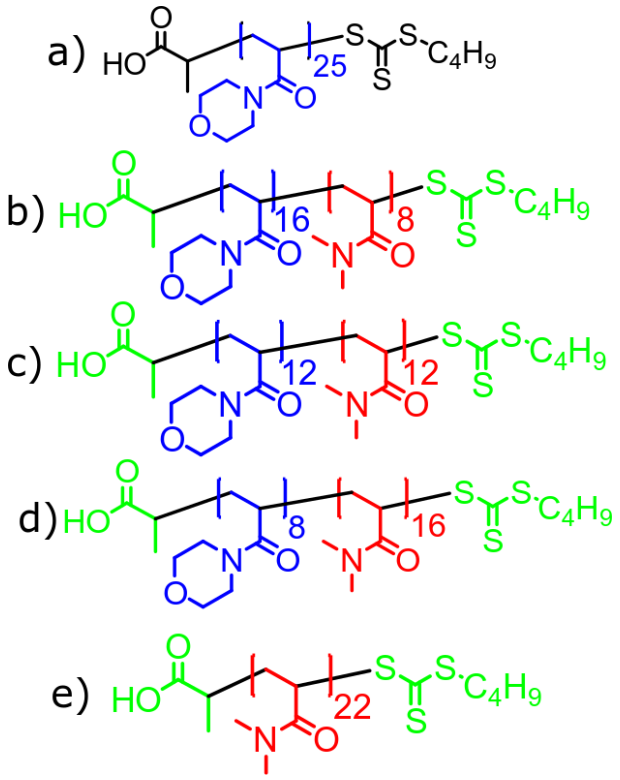

Figure 2.1: a) and b) are homopolymers of NAM and DMA respectively. c), d), and e) are copolymers constituting 66%, 50%, and 33% NAM with the rest of the polymer mass present from DMA. The end groups remain constant across the polymers and are present as a function of the RAFT reaction process.

2.3.1. Mass spectrometry analysis

Mass spectrometry analysis of the polyacrylamides was carried out without any prior separation or fractionation. The acrylamide samples were solvated into a 99.5% solution of purified water obtained from a Direct-Q3 Ultrapure Water System (Millipore, Lutterworth, United Kingdom) at 20 µM in 0.5% formic acid (Sigma-Aldrich, Dorset, United Kingdom). All experiments were performed on a 12 T solariX Fourier transform ion cyclotron resonance mass spectrometer (Bruker Daltonik, GmbH, Bremen, Germany) using a nanoelectrospray (nESI) ion source in positive ion mode. All data was recorded using 4 mega-word (2^{22}, 32 bit) transients (1.6777 s) achieving approximately 400 thousand resolving power at *m/z* 400. All mass spectra were internally calibrated by the intact polymer peaks across the polymer distribution.

Copolymer spectra were phased with the use of

2.3.2. Modified Kendrick mass defect analysis

The modified Kendrick mass defect was calculated in all cases by using the NAM monomer as the homologous series. The calculation of the modified mass defect was calculated by taking the mono-isotopic peaks from the Bruker SNAP peak picking algorithm. The masses were then charge state and adduct corrected assuming protonation, Equation 2.1. The adduct correction was left out if comparison of different adduct containing species needed to be carried out or if the adducts weren't known.

$$\left(\frac{m}{z} \times z\right) - (z \times H^{+}_{mass}) = m$$

Equation 2.1: Charge and adduct correction to produce a mass equal to that of the species. The adduct correction may be removed if analysis needs to be carried out on the adducts themselves.

The Modified Kendrick mass (MKMr) can then be calculated by normalising the mass of the species to the homologous series that has been chosen. This normalises the homologous series chosen so it now has an integer mass. The IUPAC mass is the exact mass of the species, it is rounded by the round function to the closest integer in these

equations. This also changes the mass of all the other masses being compared to that of the homologous series, Equation 2.2.

$$MKMr = m \times \frac{round(IUPAC\ mass\ monomer\ unit)}{IUPAC\ mass\ monomer\ unit}$$

Equation 2.2: Calculation of the modified Kendrick mass for any species. The IUPAC monomer mass is that of the species that is being used as the homologous series for the comparison to be made.

The calculation of the modified Kendrick mass defect (MKMD) is carried out by simply rounding the MKMr and then taking the unrounded value away from it. This means that a mass defect is calculated in such a way that an integer mass maintains a mass defect equal to zero. The conversion therefore means that the homologous series, no matter what it is, has a mass defect equal to zero.

$$MKMD = round(MKMr) - MKMr$$

Equation 2.3: Calculation of the modified Kendrick mass defect, this normalises the homologous series to have a mass defect of zero and any variation from this series will now be a mass defect directly compared to the modified homologous series.

The MKMD analysis can be modified further by increasing the amount that the normalisation function affects the MKMr. Increasing the power of the normalisation function was called high resolution modified Kendrick mass defect (HRMKMD) by Sato *et al.* but importantly, this has little relation to the resolving power of the mass spectrometer but the calculation.

2.4. Results and Discussion

2.4.1. Homopolymer analysis

Nano-Electrospray analysis of the n-acryloylmorpholine (NAM) and dimethylamine (DMA) acrylamide homopolymers produces clear spectra. The polymers were protonated due to the acidification of the sample as well as nESI being used. Figure 2.2 shows the presence of a molecular dispersity present due to the polymerisation process. The polymer also exhibits multiple charge states due to the different sizes of polymer present as well as the statistical likelihood of varying charge states. Higher charges were seen on the larger molecules on average due to the inherent nature of an increased size being able to stabilize charge more effectively. Assignment tables for the p(DMA) homopolymer are found in the supplementary information of chapter 4 showing accurate mass assignments for the expected polymer species.

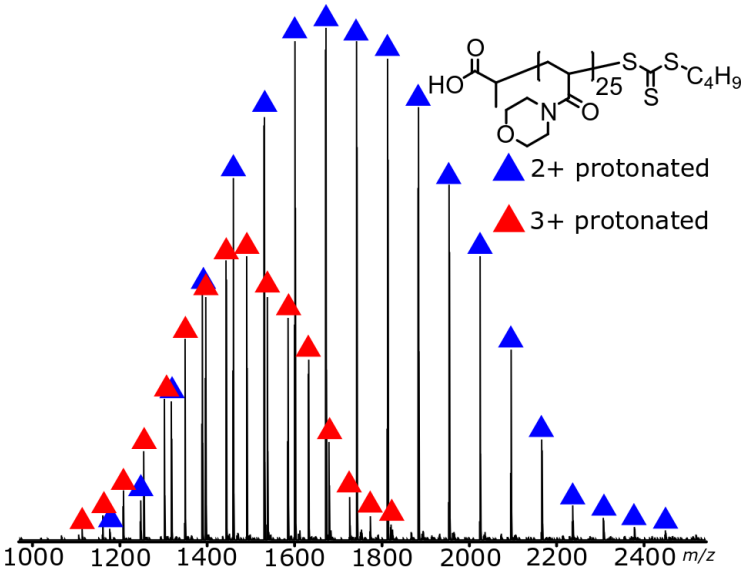

Figure 2.2: nESI analysis of a NAM polymer, this showed obvious distributions that were caused by the dispersity and charge state of the polymer. On average the larger polymer chains charged more due to their ability to stabilise an increased number of charges.

The spacing between peaks in the mass spectrum were the expected monomer spacing divided by the charge of the polymer. This was seen here as the 3+ protonation is shown to be spaced much more closely than the 2+ protonation. The amount of charge a molecule can stabilise will be inherent to its overall size, as closely

spaced charge is energetically unfavourable, and its basicity which will be a measure of effectiveness to stabilise the charge present. The analysis of NAM, Figure 2.3, shows an increased number of charge states as well as an increased number of charges with the presence of an obvious 4+ charge state even with though the polymer was smaller.

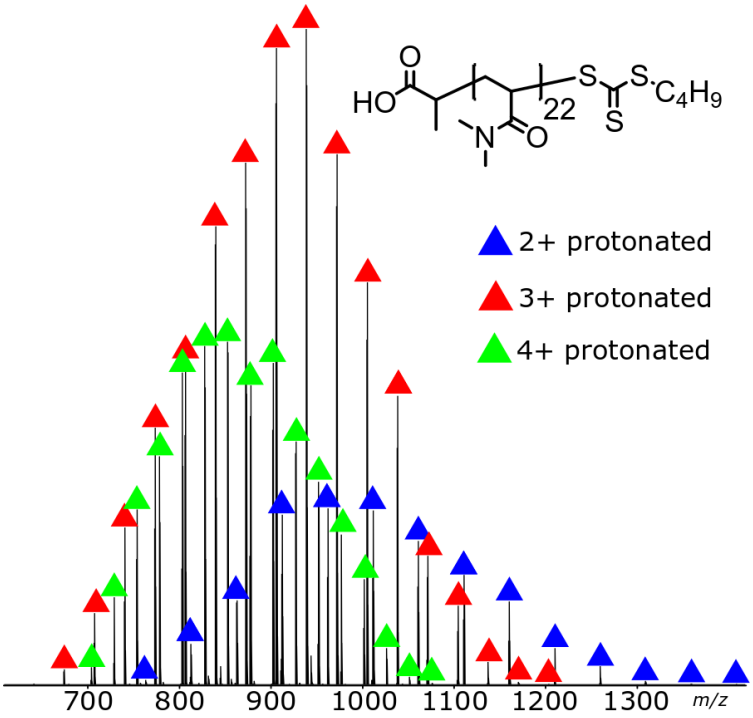

Figure 2.3: nESI analysis of a DMA polymer, this showed obvious distributions that were caused by the dispersity and charge state of the polymer. The presence of the overlapping 2+, 3+, and 4+ charge states add complexity to the spectrum.

The presence of multiple charge states added another level of dispersal complexity to the mass spectra. Although this issue could have been avoided with the use of MALDI the benefits of ESI are two-fold. There is a higher resolving power of the FT-ICR at lower m/z, meaning that the averaging effect of charge stacking on the polymer means that even high mass polymers were present at a position in the mass spectrum that allowed high resolution analysis and multiply charged ions are beneficial down-stream for fragmentation analysis. The sample preparation for the use of nESI was also trivial for the water soluble polyacrylamides used here.

Peak picking was carried out using the Bruker SNAP algorithm, this algorithm considered the presence of the isotopes to give a more accurate peak assignment to the polymer peaks that were seen. The SNAP peak picking algorithm also gave very accurate charge assignment information allowing the use of charge correction procedures on the data acquired. Direct comparison of the SNAP and acquired spectra was made, Figure 2.4, the SNAP spectrum is the theoretical isotope pattern that has been matched to the peaks that are present in the acquired spectrum.

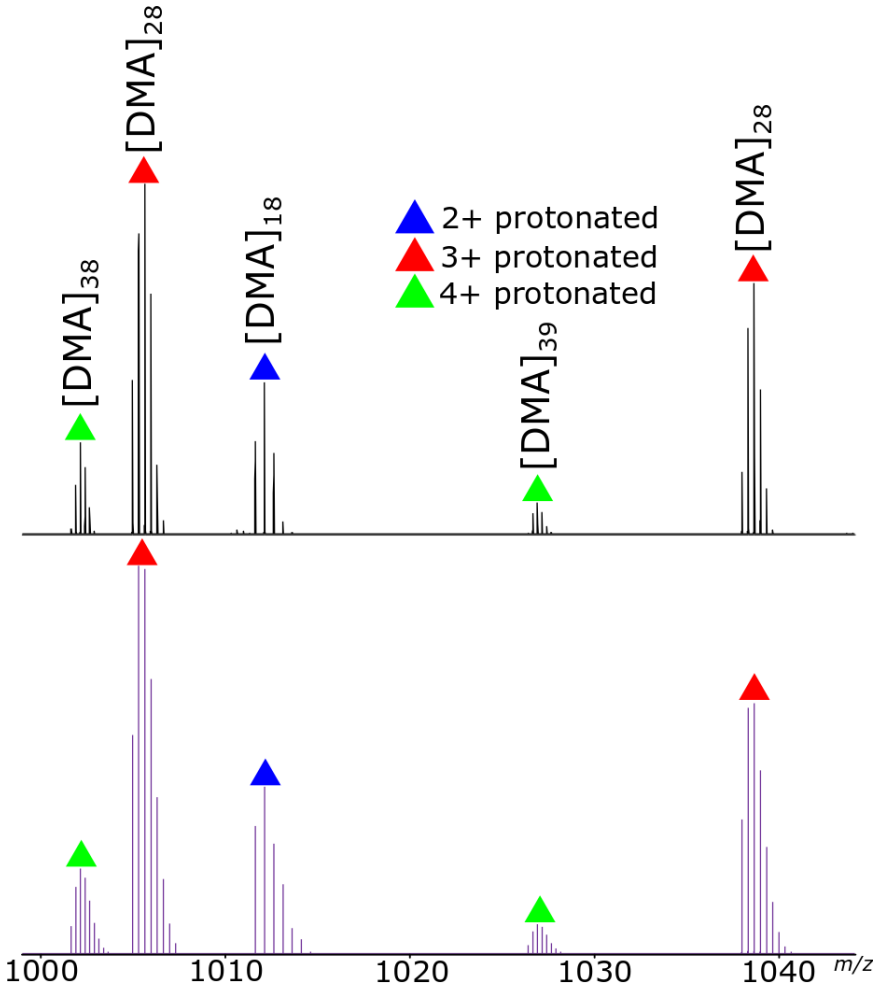

Figure 2.4: Comparison of the acquired spectrum (top) with the SNAP peak picking spectrum (bottom). This comparison allowed the direct analysis of the completeness of the SNAP peak picking to the mass spectrum itself. Importantly SNAP gave good peak picking coverage, with high accuracy due to isotope consideration as well as being able to isotope envelopes that overlap with one another.

The FT-ICR was able to achieve isotopic resolution for the entire measured dispersity of the polymer and therefore the SNAP peak picking algorithm was effective in the analysis of the mass spectrum. Another advantage afforded by SNAP peak picking is that mono-isotopes are reported taking in account the isotopes, so each species is assigned completely without the need for repeated assignment of further isotope peaks. Assignment of just mono-isotopes was also useful in simplifying the analysis of the data.

2.4.2. Copolymer Analysis

Analysis of the block copolymers gave much more complicated spectra due to the presence of multiple dispersity's coming from the natural variation of both copolymers together. The increased density of the spectra means the data is much more difficult to visualise analytically. Figure 2.5 shows the copolymer analysis of the block copolymer acrylamide (33% NAM, 67% DMA). SNAP peak picking was carried out on these data sets to produce a peak list.

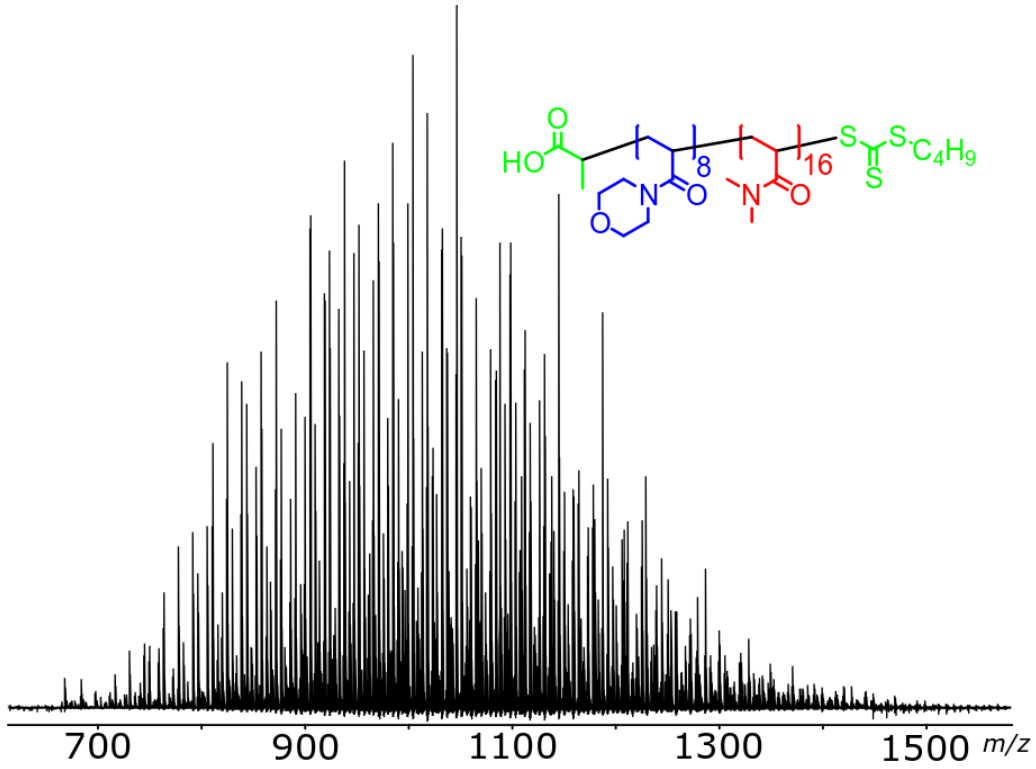

Figure 2.5: nESI copolymer spectra, analysis was carried out by electrospray giving predominately 3+ protonated charge states and

adducts. There was also the presence of lower level 2+ and 4+ charge states.

Phasing of the spectra in these data sets worked well as the spectra were highly dense allowing much more accurate phase fitting functions to be found and accurate phasing to be carried out. Phase fitting accuracy was less at the extremities of the mass distribution but overall beneficial as these peaks were almost completely unresolved in the magnitude mode spectrum.

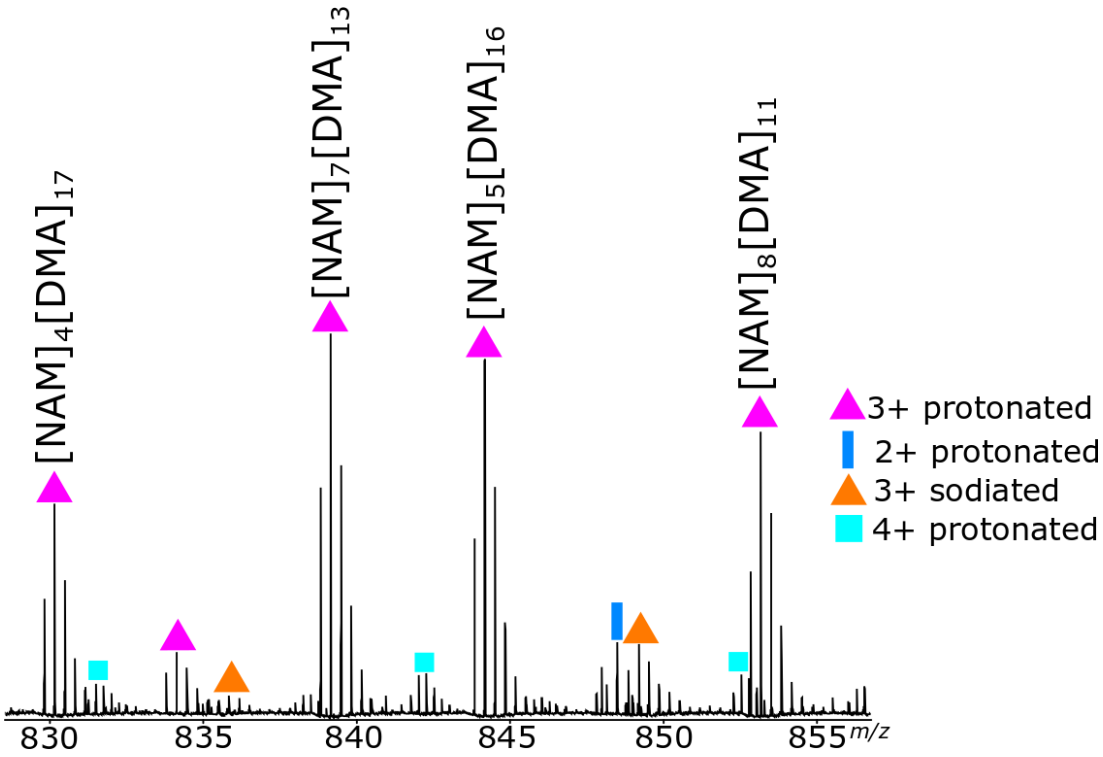

Figure 2.6: Zoom in of copolymer spectra showing the different adducted species that were present as part of the analysis.

The analysis of the other two copolymers showed similar complexity mass spectra with two further copolymer spectra produced which are almost undiscernible to the human eye. As the NAM content increases the ions observed increase in *m/z* due to both an increased mass, but also a decrease in charge density moving from NAM unit to the DMA unit.

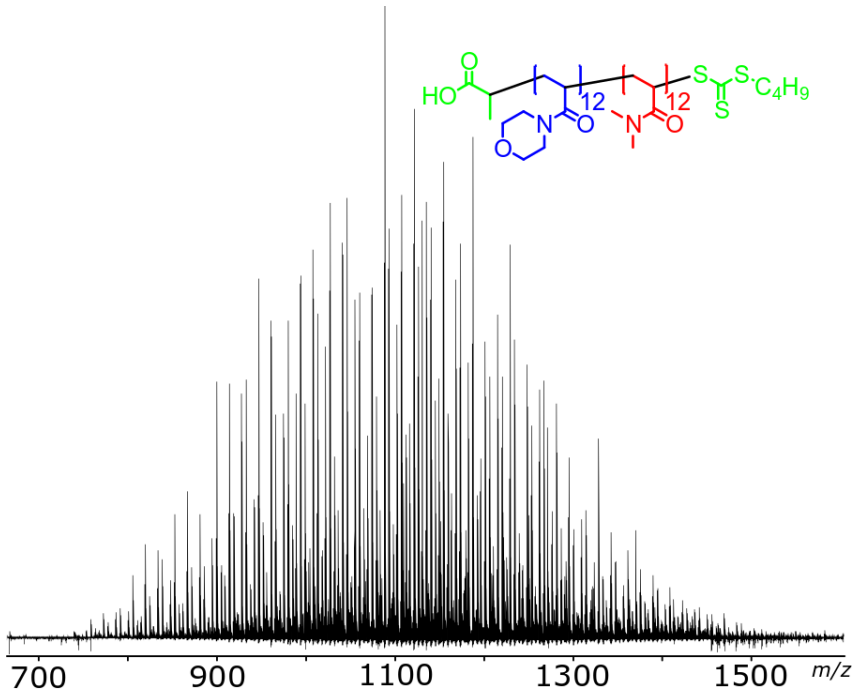

Figure 2.7: nESI copolymer spectra of a 50/50 NAM/DMA by monomer unit block copolymer.

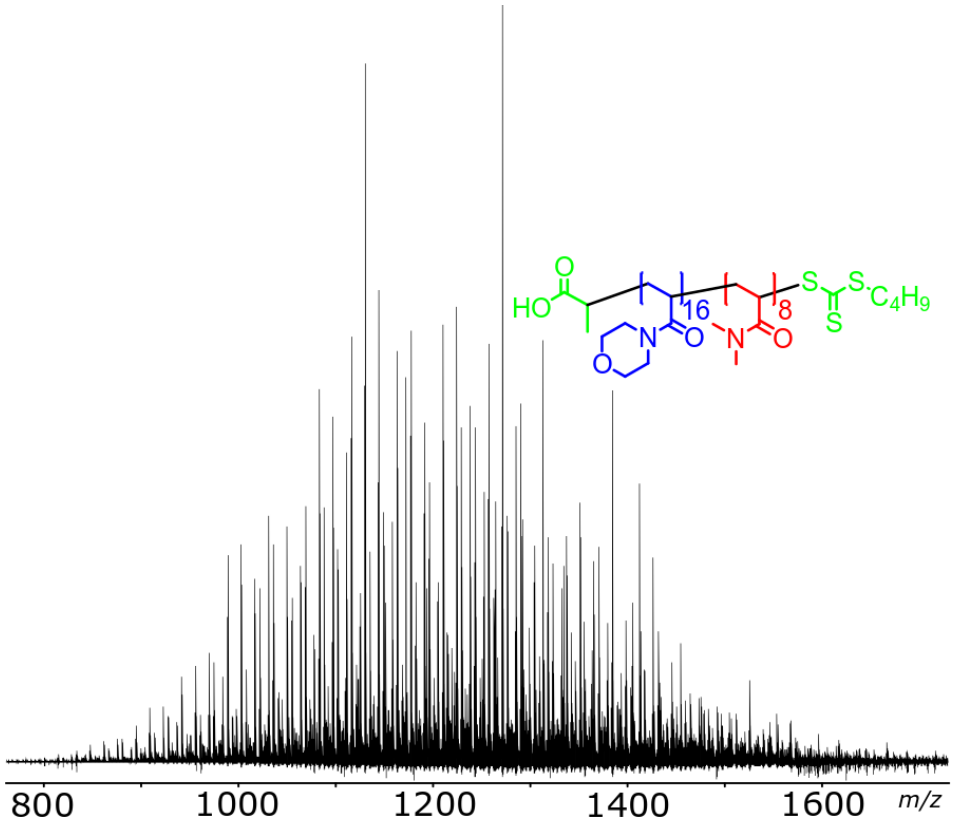

Figure 2.8: nESI copolymer spectra of a 67/33 NAM/DMA by monomer unit block copolymer.

2.4.1. Theoretical modified mass defect analysis

The effect that different copolymer compositions would have on the MKMD plots of the different species was modelled theoretically. The two homo-polymers and three copolymer could be directly compared as a function of their modified Kendrick mass defects to one another. Theoretical modelling was carried out by producing exact block copolymers of the expected chemical ratios and extrapolating these across a dispersity.

The basic premise of fitting using a MKMD plot can be described simply in terms of the IUPAC mass and fitting a theoretical ^{12}C polymer with a hydrogen atom modification to a modified mass defect. As the mass of ^{12}C is an integer with an increasing number of carbons there is no increase in mass defect. The defect is always equal to zero. Figure 2.9 shows the mass defect plot of a ^{12}C homopolymer, mass increasing on the x axis is indicative of an increasing number of ^{12}C atoms. The increasing number of ^{12}C can be seen as a dispersity of a polymer but the monomer here is simply a ^{12}C.

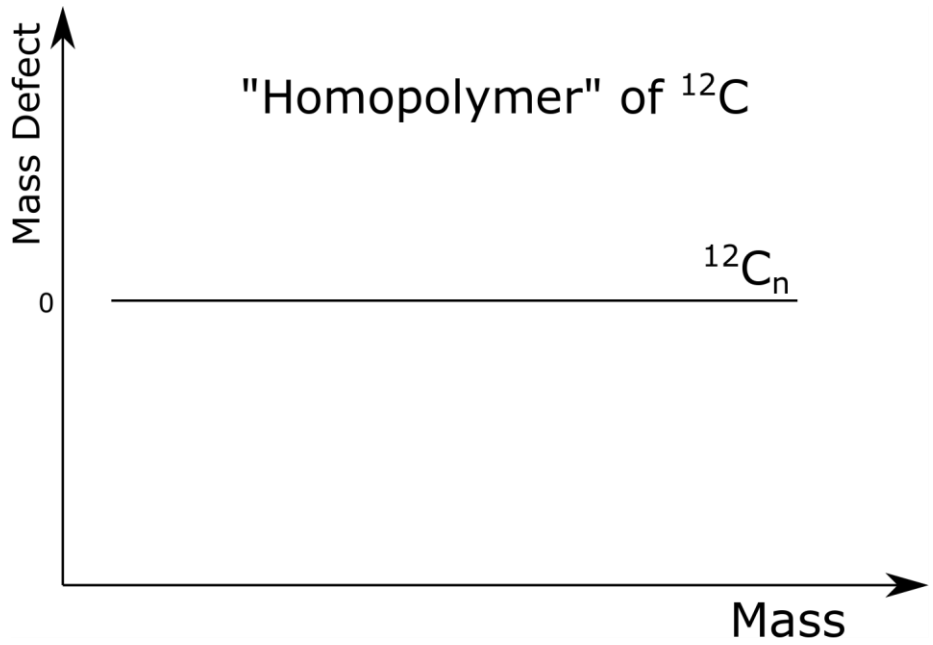

Figure 2.9: The mass defect of the theoretical ^{12}C polymer, this polymer has no mass defect as the mass of ^{12}C is an integer.

The homopolymer ^{12}C may be modified with an end group, in this case we assume hydrogen. As hydrogen has a non-integer mass the addition of a single hydrogen will cause the presence of a mass defect. The presence of a single hydrogen atom will create a single mass defect but with increasing ^{12}C there will not be an increase in mass defect.

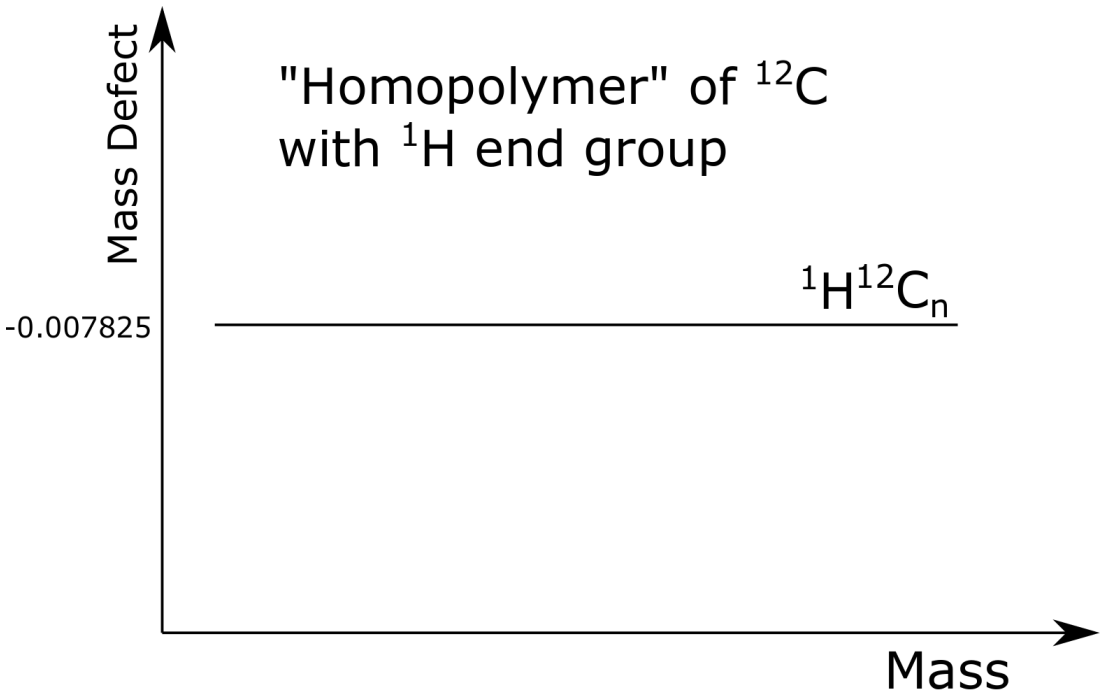

Figure 2.10: The mass defect caused by the presence of a single hydrogen atom will produce a y-intercept of the mass defect value but the gradient of the line will still be equal to zero.

The presence of a modification that is proportional to the size of the polymer will not create a proportional magnitudinal change in the mass defect across the species. This change will therefore be present as a gradient to the graph as, with increasing hydrogen modification, the mass defect will increase stepwise downwards. Assuming the polymer is long enough for this step wise to average out, a smooth linear regression line can be used which will smooth the fitting. With an increased proportional of ^{1}H there will be an increased gradient as there will be more “steps” for each ^{1}H that is present.

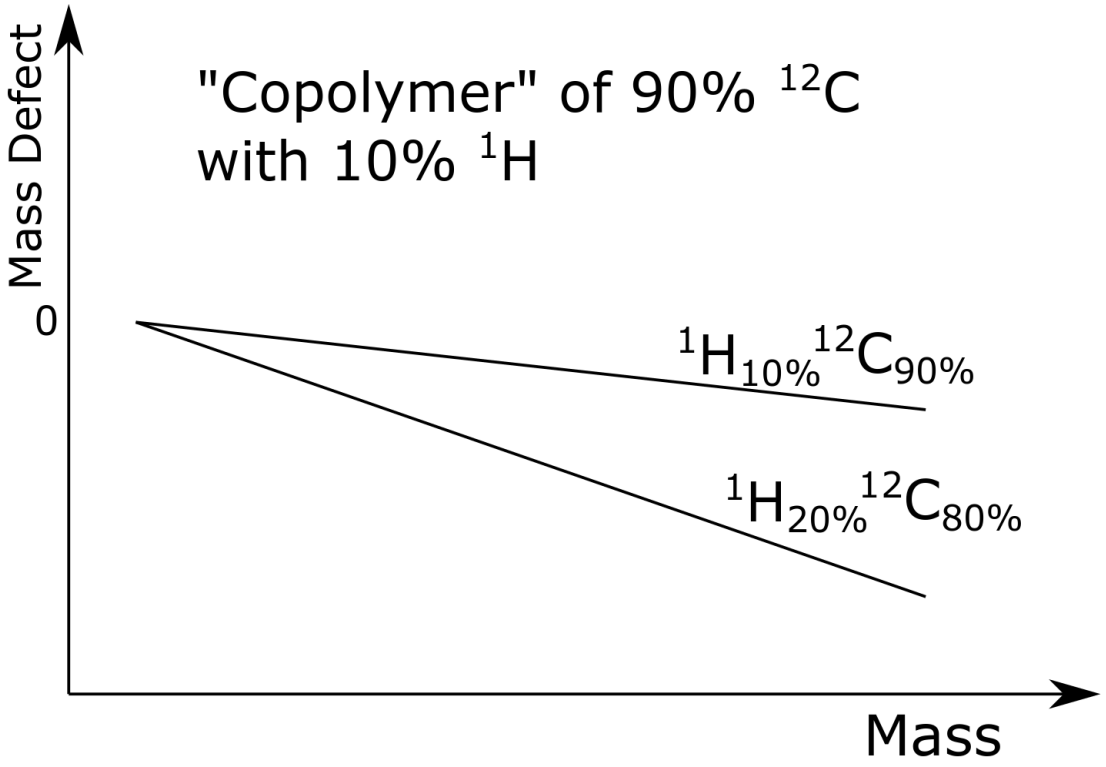

Figure 2.11: The mass defect due to the presence of a constant amount of a non-integer mass species will cause a proportional change as the mass of the molecule increases. The gradient of this change will be steeper depending on the proportion of non-integer mass present.

When using the modified Kendrick mass defect instead of ^{12}C being the integer value, the integer value is now the monomer that has been chosen as the homologous series.

Changing the ^{12}C "monomer" to now be a NAM monomer mass (setting the NAM mass to be equal to 141.00000…) gives a straight line with increasing monomer units offset in MKMD space by the mass defect of the end group.

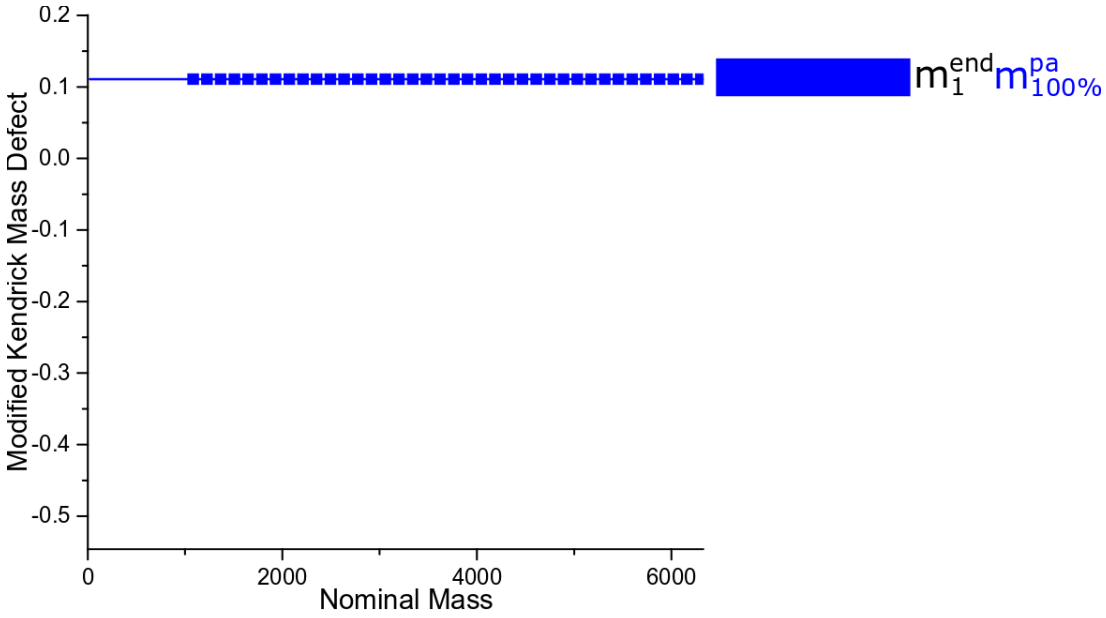

Figure 2.12: Theoretical modified Kendrick mass defect plot of an NAM polymer with an end group. The NAM mass has been normalised to an integer mass the mass defect is therefore a single value caused by the end group.

A plot of the DMA homopolymer after a modification of the integer mass to that of the NAM monomer unit shows a consistent gradient change of the mass defect with an increase in DMA units with an offset of the end group.

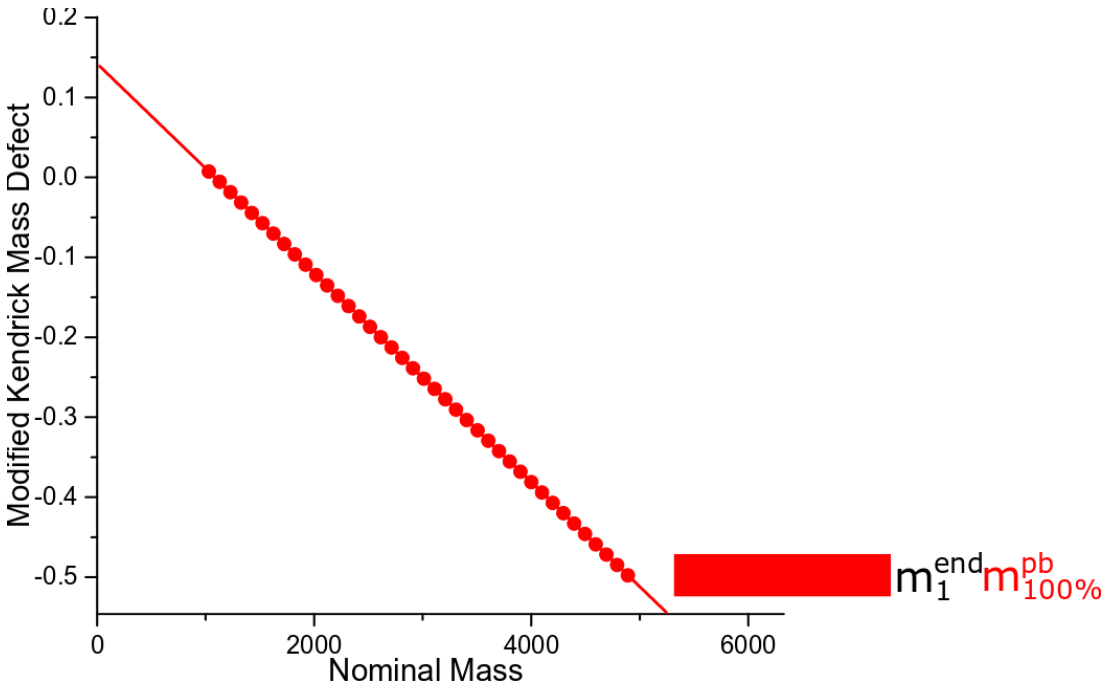

Figure 2.13: Theoretical modified Kendrick mass defect plot of a DMA polymer with an end group. The NAM mass has been normalised to an integer mass, the mass defect therefore changes with an increased number of DMA units.

The addition of a different monomer to this value which is proportional to the size of the polymer (this is always true for random copolymers, and can be made true for block copolymers) then there will be a gradient change based on the concentration of that monomer.

The results showed that for a theoretical data set the NAM polymer which was used as the homologous series had a MKMD that was equal to that of the end group, and the DMA polymer had a gradient equal to its mass defect. The copolymers formed obvious lines that intersected the homopolymer lines at the same point. This point was equal to the end group mass defect and the end group mass. The gradients of each copolymer were proportional to the total monomer composition comparing the DMA and NAM.

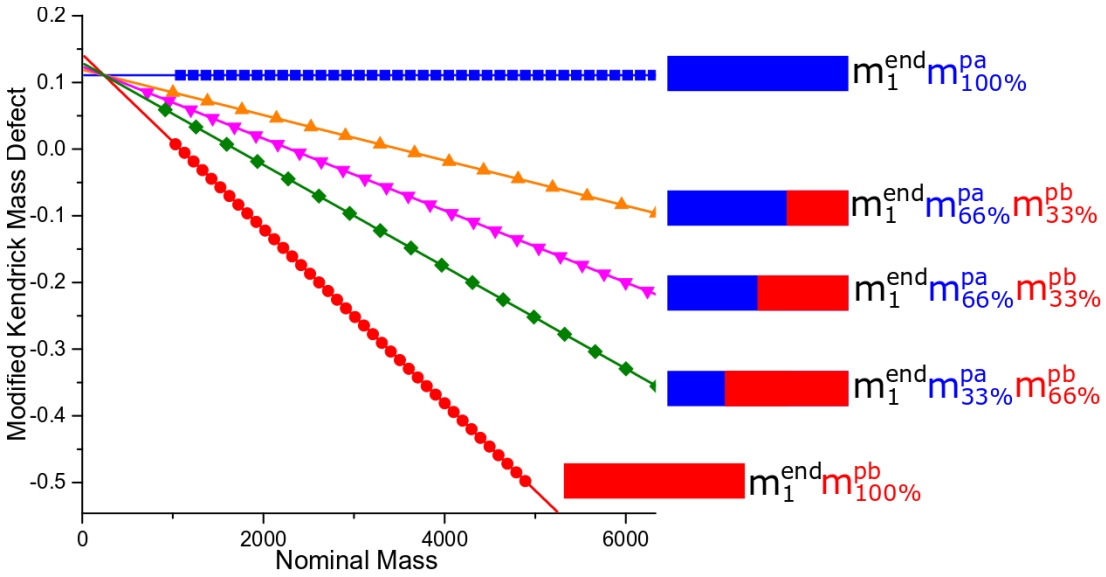

Figure 2.14: Theoretical MKMD plot of the different homo- and co-acrylamide polymers. This shows that the fitting of a line of best fit to the gradients caused by the magnitudinal change in modified Kendrick mass defect caused the formation of predictors to the analysis of the composition of the copolymers.

The theoretical data set showed how the spacing of proportions of each block plotted in a modified Kendrick mass defect graph. The intercept point of the different polymer species also produced analytically useful data in that the point of intercept contained the end group mass and mass defect. The intercept points are shown in Figure 2.15.

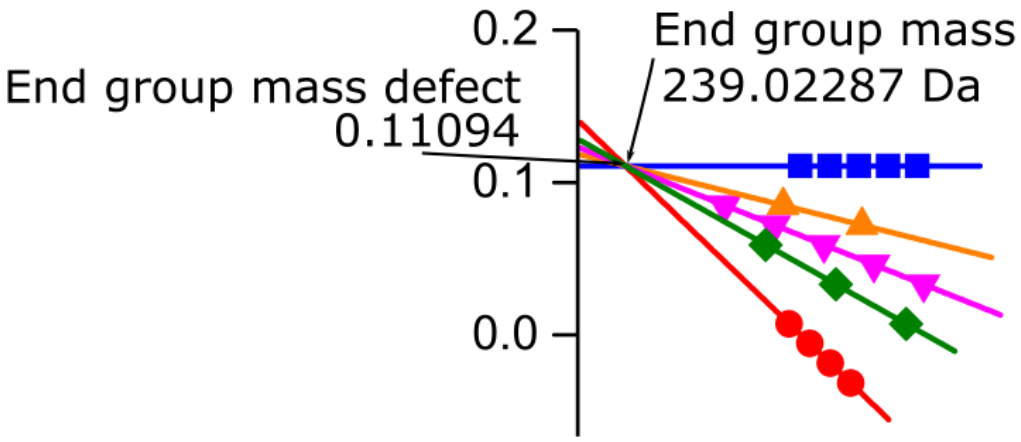

Figure 2.15: Intercept point of theoretical modified Kendrick mass defect plot of copolymers showing the intercept point is equal to the mass defect and mass of the polymer end groups.

2.4.2. Modified mass defect analysis of homopolymers

Taking the mono-isotopic list that had been assigned and carrying out charge and adduct correction meant that all of the peak assignments could be compared on a like-for-like basis. The Modified Kendrick Mass Defect (MKMD) was calculated using the NAM as the homologous series unit. With NAM as the homologous series any deviation away from NAM therefore showed as a change in the MKMD away from the zero value. The NAM homo-polymer spectra was only shifted away from the MKMD zero value by the presence of the end group. The end group structure ($C_8H_{14}O_2S_3$) has the MKMD value of 0.1109 so the MKMD graph is shifted up entirely by this value. Importantly the end group stayed the same mass and mass defect independent of the polymer length. With increasing NAM monomer content, the mass increases but there was no change in mass defect. The worked example below shows how the value is calculated, with the corresponding calculations shown above.

m/z	q	Area	mass	KMr(NAM)	NKMr(NAM)	MKMD(NAM)
a	*b*	*c*	*d*	*e*	*f*	*g*
			$(a \times b) - (b \times H^{+}_{mass})$	$d \times \frac{141}{141.078979}$	Round(*e*)	*g-f*
1812.96295	2	158337184	3623.911347	3621.882615	3622	0.117384893

Table 2.1: Worked calculation of the MKMD of an ion. The MKMD has been normalised to the NAM unit in the KMr column with the 141/141.078979 function.

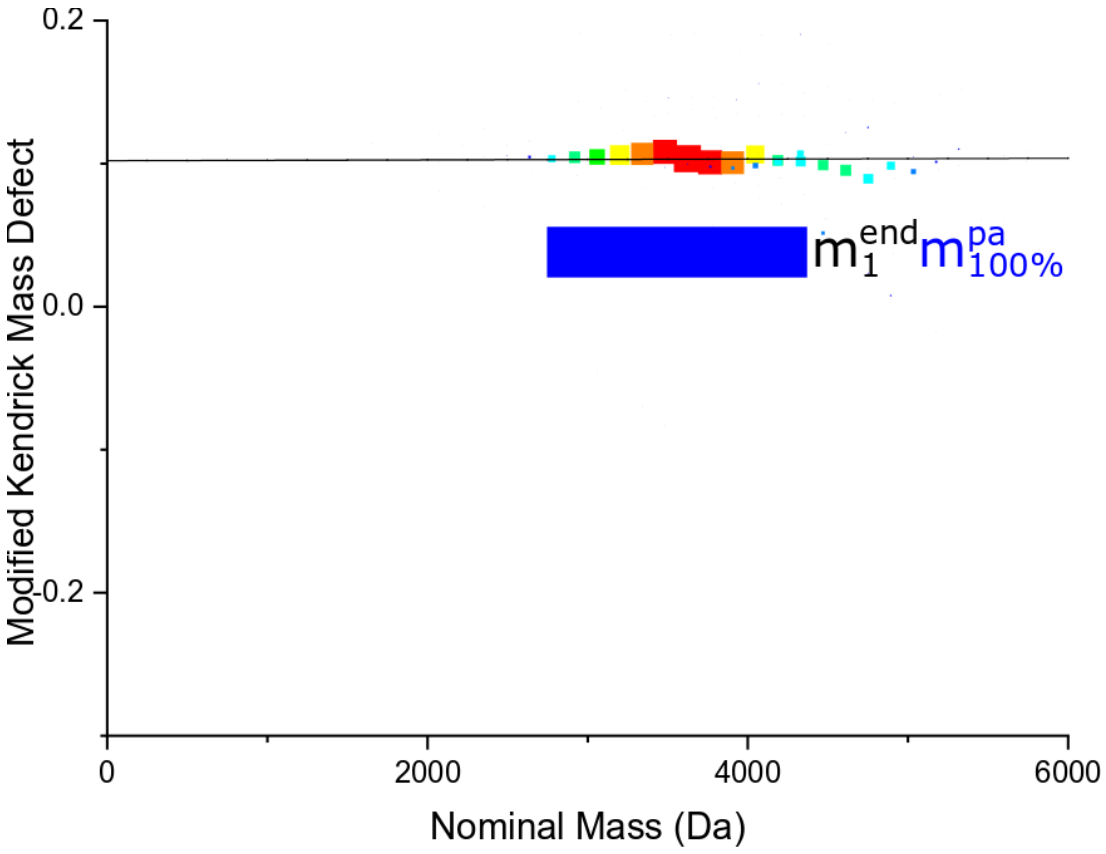

Figure 2.16: MKMD graph of the NAM homopolymer, this shows the MKMD offset caused by the presence of the end group. With increasing polymer mass due to the addition of more NAM monomer units there is no change in mass defect.

The MKMD analysis of the DMA homopolymer shows a very different relationship between the MKMD and increasing polymer mass. Importantly, the MKMD change

with polymer mass formed a constant gradient. The DMA homopolymer varied completely from the NAM homopolymer and had a MKMD value of -0.013 for every monomer unit that was present. As there is a constant change for every monomer unit added there was a constant change in MKMD with change in mass.

The gradient formed is offset from the origin as there is the presence of an end group on this polymer too meaning that there was a constant difference applied to the start of the gradient with an increase in the DMA composition there is a proportional magnitude change in the MKMD forming the gradient seen.

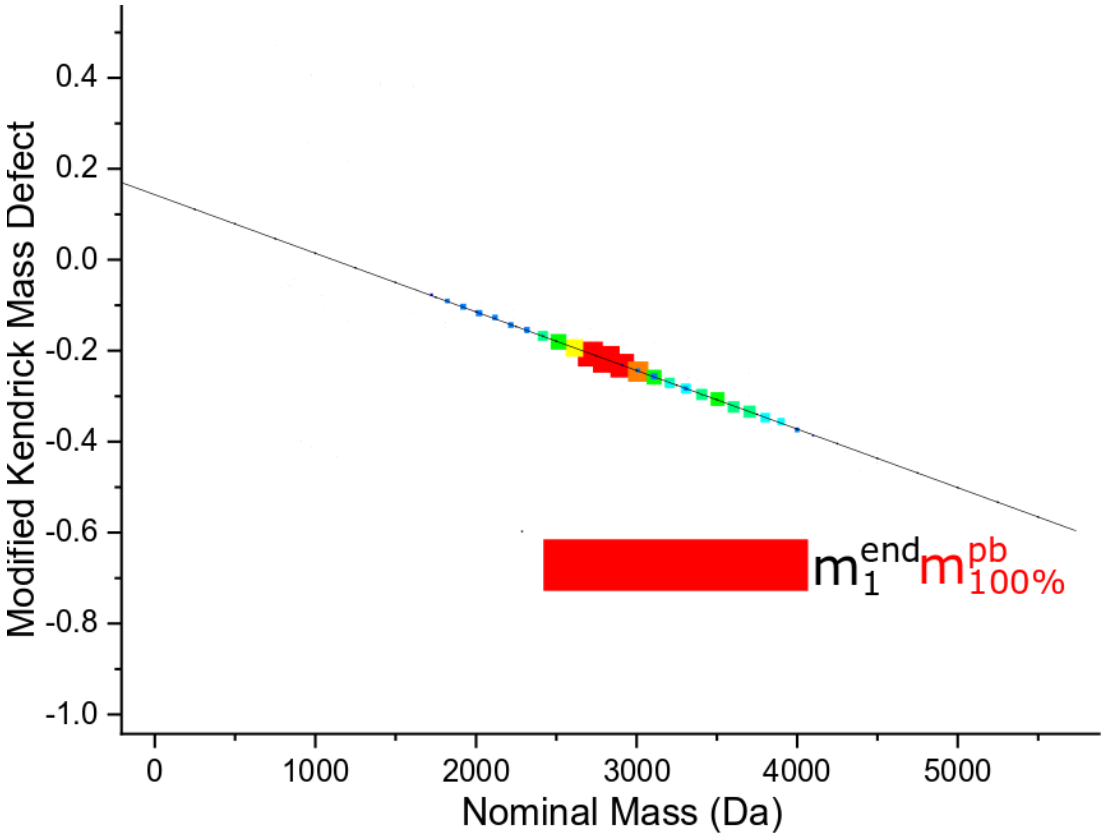

Figure 2.17: MKMD graph of the DMA homopolymer, this shows the MKMD offset caused by the presence of the end group and a constant gradient caused by the increased character of the DMA monomer. This is the maximum gradient line that can be achieved by these two species.

The gradient of the MKMD plot of a completely different monomer to that of the homologous series chosen is the maximum gradient on the MKMD plot that was achieved as the difference in polymer compositions was at a maximum. Copolymers

containing NAM will increase in mass without an increase in mass defect therefore lowering the magnitude of the gradient.

2.4.3. Modified mass defect analysis of copolymers

The analysis of the copolymers was more complex due to the necessity of the ability to accurately assign a gradient value for the distribution of the peaks based on peak size and intensity. The analysis of the different copolymers showed an obvious change in the mass of each of the copolymers as the DMA character of the copolymer increased. This is because the DMA is lighter than the NAM and the copolymers were matched by repeat unit and not mass. As the polyacrylamides gain DMA monomers the gradient of the MKMD plot becomes more negative. Figure 2.18 shows the direct comparison between the three MKMD plots. The plots themselves are colour coded showing as a heat map and point size scaled. This shows the dispersity of the copolymer in both directions. The x direction dispersity being that of the two monomers combined and the y direction being the dispersity of the monomers compared to one another. A completely uncontrolled co-polymerisation would form an increasing wider mapping of the MKMD plot.

The lines that are defining the gradient are those that are calculated as part of a weighted regression considering the peak area.

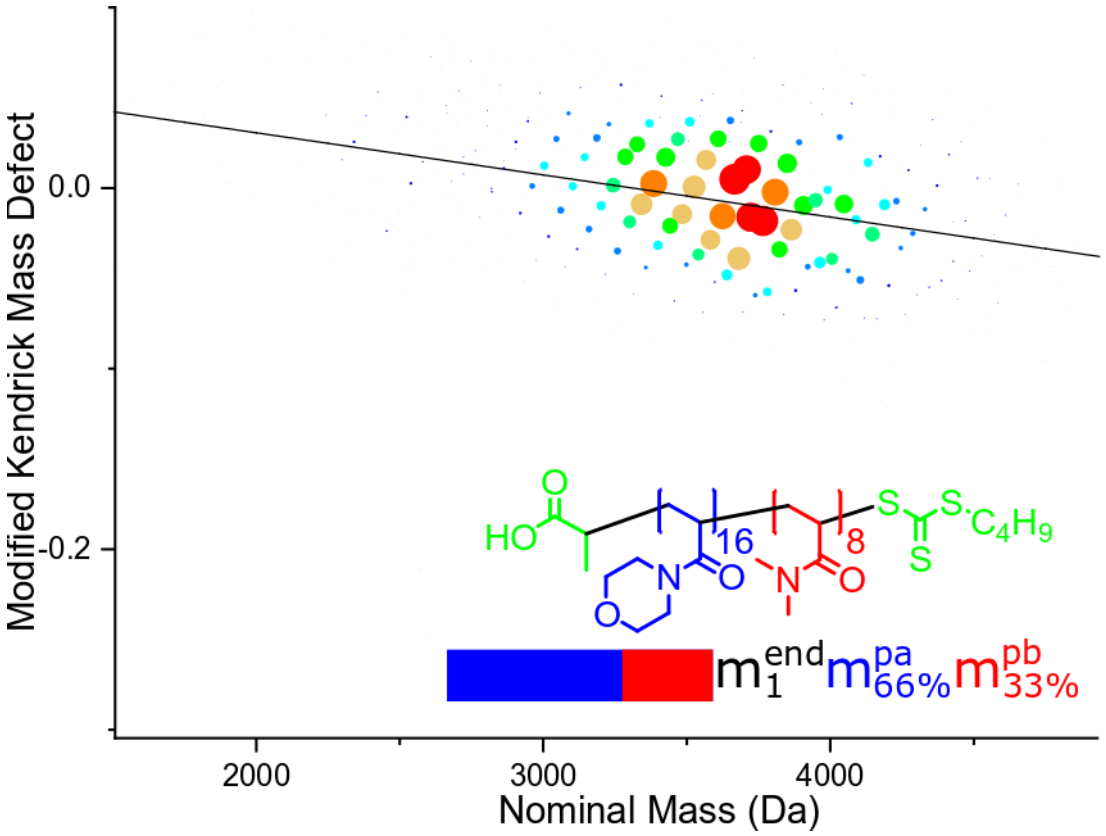
Modified Kendrick Mass Defect
0.0
-0.2
2000
3000
4000
Nominal Mass (Da)
HO
O
S
S
S
C4H9
16
8
N
O
O
m1end mpa66% mpb33%

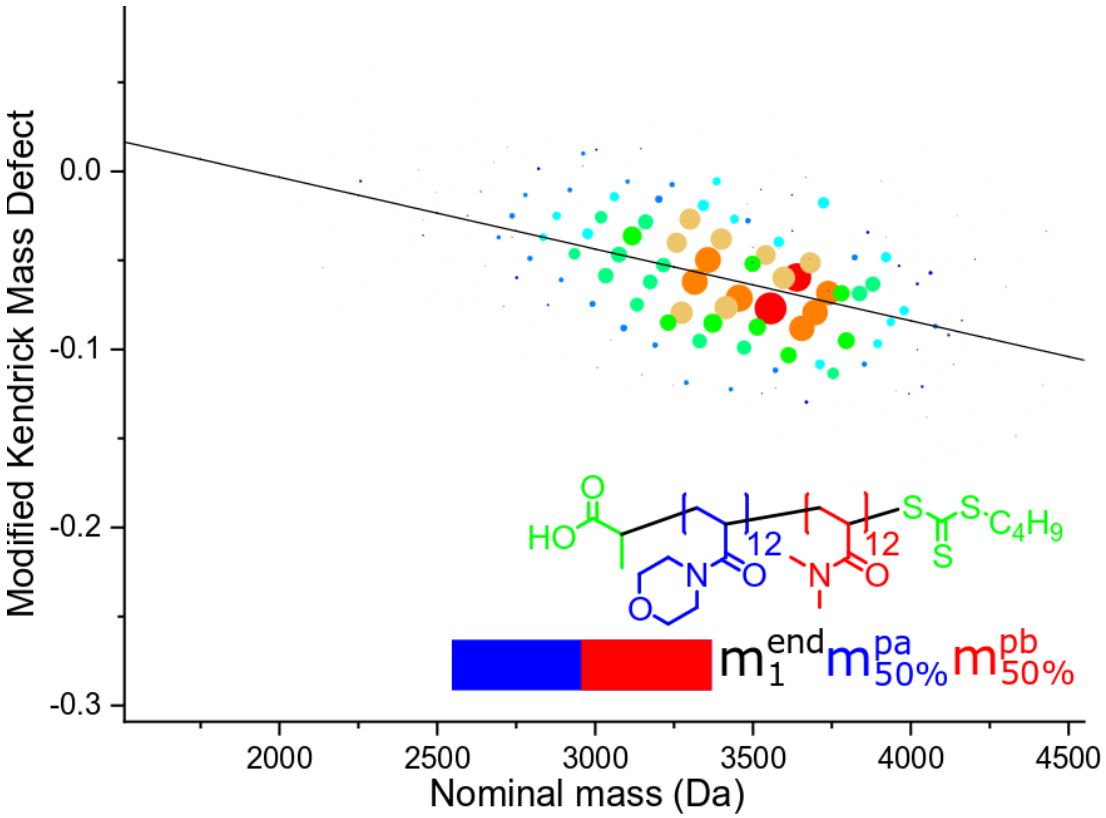
Modified Kendrick Mass Defect
0.0
-0.1
-0.2
-0.3
2000
2500
3000
3500
4000
4500
Nominal mass (Da)
HO
O
S
S
S
C4H9
12
12
N
O
O
m1end mpa50% mpb50%

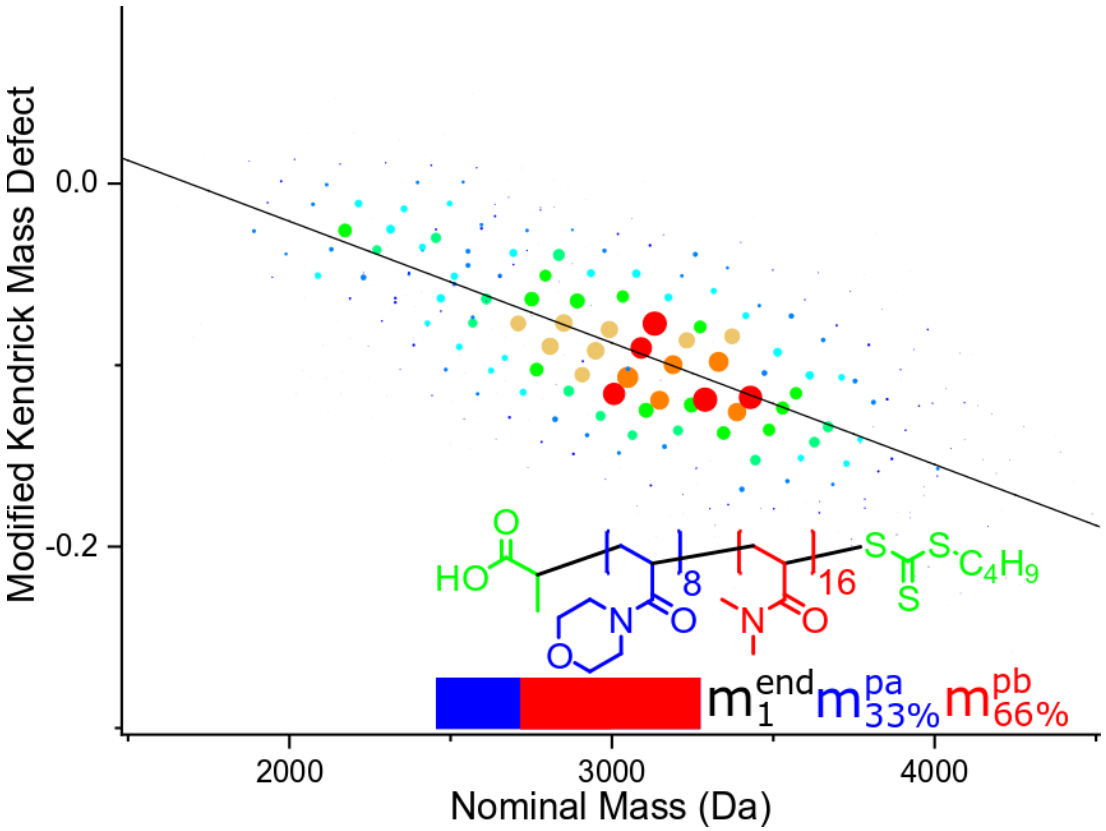

Figure 2.18 Direct comparison of the copolymer polyacrylamides, the top plot shows the MKMD plot produced from the mass analysis of a two-thirds NAM containing and one-third containing DMA copolymer. The middle plot is a 50/50 split of both monomers and the bottom plot is inversed of the top plots being one third NAM and two-thirds DMA. Importantly, the gradient of the line increases in magnitude from top to bottom as more DMA monomers are present.

The change in gradient with the change in the DMA character was then compared across all the polymer species. This showed 5 clear separations in the MKMD measurement between the different species.

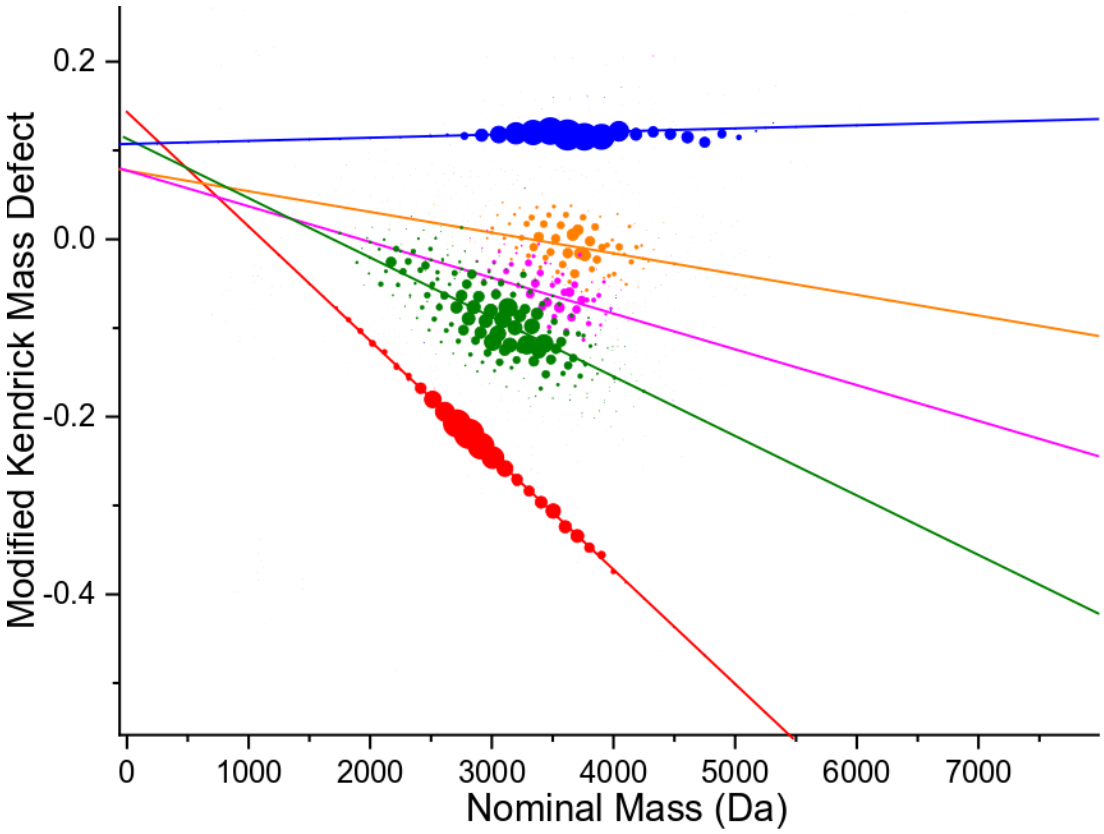

Figure 2.19: Modified Kendrick mass defect comparison of the homo- and co-polymers: it could be seen that the different copolymers formed obvious separations. The lines that are defining their character are the weighted lines of best fit calculated in R Studio.

The weighted linear regression lines do not match the theoretical values due to three main sources of error, the instrument error, fitting error, and non-uniform dispersity. The fitting error is very low, and the instrument error after internal calibration was less than 2ppm for all assignments.

The error in the analysis is likely due to the presence of dispersity in both axes causing the accurate linear fits to show the inaccuracy of the polymerisation. The gradients do shows an estimation of the copolymer composition from the monomer amounts.

Although the measurement comes with an associated error, the use of the modified Kendrick mass defect is an effective tool in the simplification and better understanding of complex polymeric data sets.

2.5. Conclusions

The analysis of homo- and co-polymer acrylamides was successfully carried out by nESI. The ultrahigh resolution instrument allowed copolymers of n = 25 monomer units to be successfully analysed across charge states. Acidification of polymer solutions also formed mostly protonated adducts, which is largely beneficial to the ease of assigning the mass spectra.

Overall, preliminary work into the use of the modified Kendrick mass defect for the analysis of polymers shows good potential as a way to characterise polymers as a function of their end groups and copolymer structure.

2.6. References

(1) Gody, G.; Barbey, R.; Danial, M.; Perrier, S. Ultrafast RAFT polymerization: multiblock copolymers within minutes *Polymer Chemistry* **2015**, *6*, 1502-1511.
(2) Martin, L.; Gody, G.; Perrier, S. Preparation of complex multiblock copolymers via aqueous RAFT polymerization at room temperature *Polymer Chemistry* **2015**, *6*, 4875-4886.
(3) Abu Lila, A. S.; Kiwada, H.; Ishida, T. The accelerated blood clearance (ABC) phenomenon: clinical challenge and approaches to manage *J. Controlled Release* **2013**, *172*, 38-47.
(4) Pelegri-O'Day, E. M.; Lin, E. W.; Maynard, H. D. Therapeutic protein-polymer conjugates: advancing beyond PEGylation *J. Am. Chem. Soc.* **2014**, *136*, 14323-14332.
(5) Engelis, N. G.; Anastasaki, A.; Nurumbetov, G.; Truong, N. P.; Nikolaou, V.; Shegiwal, A.; Whittaker, M. R.; Davis, T. P.; Haddleton, D. M. Sequence-controlled methacrylic multiblock copolymers via sulfur-free RAFT emulsion polymerization *Nature Chemistry* **2017**, *9*, 171-178.
(6) Hamidi, M.; Shahbazi, M. A.; Rostamizadeh, K. Copolymers: efficient carriers for intelligent nanoparticulate drug targeting and gene therapy *Macromolecular Bioscience* **2012**, *12*, 144-164.
(7) Liechty, W. B.; Kryscio, D. R.; Slaughter, B. V.; Peppas, N. A. Polymers for drug delivery systems *Annual Review of Chemical and Biomolecular Engineering* **2010**, *1*, 149-173.
(8) Kendrick, E. A Mass Scale Based on CH2=: 14.0000 for High Resolution Mass Spectrometry of Organic Compounds *Anal. Chem.* **1963**, *35*, 2146-2154.
(9) Sleno, L. The use of mass defect in modern mass spectrometry *J. Mass Spectrom.* **2011**, *47*, 226-236.
(10) Fouquet, T.; Nakamura, S.; Sato, H. MALDI SpiralTOF high-resolution mass spectrometry and Kendrick mass defect analysis applied to the characterization of poly(ethylene-co-vinyl acetate) copolymers *Rapid Commun. Mass Spectrom.* **2016**, *30*, 973-981.
(11) Fouquet, T.; Aizawa, H.; Sato, H. Taking MALDI SpiralTOF high-resolution mass spectrometry and mass defect analysis to the next level with ethylene vinyl acetate vinyl alcohol terpolymers *Rapid Commun. Mass Spectrom.* **2016**, *30*, 1818-1822.
(12) Fouquet, T.; Sato, H. Extension of the Kendrick Mass Defect Analysis of Homopolymers to Low Resolution and High Mass Range Mass Spectra Using Fractional Base Units *Anal. Chem.* **2017**, *89*, 2682-2686.
(13) Fouquet, T.; Shimada, H.; Maeno, K.; Ito, K.; Ozeki, Y.; Kitagawa, S.; Ohtani, H.; Sato, H. High-resolution Kendrick Mass Defect Analysis of Poly(ethylene oxide)-based Non-ionic Surfactants and Their Degradation Products *J. Oleo Sci.* **2017**, *66*, 1061-1072.
(14) Fouquet, T.; Cody, R. B.; Sato, H. Capabilities of the remainders of nominal Kendrick masses and the referenced Kendrick mass defects for copolymer ions *J. Mass Spectrom.* **2017**, *52*, 618-624.
(15) Troise, A. D.; Fiore, A.; Fogliano, V. Quantitation of acrylamide in foods by high-resolution mass spectrometry *J. Agric. Food. Chem.* **2014**, *62*, 74-79.
(16) Haler, J. R. N.; Far, J.; Aqil, A.; Claereboudt, J.; Tomczyk, N.; Giles, K.; Jerome, C.; De Pauw, E. Multiple Gas-Phase Conformations of a Synthetic Linear Poly(acrylamide) Polymer Observed Using Ion Mobility-Mass Spectrometry *J. Am. Soc. Mass. Spectrom.* **2017**, *28*, 2492-2499.
(17) Köster, C. United States, US 6188064 B1.2001.Bruker Daltonik GmbH (DE)

(18) Wootton, C. A.; Lam, Y. P. Y.; Willetts, M.; van Agthoven, M. A.; Barrow, M. P.; Sadler, P. J.; PB, O. C. Automatic assignment of metal-containing peptides in proteomic LC-MS and MS/MS data sets *Analyst* **2017**, *142*, 2029-2037.
(19) Kaur, P.; O'Connor, P. B. Algorithms for automatic interpretation of high resolution mass spectra *J. Am. Soc. Mass. Spectrom.* **2006**, *17*, 459-468.
(20) Ferguson, J. C.; Hughes, R. J.; Nguyen, D.; Pham, B. T. T.; Gilbert, R. G.; Serelis, A. K.; Such, C. H.; Hawkett, B. S. Ab Initio Emulsion polymerization by RAFT-Controlled Self-Assembly *Macromolecules* **2005**, *38*, 2191-2204.

Supplementary information

For

Introduction to modified Kendrick mass defect analysis

R-Code fit function for MKMD plots:

```
> library(readxl)

> TM21 <- read_excel("//mokey/User47/u/u1693437/Documents/Chemistry/Kendrick graphs/Kendrick Mass Defect/TM21.xlsx")

> View(TM21)

> library(readxl)

> A3DfitTM21<-read_excel("H:/Documents/Chemistry/Kendrick graphs/Kendrick Mass Defect/TM21.xlsx")

> Fit <- lm(A3DfitTM21$`NKMD(NAM)` ~ A3DfitTM21$'NKMr(NAM)', weights = A3DfitTM21$`Area`)

> Fit$coefficients
```

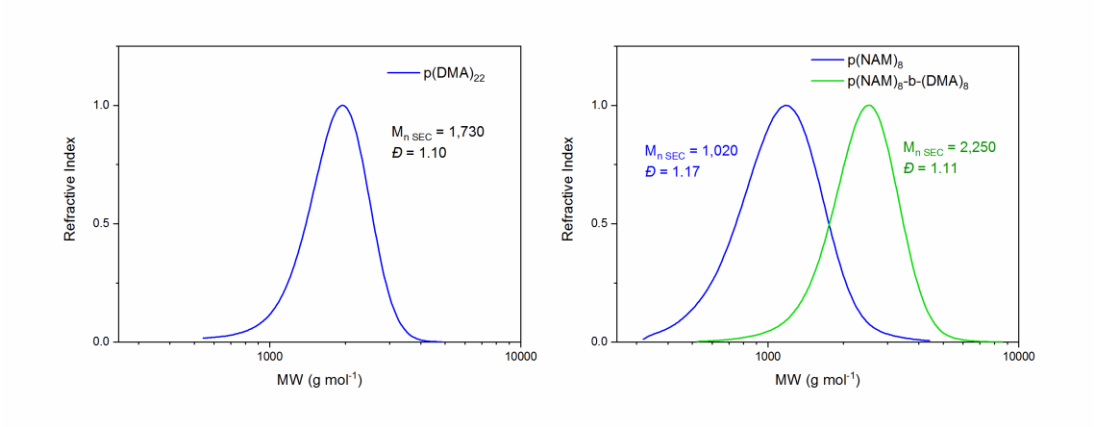

Figure S 2.1 SEC measurements in THF were performed on an Agilent Infinity II MDS instrument equipped with differential refractive index (DRI), viscometry (VS), dual angle light scatter (LS) and multiple wavelength UV detectors. The system was equipped with 2 x PLgel Mixed C columns (300 x 7.5 mm) and a PLgel 5 µm guard column. The eluent is THF with 2 % TEA (triethylamine) additive. Samples were run at 1ml/min at 30'C. Poly(methyl methacrylate standards (Agilent EasyVials) were used for calibration. Analyte samples were filtered through a GVHP membrane with 0.22 μm pore size before injection. Respectively, experimental molar mass ($M_{n,SEC}$) and dispersity ($Đ$) values of synthesized polymers were determined by conventional calibration using Agilent GPC/SEC software.

3. Electron capture dissociation tandem mass spectrometry analysis of polyoxazoline species

Tomos E. Morgan[1], Andrew Kerr[1], Remy Gavard[1], Christopher A. Wootton[1], Mark P. Barrow[1], Anthony W. T. Bristow[2], Sebastien Perrier[1], Peter B. O'Connor[1]*

[1]Department of Chemistry, University of Warwick, Coventry, Midlands, CV4 7AL, UK.

[2]Chemical Development, Pharmaceutical Technology & Development, Operations, AstraZeneca, Macclesfield, UK.

The MS, MS/MS and data analysis presented in this chapter were all carried out by the thesis author. Synthesis, purification, GPC, and NMR analysis of the polyoxazoline species was carried out by Sean H. Ellacott.

A manuscript titled: "Coupling Electron Capture Dissocaition and the modified Kendrick mass defect for sequencing of a poly(2-ethyl-2-oxazoline) polymer" by Tomos E. Morgan[1], Sean H. Ellacott[1], Christopher A. Wootton[1], Mark P. Barrow[1], Anthony W. T. Bristow[2], Sebastien Perrier[1], Peter B. O'Connor[1*] has been published in the ACS journal Analytical Chemistry. The chapter presented is directly based on this work.

3.1. Abstract

Polyoxazolines have gained a lot of interest in the pharmaceutical community as a potential conjugating polymer. The synthetic and conjugation process of polyoxazolines may cause modification of the monomer unit or the end groups. As well as incorrect termination causing the presence of unwanted termini of the finished polymer. NMR currently offers a possibility to analyse the bulk chemical characteristics of the polyoxazolinebut in the event of a low-level impurity it is unlikely that this will be detected as part of the NMR process, especially if the proton shifts are very close to one another.

This chapter focusses on the characterisation of a series of polyoxazoline species by ECD mass spectrometry. The polyoxazolines tested were all seen as potential synthetic conjugate agents for the use in peptide-polymer conjugate chemistry.

The complete backbone and end group fragmentation of polyoxazolines was carried using electron capture dissociation (ECD) fragmentation. ECD was found to target the amide bond that is present as part of the polyoxazoline monomer unit. Fragmentation from the charge reduced species also characterised the end groups.

The use of the modified Kendrick mass defect was also used extensively in this study by the taking the modified Kendrick mass defect analysis discussed in Chapter 2 and applying it to the ECD fragmentation spectra. This allowed direct comparison of backbone, internal, and end group fragmentation of the whole mass spectra and produced a much more complete assignment of the complicated fragmentation spectra.

3.2. Introduction

Polyoxazolines have recently gained interest as an alternative to poly(ethylene glycol) (PEG) based conjugate species for drug delivery.[1] polyoxazolines have benefits over PEG as they have been shown to cause less significant immune system responses[2] as well as allowing synthetic control and structural variation.[3-5] Properties of polyoxazolines are related to their chemical composition, size, and initiating and terminating end groups.[6] Due to this, there has been an increased focus on the analysis of the microstructure of polyoxazolines by tandem mass spectrometry.[7-9]

Ultra-high resolution mass spectrometry techniques such as Fourier Transform Ion Cyclotron Resonance Mass Spectrometry (FT-ICR MS) have the ability to carry out accurate fragmentation analysis of polymeric species to determine their structure. Electrospray ionisation (ESI) as a means to analyse polyoxazolines has been well established.[10,11] ESI produces multiply charged species; allowing the use of electron capture methods.[12] Electron Capture Dissociation (ECD) as a fragmentation technique has seen limited use in the analysis of polymers;[8,13-15] although ECD analysis of polymeric excipients has been carried out successfully.[16,17]

The nitrogen-carbon bond alpha to an amide group is broken when ECD fragmentation occurs in peptides and proteins,[18] making the repeating amide unit within a polyoxazoline a promising target for fragmentation analysis. The increased selectivity of ECD allows much more predictable fragmentation pathways to be present then that of other methods, such as collisional activated dissociation (CID/CAD). As ECD is a radical based rather than ergodic technique the fragmentation coverage is less affected by the presence of particularly weak covalent bonds in the molecule.[19] Analysis of polymers by CID regularly shows polymer backbone "unzipping" through a series of rearrangements.[20]

When the polymer is capable of rearrangements allowing monomer release from the major species then it is common to see near complete backbone fragmentation coverage.[21-24] There are other examples of radicals being produced as part of the ionisation process initiating fragmentation down the polymer backbone as part of a radical reaction.[25-27] CID analysis of polyoxazoline species has often been based on

the CID dissociation voltages used to produce fragmentation.[28,29] CID dissociation measurement is prone to variation between instruments and is often highly reliant on the strength of bonds within the polymer end groups, as they may fragment before elucidation of the complete polymer chain itself. Fragmentation pathways within polymer analysis can be used extensively in the characterisation of the polymer for any modifications that may occur along the polymer backbone.

Kendrick mass defect (KMD) analysis is used to characterise complex petroleum spectra by normalising the mass defect to the CH_2 group, the most common repeating unit within these samples.[30,31] Modifying the masses to the homologous series helps simplify complex spectra by grouping measured ions into classes based on their heteroatomic nature. The use of a modified mass defect has been seeing a much greater use in the analysis of polymers and complex polymeric samples, with the use of a "modified" KMD (MKMD)[32-36] and an increased use to generating high resolution plots based on a fractional base unit allowing even more resolution within MKMD analysis.[33] The use of the MKMD groups the mass defect from the pure monomer repeat unit allowing fragments to be separated based on their end group and adduct variation from different fragmentation pathways.

In this study we report the fragmentation of polyoxazolines by ECD fragmentation and how the complex fragmentation patterns can be separated using the MKMD. The use of ECD fragmentation on the polyoxazolines also showed end group fragmentation that allowed complete microstructure analysis.

3.3. Experimental

3.3.1. MS Sample preparation and analysis

The polyoxazoline sample was dissolved into a 99.5% solution of purified water obtained from a Direct-Q3 Ultrapure Water System (Millipore, Lutterworth, United Kingdom) at 20 µM in 0.5% formic acid (Sigma-Aldrich, Dorset, United Kingdom).

All experiments were performed on a 12 T solariX Fourier transform ion cyclotron resonance mass spectrometer (Bruker Daltonik, GmbH, Bremen, Germany) using a nanoelectrospray (nESI) ion source in positive ion mode. The ECD was carried out with the use of an indirectly heated hollow cathode with a current set at 1.5 A, with

a pulse length of 0.2 s and bias 1.2 eV. All data was recorded using 4 million data points (32 bit) transients (1.6777 s) achieving approximately 400 thousand resolving power at 400 *m/z*. All mass spectra were internally calibrated by the intact polymer peaks across the polymer dispersity, or by internal calibration of fragment peaks in ECD spectra (peaks used for calibration are marked). The Bruker SNAP algorithm was used for peak picking with the polyoxazoline monomer used as the repeat unit.[37,38] . The Bruker SNAP algorithm matches a calculated isotope distribution adjusted to a repeat unit with increasing mass.38-40 Adjusting the mass of the fragment to a function of the monomer was carried out by the modified Kendrick mass analysis importing the mass tables into Excel.30 Equations 1-3 shows the calculation of the HRMKMr, the value 100 is the rescaling factor linked to the monomer mass unit of the homologous series.33 The round function is to the nearest integer, up or down. The charge, z is determined by the SNAP peak picking algorithm.

$$\frac{m}{z} \times z = m$$

Equation 3.1: mass calculation of the fragment ion formed.

$$(2)\ HRMKMr = m\ \times \frac{Round\left(\frac{(Exact\ monomer\ mass)}{100}\right)}{\left(\frac{Exact\ monomer\ mass}{100}\right)}$$

Equation 3.2: High resolution modified Kendrick mass calculation using a divisor of 100 to increase spacing between Kendrick masses.

$$(3)\ HRMKMD = HRMKMr - Round(HRMKMr)$$

Equation 3.3: High resolution Kendrick mass defect of the fragment ion observed.

3.4. Results and Discussion

Nano-electrospray MS analysis presented in Figure 3.1, produced a rich spectrum due to the inherent dispersity of the polymer and multiple charge states produced. The use of the nESI device under acidified conditions produced mainly protonated ions as well as low levels of mono- and di- sodiated adduct ions. The visible charge states were assigned to protonated 2+ (blue rectangles) and 3+ (blue triangles) methyl initiated polyoxazoline ions. There was also 4+ protonated species present of a much lower intensity than the other charge and adduct species. The higher mass polymer chains showed a higher average charge state than smaller chains due to the increased ability to stabilize charge. The spacing between main peaks correspond to that of the monomer repeat unit as expected. The use of the Bruker SNAP algorithm brings a significant advantage in mass accuracy, the peak picking is based on the entire isotope pattern with an increasing mass repeat unit making this method of peak picking especially suited to polymer analysis. This analysis also showed the presence of a low level hydrogen initiated by product of the synthesis process. The major ion of the hydrogen initiated by product was the triply protonated species.

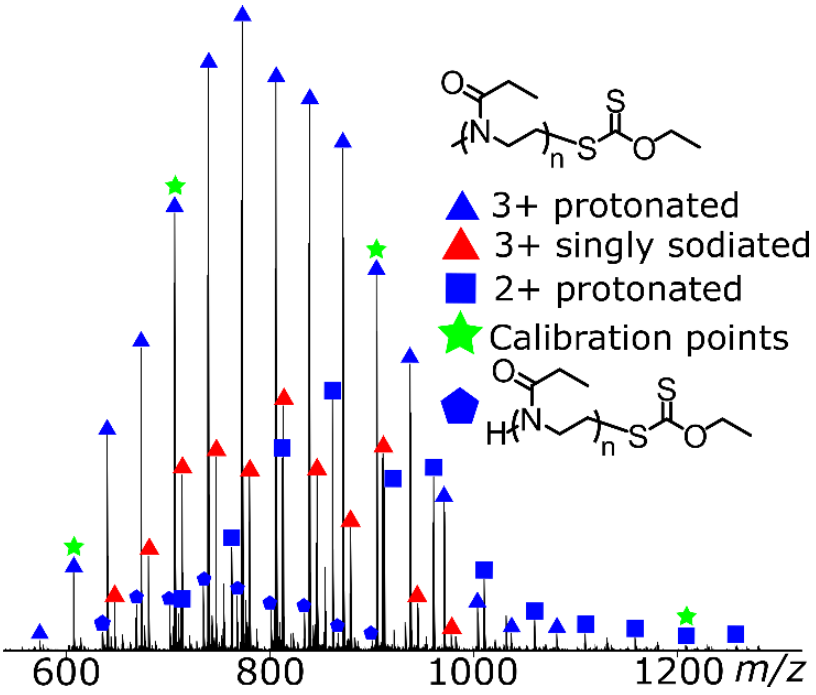

Figure 3.1 nESI Mass spectrum of the polyoxazoline species showing multiple charge states and the dispersity of the polymer. Different charge

state distributions are labelled as well as the presence of a hydrogen-initiated polymer by-product.

Isolation of the protonated methyl initiated 3+ ion at 739.81971 *m/z* (n=21) and the protonated hydrogen initiated 3+ ion at 834.21559 *m/z* (n=24) was carried out separately by both front end quadrupole isolation and multi-CHEF in-cell isolation to ensure clean isolation from the rest of the ions. The ECD event occurs before the excitation pulse, the ions are held within a close orbit and bathed in low energy fragmentation electrons (1.2 eV). Figure 3.2 presents the ECD spectra for the two isolated species. The backbone fragmentation has been labelled here.

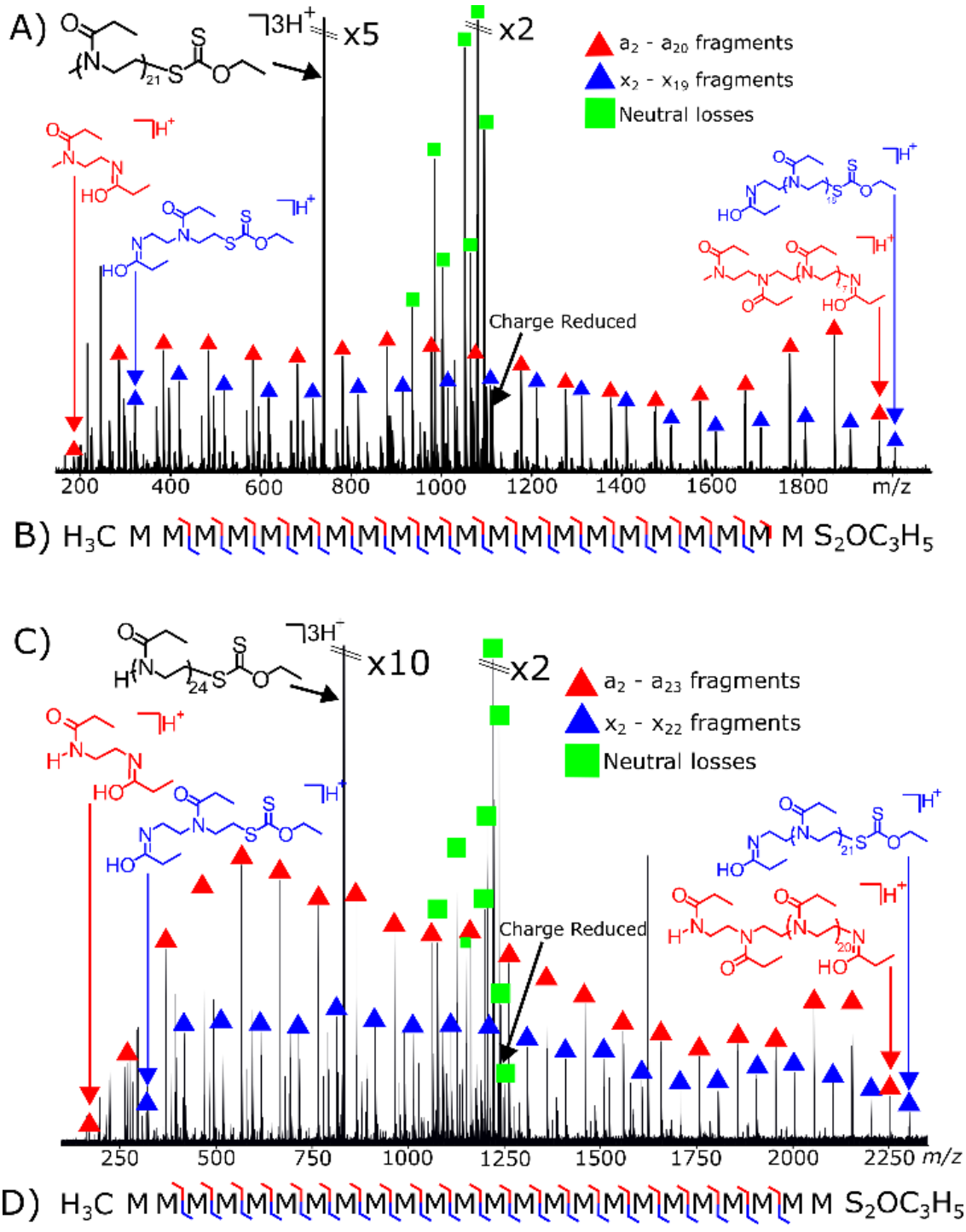

Figure 3.2 A) and C) ECD spectra of methyl initiated, and hydrogen initiated polyoxazoline respectively with fragmentation maps B) and D), this shows clear fragmentation ladders for the 2 key fragment types (marked with red (a) and blue (x) triangles), along with neutral losses indicating end groups (green squares).

The ECD event produces an odd electron charge capture ion species which can then follow numerous fragmentation pathways. Common fragmentations observed were that of neutral losses from the charge capture species as well as backbone fragmentation across the polymer. The ECD spectra of both isolated species shows two major fragmentation series, assigned to fragmentation along the polymer backbone, mainly *a* and *x* fragments (figure 3). All *a* and *x* fragments contain an end group, either the initiating methyl or hydrogen, or terminating xanthate group, and then a certain monomer repeat unit fragments, dictated by where in the polymer backbone the fragmentation took place. Both the *a* and the *x* fragmentation form a stable imidic end group.

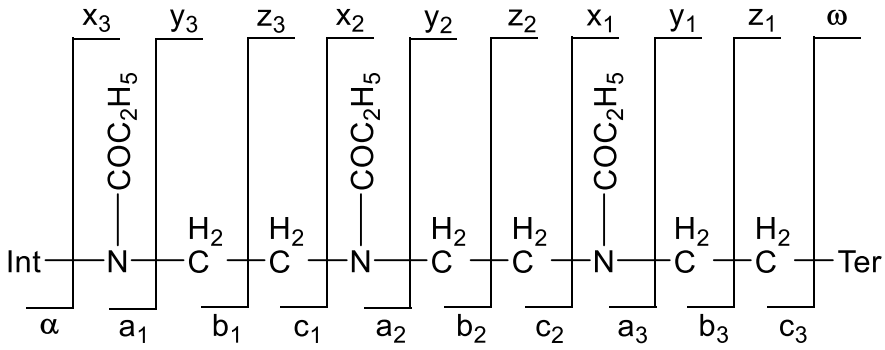

Figure 3.3 Fragmentation assignments of the polyoxazoline.

The *a* fragmentation series of the methyl initiated polyoxazoline was first observed at 187.14399 *m/z* this contains the methyl end group and two monomer units (a_2, 0.61 ppm). This fragmentation series contains 18 monomer spaced fragments ending with 1970.37582 (a_{20}, 0.13 ppm). As the series starts with two monomer units and has a further 18 monomer spaced fragments the spaces comes to a total of 20 monomer units, leaving the terminating xanthate group and a monomer unit. The last fragment in this series would be loss of an ethyl functionalized xanthate group, which is unlikely to occur as it would produce a singly charged, large polymer ion and a charged xanthate group. The xanthate containing series starts at mass 321.13011 m/z (x_2, -0.003 ppm) containing the xanthate group and two monomer repeat units. A monomer unit fragmentation series follows this ending at 2005.29034 m/z (x_{19}, 1.4 ppm) which leaves the fragmentation series the methyl end group and two monomer units short.

The *a* fragmentation series of the hydrogen initiated polyoxazoline starts at mass 173.12845 m/z (a_2, -0.02 ppm) and the series is monomer spaced to mass 2253.56340 m/z (a_{23}, -0.7 ppm) this fragmentation series therefore ends without fragmentation of the terminating xanthate group from the final monomer unit. The x fragmentation series starts with the terminating xanthate and two monomer unit 321.13007 m/z (x2, -0.1 ppm) and has a total of 19 monomer spaced fragments ending at mass 2302.43950 m/z (x22, -0.2 ppm). As the terminating xanthate group was identical between the methyl and hydrogen initiated polyoxazolines the x series fragmentation was chemically identical.

Being a radical directed MS/MS technique, rather than a slow heating process like CAD or IRMPD, ECD enabled a more evenly distributed fragment coverage of the parent species (Figure 2). Over fragmentation of polymeric species is frequently observed in slow heating processes due to the abundance and homogeneity of lower energy bonds broken, leading to abundant low m/z fragments. Whereas the ECD shown produced fragments of relatively even intensity across the entire polymer backbone and complete coverage of the target species. The charged reduced species of both polyoxazolines showed significant neutral losses indicative of the polymer end group chemistry. The charge reduced species of the methyl initiated polyoxazoline $[MeM_{21}Xan]H_3^{2+\bullet}$ (1109.22564, -0.7 ppm) and the hydrogen initiated polyoxazoline $[HM_{24}Xan]H_3^{2+\bullet}$ were both at much lower intensities than the resulting fragments. The low intensities observed suggests the charge capture species is less able to stabilize addition of the radical, contrasting to peptide/protein ECD where the charge reduced species is usually of a higher intensity then the ECD fragments.

Figure 3.4 below summarizes the neutral/radical losses from the charge reduced species of the methyl and hydrogen initiated polyoxazoline, both fragmented in very similar pathways. Fragments from the charge reduced state were often indicative of the functional groups. Many fragments observed from the charge reduced species are based on fragmentation from the α-carbon bond to the amide group, there is also significant fragmentation of the xanthate groups. Figure 3.4 shows numerous end group fragments. The doubly charged ion observed at 1102.21816 m/z corresponding to the loss of a methyl radical (α, -0.2 ppm) from the charge reduced

species. Fragments observed at 1052.36800 showed loss of the methyl group and a repeat monomer unit (a1, -0.1 ppm). Elucidation of the xanthate group occurred at two points, with fragmentation of the C-S bond, 1065.22677 *m/z* (-0.2 ppm) as well as loss of the ethyl functionalized xanthate end group 1035.22512 *m/z* (y_1, -0.2 ppm). The presence of these neutral losses from the charge capture species allow precise end group determination of the polymer species. The peak at 1081.21299 m/z can be assigned to a fragmentation of the amide bond itself. This is not a common pathway within ECD fragmentation but has been documented based on either a loss through secondary fragmentation or due to the nitrogen of the amide itself being protonated.[39]

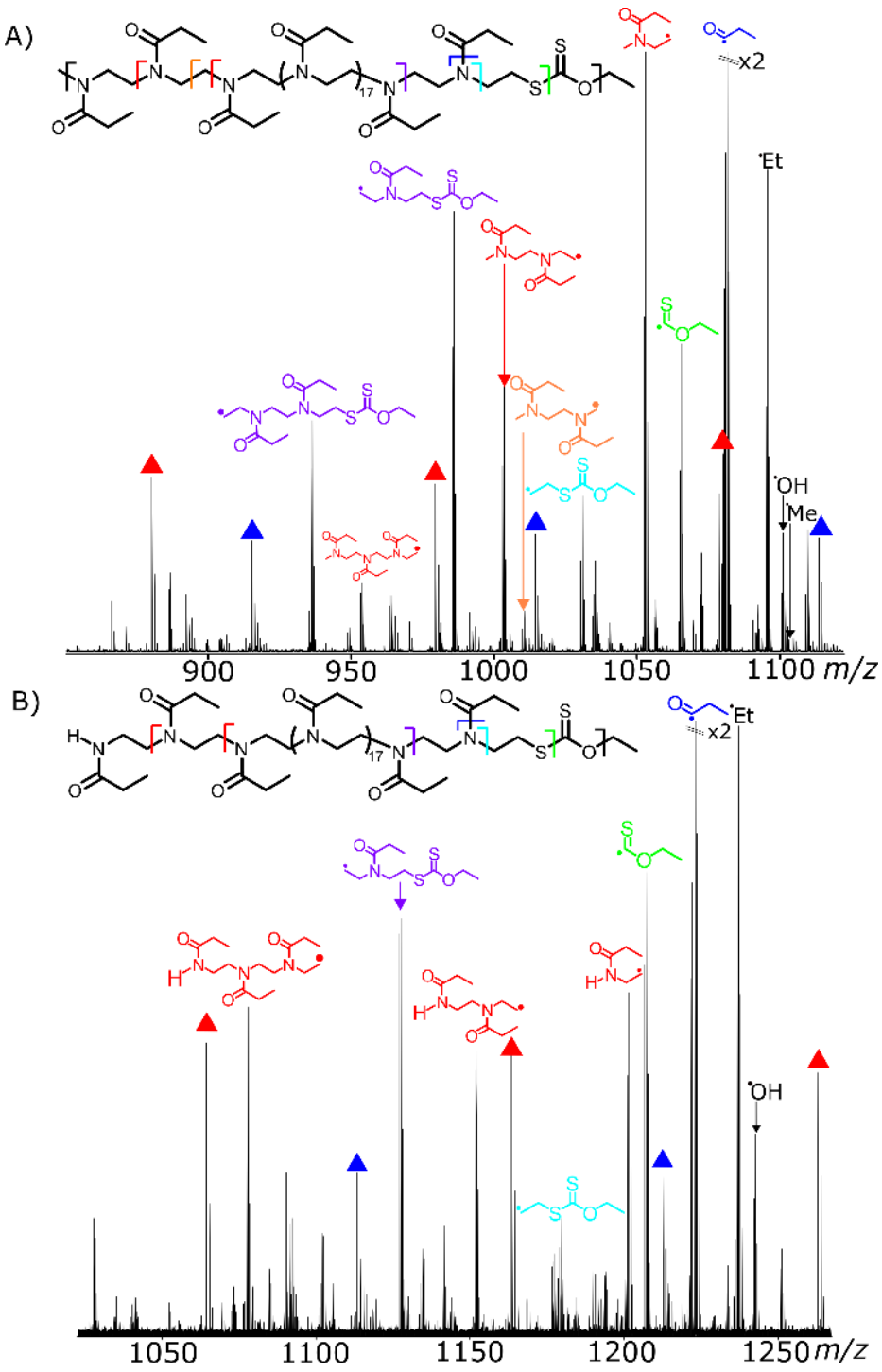

Figure 3.4 A) methylated polyoxazoline and B) hydrogen initiated polyoxazoline neutral losses showing end group losses and end groups with multiples of monomer units lost, indicating the terminal polymer chemistry.

Table 3.1 Neutral losses from the charge reduced species of the methyl initiated polyoxazoline

m/z	**Mass**	**Chemical composition**	**Loss**	**Δm/ppm**
1102.21816	2204.43632	$C_{108}H_{197}N_{21}O_{22}S_2$	CH_3	-0.17
1100.72468	2201.44932	$C_{109}H_{198}N_{21}O_{21}S_2$	OH	-0.13
1095.21026	2190.42050	$C_{107}H_{195}N_{21}O_{22}S_2$	CH_3CH_2	-0.25
1081.21301	2162.42598	$C_{106}H_{195}N_{21}O_{21}S_2$	C_3H_5O	-0.07
1065.22678	2130.45354	$C_{106}H_{195}N_{21}O_{21}S_1$	C_3H_5OS	-0.25
1052.68401	2105.36800	$C_{103}H_{188}N_{20}O_{21}S_2$	$C_6H_{12}NO$	-0.14
1035.22514	2070.45024	$C_{104}H_{191}N_{21}O_{21}$	$C_5H_9OS_2$	-0.22
1010.15772	2020.31542	$C_{99}H_{181}N_{19}O_{20}S_2$	$C_{10}H_{19}N_2O_2$	-0.05
1003.14983	2006.29964	$C_{98}H_{179}N_{19}O_{20}S_2$	$C_{11}H_{21}N_2O_2$	-0.12
985.69105	1971.38206	$C_{99}H_{182}N_{20}O_{20}$	$C_{10}H_{18}NO_2S_2$	-0.11
			Average	-0.20
			Standard Deviation	0.18

Overall, the ECD mass spectra for both molecules shows a rich coverage of backbone and end group fragmentation. Either through a and x fragmentation resulting in a 1+ backbone fragmentation series or through neutral loss from the charge capture species resulting in end group characterization. A large proportion of the fragments observed resulted from a limited number of fragmentation pathways but with a different number of monomer mass repeat unit. The simplest examples of this is the presence of a and x fragmentation pathways that contain the initiating or terminating end group and the imidic acid formed by the fragmentation itself and then a series of monomer repeat units that all form part of the fragmentation series but are from the same pathway. Grouping fragments as a function of their mass in a way which removes monomer variation means that fragments from the same pathway and end groups can be readily grouped together.

SNAP peak picking inherently provides accurate charge state information required for isotope matching, and using this charge allows a neutral mass to be calculated easily. For the MKMD analysis, the charge carriers were not corrected for as this

could lead to the potential loss of information, and subsequently can provide information on adduct influence of the various fragmentation process. Rescaling the MKMD value to the high-resolution MKMD value means there is a greater separation in the MKMD diagram compared to the non-scaled mass defects of these species. Use of the HRMKMD meant that different pathways, series, and adducts could be easily assigned to a mass defect value, allowing more obvious identification. Fragment chains with the same end group or modification but a varying number of monomer units were present as evenly spaced horizontal lines, Figure 3.5.

The presence of horizontal lines allowed rapid assignment of the fragmentation. Spacing in the y dimension is due to presence of atoms that are not part of the monomer unit and the x dimension spacing is in overall mass. Almost all the spacing present between points in the x dimension of the same MKMD value is that of a monomer mass unit. The rescaled MKMD plot showed the two major ladders as along horizontal lines moving through the length of the polymer chain and therefore the mass axis of the MKMKD plot. There were also several smaller fragmentation series that were present, spread through numerous MKMD values. As fragments in the same series will have the same repeating composition the end group, adduct, and fragmentation will be constant, allowing grouping of the whole series. The precursor (red) is present at the highest mass in the MKMD plot, as the plot has been charge corrected.

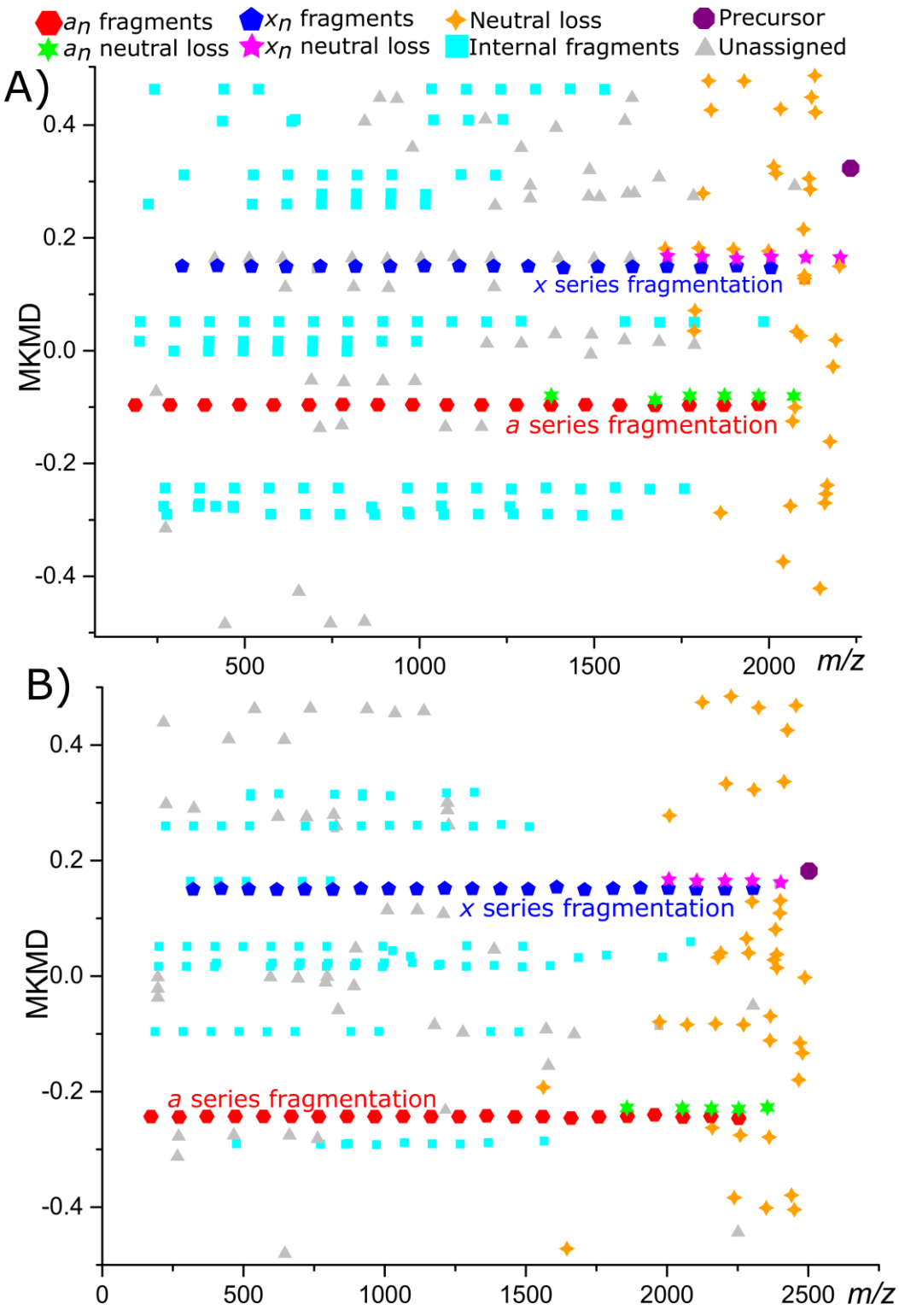

Figure 3.5 A) HRMKMD plot of the methyl-initiated species and B) hydrogen initiated by product.

For the methyl initiated polyoxazoline, the fragmentation series at MKMD value of -0.096 shown in purple contains the *a* fragmented series discussed above. The MKMD value that has been assigned for this fragmentation is based on the presence of the methyl end group and the protonation of the fragment. As the MKMD value is based purely on deviation from the homologous series chosen for the conversion the imidic end group is isobaric to the polyoxazoline repeat, so the methyl group and protonation is all that effects the mass defect. The fragments that are present as purple squares along the same MKMD value are the equally spaced monomer units of that series of fragments. The assignment of the *x* fragmentation series is the dark blue line at 0.149 MKMD. The series as shown by the MKMD value is equal to that found in the original ECD spectra (Figure 2) allowing complete visualization of the fragment series in one line. Above both *a* and *x* series, there are shorter fragment series that have also been highlighted. The fragment series above the *a* fragmentation series is coloured green, the offset in MKMD value is that of a single proton, meaning these are neutral losses that were observed from the charge capture species. The offset is due to the additional proton that is present, and as charge has been accounted for, the spacing remains the same. The presence of the complete *a* and *x* series through both fragmentation and neutral losses shows clear back bone coverage. The *x* series fragmentation line has a neutral loss line above it colored pink, which spans another 2 monomer mass units. Fragmentation of the ethyl functionalized xanthate group meant all the monomer units were accounted for when the neutral loss is included as part of the fragmentation series. With both *a* and *x* fragmentation accounted for, complete coverage of the polymer was carried out.

The *x* series for the hydrogen initiated polyoxazoline is equal to that of the methyl initiated polyoxazoline as they form the same fragments. The *x* series spans from x_2 to x_{22} at a MKMD value of 0.149. The *x* series also exhibited the presence of the neutral loss series directly above them. The *x* neutral fragment series covers fragmentation from $x_{19} – x_{23}$.The *a* series fragmentation was at an MKMD value of -0.243, colored pink, this fragmentation series, therefore, varies from the methyl initiated polyoxazoline as the end group was a hydrogen and not a methyl initiator. The fragmentation coverage was very similar, with the fragmentation coverage from

a_2 to a_{23} as well as being able to visualize the presence of neutral losses present at a_{20} – a_{23}. These two diagrams combined allow an easy method of visualizing the differences between the fragmentations of the two polymers analyzed.

Internal fragments are seen at other MKMD values (light blue), the larger internal fragment series could be assigned to numerous fragmentation pathways that are shown in the supplementary information. Internal fragmentation pathways offer some analytical use as their relative size suggests an unmodified – unbroken polyoxazoline chain.

Table 3.2 Summary of internal fragment ions, these ions represent the first fragment found in their respective series.

Structure	HRMKMD Value	Fragment mass	Error (ppm)	Assignment
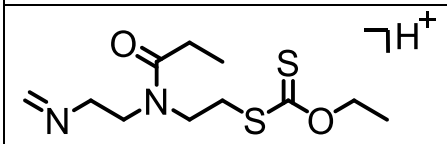	-0.290	277.10381	-0.31	io_n
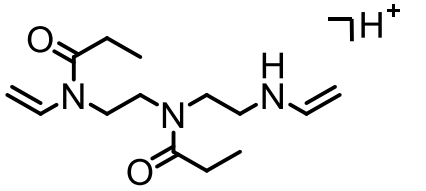	-0.276	268.20191	-0.16	ip_n
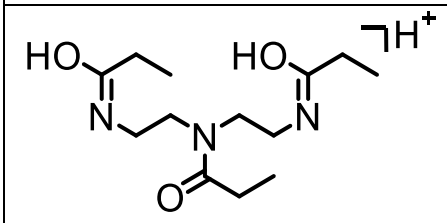	-0.244	272.19684	-0.10	Iq_n
$C_{15}H_{26}N_3O_3^+$	0.000	297.20466	-0.11	ir_n
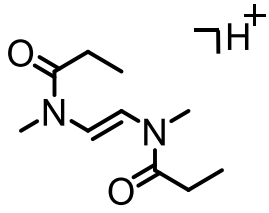	0.017	199.14398	-0.62	is_n
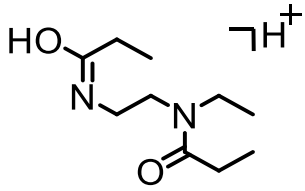	0.051	201.15964	-0.57	it_n

Neutral loss fragments, colored orange are shown to have a high deviation away from the precursor in MKMD space due to the large difference in heterogeneity the end groups have compared to the monomer repeat unit. Aliasing of the neutral losses can be seen by the diagonal line moving from -0.5 to 0.5 MKMD values. This effect means that the direct translation from a MKMD value to a mass defect value is more difficult but doesn't affect the overall grouping of ions together.

3.5. Conclusions

In conclusion, the use of electron capture dissociation to analyze polyoxazolines has been shown to be effective in achieving end group and primary structure characterization. Giving the possibility that any modification that may be made to polyoxazolines could be accurately characterized using this method of analysis. The loss of the end groups as neutral loss species greatly assisted in the identification of the terminal methyl and xanthate end groups. A significant benefit was also shown using high resolution modified Kendrick mass defect graphs to analyse these complex polymer fragmentation spectra. Separating different fragmentation routes as well as identifying ways to achieve complete backbone characterisation of the polymer due to closely related groups, based from their MKMD value. This helps to speed up the analysis time as well as being a useful tool for visualization of fragmentation spectra of polymers.

3.6. References

(1) Pelegri-O'Day, E. M.; Lin, E. W.; Maynard, H. D. Therapeutic protein-polymer conjugates: advancing beyond PEGylation *J. Am. Chem. Soc.* **2014**, *136*, 14323-14332.

(2) Qi, Y.; Chilkoti, A. Protein-polymer conjugation-moving beyond PEGylation *Curr. Opin. Chem. Biol.* **2015**, *28*, 181-193.

(3) Hartlieb, M.; Floyd, T.; Cook, A. B.; Sanchez-Cano, C.; Catrouillet, S.; Burns, J. A.; Perrier, S. Well-defined hyperstar copolymers based on a thiol–yne hyperbranched core and a poly(2-oxazoline) shell for biomedical applications *Polymer Chemistry* **2017**, *8*, 2041-2054.

(4) Rudolph, T.; von der Luhe, M.; Hartlieb, M.; Norsic, S.; Schubert, U. S.; Boisson, C.; D'Agosto, F.; Schacher, F. H. Toward Anisotropic Hybrid Materials: Directional Crystallization of Amphiphilic Polyoxazoline-Based Triblock Terpolymers *ACS Nano* **2015**, *9*, 10085-10098.

(5) Dworak, A.; Trzebicka, B.; Kowalczuk, A.; Tsvetanov, C.; Rangelov, S. Polyoxazolines — mechanism of synthesis and solution properties *Polimery* **2014**, *59*, 88-94.

(6) Viegas, T. X.; Bentley, M. D.; Harris, J. M.; Fang, Z.; Yoon, K.; Dizman, B.; Weimer, R.; Mero, A.; Pasut, G.; Veronese, F. M. Polyoxazoline: chemistry, properties, and applications in drug delivery *Bioconjugate Chem.* **2011**, *22*, 976-986.

(7) Crotty, S.; Gerislioglu, S.; Endres, K. J.; Wesdemiotis, C.; Schubert, U. S. Polymer architectures via mass spectrometry and hyphenated techniques: A review *Anal. Chim. Acta* **2016**, *932*, 1-21.

(8) Hart-Smith, G. A review of electron-capture and electron-transfer dissociation tandem mass spectrometry in polymer chemistry *Anal. Chim. Acta* **2014**, *808*, 44-55.

(9) Altuntaş, E.; Schubert, U. S. "Polymeromics": Mass spectrometry based strategies in polymer science toward complete sequencing approaches: a review *Anal. Chim. Acta* **2014**, *808*, 56-69.

(10) Altuntaş, E.; Krieg, A.; Baumgaertel, A.; Crecelius, A. C.; Schubert, U. S. ESI, APCI, and MALDI tandem mass spectrometry of poly(methyl acrylate)s: A comparison study for the structural characterization of polymers synthesized via CRP techniques and the software application to analyze MS/MS data *J. Polym. Sci., Part A: Polym. Chem.* **2013**, *51*, 1595-1605.

(11) Altuntaş, E.; Weber, C.; Kempe, K.; Schubert, U. S. Comparison of ESI, APCI and MALDI for the (tandem) mass analysis of poly(2-ethyl-2-oxazoline)s with various end-groups *Eur. Polym. J.* **2013**, *49*, 2172-2185.

(12) Yamashita, M.; Fenn, J. B. ELectrospray Ion Source. Another Vairation on the Free-Jet Theme *J. Phys. Chem.* **1984**, *88*, 4451-4459.

(13) Crecelius, A. C.; Baumgaertel, A.; Schubert, U. S. Tandem mass spectrometry of synthetic polymers *J. Mass Spectrom.* **2009**, *44*, 1277-1286.

(14) Josse, T.; De Winter, J.; Dubois, P.; Coulembier, O.; Gerbaux, P.; Memboeuf, A. A tandem mass spectrometry-based method to assess the architectural purity of synthetic polymers: a case of a cyclic polylactide obtained by click chemistry *Polymer Chemistry* **2015**, *6*, 64-69.

(15) Wesdemiotis, C.; Solak, N.; Polce, M. J.; Dabney, D. E.; Chaicharoen, K.; Katzenmeyer, B. C. Fragmentation pathways of polymer ions *Mass Spectrom. Rev.* **2011**, *30*, 523-559.

(16) Perez Hurtado, P.; Lam, P. Y.; Kilgour, D.; Bristow, A.; McBride, E.; O'Connor, P. B. Use of high resolution mass spectrometry for analysis of polymeric excipients in drug delivery formulations *Anal. Chem.* **2012**, *84*, 8579-8586.

(17) Wei, J.; Bristow, A.; McBride, E.; Kilgour, D.; O'Connor, P. B. D-alpha-tocopheryl polyethylene glycol 1000 succinate: a view from FTICR MS and tandem MS *Anal. Chem.* **2014**, *86*, 1567-1574.

(18) Qi, Y.; Volmer, D. A. Electron-based fragmentation methods in mass spectrometry: An overview *Mass Spectrom. Rev.* **2017**, *36*, 4-15.
(19) Tureček, F. N-C alpha Bond Dissociation Energies and Kinetics in Amide and Peptide Radicals. Is the Dissociation a Non-ergodic Process? *J. Am. Chem. Soc.* **2003**, *125*, 5954-5963.
(20) Baumgaertel, A.; Weber, C.; Knop, K.; Crecelius, A.; Schubert, U. S. Characterization of different poly(2-ethyl-2-oxazoline)s via matrix-assisted laser desorption/ionization time-of-flight tandem mass spectrometry *Rapid Commun. Mass Spectrom.* **2009**, *23*, 756-762.
(21) Giordanengo, R.; Viel, S.; Hidalgo, M.; Allard-Breton, B.; Thevand, A.; Charles, L. Methylation of acidic moieties in poly(methyl methacrylate-co-methacrylic acid) copolymers for end-group characterization by tandem mass spectrometry *Rapid Commun. Mass Spectrom.* **2010**, *24*, 1941-1947.
(22) Fouquet, T.; Humbel, S.; Charles, L. Tandem mass spectrometry of trimethylsilyl-terminated poly(dimethylsiloxane) ammonium adducts generated by electrospray ionization *J. Am. Soc. Mass. Spectrom.* **2011**, *22*, 649-658.
(23) Nasioudis, A.; Heeren, R. M.; van Doormalen, I.; de Wijs-Rot, N.; van den Brink, O. F. Electrospray ionization tandem mass spectrometry of ammonium cationized polyethers *J. Am. Soc. Mass. Spectrom.* **2011**, *22*, 837-844.
(24) Weidner, S. M.; Falkenhagen, J.; Knop, K.; Thunemann, A. Structure and end-group analysis of complex hexanediol-neopentylglycol-adipic acid copolyesters by matrix-assisted laser desorption/ionization collision-induced dissociation tandem mass spectrometry *Rapid Commun. Mass Spectrom.* **2009**, *23*, 2768-2774.
(25) Girod, M.; Antoine, R.; Lemoine, J.; Dugourd, P.; Charles, L. End-group characterization of poly(styrene sulfonate sodium salt) by activated electron photo-detachment dissociation *Rapid Commun. Mass Spectrom.* **2011**, *25*, 3259-3266.
(26) Polce, M. J.; Ocampo, M.; Quirk, R. P.; Wesdemiotis, C. Tandem Mass Spectrometry Characteristics of Silver-Cationized Polystyrenes: Backbone Degradation via Free Radical Chemistry *Anal. Chem.* **2008**, *2*, 347-354.
(27) Polce, M. J.; Ocampo, M.; Quirk, R. P.; Leigh, A. M.; Wesdemiotis, C. Tandem Mass Spectrometry Characteristics of Silver-Cationized Polystyrenes: Internal Energy, Size, and Chain End versus Backbone Substituent Effects *Anal. Chem.* **2008**, *80*, 355-362.
(28) Altuntaş, E.; Weber, C.; Schubert, U. S. Detailed characterization of poly(2-ethyl-2oxazoline)s by energy variable collision-induced dissociation study *Rapid Commun. Mass Spectrom.* **2013**, *27*, 1095-1100.
(29) Baumgaertel, A.; Scheubert, K.; Pietsch, B.; Kempe, K.; Crecelius, A. C.; Bocker, S.; Schubert, U. S. Analysis of different synthetic homopolymers by the use of a new calculation software for tandem mass spectra *Rapid Commun. Mass Spectrom.* **2011**, *25*, 1765-1778.
(30) Kendrick, E. A Mass Scale Based on CH2=: 14.0000 for High Resolution Mass Spectrometry of Organic Compounds *Anal. Chem.* **1963**, *35*, 2146-2154.
(31) Sleno, L. The use of mass defect in modern mass spectrometry *J. Mass Spectrom.* **2011**, *47*, 226-236.
(32) Qi, Y.; Hempelmann, R.; Volmer, D. A. Two-dimensional mass defect matrix plots for mapping genealogical links in mixtures of lignin depolymerisation products *Anal. Bioanal. Chem.* **2016**, *408*, 4835-4843.
(33) Fouquet, T.; Sato, H. Extension of the Kendrick Mass Defect Analysis of Homopolymers to Low Resolution and High Mass Range Mass Spectra Using Fractional Base Units *Anal. Chem.* **2017**, *89*, 2682-2686.
(34) Fouquet, T.; Cody, R. B.; Sato, H. Capabilities of the remainders of nominal Kendrick masses and the referenced Kendrick mass defects for copolymer ions *J. Mass Spectrom.* **2017**, *52*, 618-624.

(35) Fouquet, T.; Nakamura, S.; Sato, H. MALDI SpiralTOF high-resolution mass spectrometry and Kendrick mass defect analysis applied to the characterization of poly(ethylene-co-vinyl acetate) copolymers *Rapid Commun. Mass Spectrom.* **2016**, *30*, 973-981.
(36) Fouquet, T.; Shimada, H.; Maeno, K.; Ito, K.; Ozeki, Y.; Kitagawa, S.; Ohtani, H.; Sato, H. High-resolution Kendrick Mass Defect Analysis of Poly(ethylene oxide)-based Non-ionic Surfactants and Their Degradation Products *J. Oleo Sci.* **2017**, *66*, 1061-1072.
(37) Köster, C. United States, US 6188064 B1.2001.Bruker Daltonik GmbH (DE)
(38) Wootton, C. A.; Lam, Y. P. Y.; Willetts, M.; van Agthoven, M. A.; Barrow, M. P.; Sadler, P. J.; PB, O. C. Automatic assignment of metal-containing peptides in proteomic LC-MS and MS/MS data sets *Analyst* **2017**, *142*, 2029-2037.
(39) Cooper, H. J. Investigation of the presence of b ions in electron capture dissociation mass spectra *J. Am. Soc. Mass. Spectrom.* **2005**, *16*, 1932-1940.

Supplementary information

For

Coupling electron capture dissociation and the modified Kendrick mass defect for sequencing of a poly(2-ethyl-2-oxazoline) polymer

by

Tomos E. Morgan[1], Sean H. Ellacott[1], Christopher A. Wootton[1], Mark P. Barrow[1], Anthony W. T. Bristow[2], Sebastien Perrier[1], Peter B. O'Connor[1*]

[1]Department of Chemistry, University of Warwick, Coventry, Midlands, CV4 7AL, UK.

[2]Chemical Development, Pharmaceutical Technology & Development, Operations, AstraZeneca, Macclesfield, UK.

*Corresponding authors: Peter O'Connor [redacted]

Synthesis of poly(2-ethyl-2-oxazoline)

Synthesis of poly(2-ethyl-2-oxazoline): 2-ethyl-2-oxazoline (99%, Sigma Aldrich, Dorset, United Kingdom EtOx) was dried over barium oxide and distilled under reduced pressure then kept in a Schlenk flask prior to use. Methyl p-toluenesulfonate (98%, VWR International Ltd., Lutterworth, United Kingdom), MeTos was distilled under reduced pressure and kept under a nitrogen atmosphere.

Potassium ethyl xanthogenae (96%, Sigma Aldrich, Dorset, United Kingdom, potassium ethyl xanthate) Acetonitrile Extra Dry (99.9%+, Fisher Scientific, Acros Organics, Loughborough, United Kingdom) were used as purchased. ^{1}H NMR spectra were measured using Bruker DPX-400 NMR spectrometer which operated at 400.05 MHz. Size exclusion chromatography (SEC) measurements in chloroform ($CHCl_3$) were performed using an Agilent 390-LC MDS (Agilent Technologies LDA UK, Cheadle, United Kingdom) with differential refractive index (DRI), viscometry (VS), dual-angle light scatter (LS) and two wavelength UV detectors. The system was equipped with 2 x PLgel Mixed D columns (300 x 7.5 mm, linear operating range between 200 and 400,000 g mol^{-1}) and a PLgel 5 µm guard column (Agilent Technologies LDA UK,

Cheadle, United Kingdom). The eluent was $CHCl_3$ with 2% triethylamine additive. SEC used Polystyrene standards (Agilent Easy Vials (Agilent Technologies LDA UK, Cheadle, United Kingdom) were used for calibration (150-350,000 g mol^{-1}).

Polymerisations of 2-ethyl-2-oxazoline were carried on a Biotage Initiator+ microwave synthesizer (Biotage, Uppsala, Sweden). Dry methyl tosylate (0.186 g, 1 mmol), dry 2-ethyl-2-oxazoline (1.983 g, 20 mmol) and extra dry acetonitrile (2.83 mL) were added to a pre-dried Biotage microwave vial, under a constant flux of nitrogen. The vial was sealed, left to stir for 30 s before being heated at 140 °C for 3 min. After cooling, a 2 mL solution of potassium ethyl xanthate (0.192 g, 1.2 mmol) in extra dry acetonitrile was added with a syringe to the polymer mixture for end-capping of the polymer. The solution was left stirring at room temperature for 48 h. Chloroform (50 mL) was and the organic phase was washed three times with a saturated solution of sodium hydrogen carbonate, with brine and dried on magnesium sulfate. The polymer was reconstituted in 10 mL of dichloromethane before precipitation in diethyl ether and dried overnight in a vacuum oven at 40 °C (yield 1.44 g).

^1H NMR (400 MHz, $CDCl_3$) δ ppm: 3.75 – 3.13 (m, 80 H, backbone), 3.10 - 2.92 (m, 3 H, Methyl group (α-end)), 2.54 - 2.13 (m, 40 H, CH_2 side chain), 1.44 (t, 2.4 H, Methyl group (xanthate)), 1.23 – 0.98 (m, 60 H, CH_3 side chain).

SEC (CHCl3, trimethylamine, PS calibration): M_n = 2,700 g mol^{-1}, Đ = 1.13.

Table S 3.1: MS assignment of polyoxazoline polymer Figure 3.1

m/z	z	Chemical formula assigned	Formula	error (ppm)	notes
723.94274	2	$C_{69}H_{125}N_{13}O_{14}S_2H^+_1Na^+_1$	$EGP_{13}H^+_1Na^+_1$	-1.8	2^+ singly sodiated
773.47806	2	$C_{74}H_{134}N_{14}O_{15}S_2H^+_1Na^+_1$	$EGP_{14}H^+_1Na^+_1$	-0.24	
823.0112	2	$C_{79}H_{143}N_{15}O_{16}S_2H^+_1Na^+_1$	$EGP_{15}H^+_1Na^+_1$	-1.53	
872.54583	2	$C_{84}H_{152}N_{16}O_{17}S_2H^+_1Na^+_1$	$EGP_{16}H^+_1Na^+_1$	-0.95	
922.08002	2	$C_{89}H_{161}N_{17}O_{18}S_2H^+_1Na^+_1$	$EGP_{17}H^+_1Na^+_1$	-0.92	
971.61459	2	$C_{94}H_{170}N_{18}O_{19}S_2H^+_1Na^+_1$	$EGP_{18}H^+_1Na^+_1$	-0.5	
1021.14875	2	$C_{99}H_{179}N_{19}O_{20}S_2H^+_1Na^+_1$	$EGP_{19}H^+_1Na^+_1$	-0.52	
1070.68453	2	$C_{104}H_{188}N_{20}O_{21}S_2H^+_1Na^+_1$	$EGP_{20}H^+_1Na^+_1$	0.97	
1120.21661	2	$C_{109}H_{197}N_{21}O_{22}S_2H^+_1Na^+_1$	$EGP_{21}H^+_1Na^+_1$	-0.97	
1169.75224	2	$C_{114}H_{206}N_{22}O_{23}S_2H^+_1Na^+_1$	$EGP_{22}H^+_1Na^+_1$	0.29	
1219.28656	2	$C_{119}H_{215}N_{23}O_{24}S_2H^+_1Na^+_1$	$EGP_{23}H^+_1Na^+_1$	0.37	
615.05684	3	$C_{89}H_{161}N_{17}O_{18}S_2H^+_2Na^+_1$	$EGP_{17}H^+_2Na^+_1$	0.82	3^+ singly sodiated
648.07852	3	$C_{94}H_{170}N_{18}O_{19}S_2H^+_2Na^+_1$	$EGP_{18}H^+_2Na^+_1$	-0.96	
681.10134	3	$C_{99}H_{179}N_{19}O_{20}S_2H^+_2Na^+_1$	$EGP_{19}H^+_2Na^+_1$	-0.89	
714.12405	3	$C_{104}H_{188}N_{20}O_{21}S_2H^+_2Na^+_1$	$EGP_{20}H^+_2Na^+_1$	-0.98	
780.16968	3	$C_{114}H_{206}N_{22}O_{23}S_2H^+_2Na^+_1$	$EGP_{22}H^+_2Na^+_1$	-0.87	
813.19231	3	$C_{119}H_{215}N_{23}O_{24}S_2H^+_2Na^+_1$	$EGP_{23}H^+_2Na^+_1$	-1.05	
846.21527	3	$C_{124}H_{224}N_{24}O_{25}S_2H^+_2Na^+_1$	$EGP_{24}H^+_2Na^+_1$	-0.83	
879.23827	3	$C_{129}H_{233}N_{25}O_{26}S_2H^+_2Na^+_1$	$EGP_{25}H^+_2Na^+_1$	-0.58	
912.26021	3	$C_{134}H_{242}N_{26}O_{27}S_2H^+_2Na^+_1$	$EGP_{26}H^+_2Na^+_1$	-1.5	
945.28339	3	$C_{139}H_{251}N_{27}O_{28}S_2H^+_2Na^+_1$	$EGP_{27}H^+_2Na^+_1$	-1.05	
978.30645	3	$C_{144}H_{260}N_{28}O_{29}S_2H^+_2Na^+_1$	$EGP_{28}H^+_2Na^+_1$	-0.76	
1044.35225	3	$C_{154}H_{278}N_{30}O_{31}S_2H^+_2Na^+_1$	$EGP_{30}H^+_2Na^+_1$	-0.53	
1077.37612	3	$C_{159}H_{287}N_{31}O_{32}S_2H^+_2Na^+_1$	$EGP_{31}H^+_2Na^+_1$	0.48	
784.46850	2	$C_{74}H_{134}N_{14}O_{15}S_2H^+_0Na^+_2$	$EGP_{14}H^+_0Na^+_2$	-1.27	2^+ doubly sodiated
834.00264	2	$C_{79}H_{143}N_{15}O_{16}S_2H^+_0Na^+_2$	$EGP_{15}H^+_0Na^+_2$	-1.27	
883.53663	2	$C_{84}H_{152}N_{16}O_{17}S_2H^+_0Na^+_2$	$EGP_{16}H^+_0Na^+_2$	-1.45	
933.07071	2	$C_{89}H_{161}N_{17}O_{18}S_2H^+_0Na^+_2$	$EGP_{17}H^+_0Na^+_2$	-1.51	
982.60552	2	$C_{94}H_{170}N_{18}O_{19}S_2H^+_0Na^+_2$	$EGP_{18}H^+_0Na^+_2$	-0.82	
1032.1398	2	$C_{99}H_{179}N_{19}O_{20}S_2H^+_0Na^+_2$	$EGP_{19}H^+_0Na^+_2$	-0.71	
1081.67341	2	$C_{104}H_{188}N_{20}O_{21}S_2H^+_0Na^+_2$	$EGP_{20}H^+_0Na^+_2$	-1.23	
1131.20783	2	$C_{109}H_{197}N_{21}O_{22}S_2H^+_0Na^+_2$	$EGP_{21}H^+_0Na^+_2$	-0.98	
1180.74157	2	$C_{114}H_{206}N_{22}O_{23}S_2H^+_0Na^+_2$	$EGP_{22}H^+_0Na^+_2$	-1.34	
1230.27663	2	$C_{119}H_{215}N_{23}O_{24}S_2H^+_0Na^+_2$	$EGP_{23}H^+_0Na^+_2$	-0.59	
655.40628	3	$C_{94}H_{170}N_{18}O_{19}S_2H^+_1Na^+_2$	$EGP_{18}H^+_1Na^+_2$	-0.55	3^+ doubly sodiated
688.42862	3	$C_{99}H_{179}N_{19}O_{20}S_2H^+_1Na^+_2$	$EGP_{19}H^+_1Na^+_2$	-1.2	
721.45124	3	$C_{104}H_{188}N_{20}O_{21}S_2H^+_1Na^+_2$	$EGP_{20}H^+_1Na^+_2$	-1.4	
754.47424	3	$C_{109}H_{197}N_{21}O_{22}S_2H^+_1Na^+_2$	$EGP_{21}H^+_1Na^+_2$	-1.08	
787.49692	3	$C_{114}H_{206}N_{22}O_{23}S_2H^+_1Na^+_2$	$EGP_{22}H^+_1Na^+_2$	-1.19	
820.51975	3	$C_{119}H_{215}N_{23}O_{24}S_2H^+_1Na^+_2$	$EGP_{23}H^+_1Na^+_2$	-1.11	
853.54251	3	$C_{124}H_{224}N_{24}O_{25}S_2H^+_1Na^+_2$	$EGP_{24}H^+_1Na^+_2$	-1.12	
919.58793	3	$C_{134}H_{242}N_{26}O_{27}S_2H^+_1Na^+_2$	$EGP_{26}H^+_1Na^+_2$	-1.25	

					Hydrogen initiated 2^+
606.87669	2	$C_{58}H_{105}N_{11}O_{12}S_2H^+_2$	$EGP_{11}H^+_2$	0.22	protonated
656.41077	2	$C_{63}H_{114}N_{12}O_{13}S_2H^+_2$	$EGP_{12}H^+_2$	0.01	
755.47818	2	$C_{73}H_{132}N_{14}O_{15}S_2H^+_2$	$EGP_{14}H^+_2$	-1.32	
854.54706	2	$C_{83}H_{150}N_{16}O_{17}S_2H^+_2$	$EGP_{16}H^+_2$	-0.62	
953.61554	2	$C_{93}H_{168}N_{18}O_{19}S_2H^+_2$	$EGP_{18}H^+_2$	-0.49	
1003.1494	2	$C_{98}H_{177}N_{19}O_{20}S_2H^+_2$	$EGP_{19}H^+_2$	-0.81	
1052.68453	2	$C_{103}H_{186}N_{20}O_{21}S_2H^+_2$	$EGP_{20}H^+_2$	0.11	
1151.75245	2	$C_{113}H_{204}N_{22}O_{23}S_2H^+_2$	$EGP_{22}H^+_2$	-0.33	
1201.28794	2	$C_{118}H_{213}N_{23}O_{24}S_2H^+_2$	$EGP_{23}H^+_2$	0.75	
					Hydrogen initiated 3^+
603.05681	3	$C_{88}H_{159}N_{17}O_{18}S_2H^+_3$	$EGP_{17}H^+_3$	-0.24	protonated
636.07941	3	$C_{93}H_{168}N_{18}O_{19}S_2H^+_3$	$EGP_{18}H^+_3$	-0.55	
669.10206	3	$C_{98}H_{177}N_{19}O_{20}S_2H^+_3$	$EGP_{19}H^+_3$	-0.76	
702.12487	3	$C_{103}H_{186}N_{20}O_{21}S_2H^+_3$	$EGP_{20}H^+_3$	-0.71	
735.14740	3	$C_{108}H_{195}N_{21}O_{22}S_2H^+_3$	$EGP_{21}H^+_3$	-1.06	
768.170300	3	$C_{113}H_{204}N_{22}O_{23}S_2H^+_3$	$EGP_{22}H^+_3$	-0.89	
801.19269	3	$C_{118}H_{213}N_{23}O_{24}S_2H^+_3$	$EGP_{23}H^+_3$	-1.37	
834.21588	3	$C_{123}H_{222}N_{24}O_{25}S_2H^+_3$	$EGP_{24}H^+_3$	-0.85	
867.23888	3	$C_{128}H_{231}N_{25}O_{26}S_2H^+_3$	$EGP_{25}H^+_3$	-0.59	
900.26204	3	$C_{133}H_{240}N_{26}O_{27}S_2H^+_3$	$EGP_{26}H^+_3$	-0.18	
933.28417	3	$C_{138}H_{249}N_{27}O_{28}S_2H^+_3$	$EGP_{27}H^+_3$	-0.89	
966.30747	3	$C_{143}H_{258}N_{28}O_{29}S_2H^+_3$	$EGP_{28}H^+_3$	-0.35	
613.88422	2	$C_{59}H_{107}N_{11}O_{12}S_2H^+_2$	$EGP_{11}H^+_2$	-0.26	2^+ protonated
663.41866	2	$C_{64}H_{116}N_{12}O_{13}S_2H^+_2$	$EGP_{12}H^+_2$	0.11	
712.95305	2	$C_{69}H_{125}N_{13}O_{14}S_2H^+_2$	$EGP_{13}H^+_2$	0.36	
762.48679	2	$C_{74}H_{134}N_{14}O_{15}S_2H^+_2$	$EGP_{14}H^+_2$	-0.28	
861.55517	2	$C_{84}H_{152}N_{16}O_{17}S_2H^+_2$	$EGP_{16}H^+_2$	-0.29	
911.08964	2	$C_{89}H_{161}N_{17}O_{18}S_2H^+_2$	$EGP_{17}H^+_2$	0.02	
960.62319	2	$C_{94}H_{170}N_{18}O_{19}S_2H^+_2$	$EGP_{18}H^+_2$	-0.67	
1010.15766	2	$C_{99}H_{179}N_{19}O_{20}S_2H^+_2$	$EGP_{19}H^+_2$	-0.37	
1059.69233	2	$C_{104}H_{188}N_{20}O_{21}S_2H^+_2$	$EGP_{20}H^+_2$	0.08	
1109.22643	2	$C_{109}H_{197}N_{21}O_{22}S_2H^+_2$	$EGP_{21}H^+_2$	-0.02	
1158.75944	2	$C_{114}H_{206}N_{22}O_{23}S_2H^+_2$	$EGP_{22}H^+_2$	-1.05	
1208.2929	2	$C_{119}H_{215}N_{23}O_{24}S_2H^+_2$	$EGP_{23}H^+_2$	-1.63	
1257.82908	2	$C_{124}H_{224}N_{24}O_{25}S_2H^+_2$	$EGP_{24}H^+_2$	0.01	
574.70604	3	$C_{84}H_{152}N_{16}O_{17}S_2H^+_3$	$EGP_{16}H^+_3$	0.01	3^+ protonated
607.72900	3	$C_{89}H_{161}N_{17}O_{18}S_2H^+_3$	$EGP_{17}H^+_3$	0.26	
640.75163	3	$C_{94}H_{170}N_{18}O_{19}S_2H^+_3$	$EGP_{18}H^+_3$	-0.02	
673.77447	3	$C_{99}H_{179}N_{19}O_{20}S_2H^+_3$	$EGP_{19}H^+_3$	0.03	
706.79707	3	$C_{104}H_{188}N_{20}O_{21}S_2H^+_3$	$EGP_{20}H^+_3$	-0.26	
739.82002	3	$C_{109}H_{197}N_{21}O_{22}S_2H^+_3$	$EGP_{21}H^+_3$	-0.05	
772.84286	3	$C_{114}H_{206}N_{22}O_{23}S_2H^+_3$	$EGP_{22}H^+_3$	-0.01	
805.86578	3	$C_{119}H_{215}N_{23}O_{24}S_2H^+_3$	$EGP_{23}H^+_3$	0.14	
838.88855	3	$C_{124}H_{224}N_{24}O_{25}S_2H^+_3$	$EGP_{24}H^+_3$	0.09	
871.91119	3	$C_{129}H_{233}N_{25}O_{26}S_2H^+_3$	$EGP_{25}H^+_3$	-0.1	

904.93384	3	$C_{134}H_{242}N_{26}O_{27}S_2H^+_3$	$EGP_{26}H^+_3$	-0.27	
937.95656	3	$C_{139}H_{251}N_{27}O_{28}S_2H^+_3$	$EGP_{27}H^+_3$	-0.35	
970.97921	3	$C_{144}H_{260}N_{28}O_{29}S_2H^+_3$	$EGP_{28}H^+_3$	-0.5	
1004.00232	3	$C_{149}H_{269}N_{29}O_{30}S_2H^+_3$	$EGP_{29}H^+_3$	-0.18	
1070.04829	3	$C_{159}H_{287}N_{31}O_{32}S_2H^+_3$	$EGP_{31}H^+_3$	0.17	
1103.07258	3	$C_{164}H_{296}N_{32}O_{33}S_2H^+_3$	$EGP_{32}H^+_3$	1.51	
703.71878	4	$C_{139}H_{251}N_{27}O_{28}S_2H^+_4$	$EGP_{27}H^+_4$	-1	4^+ protonated
728.48580	4	$C_{144}H_{260}N_{28}O_{29}S_2H^+_4$	$EGP_{28}H^+_4$	-1.08	
753.25276	4	$C_{149}H_{269}N_{29}O_{30}S_2H^+_4$	$EGP_{29}H^+_4$	-1.24	
778.01942	4	$C_{154}H_{278}N_{30}O_{31}S_2H^+_4$	$EGP_{30}H^+_4$	-1.77	
802.78692	4	$C_{159}H_{287}N_{31}O_{32}S_2H^+_4$	$EGP_{31}H^+_4$	-1.22	
827.55444	4	$C_{164}H_{296}N_{32}O_{33}S_2H^+_4$	$EGP_{32}H^+_4$	-0.68	
852.32099	4	$C_{169}H_{305}N_{33}O_{34}S_2H^+_4$	$EGP_{33}H^+_4$	-1.31	
766.46975	2	$C_{73}H_{132}N_{14}O_{15}S_2H^+_1Na^+_1$	$EGP_{14}H^+_1Na^+_1$	-0.88	
865.53879	2	$C_{83}H_{150}N_{16}O_{17}S_2H^+_1Na^+_1$	$EGP_{16}H^+_1Na^+_1$	-0.05	
915.07232	2	$C_{88}H_{159}N_{17}O_{18}S_2H^+_1Na^+_1$	$EGP_{17}H^+_1Na^+_1$	-0.79	
964.60703	2	$C_{93}H_{168}N_{18}O_{19}S_2H^+_1Na^+_1$	$EGP_{18}H^+_1Na^+_1$	-0.23	
				Average error (ppm)	-0.55
				Standard Deviation error (ppm)	0.68

Table S 3.2: ECD assignments of a and x series along with internal fragments Figure 3.2

m/z	charge	Chemical	error (ppm)	Series
277.10381	1	$C_{11}H_{20}N_2O_2S_2H_{+1}$	-0.31	io_2
574.30917	1	$C_{26}H_{47}N_5O_5S_2H_{+1}$	0.06	io_3
673.37769	1	$C_{31}H_{56}N_6O_6S_2H_{+1}$	0.2	io_4
772.44594	1	$C_{36}H_{65}N_7O_7S_2H_{+1}$	-0.03	io_5
871.51433	1	$C_{41}H_{74}N_8O_8S_2H_{+1}$	-0.06	io_6
970.58297	1	$C_{46}H_{83}N_9O_9S_2H_{+1}$	0.18	io_7
1069.65107	1	$C_{51}H_{92}N_{10}O_{10}S_2H_{+1}$	-0.13	io_8
1168.71994	1	$C_{56}H_{101}N_{11}O_{11}S_2H_{+1}$	0.27	io_9
1267.78864	1	$C_{61}H_{110}N_{12}O_{12}S_2H_{+1}$	0.48	io_{10}
1366.85692	1	$C_{66}H_{119}N_{13}O_{13}S_2H_{+1}$	0.34	io_{11}
1465.92348	1	$C_{71}H_{128}N_{14}O_{14}S_2H_{+1}$	-0.94	io_{12}
1564.99274	1	$C_{76}H_{137}N_{15}O_{15}S_2H_{+1}$	-0.34	io_{13}
268.20191	1	$C_{14}H_{25}N_3O_2S_0H_{+1}$	-0.16	ip_2
367.27029	1	$C_{19}H_{34}N_4O_3S_0H_{+1}$	-0.21	ip_3
466.33892	1	$C_{24}H_{43}N_5O_4S_0H_{+1}$	0.3	ip_4
862.61142	1	$C_{44}H_{79}N_9O_8S_0H_{+1}$	-1.18	ip_8
1258.88559	1	$C_{64}H_{115}N_{13}O_{12}S_0H_{+1}$	-0.4	ip_{12}
272.19684	1	$C_{13}H_{25}N_3O_3S_0H_{+1}$	-0.1	iq_2
371.26528	1	$C_{18}H_{34}N_4O_4S_0H_{+1}$	-0.01	iq_3
470.33369	1	$C_{23}H_{43}N_5O_5S_0H_{+1}$	-0.01	iq_4
569.40212	1	$C_{28}H_{52}N_6O_6S_0H_{+1}$	0.02	iq_5
668.47053	1	$C_{33}H_{61}N_7O_7S_0H_{+1}$	0.01	iq_6
767.53890	1	$C_{38}H_{70}N_8O_8S_0H_{+1}$	-0.05	iq_7
965.67579	1	$C_{48}H_{88}N_{10}O_{10}S_0H_{+1}$	0.03	iq_9
1064.74437	1	$C_{53}H_{97}N_{11}O_{11}S_0H_{+1}$	0.18	iq_{10}
1163.81262	1	$C_{58}H_{106}N_{12}O_{12}S_0H_{+1}$	0.02	iq_{11}
1262.87932	1	$C_{63}H_{115}N_{13}O_{13}S_0H_{+1}$	-1.34	iq_{12}
1361.94956	1	$C_{68}H_{124}N_{14}O_{14}S_0H_{+1}$	0.1	iq_{13}
1461.01617	1	$C_{73}H_{133}N_{15}O_{15}S_0H_{+1}$	-1.14	iq_{14}
1560.08706	1	$C_{78}H_{142}N_{16}O_{16}S_0H_{+1}$	0.52	iq_{15}
1659.15251	1	$C_{83}H_{151}N_{17}O_{17}S_0H_{+1}$	-1.3	iq_{16}
1758.22187	1	$C_{88}H_{160}N_{18}O_{18}S_0H_{+1}$	-0.69	iq_{17}
187.14399	1	$C_9H_{18}N_2O_2S_0H_{+1}$	-0.61	a_2
286.21252	1	$C_{14}H_{27}N_3O_3S_0H_{+1}$	0.01	a_3
385.28096	1	$C_{19}H_{36}N_4O_4S_0H_{+1}$	0.07	a_4
484.34935	1	$C_{24}H_{45}N_5O_5S_0H_{+1}$	0.01	a_5
583.41776	1	$C_{29}H_{54}N_6O_6S_0H_{+1}$	0	a_6
682.48624	1	$C_{34}H_{63}N_7O_7S_0H_{+1}$	0.1	a_7
781.55455	1	$C_{39}H_{72}N_8O_8S_0H_{+1}$	-0.05	a_8
880.62319	1	$C_{44}H_{81}N_9O_9S_0H_{+1}$	0.21	a_9
979.69159	1	$C_{49}H_{90}N_{10}O_{10}S_0H_{+1}$	0.18	a_{10}
1078.75997	1	$C_{54}H_{99}N_{11}O_{11}S_0H_{+1}$	0.13	a_{11}
1177.82824	1	$C_{59}H_{108}N_{12}O_{12}S_0H_{+1}$	0	a_{12}

1276.89664	1	$C_{64}H_{117}N_{13}O_{13}S_0H+_1$	-0.01	a_{13}
1375.96458	1	$C_{69}H_{126}N_{14}O_{14}S_0H+_1$	-0.36	a_{14}
1475.03329	1	$C_{74}H_{135}N_{15}O_{15}S_0H+_1$	-0.13	a_{15}
1574.10174	1	$C_{79}H_{144}N_{16}O_{16}S_0H+_1$	-0.1	a_{16}
1673.16892	1	$C_{84}H_{153}N_{17}O_{17}S_0H+_1$	-0.83	a_{17}
1772.23795	1	$C_{89}H_{162}N_{18}O_{18}S_0H+_1$	-0.44	a_{18}
1871.306	1	$C_{94}H_{171}N_{19}O_{19}S_0H+_1$	-0.61	a_{19}
1970.37582	1	$C_{99}H_{180}N_{20}O_{20}S_0H+_1$	0.13	a_{20}
837.08491	2	$C_{84}H_{153}N_{17}O_{17}S_0H+_2$	-4.64	a_{17}
886.62253	2	$C_{89}H_{162}N_{18}O_{18}S_0H+_2$	-0.53	a_{18}
936.15684	2	$C_{94}H_{171}N_{19}O_{19}S_0H+_2$	-0.39	a_{19}
985.69105	2	$C_{99}H_{180}N_{20}O_{20}S_0H+_2$	-0.37	a_{20}
1035.22514	2	$C_{104}H_{189}N_{21}O_{21}S_0H+_2$	-0.47	a_{21}
297.20466	1	$C_{15}H_{26}N_3O_3S_0H+_1$	-0.11	ir_2
396.27310	1	$C_{20}H_{35}N_4O_4S_0H+_1$	-0.02	ir_3
495.34155	1	$C_{25}H_{44}N_5O_5S_0H+_1$	0.06	ir_4
594.41006	1	$C_{30}H_{53}N_6O_6S_0H+_1$	0.21	ir_5
693.47826	1	$C_{35}H_{62}N_7O_7S_0H+_1$	-0.13	ir_6
792.54627	1	$C_{40}H_{71}N_8O_8S_0H+_1$	-0.62	ir_7
199.14398	1	$C_{10}H_{18}N_2O_2S_0H+_1$	-0.62	is_2
397.28091	1	$C_{20}H_{36}N_4O_4S_0H+_1$	-0.06	is_3
496.34939	1	$C_{25}H_{45}N_5O_5S_0H+_1$	0.09	is_4
595.41776	1	$C_{30}H_{54}N_6O_6S_0H+_1$	0	is_5
694.48635	1	$C_{35}H_{63}N_7O_7S_0H+_1$	0.25	is_6
793.55479	1	$C_{40}H_{72}N_8O_8S_0H+_1$	0.25	is_7
892.62304	1	$C_{45}H_{81}N_9O_9S_0H+_1$	0.04	is_8
991.69132	1	$C_{50}H_{90}N_{10}O_{10}S_0H+_1$	-0.1	is_9
201.15964	1	$C_{10}H_{20}N_2O_2S_0H+_1$	-0.57	it_2
300.22814	1	$C_{15}H_{29}N_3O_3S_0H+_1$	-0.09	it_3
399.29658	1	$C_{20}H_{38}N_4O_4S_0H+_1$	-0.01	it_4
498.36501	1	$C_{25}H_{47}N_5O_5S_0H+_1$	0.03	it_5
597.43347	1	$C_{30}H_{56}N_6O_6S_0H+_1$	0.1	it_6
696.50182	1	$C_{35}H_{65}N_7O_7S_0H+_1$	-0.01	it_7
795.57041	1	$C_{40}H_{74}N_8O_8S_0H+_1$	0.22	it_8
894.63881	1	$C_{45}H_{83}N_9O_9S_0H+_1$	0.18	it_9
993.70692	1	$C_{50}H_{92}N_{10}O_{10}S_0H+_1$	-0.15	it_{10}
1092.77545	1	$C_{55}H_{101}N_{11}O_{11}S_0H+_1$	-0.03	it_{11}
1191.84352	1	$C_{60}H_{110}N_{12}O_{12}S_0H+_1$	-0.31	it_{12}
1290.91315	1	$C_{65}H_{119}N_{13}O_{13}S_0H+_1$	0.65	it_{13}
1588.11791	1	$C_{80}H_{146}N_{16}O_{16}S_0H+_1$	0.23	it_{14}
1687.18495	1	$C_{85}H_{155}N_{17}O_{17}S_0H+_1$	-0.6	it_{15}
1786.25356	1	$C_{90}H_{164}N_{18}O_{18}S_0H+_1$	-0.46	it_{16}
1984.39132	1	$C_{100}H_{182}N_{20}O_{20}S_0H+_1$	0.06	it_{18}
321.13011	1	$C_{13}H_{24}N_2O_3S_2H+_1$	0	x_2
420.19854	1	$C_{18}H_{33}N_3O_4S_2H+_1$	0.04	x_3
519.26700	1	$C_{23}H_{42}N_4O_5S_2H+_1$	0.12	x_4

618.33544	1	$C_{28}H_{51}N_5O_6S_2H+_1$	0.14	x_5
717.40375	1	$C_{33}H_{60}N_6O_7S_2H+_1$	-0.02	x_6
816.47225	1	$C_{38}H_{69}N_7O_8S_2H+_1$	0.08	x_7
915.54071	1	$C_{43}H_{78}N_8O_9S_2H+_1$	0.13	x_8
1014.60903	1	$C_{48}H_{87}N_9O_{10}S_2H+_1$	0.02	x_9
1113.67740	1	$C_{53}H_{96}N_{10}O_{11}S_2H+_1$	-0.02	x_{10}
1212.74625	1	$C_{58}H_{105}N_{11}O_{12}S_2H+_1$	0.34	x_{11}
1311.81443	1	$C_{63}H_{114}N_{12}O_{13}S_2H+_1$	0.14	x_{12}
1410.88015	1	$C_{68}H_{123}N_{13}O_{14}S_2H+_1$	-1.78	x_{13}
1509.95097	1	$C_{73}H_{132}N_{14}O_{15}S_2H+_1$	-0.07	x_{14}
1609.01932	1	$C_{78}H_{141}N_{15}O_{16}S_2H+_1$	-0.11	x_{15}
1708.08733	1	$C_{83}H_{150}N_{16}O_{17}S_2H+_1$	-0.34	x_{16}
1807.15479	1	$C_{88}H_{159}N_{17}O_{18}S_2H+_1$	-0.85	x_{17}
1906.22600	1	$C_{93}H_{168}N_{18}O_{19}S_2H+_1$	0.66	x_{18}
2005.29034	1	$C_{98}H_{177}N_{19}O_{20}S_2H+_1$	-1.4	x_{19}
224.15188	1	$C_{12}H_{19}N_2O_2S_0H+_1$	-0.22	Internal
521.35717	1	$C_{27}H_{46}N_5O_5S_0H+_1$	0	
620.42574	1	$C_{32}H_{55}N_6O_6S_0H+_1$	0.25	
719.49419	1	$C_{37}H_{64}N_7O_7S_0H+_1$	0.27	
818.56270	1	$C_{42}H_{73}N_8O_8S_0H+_1$	0.35	
917.63102	1	$C_{47}H_{82}N_9O_9S_0H+_1$	0.21	
1016.69921	1	$C_{52}H_{91}N_{10}O_{10}S_0H+_1$	-0.03	
326.24384	1	$C_{17}H_{31}N_3O_3S_0H+_1$	0.07	Internal
524.38069	1	$C_{27}H_{49}N_5O_5S_0H+_1$	0.08	
623.44900	1	$C_{32}H_{58}N_6O_6S_0H+_1$	-0.1	
722.51725	1	$C_{37}H_{67}N_7O_7S_0H+_1$	-0.31	
821.58578	1	$C_{42}H_{76}N_8O_8S_0H+_1$	-0.13	
920.65460	1	$C_{47}H_{85}N_9O_9S_0H+_1$	0.32	
1118.79160	1	$C_{57}H_{103}N_{11}O_{11}S_0H+_1$	0.42	
1217.85926	1	$C_{62}H_{112}N_{12}O_{12}S_0H+_1$	-0.23	
436.30439	1	$C_{23}H_{39}N_4O_4S_0H+_1$	-0.04	
634.44048	1	$C_{33}H_{57}N_6O_6S_0H+_1$	-1.19	
242.18625	1	$C_{12}H_{23}N_3O_2S_0H+_1$	-0.22	Internal
440.32316	1	$C_{22}H_{41}N_5O_4S_0H+_1$	0.07	
539.39150	1	$C_{27}H_{50}N_6O_5S_0H+_1$	-0.08	
1034.73411	1	$C_{52}H_{95}N_{11}O_{10}S_0H+_1$	0.48	
1133.80179	1	$C_{57}H_{104}N_{12}O_{11}S_0H+_1$	-0.21	
1232.87041	1	$C_{62}H_{113}N_{13}O_{12}S_0H+_1$	-0.03	
1331.93899	1	$C_{67}H_{122}N_{14}O_{13}S_0H+_1$	0.1	
1431.00768	1	$C_{72}H_{131}N_{15}O_{14}S_0H+_1$	0.29	
1530.07521	1	$C_{77}H_{140}N_{16}O_{15}S_0H+_1$	-0.31	
			Average error (ppm)	-0.12
			Standard Deviation error (ppm)	0.41

Table S 3.3: ECD assignments of a and x series of hydrogen initiated polyoxazoline along with internal fragments Figure 3.2

m/z	z	Formula	error	Fragmentation	
272.19692	1	$C_8H_{16}N_2O_2S_0H^+_1$	-0.02		a_2
371.26529	1	$C_{13}H_{25}N_3O_3S_0H^+_1$	0.19		a_3
470.33368	1	$C_{18}H_{34}N_4O_4S_0H^+_1$	0.02		a_4
569.40202	1	$C_{23}H_{43}N_5O_5S_0H^+_1$	-0.03		a_5
668.47052	1	$C_{28}H_{52}N_6O_6S_0H^+_1$	-0.16		a_6
767.53889	1	$C_{33}H_{61}N_7O_7S_0H^+_1$	-0.01		a_7
866.60772	1	$C_{38}H_{70}N_8O_8S_0H^+_1$	-0.06		a_8
965.67589	1	$C_{43}H_{79}N_9O_9S_0H^+_1$	0.43		a_9
1064.74423	1	$C_{48}H_{88}N_{10}O_{10}S_0H^+_1$	0.13		a_{10}
1163.81253	1	$C_{53}H_{97}N_{11}O_{11}S_0H^+_1$	0.05		a_{11}
1262.88104	1	$C_{58}H_{106}N_{12}O_{12}S_0H^+_1$	-0.05		a_{12}
1361.95028	1	$C_{63}H_{115}N_{13}O_{13}S_0H^+_1$	0.03		a_{13}
1461.01763	1	$C_{68}H_{124}N_{14}O_{14}S_0H^+_1$	0.63		a_{14}
1560.08600	1	$C_{73}H_{133}N_{15}O_{15}S_0H^+_1$	-0.14		a_{15}
1659.15248	1	$C_{78}H_{142}N_{16}O_{16}S_0H^+_1$	-0.16		a_{16}
1758.22349	1	$C_{83}H_{151}N_{17}O_{17}S_0H^+_1$	-1.32		a_{17}
1857.29534	1	$C_{88}H_{160}N_{18}O_{18}S_0H^+_1$	0.23		a_{18}
1956.36348	1	$C_{93}H_{169}N_{19}O_{19}S_0H^+_1$	2.07		a_{19}
2055.42845	1	$C_{98}H_{178}N_{20}O_{20}S_0H^+_1$	1.83		a_{20}
2154.49923	1	$C_{103}H_{187}N_{21}O_{21}S_0H^+_1$	0.06		a_{21}
2253.56343	1	$C_{108}H_{196}N_{22}O_{22}S_0H^+_1$	1.16		a_{22}
196.12062	1	$C_{113}H_{205}N_{23}O_{23}S_0H^+_1$	-0.76		a_{23}
298.21253	1	$C_{10}H_{18}N_2O_2S_0H^+_1$	-0.07	internal	
397.28089	1	$C_{15}H_{27}N_3O_3S_0H^+_1$	0.04		
595.41781	1	$C_{20}H_{36}N_4O_4S_0H^+_1$	-0.11		
694.48697	1	$C_{30}H_{54}N_6O_6S_0H^+_1$	0.08		
793.55477	1	$C_{35}H_{63}N_7O_7S_0H^+_1$	1.15		
892.62397	1	$C_{40}H_{72}N_8O_8S_0H^+_1$	0.23		
991.69105	1	$C_{45}H_{81}N_9O_9S_0H^+_1$	1.08		
1189.82981	1	$C_{50}H_{90}N_{10}O_{10}S_0H^+_1$	-0.37		
1288.89688	1	$C_{60}H_{108}N_{12}O_{12}S_0H^+_1$	1.32		
1387.96680	1	$C_{65}H_{117}N_{13}O_{13}S_0H^+_1$	0.17		
1487.03275	1	$C_{70}H_{126}N_{14}O_{14}S_0H^+_1$	1.25		
1586.10303	1	$C_{75}H_{135}N_{15}O_{15}S_0H^+_1$	-0.49		
404.22132	1	$C_{80}H_{144}N_{16}O_{16}S_0H^+_1$	0.71		
300.22819	1	$C_{10}H_{20}N_2O_2S_0H^+_1$	-0.02		c_3
399.29659	1	$C_{15}H_{29}N_3O_3S_0H^+_1$	0.07		c_4
498.36490	1	$C_{20}H_{38}N_4O_4S_0H^+_1$	0.02		c_5
597.43344	1	$C_{25}H_{47}N_5O_5S_0H^+_1$	-0.19		c_6
696.50180	1	$C_{30}H_{56}N_6O_6S_0H^+_1$	0.05		c_7
795.57035	1	$C_{35}H_{65}N_7O_7S_0H^+_1$	-0.03		c_8
993.70744	1	$C_{40}H_{74}N_8O_8S_0H^+_1$	0.14		c_{10}

1290.91343	1	$C_{50}H_{92}N_{10}O_{10}S_0H^+_1$	0.38		c_{12}
420.19845	1	$C_{13}H_{24}N_2O_3S_2H^+_1$	-0.13		x_3
519.26692	1	$C_{18}H_{33}N_3O_4S_2H^+_1$	-0.18		x_4
618.33495	1	$C_{23}H_{42}N_4O_5S_2H^+_1$	-0.04		x_5
717.40375	1	$C_{28}H_{51}N_5O_6S_2H^+_1$	-0.65		x_6
816.47092	1	$C_{33}H_{60}N_6O_7S_2H^+_1$	-0.02		x_7
915.54061	1	$C_{38}H_{69}N_7O_8S_2H^+_1$	-1.54		x_8
1014.60909	1	$C_{43}H_{78}N_8O_9S_2H^+_1$	0.02		x_9
1113.67738	1	$C_{48}H_{87}N_9O_{10}S_2H^+_1$	0.08		x_{10}
1212.74642	1	$C_{53}H_{96}N_{10}O_{11}S_2H^+_1$	-0.04		x_{11}
1311.81434	1	$C_{58}H_{105}N_{11}O_{12}S_2H^+_1$	0.48		x_{12}
1410.88324	1	$C_{63}H_{114}N_{12}O_{13}S_2H^+_1$	0.07		x_{13}
1509.95028	1	$C_{68}H_{123}N_{13}O_{14}S_2H^+_1$	0.41		x_{14}
1609.02168	1	$C_{73}H_{132}N_{14}O_{15}S_2H^+_1$	-0.53		x_{15}
1708.08618	1	$C_{78}H_{141}N_{15}O_{16}S_2H^+_1$	1.36		x_{16}
1807.15634	1	$C_{83}H_{150}N_{16}O_{17}S_2H^+_1$	-1.01		x_{17}
1906.22596	1	$C_{88}H_{159}N_{17}O_{18}S_2H^+_1$	0.01		x_{18}
2005.29377	1	$C_{93}H_{168}N_{18}O_{19}S_2H^+_1$	0.64		x_{19}
2104.36165	1	$C_{98}H_{177}N_{19}O_{20}S_2H^+_1$	0.31		x_{20}
2203.42949	1	$C_{103}H_{186}N_{20}O_{21}S_2H^+_1$	0.04		x_{21}
2302.50202	1	$C_{108}H_{195}N_{21}O_{22}S_2H^+_1$	-0.22		x_{22}
312.22826	1	$C_{113}H_{204}N_{22}O_{23}S_2H^+_1$	1.58		
411.29647	1	$C_{16}H_{29}N_3O_3S_0H^+_1$	0.29	internal	
510.36478	1	$C_{21}H_{38}N_4O_4S_0H^+_1$	-0.27		
708.50162	1	$C_{26}H_{47}N_5O_5S_0H^+_1$	-0.42		
807.57092	1	$C_{36}H_{65}N_7O_7S_0H^+_1$	-0.29		
224.15195	1	$C_{41}H_{74}N_8O_8S_0H^+_1$	0.84		
323.22033	1	$C_{12}H_{19}N_2O_2S_0H^+_1$	0.09		
422.28889	1	$C_{17}H_{28}N_3O_3S_0H^+_1$	-0.04		
521.35735	1	$C_{22}H_{37}N_4O_4S_0H^+_1$	0.31		
719.49385	1	$C_{27}H_{46}N_5O_5S_0H^+_1$	0.34		
818.56279	1	$C_{37}H_{64}N_7O_7S_0H^+_1$	-0.21		
917.63100	1	$C_{42}H_{73}N_8O_8S_0H^+_1$	0.46		
1016.70036	1	$C_{47}H_{82}N_9O_9S_0H^+_1$	0.19		
1115.76915	1	$C_{52}H_{91}N_{10}O_{10}S_0H^+_1$	1.1		
1214.83526	1	$C_{57}H_{100}N_{11}O_{11}S_0H^+_1$	1.34		
1313.90418	1	$C_{62}H_{109}N_{12}O_{12}S_0H^+_1$	-0.67		
1412.97555	1	$C_{67}H_{118}N_{13}O_{13}S_0H^+_1$	-0.23		
1512.04020	1	$C_{72}H_{127}N_{14}O_{14}S_0H^+_1$	1.88		
524.38022	1	$C_{77}H_{136}N_{15}O_{15}S_0H^+_1$	-0.73		
286.21255	1	$C_9H_{18}N_2O_2S_0H^+_1$	-0.08	internal	
385.28095	1	$C_{14}H_{27}N_3O_3S_0H^+_1$	0.11		
484.34936	1	$C_{19}H_{36}N_4O_4S_0H^+_1$	0.05		
583.41738	1	$C_{24}H_{45}N_5O_5S_0H^+_1$	0.03		
682.48623	1	$C_{29}H_{54}N_6O_6S_0H^+_1$	-0.65		
880.62309	1	$C_{34}H_{63}N_7O_7S_0H^+_1$	0.08		

979.69176	1	$C_{44}H_{81}N_9O_9S_0H^+_1$	0.1		
1375.96510	1	$C_{49}H_{90}N_{10}O_{10}S_0H^+_1$	0.35		
1475.03289	1	$C_{69}H_{126}N_{14}O_{14}S_0H^+_1$	0.02		
834.21559	3	$C_{74}H_{135}N_{15}O_{15}S_0H^+_1$	-0.4		
396.27313	2	$C_{123}H_{222}N_{24}O_{25}S_2H^+_3$	-1.2		
			Average		0.04
			Standard Deviation	0.71	

Table S 3.4: Neutral loss assignments of the hydrogen initiated polyoxazoline from the charged reduced species

m/z	mass	Chemical Formula	loss	ppm error
1250.82082	2501.64249	$C_{123}H_{221}N_{24}O_{25}S_2H^+_3$	CH_3	-0.61
1242.31712	2484.63921	$C_{123}H_{220}N_{24}O_{24}S_2H^+_3$	OH	-0.99
1236.80392	2473.61064	$C_{121}H_{217}N_{24}O_{25}S_2H^+_3$	CH_3CH_2	-0.1
1222.30363	2444.60791	$C_{120}H_{216}N_{24}O_{24}S_2H^+_3$	C_3H_5O	0.84
1206.81998	2413.64366	$C_{120}H_{217}N_{24}O_{24}S_1H^+_3$	C_3H_5OS	-0.37
1201.28553	2402.57353	$C_{118}H_{212}N_{23}O_{24}S_2H^+_3$	$C_5H_{10}NO$	-0.14
1176.82030	2353.64029	$C_{118}H_{213}N_{24}O_{24}S_0H^+_3$	$C_5H_9OS_2$	0.13
1151.75080	2303.50512	$C_{113}H_{203}N_{22}O_{23}S_2H^+_3$	$C_{10}H_{19}N_2O_2$	-0.28
1141.30014	2282.60317	$C_{115}H_{208}N_{23}O_{23}S_0H^+_3$	$C_8H_{14}NO_2S_2$	-0.01
1127.28462	2254.57187	$C_{113}H_{204}N_{23}O_{23}S_0H^+_3$	$C_{10}H_{18}NO_2S_2$	-0.05
			Average	-0.17
			Standard Deviation	0.57

Table S 3.5: Example of HRMKMD values and fragments of internal fragments for hydrogen terminated species

Structure	**HRMKMD Value**	**Fragment mass**	**Error (ppm)**
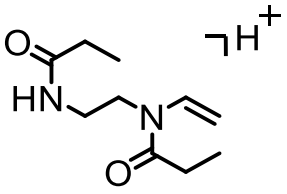	0.0167	199.14409	-0.07
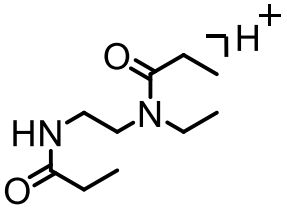	0.05	201.15975	-0.02
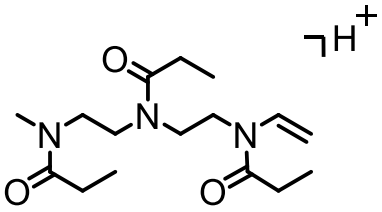	0.164	312.22826	0.29

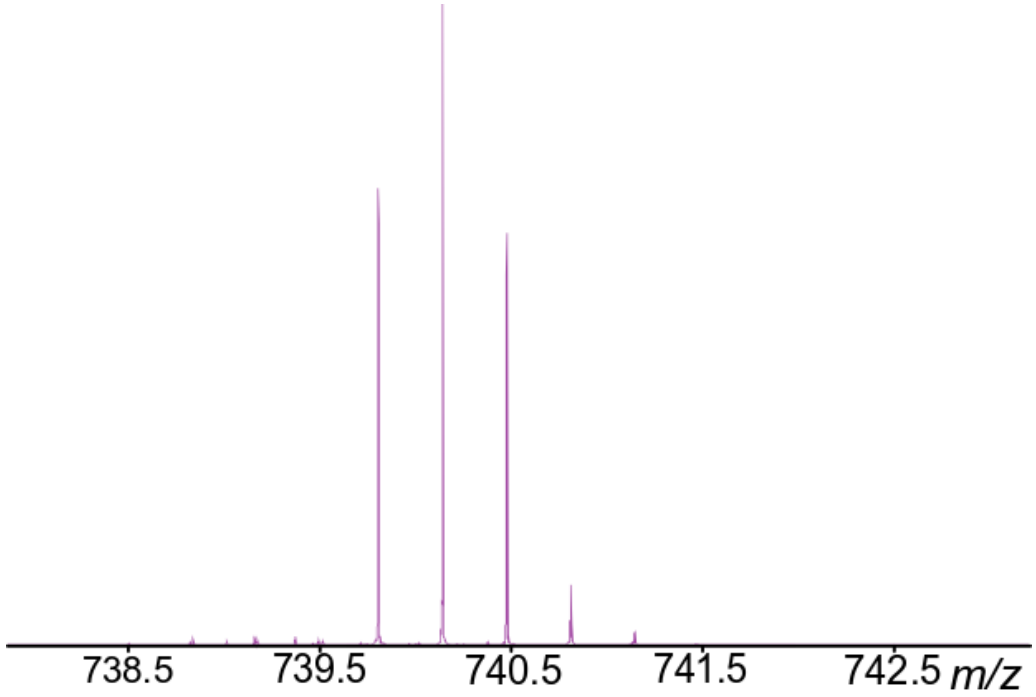

Figure S 3.1 Isolation Window spectrum of methyl initiated polyoxazoline

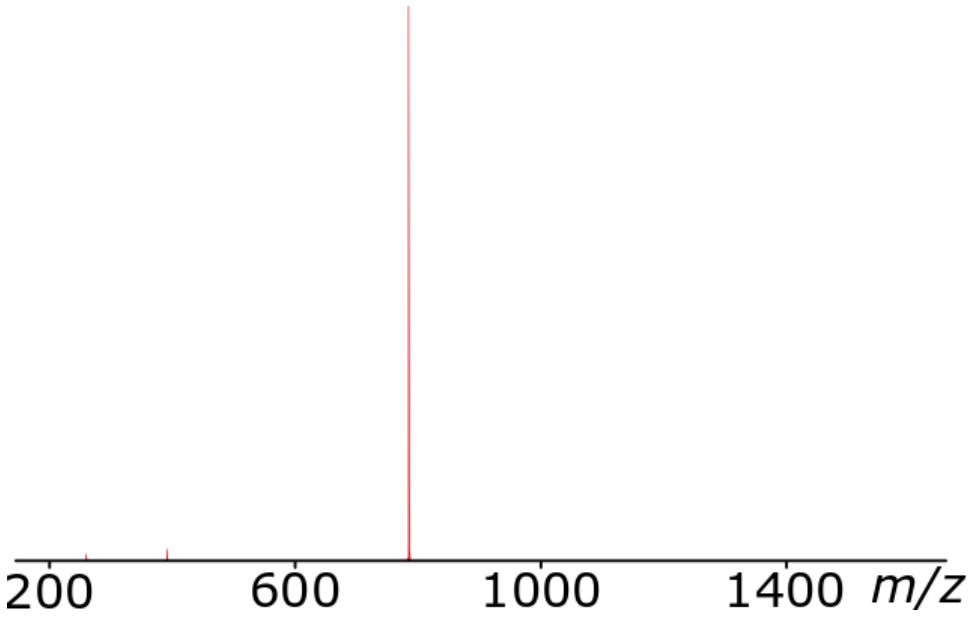

Figure S 3.2 Full isolation spectrum of the methyl initiated polyoxazoline precursor

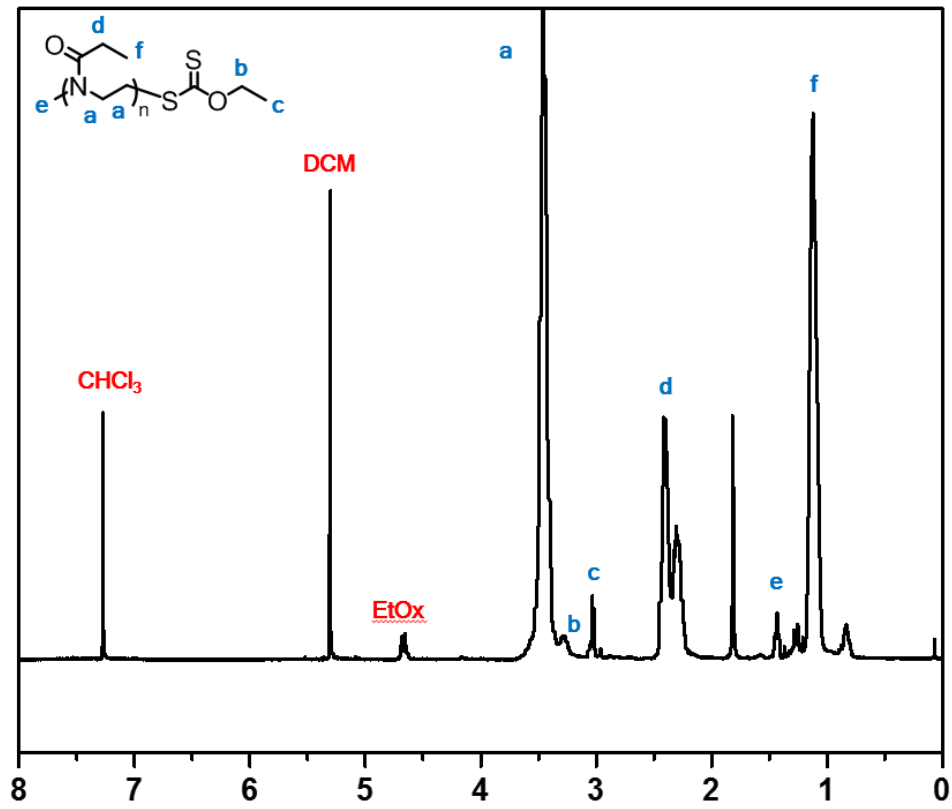

Figure S 3.3 ^{1}H-NMR spectrum of the polyoxazoline.

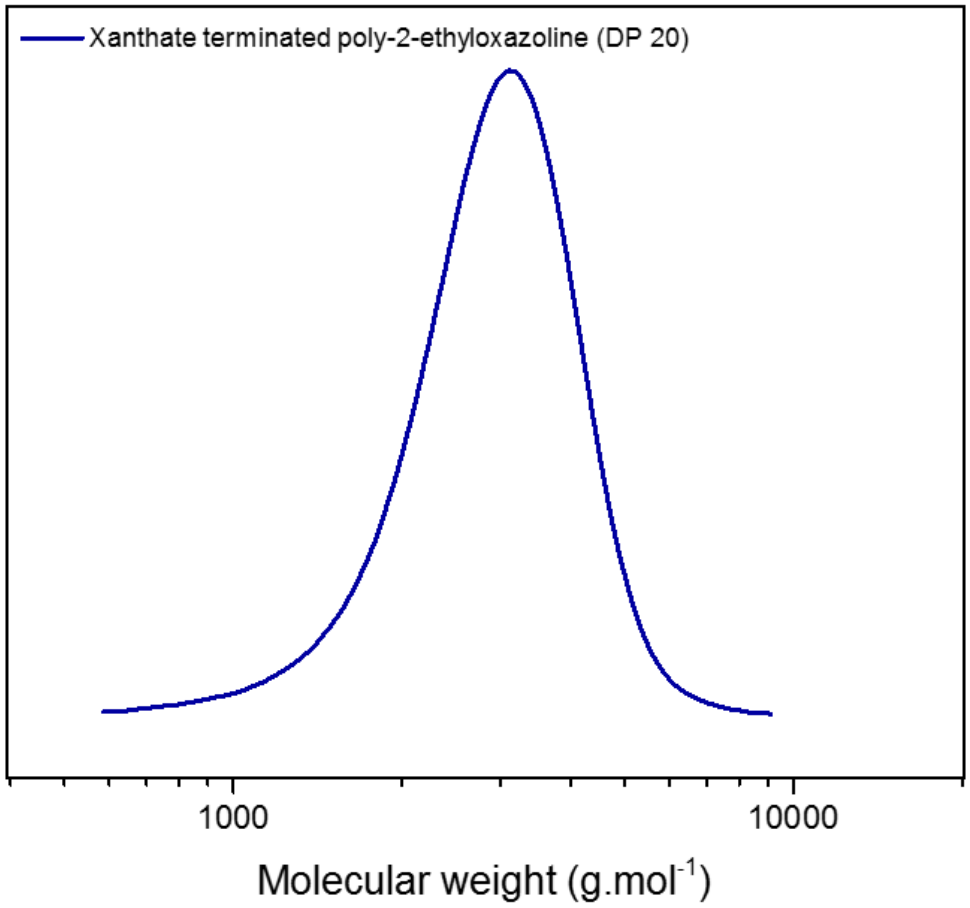

Figure S 3.4 SEC characterisation of the described poly-2-ethyloxazoline. Measurement was performed in chloroform with 2% trimethylamine additive, a polystyrene calibration was used as described in the Experimental section.

4. Electron capture dissociation tandem of trithiocarbonate terminated acrylamide homo- and co-polymers: An atom directed mechanism?

Tomos E. Morgan[1], Andrew Kerr[1], Christopher A. Wootton[1], Mark P. Barrow[1], Anthony W. T. Bristow[2], Sebastien Perrier[1], Peter B. O'Connor[1]*

[1]Department of Chemistry, University of Warwick, Coventry, Midlands, CV4 7AL, UK.

[2]Chemical Development, Pharmaceutical Technology & Development, Operations, AstraZeneca, Macclesfield, UK.

The MS, MS/MS, and analysis presented in this chapter were all carried out by the thesis author. Dr. Kerr synthesised and purified all the polymers presented in this chapter as well as NMR and GPC analysis.

The work presented in this chapter has been prepared for publication in ACS Analytical chemistry by authors Tomos E. Morgan, Andrew Kerr, Christopher A. Wootton, Mark P. Barrow, Anthony W. T. Bristow, Sebastien Perrier, Peter B. O'Connor.

4.1. Abstract

Structure and sequence elucidation of complex homo- and co-polymers is key for further understanding of polymers, polymer synthesis, and polymer interactions in biological processes. In this contribution, poly(dimethylacrylamide) homo- and dimethylacrylamide/4-acryloylmorpholine block co-polymers were synthesized and analyzed by electron capture dissociation (ECD) Fourier transform ion cyclotron resonance (FT-ICR) tandem mass spectrometry. A novel radical dissociation process is presented, electron capture caused specific cleavage at the terminal butyl-trithiocarbonate group which initiated a free radical dissociation process.

4.2. Introduction

Recent advances in the efficiency and control of various reversible addition-fragmentation chain transfer (RAFT) polymerization techniques has created a large increase in the variation and complexity of homo- and co-polymer structures which can be produced.[1,2] Bioconjugation of polymers to various bio-targets such as proteins, antibodies and so on, improve their activity, circulation time, and cell interactions.[3]

Although poly(ethylene glycol) (PEG) is by far the most used material in this field,[4,5] it has a number of drawbacks, including accelerated blood clearance phenomena, and limited opportunities to modify the polymer backbone.[5] In that respect, well-defined polymers obtained by RAFT polymerization offer attractive alternatives, and in particular polyacrylamides which are biocompatible, functional and hydrolytically stable.[6] As these polymers find an increased use in biological and medicinal applications[7] there has been an increased interest in their accurate chemical analysis.[8] For instance, copolymer architectures grafted on peptides or proteins have shown strong biological utility due to the ability to control chemical properties, such as stability and solubility.[9,10]

The use of random or block copolymers allows increased fine tuning of chemical properties.[11] Analysis is often carried out by two-dimensional chromatography separation methods,[12,13] but there are limitations, thus calling for more powerful analytical methods.[14,15] Mass spectrometry is effective in the analysis of homo- and co-polymers for sequence analysis,[16-19] particularly by multimodal fragmentation methods.[20] Synthetic insight of acrylamides by mass spectrometry analysis has come from the use of matrix assisted laser desorption mass spectrometry (MALDI)[21] and electrospray ionization (ESI) techniques.[22] Direct mass spectrometry analysis of copolymer species has been improved with the use of a modified Kendrick analysis[23,24] developed by Fouquet *et al*. [25-27] by normalizing to a homologous series.[28-30] Sequence and end group analysis of polymers by fragmenting the polymer into smaller oligomer units[31-33] allows direct testing of synthetic procedures and modifications.[34-36]

Site specific fragmentation has been observed in collisionally induced fragmentation (CID/CAD) and UV dissociation. MALDI-CAD induced radical dissociation of poly(styrenes) and poly(acrylates) backbones after radical generation by homolytic cleavage of an alkene.[18,37-39] UV dissociation can generate site specific radical formation with the use of a carbon –halide bond incorporated into Tyr59 for protein dissociation.[40] An advantage of atom directed methods allows controlled radical production that can be used to probe structures.[41]

Usually, electron capture dissociation (ECD) analysis is carried out on proteins. Polymer fragmentation by ECD[42,43] has been carried out successfully, where amide groups are not directly part of the backbone.[44,45] Evidence of higher order radical dissociation mechanisms have been shown in proteins and peptides where radical fragments are present,[46,47] furthering the Utah-Washington mechanism with secondary radical reactions, *i.e.* the free radical cascade.[48,49] Radical capture favorability has been studied with the fragmentation of disulfide bonds in proteins, although there is no evidence of further radical transfer after disulfide fragmentation.[50]

ECD initiated radical depolymerisation of species that don't contain amide backbones, such as polyacrylamides, is little understood. In this study we report the characterization of a dimethylacrylamide (pDMA) homopolymer and a dimethylacrylamide/4-acryloylmorpholine (p(NAM-*b*-DMA)) block copolymer, by nESI and ECD. The use of ECD fragmentation of the acrylamides showed end group and sequence coverage of the copolymer allowing determination of the block lengths of the copolymer itself. Double resonance experiments were carried out, ejecting the radical ion intermediates to reveal the fragmentation mechanism.[51-54] The fragmentation mechanism inferred from the double resonance studies offers insight into a novel atom directed dissociation mechanism as well as confirming free radical cascade observations from previous studies.

4.3. Methods

Synthesis of Acrylamides was carried out according to previous literature.[55]

MS Sample Preparation: The polyacrylamide samples were dissolved into a 99.5% solution of purified water obtained from a Direct-Q3 Ultrapure Water System (Millipore, Lutterworth, United Kingdom) at 20 µM in 0.5% formic acid (Sigma-Aldrich, Dorset, United Kingdom).

FT-ICR MS analysis: All experiments were performed on a 12 T solariX Fourier transform ion cyclotron resonance mass spectrometer (Bruker Daltonik, GmbH, Bremen, Germany) fitted with the Infinity cell, using a nanoelectrospray (nESI) ion source in positive ion mode. The ECD was carried out with the use of an indirectly heated hollow cathode with the heater current set at 1.5 A, with a pulse length of 0.2 s and bias 1.0 – 1.2 eV. MS data was recorded using 4 mega-word (2^{22}, 22 bit) transients (1.6777 s) achieving approximately 400,000 resolving power FWHM at *m/z* 400. ECD MS data was recorded at a lower *m/z* cutoff using 4 mega-word (2^{22}, 22 bit) transients (1.185 s) achieving approximately 280,000 resolving power FWHM at *m/z* 400.

All mass spectra were internally calibrated by the intact polymer peaks across the polymer distribution, or fragment peaks in ECD spectra. The copolymer MS spectrum was converted to absorption mode using Bruker FTMS Processing (Bruker Daltonics, Billerica, USA). The Bruker SNAP algorithm was used for peak picking with the dimethylamine polyacrylamide monomer used as the repeat unit. The Bruker SNAP algorithm matches a calculated isotope distribution adjusted to a repeat unit with increasing mass.[56,57] Simplified data visualization was carried out by adjusting the mass of the fragment to a function of the monomer, as shown previously.[30]

Double resonance (ion ejection) experiments were carried out by producing a resonant ejection pulse at the specified frequency of the ion being ejected during the ECD MS/MS fragmentation event within the ICR cell.[51]

4.4. Results and Discussion

Nano-electrospray ionization (nESI) of the polyacrylamides, Figure 4.1 A) nESI of the DMA homopolymer showing up to 4+ protonated charge state, B) nESI spectrum of p(NAM-b-DMA) copolymer, C) zoom in spectra of B, showing resolution and presence of selected ions, D) fractional Kendrick mass (HRMKMD) plot allowing rapid assignment of copolymer species.

A and B, showed a clear polymer dispersity for homopolymer poly(N-N-dimethylacrylamide), pDMA. The pDMA produced 2+, 3+, and 4+ protonated species, a weight average of 3030 Da and dispersity 1.1. The mass spectrum for the block copolymer, p(NAM-*b*-DMA) Figure 4.1 A) nESI of the DMA homopolymer showing up to 4+ protonated charge state, B) nESI spectrum of p(NAM-b-DMA) copolymer, C) zoom in spectra of B, showing resolution and presence of selected ions, D) fractional Kendrick mass (HRMKMD) plot allowing rapid assignment of copolymer species.

B, was much more complex due to the presence of multiple dispersities caused by different block lengths. Overall, 2+, 3+, and 4+ species were observed of the copolymer.

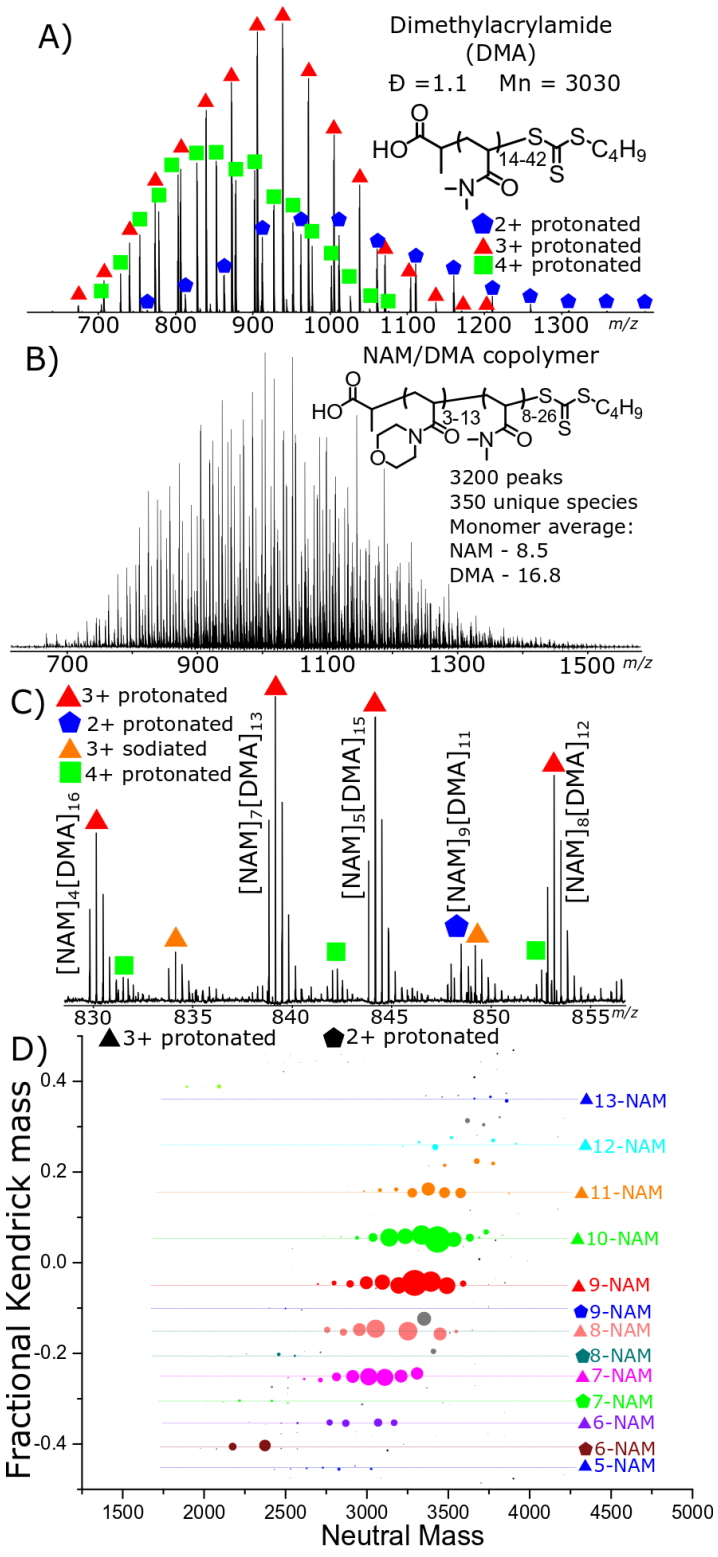

Figure 4.1 A) nESI of the DMA homopolymer showing up to 4+ protonated charge state, B) nESI spectrum of p(NAM-b-DMA) copolymer, C) zoom in spectra of B, showing resolution and presence of selected ions, D) fractional Kendrick mass (HRMKMD) plot allowing rapid assignment of copolymer species.

Over 3200 peaks were observed as part of the mass spectrum and with the use of SNAP peak picking approximately 350 unique species were assigned. The spectral complexity can be analyzed and visualized by Kendrick analysis. The fractional Kendrick mass (HRMKMD) was taken and plotted as a function of the mass of the ions, Figure 1D. The DMA monomer (monomer A) was used for the normalization of the homologous series in the analysis of the p(NAM-*b*-DMA) copolymer. By normalizing to the DMA monomer the presence of end groups, adducts, and the NAM (monomer B) caused a change in the fKm. As the end group is constant and the adduct will only differ by a proton, the main change in the fKm value is the presence of a differing number of NAM monomers causing a difference in the heteroatom content.

As the HRMKMD is plotted in the vertical dimension, a difference in the number of NAM units are seen as horizontal lines. The most common species were triply protonated copolymer containing 7-11 NAM units. Taking an average number of NAM and DMA units of the assignments gives a NAM monomer unit value of 8.6 ± 0.1 and DMA monomer repeat unit value of 16.6 ± 0.2.

An advantage offered by analyzing complex copolymer spectra in this way means that direct measurement of the NAM/DMA ratio and distribution of the copolymer species can be made without analysis during the synthetic procedure, such as gel permeation chromatography.

Figure 4.2 shows the expected and observed fragmentation caused by the radical dissociation of p(DMA).

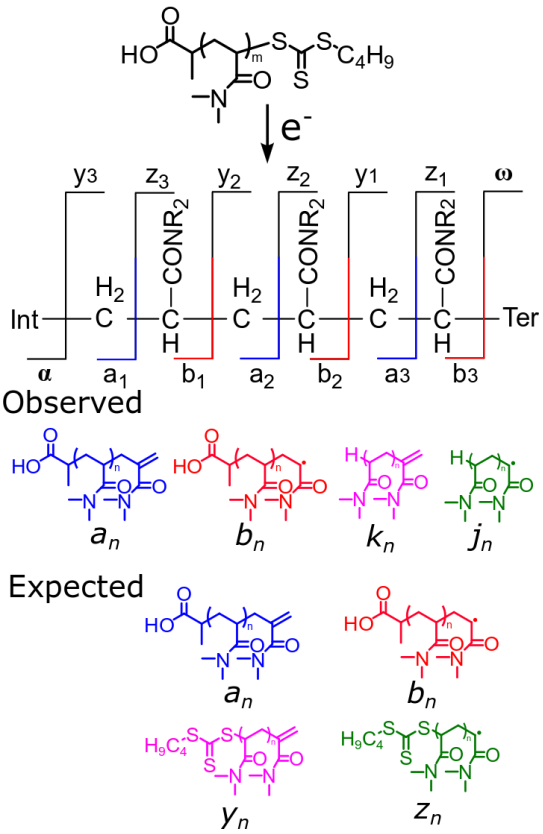

Figure 4.2 A) Fragmentation of p(DMA) through ECD dissociation. a, b, k, and j, are observed fragment series.

Nano-electrospray ionization (nESI) of poly(N-N-dimethylacrylamide), pDMA, produced 2+, 3+, and 4+ protonated species, with a weight average of 3030 Da and dispersity 1.1, see section S1 in SI. A quadrupole isolated 3+ protonated species at *m/z* 872.89190 corresponding to n = 24 repeat units was trapped within the ICR cell and reacted with low energy electrons (cathode voltage 1.0 eV) forming a charge reduced radical species. Radical dissociation produced a rich spectrum, Figure 1A, with four main fragmentation series across the mass range of the polymer and numerous side chain neutral losses from the charge reduced state.

The *a* and *b* series contain the carboxylic acid terminus. The *b* series started at b_3 (*m/z* 371.24129, -0.5 ppm) and finished at b_{21} (*m/z* 2154.47417, 0.5 ppm). The *a* series was more complete, and resolved from the j series, Figure 1B, starting at a_2 (*m/z* 285.18079, -0.3 ppm) and finishing at a_{23} (*m/z* 2266.55137, 1 ppm). The *j* series are an internal fragment series that don't contain either terminus. The *j* series began with the fragment ion j_2 (*m/z* 186.13624, -0.2 ppm), intensity reduced at higher oligomer units finishing with j_{10} (978.68401, 0.4 ppm). The *k* fragment series began

at k_2 (*m/z* 199.14406, -0.2 ppm) with a very intense signal at k_3 (*m/z* 298.21240, -0.4 ppm), the final fragment of the *k* series was *m/z* 1982.37421 (k_{20}, -0.6 ppm). The second largest intensity fragment was the ion present after butyl-trithiocarbonate end group loss (*m/z* 1226.34329, 0.7 ppm, mass loss 165.98 Da). Other fragments were loss of multiple side chain or end groups.

Due to the large number of trapped ions the fragment quantities produced will be statistically distributed based on their corresponding fragment pathway likelihood. The relative intensities of the fragments is an indirect measure of the fragment stability and the likelihood of the fragment production during radical dissociation. The fragment intensities show that *j* fragmentation is the least stable fragment due to consistently lower intensities and *k* and *a* are the most stable fragments. *k* and *a* fragment stabilities are likely due to their cyclic or double bonded nature, as *b* and *j* fragments retain the radical. No fragments containing the terminal butyl-trithiocarbonate were observed, although homolytic cleaveage of the backbone would produce butyl-trithiocarbonate containing fragments. Importantly, no fragments containing the butyl-trithiocarbonate were observed across the spectrum, including neutral loss fragments.

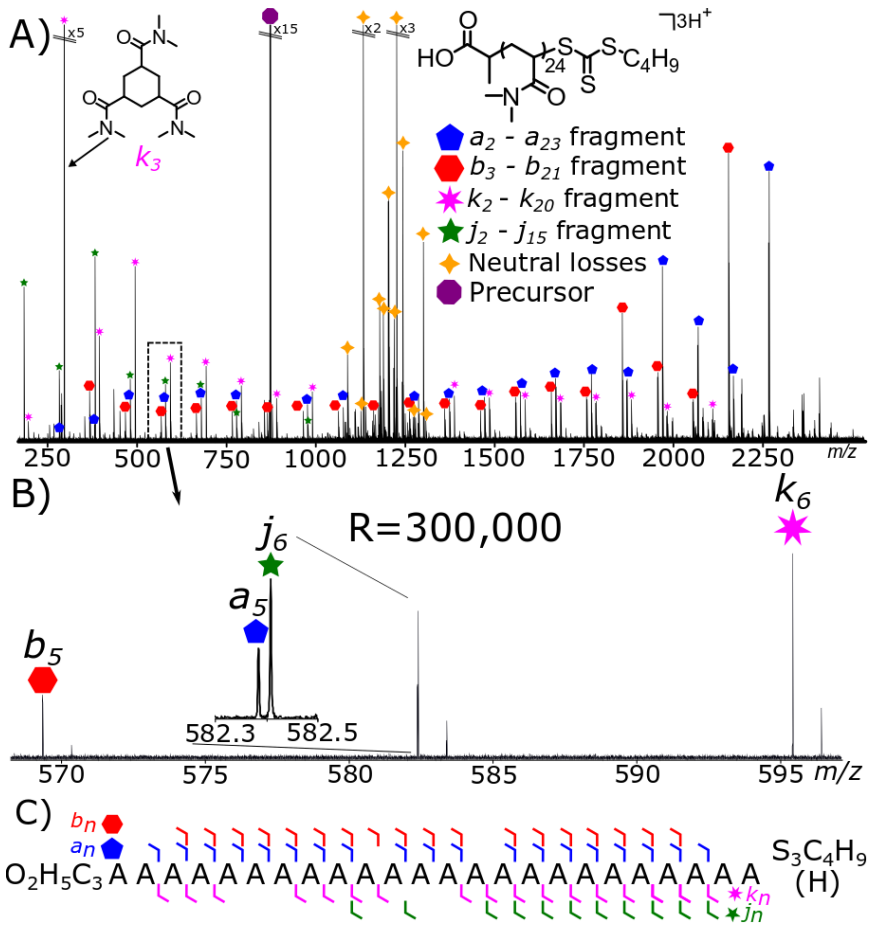

Figure 4.3 A) p(DMA) fragmentation spectrum after electron capture and radical dissociation. B) resolution of a and j series. C) fragmentation map of p(DMA).

The lack of terminal butyl-trithiocarbonate suggest that fragmentation may be caused by the loss of the butyl-trithiocarbonate group or that loss of the butyl-trithiocarbonate group is the most favored pathway. A double resonance experiment can be carried out to determine if loss of the butyl-trithiocarbonate group produces an intermediate which leads to further fragmentation.

The ECD process involves capture of an electron to form a radical species. The lifetime of the radical species allows possible dissociation pathways to be interrogated by removing the intermediate species from the ICR cell before the radical dissociation may occur, called double resonance for historical reasons.[51] Possible intermediates were predicted and removed from the cell individually, before further dissociation was possible. By ejecting the ions at a particular *m/z* ratio that corresponds to the intermediate, any secondary products formed from the ejected

intermediates will have a reduction in intensity. The analysis of the intensity changes elucidated the dissociation pathways. Scheme 2 gives an overview of the experiment.

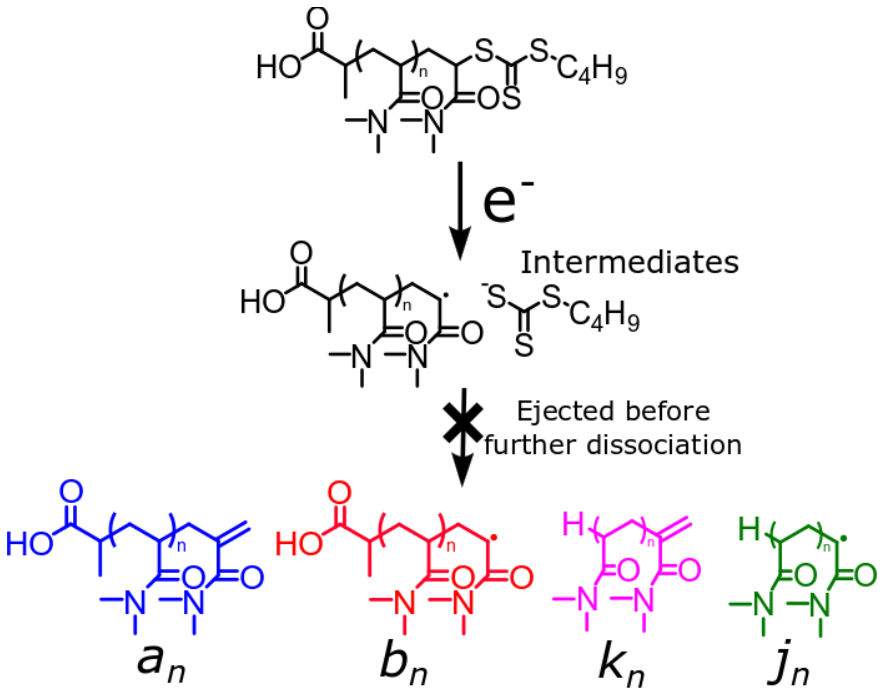

Figure 4.4 Double resonance experiment parameters.

Figure 2A shows ejection of a side chain radical after neutral loss of the dimethylamine ($(CH_3)_2N$) from the parent ion, *m/z* 1286.81106. The formation of further sequence fragments ions was generally unaffected by the ejection of the side chain radical remaining after dimethylamine loss. Unaffected sequence ion intensity indicates that side chain radical formation is not necessary for formation of secondary sequence fragment ions.

In contrast, ejection of the backbone radical ($C_{127}H_{217}N_{22}O_{31}^{\bullet}$) after terminal butyl-trithiocarbonate loss ($C_5H_9S_3$), Figure 4.5B, showed a dramatic decrease in the number of sequence fragments present and also in their corresponding intensities, compared to Figure 4.2B. Figure 4.5C shows the normalized average fragment intensity which shows a drop of approximately 80% for the sequence ions present after the backbone radical has been ejected. Thus, the major fragmentation pathway involves the primary loss of the trithiocarbonate group producing a backbone radical. The secondary radical-driven rearrangements result in cleavages along the backbone.

The drop in fragment intensity witnessed for the side chain radical fragment was consistent with all the other experiments carried out, shown in the supplementary information. Slight variations in the intensity of fragments also occurs in double resonance experiments due to the ICR cell and pulse sequence changes to accommodate a double-resonance pulse, but full comparisons of the different fragments ejected are shown in the supplementary information.

The loss of the butyl-trithiocarbonate end group will form a radical on the terminal position of the polymer which can then undergo hydrogen atom transfer backbiting onto the polymer backbone. The radical species after hydrogen transfer can then dissociate forming the corresponding sequence fragments.

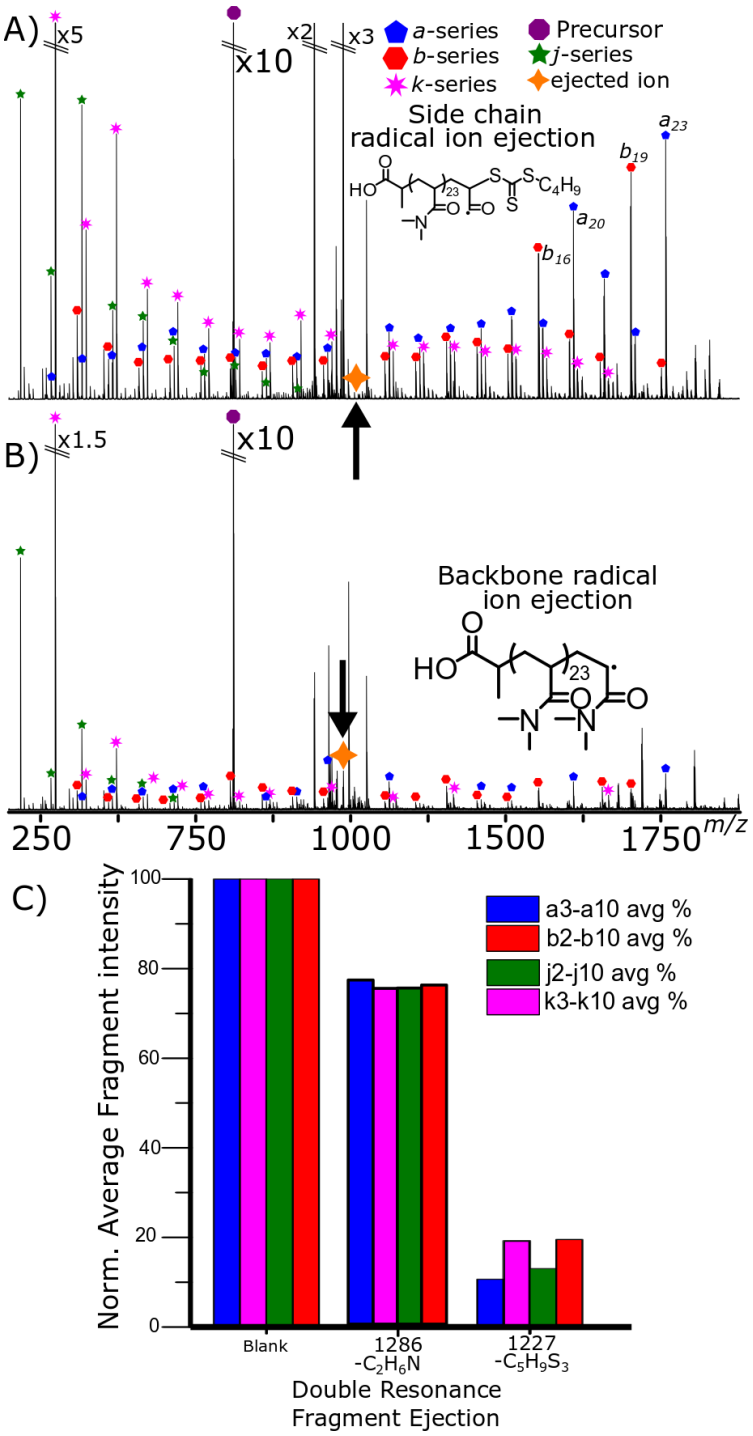

Figure 4.5 Normalized fragment intensity spectra of A) ECD spectrum after ejection of a side chain radical ion after loss of a dime-thylamine group. B) ECD spectrum after ejection of ion formed after backbone radical formation. C) Normalized fragment intensity after backbone radical ejection. Comparison of all double resonance experiments are present in Figure S 4.3 Ion intensity of individual fragmentation series showing difference caused by ejection of ions.Figure S 4.3.

Intense a_{23} and b_{21} fragments can be clearly seen in the p(DMA) spectrum regardless of the ejection of the side chain radical ejection, Figure 4.2A, the fragment positions occurs due to the favoured formation of a five membered ring from the initial radical loss.

Intense fragment peaks at a_{20} and b_{16} correspond to the loss of two six membered rings from the precursor ion. Such distinct fragment patters suggests that initial fragmentation is occurring from radical formation at the ω terminus. Once fragmentation is occurring further than n=6 monomer units from the ω terminus, there is a loss of the six membered ring fragmentation pattern.

Obvious fragmentation patterns centred on three monomer species, suggest that the initial, and most intense, fragmentation is occurring from one position, the end monomer unit caused by loss of the terminal butyl-trithiocarbonate. Consistent abundances of fragment ions past n=6 monomer units from the end group shows that the fragmentation is no longer sterically driven across these molecular distances. Figure 4.6 describes the fragmentation forming the higher intensity fragments. The relative stabilities of the fragments formed can explain the differences in the intensities of the fragments compared to one another. The *a* fragment is more stable on the experiment time scale as it doesn't contain a radical, the *b* fragment dissociates further reducing its intensity.

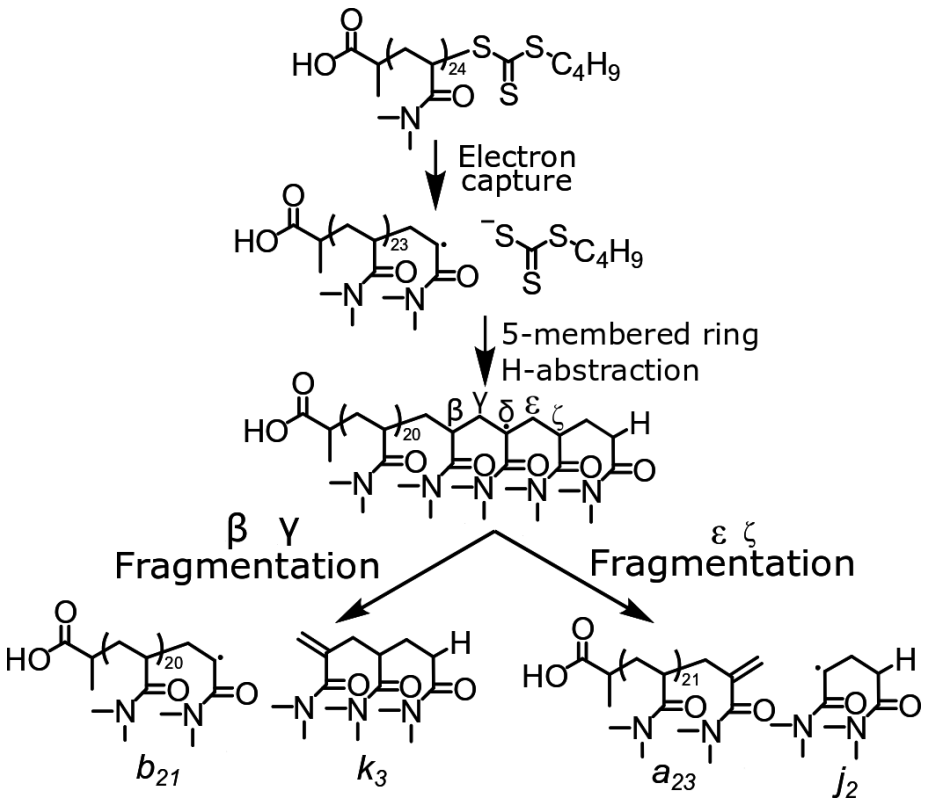

Figure 4.6 Favored five membered ring radical transfer creates increased intensity of b_{21}, k_3, a_{23}, and j_2 fragments.

ECD analysis was also carried out on the block copolymer, p(NAM$_7$-*b*-DMA$_{14}$), shown in Figure 4.7. Fragmentation occurred through both the DMA/NAM blocks of the chain. Three key observations were made:

α terminus sequence ions - Fragmentation coverage started at *m/z* 369.20197 (a_3, -0.3 ppm) fragmenting the NAM block to a_8 (*m/z* 1074.59691, 0.0 ppm) and then across the DAM block to a_{22} (*m/z* 2362.48869, 1.1 ppm), therefore the *a* fragmentation series is complete across the DMA block, only missing the butyl-trithiocarbonate group. The *b* series fragments from *m/z* 497.27304 (b_3, -0.3 ppm) to the b_{20} (*m/z* 2250.40997, 0.0 ppm) fragment, the NAM/DMA crossing is seen through the NAM block fragment (b_7, *m/z* 1061.58914, 0.1 ppm). The coverage of the *b* fragment series is extensive, only one DMA unit short of the butyl-trithiocarbonate group.

Internal fragments - The presence of *j* and *k* and lack of *y* and *z* fragmentation series suggest identical fragmentation pathways for p(DMA) and p(NAM-*b*-DMA). The *k* series finishes at the k_{15} fragment (*m/z* 1487.03317, -0.2 ppm) fragment which

matches the total number of DMA units. The *j* fragment series coverage finishes at j_{14} (*m/z* 1474.02602, 0.2 ppm). In both cases the *k* and *j* series primarily contained DMA.

Higher order dissociation - A fragment at *m/z* 424.24422 (0.02 ppm) is the equivalent of a *k3* fragment but for a NAM homopolymer, and a peak at *m/z* 270.17338 represents an internal j_2 fragment containing two NAM units. A fragment at *m/z* 340.22301 contained two DMA units and a NAM unit.

Neither p(DMA) and p(NAM-*b*-DMA) fragmentation pathways include fragments that contained the butyl trithiocarbonate terminus. Thus, the block copolymer was characterized using the α terminus.

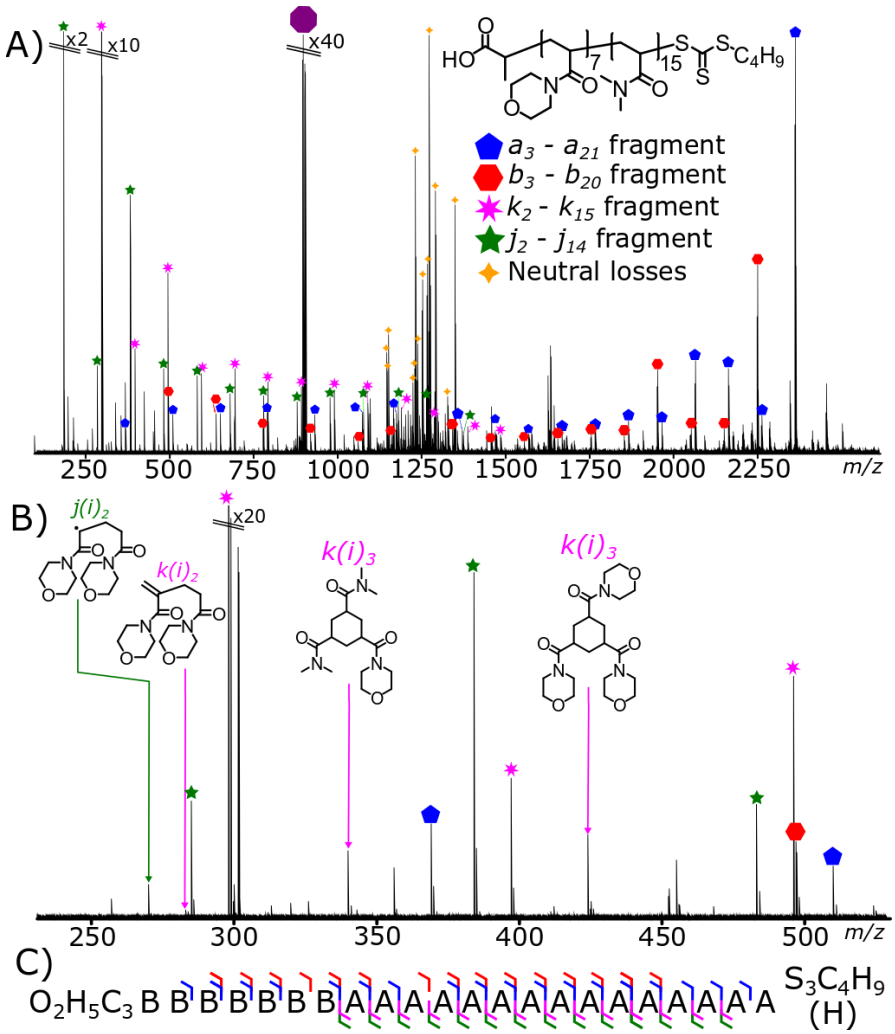

Figure 4.7 A) ECD analysis of p(NAM$_7$-*b*-DMA$_{14}$), B) inset showing further internal fragments, containing NAM or DMA/NAM mixtures. C) Fragmentation coverage diagram of the p(NAM-*b*-DMA) showing the A/B boundary has been characterized.

The fragmentation observed in Figure 4.7A and Figure 4.7B suggest the radical formation from loss of the butyl-trithiocarbonate group dissociations further with radical migration and hydrogen abstraction down the polymer chain, followed by cleavage adjacent to the new radical site. Figure 4.8 shows that the further fragmentation of the radical containing *b* ion will generate *a* and *b* fragments that are identical to the *a* and *b* fragments formed at any stage in the dissociation, but in p(NAM-*b*-DMA) unique internal *j* and *k* fragments are produced, depending on the fragmentation position.

The radical dissociation process as well as multiple radical dissociation events explains the intense k_3 ion. The formation of a six membered ring in a concerted radical dissociation step is energetically favourable, and if multiple fragmentation events occur, the presence of a more intense k_3 is highly likely. The formation of smaller *k* and *j* fragments which contain the mixed NAM/DMA monomer units indicates *at least* secondary backbone radical cleavage is occurring. Altogether, the double resonance experiment shows formation of a radical on one terminus, the presence of sequence fragments shows a secondary dissociation caused by radical cleavage and the internal, mixed DMA/NAM containing, *k* fragments show that tertiary dissociation of the radical containing species occurred. The formation of all the observations are explained by a free radical cascade occurring down the polymer chain, one that is initiated by butyl trithiocarbonate loss at one terminus.

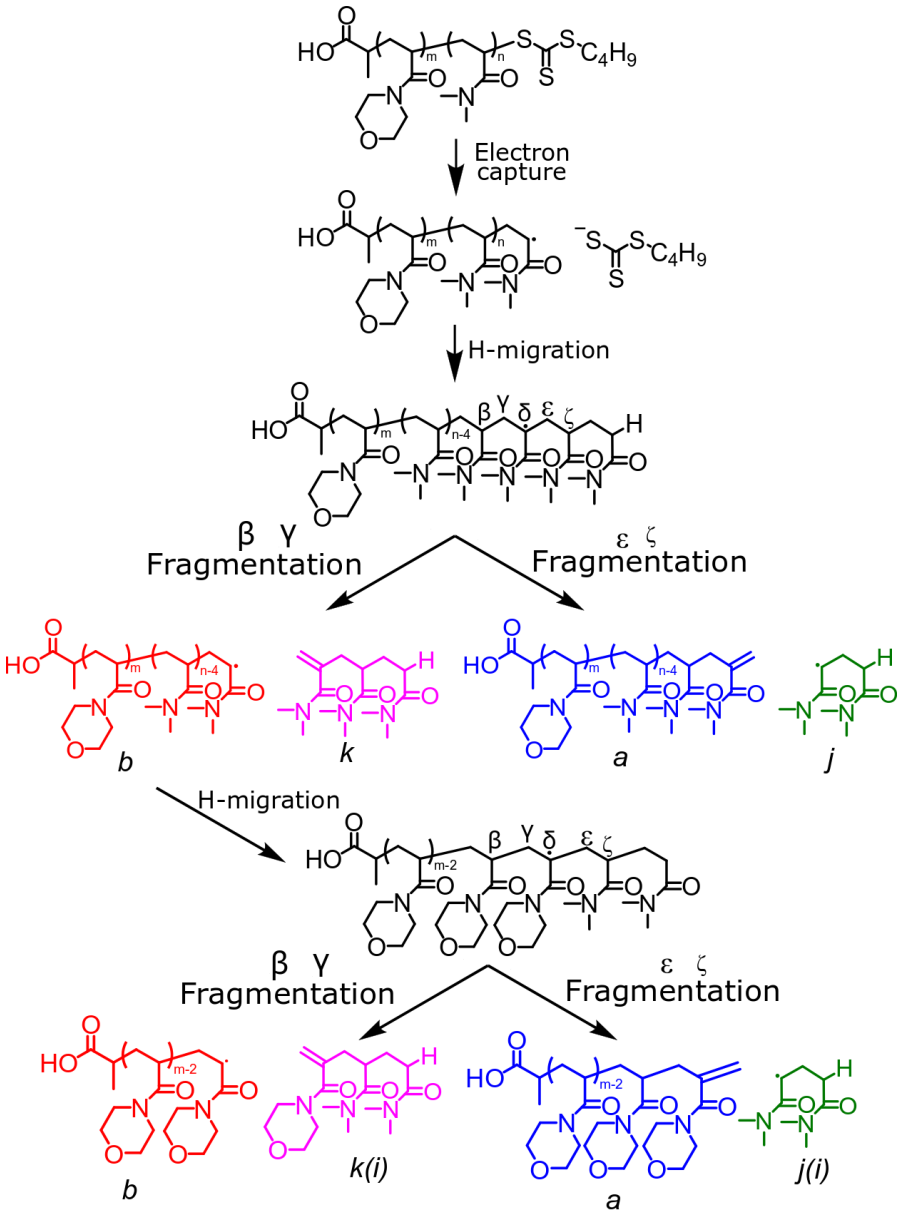

Figure 4.8 Radical dissociation process of the acrylamide polymer showing formation of the four sequence ions. Further dissociation may occur from the radical-containing *b* fragment.

Substitution of the terminal butyl-trithiocarbonate group for hydrogen end groups was carried out in order to eliminate the presence of the terminal butyl-trithiocarbonate group and determine whether the loss of the butyl-trithiocarbonate group was directing the radical dissociation mechanism proposed. Figure 4.9 shows the ECD spectra of both hydrogen capped homo- and co-polymers.

Hydrogen substituted polyacrylamides dissociated producing intense *a*, *b*, *k*, and *j* fragment series. The difference in the fragment patterns was obvious with a

decreasing fragment ion intensity across the spectrum rather than three monomer unit stacking at either end. Comparison of the k_3 fragment shows a clear relationship. The k_3 fragment by is only two or three times more abundant than the other sequence ions, in contrast to ten times more abundant than the experiments carried out with the butyl-trithiocarbonate end group. Formation of $k(i)_3$ (*m/z* 424.24413, -0.2 ppm) fragments from the hydrogen capped copolymer showed that the secondary reactions from the *b* fragmentation were still occurring. Sequence coverage is similar to those of the butyl-trithiocarbonate containing end group polymers showing that the butyl-trithiocarbonate group is not needed for the fragmentation of the acrylamide polymers.

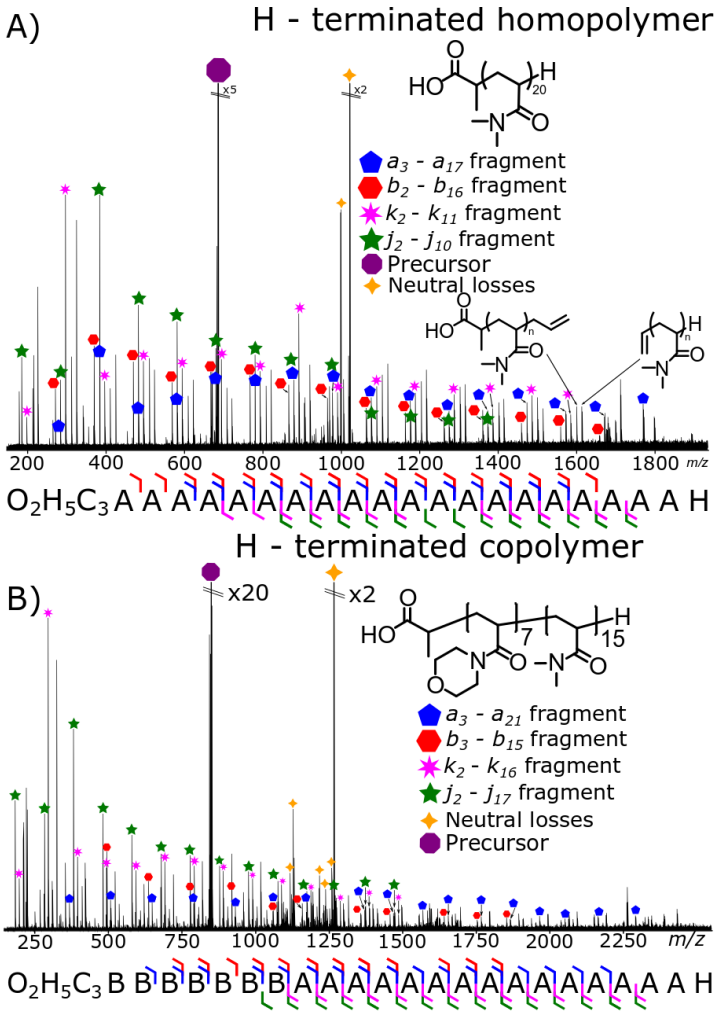

Figure 4.9 Radical dissociation of the A) hydrogen capped p(DMA) species. B) hydrogen capped copolymer species. Both spectra show that the trithiocarbonate is not required for fragmentation to occur.

The hydrogen capped polymers produce fragments with identical composition due to the fragments formed by hydrogen migration, *j* and *k* fragments, being indistinguishable from the ω terminus containing fragments, *y* and *z*. Fragmentation of the hydrogen capped NAM/DMA block copolymer produced near complete sequence coverage through the *a* fragment ion series and all fragment ion series covered the both monomer blocks allowing the total block size to be determined.

Analysis of the OH terminated p(NAM-*b*-DMA) by the same ECD method is shown in Figure 4.10. Sequence coverage is similar to those of the butyl-trithiocarbonate containing end group polymers showing that the butyl-trithiocarbonate group is not needed for the fragmentation of the acrylamide polymers, but the spectrum shows many more fragmentation channels, and overall lower intensity of fragmentation.

Dissociation of the hydroxyl capped block copolymer species showed the presence of *y* and *z* fragments. The *y* fragment series started at *m/z* 314.20740 (-0.1 ppm) and continued to y_{13} (*m/z* 1304.89079, (-0.6 ppm). The *z* fragment series started at z_3 (*m/z* 301.19989, -0.4 ppm) and continued to *m/z* 1291.88507 (z_{13}, 1 ppm). The presence of the *j* and *k* fragment series shows that secondary radical dissociation is occurring.

Internal *j* and *k* fragments (*m/z* 424.24409, $k(i)_3$, -0.2 ppm) were also present in the block copolymer dissociation again showing that further orders of dissociation are possible even without the presence of radical formation from the loss of a butyl-trithiocarbonate group.

Observation of fragments containing both termini of the polymer suggest that the radical capture was occurring across the polymer and fragmentation was occurring at every possible position. The presence of internal fragments show that higher order dissociation was still occurring even in species that didn't contain the butyl trithiocarbonate group.

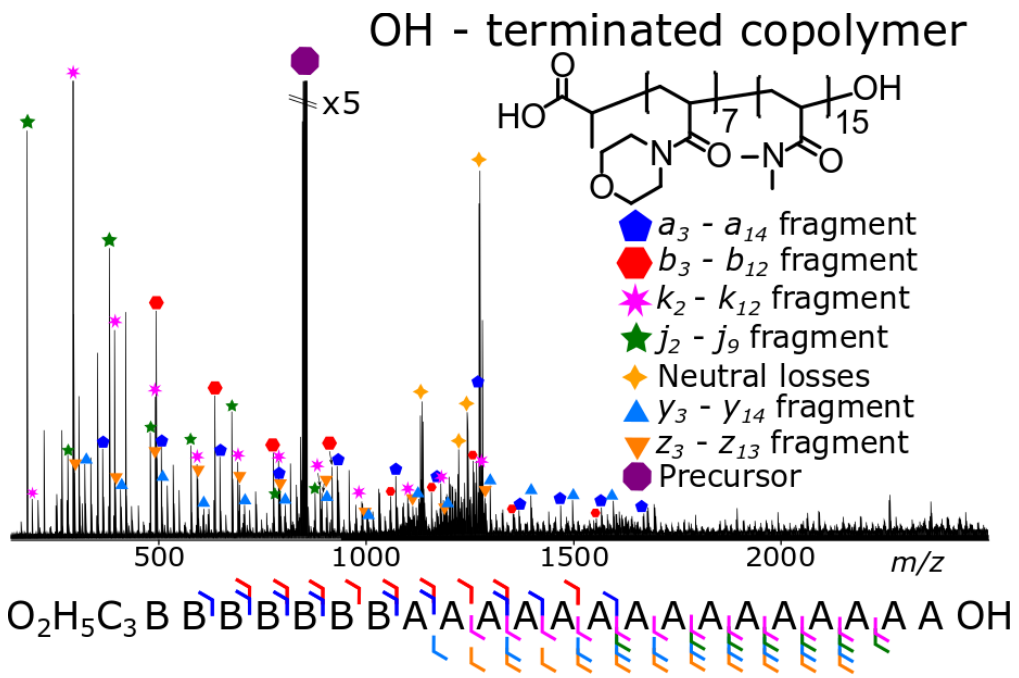

Figure 4.10 Fragmentation of the hydroxyl capped copolymer, with respective fragmentation diagram.

4.5. Conclusions

In conclusion, the formation of radicals through the loss of the butyl-trithiocarbonate group showed a form of radical directed dissociation which is previously unexplored in electron capture dissociation. Although dissociation could occur across the molecule, the presence of the butyl-trithiocarbonate group meant that initial dissociation occurred from the same point, showing mechanistic similarity to previous studies using radical directed UV dissociation.[41] The corresponding radical dissociation generated multiple fragment types of which some dissociated further, at least tertiary fragmentation could be observed aligning with a free radical cascade mechanism. The radical dissociation shown produced almost total sequence coverage across the copolymers analyzed. The fragmentation coverage of ECD consistently allowed effective analysis of the copolymer for end groups and overall block size.

4.6. References

(1) Keddie, D. J. A guide to the synthesis of block copolymers using reversible-addition fragmentation chain transfer (RAFT) polymerization *Chem. Soc. Rev.* **2014**, *43*, 496-505.
(2) Perrier, S. 50th Anniversary Perspective: RAFT Polymerization—A User Guide *Macromolecules* **2017**, *50*, 7433-7447.
(3) Ekladious, I.; Colson, Y. L.; Grinstaff, M. W. Polymer-drug conjugate therapeutics: advances, insights and prospects *Nat. Rev. Drug Discov.* **2019**, *18*, 273-294.
(4) Abu Lila, A. S.; Kiwada, H.; Ishida, T. The accelerated blood clearance (ABC) phenomenon: clinical challenge and approaches to manage *J. Controlled Release* **2013**, *172*, 38-47.
(5) Pelegri-O'Day, E. M.; Lin, E. W.; Maynard, H. D. Therapeutic protein-polymer conjugates: advancing beyond PEGylation *J. Am. Chem. Soc.* **2014**, *136*, 14323-14332.
(6) Palivan, C. G.; Goers, R.; Najer, A.; Zhang, X.; Car, A.; Meier, W. Bioinspired polymer vesicles and membranes for biological and medical applications *Chem. Soc. Rev.* **2016**, *45*, 377-411.
(7) Hamidi, M.; Shahbazi, M. A.; Rostamizadeh, K. Copolymers: efficient carriers for intelligent nanoparticulate drug targeting and gene therapy *Macromolecular Bioscience* **2012**, *12*, 144-164.
(8) Liechty, W. B.; Kryscio, D. R.; Slaughter, B. V.; Peppas, N. A. Polymers for drug delivery systems *Annual Review of Chemical and Biomolecular Engineering* **2010**, *1*, 149-173.
(9) Obermeyer, A. C.; Olsen, B. D. Synthesis and Application of Protein-Containing Block Copolymers *ACS Macro Letters* **2015**, *4*, 101-110.
(10) Ghosh, S.; Basu, S.; Thayumanavan, S. Simultaneous and Reversible Functionalization of Copolymers for Biological Applications *Macromolecules* **2006**, *39*, 5595-5597.
(11) Cobo, I.; Li, M.; Sumerlin, B. S.; Perrier, S. Smart hybrid materials by conjugation of responsive polymers to biomacromolecules *Nat. Mater.* **2015**, *14*, 143-159.
(12) Radke, W. Polymer separations by liquid interaction chromatography: principles - prospects - limitations *J. Chromatogr. A* **2014**, *1335*, 62-79.
(13) Baumgaertel, A.; Altuntaş, E.; Schubert, U. S. Recent developments in the detailed characterization of polymers by multidimensional chromatography *J. Chromatogr. A* **2012**, *1240*, 1-20.
(14) Altuntaş, E.; Schubert, U. S. "Polymeromics": Mass spectrometry based strategies in polymer science toward complete sequencing approaches: a review *Anal. Chim. Acta* **2014**, *808*, 56-69.
(15) Crotty, S.; Gerislioglu, S.; Endres, K. J.; Wesdemiotis, C.; Schubert, U. S. Polymer architectures via mass spectrometry and hyphenated techniques: A review *Anal. Chim. Acta* **2016**, *932*, 1-21.
(16) Hart-Smith, G. A review of electron-capture and electron-transfer dissociation tandem mass spectrometry in polymer chemistry *Anal. Chim. Acta* **2014**, *808*, 44-55.
(17) Crecelius, A. C.; Baumgaertel, A.; Schubert, U. S. Tandem mass spectrometry of synthetic polymers *J. Mass Spectrom.* **2009**, *44*, 1277-1286.
(18) Wesdemiotis, C.; Solak, N.; Polce, M. J.; Dabney, D. E.; Chaicharoen, K.; Katzenmeyer, B. C. Fragmentation pathways of polymer ions *Mass Spectrom. Rev.* **2011**, *30*, 523-559.
(19) Li, X.; Guo, L.; Casiano-Maldonado, M.; Zhang, D.; Wesdemiotis, C. Top-Down Multidimensional Mass Spectrometry Methods for Synthetic Polymer Analysis *Macromolecules* **2011**, *44*, 4555-4564.

(20) Crotty, S.; Weber, C.; Baumgaertel, A.; Fritz, N.; Altuntaş, E.; Kempe, K.; Schubert, U. S. Semi-automated multi-dimensional characterization of synthetic copolymers *Eur. Polym. J.* **2014**, *60*, 153-162.
(21) Favier, A.; Ladaviere, C.; Charreyre, M.-T.; Pichot, C. MALDI-TOF MS Investigation of the RAFT polymerisation of water-soluble acrylamide derivative *Macromolecules* **2004**, *37*, 2026-2034.
(22) Haler, J. R. N.; Far, J.; Aqil, A.; Claereboudt, J.; Tomczyk, N.; Giles, K.; Jerome, C.; De Pauw, E. Multiple Gas-Phase Conformations of a Synthetic Linear Poly(acrylamide) Polymer Observed Using Ion Mobility-Mass Spectrometry *J. Am. Soc. Mass. Spectrom.* **2017**, *28*, 2492-2499.
(23) Kendrick, E. A Mass Scale Based on CH2=: 14.0000 for High Resolution Mass Spectrometry of Organic Compounds *Anal. Chem.* **1963**, *35*, 2146-2154.
(24) Qi, Y.; Hempelmann, R.; Volmer, D. A. Two-dimensional mass defect matrix plots for mapping genealogical links in mixtures of lignin depolymerisation products *Anal. Bioanal. Chem.* **2016**, *408*, 4835-4843.
(25) Fouquet, T.; Sato, H. Extension of the Kendrick Mass Defect Analysis of Homopolymers to Low Resolution and High Mass Range Mass Spectra Using Fractional Base Units *Anal. Chem.* **2017**, *89*, 2682-2686.
(26) Fouquet, T.; Cody, R. B.; Sato, H. Capabilities of the remainders of nominal Kendrick masses and the referenced Kendrick mass defects for copolymer ions *J. Mass Spectrom.* **2017**, *52*, 618-624.
(27) Fouquet, T.; Nakamura, S.; Sato, H. MALDI SpiralTOF high-resolution mass spectrometry and Kendrick mass defect analysis applied to the characterization of poly(ethylene-co-vinyl acetate) copolymers *Rapid Commun. Mass Spectrom.* **2016**, *30*, 973-981.
(28) Fouquet, T.; Shimada, H.; Maeno, K.; Ito, K.; Ozeki, Y.; Kitagawa, S.; Ohtani, H.; Sato, H. High-resolution Kendrick Mass Defect Analysis of Poly(ethylene oxide)-based Non-ionic Surfactants and Their Degradation Products *J. Oleo Sci.* **2017**, *66*, 1061-1072.
(29) Fouquet, T. N. J.; Cody, R. B.; Ozeki, Y.; Kitagawa, S.; Ohtani, H.; Sato, H. On the Kendrick Mass Defect Plots of Multiply Charged Polymer Ions: Splits, Misalignments, and How to Correct Them *J. Am. Soc. Mass. Spectrom.* **2018**, *29*, 1611-1626.
(30) Morgan, T. E.; Ellacott, S. H.; Wootton, C. A.; Barrow, M. P.; Bristow, A. W. T.; Perrier, S.; O'Connor, P. B. Coupling Electron Capture Dissociation and the Modified Kendrick Mass Defect for Sequencing of a Poly(2-ethyl-2-oxazoline) Polymer *Anal. Chem.* **2018**, *90*, 11710-11715.
(31) Giordanengo, R.; Viel, S.; Hidalgo, M.; Allard-Breton, B.; Thevand, A.; Charles, L. Methylation of acidic moieties in poly(methyl methacrylate-co-methacrylic acid) copolymers for end-group characterization by tandem mass spectrometry *Rapid Commun. Mass Spectrom.* **2010**, *24*, 1941-1947.
(32) Nasioudis, A.; Heeren, R. M.; van Doormalen, I.; de Wijs-Rot, N.; van den Brink, O. F. Electrospray ionization tandem mass spectrometry of ammonium cationized polyethers *J. Am. Soc. Mass. Spectrom.* **2011**, *22*, 837-844.
(33) Girod, M.; Antoine, R.; Lemoine, J.; Dugourd, P.; Charles, L. End-group characterization of poly(styrene sulfonate sodium salt) by activated electron photo-detachment dissociation *Rapid Commun. Mass Spectrom.* **2011**, *25*, 3259-3266.
(34) Altuntaş, E.; Weber, C.; Schubert, U. S. Detailed characterization of poly(2-ethyl-2oxazoline)s by energy variable collision-induced dissociation study *Rapid Commun. Mass Spectrom.* **2013**, *27*, 1095-1100.
(35) Town, J. S.; Jones, G. R.; Haddleton, D. M. MALDI-LID-ToF/ToF analysis of statistical and diblock polyacrylate copolymers *Polymer Chemistry* **2018**, *9*, 4631-4641.

(36) Town, J. S.; Jones, G. R.; Hancox, E.; Shegiwal, A.; Haddleton, D. M. Tandem Mass Spectrometry for Polymeric Structure Analysis: A Comparison of Two Common MALDI-ToF/ToF Techniques *Macromol. Rapid Commun.* **2019**, 1900088-1900094.
(37) Polce, M. J.; Ocampo, M.; Quirk, R. P.; Wesdemiotis, C. Tandem Mass Spectrometry Characteristics of Silver-Cationized Polystyrenes: Backbone Degradation via Free Radical Chemistry *Anal. Chem.* **2008**, *2*, 347-354.
(38) Polce, M. J.; Ocampo, M.; Quirk, R. P.; Leigh, A. M.; Wesdemiotis, C. Tandem Mass Spectrometry Characteristics of Silver-Cationized Polystyrenes: Internal Energy, Size, and Chain End versus Backbone Substituent Effects *Anal. Chem.* **2008**, *80*, 355-362.
(39) Chaicharoen, K.; Polce, M. J.; Singh, A.; Pugh, C.; Wesdemiotis, C. Characterization of linear and branched polyacrylates by tandem mass spectrometry *Anal. Bioanal. Chem.* **2008**, *392*, 595-607.
(40) Ly, T.; Julian, R. R. Elucidating the tertiary structure of protein ions in vacuo with site specific photoinitiated radical reactions *J. Am. Chem. Soc.* **2010**, *132*, 8602-8609.
(41) Ly, T.; Julian, R. R. Residue-specific radical-directed dissociation of whole proteins in the gas phase *J. Am. Chem. Soc.* **2008**, *130*, 351-358.
(42) Cerda, B. A.; Breuker, K.; Horn, D. M.; McLafferty, F. W. Charge/Radical Site initiation versus coulombic repulsion for cleavage of multiply charged ions. Charge solvation in Poly(alkene glycol) ions *J. Am. Soc. Mass. Spectrom.* **2001**, *12*, 565-570.
(43) Koster, S.; Duursma, M. C.; Boon, J. J.; Heeren, R. M. A.; Ingemann, S.; Benthem, R. A. T. M.; Koster, C. G. Electron capture and collisionally activated dissociation mass spectrometry of doubly charged hyperbranched polyesteramides *J. Am. Soc. Mass. Spectrom.* **2003**, *14*, 332-341.
(44) Perez Hurtado, P.; Lam, P. Y.; Kilgour, D.; Bristow, A.; McBride, E.; O'Connor, P. B. Use of high resolution mass spectrometry for analysis of polymeric excipients in drug delivery formulations *Anal. Chem.* **2012**, *84*, 8579-8586.
(45) Wei, J.; Bristow, A.; McBride, E.; Kilgour, D.; O'Connor, P. B. D-alpha-tocopheryl polyethylene glycol 1000 succinate: a view from FTICR MS and tandem MS *Anal. Chem.* **2014**, *86*, 1567-1574.
(46) Leymarie, N.; Costello, C. E.; O'Connor, P. B. Electron Capture Dissociation Initiates a Free Radical Reaction Cascade *J. Am. Chem. Soc.* **2003**, *125*, 8949-8958.
(47) Breuker, K.; HanBin, O.; Lin, C.; Carpenter, B. K.; McLafferty, F. W. Nonergodic and conformational control of theelectron capture dissociation of protein cations *Proc. Natl. Acad. Sci. U.S.A* **2004**, *101*, 14011-14016.
(48) Tureček, F. N-C alpha Bond Dissociation Energies and Kinetics in Amide and Peptide Radicals. Is the Dissociation a Non-ergodic Process? *J. Am. Chem. Soc.* **2003**, *125*, 5954-5963.
(49) Zubarev, R. A.; Kelleher, N. L.; McLafferty, F. W. Electron Capture Dissocaition of Multiply Charged Protein Cations. A nonergodic Process *J. Am. Chem. Soc.* **1998**, *120*, 3265-3266.
(50) Moore, B. N.; Ly, T.; Julian, R. R. Radical conversion and migration in electron capture dissociation *J. Am. Chem. Soc.* **2011**, *133*, 6997-7006.
(51) Lin, C.; Cournoyer, J. J.; O'Connor, P. B. Use of a double resonance electron capture dissociation experiment to probe fragment intermediate lifetimes *J. Am. Soc. Mass. Spectrom.* **2006**, *17*, 1605-1615.
(52) Gauthier, J. W.; Trautman, T. R.; Jacobson, D. B. Sustained off-resonance irradiation for collision-activated dissociation involving Fourier transform mass spectrometry. Collision-activated dissociation technique that emulates infrared multiphoton dissociation *Anal. Chim. Acta* **1991**, *246*, 211-225.
(53) Asam, M. R.; Glish, G. L. Determination of the Dissociation Kinetics ofa Transient Intermediate *J. Am. Soc. Mass. Spectrom.* **1999**, *10*, 119-125.
(54) Anders, L. R.; Beauchamp, J. L.; Dunbar, R. C.; Baldeschwieler, J. D. Ion-Cyclotron Double Resonance *J. Chem. Phys.* **1966**, *45*, 1062-1063.

(55) Ferguson, J. C.; Hughes, R. J.; Nguyen, D.; Pham, B. T. T.; Gilbert, R. G.; Serelis, A. K.; Such, C. H.; Hawkett, B. S. Ab Initio Emulsion polymerization by RAFT-Controlled Self-Assembly *Macromolecules* **2005**, *38*, 2191-2204.
(56) Köster, C. United States, US 6188064 B1.2001.Bruker Daltonik GmbH (DE)
(57) Wootton, C. A.; Lam, Y. P. Y.; Willetts, M.; van Agthoven, M. A.; Barrow, M. P.; Sadler, P. J.; PB, O. C. Automatic assignment of metal-containing peptides in proteomic LC-MS and MS/MS data sets *Analyst* **2017**, *142*, 2029-2037.

SUPPORTING INFORMATION

to

Electron capture dissociation of trithiocarbonate terminated acrylamide homo- and co-polymers: An atom directed mechanism?

Tomos E. Morgan[1], Andrew Kerr[1], Christopher A. Wootton[1], Mark P. Barrow[1], Anthony W. T. Bristow[2], Sebastien Perrier[1], Peter B. O'Connor[1]*

[1]Department of Chemistry, University of Warwick, Coventry, Midlands, CV4 7AL, UK.

[2]Chemical Development, Pharmaceutical Technology & Development, Operations, AstraZeneca, Macclesfield, UK.

*Corresponding authors: Peter O'Connor [redacted]

N-N-dimethylacrylamide (DMA, Sigma Aldrich, 99%), and N-Acryloylmorpoline (NAM, Sigma Aldrich, 97%) were passed through a column of basic alumina prior to use. 1,4-dioxane (Fisher Scientific), dimethyl sulfoxide-d6 (Sigma Aldrich, 99.9% D atom), chloroform-d (Sigma Aldrich, 99.8% D atom), and 2,2'-azobis[2-(2-imidazolin-2-yl)propane]dihydrochloride (VA-044, >98%, Wako) were used as received. 2-(((butylthio)carbonothioyl)thio) propanoic acid (PABTC) was synthesised according to the literature procedure.1

SEC measurements in THF were performed on an Agilent Infinity II MDS instrument equipped with differential refractive index (DRI), viscometry (VS), dual angle light scatter (LS) and multiple wavelength UV detectors. The system was equipped with 2 x PLgel Mixed C columns (300 x 7.5 mm) and a PLgel 5 µm guard column. The eluent is THF with 2 % TEA (triethylamine) additive. Samples were run at 1ml/min at 30'C. Poly(methyl methacrylate standards (Agilent EasyVials) were used for calibration. Analyte samples were filtered through a GVHP membrane with 0.22 µm pore size before injection. Respectively, experimental molar mass (Mn,SEC) and dispersity (Đ) values of synthesized polymers were determined by conventional calibration using Agilent GPC/SEC software.

Synthesis of poly(DMA)22

Dimethylacrylamide (500 mg, 5.04 mmol), PABTC (40.1 mg, 0.168 mmol), VA-044 (0.5 mg, 1.68*10-3 mmol), 1,4-dioxane (232 µl) and deionised water (657 µl) were added to a 3 ml vial fitted with a stirrer bar and rubber septum. The reaction mixture was degassed under nitrogen for 15 minutes and placed in an oil bath heated to 70°C for 2h. A sample was taken to determine monomer conversion by NMR, after which the reaction mixture was concentrated under vacuum, redissolved in 1,4-dioxane and precipitated three times into ice cold diethyl ether. The solid was collected and dried in vacuum overnight at 40°C to yield a pale yellow powder.

SEC (THF) Mn = 1,730 g mol-1, Đ = 1.1

Synthesis of poly(NAM)8-b-(DMA)16

N-acryloylmorpholine (450 mg, 3.19 mmol), PABTC (95 mg, 0.398 mmol), VA-044 (0.3 mg, 1.06*10-3 mmol), 1,4-dioxane (132 µl) and deionised water (357 µl) were added to a 3 ml vial fitted with a stirrer bar and rubber septum. The reaction mixture was degassed under nitrogen for 15

minutes and placed in an oil bath heated to 70°C for 2h. A sample was taken to determine full consumption of monomer by NMR, and then a degassed solution of DMA (632 mg, 6.28 mmol), VA-044 (0.7 mg, 2.13*10-3 mmol) and deioinised water (300 µl) was added to the reaction mixture via syringe. The vial was heated at 70°C for a further 2h, after which the reaction mixture was concentrated under vacuum, redissolved in 1,4-dioxane and precipitated three times into ice cold diethyl ether. The solid was collected and dried in vacuum overnight at 40°C to yield a pale yellow powder.

Block 1 SEC (THF) Mn = 1,020 g mol-1, Đ = 1.17

Block 2 SEC (THF) Mn = 2,250 g mol-1, Đ = 1.11

Table S 4.1: MS assignment of the p(DMA); Figure 4.1A

m/z	charge	Chemical Composition	DMA units	error	Assignment
641.73407	3	$C_{93}H_{167}N_{17}O_{19}S_3H^+_3$	17	0.91	3^+ protonated
674.75652	3	$C_{98}H_{176}N_{18}O_{20}S_3H^+_3$	18	0.34	3^+ protonated
707.77910	3	$C_{103}H_{185}N_{19}O_{21}S_3H^+_3$	19	0.01	3^+ protonated
740.80185	3	$C_{108}H_{194}N_{20}O_{22}S_3H^+_3$	20	0.07	3^+ protonated
773.82453	3	$C_{113}H_{203}N_{21}O_{23}S_3H^+_3$	21	0.23	3^+ protonated
806.84773	3	$C_{118}H_{212}N_{22}O_{24}S_3H^+_3$	22	0.27	3^+ protonated
839.87045	3	$C_{123}H_{221}N_{23}O_{25}S_3H^+_3$	23	0.16	3^+ protonated
872.8935	3	$C_{128}H_{230}N_{24}O_{26}S_3H^+_3$	24	0.44	3^+ protonated
905.91639	3	$C_{133}H_{239}N_{25}O_{27}S_3H^+_3$	25	0.52	3^+ protonated
938.93881	3	$C_{138}H_{248}N_{26}O_{28}S_3H^+_3$	26	0.09	3^+ protonated
971.96191	3	$C_{143}H_{257}N_{27}O_{29}S_3H^+_3$	27	0.39	3^+ protonated
1004.98471	3	$C_{148}H_{266}N_{28}O_{30}S_3H^+_3$	28	0.37	3^+ protonated
1038.00731	3	$C_{153}H_{275}N_{29}O_{31}S_3H^+_3$	29	0.16	3^+ protonated
1071.03087	3	$C_{158}H_{284}N_{30}O_{32}S_3H^+_3$	30	0.86	3^+ protonated
1104.05270	3	$C_{163}H_{293}N_{31}O_{33}S_3H^+_3$	31	0.05	3^+ protonated
1137.07599	3	$C_{168}H_{302}N_{32}O_{34}S_3H^+_3$	32	0.38	3^+ protonated
679.69003	4	$C_{133}H_{239}N_{25}O_{27}S_3H^+_4$	25	1.87	4^+ protonated
679.68838	4	$C_{133}H_{239}N_{25}O_{27}S_3H^+_4$	25	0.56	4^+ protonated
704.45580	4	$C_{138}H_{248}N_{26}O_{28}S_3H^+_4$	26	0.09	4^+ protonated
729.22281	4	$C_{143}H_{257}N_{27}O_{29}S_3H^+_4$	27	0.22	4^+ protonated
753.98975	4	$C_{148}H_{266}N_{28}O_{30}S_3H^+_4$	28	0.43	4^+ protonated
778.75679	4	$C_{153}H_{275}N_{29}O_{31}S_3H^+_4$	29	0.50	4^+ protonated
803.52420	4	$C_{158}H_{284}N_{30}O_{32}S_3H^+_4$	30	0.10	4^+ protonated
828.29133	4	$C_{163}H_{293}N_{31}O_{33}S_3H^+_4$	31	0.06	4^+ protonated
853.05839	4	$C_{168}H_{302}N_{32}O_{34}S_3H^+_4$	32	0.11	4^+ protonated
877.82472	4	$C_{173}H_{311}N_{33}O_{35}S_3H^+_4$	33	0.99	4^+ protonated
902.59304	4	$C_{178}H_{320}N_{34}O_{36}S_3H^+_4$	34	0.38	4^+ protonated
927.35946	4	$C_{183}H_{329}N_{35}O_{37}S_3H^+_4$	35	0.36	4^+ protonated
952.12662	4	$C_{188}H_{338}N_{36}O_{38}S_3H^+_4$	36	0.29	4^+ protonated
976.89255	4	$C_{193}H_{347}N_{37}O_{39}S_3H^+_4$	37	1.49	4^+ protonated
1001.66108	4	$C_{198}H_{356}N_{38}O_{40}S_3H^+_4$	38	0.03	4^+ protonated
1026.42808	4	$C_{203}H_{365}N_{39}O_{41}S_3H^+_4$	39	0.13	4^+ protonated
1100.72846	4	$C_{218}H_{392}N_{42}O_{44}S_3H^+_4$	42	0.96	4^+ protonated
813.49418	2	$C_{78}H_{140}N_{14}O_{16}S_3H^+_2$	14	0.26	2^+ protonated
863.02844	2	$C_{83}H_{149}N_{15}O_{17}S_3H^+_2$	15	0.30	2^+ protonated
912.56296	2	$C_{88}H_{158}N_{16}O_{18}S_3H^+_2$	16	0.63	2^+ protonated
962.09708	2	$C_{93}H_{167}N_{17}O_{19}S_3H^+_2$	17	0.51	2^+ protonated
1011.63183	2	$C_{98}H_{176}N_{18}O_{20}S_3H^+_2$	18	1.02	2^+ protonated
1061.16435	2	$C_{103}H_{185}N_{19}O_{21}S_3H^+_2$	19	0.62	2^+ protonated
1110.70051	2	$C_{108}H_{194}N_{20}O_{22}S_3H^+_2$	20	1.17	2^+ protonated
1160.23485	2	$C_{113}H_{203}N_{21}O_{23}S_3H^+_2$	21	1.23	2^+ protonated
1209.76764	2	$C_{118}H_{212}N_{22}O_{24}S_3H^+_2$	22	0.01	2^+ protonated
1308.83978	2	$C_{128}H_{230}N_{24}O_{26}S_3H^+_2$	24	2.86	2^+ protonated

m/z	charge	Chemical Composition	DMA units	error	Assignment
781.71912	5	$C_{193}H_{347}N_{37}O_{39}S_3H^+_5$	37	3.15	5^+ protonated
781.7161	5	$C_{193}H_{347}N_{37}O_{39}S_3H^+_5$	37	0.71	5^+ protonated
801.52944	5	$C_{198}H_{356}N_{38}O_{40}S_3H^+_5$	38	1.12	5^+ protonated
920.41072	5	$C_{228}H_{410}N_{44}O_{46}S_3H^+_5$	44	1.87	5^+ protonated
833.78814	4	$C_{163}H_{293}N_{31}O_{33}S_3H^+_3$	31	1.52	3^+ singly sodiated
946.26418	3	$C_{138}H_{248}N_{26}O_{28}S_3H^+_2$	26	1.97	2^+ singly sodiated
847.19583	3	$C_{123}H_{221}N_{23}O_{25}S_3H^+_2$	23	2.12	2^+ singly sodiated
			Average	0.71	
			Std dev	1.0	

Table S 4.2: MS assignment of the p(NAM-b-DMA); Figure 4.1B

m/z	charge	NAM	DMA	Chemical Composition	Error (ppm)
749.78759	3	3	15	$C_{109}H_{191}N_{19}O_{24}S_3H^+_3$	-2.76
782.81164	3	3	16	$C_{114}H_{200}N_{20}O_{25}S_3H^+_3$	-1.05
815.83405	3	3	17	$C_{119}H_{209}N_{21}O_{26}S_3H^+_3$	-1.49
881.87891	3	3	18	$C_{129}H_{227}N_{23}O_{28}S_3H^+_3$	-2.23
914.90319	3	3	20	$C_{134}H_{236}N_{24}O_{29}S_3H^+_3$	-0.54
796.81504	3	3	21	$C_{116}H_{202}N_{20}O_{26}S_3H^+_3$	-1.19
829.83842	3	4	16	$C_{121}H_{211}N_{21}O_{27}S_3H^+_3$	-0.45
862.86089	3	4	17	$C_{126}H_{220}N_{22}O_{28}S_3H^+_3$	-0.82
895.88493	3	4	18	$C_{131}H_{229}N_{23}O_{29}S_3H^+_3$	0.59
961.92955	3	4	19	$C_{141}H_{247}N_{25}O_{31}S_3H^+_3$	-0.48
994.95256	3	4	21	$C_{146}H_{256}N_{26}O_{32}S_3H^+_3$	-0.26
777.79552	3	5	14	$C_{113}H_{195}N_{19}O_{26}S_3H^+_3$	-1.52
810.81899	3	5	15	$C_{118}H_{204}N_{20}O_{27}S_3H^+_3$	-0.64
843.84218	3	5	16	$C_{123}H_{213}N_{21}O_{28}S_3H^+_3$	-0.16
876.86542	3	5	17	$C_{128}H_{222}N_{22}O_{29}S_3H^+_3$	0.35
909.88861	3	5	18	$C_{133}H_{231}N_{23}O_{30}S_3H^+_3$	0.76
942.91039	3	5	19	$C_{138}H_{240}N_{24}O_{31}S_3H^+_3$	-0.36
975.93620	3	5	20	$C_{143}H_{249}N_{25}O_{32}S_3H^+_3$	2.73
1008.95620	3	5	21	$C_{148}H_{258}N_{26}O_{33}S_3H^+_3$	-0.13
939.52585	2	6	8	$C_{90}H_{152}N_{14}O_{22}S_3H^+_2$	0.20
989.06010	2	6	9	$C_{95}H_{161}N_{15}O_{23}S_3H^+_2$	0.23
1038.59368	2	6	10	$C_{100}H_{170}N_{16}O_{24}S_3H^+_2$	-0.38
1088.13030	2	6	12	$C_{105}H_{179}N_{17}O_{25}S_3H^+_2$	1.85
1187.19999	2	6	13	$C_{115}H_{197}N_{19}O_{27}S_3H^+_2$	2.77
1236.73096*	2	6	14	$C_{120}H_{206}N_{20}O_{28}S_3H^+_2$	0.04
824.82258	3	6	14	$C_{120}H_{206}N_{20}O_{28}S_3H^+_3$	-0.54
1286.26487	2	6	15	$C_{125}H_{215}N_{21}O_{29}S_3H^+_2$	-0.19
857.84550	3	6	15	$C_{125}H_{215}N_{21}O_{29}S_3H^+_3$	-0.39
923.89158	3	6	17	$C_{135}H_{233}N_{23}O_{31}S_3H^+_3$	0.15
956.91384	3	6	18	$C_{140}H_{242}N_{24}O_{32}S_3H^+_3$	-0.43
1022.95983*	3	6	19	$C_{150}H_{260}N_{26}O_{34}S_3H^+_3$	-0.03

m/z	charge	NAM	DMA	Chemical Composition	Error (ppm)
1055.98256	3	6	20	$C_{155}H_{269}N_{27}O_{35}S_3H^+_3$	-0.10
1010.06564	2	7	8	$C_{97}H_{163}N_{15}O_{24}S_3H^+_2$	0.48
1059.59978	2	7	9	$C_{102}H_{172}N_{16}O_{25}S_3H^+_2$	0.40
1109.13539	2	7	10	$C_{107}H_{181}N_{17}O_{26}S_3H^+_2$	1.64
772.77939	3	7	11	$C_{112}H_{190}N_{18}O_{27}S_3H^+_3$	-2.01
1208.20363	2	7	12	$C_{117}H_{199}N_{19}O_{28}S_3H^+_2$	1.36
805.80286	3	7	12	$C_{117}H_{199}N_{19}O_{28}S_3H^+_3$	-1.10
1257.73551	2	7	13	$C_{122}H_{208}N_{20}O_{29}S_3H^+_2$	-0.54
838.82573	3	7	13	$C_{122}H_{208}N_{20}O_{29}S_3H^+_3$	-0.98
871.84749	3	7	14	$C_{127}H_{217}N_{21}O_{30}S_3H^+_3$	-2.14
904.86961	3	7	15	$C_{132}H_{226}N_{22}O_{31}S_3H^+_3$	-2.82
937.89464	3	7	16	$C_{137}H_{235}N_{23}O_{32}S_3H^+_3$	-0.35
970.91772*	3	7	17	$C_{142}H_{244}N_{24}O_{33}S_3H^+_3$	-0.05
1003.94036	3	7	18	$C_{147}H_{253}N_{25}O_{34}S_3H^+_3$	-0.21
1036.96273	3	7	19	$C_{152}H_{262}N_{26}O_{35}S_3H^+_3$	-0.63
1069.98641	3	7	20	$C_{157}H_{271}N_{27}O_{36}S_3H^+_3$	0.21
1103.01105	3	7	21	$C_{162}H_{280}N_{28}O_{37}S_3H^+_3$	1.87
1080.60391	2	8	7	$C_{104}H_{174}N_{16}O_{26}S_3H^+_2$	-0.68
1130.14125	2	8	8	$C_{109}H_{183}N_{17}O_{27}S_3H^+_2$	2.12
1229.20933	2	8	9	$C_{119}H_{201}N_{19}O_{29}S_3H^+_2$	1.68
1278.74194	2	8	10	$C_{124}H_{210}N_{20}O_{30}S_3H^+_2$	0.37
885.85242	3	8	12	$C_{129}H_{219}N_{21}O_{31}S_3H^+_3$	-0.52
918.87598	3	8	13	$C_{134}H_{228}N_{22}O_{32}S_3H^+_3$	0.32
951.89718	3	8	14	$C_{139}H_{237}N_{23}O_{33}S_3H^+_3$	-1.37
984.92172	3	8	15	$C_{144}H_{246}N_{24}O_{34}S_3H^+_3$	0.44
1017.94518	3	8	16	$C_{149}H_{255}N_{25}O_{35}S_3H^+_3$	1.07
1083.98909	3	8	17	$C_{159}H_{273}N_{27}O_{37}S_3H^+_3$	-0.57
1150.03274	3	8	18	$C_{169}H_{291}N_{29}O_{39}S_3H^+_3$	-2.24
1183.05727	3	8	19	$C_{174}H_{300}N_{30}O_{40}S_3H^+_3$	-0.72
1216.08101	3	8	20	$C_{179}H_{309}N_{31}O_{41}S_3H^+_3$	0.07
912.31315	4	8	21	$C_{179}H_{309}N_{31}O_{41}S_3H^+_4$	0.70
947.05020	2	8	22	$C_{91}H_{157}N_{15}O_{21}S_3H^+_2$	0.94
996.58392	2	8	23	$C_{96}H_{166}N_{16}O_{22}S_3H^+_2$	0.41
937.07851	4	8	23	$C_{184}H_{318}N_{32}O_{42}S_3H^+_4$	-1.18
1046.11887	2	8	24	$C_{101}H_{175}N_{17}O_{23}S_3H^+_2$	1.10
961.84642	4	8	24	$C_{189}H_{327}N_{33}O_{43}S_3H^+_4$	-0.31
1095.65020	2	8	25	$C_{106}H_{184}N_{18}O_{24}S_3H^+_2$	-1.58
1011.38274	4	8	25	$C_{199}H_{345}N_{35}O_{45}S_3H^+_4$	1.79
852.82848	3	8	26	$C_{124}H_{210}N_{20}O_{30}S_3H^+_3$	-1.87
913.86070	3	8	26	$C_{133}H_{223}N_{21}O_{33}S_3H^+_3$	0.85
1200.68085	2	9	8	$C_{116}H_{194}N_{18}O_{29}S_3H^+_2$	2.09
1250.21425	2	9	9	$C_{121}H_{203}N_{19}O_{30}S_3H^+_2$	1.36
1299.74703	2	9	10	$C_{126}H_{212}N_{20}O_{31}S_3H^+_2$	0.21
847.97910	2	9	11	$C_{81}H_{139}N_{13}O_{19}S_3H^+_2$	-2.11
866.83433	3	9	11	$C_{126}H_{212}N_{20}O_{31}S_3H^+_3$	0.85

m/z	charge	NAM	DMA	Chemical Composition	Error (ppm)
899.85643*	3	9	12	$C_{131}H_{221}N_{21}O_{32}S_3H^+_3$	0.03
932.87999	3	9	13	$C_{136}H_{230}N_{22}O_{33}S_3H^+_3$	0.84
965.90216	3	9	14	$C_{141}H_{239}N_{23}O_{34}S_3H^+_3$	0.16
998.92571	3	9	15	$C_{146}H_{248}N_{24}O_{35}S_3H^+_3$	0.90
1031.94896	3	9	16	$C_{151}H_{257}N_{25}O_{36}S_3H^+_3$	1.30
1064.96947	3	9	17	$C_{156}H_{266}N_{26}O_{37}S_3H^+_3$	-0.89
1097.99406	3	9	18	$C_{161}H_{275}N_{27}O_{38}S_3H^+_3$	0.76
1131.01774	3	9	19	$C_{166}H_{284}N_{28}O_{39}S_3H^+_3$	1.51
1164.03776	3	9	20	$C_{171}H_{293}N_{29}O_{40}S_3H^+_3$	-0.92
1197.06192	3	9	21	$C_{176}H_{302}N_{30}O_{41}S_3H^+_3$	0.23
1230.08143	3	9	22	$C_{181}H_{311}N_{31}O_{42}S_3H^+_3$	-2.45
1263.11104	3	9	23	$C_{186}H_{320}N_{32}O_{43}S_3H^+_3$	3.00
716.76403	3	10	9	$C_{104}H_{182}N_{18}O_{23}S_3H^+_3$	-3.94
946.88356	3	10	11	$C_{138}H_{232}N_{22}O_{34}S_3H^+_3$	0.88
979.90561	3	10	12	$C_{143}H_{241}N_{23}O_{35}S_3H^+_3$	0.08
1012.92869	3	10	13	$C_{148}H_{250}N_{24}O_{36}S_3H^+_3$	0.35
1045.9514	3	10	14	$C_{153}H_{259}N_{25}O_{37}S_3H^+_3$	0.25
1078.9751	3	10	15	$C_{158}H_{268}N_{26}O_{38}S_3H^+_3$	1.07
1111.99879	3	10	16	$C_{163}H_{277}N_{27}O_{39}S_3H^+_3$	1.84
1145.0185	3	10	17	$C_{168}H_{286}N_{28}O_{40}S_3H^+_3$	-0.92
1178.0413	3	10	18	$C_{173}H_{295}N_{29}O_{41}S_3H^+_3$	-0.90
1211.06537	3	10	19	$C_{178}H_{304}N_{30}O_{42}S_3H^+_3$	0.17
1244.09265	3	10	20	$C_{183}H_{313}N_{31}O_{43}S_3H^+_3$	3.76
1277.11273	3	10	21	$C_{188}H_{322}N_{32}O_{44}S_3H^+_3$	1.53
791.79888	3	10	22	$C_{115}H_{197}N_{19}O_{27}S_3H^+_3$	-1.70
927.86221	3	11	10	$C_{135}H_{225}N_{21}O_{34}S_3H^+_3$	-1.33
960.88669	3	11	11	$C_{140}H_{234}N_{22}O_{35}S_3H^+_3$	0.46
993.90947	3	11	12	$C_{145}H_{243}N_{23}O_{36}S_3H^+_3$	0.42
1026.93292	3	11	13	$C_{150}H_{252}N_{24}O_{37}S_3H^+_3$	1.04
1059.95629	3	11	14	$C_{155}H_{261}N_{25}O_{38}S_3H^+_3$	1.54
1092.97668	3	11	15	$C_{160}H_{270}N_{26}O_{39}S_3H^+_3$	-0.72
1126.00391	3	11	16	$C_{165}H_{279}N_{27}O_{40}S_3H^+_3$	3.23
1159.02251	3	11	17	$C_{170}H_{288}N_{28}O_{41}S_3H^+_3$	-0.49
1192.04501	3	11	18	$C_{175}H_{297}N_{29}O_{42}S_3H^+_3$	-0.73
1291.11300	3	11	20	$C_{190}H_{324}N_{32}O_{45}S_3H^+_3$	-1.00
974.88910	3	12	10	$C_{142}H_{236}N_{22}O_{36}S_3H^+_3$	-0.69
1007.91256	3	12	11	$C_{147}H_{245}N_{23}O_{37}S_3H^+_3$	-0.01
1073.95772	3	12	12	$C_{157}H_{263}N_{25}O_{39}S_3H^+_3$	-0.43
1106.98336	3	12	13	$C_{162}H_{272}N_{26}O_{40}S_3H^+_3$	2.14
1140.00269	3	12	14	$C_{167}H_{281}N_{27}O_{41}S_3H^+_3$	-0.97
1173.03219	3	12	15	$C_{172}H_{290}N_{28}O_{42}S_3H^+_3$	4.77
1120.98700	3	13	13	$C_{164}H_{274}N_{26}O_{41}S_3H^+_3$	2.22
1154.00907	3	13	14	$C_{169}H_{283}N_{27}O_{42}S_3H^+_3$	1.52
1187.03283	3	13	15	$C_{174}H_{292}N_{28}O_{43}S_3H^+_3$	2.29
1220.05348	3	13	16	$C_{179}H_{301}N_{29}O_{44}S_3H^+_3$	0.46

m/z	charge	NAM	DMA	Chemical Composition	Error (ppm)
1253.07753	3	13	17	$C_{184}H_{310}N_{30}O_{45}S_3H^+_3$	1.44
1286.09746	3	13	18	$C_{189}H_{319}N_{31}O_{46}S_3H^+_3$	-0.83

Table S 4.3: ECD assignments of the p(DMA); Figure 4.3

m/z	charge	Chemical Composition	Error (ppm)	assignment
371.24129	1	$C_{18}H_{32}N_3O_5S_0H^+_1$	-0.49	b_3
470.30970	1	$C_{23}H_{41}N_4O_6S_0H^+_1$	-0.40	b_4
569.37810	1	$C_{28}H_{50}N_5O_7S_0H^+_1$	-0.35	b_5
668.44652	1	$C_{33}H_{59}N_6O_8S_0H^+_1$	-0.29	b_6
767.51530	1	$C_{38}H_{68}N_7O_9S_0H^+_1$	0.22	b_7
866.58342	1	$C_{43}H_{77}N_8O_{10}S_0H^+_1$	-0.14	b_8
965.65182	1	$C_{48}H_{86}N_9O_{11}S_0H^+_1$	-0.14	b_9
1064.72024	1	$C_{53}H_{95}N_{10}O_{12}S_0H^+_1$	-0.12	b_{10}
1163.78818	1	$C_{58}H_{104}N_{11}O_{13}S_0H^+_1$	-0.52	b_{11}
1262.85724	1	$C_{63}H_{113}N_{12}O_{14}S_0H^+_1$	0.03	b_{12}
1361.92536	1	$C_{68}H_{122}N_{13}O_{15}S_0H^+_1$	-0.18	b_{13}
1560.06286	1	$C_{78}H_{140}N_{15}O_{17}S_0H^+_1$	0.27	b_{14}
1659.13036	1	$C_{83}H_{149}N_{16}O_{18}S_0H^+_1$	-0.30	b_{15}
1758.19902	1	$C_{88}H_{158}N_{17}O_{19}S_0H^+_1$	-0.14	b_{16}
1857.26790	1	$C_{93}H_{167}N_{18}O_{20}S_0H^+_1$	0.12	b_{17}
1956.33745	1	$C_{98}H_{176}N_{19}O_{21}S_0H^+_1$	0.69	b_{18}
2055.40395	1	$C_{103}H_{185}N_{20}O_{22}S_0H^+_1$	-0.27	b_{19}
2154.47417	1	$C_{108}H_{194}N_{21}O_{23}S_0H^+_1$	0.58	b_{20}
285.18079	1	$C_{14}H_{24}N_2O_4S_0H^+_1$	-0.33	a_2
384.24917	1	$C_{19}H_{33}N_3O_5S_0H^+_1$	-0.33	a_3
483.31757	1	$C_{24}H_{42}N_4O_6S_0H^+_1$	-0.29	a_4
582.38589	1	$C_{29}H_{51}N_5O_7S_0H^+_1$	-0.40	a_5
681.45460	1	$C_{34}H_{60}N_6O_8S_0H^+_1$	0.09	a_6*
780.52287	1	$C_{39}H_{69}N_7O_9S_0H^+_1$	-0.11	a_7
879.59156	1	$C_{44}H_{78}N_8O_{10}S_0H^+_1$	0.22	a_8
978.66014	1	$C_{49}H_{87}N_9O_{11}S_0H^+_1$	0.37	a_{10}
1176.79471	1	$C_{59}H_{105}N_{11}O_{13}S_0H^+_1$	-1.61	a_{12}
1275.86497	1	$C_{64}H_{114}N_{12}O_{14}S_0H^+_1$	-0.04	a_{13}*
1374.93286	1	$C_{69}H_{123}N_{13}O_{15}S_0H^+_1$	-0.42	a_{14}
1573.06819	1	$C_{79}H_{141}N_{15}O_{17}S_0H^+_1$	-1.32	a_{16}
1672.13615	1	$C_{84}H_{150}N_{16}O_{18}S_0H^+_1$	-1.51	a_{17}
1771.20407	1	$C_{89}H_{159}N_{17}O_{19}S_0H^+_1$	-1.71	a_{18}
1870.27147	1	$C_{94}H_{168}N_{18}O_{20}S_0H^+_1$	-2.16	a_{19}
1969.34336	1	$C_{99}H_{177}N_{19}O_{21}S_0H^+_1$	-0.28	a_{20}
2068.40868	1	$C_{104}H_{186}N_{20}O_{22}S_0H^+_1$	-1.77	a_{21}
2167.48100	1	$C_{109}H_{195}N_{21}O_{23}S_0H^+_1$	0.12	a_{22}*
2266.55137	1	$C_{114}H_{204}N_{22}O_{24}S_0H^+_1$	0.97	a_{23}
199.144060	1	$C_{10}H_{18}N_2O_2S_0H^+_1$	-0.22	k_2*

m/z	charge	Chemical Composition	Error (ppm)	assignment
298.21240	1	$C_{15}H_{27}N_3O_3S_0H^+_1$	-0.40	k_3
397.28076	1	$C_{20}H_{36}N_4O_4S_0H^+_1$	-0.43	k_4
496.34912	1	$C_{25}H_{45}N_5O_5S_0H^+_1$	-0.46	k_5
595.41760	1	$C_{30}H_{54}N_6O_6S_0H^+_1$	-0.27	k_6
694.48603	1	$C_{35}H_{63}N_7O_7S_0H^+_1$	-0.21	k_7
793.55478	1	$C_{40}H_{72}N_8O_8S_0H^+_1$	0.24	k_8
892.62278	1	$C_{45}H_{81}N_9O_9S_0H^+_1$	-0.25	k_9
991.69129	1	$C_{50}H_{90}N_{10}O_{10}S_0H^+_1$	-0.13	k_{10}
1288.89582	1	$C_{65}H_{117}N_{13}O_{13}S_0H^+_1$	-0.65	k_{13}
1387.96442	1	$C_{70}H_{126}N_{14}O_{14}S_0H^+_1$	-0.47	k_{14}
1487.03252	1	$C_{75}H_{135}N_{15}O_{15}S_0H^+_1$	-0.65	k_{15}
1586.10278	1	$C_{80}H_{144}N_{16}O_{16}S_0H^+_1$	0.56	k_{16}
1883.30806	1	$C_{95}H_{171}N_{19}O_{19}S_0H^+_1$	0.49	k_{19}
1982.37421	1	$C_{100}H_{180}N_{20}O_{20}S_0H^+_1$	-0.68	k_{20}
2081.43669	1	$C_{105}H_{189}N_{21}O_{21}S_0H^+_1$	-3.50	k_{21}
186.13624	1	$C_9H_{17}N_2O_2S_0H^+_1$	-0.21	j_2
285.20460	1	$C_{14}H_{26}N_3O_3S_0H^+_1$	-0.33	j_3
384.27293	1	$C_{19}H_{35}N_4O_4S_0H^+_1$	-0.46	j_4
483.34134	1	$C_{24}H_{44}N_5O_5S_0H^+_1$	-0.37	j_5
582.40977	1	$C_{29}H_{53}N_6O_6S_0H^+_1$	-0.28	j_6
681.47818	1	$C_{34}H_{62}N_7O_7S_0H^+_1$	-0.25	j_7
780.54653	1	$C_{39}H_{71}N_8O_8S_0H^+_1$	-0.30	j_8
879.61511	1	$C_{44}H_{80}N_9O_9S_0H^+_1$	-0.08	j_9
978.68401	1	$C_{49}H_{89}N_{10}O_{10}S_0H^+_1$	0.43	j_{10}
270.18115	1	$C_{13}H_{23}N_3O_3S_0H^+_1$	-0.25	
369.24964	1	$C_{18}H_{32}N_4O_4S_0H^+_1$	0.02	
468.31798	1	$C_{23}H_{41}N_5O_5S_0H^+_1$	-0.14	
567.38635	1	$C_{28}H_{50}N_6O_6S_0H^+_1$	-0.19	
		Average error (ppm)	0.78	
		Std dev error (ppm)	1.1	

Table S 4.4: Neutral losses from Charge reduced species of p(DMA); Figure 4.3

m/z	charge	Chemical Composition	Error (ppm)	Loss
872.8919	3	$C_{128}H_{230}N_{24}O_{26}S_3H^+_3$	-1.40	Charge reduced
1308.33207	2	$C_{128}H_{228}N_{24}O_{26}S_3H^+_3$	0.17	-2H
1301.32509	2	$C_{127}H_{226}N_{24}O_{26}S_3H^+_3$	0.82	$-CH_3$-H
1286.81106	2	$C_{126}H_{223}N_{23}O_{26}S_3H^+_3$	0.24	C_2H_6N-H
1279.29828	2	$C_{125}H_{220}N_{23}O_{26}S_3H^+_3$	-0.58	C_2H_6N-CH_3-H
1272.81284	2	$C_{125}H_{223}N_{23}O_{25}S_3H^+_3$	-0.36	C_3H_6NO-H
1266.80612	2	$C_{123}H_{221}N_{24}O_{25}S_3H^+_3$	-0.70	C_4H_9-CO
1264.28174	2	$C_{124}H_{216}N_{22}O_{26}S_3H^+_3$	-0.29	2 x C_2H_6N
1258.27347	2	$C_{122}H_{214}N_{23}O_{26}S_3H^+_3$	-1.65	C_4H_9-C_2H_6N-H
1250.78691	2	$C_{123}H_{217}N_{22}O_{25}S_3H^+_3$	-1.10	C_3H_6NO-C_2H_6N-H
1244.27755	2	$C_{121}H_{214}N_{23}O_{25}S_3H^+_3$	-0.43	C_4H_9-C_3H_6NO-H
1242.32968	2	$C_{123}H_{220}N_{24}O_{26}S_1H^+_3$	0.74	$C_5H_9S_2$-H
1226.34329	2	$C_{123}H_{220}N_{24}O_{26}S_0H^+_3$	0.69	$C_5H_9S_3$-H
1219.79906	2	$C_{121}H_{213}N_{23}O_{26}S_1H^+_3$	-0.41	C_2H_6N $C_5H_9S_2$ -2H
1203.81356	2	$C_{121}H_{213}N_{23}O_{26}S_0H^+_3$	0.03	$C_5H_9S_3$-C_2H_6N-2H
1197.27138	2	$C_{119}H_{206}N_{22}O_{26}S_1H^+_3$	0.62	$C_5H_9S_2$- 2 x C_2H_6N -3H
1189.81564	2	$C_{120}H_{213}N_{23}O_{25}S_0H^+_3$	-0.36	C_3H_6NO - $C_5H_9S_3$ - 2H
1181.28668	2	$C_{119}H_{206}N_{22}O_{26}S_0H^+_3$	1.76	$C_5H_9S_3$ - 2xC_2H_6N -2H
1167.28877	2	$C_{118}H_{206}N_{22}O_{25}S_0H^+_3$	1.40	C_3H_6NO - $C_5H_9S_3$ - C_2H_6N - 3H
1158.75827	2	$C_{117}H_{199}N_{21}O_{26}S_0H^+_3$	2.24	C_3H_6NO - $C_5H_9S_3$ -2 x C_2H_6N - 3H
1133.27522	2	$C_{114}H_{202}N_{22}O_{24}S_0H^+_3$	0.81	$C_{14}H_{25}N_2O_2S_3$ - 3H

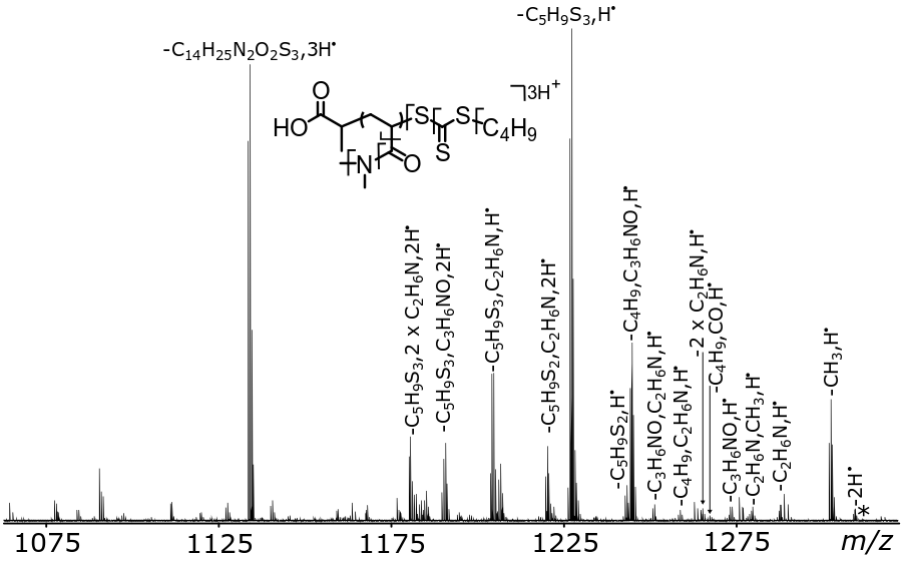

Figure S 4.1 Zoomed region of the neutral losses from the charged reduced species of p(DMA).

Table S 4.5: ECD assignments of p(NAM-b-DMA), Figure 4.7.

m/z	charge	chemical composition	error	assignment
369.20197	1	$C_{18}H_{28}N_2O_6S_0H^+_1$	-0.12	a_3
510.28081	1	$C_{25}H_{39}N_3O_8S_0H^+_1$	-0.36	a_4
651.36001	1	$C_{32}H_{50}N_4O_{10}S_0H^+_1$	0.06	a_5
792.43903	1	$C_{39}H_{61}N_5O_{12}S_0H^+_1$	0.10	a_6
933.51777	1	$C_{46}H_{72}N_6O_{14}S_0H^+_1$	-0.17	a_8
1074.59691	1	$C_{53}H_{83}N_7O_{16}S_0H^+_1$	0.00	a_9
1173.66524	1	$C_{58}H_{92}N_8O_{17}S_0H^+_1$	-0.07	a_{10}
1371.80226	1	$C_{68}H_{110}N_{10}O_{19}S_0H^+_1$	0.08	a_{12}
1470.87025	1	$C_{73}H_{119}N_{11}O_{20}S_0H^+_1$	-0.21	a_{13}
1569.93595	1	$C_{78}H_{128}N_{12}O_{21}S_0H^+_1$	-1.93	a_{14}
1669.00393	1	$C_{83}H_{137}N_{13}O_{22}S_0H^+_1$	-2.07	a_{15}
1768.07334	1	$C_{88}H_{146}N_{14}O_{23}S_0H^+_1$	-1.39	a_{16}
1867.14111	1	$C_{93}H_{155}N_{15}O_{24}S_0H^+_1$	-1.66	a_{17}
1966.21097	1	$C_{98}H_{164}N_{16}O_{25}S_0H^+_1$	-0.84	a_{18}
2065.28066	1	$C_{103}H_{173}N_{17}O_{26}S_0H^+_1$	-0.19	a_{19}*
2164.34664	1	$C_{108}H_{182}N_{18}O_{27}S_0H^+_1$	-1.30	a_{20}
2263.41355	1	$C_{113}H_{191}N_{19}O_{28}S_0H^+_1$	-1.91	a_{21}
2362.48869	1	$C_{118}H_{200}N_{20}O_{29}S_0H^+_1$	1.02	a_{22}
497.27304	1	$C_{24}H_{38}N_3O_8S_0H^+_1$	-0.25	b_3
638.35211	1	$C_{31}H_{49}N_4O_{10}S_0H^+_1$	-0.06	b_4
779.43076	1	$C_{38}H_{60}N_5O_{12}S_0H^+_1$	-0.47	b_5
920.51045	1	$C_{45}H_{71}N_6O_{14}S_0H^+_1$	0.38	b_6
1061.58914	1	$C_{52}H_{82}N_7O_{16}S_0H^+_1$	0.06	b_7
1160.65906	1	$C_{57}H_{91}N_8O_{17}S_0H^+_1$	1.35	b_8
1259.72376	1	$C_{62}H_{100}N_9O_{18}S_0H^+_1$	-1.71	b_9
1457.86296	1	$C_{72}H_{118}N_{11}O_{20}S_0H^+_1$	0.15	b_{11}
1556.92961	1	$C_{77}H_{127}N_{12}O_{21}S_0H^+_1$	-0.99	b_{12}
1656.00028	1	$C_{82}H_{136}N_{13}O_{22}S_0H^+_1$	0.43	b_{13}
1755.06654	1	$C_{87}H_{145}N_{14}O_{23}S_0H^+_1$	-0.82	b_{14}
1854.13648	1	$C_{92}H_{154}N_{15}O_{24}S_0H^+_1$	0.05	b_{15}*
1953.20463	1	$C_{97}H_{163}N_{16}O_{25}S_0H^+_1$	-0.09	b_{16}
2052.26855	1	$C_{102}H_{172}N_{17}O_{26}S_0H^+_1$	-2.28	b_{17}
2151.33685	1	$C_{107}H_{181}N_{18}O_{27}S_0H^+_1$	-2.22	b_{18}
2250.40997	1	$C_{112}H_{190}N_{19}O_{28}S_0H^+_1$	-0.03	b_{19}
186.13622	1	$C_9H_{17}N_2O_2S_0H^+_1$	-0.32	j_2
285.20465	1	$C_{14}H_{26}N_3O_3S_0H^+_1$	-0.15	j_3
384.27303	1	$C_{19}H_{35}N_4O_4S_0H^+_1$	-0.20	j_4
483.34143	1	$C_{24}H_{44}N_5O_5S_0H^+_1$	-0.19	j_5
582.40981	1	$C_{29}H_{53}N_6O_6S_0H^+_1$	-0.21	j_6
681.47819	1	$C_{34}H_{62}N_7O_7S_0H^+_1$	-0.23	j_7
780.54670	1	$C_{39}H_{71}N_8O_8S_0H^+_1$	-0.08	j_8
879.61542	1	$C_{44}H_{80}N_9O_9S_0H^+_1$	0.28	j_9
978.68365	1	$C_{49}H_{89}N_{10}O_{10}S_0H^+_1$	0.06	j_{10}

m/z	charge	chemical composition	error	assignment
1077.75165	1	$C_{54}H_{98}N_{11}O_{11}S_0H^+_1$	-0.33	j_{11}
1176.82065	1	$C_{59}H_{107}N_{12}O_{12}S_0H^+_1$	0.20	j_{12}
1374.95559	1	$C_{69}H_{125}N_{14}O_{14}S_0H^+_1$	-1.20	j_{13}
1474.02602	1	$C_{74}H_{134}N_{15}O_{15}S_0H^+_1$	0.24	j_{14}
199.14420	1	$C_{10}H_{18}N_2O_2S_0H^+_1$	0.48	k_2
298.21243	1	$C_{15}H_{27}N_3O_3S_0H^+_1$	-0.30	k_3
397.28085	1	$C_{20}H_{36}N_4O_4S_0H^+_1$	-0.21	k_4
496.34933	1	$C_{25}H_{45}N_5O_5S_0H^+_1$	-0.03	k_5
595.41777	1	$C_{30}H_{54}N_6O_6S_0H^+_1$	0.02	k_6*
694.48623	1	$C_{35}H_{63}N_7O_7S_0H^+_1$	0.08	k_7
793.55466	1	$C_{40}H_{72}N_8O_8S_0H^+_1$	0.09	k_8
892.62311	1	$C_{45}H_{81}N_9O_9S_0H^+_1$	0.12	k_9
991.69144	1	$C_{50}H_{90}N_{10}O_{10}S_0H^+_1$	0.02	k_{10}*
1090.75987	1	$C_{55}H_{99}N_{11}O_{11}S_0H^+_1$	0.04	k_{11}
1189.82829	1	$C_{60}H_{108}N_{12}O_{12}S_0H^+_1$	0.04	k_{12}
1288.89617	1	$C_{65}H_{117}N_{13}O_{13}S_0H^+_1$	-0.38	k_{13}
1387.96459	1	$C_{70}H_{126}N_{14}O_{14}S_0H^+_1$	-0.35	k_{14}
1487.03317	1	$C_{75}H_{135}N_{15}O_{15}S_0H^+_1$	-0.21	k_{15}
283.16520	1	$C_{14}H_{22}N_2O_4S_0H^+_1$	-0.12	$k(i)_2$
340.22301	1	$C_{17}H_{29}N_3O_4S_0H^+_1$	-0.21	$k(i)_3$
424.24422	1	$C_{21}H_{33}N_3O_6S_0H^+_1$	0.02	$k(i)_3$
270.15733	1	$C_{13}H_{21}N_2O_4S_0H^+_1$	-0.29	$j(i)_2$
552.31531	1	$C_{27}H_{43}N_4O_8S_0H^+_1$	-0.10	$j(i)_4$
		Average error (ppm)	0.49	
		Std dev error (ppm)	0.7	

*Table S 4.6: Neutral losses from Charged reduced species of p(NAM-*b*-DMA) Figure 4.7.*

m/z	charge	Error (ppm)	Assignment	notes
904.87104	3	-1.24	$C_{132}H_{226}N_{22}O_{31}S_3H^+_3$	Charge Reduced species
1356.8017	2	-1.94	$C_{132}H_{225}N_{22}O_{31}S_3H^+_3$	Me
1349.7955	2	-0.74	$C_{131}H_{223}N_{22}O_{31}S_3H^+_3$	C_3H_6NO-H
1320.78056	2	-0.98	$C_{129}H_{219}N_{21}O_{30}S_3H^+_3$	C_4H_9-CO
1314.77462	2	-0.72	$C_{127}H_{217}N_{22}O_{30}S_3H^+_3$	C_4H_9-C_2H_6N-H
1306.24242	2	-1.29	$C_{126}H_{210}N_{21}O_{31}S_3H^+_3$	$C_5H_8NO_2$ - H
1299.77564	2	-0.72	$C_{127}H_{217}N_{21}O_{29}S_3H^+_3$	C_4H_9-C_3H_6NO-H
1292.24583	2	-0.63	$C_{125}H_{210}N_{21}O_{30}S_3H^+_3$	$C_5H_9S_2$
1290.79987	2	-0.84	$C_{127}H_{217}N_{22}O_{31}S_1H^+_3$	$C_5H_9S_3$
1274.81438	2	-0.42	$C_{127}H_{217}N_{22}O_{31}S_0H^+_3$	C_3H_6NO - $C_5H_9S_3$ - H
1238.28825	2	-0.23	$C_{124}H_{210}N_{21}O_{30}S_0H^+_3$	C_4H_9-CO-$C_5H_9S_3$
1232.28750	2	-0.84	$C_{123}H_{210}N_{21}O_{30}S_0H^+_3$	C_4H_9-CO-$C_5H_9S_4$

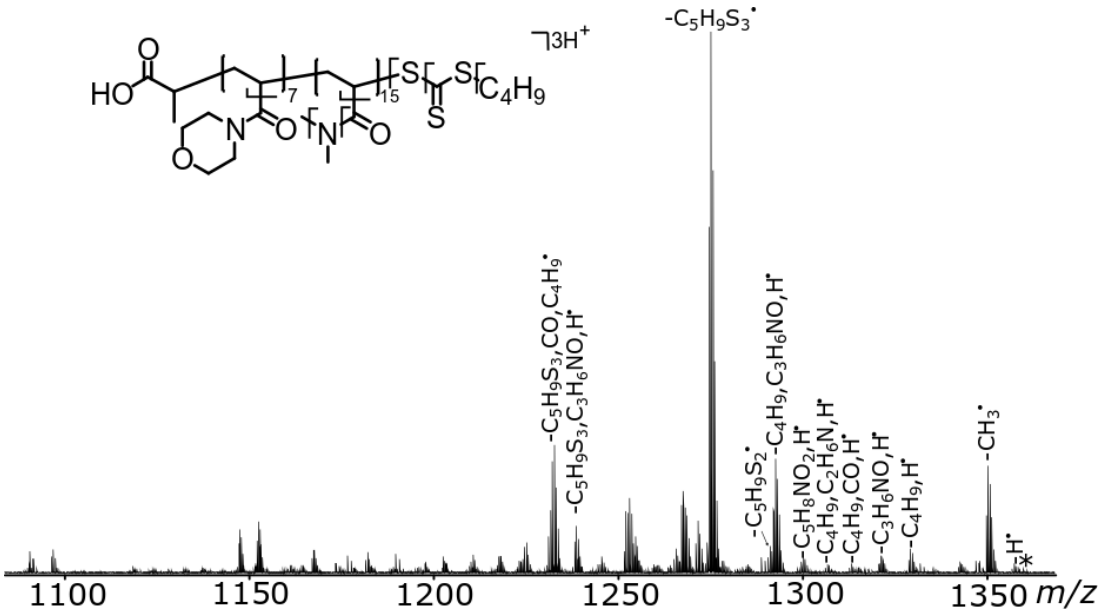

*Figure S 4.2 Zoomed region of the neutral losses from the charged reduced species of p(NAM-*b*-DMA).*

*Table S 4.7: Effect of double Neutral losses from Charged reduced species of p(NAM-*b*-DMA) Figure 4.5.*

DR ex	a3-a10 avg %	k3-k10 avg %	j2-j10 avg %	b2-b10 avg %
2900-Blank	100.0	100.0	100.0	100.0
1227 - C5H9S3	10.7	19.2	13.1	19.5
1242 - C5H9S2	52.9	63.2	49.7	50.9
1190 - C3H6NO -C5H9S3	89.8	84.3	80.4	84.7
1302 -CH3	84.1	81.9	81.6	83.1
1286 -C2H6N	78.8	70.3	70.3	74.8
1134 -C14H25N2O2S3	69.2	73.5	82.7	71.4
1265 -C4H9	86.8	84.8	79.7	75.0

Table S 4.8: Assignments of "blank" ion ejection at ejection m/z 2900

m/z	Peak area	error	assignment
285.18089	1875	0.02	a_3
384.24933	14829	0.08	a_4
483.31773	34341	0.04	a_5
582.38615	52136	0.04	a_6
681.45454	79822	0.00	a_7
780.52296	111117	0.01	a_8
879.59130	139223	-0.08	a_9
978.65969	176715	-0.09	a_{10}
1077.72808	266492	-0.11	a_{11}
1176.79659	308188	-0.02	a_{12}
1275.86500	393782	-0.02	a_{13}
1374.93347	589432	0.02	a_{14}
1474.00179	514866	-0.04	a_{15}
1573.0697	605114	-0.36	a_{16}
1672.13827	808928	-0.24	a_{17}
1771.20662	942345	-0.27	a_{18}
1870.27516	803382	-0.19	a_{19}
1969.34308	2160207	-0.43	a_{20}
2068.41013	1257425	-1.07	a_{21}
2167.47981	754470	-0.43	a_{22}
2266.54783	3340357	-0.59	a_{23}
199.14410	5476	-0.02	k_2
298.21249	955121	-0.09	k_3
397.28095	107892	0.05	k_4
496.34935	258441	0.01	k_5
595.41776	155421	0.00	k_6
694.48616	199006	-0.02	k_7
793.55459	188252	0.00	k_8
892.62301	214181	0.01	k_9

m/z	Peak area	error	assignment
991.69135	251439	-0.07	k_{10}
1288.89658	377226	-0.06	k_{13}
1387.96492	377878	-0.11	k_{14}
1487.03327	444063	-0.14	k_{15}
1586.1019	455304	0.00	k_{16}
1685.17063	445698	0.19	k_{17}
1784.23856	472456	-0.09	k_{18}
1883.30763	492222	0.26	k_{19}
1982.37636	385759	0.41	k_{20}
2081.44433	263599	0.17	k_{21}
2180.51239	82861	0.00	k_{22}
186.13627	47972	-0.05	j_{2}
285.20470	43866	0.02	j_{3}
384.27312	181297	0.03	j_{4}
483.34152	82187	0.00	j_{5}
582.40992	113165	-0.03	j_{6}
681.47831	106344	-0.06	j_{7}
780.54673	130754	-0.04	j_{8}
879.61514	153929	-0.04	j_{9}
978.68365	164371	0.06	j_{10}
1077.75201	183012	0.01	j_{11}
1176.8206	242085	0.15	j_{12}
1275.88892	241959	0.07	j_{13}
1374.95732	237619	0.05	j_{14}
1474.02567	287693	0.01	j_{15}
371.24149	21389	0.05	b_{3}
470.30990	36509	0.03	b_{4}
569.37830	42719	0.00	b_{5}
668.44674	62528	0.04	b_{6}
767.51509	89527	-0.05	b_{7}
866.58356	115988	0.02	b_{8}
965.65182	160525	-0.14	b_{9}
1064.72016	181216	-0.20	b_{10}
1163.78874	209320	-0.04	b_{11}
1262.85705	348359	-0.12	b_{12}
1361.92545	268864	-0.12	b_{13}
1460.99369	394880	-0.23	b_{14}
1560.06213	514773	-0.20	b_{15}
1659.13052	503959	-0.20	b_{16}
1758.19860	456751	-0.38	b_{17}
1857.26753	1679880	-0.08	b_{18}
1956.33565	740260	-0.23	b_{19}
2055.40289	471324	-0.79	b_{20}
2154.47258	2721763	-0.16	b_{21}
2253.53545	752828	-2.61	b_{22}

m/z	Peak area	error	assignment
	Average error (ppm)	0.16	
	Std dev error (ppm)	0.33	

Table S 4.9: Assignments of trithiocarbonate $C_5H_9S_3$ ion ejection at ejection m/z *1227*

m/z	Peak Area	error	Source
285.18090	364	0.06	a_3
384.24937	1399	0.19	a_4
483.31772	3245	0.02	a_5
582.38624	3896	0.20	a_6
681.45448	6631	-0.09	a_7
780.52268	11142	-0.35	a_8
879.59134	16656	-0.03	a_9
978.65981	21868	0.03	a_{10}
1275.86411	60100	-0.72	a_{12}
1374.93318	172018	-0.19	a_{13}
1473.99866	51726	-2.16	a_{14}
1573.06997	43624	-0.19	a_{15}
1672.13700	55913	-1.00	a_{16}
1771.20733	37522	0.13	a_{17}
1870.27498	34472	-0.28	a_{18}
2068.40880	63776	-1.71	a_{19}
2167.47855	52668	-1.01	a_{20}
2266.54654	351138	-1.16	a_{21}
199.14410	933	-0.02	k_2
298.21253	304095	0.04	k_3
397.28096	12622	0.07	k_4
496.34937	41076	0.05	k_5
595.41777	11498	0.02	k_6
694.48618	17955	0.01	k_7
793.55437	20172	-0.27	k_8
892.62281	22936	-0.21	k_9
991.69150	17809	0.09	k_{10}
1090.76025	25928	0.39	k_{11}
1189.82754	36706	-0.59	k_{12}
1288.89674	31707	0.06	k_{13}
1387.96402	43950	-0.76	k_{14}
1487.03340	25786	-0.06	k_{15}
1586.10097	33208	-0.59	k_{16}
1685.17183	18695	0.90	k_{17}
1784.23861	32750	-0.07	k_{18}
1883.30725	28082	0.06	k_{19}

m/z	Peak Area	error	Source
186.13627	18689	-0.05	j_2
285.20471	5992	0.06	j_3
384.27314	31416	0.09	j_4
483.34147	9957	-0.11	j_5
582.40989	12611	-0.08	j_6
681.47822	11103	-0.19	j_7
780.54683	11579	0.09	j_8
879.61483	13796	-0.39	j_9
978.68315	18623	-0.45	j_{10}
1077.75126	18566	-0.69	j_{11}
1176.82049	29161	0.06	j_{12}
1275.8882	25058	-0.50	j_{13}
1374.9572	20126	-0.03	j_{14}
1474.02474	57220	-0.62	j_{15}
371.24150	3398	0.07	b_3
470.30992	3623	0.07	b_4
569.37827	5806	-0.05	b_5
668.44667	9682	-0.07	b_6
767.51480	13785	-0.43	b_7
866.58309	18434	-0.52	b_8
965.65102	42731	-0.97	b_9
1064.72009	41322	-0.26	b_{10}
1163.78877	33377	-0.01	b_{11}
1262.85594	108958	-1.00	b_{12}
1361.92497	45017	-0.47	b_{13}
1460.99124	48904	-1.91	b_{14}
1560.06283	102116	0.25	b_{15}
1659.12795	78990	-1.75	b_{16}
1758.19816	36451	-0.63	b_{17}
1857.26540	169230	-1.23	b_{18}
1956.33308	77588	-1.54	b_{19}
2055.40201	59338	-1.22	b_{20}
2154.46919	214201	-1.73	b_{21}
2253.53430	201910	-3.12	b_{22}
	Average error (ppm)	0.49	
	Std dev error (ppm)	0.68	

Table S 4.10: Assignments of CH_3 loss ion ejection at ejection m/z *1302*

m/z	Peak Area	error	Source
285.18089	1732	0.02	a_3
384.24930	15809	0.01	a_4

m/z	Peak Area	error	Source
483.31771	30531	0.00	a_5
582.38613	48054	0.01	a_6
681.45453	71783	-0.01	a_7
780.52300	101436	0.06	a_8
879.59140	134442	0.04	a_9
978.65988	168234	0.10	a_{10}
1077.72814	246716	-0.05	a_{11}
1176.79649	292206	-0.10	a_{12}
1275.86438	308479	-0.50	a_{13}
1374.93324	547791	-0.14	a_{14}
1474.00171	481155	-0.10	a_{15}
1573.06989	618611	-0.24	a_{16}
1672.13844	811385	-0.14	a_{17}
1771.20691	945384	-0.10	a_{18}
1870.2752	867722	-0.16	a_{19}
1969.34391	2422065	-0.01	a_{20}
2167.47995	874445	-0.37	a_{21}
2266.54899	3943276	-0.08	a_{22}
199.14410	5124	-0.02	k_2
298.21250	878163	-0.06	k_3
397.28094	93673	0.02	k_4
496.34934	240091	-0.01	k_5
595.41776	139106	0.00	k_6
694.48622	178695	0.07	k_7
793.55465	166876	0.08	k_8
892.62301	192814	0.01	k_9
991.69142	237366	0.00	k_{10}
1288.89682	54173	0.13	k_{12}
1387.9652	369096	0.09	k_{13}
1487.03347	425970	-0.01	k_{14}
1685.17016	490411	-0.09	k_{15}
1784.2392	524230	0.27	k_{16}
1883.30686	565787	-0.15	k_{17}
1982.37613	433837	0.29	k_{18}
2081.44368	304148	-0.14	k_{19}
2180.5124	114200	0.01	k_{20}
186.13628	46837	0.00	j_2
285.20470	40879	0.02	j_3
384.27311	162367	0.01	j_4
483.34152	77813	0.00	j_5
582.40993	103794	-0.01	j_6
681.47834	98707	-0.01	j_7
780.54676	109373	0.00	j_8
879.61522	141571	0.05	j_9
978.68351	150846	-0.08	j_{10}

m/z	Peak Area	error	Source
1077.75215	192732	0.14	j_{11}
1176.82032	224439	-0.08	j_{12}
1275.88837	196542	-0.36	j_{13}
1374.95740	242451	0.11	j_{14}
1474.02606	252749	0.27	j_{15}
1573.09486	221755	0.50	j_{16}
272.17306	1285	0.00	b_2
371.24148	21265	0.02	b_3
470.30987	32381	-0.04	b_4
569.37827	39799	-0.05	b_5
668.44673	63504	0.02	b_6
767.51510	89033	-0.04	b_7
866.58351	106286	-0.04	b_8
965.65192	145608	-0.04	b_9
1064.72007	160057	-0.28	b_{10}
1163.78842	190757	-0.31	b_{11}
1262.85692	343647	-0.22	b_{12}
1361.92546	271981	-0.11	b_{13}
1460.99369	306369	-0.23	b_{14}
1560.0624	534783	-0.03	b_{15}
1659.13083	556603	-0.01	b_{16}
1758.19947	547048	0.12	b_{17}
1857.26798	1996903	0.16	b_{18}
1956.33608	825390	-0.01	b_{19}
2055.4059	512945	0.68	b_{20}
2154.47332	3358629	0.18	b_{21}
2253.53916	497780	-0.97	b_{22}
	Average error (ppm)	0.12	
	Std dev error (ppm)	0.20	

Table S 4.11: Assignments of C_2H_6N loss ion ejection at ejection m/z *1286*

m/z	Peak Area	error	Source
285.18088	1833	-0.01	a_3
384.24930	14419	0.01	a_4
483.31772	29091	0.02	a_5
582.38611	56352	-0.03	a_6
681.45454	78624	0.00	a_7
780.52293	123973	-0.03	a_8
879.59130	139519	-0.08	a_9
978.65969	181154	-0.09	a_{10}
1077.72799	243601	-0.19	a_{11}

m/z	Peak Area	error	Source
1176.79641	312974	-0.17	a_{12}
1275.86485	47443	-0.14	a_{13}
1374.9332	628279	-0.17	a_{14}
1474.00122	524444	-0.43	a_{15}
1573.06938	646533	-0.56	a_{16}
1672.13773	924911	-0.57	a_{17}
1771.20618	1160532	-0.52	a_{18}
1870.27395	1049019	-0.83	a_{19}
1969.34269	2897272	-0.62	a_{20}
2068.40939	1780712	-1.42	a_{21}
2167.47925	995129	-0.69	a_{22}
2266.54768	4775251	-0.65	a_{23}
199.14410	5226	-0.02	k_{2}
298.21250	842543	-0.06	k_{3}
397.28094	102518	0.02	k_{4}
496.34935	230852	0.01	k_{5}
595.41775	147190	-0.02	k_{6}
694.48617	182642	-0.01	k_{7}
793.55456	179768	-0.03	k_{8}
892.62296	204711	-0.05	k_{9}
991.69130	239970	-0.12	k_{10}
1288.89709	49797	0.34	k_{13}
1387.96463	434300	-0.32	k_{14}
1487.03303	483562	-0.31	k_{15}
1586.10152	507728	-0.24	k_{16}
1685.16997	526593	-0.20	k_{17}
1784.23811	594716	-0.35	k_{18}
1883.30667	608202	-0.25	k_{19}
1982.37517	501711	-0.19	k_{20}
2081.44272	356369	-0.60	k_{21}
2180.51251	98129	0.06	k_{22}
186.13628	45867	0.00	j_{2}
285.20470	38082	0.02	j_{3}
384.27311	167658	0.01	j_{4}
483.34152	74766	0.00	j_{5}
582.40993	106328	-0.01	j_{6}
681.47833	98094	-0.03	j_{7}
780.54674	120009	-0.03	j_{8}
879.61515	146100	-0.03	j_{9}
978.68348	138770	-0.11	j_{10}
1077.75190	183889	-0.10	j_{11}
1176.82038	226663	-0.03	j_{12}
1275.88813	52512	-0.55	j_{13}
1374.95698	270229	-0.19	j_{14}
1474.02558	314099	-0.05	j_{15}

m/z	Peak Area	error	Source
1573.09391	290520	-0.10	j_{16}
272.17308	1373	0.08	b_2
371.24149	21871	0.05	b_3
470.30989	31425	0.01	b_4
569.37829	38337	-0.02	b_5
668.44672	62075	0.01	b_6
767.51513	93616	0.00	b_7
866.58351	111234	-0.04	b_8
965.65175	164707	-0.21	b_9
1064.72022	167481	-0.14	b_{10}
1163.78849	193148	-0.25	b_{11}
1262.85663	282431	-0.45	b_{12}
1361.92511	304902	-0.37	b_{13}
1460.99353	337335	-0.34	b_{14}
1560.06194	631278	-0.32	b_{15}
1659.13011	662741	-0.45	b_{16}
1758.19831	611496	-0.54	b_{17}
1857.26696	2259255	-0.39	b_{18}
1956.3352	1032353	-0.46	b_{19}
2055.40335	624693	-0.56	b_{20}
2154.47154	4092778	-0.64	b_{21}
2253.53552	640392	-2.58	b_{22}
	Average error (ppm)	0.26	
	Std dev error (ppm)	0.38	

Table S 4.12: Assignments of C5H9S2 loss ion ejection at ejection m/z 1242

m/z	Peak Area	error	Source
285.18090	792	0.06	a_3
384.24931	8777	0.03	a_4
483.31772	17999	0.02	a_5
582.38612	30195	-0.01	a_6
681.45454	46633	0.00	a_7
780.52295	65780	0.00	a_8
879.59141	91786	0.05	a_9
978.65973	112372	-0.05	a_{10}
1077.72815	140974	-0.04	a_{11}
1275.86508	117608	0.04	a_{12}
1374.93372	389740	0.21	a_{13}
1474.00156	324108	-0.20	a_{14}
1573.07008	379427	-0.12	a_{15}
1672.13842	631910	-0.15	a_{16}

m/z	Peak Area	error	Source
1771.20644	574933	-0.37	a_{17}
1870.27419	551837	-0.70	a_{18}
1969.34339	2215512	-0.27	a_{19}
2068.41039	852146	-0.94	a_{20}
2167.47983	695587	-0.42	a_{21}
2266.54864	3182451	-0.23	a_{22}
199.14410	4139	-0.02	k_{2}
298.21252	873735	0.01	k_{3}
397.28094	71489	0.02	k_{4}
496.34936	198699	0.03	k_{5}
595.41776	100115	0.00	k_{6}
694.48618	102857	0.01	k_{7}
793.55459	110575	0.00	k_{8}
892.62296	119199	-0.05	k_{9}
991.69121	129604	-0.21	k_{10}
1288.89648	106732	-0.14	k_{13}
1387.96523	158530	0.11	k_{14}
1487.03354	194073	0.04	k_{15}
1586.10173	253016	-0.11	k_{16}
1685.1703	262830	-0.01	k_{17}
1784.23798	285094	-0.42	k_{18}
1883.30679	318057	-0.19	k_{19}
1982.37558	244271	0.01	k_{20}
2081.44272	161747	-0.60	k_{21}
186.13628	48917	0.00	j_{2}
285.20470	28922	0.02	j_{3}
384.27312	125508	0.03	j_{4}
483.34153	46769	0.02	j_{5}
582.40994	64319	0.01	j_{6}
681.47836	53743	0.02	j_{7}
780.54673	66234	-0.04	j_{8}
879.61517	76453	-0.01	j_{9}
978.68363	78969	0.04	j_{10}
1077.75248	80653	0.44	j_{11}
1176.82079	87579	0.32	j_{12}
1275.88915	73845	0.25	j_{13}
1374.95784	101946	0.43	j_{14}
1474.02594	169960	0.19	j_{15}
1573.0948	152565	0.46	j_{16}
1672.16359	128353	0.66	j_{17}
272.17307	1054	0.04	b_{2}
371.24149	13457	0.05	b_{3}
470.30991	21457	0.05	b_{4}
569.37831	22224	0.02	b_{5}
668.44672	36857	0.01	b_{6}

m/z	Peak Area	error	Source
767.51515	55257	0.03	b_7
866.58347	62973	-0.08	b_8
965.65183	94747	-0.13	b_9
1064.72025	111635	-0.11	b_{10}
1163.78846	126360	-0.28	b_{11}
1262.85711	166814	-0.07	b_{12}
1361.92534	173855	-0.20	b_{13}
1460.99422	171324	0.13	b_{14}
1560.06223	459413	-0.13	b_{15}
1659.13056	397485	-0.18	b_{16}
1758.19847	362672	-0.45	b_{17}
1857.26722	1903984	-0.25	b_{18}
1956.3347	714979	-0.71	b_{19}
2055.40318	414531	-0.65	b_{20}
2154.47186	2496187	-0.49	b_{21}
2253.53719	386908	-1.84	b_{22}
	Average error (ppm)	0.20	
	Std dev error (ppm)	0.33	

Table S 4.13: Assignments of C14H25S3 loss ion ejection at ejection m/z 1134

m/z	Peak Area	error	Source
285.18084	1561	-0.15	a_3
384.24922	11404	-0.20	a_4
483.31761	23743	-0.21	a_5
582.38607	39098	-0.10	a_6
681.45453	60565	-0.01	a_7
780.52295	76375	0.00	a_8
879.59115	93272	-0.25	a_9
978.65985	116111	0.07	a_{10}
1077.72715	176961	-0.97	a_{11}
1176.79583	189856	-0.66	a_{12}
1275.86593	238856	0.71	a_{13}
1374.93270	358577	-0.54	a_{14}
1473.99997	261386	-1.28	a_{15}
1573.06746	352808	-1.78	a_{16}
1672.13473	453221	-2.36	a_{17}
1771.20337	542791	-2.10	a_{18}
1870.27092	502285	-2.45	a_{19}
1969.34100	1659998	-1.48	a_{20}

m/z	Peak Area	error	Source
2068.40878	956003	-1.72	a_{21}
2167.47393	660441	-3.15	a_{22}
2266.53982	1495810	-4.12	a_{23}
199.1441	4870	-0.02	k_2
298.21245	740236	-0.23	k_3
397.28084	77497	-0.23	k_4
496.34925	196985	-0.19	k_5
595.41768	111168	-0.13	k_6
694.48615	135924	-0.03	k_7
793.5546	130134	0.02	k_8
892.62307	147571	0.08	k_9
991.69148	172819	0.06	k_{10}
1288.8962	248526	-0.35	k_{13}
1387.96409	266636	-0.71	k_{14}
1487.03253	296947	-0.64	k_{15}
1586.09904	323128	-1.80	k_{16}
1685.1705	340046	0.11	k_{17}
1784.23554	371454	-1.79	k_{18}
1883.30704	379013	-0.05	k_{19}
1982.37707	315293	0.76	k_{20}
2180.51308	62622	0.32	k_{21}
186.13628	43409	0.00	j_2
285.20465	34581	-0.15	j_3
384.27302	132305	-0.23	j_4
483.34142	60511	-0.21	j_5
582.40984	83058	-0.16	j_6
681.47832	73901	-0.04	j_7
780.54668	95114	-0.11	j_8
879.61510	108600	-0.09	j_9
978.68368	118198	0.09	j_{10}
1077.75223	140780	0.21	j_{11}
1176.8207	157999	0.24	j_{12}
1275.88946	168492	0.49	j_{13}
1374.95977	154389	1.84	j_{14}
1474.02518	184216	-0.33	j_{15}
1573.09575	152300	1.07	j_{16}
1672.16857	121637	3.64	j_{17}
272.17304	978	-0.07	b_2
371.24140	16366	-0.20	b_3
470.30980	25544	-0.18	b_4
569.37820	30526	-0.18	b_5
668.44663	50393	-0.13	b_6
767.51513	63482	0.00	b_7
866.5835	86350	-0.05	b_8
965.65194	112959	-0.02	b_9

m/z	Peak Area	error	Source
1064.72129	127629	0.86	b_{10}
1163.78725	120252	-1.32	b_{11}
1262.85694	233658	-0.20	b_{12}
1361.92411	193274	-1.10	b_{13}
1460.99205	225640	-1.35	b_{14}
1560.06027	375796	-1.39	b_{15}
1659.13101	416431	0.09	b_{16}
1758.19508	385869	-2.38	b_{17}
1857.2666	1434900	-0.58	b_{18}
1956.3335	603989	-1.33	b_{19}
2055.39817	490215	-3.08	b_{20}
2154.46875	2516833	-1.94	b_{21}
	Average error (ppm)	0.76	
	Std dev error (ppm)	1.1	

Table S 4.14: Assignments of C_4H_9 loss ion ejection at ejection m/z *1265*

m/z	Peak Area	error	Source
285.18086	1709	-0.08	a_3
384.24925	13429	-0.12	a_4
483.31766	32256	-0.11	a_5
582.38608	47013	-0.08	a_6
681.45451	73150	-0.04	a_7
780.52302	92154	0.09	a_8
879.59137	114225	0.00	a_9
978.65995	155590	0.17	a_{10}
1077.72799	173551	-0.19	a_{11}
1176.79662	243003	0.01	a_{12}
1275.86462	41968	-0.32	a_{13}
1374.93339	514075	-0.03	a_{14}
1474.0018	426370	-0.03	a_{15}
1573.06925	545395	-0.64	a_{16}
1672.13858	786046	-0.06	a_{17}
1771.20637	955004	-0.41	a_{18}
1870.27405	928077	-0.78	a_{19}
1969.34333	2555772	-0.30	a_{20}
2068.40947	1621807	-1.38	a_{21}
2167.4804	1029829	-0.16	a_{22}
2266.54835	4605071	-0.36	a_{23}
199.14410	5220	-0.02	k_2
298.21248	831909	-0.13	k_3
397.28089	88950	-0.11	k_4

m/z	Peak Area	error	Source
496.34929	212683	-0.11	k_5
595.41771	138771	-0.08	k_6
694.48614	164943	-0.05	k_7
793.55459	153113	0.00	k_8
892.62304	176952	0.04	k_9
991.69152	207322	0.11	k_{10}
1288.89538	141706	-0.99	k_{13}
1387.96505	359523	-0.02	k_{14}
1487.03379	429067	0.20	k_{15}
1586.10218	464554	0.18	k_{16}
1685.17038	488138	0.04	k_{17}
1784.23817	523417	-0.31	k_{18}
1883.30770	565801	0.30	k_{19}
1982.37559	444355	0.02	k_{20}
2081.44350	334881	-0.23	k_{21}
2180.50822	93847	-1.91	k_{22}
186.13629	44034	0.06	j_2
285.20468	37654	-0.05	j_3
384.27306	146566	-0.12	j_4
483.34146	70617	-0.13	j_5
582.40989	103307	-0.08	j_6
681.47828	80697	-0.10	j_7
780.54676	97971	0.00	j_8
879.6152	121811	0.03	j_9
978.68383	113866	0.24	j_{10}
1176.82054	185916	0.10	j_{12}
1275.88902	44489	0.15	j_{13}
1374.95860	232897	0.98	j_{14}
1474.02714	285643	1.00	j_{15}
1573.09485	243724	0.49	j_{16}
272.17304	1298	-0.07	b_2
371.24143	20827	-0.11	b_3
470.30984	33021	-0.10	b_4
569.37824	35246	-0.11	b_5
668.44672	53472	0.01	b_6
767.51514	74348	0.02	b_7
866.58359	94063	0.06	b_8
965.65186	85122	-0.10	b_9
1064.72061	136123	0.23	b_{10}
1163.78843	158584	-0.30	b_{11}
1262.85764	39595	0.35	b_{12}
1361.92607	260446	0.34	b_{13}
1460.99420	320338	0.12	b_{14}
1560.06213	533822	-0.20	b_{15}
1659.13089	563718	0.02	b_{16}

m/z	Peak Area	error	Source
1758.19895	566512	-0.18	b_{17}
1857.26796	2069835	0.15	b_{18}
1956.33621	1004580	0.06	b_{19}
2055.40490	590213	0.19	b_{20}
2154.47194	4066120	-0.46	b_{21}
2253.53736	653293	-1.76	b_{22}
	Average error (ppm)	0.25	
	Std dev error (ppm)	0.43	

Table S 4.15: Assignments of C3H6NO-C5H9S3 (1190) loss ion ejection at ejection m/z 1190

m/z	Peak Area	error	Source
285.18087	1681	-0.05	a_3
384.24929	15548	-0.02	a_4
483.31771	28285	0.00	a_5
582.38616	48011	0.06	a_6
681.4546	71190	0.09	a_7
780.52313	88846	0.23	a_8
879.59142	129129	0.06	a_9
978.65970	158587	-0.08	a_{10}
1176.79554	30925	-0.91	a_{12}
1275.86514	317111	0.09	a_{13}
1374.93357	497412	0.10	a_{14}
1474.00089	434011	-0.65	a_{15}
1573.06962	539637	-0.41	a_{16}
1672.13783	766168	-0.51	a_{17}
1771.20602	979856	-0.61	a_{18}
1870.27326	887159	-1.20	a_{19}
1969.34227	2590571	-0.84	a_{20}
2068.40859	1581454	-1.81	a_{21}
2167.47699	948337	-1.73	a_{22}
2266.54696	5495253	-0.97	a_{23}
199.14410	5393	-0.02	k_2
298.21250	817039	-0.06	k_3
397.28091	88669	-0.06	k_4
496.34935	221999	0.01	k_5
595.41776	131935	0.00	k_6
694.48621	160985	0.05	k_7
793.55457	154130	-0.02	k_8
892.62309	166677	0.10	k_9

m/z	Peak Area	error	Source
991.69165	197196	0.24	k_{10}
1189.82822	31386	-0.02	k_{12}
1288.89697	312905	0.24	k_{13}
1387.96501	342772	-0.04	k_{14}
1487.03298	400829	-0.34	k_{15}
1586.10178	447702	-0.08	k_{16}
1685.16979	459582	-0.31	k_{17}
1784.23814	516125	-0.33	k_{18}
1883.30532	501341	-0.97	k_{19}
1982.37558	407694	0.01	k_{20}
2081.44133	304572	-1.27	k_{21}
186.13628	47697	0.00	j_{2}
285.20469	37412	-0.01	j_{3}
384.27310	150404	-0.02	j_{4}
483.34150	68086	-0.04	j_{5}
582.40993	91490	-0.01	j_{6}
681.47836	81040	0.02	j_{7}
780.54668	97785	-0.11	j_{8}
879.61522	104113	0.05	j_{9}
978.68362	134629	0.03	j_{10}
1077.75225	159699	0.23	j_{11}
1176.82079	41442	0.32	j_{12}
1275.88932	214983	0.38	j_{13}
1374.95737	231863	0.09	j_{14}
1474.02598	268876	0.22	j_{15}
1573.09473	218499	0.42	j_{16}
1672.16454	203883	1.23	j_{17}
272.17307	1141	0.04	b_{2}
371.24147	20204	-0.01	b_{3}
470.30988	31011	-0.01	b_{4}
569.37829	34667	-0.02	b_{5}
668.44670	58162	-0.02	b_{6}
767.51516	77671	0.04	b_{7}
866.58353	95088	-0.01	b_{8}
965.65226	124516	0.31	b_{9}
1064.72044	152656	0.07	b_{10}
1163.78806	151243	-0.62	b_{11}
1262.85728	281754	0.07	b_{12}
1361.92507	273246	-0.40	b_{13}
1460.99381	303153	-0.15	b_{14}
1560.06232	558953	-0.08	b_{15}
1659.12973	588956	-0.68	b_{16}
1758.19822	617119	-0.60	b_{17}
1857.26682	2100291	-0.46	b_{18}
1956.33453	954208	-0.80	b_{19}

m/z	Peak Area	error	Source
2055.40193	478967	-1.25	b_{20}
2154.47113	3743265	-0.83	b_{21}
	Average error (ppm)	0.32	
	Std dev error (ppm)	0.10	

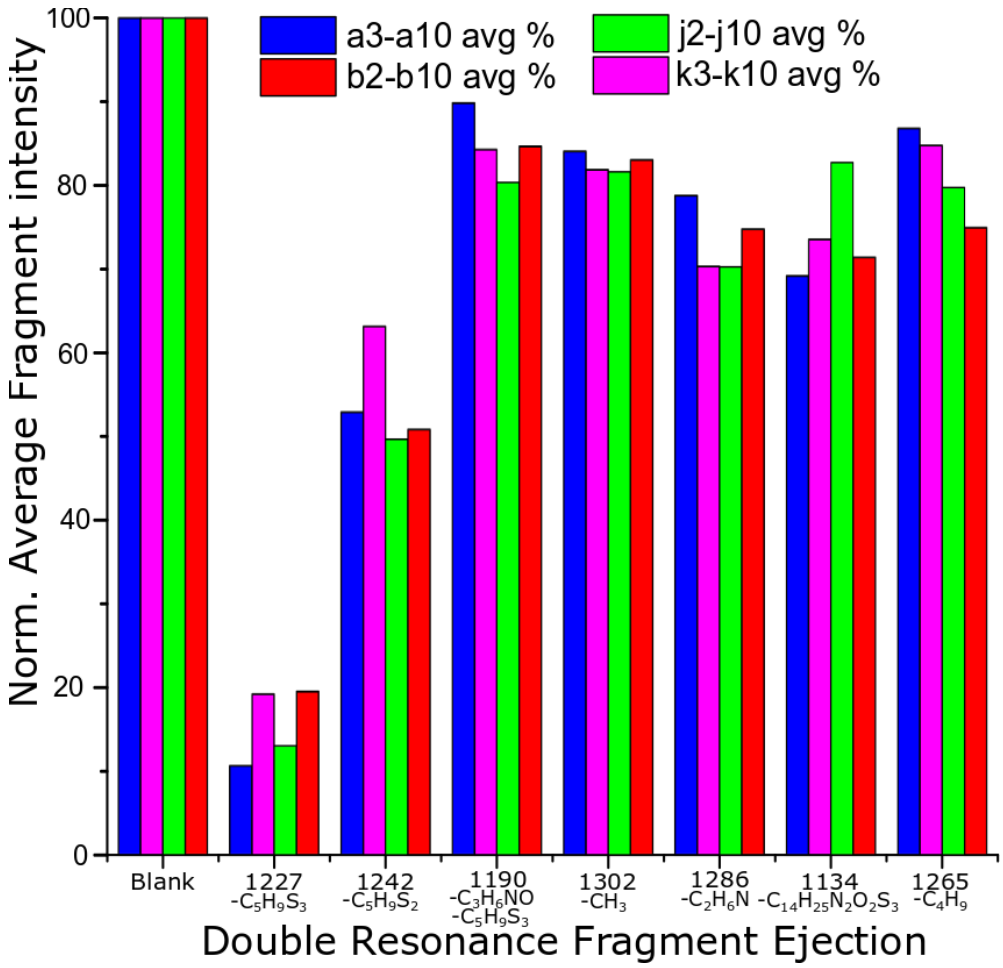

Figure S 4.3 Ion intensity of individual fragmentation series showing difference caused by ejection of ions.

Table S 4.16: Fragment assignments for the fragmentation of the H-terminated p(DMA)

m/z	charge	Chemical Formula	error	assignment
272.17298	1	$C_{13}H_{23}N_2O_4S_0H^+_1$	-0.29	b_2
371.24139	1	$C_{18}H_{32}N_3O_5S_0H^+_1$	-0.22	b_3
470.30991	1	$C_{23}H_{41}N_4O_6S_0H^+_1$	0.05	b_4
569.37885	1	$C_{28}H_{50}N_5O_7S_0H^+_1$	0.97	b_5
668.44667	1	$C_{33}H_{59}N_6O_8S_0H^+_1$	-0.07	b_6
767.51513	1	$C_{38}H_{68}N_7O_9S_0H^+_1$	0.00	b_7
866.58338	1	$C_{43}H_{77}N_8O_{10}S_0H^+_1$	-0.19	b_8
965.65198	1	$C_{48}H_{86}N_9O_{11}S_0H^+_1$	0.02	b_9
1064.72063	1	$C_{53}H_{95}N_{10}O_{12}S_0H^+_1$	0.24	b_{10}
1163.78786	1	$C_{58}H_{104}N_{11}O_{13}S_0H^+_1$	-0.79	b_{11}
1262.85627	1	$C_{63}H_{113}N_{12}O_{14}S_0H^+_1$	-0.73	b_{12}
1361.92474	1	$C_{68}H_{122}N_{13}O_{15}S_0H^+_1$	-0.64	b_{13}
1460.99942	1	$C_{73}H_{131}N_{14}O_{16}S_0H^+_1$	3.69	b_{14}
1560.06584	1	$C_{78}H_{140}N_{15}O_{17}S_0H^+_1$	2.18	b_{15}
1659.1336	1	$C_{83}H_{149}N_{16}O_{18}S_0H^+_1$	1.66	b_{16}
285.18078	1	$C_{14}H_{24}N_2O_4S_0H^+_1$	-0.36	a_2
384.24924	1	$C_{19}H_{33}N_3O_5S_0H^+_1$	-0.15	a_3
483.31754	1	$C_{24}H_{42}N_4O_6S_0H^+_1$	-0.35	a_4
582.38723	1	$C_{29}H_{51}N_5O_7S_0H^+_1$	1.90	a_5
681.45425	1	$C_{34}H_{60}N_6O_8S_0H^+_1$	-0.42	a_6
780.52319	1	$C_{39}H_{69}N_7O_9S_0H^+_1$	0.30	a_7
879.59199	1	$C_{44}H_{78}N_8O_{10}S_0H^+_1$	0.71	a_8
978.65954	1	$C_{49}H_{87}N_9O_{11}S_0H^+_1$	-0.25	a_9
1077.72843	1	$C_{54}H_{96}N_{10}O_{12}S_0H^+_1$	0.22	a_{10}
1176.79697	1	$C_{59}H_{105}N_{11}O_{13}S_0H^+_1$	0.31	a_{11}
1275.86353	1	$C_{64}H_{114}N_{12}O_{14}S_0H^+_1$	-1.17	a_{12}
1374.93266	1	$C_{69}H_{123}N_{13}O_{15}S_0H^+_1$	-0.56	a_{13}
1474.00235	1	$C_{74}H_{132}N_{14}O_{16}S_0H^+_1$	0.34	a_{14}
1573.06938	1	$C_{79}H_{141}N_{15}O_{17}S_0H^+_1$	-0.56	a_{15}
1672.13839	1	$C_{84}H_{150}N_{16}O_{18}S_0H^+_1$	-0.17	a_{16}*
1771.20782	1	$C_{89}H_{159}N_{17}O_{19}S_0H^+_1$	0.41	a_{17}
199.14410	1	$C_{10}H_{18}N_2O_2S_0H^+_1$	-0.02	k_2*
298.21246	1	$C_{15}H_{27}N_3O_3S_0H^+_1$	-0.20	k_3
397.28082	1	$C_{20}H_{36}N_4O_4S_0H^+_1$	-0.28	k_4
496.34936	1	$C_{25}H_{45}N_5O_5S_0H^+_1$	0.03	k_5
595.41783	1	$C_{30}H_{54}N_6O_6S_0H^+_1$	0.12	k_6
694.48616	1	$C_{35}H_{63}N_7O_7S_0H^+_1$	-0.02	k_7*
793.55439	1	$C_{40}H_{72}N_8O_8S_0H^+_1$	-0.25	k_8
1090.75975	1	$C_{55}H_{99}N_{11}O_{11}S_0H^+_1$	-0.07	k_{11}
1189.82713	1	$C_{60}H_{108}N_{12}O_{12}S_0H^+_1$	-0.94	k_{12}
1288.89664	1	$C_{65}H_{117}N_{13}O_{13}S_0H^+_1$	-0.01	k_{13}*
1387.96426	1	$C_{70}H_{126}N_{14}O_{14}S_0H^+_1$	-0.58	k_{14}
1487.03473	1	$C_{75}H_{135}N_{15}O_{15}S_0H^+_1$	0.84	k_{15}

m/z	charge	Chemical Formula	error	assignment
1586.10207	1	$C_{80}H_{144}N_{16}O_{16}S_0H^+_1$	0.11	k_{16}
1685.17155	1	$C_{85}H_{153}N_{17}O_{17}S_0H^+_1$	0.73	k_{17}
186.13628	1	$C_9H_{17}N_2O_2S_0H^+_1$	0.00	j_2
285.2046	1	$C_{14}H_{26}N_3O_3S_0H^+_1$	-0.33	j_3
384.27307	1	$C_{19}H_{35}N_4O_4S_0H^+_1$	-0.10	j_4
483.34154	1	$C_{24}H_{44}N_5O_5S_0H^+_1$	0.04	j_5
582.40994	1	$C_{29}H_{53}N_6O_6S_0H^+_1$	0.01	j_6
681.47865	1	$C_{34}H_{62}N_7O_7S_0H^+_1$	0.44	j_7
780.54646	1	$C_{39}H_{71}N_8O_8S_0H^+_1$	-0.39	j_8
879.61525	1	$C_{44}H_{80}N_9O_9S_0H^+_1$	0.08	j_9
978.68300	1	$C_{49}H_{89}N_{10}O_{10}S_0H^+_1$	-0.60	j_{10}
1077.75238	1	$C_{54}H_{98}N_{11}O_{11}S_0H^+_1$	0.35	j_{11}
1176.82014	1	$C_{59}H_{107}N_{12}O_{12}S_0H^+_1$	-0.24	j_{12}
1275.88848	1	$C_{64}H_{116}N_{13}O_{13}S_0H^+_1$	-0.28	j_{13}
1374.95827	1	$C_{69}H_{125}N_{14}O_{14}S_0H^+_1$	0.74	j_{14}
313.21211	1	$C_{16}H_{28}N_2O_4S_0H^+_1$	-0.24	internal
412.28055	1	$C_{21}H_{37}N_3O_5S_0H^+_1$	-0.12	internal
511.34904	1	$C_{26}H_{46}N_4O_6S_0H^+_1$	0.06	internal
610.41732	1	$C_{31}H_{55}N_5O_7S_0H^+_1$	-0.17	internal
709.48577	1	$C_{36}H_{64}N_6O_8S_0H^+_1$	-0.10	internal
808.55407	1	$C_{41}H_{73}N_7O_9S_0H^+_1$	-0.23	internal
907.62235	1	$C_{46}H_{82}N_8O_{10}S_0H^+_1$	-0.35	internal
1105.75926	1	$C_{56}H_{100}N_{10}O_{12}S_0H^+_1$	-0.21	internal
1204.82773	1	$C_{61}H_{109}N_{11}O_{13}S_0H^+_1$	-0.15	internal
1303.89604	1	$C_{66}H_{118}N_{12}O_{14}S_0H^+_1$	-0.22	internal
1402.96498	1	$C_{71}H_{127}N_{13}O_{15}S_0H^+_1$	0.17	internal
1502.03338	1	$C_{76}H_{136}N_{14}O_{16}S_0H^+_1$	0.15	internal
1601.10068	1	$C_{81}H_{145}N_{15}O_{17}S_0H^+_1$	-0.55	internal
1700.17018	1	$C_{86}H_{154}N_{16}O_{18}S_0H^+_1$	0.12	internal
1799.23939	1	$C_{91}H_{163}N_{17}O_{19}S_0H^+_1$	0.55	internal
227.17540	1	$C_{12}H_{22}N_2O_2S_0H^+_1$	-0.02	internal
326.24374	1	$C_{17}H_{31}N_3O_3S_0H^+_1$	-0.24	internal
425.31231	1	$C_{22}H_{40}N_4O_4S_0H^+_1$	0.18	internal
524.38071	1	$C_{27}H_{49}N_5O_5S_0H^+_1$	0.12	internal
623.44896	1	$C_{32}H_{58}N_6O_6S_0H^+_1$	-0.16	internal
722.51710	1	$C_{37}H_{67}N_7O_7S_0H^+_1$	-0.52	internal
821.58582	1	$C_{42}H_{76}N_8O_8S_0H^+_1$	-0.08	internal
920.65398	1	$C_{47}H_{85}N_9O_9S_0H^+_1$	-0.35	internal
1019.72262	1	$C_{52}H_{94}N_{10}O_{10}S_0H^+_1$	-0.09	internal
1118.79115	1	$C_{57}H_{103}N_{11}O_{11}S_0H^+_1$	0.02	internal
1217.86007	1	$C_{62}H_{112}N_{12}O_{12}S_0H^+_1$	0.43	internal
1316.92831	1	$C_{67}H_{121}N_{13}O_{13}S_0H^+_1$	0.27	internal
1415.99598	1	$C_{72}H_{130}N_{14}O_{14}S_0H^+_1$	-0.28	internal
1515.06635	1	$C_{77}H_{139}N_{15}O_{15}S_0H^+_1$	1.03	internal
1614.13479	1	$C_{82}H_{148}N_{16}O_{16}S_0H^+_1$	0.99	internal

m/z	charge	Chemical Formula	error	assignment
1713.20338	1	$C_{87}H_{157}N_{17}O_{17}S_0H^+_1$	1.03	internal
		Average error (ppm)	0.41	
		Std dev error (ppm)	0.67	

Table S 4.17: Fragment assignments for the H-terminated p(NAM-b-DMA)

m/z	charge	chemical formula	error	assignment
186.1363	1	$C_9H_{17}N_2O_2S_0H^+_1$	0.00	j_2*
285.2046	1	$C_{14}H_{26}N_3O_3S_0H^+_1$	-0.22	j_3
384.2731	1	$C_{19}H_{35}N_4O_4S_0H^+_1$	-0.02	j_4
483.3415	1	$C_{24}H_{44}N_5O_5S_0H^+_1$	0.00	j_5
582.4099	1	$C_{29}H_{53}N_6O_6S_0H^+_1$	-0.13	j_6
681.4784	1	$C_{34}H_{62}N_7O_7S_0H^+_1$	0.05	j_7
780.5466	1	$C_{39}H_{71}N_8O_8S_0H^+_1$	-0.20	j_8
879.6152	1	$C_{44}H_{80}N_9O_9S_0H^+_1$	0.04	j_9*
978.6834	1	$C_{49}H_{89}N_{10}O_{10}S_0H^+_1$	-0.19	j_{10}
1077.751	1	$C_{54}H_{98}N_{11}O_{11}S_0H^+_1$	-0.97	j_{11}
1176.82	1	$C_{59}H_{107}N_{12}O_{12}S_0H^+_1$	0.00	j_{12}
1275.889	1	$C_{64}H_{116}N_{13}O_{13}S_0H^+_1$	-0.02	j_{13}
1374.958	1	$C_{69}H_{125}N_{14}O_{14}S_0H^+_1$	0.34	j_{14}
1474.025	1	$C_{74}H_{134}N_{15}O_{15}S_0H^+_1$	-0.41	j_{15}
1756.184	1	$C_{88}H_{156}N_{17}O_{19}S_0H^+_1$	0.17	j_{16}
369.2021	1	$C_{18}H_{28}N_2O_6S_0H^+_1$	0.18	a_3
510.281	1	$C_{25}H_{39}N_3O_8S_0H^+_1$	-0.08	a_4
651.3595	1	$C_{32}H_{50}N_4O_{10}S_0H^+_1$	-0.69	a_5
792.4389	1	$C_{39}H_{61}N_5O_{12}S_0H^+_1$	-0.11	a_6
933.5177	1	$C_{46}H_{72}N_6O_{14}S_0H^+_1$	-0.30	a_8
1074.597	1	$C_{53}H_{83}N_7O_{16}S_0H^+_1$	-0.06	a_9
1173.666	1	$C_{58}H_{92}N_8O_{17}S_0H^+_1$	0.81	a_{10}
1272.732	1	$C_{63}H_{101}N_9O_{18}S_0H^+_1$	-1.40	a_{11}
1371.802	1	$C_{68}H_{110}N_{10}O_{19}S_0H^+_1$	0.12	a_{12}
1470.869	1	$C_{73}H_{119}N_{11}O_{20}S_0H^+_1$	-1.30	a_{13}
1569.938	1	$C_{78}H_{128}N_{12}O_{21}S_0H^+_1$	-0.83	a_{14}
1669.005	1	$C_{83}H_{137}N_{13}O_{22}S_0H^+_1$	-1.23	a_{15}
1768.077	1	$C_{88}H_{146}N_{14}O_{23}S_0H^+_1$	0.84	a_{16}
1867.142	1	$C_{93}H_{155}N_{15}O_{24}S_0H^+_1$	-1.10	a_{17}
1966.212	1	$C_{98}H_{164}N_{16}O_{25}S_0H^+_1$	-0.13	a_{18}
2164.347	1	$C_{108}H_{182}N_{18}O_{27}S_0H^+_1$	-0.97	a_{20}
2263.421	1	$C_{113}H_{191}N_{19}O_{28}S_0H^+_1$	1.57	a_{21}
199.1441	1	$C_{10}H_{18}N_2O_2S_0H^+_1$	-0.07	k_2

m/z	charge	chemical formula	error	assignment
298.2125	1	$C_{15}H_{27}N_3O_3S_0H+_1$	-0.16	k_3
397.2809	1	$C_{20}H_{36}N_4O_4S_0H+_1$	-0.18	k_4
496.3493	1	$C_{25}H_{45}N_5O_5S_0H+_1$	-0.07	k_5
595.4178	1	$C_{30}H_{54}N_6O_6S_0H+_1$	0.03	k_6
694.4861	1	$C_{35}H_{63}N_7O_7S_0H+_1$	-0.05	k_7
793.5546	1	$C_{40}H_{72}N_8O_8S_0H+_1$	0.05	k_8
892.623	1	$C_{45}H_{81}N_9O_9S_0H+_1$	-0.04	k_9
991.6908	1	$C_{50}H_{90}N_{10}O_{10}S_0H^+_1$	-0.65	k_{10}
1090.76	1	$C_{55}H_{99}N_{11}O_{11}S_0H^+_1$	-0.23	k_{11}
1189.827	1	$C_{60}H_{108}N_{12}O_{12}S_0H^+_1$	-0.69	k_{12}
1288.896	1	$C_{65}H_{117}N_{13}O_{13}S_0H^+_1$	-0.26	k_{13}
1387.965	1	$C_{70}H_{126}N_{14}O_{14}S_0H^+_1$	-0.38	k_{14}
1487.033	1	$C_{75}H_{135}N_{15}O_{15}S_0H^+_1$	-0.02	k_{15}*
497.2733	1	$C_{24}H_{38}N_3O_8S_0H^+_1$	0.29	b_3
638.3521	1	$C_{31}H_{49}N_4O_{10}S_0H^+_1$	-0.13	b_4
779.4312	1	$C_{38}H_{60}N_5O_{12}S_0H^+_1$	0.08	b_5
920.5101	1	$C_{45}H_{71}N_6O_{14}S_0H^+_1$	-0.04	b_6
1061.589	1	$C_{52}H_{82}N_7O_{16}S_0H^+_1$	-0.11	b_7
1160.657	1	$C_{57}H_{91}N_8O_{17}S_0H^+_1$	-0.81	b_8
1259.725	1	$C_{62}H_{100}N_9O_{18}S_0H^+_1$	-0.59	b_9
1358.794	1	$C_{67}H_{109}N_{10}O_{19}S_0H^+_1$	-0.30	b_{10}
1457.864	1	$C_{72}H_{118}N_{11}O_{20}S_0H^+_1$	1.07	b_{11}
1655.999	1	$C_{82}H_{136}N_{13}O_{22}S_0H^+_1$	-0.50	b_{13}
1755.068	1	$C_{87}H_{145}N_{14}O_{23}S_0H^+_1$	0.02	b_{14}*
1854.134	1	$C_{92}H_{154}N_{15}O_{24}S_0H^+_1$	-1.16	b_{15}
2053.269	1	$C_{102}H_{172}N_{17}O_{26}S_0H^+_1$	-3.68	b_{17} 2nd iso
227.1753	1	$C_{12}H_{22}N_2O_2S_0H^+_1$	-0.33	internal
326.2438	1	$C_{17}H_{31}N_3O_3S_0H^+_1$	-0.09	internal
425.3122	1	$C_{22}H_{40}N_4O_4S_0H^+_1$	-0.08	internal
524.3807	1	$C_{27}H_{49}N_5O_5S_0H^+_1$	0.06	internal
623.449	1	$C_{32}H_{58}N_6O_6S_0H^+_1$	-0.05	internal
722.5174	1	$C_{37}H_{67}N_7O_7S_0H^+_1$	-0.17	internal
821.5858	1	$C_{42}H_{76}N_8O_8S_0H^+_1$	-0.14	internal
920.6543	1	$C_{47}H_{85}N_9O_9S_0H^+_1$	-0.02	internal
1019.722	1	$C_{52}H_{94}N_{10}O_{10}S_0H^+_1$	-0.28	internal
1118.792	1	$C_{57}H_{103}N_{11}O_{11}S_0H^+_1$	0.44	internal
1217.858	1	$C_{62}H_{112}N_{12}O_{12}S_0H^+_1$	-1.26	internal
1316.928	1	$C_{67}H_{121}N_{13}O_{13}S_0H^+_1$	-0.10	internal
1415.996	1	$C_{72}H_{130}N_{14}O_{14}S_0H^+_1$	-0.27	internal
283.1652	1	$C_{14}H_{22}N_2O_4S_0H^+_1$	-0.19	k'2
424.2441	1	$C_{21}H_{33}N_3O_6S_0H^+_1$	-0.19	k'3
270.1574	1	$C_{13}H_{21}N_2O_4S_0H^+_1$	-0.22	j'2
		Average error (ppm)	0.40	
		Std dev error (ppm)	0.55	

Table S 4.18: Fragment assignments of the OH-terminated p(NAM-b-DMA)

m/z	charge	chemical formula	error	assignment
186.1363	1	$C_9H_{17}N_2O_2S_0H^+_1$	0.11	j_2
285.20461	1	$C_{14}H_{26}N_3O_3S_0H^+_1$	-0.29	j_3
384.27301	1	$C_{19}H_{35}N_4O_4S_0H^+_1$	-0.25	j_4
483.34149	1	$C_{24}H_{44}N_5O_5S_0H^+_1$	-0.06	j_5
582.41003	1	$C_{29}H_{53}N_6O_6S_0H^+_1$	0.16	j_6
681.47869	1	$C_{34}H_{62}N_7O_7S_0H^+_1$	0.50	j_7
879.61521	1	$C_{44}H_{80}N_9O_9S_0H^+_1$	0.04	j_9
1077.75176	1	$C_{54}H_{98}N_{11}O_{11}S_0H^+_1$	-0.23	j_{11}
199.1441	1	$C_{10}H_{18}N_2O_2S_0H^+_1$	-0.02	k_2*
298.21242	1	$C_{15}H_{27}N_3O_3S_0H^+_1$	-0.33	k_3
397.28077	1	$C_{20}H_{36}N_4O_4S_0H^+_1$	-0.41	k_4
496.34934	1	$C_{25}H_{45}N_5O_5S_0H^+_1$	-0.01	k_5
595.41789	1	$C_{30}H_{54}N_6O_6S_0H^+_1$	0.22	k_6
694.48617	1	$C_{35}H_{63}N_7O_7S_0H^+_1$	-0.01	k_7*
793.55465	1	$C_{40}H_{72}N_8O_8S_0H^+_1$	0.08	k_8
892.62373	1	$C_{45}H_{81}N_9O_9S_0H^+_1$	0.82	k_9
991.69228	1	$C_{50}H_{90}N_{10}O_{10}S_0H^+_1$	0.87	k_{10}
1090.76119	1	$C_{55}H_{99}N_{11}O_{11}S_0H^+_1$	1.25	k_{11}
1189.8282	1	$C_{60}H_{108}N_{12}O_{12}S_0H^+_1$	-0.04	k_{12}*
1288.90117	1	$C_{65}H_{117}N_{13}O_{13}S_0H^+_1$	3.50	k_{13}
301.19948	1	$C_{14}H_{26}N_3O_4S_0H^+_1$	-0.42	z_3
400.26792	1	$C_{19}H_{35}N_4O_5S_0H^+_1$	-0.25	z_4
499.33641	1	$C_{24}H_{44}N_5O_6S_0H^+_1$	-0.05	z_5
598.4049	1	$C_{29}H_{53}N_6O_7S_0H^+_1$	0.08	z_6
697.47292	1	$C_{34}H_{62}N_7O_8S_0H^+_1$	-0.49	z_7
796.54135	1	$C_{39}H_{71}N_8O_9S_0H^+_1$	-0.41	z_8
895.61054	1	$C_{44}H_{80}N_9O_{10}S_0H^+_1$	0.50	z_9
994.6793	1	$C_{49}H_{89}N_{10}O_{11}S_0H^+_1$	0.80	z_{10}
1093.74922	1	$C_{54}H_{98}N_{11}O_{12}S_0H^+_1$	2.10	z_{11}
1192.81778	1	$C_{59}H_{107}N_{12}O_{13}S_0H^+_1$	2.05	z_{12}
1291.88507	1	$C_{64}H_{116}N_{13}O_{14}S_0H^+_1$	1.02	z_{13}
314.2074	1	$C_{15}H_{27}N_3O_4S_0H^+_1$	-0.10	y_3
413.27574	1	$C_{20}H_{36}N_4O_5S_0H^+_1$	-0.26	y_4
512.34411	1	$C_{25}H_{45}N_5O_6S_0H^+_1$	-0.29	y_5
611.4124	1	$C_{30}H_{54}N_6O_7S_0H^+_1$	-0.45	y_6
710.4813	1	$C_{35}H_{63}N_7O_8S_0H^+_1$	0.30	y_7
809.54943	1	$C_{40}H_{72}N_8O_9S_0H^+_1$	-0.09	y_8
908.61886	1	$C_{45}H_{81}N_9O_{10}S_0H^+_1$	1.04	y_9
1007.68611	1	$C_{50}H_{90}N_{10}O_{11}S_0H^+_1$	-0.22	y_{10}
1106.75812	1	$C_{55}H_{99}N_{11}O_{12}S_0H^+_1$	3.05	y_{11}
1205.82623	1	$C_{60}H_{108}N_{12}O_{13}S_0H^+_1$	2.55	y_{12}

m/z	charge	chemical formula	error	assignment
1304.89079	1	$C_{65}H_{117}N_{13}O_{14}S_0H^+_1$	-0.60	y_{13}
1403.95589	1	$C_{70}H_{126}N_{14}O_{15}S_0H^+_1$	-2.92	y_{14}
369.20194	1	$C_{18}H_{28}N_2O_6S_0H^+_1$	-0.20	a_3
510.28086	1	$C_{25}H_{39}N_3O_8S_0H^+_1$	-0.26	a_4
651.36016	1	$C_{32}H_{50}N_4O_{10}S_0H^+_1$	0.29	a_5
792.43897	1	$C_{39}H_{61}N_5O_{12}S_0H^+_1$	0.03	a_6*
933.51784	1	$C_{46}H_{72}N_6O_{14}S_0H^+_1$	-0.09	a_8
1074.59672	1	$C_{53}H_{83}N_7O_{16}S_0H^+_1$	-0.17	a_9
1173.66419	1	$C_{58}H_{92}N_8O_{17}S_0H^+_1$	-0.96	a_{10}
1272.73159	1	$C_{63}H_{101}N_9O_{18}S_0H^+_1$	-1.68	a_{11}
1371.79959	1	$C_{68}H_{110}N_{10}O_{19}S_0H^+_1$	-1.86	a_{12}
1470.87812	1	$C_{73}H_{119}N_{11}O_{20}S_0H^+_1$	5.14	a_{13}
1569.93721	1	$C_{78}H_{128}N_{12}O_{21}S_0H^+_1$	-1.12	a_{14}
1669.01776	1	$C_{83}H_{137}N_{13}O_{22}S_0H^+_1$	6.21	a_{15}
497.27316	1	$C_{24}H_{38}N_3O_8S_0H^+_1$	-0.01	b_3
638.35235	1	$C_{31}H_{49}N_4O_{10}S_0H^+_1$	0.32	b_4
779.43132	1	$C_{38}H_{60}N_5O_{12}S_0H^+_1$	0.25	b_5
920.51063	1	$C_{45}H_{71}N_6O_{14}S_0H^+_1$	0.57	b_6
1061.58931	1	$C_{52}H_{82}N_7O_{16}S_0H^+_1$	0.22	b_7
1160.65536	1	$C_{57}H_{91}N_8O_{17}S_0H^+_1$	-1.84	b_8
1259.72154	1	$C_{62}H_{100}N_9O_{18}S_0H^+_1$	-3.47	b_9
1358.79286	1	$C_{67}H_{109}N_{10}O_{19}S_0H^+_1$	-1.08	b_{10}
1556.93205	1	$C_{77}H_{127}N_{12}O_{21}S_0H^+_1$	0.58	b_{12}
283.16514	1	$C_{14}H_{22}N_2O_4S_0H^+_1$	-0.33	k'_2
424.24409	1	$C_{21}H_{33}N_3O_6S_0H^+_1$	-0.29	k'_3
270.15731	1	$C_{13}H_{21}N_2O_4S_0H^+_1$	-0.37	j'_2
		Average error (ppm)	0.53	
		Std dev error (ppm)	0.80	

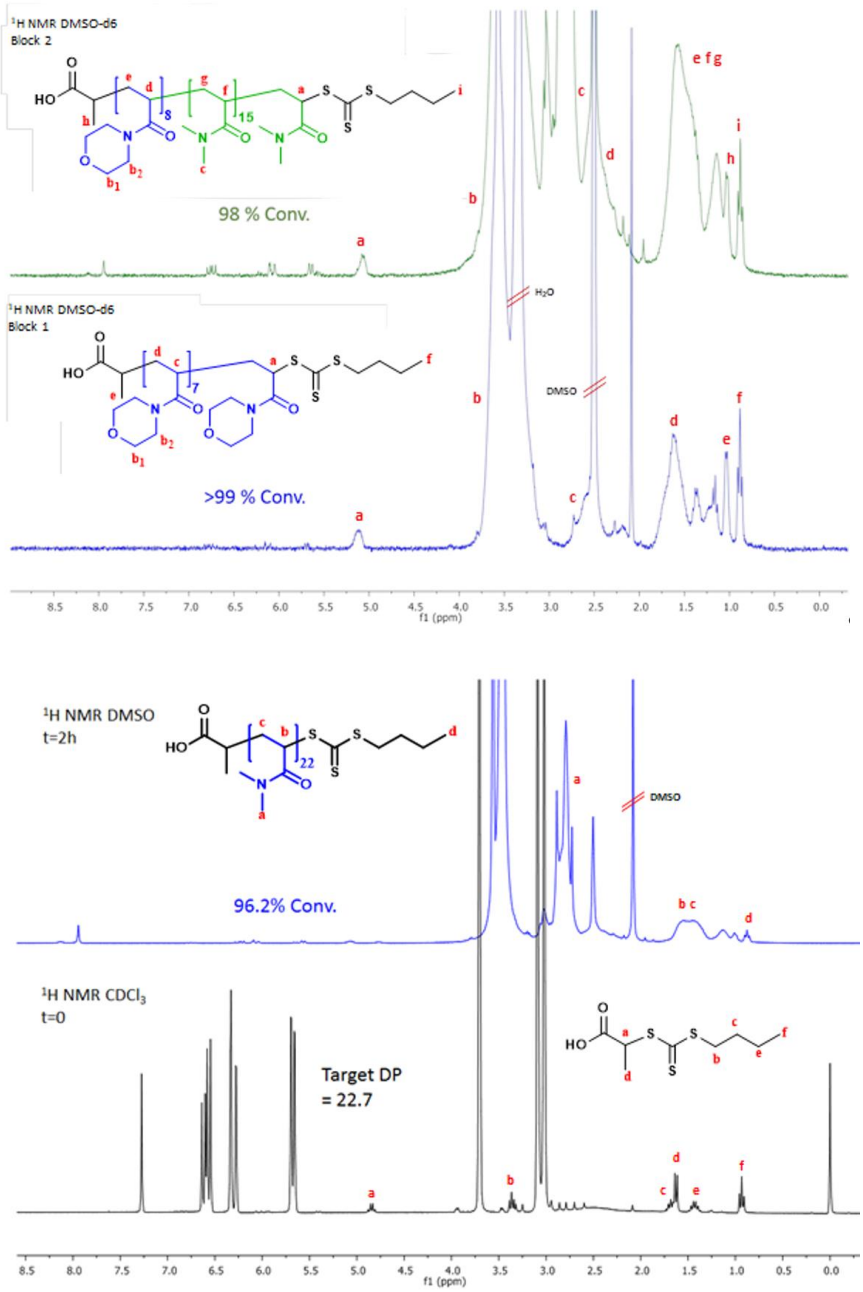

*Figure S 4.4 ^{1}H NMR spectrum of p(DMA) and p(NAM-*b*-DMA) carried out on a 400 MHz NMR instrument in $CDCl_3$ as a solvent.*

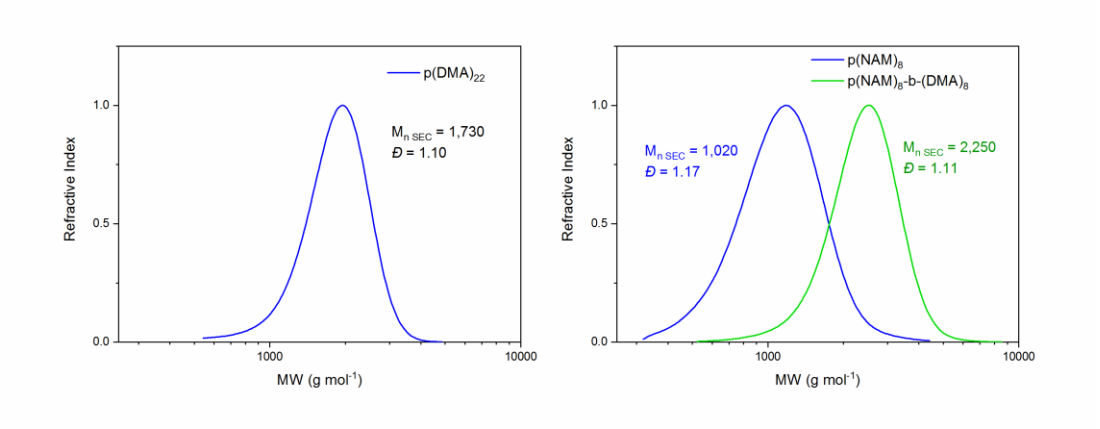

Figure S 4.5 SEC characterisation of the polyacrylamides. Measurement was performed in THF as described in the experimental section.

5. Influence of select terminal groups on poly(2-oxazoline) hydrolysis

Tomos E. Morgan[1], Thomas Floyd[1], Bryan Marzullo[1], Christopher A. Wootton[1], Mark P. Barrow[1], Anthony W. T. Bristow[2], Sebastien Perrier[1], Peter B. O'Connor[1]*

[1]Department of Chemistry, University of Warwick, Coventry, Midlands, CV4 7AL, UK.

[2]Chemical Development, Pharmaceutical Technology & Development, Operations, AstraZeneca, Macclesfield, UK.

The MS, MS/MS, and analysis presented in this chapter were all carried out by the thesis author. Thomas Floyd carried out the synthesis, purification, and GPC and NMR analysis of the polyoxazoline species.

The work presented in this chapter has been prepared for publication in ACS Analytical chemistry by authors Tomos E. Morgan, Thomas Floyd, Bryan P. Marzullo, Christopher A. Wootton, Mark P. Barrow, Anthony W. T. Bristow, Sébastien Perrier, Peter B. O'Connor.

5.1. Abstract

Understanding modification of synthetic polymer structures is important in furthering their synthesis and applications. In this contribution, a series of hydrolyzed poly(2-oxazoline) species were produced forming [(2-polyoxazoline)-*co*-(ethylenimine)]. P(Ox-*co*-EI) copolymers, PEI being the hydrolyzed product of POx. The copolymers were analyzed by mass spectrometry to achieve characterization of PEI content which closely agreed to the NMR data.

Kendrick analysis of the data greatly simplified the assignment of complex copolymer fragmentation spectra. Analysis of the copolymers by electron capture dissociation fragmentation gave a large insight into the characterization of the species end groups and location of hydrolysis events. Hydrolysis levels from each fragment were calculated theoretically and compared to the practical data showing close alignment between the predicted and measured hydrolysis levels. Analysis of the hydrolyzed polyoxazolines showed that presence of an OH terminus resulted in a hydrolysis event on the adjacent monomer unit, giving direct molecular insight to the hydrolysis of the polyoxazoline polymer.

5.2. Introduction

The use of biocompatible poly(2-oxazoline)s (POx) as an alternative to poly(ethylene glycol) (PEG)-based bioconjugation species is well established due to their favourable immunogenic properties[1-3] and ease of introducing functionality.[4,5] Chemical modification of POxs by hydrolysis to the polyethyleneimine (PEI) species offers a significant advantage as further post polymerization modification of the resulting P(Ox-*co*-EI) copolymers[6] increase their biocompatibility and fine tuning their biological response.[7-10] Post polymerization modification allows more complex copolymer structures to be produced allowing a greater control of chemical properties and conjugation frameworks.[11,12] The ethyleneimine sections of the copolymer can carry a positive charge in biological media allowing the resulting copolymer to bind to negatively charged species, such as DNA and RNA.[10] Therefore Poly[(oxazoline)-*co*-(ethylenimine)] (P(Ox-*co*-EI)) acts as a potential carrier of siRNA as a therapeutic agent, increasing siRNA half-lives and the biocompatibility of the transfection vector.[13-15] The biological properties of the resulting copolymer species are based on the size, terminating and initiating groups, and the levels and distribution of PEI present.[16,17]

The use of electrospray ionisation (ESI) as a means to analyse polyoxazolines and poly(ethylenimine)s polymers has been previously studied.[18,19] Coupling ESI to ultra-high resolution mass spectrometry techniques, such as Fourier-transform ion cyclotron resonance mass spectrometry (FT-ICR MS) produces accurate mass analysis and the ability to fragment polymers to better understand their sequence.[20-24] The analysis of copolymeric species to better understand the reactivity ratios between monomer units can be very useful to synthetic polymer chemists in understanding synthesis of more complex polymeric species.[25]

Multiple fragmentation methods for the sequence analysis of POxs have been shown including collision induced/activated dissociation (CAD/CID),[26,27] fragmentation of PEI has been carried out by similar methods.[18,28] The use of electron capture dissociation (ECD) techniques has been shown to provide near complete sequence coverage as well as initiating and terminating end group information.[20,21,29] The partial hydrolysis of a POx to PEI can be well controlled,[10,30] with the resulting

copolymer ratio measured by nuclear magnetic resonance (NMR). NMR analysis provides accurate hydrolysis percentages but cannot provide information about the variation in hydrolysis with polymer size, or where the hydrolysis occurs across individual polymer chains.

Copolymer mass spectrometry can be analysed with the use of Kendrick mass analysis,[31-36] the analysis relies on the difference in fractional mass of different monomers present in the copolymer species. The separation of different fragmentation pathways and monomer unit composition allows the rapid *de novo* elucidation of highly complex tandem MS spectra.

In this study, we report the characterisation of P(Ox-*co*-EI)-OH and P(Ox-*co*-EI)-N_3 copolymers as well as fragmentation data to elucidate sequence information of the copolymers generated. The total hydrolysis ratio mass spectrometry data aligned closely with the NMR results. The sequence and end group coverage produced by tandem mass spectrometry gave insight into the random distribution of the EI species as well as showing the effects of the terminal group on the hydrolysis.

5.3. Experimental and methods

Cationic ring opening polymerisation of 2-ethyl oxazoline was carried out producing a methyl- and hydroxyl- capped poly(2-ethyl-2-oxazoline), section S1 in supplementary information. The resulting poly(2-ethyl-2-oxazoline) was hydrolysed by microwave heating for 30 minutes into a poly(2-ethyl-2-oxazoline) and polyethyleneimine copolymer. The total amount of hydrolysis was calculated by NMR.

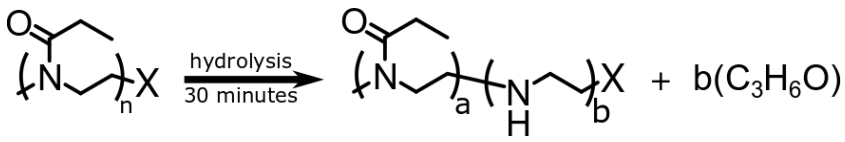

Figure 5.1 A) Overview of synthesis of P(Ox-co-EI)-OH, through hydrolysis of POx.

The hydrolysed sample was dissolved into a 99.5% solution of purified water obtained from a Direct-Q3 Ultrapure Water System (Millipore, Lutterworth, United Kingdom) at 20 µM in 0.5% formic acid (Sigma- Aldrich, Dorset, United Kingdom). All experiments were performed on a 12 T solariX Fourier transform ion cyclotron resonance mass spectrometer (Bruker Daltonik, GmbH, Bremen, Germany) using a nanoelectrospray (nESI) ion source in positive ion mode. The ECD was carried out with the use of an indirectly heated hollow cathode with a current set at 1.5 A, with a pulse length of 0.2 s and bias 1.2 eV. All data were recorded using 4 mega-word (2^{22}, 22 bit) transients (1.6777 s) achieving approximately 400 000 resolving power at *m/z* 400. All mass spectra were internally calibrated by the intact polymer peaks across the polymer distribution, or by internal calibration of fragment peaks in ECD spectra (peaks used for calibration are marked). The peaks used for internal calibration were crosschecked using both the *a* and *x* fragment series. The Bruker SNAP algorithm was used for peak picking with the polyoxazoline monomer used as the repeat unit. The Bruker SNAP algorithm matches a calculated isotope distribution adjusted to a repeat unit with increasing mass. [37-39]

The fragmentation data was compared to the statistically distributed fragmentation patterns. The statistically distributed hydrolysis maps were calculated by combination of PEI units within a polymer chain using a modified Heap's algorithm.[40] The total number of arrangements was calculated and the fragment intensities were calculated by code included in the SI. Figure 5.2 shows a theoretical model of 2 EI units evenly distributed across five monomer units using the Heap's algorithm and how, at different fragmentation points, the total proportion of each species will vary. Put simply:

Random hydrolysis events (H) will evenly distribute across all possible combinations. All possible combinations will be statistically represented during the analysis. At

monomer position **1** measuring back to the α (left) methyl terminus 40% of fragments have one hydrolysis event (H) as only one monomer unit is present; a doubly hydrolysed species can't be present. The remaining 60% of fragments possible have not undergone a hydrolysis event.

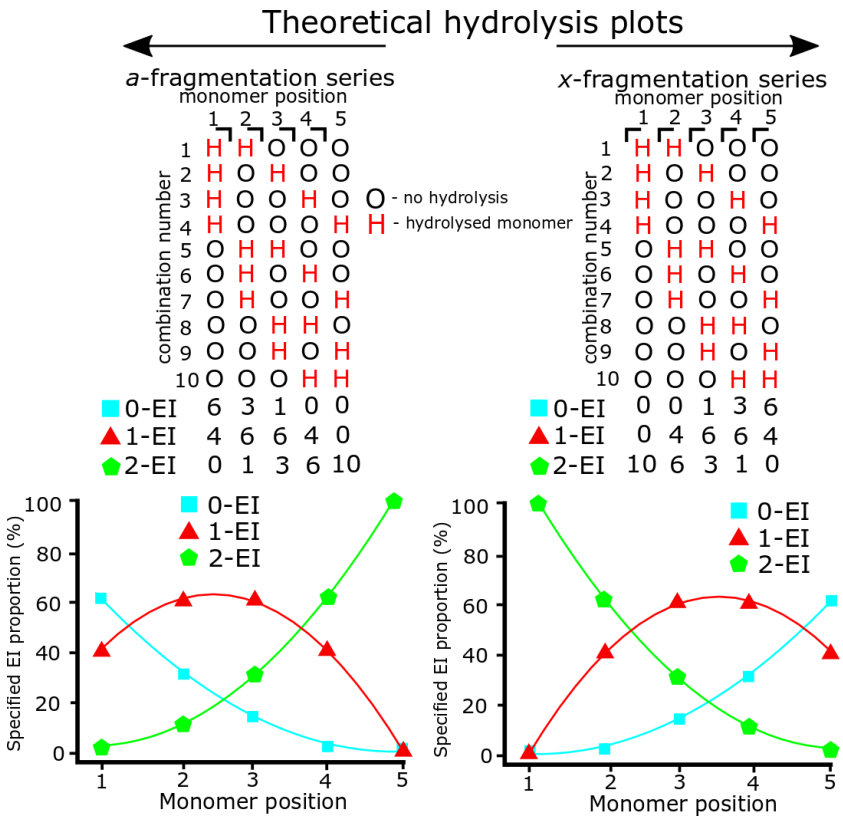

Figure 5.2 A) Theoretical plots of all possible combinations of hydrolysed species (H) and unhydrolysed species (O) for a 5 monomer polymer where 2 units are hydrolysed. Each monomer position is counting back to the corresponding a/x terminus. Plotting the intensities shows the distribution of EI based on a random hydrolysis chance. Deviations from the theoretical distribution is evidence that hydrolysis is not a random process. The x-series will be mirror imaged of the a series in a random process.

Moving to monomer position **2** 60% of measured fragment oligomers contain one hydrolysis event (H). 30% of fragments contain no hydrolysis events and 10% of fragments contained 2 hydrolysis events. Fragmentation at each monomer and the resulting oligomer unit can be analyzed in the same way and the proportions compared. If the practical data shows similar binomial distribution to the theoretical

plot then they hydrolysis is random, if there is a large shift in the distribution then it is not random.

5.4. Results and Discussion

MS analysis of the hydrolysed POx species are shown in Figure 2. The analysis showed mainly protonated adduct species between charges 2+ and 4+. The weighted average hydrolysis value closely aligned to the amounts measured by NMR, presented in the SI. The increased complexity caused by the presence of multiple copolymer species was resolved within the FT-ICR MS. Over 100 assignments were made for each of the copolymer species.

Heat maps corresponding to the POx and PEI content shows the distribution of hydrolysis with increasing mass. The mass range of P(Ox-*co*-EI)-OH, Figure 5.3, started with a detected mass of 1337 Da consisting of 5-PEI units and 11-Pox units. The highest mass was detected at 2568 Da containing 6-PEI and 23-POx units. The smallest chain detected was formed of 9-POx and 2-PEI units. The NMR data showed average bulk hydrolysis level of P(Ox-*co*-EI)-OH to be 25%. By MS the weighted peak averages gives the Ox/EI ratio of 25.8% showing that mass spectrometry is capable of achieving species-specific and bulk measurement of the modified polymers in addition to the distribution of the hydrolysis by mass.

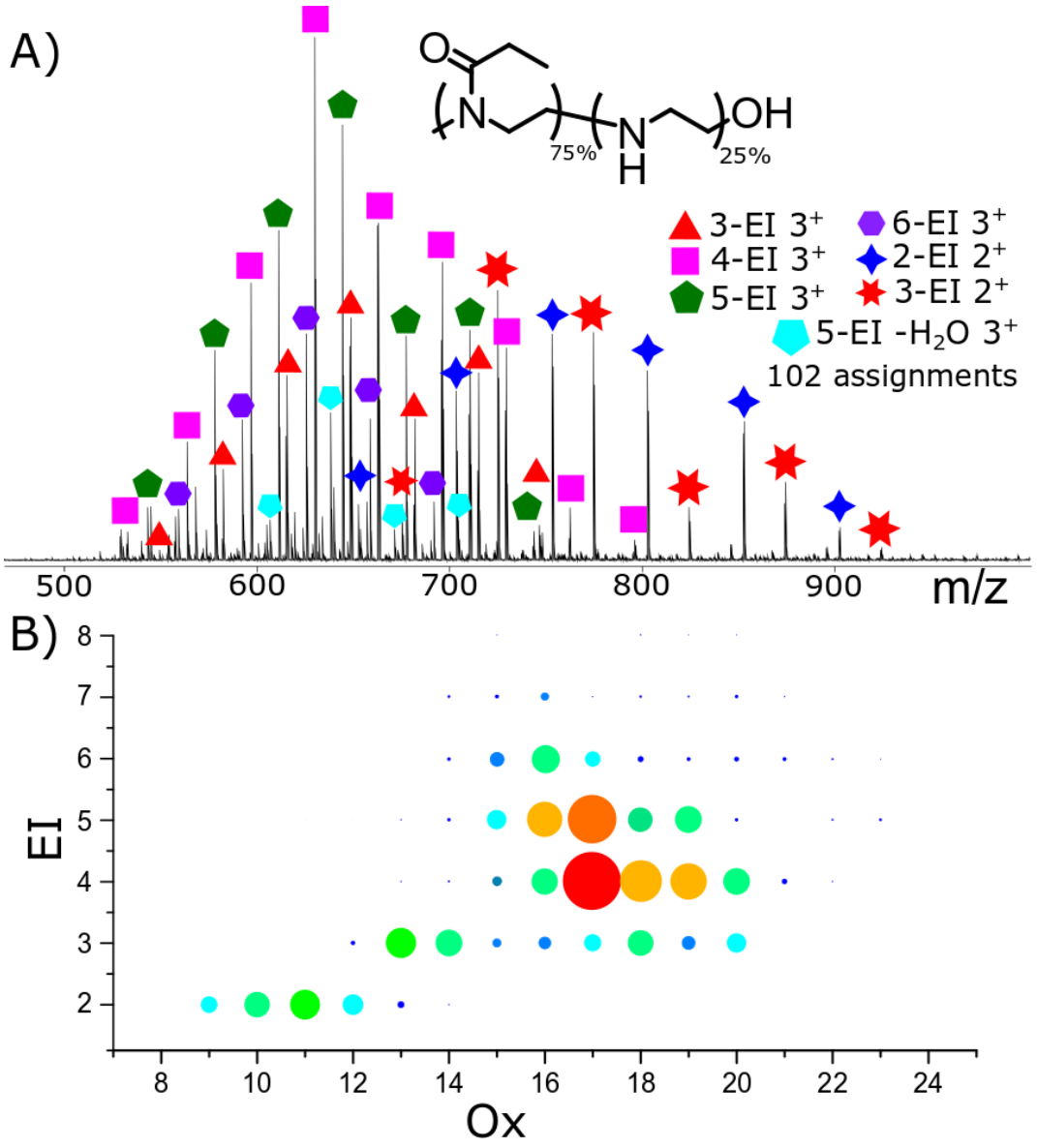

Figure 5.3 A) nESI analysis of P(Ox-*co*-EI)-OH, with B) Heat map of POx units to EI units spot size directly relates to peak area in MS.

The sample of P(Ox-*co*-EI)-N_3 contained both P(Ox-*co*-EI)-N_3 and P(Ox-*co*-EI)-OH. Both copolymer species could be separated by mass and their individual hydrolysis levels measured. There is a great advantage in the ability to analyse the two different polymer species as opposed to a bulk measurement by NMR.

The P(Ox-*co*-EI)-N_3 consisted of the largest detected chain of 25 Ox units and 4 EI units and highest mass of 2704 Da. The smallest chain contained 10 Ox units and 2 EI units and was also the lowest mass at 1232 Da.

NMR can be used to achieve analysis of a bulk measurement with comparisons to the mass spectrometry results. Figure 5.4 shows the NMR that compares the protons from the EI environment to that of the Ox environment. Although this gives a very accurate measurement of the total hydrolysis amount, the NMR does not give an accurate measurement of how that might be distributed across a polymer distribution.

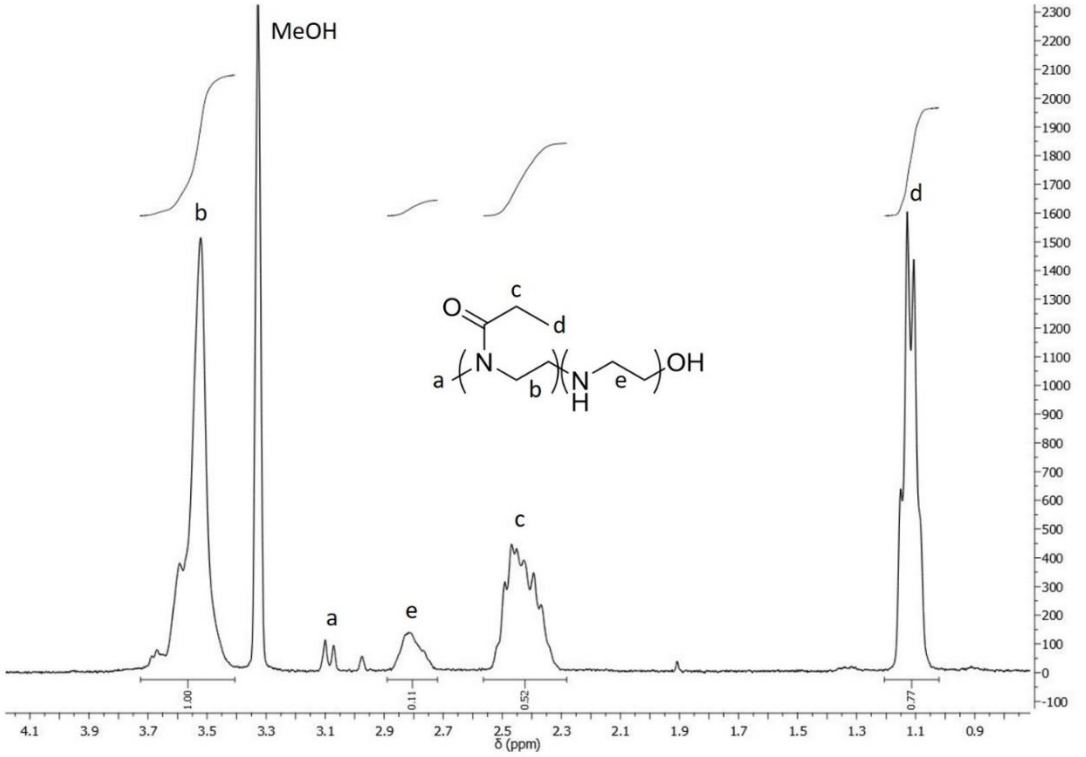

Figure 5.4 NMR of the p(Ox-*co*-EI)-OH, the EI protons (e) and the Ox protons (b) can be integrated and compared. Broadness of peaks is caused by the range of proton environments that are present within the polymer.

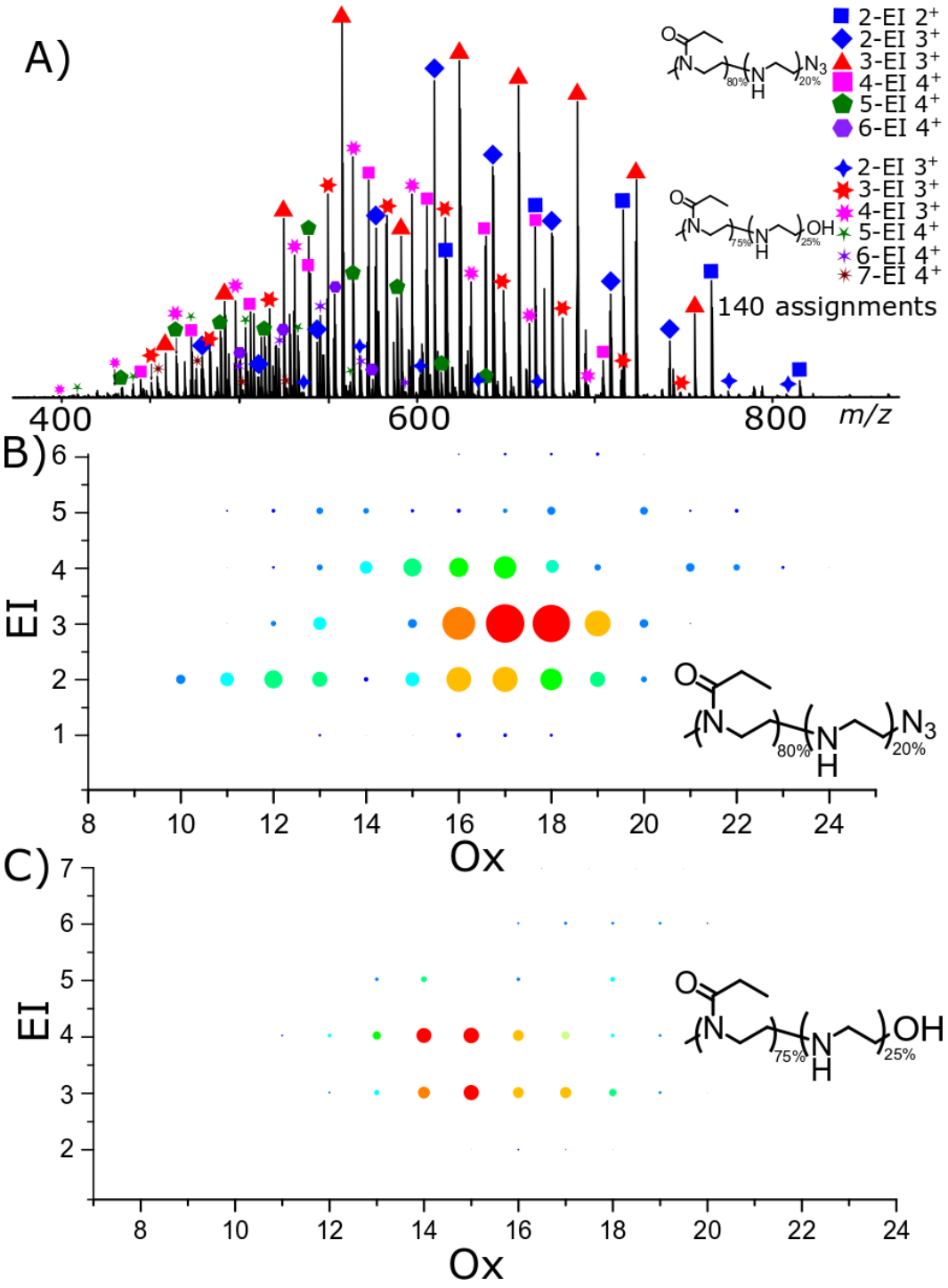

Figure 5.5 A) nESI analysis of P(Ox-*co*-EI)-N_3 B) and C) corresponding heat maps to the same scale showing more N_3 terminated copolymer compared to OH terminated.

Analysis of the hydrolysis positioning by tandem mass spectrometry experiments was carried out using electron capture dissociation[41] (ECD) on a number of hydrolysed copolymer species. The fragmentation of the copolymers by ECD gave two fragment

ion series *a* and *x*. The fragment series contain a number of monomer units, forming an fragmented oligomer of the polymer, and a terminus. Figure 5.6 shows that the *a* fragmentation series will contain the α terminus, in both of the copolymer cases the α terminus is the methyl group. The *x* series contains the ω terminus, OH or N_3 depending on the polymer analysed.

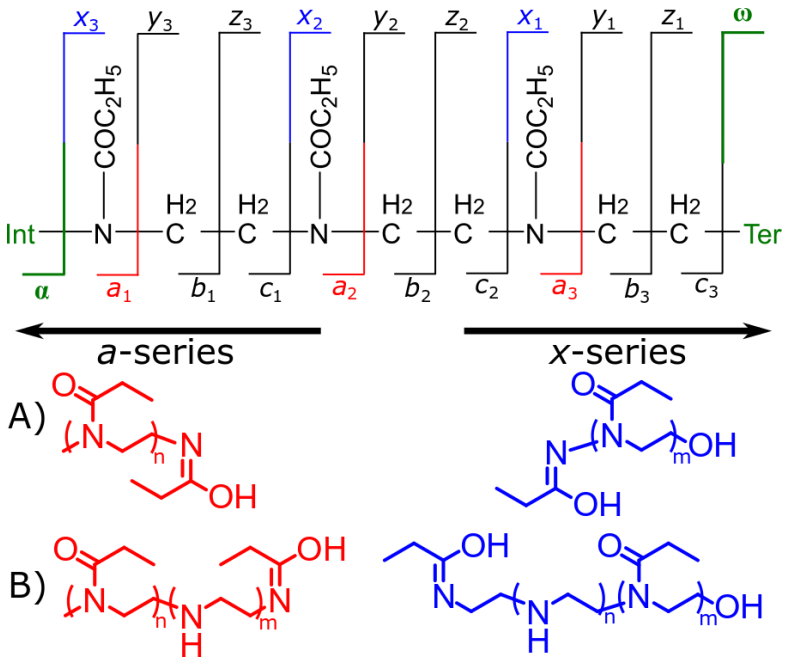

Figure 5.6 A) Cleavage diagram of a polyoxazoline polymer with the observed *a*- and *x*- series fragments , A) shows the expected *a*-series and *x*-series fragments produced from a homopolymer and B) the expected *a*-series and *x*-series fragments produced from a EI/Ox copolymer.

The proportions represented in Figure 5.7 are the fragment intensities comparing the peak area of the 0-EI containing fragment and the 1-EI containing fragment at each monomer position. By calculating the total peak area of fragments at each monomer unit the relative proportions of differing EI amounts can be compared to one another generating a plot, Figure 5.7C. The theoretical plot, Figure 5.7D, assumes completely random hydrolysis. Deviation from the theoretical plots indicates deviation from completely random hydrolysis events.

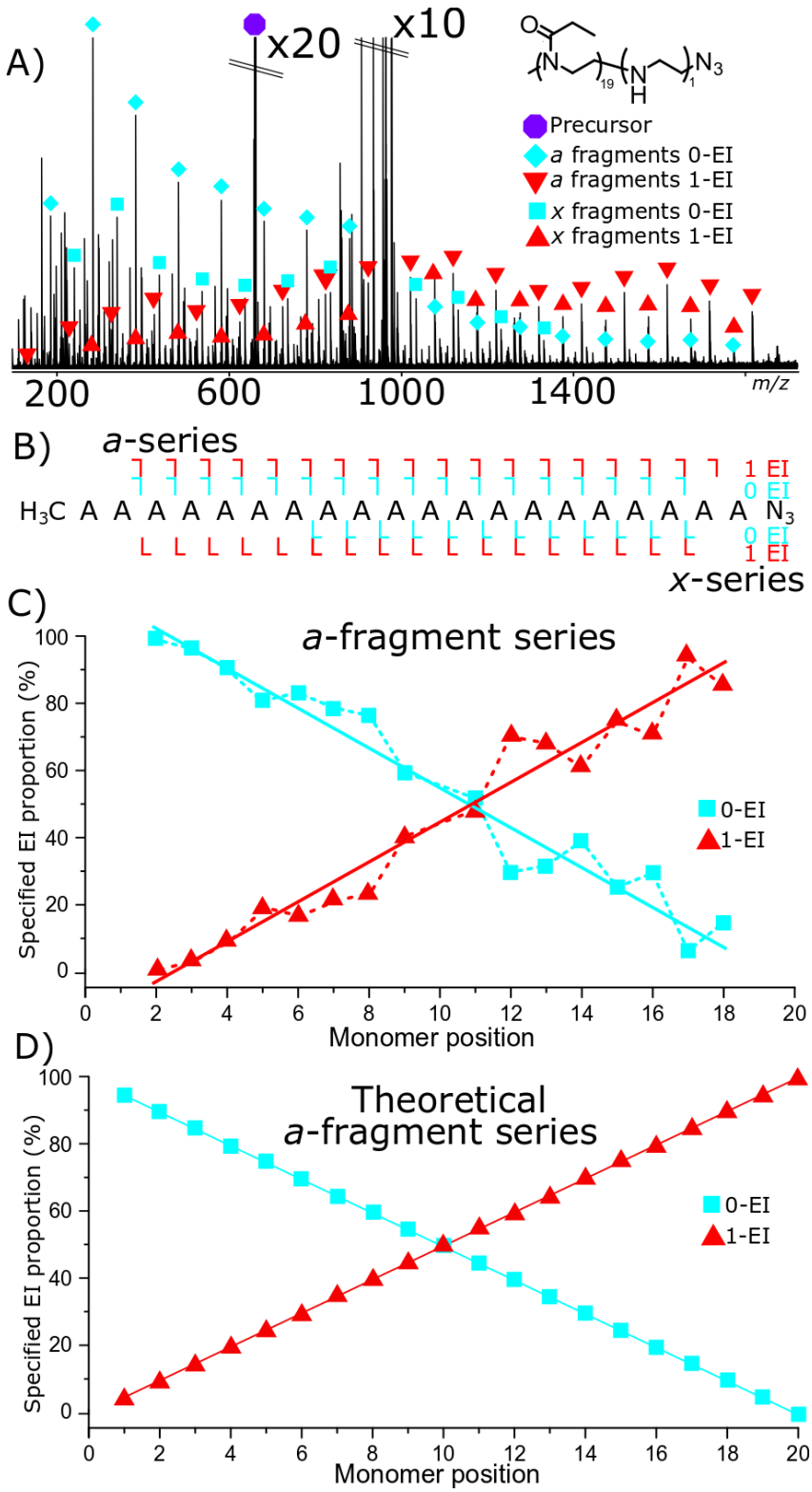

Figure 5.7 A) ECD fragmentation of a 20 monomer copolymer species containing 1 EI unit. Main fragment series are highlighted. B) Fragment coverage diagram showing all fragments. C) Plot of EI content on the *a*-series as a function of fragment intensity. D) Theoretical plot of fragment intensity between the two EI values. Showing good agreement with C).

Isolation and fragmentation of P(Ox_{19}-*co*-EI_1)-N_3 gave the four expected fragmentation pathways, Figure 5.7. The *a*-series consisted of the methyl terminus and two fragment series, one fragment series contained 0-EI units and the other containing 1-EI unit. The *x*-series contained the N_3 terminus and 0-EI units and a 1-EI unit series. Figure 5.7C shows the *a*-series fragments plotted together. The *a*-series fragments contain the methyl end group and a number of monomer units. As the measurement occurred from the methyl end group the likelihood of observing an EI unit increased moving right across the molecule, towards the N_3 terminus.

Total coverage in the *a* series for 0-EI units was from a_2 (2-POx, *m/z* 187.14410) to a_{18} (18-Ox, *m/z* 1772.24155). The 1-EI series extended from a_2 (1-Ox 1-EI, *m/z* 131.11793) to a_{19} (18-Ox 1-EI, *m/z* 1815.28096). Figure 5.7C shows the plot by comparing the area of each peak. The total areas of the a_n peaks in both the 0-EI and 1-EI series were summed at the ratio between the two compared.

The results, presented in Figure 5.7, closely align with the theoretical plot, Figure 5.7D. Showing the presence of the 1-EI group trending upwards linearly across the length of the polymer chain. The analysis shows that it seems likely that the hydrolysis events forming EI monomer species in the copolymer were based on a random process.

Comparing Figure 5.7 to Figure 5.8 shows the inverted relationship between the *a*- and *x*- series fragments. Again, the *x*-series closely aligns to that of the theoretical plot shown below.

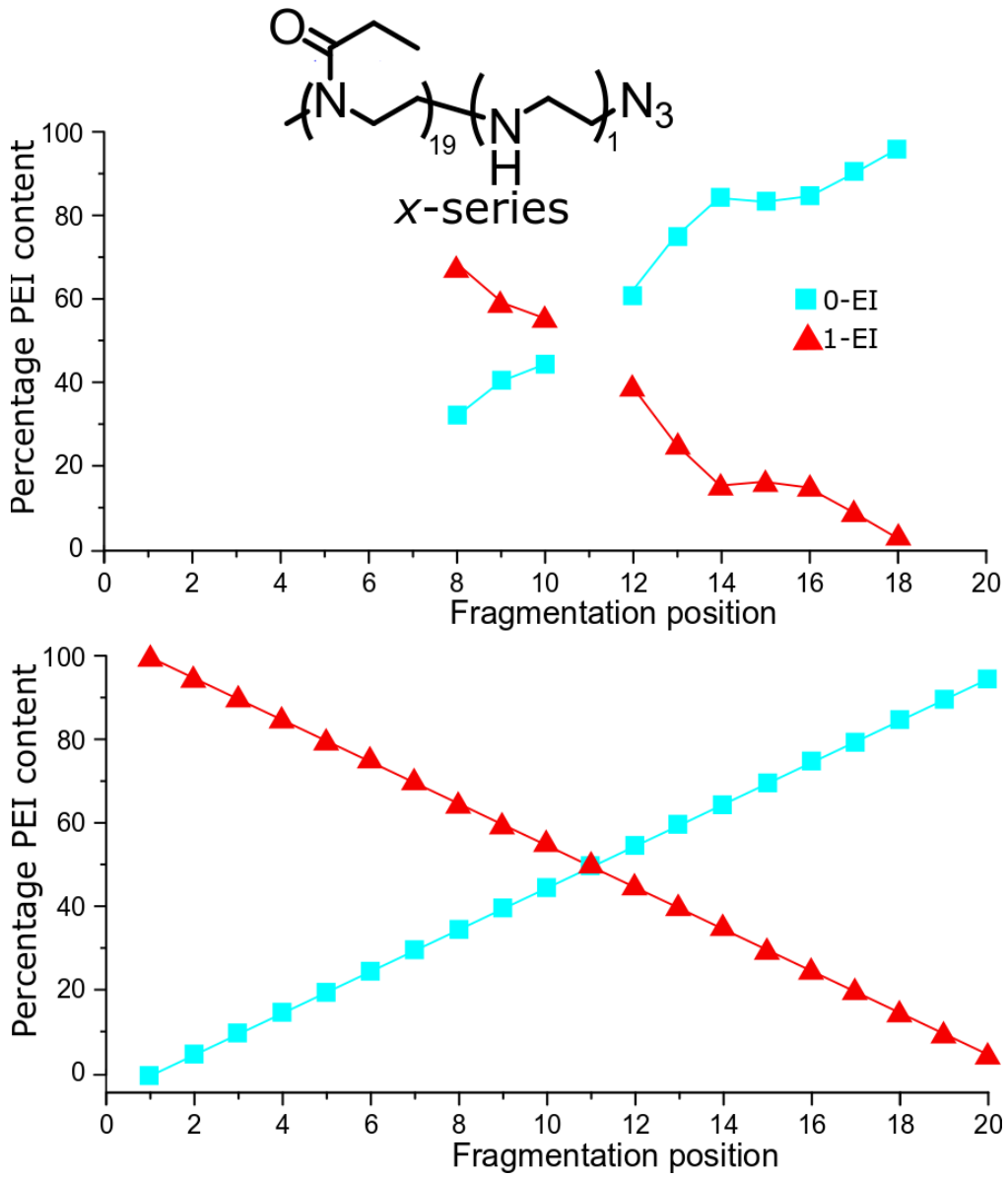

Figure 5.8 ECD fragmentation of P(Ox$_{19}$-*co*-EI$_1$)-OH with the *x-series* fragment comparison, the *x-series* forms a mirror image of the *a-series* shown in Figure 5.7.

The analysis of P(Ox$_{19}$-*co*-EI$_1$)-N$_3$ showed the expected hydrolysis distribution based on a random hydrolysis event. With complementary information produced through the *a*- and *x*- series the ability to characterize the hydrolysis events across the polymer was possible.

Changing the ω terminus from an N$_3$ to an OH functionalisation gave very different results. Quadrupole isolation of a singly hydrolysed copolymer P(Ox$_{19}$-*co*-EI$_1$)-OH showed no *x*-fragments containing 0-EI units. Only *x*-fragments containing 1-EI unit

were observed. Conversely, the *a*-fragment series showd mostly species consisting of 1-EI containing units. The lack of 0-EI oligomer units generated from the OH terminus suggests that hydrolysis is occurring in the monomer directly next to the OH terminus at a much higher rate than all other sites.

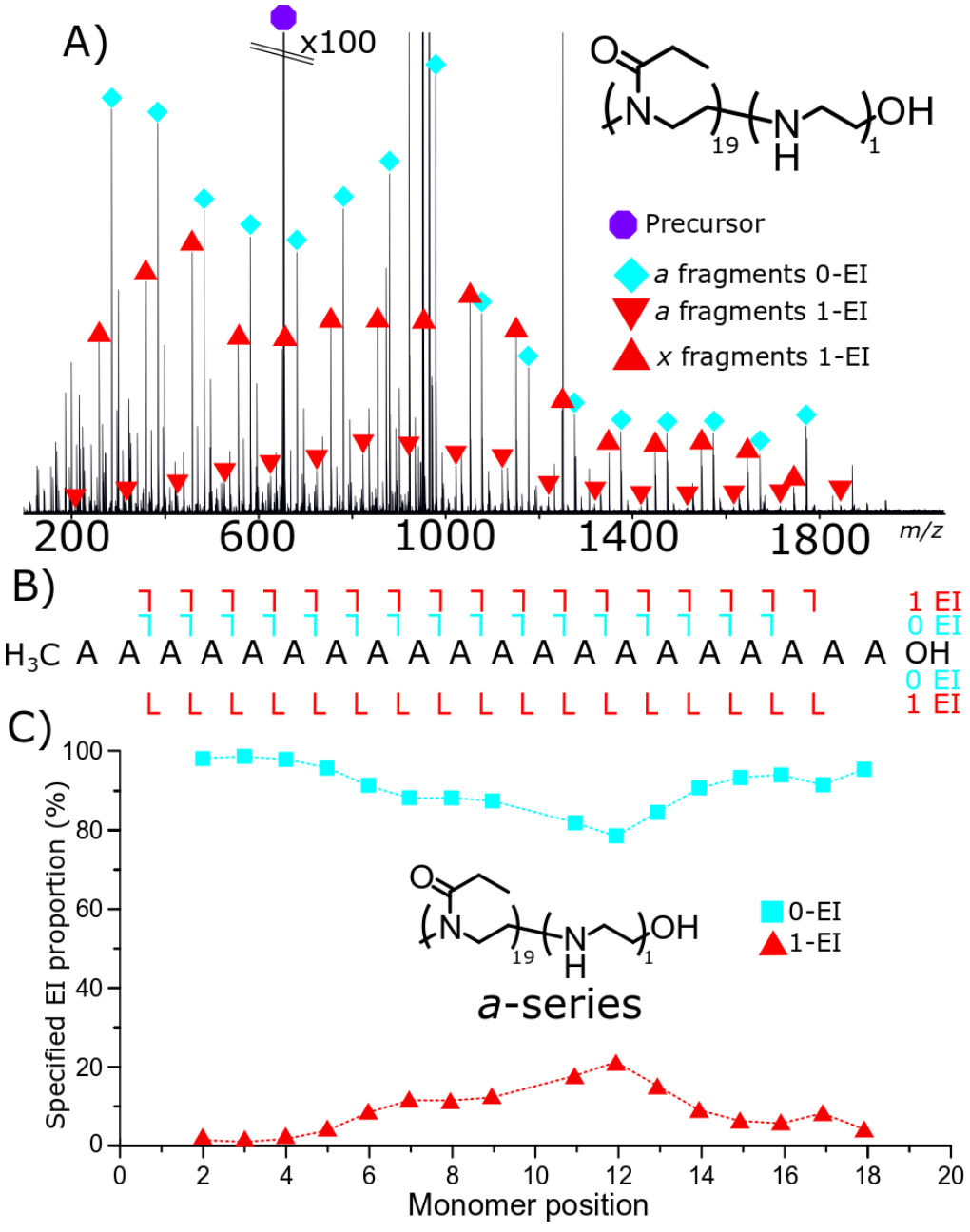

Figure 5.9 A) ECD fragmentation of P(Ox$_{19}$-*co*-EI$_1$)-OH B) Fragment coverage showing no OH terminated 0-PEI species. C) Shows the distribution of the a-series.

The OH terminus increased the frequency of hydrolysis events occurring at the terminal monomer. The same amount of 1-EI containing *a* series shows that the

formation of hydrolysis at any other position in the polymer chain is much less favoured, relatively. Comparing the plot of Figure 5.9C to that of the theoretical (Figure 5.7D) shows how the distribution is far separated from the random process projected values indicating a synergistic effect of the terminus on the hydrolysis event.

At higher levels of hydrolysis the same terminal effects were observed, testing higher levels of hydrolysis showed that there was no increase in the in the number of hydrolysis events at neighbouring POx units. By fragmenting a P(Ox_{22}-*co*-EI_2)-OH polymer it became clear to see the lack of neighbouring group effects but the same terminal hydrolysis event caused by the presence of the OH terminus. The effect of the constant hydrolysis event on the OH terminus becomes clear in Figure 5.10 where no 2-EI fragments are observed from the *a*-series (methyl terminus) and no 0-EI species are observed in the *x*-series (OH terminus). Plotting the *a*-series Figure 5.10B shows a close link to the theoretical plot Figure 5.10C assuming only one hydrolysis event. The most obvious difference is within the fragmentation map Figure 5.10D shows the lack of 0-EI *x*-series and 2-EI *a*-series fragments.

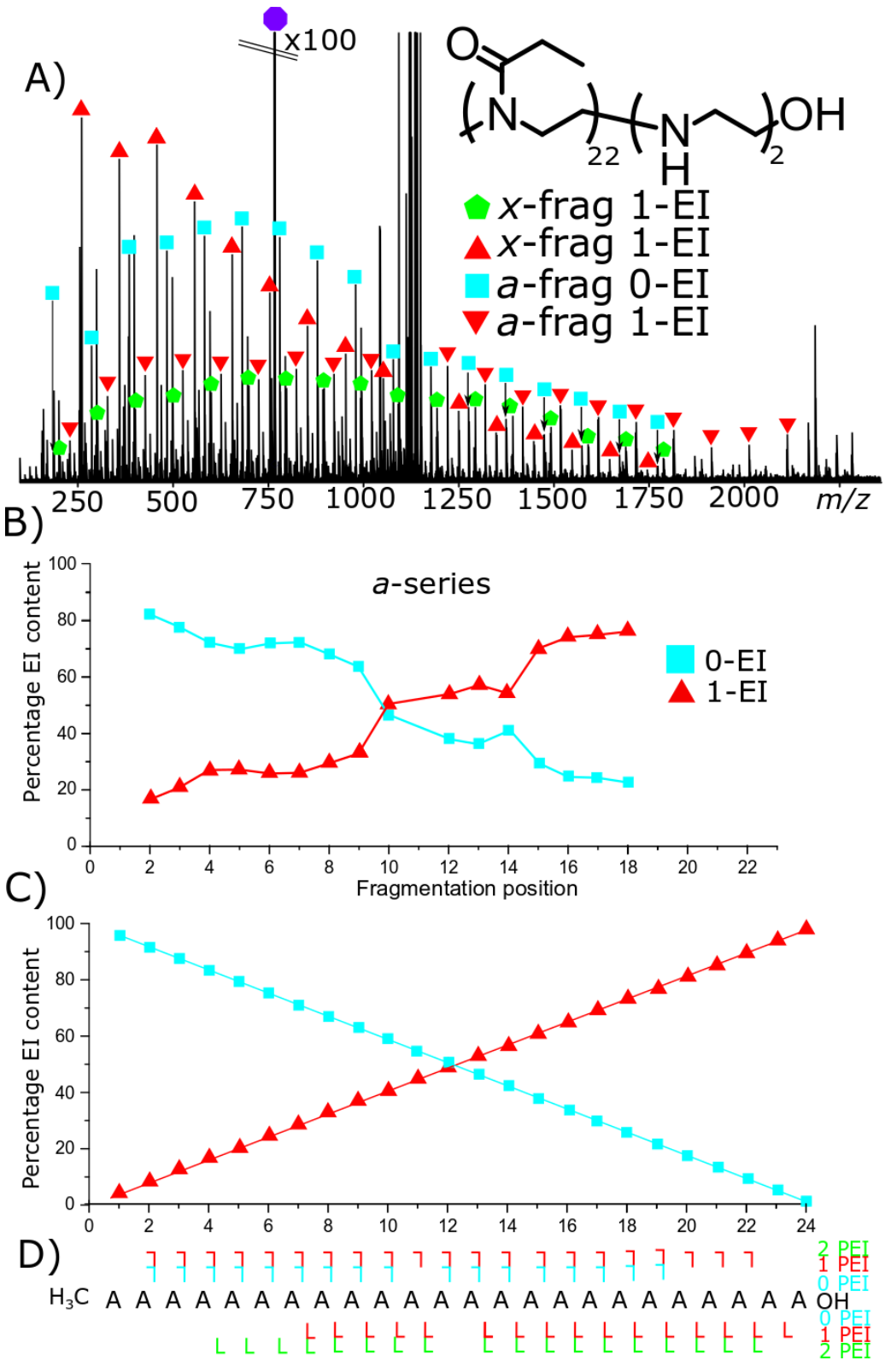

Figure 5.10 A) ECD fragmentation of P(Ox$_{22}$-*co*-EI$_2$)-OH B) Fragment EI content comparison, C) Theoretical plot assuming one hydrolysis event. D) Fragmentation map showing EI containing fragments.

The *x*-series showed a two hydrolysis events but with one of the events always occurring at the OH terminus. There are two distinct features:

Shifted hydrolysis event- A single hydrolysis event always occurs at the OH terminus and is seen as a clear shift as there are no 0-EI containing units.

No evidence of neighbouring effect- There is no evidence of a change in hydrolysis event rate with hydrolysis. Assuming hydrolysis always occurs at the OH terminus position there would be increased change from 1-EI to 2-EI resulting in an increased gradient closer to the terminus. As the gradient is relatively constant throughout the first ten positions it is unlikely that a neighbouring effect is present.

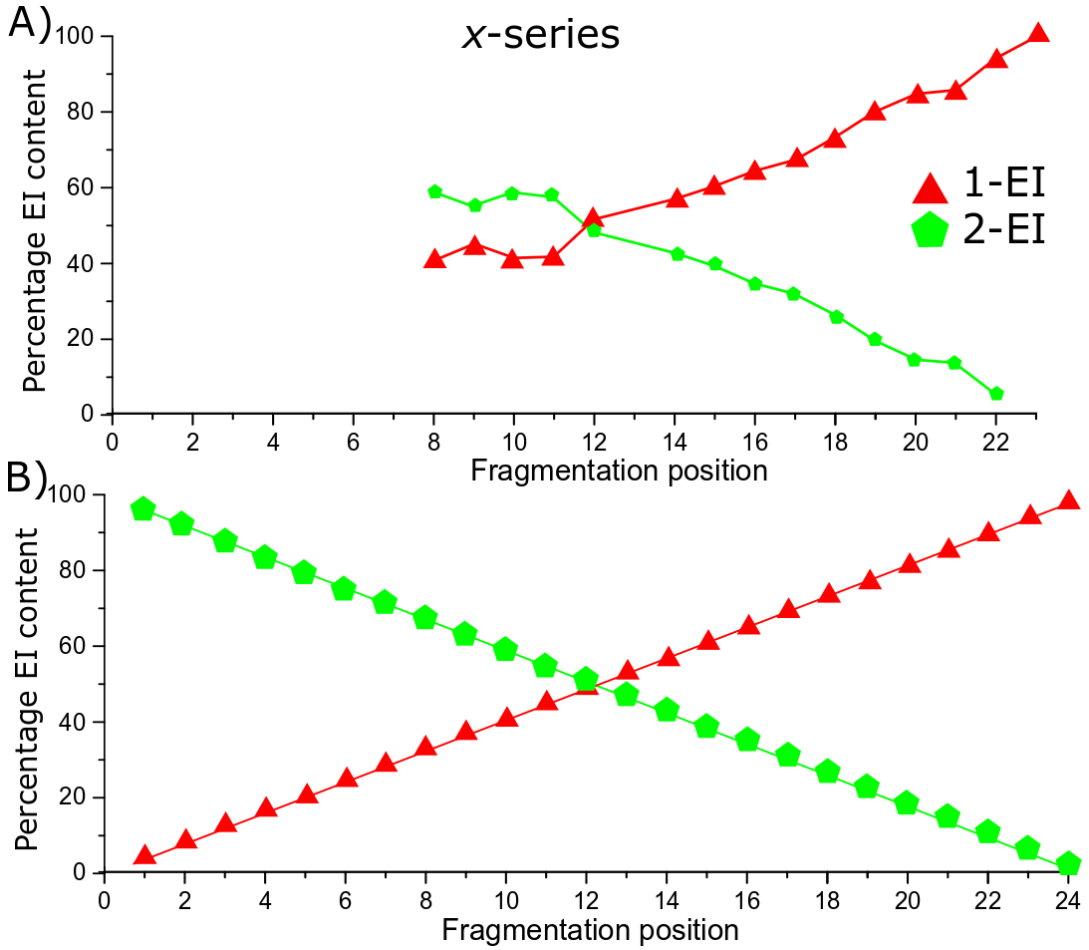

Figure 5.11 ECD fragmentation of P(Ox$_{22}$-*co*-EI$_2$)-OH A) Fragment EI content comparison, C) Theoretical plot assuming one hydrolysis event but with a one hydrolysis event shift.

The analysis of a P(Ox_{17}-*co*-EI_4)-OH polymer by ECD, Figure 5.12, results in the observation of no 0-EI OH terminated, *x*-series oligomers. Figure 5.12A shows the large number of peaks generated in the analysis due to the random copolymer fragmentation. The complexity of the ECD spectrum is not only increased by the many different EI containing *a*- and *x*-series fragments but also their related internal fragments. Although increasing complexity makes the analysis more challenging the high resolving power achieved allowed the fragments to be separated from one another.

***x*-series fragments:** The *x*-series fragments consisted of 1-EI to 4-EI containing oligomer fragments. The 1-EI species were present from x_2 to x_8 (*m/z* 161.12847, 0.0 ppm; *m/z* 854.60736, 0.0 ppm respectively). 2-EI species were observed from x_2 (*m/z* 105.10229, 0.48 ppm) to x_{13} (*m/z* 1194.8543, -0.41 ppm). 3-EI oligomers were present from x_4 to x_{18} (*m/z* 148.14447, 0.21 ppm; *m/z* 1535.10141, -0.50 ppm respectively), and the maximum hydrolysis level 4-EI oligomers were observed from x_5 (*m/z* 191.18667, 0.16 ppm) to x_{16} (*m/z* 1380.00773, 0.1 ppm).

***a*-series fragments:** Conversely the *a*-series fragments consisted of a 0-EI containing fragment series from a_2 to a_{11}, (*m/z* 187.14410, -0.08 ppm; *m/z* 1177.82781, 0.0 ppm respectively). The 1-EI containing oligomers were present from x_2 (*m/z* 131.11792, 0.23 ppm) to x_{16} (*m/z* 1518.07434, -0.88 ppm). The 2-EI species from a_3 to a_{18} (*m/z* 174.16009, -0.2 ppm; *m/z* 1660.18170, -2.7 ppm). The final hydrolysis level observed was 3-EI containing species consisting of a_5 (*m/z* 316.27076, 0.18 ppm) to a_{17} (*m/z* 1604.15787, -1.37 ppm).

Figure 5.12C shows the fragmentation map of the hydrolysed polymer. The presence of many 4-EI oligomers in the *x*-series and no detected 0-EI oligomers indicated that hydrolysis occurred preferentially at the OH terminus. After the initial hydrolysis at the OH terminus there seems to be little increase overall in the rate of hydrolysis at closer monomer units.

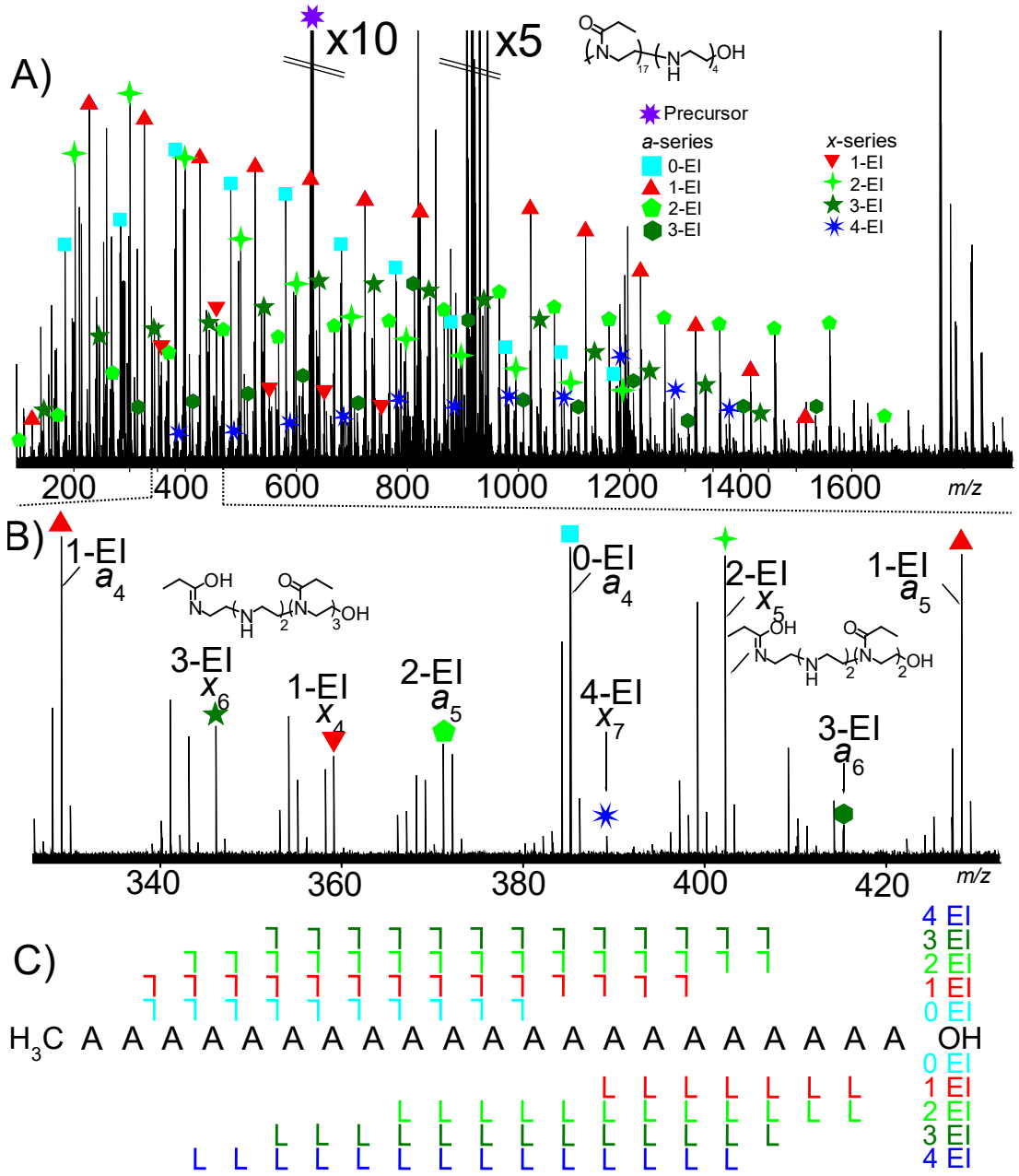

Figure 5.12 A) ECD fragmentation of P(Ox$_{17}$-*co*-EI$_4$)-OH B) zoom of region C) Fragment coverage showing no OH terminated 0-EI species. D) Theoretical *x*-series plot based on randomised hydrolysis process. E) fragment proportion showing fragment hydrolysis distribution F) is a shifted plot with 0-EI units substituted with 1-EI unit to better match the observed fragmentation.

Matching the 4-EI fragmentation with the corresponding fragment intensities of the *x*-series produces the following plots, Figure 5.13. The theoretical plot A) shows completely random hydrolysis events. B) is the measured hydrolysis distribution,

showing that there is still the presence of a 1-EI at the terminus of the polymer chain. The shifted plot can be substituted with 1-EI unit and compared: C). The comparison shows a much closer agreement between B) and C) compared with A) and B) showing the 1-EI shift at the terminus.

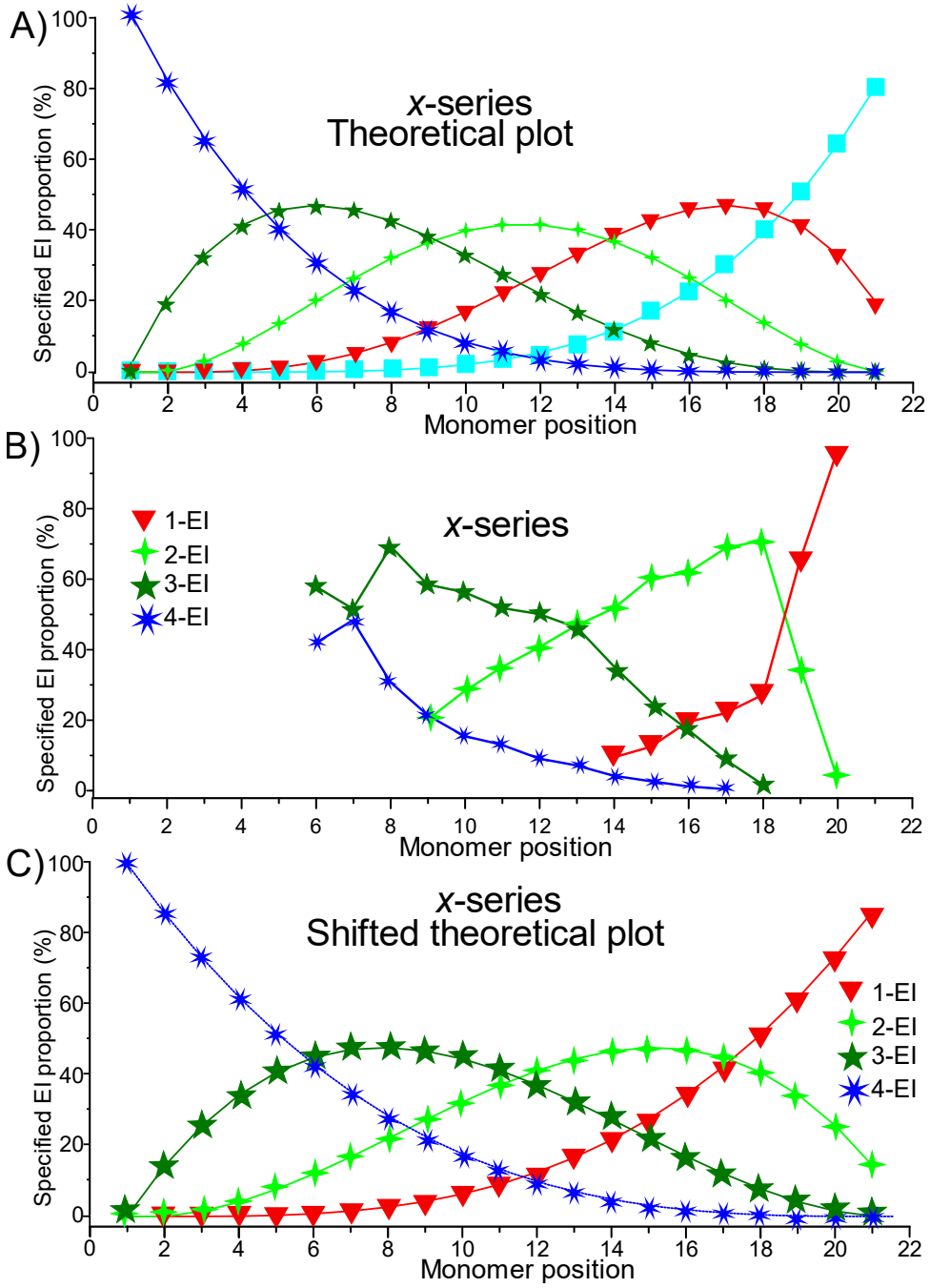

Figure 5.13 A) Theoretical *x*-series plot based on randomised hydrolysis process. B) fragment proportion showing fragment hydrolysis distribution C) is a shifted plot with 0-EI units substituted with 1-EI unit to better match the observed fragmentation.

Comparing the same molecule but as an *a*-series graph shows similar agreement and also the presence of 0-EI and a lack of 4-EI units from the methyl termination showing that hydrolysis is not being observed consistently at the terminus adjacent to the methyl group. By correcting for the lack of 4-EI fragments a much closer match is found between the two hydrolysis plots.

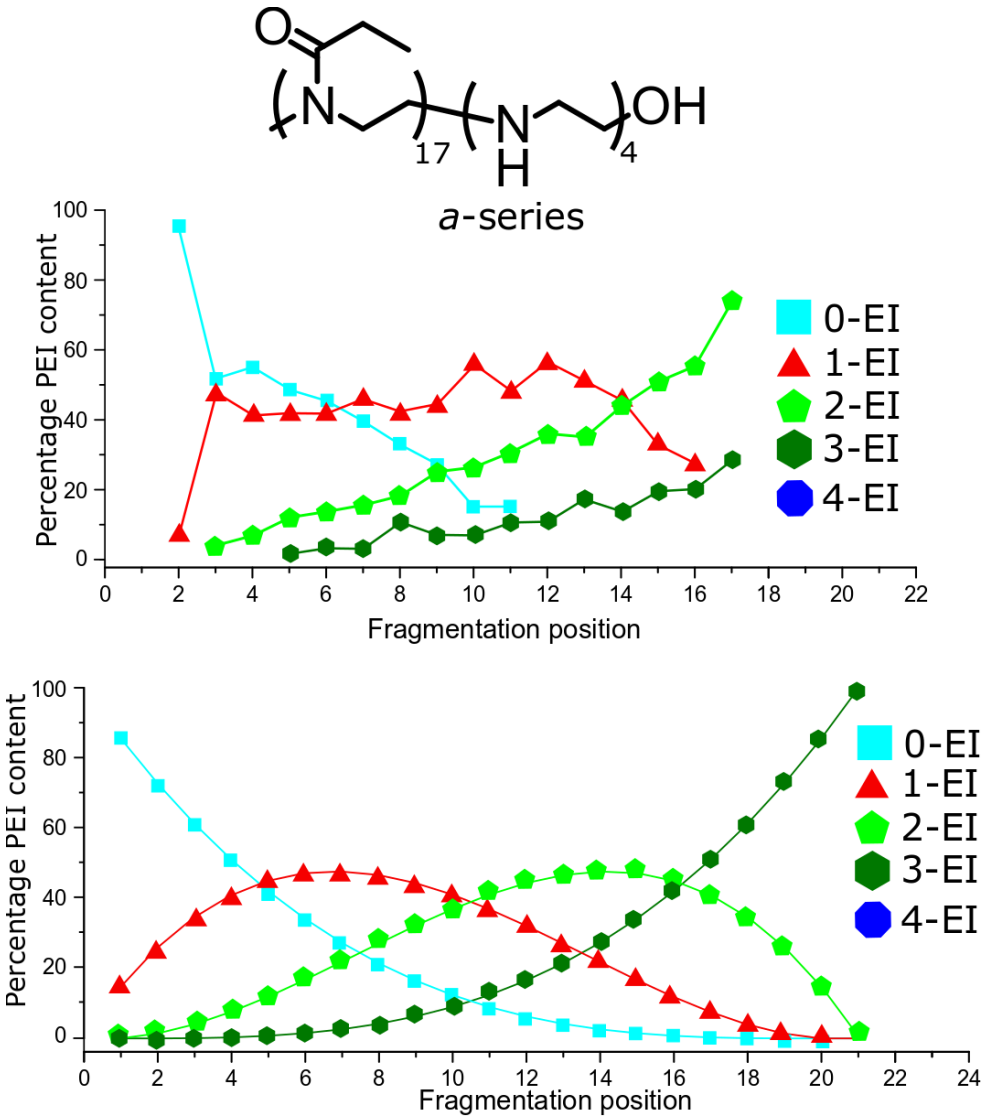

Figure 5.14 A) ECD fragmentation of P(Ox$_{17}$-*co*-EI$_4$)-OH showing *a*-series fragments, the top figure shows the observed hydrolysis events and the bottom shows a theoretical hydrolysis series assuming one hydrolysis less than the total amount (due to hydrolysis always occurring at the other terminus).

5.5. Conclusions

In conclusion, tandem mass spectrometry can be used to gain greater information into the molecular make up of modified polyoxazolines. The bulk hydrolysis levels of a hydrolyzed polyoxazoline can be analyzed by mass spectrometry, producing results that align closely to NMR. An added advantage comes from the analysis being carried out in a species specific manner, allowing the distribution of EI based on polymer chain size to be measured.

The randomness of the hydrolysis process can modelled and tested using combination theory and then tested practically by ECD of the poly[(oxazoline)-*co*-(ethylenimine)] copolymer. The modeling of random hydrolysis events allows direct comparison to practical data, differences between the two give information on the hydrolysis process. The presence of an OH terminus causes a much larger increase in the rate of hydrolysis on the polyoxazoline group directly adjacent to it. Increased knowledge of the molecular structure of modified polymers allows their biological properties to be understood to a much higher degree.

5.6. References

(1) Viegas, T. X.; Bentley, M. D.; Harris, J. M.; Fang, Z.; Yoon, K.; Dizman, B.; Weimer, R.; Mero, A.; Pasut, G.; Veronese, F. M. Polyoxazoline: chemistry, properties, and applications in drug delivery *Bioconjugate Chem.* **2011**, *22*, 976-986.
(2) Dworak, A.; Trzebicka, B.; Kowalczuk, A.; Tsvetanov, C.; Rangelov, S. Polyoxazolines — mechanism of synthesis and solution properties *Polimery* **2014**, *59*, 88-94.
(3) Bauer, M.; Lautenschlaeger, C.; Kempe, K.; Tauhardt, L.; Schubert, U. S.; Fischer, D. Poly(2-ethyl-2-oxazoline) as alternative for the stealth polymer poly(ethylene glycol): comparison of in vitro cytotoxicity and hemocompatibility *Macromolecular Bioscience* **2012**, *12*, 986 - 998.
(4) Guillerm, B.; Monge, S.; Lapinte, V.; Robin, J. J. How to modulate the chemical structure of polyoxazolines by appropriate functionalization *Macromol. Rapid Commun.* **2012**, *33*, 1600-1612.
(5) Glassner, M.; Vergaelen, M.; Hoogenboom, R. Poly(2-oxazoline)s: A comprehensive overview of polymer structures and their physical properties *Polym. Int.* **2018**, *67*, 32-45.
(6) Sedlacek, O.; Janouskova, O.; Verbraeken, B.; Hoogenboom, R. Straightforward Route to Superhydrophilic Poly(2-oxazoline)s via Acylation of Well-Defined Polyethylenimine *Biomacromolecules* **2019**, *20*, 222-230.
(7) Brissault, B.; Kichler, A.; Guis, C.; Leborgne, C.; Danos, O.; Cheradame, H. Synthesis of Linear Polyethylenimine Derivatives for DNA transfection *Bioconjugate Chem.* **2003**, *14*, 581-587.
(8) Tauhardt, L.; Kempe, K.; Knop, K.; Altuntaş, E.; Jäger, M.; Schubert, S.; Fischer, D.; Schubert, U. S. Linear Polyethyleneimine: Optimized Synthesis and Characterization - On the Way to “Pharmagrade” Batches *Macromol. Chem. Phys.* **2011**, 1918-1924.
(9) Yol, A. M.; Janoski, J.; Quirk, R. P.; Wesdemiotis, C. Sequence analysis of styrenic copolymers by tandem mass spectrometry *Anal. Chem.* **2014**, *86*, 9576-9582.
(10) Mees, M. A.; Hoogenboom, R. Full and partial hydrolysis of poly(2-oxazoline)s and the subsequent post-polymerization modification of the resulting polyethylenimine (co)polymers *Polymer Chemistry* **2018**, *9*, 4968-4978.
(11) Obermeyer, A. C.; Olsen, B. D. Synthesis and Application of Protein-Containing Block Copolymers *ACS Macro Letters* **2015**, *4*, 101-110.
(12) Ghosh, S.; Basu, S.; Thayumanavan, S. Simultaneous and Reversible Functionalization of Copolymers for Biological Applications *Macromolecules* **2006**, *39*, 5595-5597.
(13) Taranejoo, S.; Liu, J.; Verma, P.; Hourigan, K. A review of the developments of characteristics of PEI derivatives for gene delivery applications *J. Appl. Polym. Sci.* **2015**, *132*, 42096-42104.
(14) Hobel, S.; Aigner, A. Polyethylenimines for siRNA and miRNA delivery in vivo *WIREs Nanomed. Nanobiotechnol.* **2013**, *5*, 484-501.
(15) Lungwitz, U.; Breunig, M.; Blunk, T.; Gopferich, A. Polyethylenimine-based non-viral gene delivery systems *European journal of pharmaceutics and Biopharmaceutics* **2005**, *60*, 247-266.
(16) Adams, N.; Schubert, U. S. Poly(2-oxazolines) in biological and biomedical application contexts *Advanced Drug Delivery Reviews* **2007**, *59*, 1504-1520.
(17) Weber, C.; Becer, R. C.; Baumgaertel, A.; Hoogenboom, R.; Schubert, U. S. Preparation of Methacrylate End-Functionalized Poly(2-ethyl-2-oxazoline) Macromonomers *Designed Monomers and Polymers* **2012**, *12*, 149-165.
(18) Altuntaş, E.; Knop, K.; Tauhardt, L.; Kempe, K.; Crecelius, A. C.; Jager, M.; Hager, M. D.; Schubert, U. S. Tandem mass spectrometry of poly(ethylene imine)s

by electrospray ionization (ESI) and matrix-assisted laser desorption/ionization (MALDI) *J. Mass Spectrom.* **2012**, *47*, 105-114.
(19) Altuntaş, E.; Weber, C.; Kempe, K.; Schubert, U. S. Comparison of ESI, APCI and MALDI for the (tandem) mass analysis of poly(2-ethyl-2-oxazoline)s with various end-groups *Eur. Polym. J.* **2013**, *49*, 2172-2185.
(20) Perez Hurtado, P.; Lam, P. Y.; Kilgour, D.; Bristow, A.; McBride, E.; O'Connor, P. B. Use of high resolution mass spectrometry for analysis of polymeric excipients in drug delivery formulations *Anal. Chem.* **2012**, *84*, 8579-8586.
(21) Wei, J.; Bristow, A.; McBride, E.; Kilgour, D.; O'Connor, P. B. D-alpha-tocopheryl polyethylene glycol 1000 succinate: a view from FTICR MS and tandem MS *Anal. Chem.* **2014**, *86*, 1567-1574.
(22) Altuntaş, E.; Schubert, U. S. "Polymeromics": Mass spectrometry based strategies in polymer science toward complete sequencing approaches: a review *Anal. Chim. Acta* **2014**, *808*, 56-69.
(23) Crotty, S.; Gerislioglu, S.; Endres, K. J.; Wesdemiotis, C.; Schubert, U. S. Polymer architectures via mass spectrometry and hyphenated techniques: A review *Anal. Chim. Acta* **2016**, *932*, 1-21.
(24) Town, J. S.; Jones, G. R.; Hancox, E.; Shegiwal, A.; Haddleton, D. M. Tandem Mass Spectrometry for Polymeric Structure Analysis: A Comparison of Two Common MALDI-ToF/ToF Techniques *Macromol. Rapid Commun.* **2019**, 1900088-1900094.
(25) Town, J. S.; Jones, G. R.; Haddleton, D. M. MALDI-LID-ToF/ToF analysis of statistical and diblock polyacrylate copolymers *Polymer Chemistry* **2018**, *9*, 4631-4641.
(26) Altuntaş, E.; Weber, C.; Schubert, U. S. Detailed characterization of poly(2-ethyl-2oxazoline)s by energy variable collision-induced dissociation study *Rapid Commun. Mass Spectrom.* **2013**, *27*, 1095-1100.
(27) Baumgaertel, A.; Scheubert, K.; Pietsch, B.; Kempe, K.; Crecelius, A. C.; Bocker, S.; Schubert, U. S. Analysis of different synthetic homopolymers by the use of a new calculation software for tandem mass spectra *Rapid Commun. Mass Spectrom.* **2011**, *25*, 1765-1778.
(28) Rivera-Tirado, E.; Wesdemiotis, C. Characterization of polyethylenimine by electrospray ionization and matrix-assisted laser desorption/ionization *J. Mass Spectrom.* **2011**, *46*, 876-883.
(29) Morgan, T. E.; Ellacott, S. H.; Wootton, C. A.; Barrow, M. P.; Bristow, A. W. T.; Perrier, S.; O'Connor, P. B. Coupling Electron Capture Dissociation and the Modified Kendrick Mass Defect for Sequencing of a Poly(2-ethyl-2-oxazoline) Polymer *Anal. Chem.* **2018**, *90*, 11710-11715.
(30) de la Rosa, V. R.; Bauwens, E.; Monnery, B. D.; De Geest, B. G.; Hoogenboom, R. Fast and accurate partial hydrolysis of poly(2-ethyl-2-oxazoline) into tailored linear polyethylenimine copolymers *Polymer Chemistry* **2014**, *5*, 4957-4964.
(31) Qi, Y.; Hempelmann, R.; Volmer, D. A. Two-dimensional mass defect matrix plots for mapping genealogical links in mixtures of lignin depolymerisation products *Anal. Bioanal. Chem.* **2016**, *408*, 4835-4843.
(32) Fouquet, T.; Sato, H. Extension of the Kendrick Mass Defect Analysis of Homopolymers to Low Resolution and High Mass Range Mass Spectra Using Fractional Base Units *Anal. Chem.* **2017**, *89*, 2682-2686.
(33) Fouquet, T.; Cody, R. B.; Sato, H. Capabilities of the remainders of nominal Kendrick masses and the referenced Kendrick mass defects for copolymer ions *J. Mass Spectrom.* **2017**, *52*, 618-624.
(34) Fouquet, T.; Nakamura, S.; Sato, H. MALDI SpiralTOF high-resolution mass spectrometry and Kendrick mass defect analysis applied to the characterization of poly(ethylene-co-vinyl acetate) copolymers *Rapid Commun. Mass Spectrom.* **2016**, *30*, 973-981.

(35) Fouquet, T.; Shimada, H.; Maeno, K.; Ito, K.; Ozeki, Y.; Kitagawa, S.; Ohtani, H.; Sato, H. High-resolution Kendrick Mass Defect Analysis of Poly(ethylene oxide)-based Non-ionic Surfactants and Their Degradation Products *J. Oleo Sci.* **2017**, *66*, 1061-1072.
(36) Fouquet, T. N. J.; Cody, R. B.; Ozeki, Y.; Kitagawa, S.; Ohtani, H.; Sato, H. On the Kendrick Mass Defect Plots of Multiply Charged Polymer Ions: Splits, Misalignments, and How to Correct Them *J. Am. Soc. Mass. Spectrom.* **2018**, *29*, 1611-1626.
(37) Köster, C. United States, US 6188064 B1.2001.Bruker Daltonik GmbH (DE)
(38) Wootton, C. A.; Lam, Y. P. Y.; Willetts, M.; van Agthoven, M. A.; Barrow, M. P.; Sadler, P. J.; PB, O. C. Automatic assignment of metal-containing peptides in proteomic LC-MS and MS/MS data sets *Analyst* **2017**, *142*, 2029-2037.
(39) Kaur, P.; O'Connor, P. B. Algorithms for automatic interpretation of high resolution mass spectra *J. Am. Soc. Mass. Spectrom.* **2006**, *17*, 459-468.
(40) Heap, B. R. Permutations by Interchanges *The Computer Journal* **1963**, *6*, 293-294.
(41) Zubarev, R. A.; Kelleher, N. L.; McLafferty, F. W. Electron Capture Dissocaition of Multiply Charged Protein Cations. A nonergodic Process *J. Am. Chem. Soc.* **1998**, *120*, 3265-3266.

SUPPORTING INFORMATION

to

Influence of select terminal groups on poly(2-oxazoline) hydrolysis

by

Tomos E. Morgan[1], Thomas Floyd[1], Bryan Marzullo[1], Christopher A. Wootton[1], Mark P. Barrow[1], Anthony W. T. Bristow[2], Sebastien Perrier[1], Peter B. O'Connor[1]*

[1]Department of Chemistry, University of Warwick, Coventry, Midlands, CV4 7AL, UK.

[2]Chemical Development, Pharmaceutical Technology & Development, Operations, AstraZeneca, Macclesfield, UK.

*Corresponding authors: Peter O'Connor [redacted]

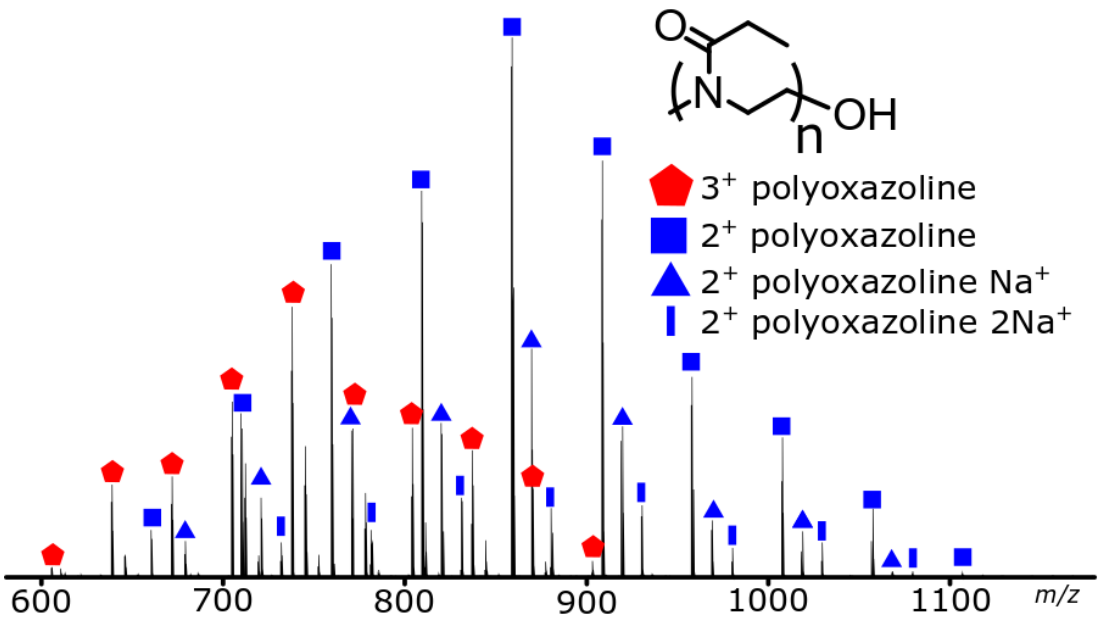

Figure S 5.1 : nESI mass spectrum of the unhydrolysed POx.

Table S 5.1: MS assignment of the unhydrolysed POx

m/z	z	Chemical formula assigned	Formula	error (ppm)
561.89666	2	$C_{56}H_{103}N_{11}O_{12}S_0H^+_2$	p(EtOx$_{11}$)	-0.00
611.43126	2	$C_{61}H_{112}N_{12}O_{13}S_0H^+_2$	p(EtOx$_{12}$)	0.64
660.96551	2	$C_{66}H_{121}N_{13}O_{14}S_0H^+_2$	p(EtOx$_{13}$)	0.66
710.4993	2	$C_{71}H_{130}N_{14}O_{15}S_0H^+_2$	p(EtOx$_{14}$)	0.03
760.03348	2	$C_{76}H_{139}N_{15}O_{16}S_0H^+_2$	p(EtOx$_{15}$)	-0.01
809.56694	2	$C_{81}H_{148}N_{16}O_{17}S_0H^+_2$	p(EtOx$_{16}$)	-0.93
859.10109	2	$C_{86}H_{157}N_{17}O_{18}S_0H^+_2$	p(EtOx$_{17}$)	-0.94
908.63607	2	$C_{91}H_{166}N_{18}O_{19}S_0H^+_2$	p(EtOx$_{18}$)	-0.04
958.17043	2	$C_{96}H_{175}N_{19}O_{20}S_0H^+_2$	p(EtOx$_{19}$)	0.12
1007.70666	2	$C_{101}H_{184}N_{20}O_{21}S_0H^+_2$	p(EtOx$_{20}$)	2.12
1057.2414	2	$C_{106}H_{193}N_{21}O_{22}S_0H^+_2$	p(EtOx$_{21}$)	2.52
1106.77296	2	$C_{111}H_{202}N_{22}O_{23}S_0H^+_2$	p(EtOx$_{22}$)	0.02
1156.30574	2	$C_{116}H_{211}N_{23}O_{24}S_0H^+_2$	p(EtOx$_{23}$)	-1.21
1205.84014	2	$C_{121}H_{220}N_{24}O_{25}S_0H^+_2$	p(EtOx$_{24}$)	-1.00
613.42091	3	$C_{91}H_{166}N_{18}O_{19}S_0H^+_2Na^+_1$	p(EtOx$_{18}$)	0.40
646.44391	3	$C_{96}H_{175}N_{19}O_{20}S_0H^+_2Na^+_1$	p(EtOx$_{19}$)	0.69
679.46624	3	$C_{101}H_{184}N_{20}O_{21}S_0H^+_2Na^+_1$	p(EtOx$_{20}$)	-0.04
712.48856	3	$C_{106}H_{193}N_{21}O_{22}S_0H^+_2Na^+_1$	p(EtOx$_{21}$)	-0.72
745.51177	3	$C_{111}H_{202}N_{22}O_{23}S_0H^+_2Na^+_1$	p(EtOx$_{22}$)	-0.15
778.53421	3	$C_{116}H_{211}N_{23}O_{24}S_0H^+_2Na^+_1$	p(EtOx$_{23}$)	-0.61
811.55656	3	$C_{121}H_{220}N_{24}O_{25}S_0H^+_2Na^+_1$	p(EtOx$_{24}$)	-1.14
844.58147	3	$C_{126}H_{229}N_{25}O_{26}S_0H^+_2Na^+_1$	p(EtOx$_{25}$)	1.39
877.60487	3	$C_{131}H_{238}N_{26}O_{27}S_0H^+_2Na^+_1$	p(EtOx$_{26}$)	2.01
633.41243	2	$C_{61}H_{112}N_{12}O_{13}S_0H^+_0Na^+_2$	p(EtOx$_{12}$)	-1.46
682.94599	2	$C_{66}H_{121}N_{13}O_{14}S_0H^+_0Na^+_2$	p(EtOx$_{13}$)	-2.31

732.48089	2	$C_{71}H_{130}N_{14}O_{15}S_0H^+_0Na^+_2$	p($EtOx_{14}$)	-1.20
782.01534	2	$C_{76}H_{139}N_{15}O_{16}S_0H^+_0Na^+_2$	p($EtOx_{15}$)	-0.82
831.54886	2	$C_{81}H_{148}N_{16}O_{17}S_0H^+_0Na^+_2$	p($EtOx_{16}$)	-1.60
881.08534	2	$C_{86}H_{157}N_{17}O_{18}S_0H^+_0Na^+_2$	p($EtOx_{17}$)	1.07
930.61741	2	$C_{91}H_{166}N_{18}O_{19}S_0H^+_0Na^+_2$	p($EtOx_{18}$)	-1.28
980.14945	2	$C_{96}H_{175}N_{19}O_{20}S_0H^+_0Na^+_2$	p($EtOx_{19}$)	-3.42
1029.68503	2	$C_{101}H_{184}N_{20}O_{21}S_0H^+_0Na^+_2$	p($EtOx_{20}$)	-1.93
1079.21934	2	$C_{106}H_{193}N_{21}O_{22}S_0H^+_0Na^+_2$	p($EtOx_{21}$)	-1.74
1128.75408	2	$C_{111}H_{202}N_{22}O_{23}S_0H^+_0Na^+_2$	p($EtOx_{22}$)	-1.19
1178.28987	2	$C_{116}H_{211}N_{23}O_{24}S_0H^+_0Na^+_2$	p($EtOx_{23}$)	0.12
1227.82471	2	$C_{121}H_{220}N_{24}O_{25}S_0H^+_0Na^+_2$	p($EtOx_{24}$)	0.71
919.6286	2	$C_{91}H_{166}N_{18}O_{19}S_0H^+_1Na^+_1$	p($EtOx_{18}$)	1.35
969.16407	2	$C_{96}H_{175}N_{19}O_{20}S_0H^+_1Na^+_1$	p($EtOx_{19}$)	2.59
1018.69935	2	$C_{101}H_{184}N_{20}O_{21}S_0H^+_1Na^+_1$	p($EtOx_{20}$)	3.51
1117.76671	2	$C_{111}H_{202}N_{22}O_{23}S_0H^+_1Na^+_1$	p($EtOx_{21}$)	2.26
620.74707	3	$C_{91}H_{166}N_{18}O_{19}S_0H^+_1Na^+_2$	p($EtOx_{22}$)	-1.75
653.7703	3	$C_{96}H_{175}N_{19}O_{20}S_0H^+_1Na^+_2$	p($EtOx_{23}$)	-1.02
686.79319	3	$C_{101}H_{184}N_{20}O_{21}S_0H^+_1Na^+_2$	p($EtOx_{24}$)	-0.84
719.81619	3	$C_{106}H_{193}N_{21}O_{22}S_0H^+_1Na^+_2$	p($EtOx_{25}$)	-0.53
752.83892	3	$C_{111}H_{202}N_{22}O_{23}S_0H^+_1Na^+_2$	p($EtOx_{26}$)	-0.61
785.86062	3	$C_{116}H_{211}N_{23}O_{24}S_0H^+_1Na^+_2$	p($EtOx_{27}$)	-1.99
818.88328	3	$C_{121}H_{220}N_{24}O_{25}S_0H^+_1Na^+_2$	p($EtOx_{28}$)	-2.08
851.90546	3	$C_{126}H_{229}N_{25}O_{26}S_0H^+_1Na^+_2$	p($EtOx_{29}$)	-2.73
884.92835	3	$C_{131}H_{238}N_{26}O_{27}S_0H^+_1Na^+_2$	p($EtOx_{30}$)	-2.53
			average error (ppm)	-0.11
			standard dev error (ppm)	1.31

Table S 5.2: MS assignment of P(Ox75%-co-EI25%)-OH, Figure 5.3 in chapter text

m/z	q	Pox	PEI	chemical formula	error	area
531.39202	3	14	4	$C_{79}H_{150}N_{18}O_{15}H^{+}_{3}$	0.89	32556
564.4145	3	15	4	$C_{84}H_{159}N_{19}O_{16}H^{+}_{3}$	0.27	252229
597.43731	3	16	4	$C_{89}H_{168}N_{20}O_{17}H^{+}_{3}$	0.26	744042
630.46014	3	17	4	$C_{94}H_{177}N_{21}O_{18}H^{+}_{3}$	0.29	1611874
663.4829	3	18	4	$C_{99}H_{186}N_{22}O_{19}H^{+}_{3}$	0.21	1172455
696.50622	3	19	4	$C_{104}H_{195}N_{23}O_{20}H^{+}_{3}$	0.94	1038064
729.52893	3	20	4	$C_{109}H_{204}N_{24}O_{21}H^{+}_{3}$	0.76	777592
762.55132	3	21	4	$C_{114}H_{213}N_{25}O_{22}H^{+}_{3}$	0.19	163225
795.574	3	22	4	$C_{119}H_{222}N_{26}O_{23}H^{+}_{3}$	0.02	40505
591.43319	3	15	4	$C_{89}H_{166}N_{20}O_{16}H^{+}_{3}$	-0.75	23945
624.45609	3	16	4	$C_{94}H_{175}N_{21}O_{17}H^{+}_{3}$	-0.56	95570
657.47839	3	17	4	$C_{99}H_{184}N_{22}O_{18}H^{+}_{3}$	-1.30	134700
690.50133	3	18	4	$C_{104}H_{193}N_{23}O_{19}H^{+}_{3}$	-1.04	67374
669.50093	2	11	5	$C_{66}H_{128}N_{16}O_{12}H^{+}_{2}$	-1.83	10744
719.03834	2	12	5	$C_{71}H_{137}N_{17}O_{13}H^{+}_{2}$	2.75	14354
768.56906	2	13	5	$C_{76}H_{146}N_{18}O_{14}H^{+}_{2}$	-1.97	39222
818.10297	2	14	5	$C_{81}H_{155}N_{19}O_{15}H^{+}_{2}$	-2.21	29967
867.64426	2	15	5	$C_{86}H_{164}N_{20}O_{16}H^{+}_{2}$	6.08	40470
917.17618	2	16	5	$C_{91}H_{173}N_{21}O_{17}H^{+}_{2}$	3.26	36302
545.73892	3	14	5	$C_{81}H_{155}N_{19}O_{15}H^{+}_{3}$	-0.05	103531
578.76179	3	15	5	$C_{86}H_{164}N_{20}O_{16}H^{+}_{3}$	0.07	524084
611.78461	3	16	5	$C_{91}H_{173}N_{21}O_{17}H^{+}_{3}$	0.09	927185
644.80738	3	17	5	$C_{96}H_{182}N_{22}O_{18}H^{+}_{3}$	0.03	1366747
677.8301	3	18	5	$C_{101}H_{191}N_{23}O_{19}H^{+}_{3}$	-0.09	655737
710.85242	3	19	5	$C_{106}H_{200}N_{24}O_{20}H^{+}_{3}$	-0.77	765933
743.87662	3	20	5	$C_{111}H_{209}N_{25}O_{21}H^{+}_{3}$	1.14	87662
704.0068	2	9	2	$C_{70}H_{131}N_{15}O_{14}H^{+}_{2}$	-0.67	481861
753.54251	2	10	2	$C_{75}H_{140}N_{16}O_{15}H^{+}_{2}$	1.37	733586
803.07649	2	11	2	$C_{80}H_{149}N_{17}O_{16}H^{+}_{2}$	1.00	860961
852.60957	2	12	2	$C_{85}H_{158}N_{18}O_{17}H^{+}_{2}$	-0.38	594528
902.14495	2	13	2	$C_{90}H_{167}N_{19}O_{18}H^{+}_{2}$	0.94	199016
951.67931	2	14	2	$C_{95}H_{176}N_{20}O_{19}H^{+}_{2}$	1.05	45720
675.99343	2	12	3	$C_{67}H_{127}N_{15}O_{13}H^{+}_{2}$	-1.09	133985
725.52877	2	13	3	$C_{72}H_{136}N_{16}O_{14}H^{+}_{2}$	0.55	870220
775.0626	2	14	3	$C_{77}H_{145}N_{17}O_{15}H^{+}_{2}$	0.03	774867
824.5986	2	15	3	$C_{82}H_{154}N_{18}O_{16}H^{+}_{2}$	2.20	262327
874.13361	2	16	3	$C_{87}H_{163}N_{19}O_{17}H^{+}_{2}$	2.99	359251
923.66472	2	17	3	$C_{92}H_{172}N_{20}O_{18}H^{+}_{2}$	-0.52	66105
550.06689	3	16	3	$C_{82}H_{154}N_{18}O_{16}H^{+}_{3}$	-0.11	20980
616.11272	3	17	3	$C_{92}H_{172}N_{20}O_{18}H^{+}_{3}$	0.26	471137
649.13559	3	18	3	$C_{97}H_{181}N_{21}O_{19}H^{+}_{3}$	0.35	741345
682.15857	3	19	3	$C_{102}H_{190}N_{22}O_{20}H^{+}_{3}$	0.59	389137
715.18145	3	20	3	$C_{107}H_{199}N_{23}O_{21}H^{+}_{3}$	0.67	558522

601.45281	3	14	7	$C_{90}H_{172}N_{22}O_{15}H^{+}_{3}$	-0.36	31366
634.47553	3	15	7	$C_{95}H_{181}N_{23}O_{16}H^{+}_{3}$	-0.48	96855
667.49811	3	16	7	$C_{100}H_{190}N_{24}O_{17}H^{+}_{3}$	-0.79	20275
700.52024	3	17	7	$C_{105}H_{199}N_{25}O_{18}H^{+}_{3}$	-1.71	31739
733.54346	3	18	7	$C_{110}H_{208}N_{26}O_{19}H^{+}_{3}$	-1.07	17758
697.51418	2	13	4	$C_{69}H_{132}N_{16}O_{13}H^{+}_{2}$	-1.56	41579
796.5814	2	14	4	$C_{79}H_{150}N_{18}O_{15}H^{+}_{2}$	-2.86	58447
846.1203	2	15	4	$C_{84}H_{159}N_{19}O_{16}H^{+}_{2}$	2.85	80179
895.65248	2	16	4	$C_{89}H_{168}N_{20}O_{17}H^{+}_{2}$	0.43	77660
945.18603	2	17	4	$C_{94}H_{177}N_{21}O_{18}H^{+}_{2}$	-0.29	54768
560.08635	3	14	6	$C_{83}H_{160}N_{20}O_{15}H^{+}_{3}$	0.01	107125
593.10908	3	15	6	$C_{88}H_{169}N_{21}O_{16}H^{+}_{3}$	-0.12	371318
626.13174	3	16	6	$C_{93}H_{178}N_{22}O_{17}H^{+}_{3}$	-0.34	738401
659.15459	3	17	6	$C_{98}H_{187}N_{23}O_{18}H^{+}_{3}$	-0.26	412014
692.17698	3	18	6	$C_{103}H_{196}N_{24}O_{19}H^{+}_{3}$	-0.84	173682
758.22199	3	19	6	$C_{113}H_{214}N_{26}O_{21}H^{+}_{3}$	-1.56	39683
574.43385	3	14	7	$C_{85}H_{165}N_{21}O_{15}H^{+}_{3}$	0.18	81219
607.4566	3	15	7	$C_{90}H_{174}N_{22}O_{16}H^{+}_{3}$	0.08	118453
640.47921	3	16	7	$C_{95}H_{183}N_{23}O_{17}H^{+}_{3}$	-0.22	239348
673.50183	3	17	7	$C_{100}H_{192}N_{24}O_{18}H^{+}_{3}$	-0.49	33577
706.52647	3	18	7	$C_{105}H_{201}N_{25}O_{19}H^{+}_{3}$	2.13	29888
739.54723	3	19	7	$C_{110}H_{210}N_{26}O_{20}H^{+}_{3}$	-0.73	8516
519.38538	4	18	6	$C_{103}H_{196}N_{24}O_{19}H^{+}_{4}$	0.75	21388
544.15215	4	19	6	$C_{108}H_{205}N_{25}O_{20}H^{+}_{4}$	0.10	110539
568.91923	4	20	6	$C_{113}H_{214}N_{26}O_{21}H^{+}_{4}$	0.06	149344
593.68627	4	21	6	$C_{118}H_{223}N_{27}O_{22}H^{+}_{4}$	-0.05	111628
618.45373	4	22	6	$C_{123}H_{232}N_{28}O_{23}H^{+}_{4}$	0.52	57899
643.21939	4	23	6	$C_{128}H_{241}N_{29}O_{24}H^{+}_{4}$	-1.74	34332
587.10544	3	14	6	$C_{88}H_{167}N_{21}O_{15}H^{+}_{3}$	-0.32	20425
620.12845	3	15	6	$C_{93}H_{176}N_{22}O_{16}H^{+}_{3}$	0.03	136030
653.15086	3	16	6	$C_{98}H_{185}N_{23}O_{17}H^{+}_{3}$	-0.58	164385
686.17328	3	17	6	$C_{103}H_{194}N_{24}O_{18}H^{+}_{3}$	-1.11	59136
719.19522	3	18	6	$C_{108}H_{203}N_{25}O_{19}H^{+}_{3}$	-2.26	27738
861.14651	2	14	7	$C_{85}H_{165}N_{21}O_{15}H^{+}_{2}$	-0.54	19639
621.80311	3	15	8	$C_{92}H_{179}N_{23}O_{16}H^{+}_{3}$	-1.35	26412
533.39189	4	19	5	$C_{106}H_{200}N_{24}O_{20}H^{+}_{4}$	0.65	63464
558.15881	4	20	5	$C_{111}H_{209}N_{25}O_{21}H^{+}_{4}$	0.29	88228
607.69245	4	22	5	$C_{121}H_{227}N_{27}O_{23}H^{+}_{4}$	-0.67	57746
632.45936	4	23	5	$C_{126}H_{236}N_{28}O_{24}H^{+}_{4}$	-0.95	80369
572.75773	3	14	5	$C_{86}H_{162}N_{20}O_{15}H^{+}_{3}$	-0.87	29696
605.78086	3	15	5	$C_{91}H_{171}N_{21}O_{16}H^{+}_{3}$	-0.28	96267
638.80398	3	16	5	$C_{96}H_{180}N_{22}O_{17}H^{+}_{3}$	0.22	412849
671.82665	3	17	5	$C_{101}H_{189}N_{23}O_{18}H^{+}_{3}$	0.01	112816
704.84953	3	18	5	$C_{106}H_{198}N_{24}O_{19}H^{+}_{3}$	0.12	145144
737.87214	3	19	5	$C_{111}H_{207}N_{25}O_{20}H^{+}_{3}$	-0.15	55128
770.89441	3	20	5	$C_{116}H_{216}N_{26}O_{21}H^{+}_{3}$	-0.84	24756

505.37859	4	17	7	$C_{100}H_{192}N_{24}O_{18}H^{+}_{4}$	0.30	8835
530.14579	4	18	7	$C_{105}H_{201}N_{25}O_{19}H^{+}_{4}$	0.47	67299
554.91268	4	19	7	$C_{110}H_{210}N_{26}O_{20}H^{+}_{4}$	0.06	66539
579.67986	4	20	7	$C_{115}H_{219}N_{27}O_{21}H^{+}_{4}$	0.19	101139
604.44696	4	21	7	$C_{120}H_{228}N_{28}O_{22}H^{+}_{4}$	0.18	39485
516.13936	4	17	8	$C_{102}H_{197}N_{25}O_{18}H^{+}_{4}$	0.72	7406
540.90622	4	18	8	$C_{107}H_{206}N_{26}O_{19}H^{+}_{4}$	0.24	43703
565.67288	4	19	8	$C_{112}H_{215}N_{27}O_{20}H^{+}_{4}$	-0.56	36012
590.44029	4	20	8	$C_{117}H_{224}N_{28}O_{21}H^{+}_{4}$	-0.01	28392
				Average error (ppm)	0.01	
				Standard deviation (ppm)	1.23	
				Sum weighted PEI	99113345	
				Sum weighted Pox	384740786	
				Ratio	25.76%	

Table S 5.3: MS assignment of P(Ox75%-co-EI25%)-N3 Figure 5.5 in chapter text

m/z	q	Pox	PEI	chemical formula	error	area	OH/N_3
562.72908	3	15	1	$C_{83}H_{152}N_{20}O_{16}H^{+}_{3}$	-2.43	15989	N_3
595.75285	3	16	1	$C_{88}H_{161}N_{21}O_{17}H^{+}_{3}$	-0.68	140335	N_3
628.77448	3	17	1	$C_{93}H_{170}N_{22}O_{18}H^{+}_{3}$	-2.51	122452	N_3
661.79912	3	18	1	$C_{98}H_{179}N_{23}O_{19}H^{+}_{3}$	0.39	97772	N_3
727.84634	3	20	1	$C_{108}H_{197}N_{25}O_{21}H^{+}_{3}$	2.57	12386	N_3
478.0082	3	12	2	$C_{70}H_{130}N_{18}O_{13}H^{+}_{3}$	-2.58	2001	N_3
511.03185	3	13	2	$C_{75}H_{139}N_{19}O_{14}H^{+}_{3}$	-0.76	42133	N_3
544.05481	3	14	2	$C_{80}H_{148}N_{20}O_{15}H^{+}_{3}$	-0.43	143444	N_3
577.07793	3	15	2	$C_{85}H_{157}N_{21}O_{16}H^{+}_{3}$	0.14	424300	N_3
610.1002	3	16	2	$C_{90}H_{166}N_{22}O_{17}H^{+}_{3}$	-0.74	749273	N_3
643.12318	3	17	2	$C_{95}H_{175}N_{23}O_{18}H^{+}_{3}$	-0.43	761914	N_3
676.14667	3	18	2	$C_{100}H_{184}N_{24}O_{19}H^{+}_{3}$	0.60	665552	N_3
709.16868	3	19	2	$C_{105}H_{193}N_{25}O_{20}H^{+}_{3}$	-0.55	469230	N_3
742.19033	3	20	2	$C_{110}H_{202}N_{26}O_{21}H^{+}_{3}$	-2.08	187834	N_3
775.21184	3	21	2	$C_{115}H_{211}N_{27}O_{22}H^{+}_{3}$	-3.66	10535	N_3
808.23529	3	22	2	$C_{120}H_{220}N_{28}O_{23}H^{+}_{3}$	-2.71	8248	N_3
459.33448	3	11	3	$C_{67}H_{126}N_{18}O_{12}H^{+}_{3}$	0.98	21219	N_3
492.35682	3	12	3	$C_{72}H_{135}N_{19}O_{13}H^{+}_{3}$	-0.03	169770	N_3
525.37949	3	13	3	$C_{77}H_{144}N_{20}O_{14}H^{+}_{3}$	-0.28	393136	N_3
591.426	3	15	3	$C_{87}H_{162}N_{22}O_{16}H^{+}_{3}$	1.27	273630	N_3
624.4478	3	16	3	$C_{92}H_{171}N_{23}O_{17}H^{+}_{3}$	-0.41	994471	N_3
657.47081	3	17	3	$C_{97}H_{180}N_{24}O_{18}H^{+}_{3}$	-0.07	1153729	N_3
690.49364	3	18	3	$C_{102}H_{189}N_{25}O_{19}H^{+}_{3}$	-0.03	1120444	N_3
723.51648	3	19	3	$C_{107}H_{198}N_{26}O_{20}H^{+}_{3}$	0.02	785368	N_3
756.53814	3	20	3	$C_{112}H_{207}N_{27}O_{21}H^{+}_{3}$	-1.50	255919	N_3
789.5645	3	21	3	$C_{117}H_{216}N_{28}O_{22}H^{+}_{3}$	3.07	45949	N_3
822.58535	3	22	3	$C_{122}H_{225}N_{29}O_{23}H^{+}_{3}$	0.57	8628	N_3

440.65862	3	11	4	$C_{64}H_{122}N_{18}O_{11}H^{+}_{3}$	-0.01	16252	N_3
473.68101	3	12	4	$C_{69}H_{131}N_{19}O_{12}H^{+}_{3}$	-0.89	82051	N_3
506.70414	3	13	4	$C_{74}H_{140}N_{20}O_{13}H^{+}_{3}$	-0.19	189057	N_3
539.72699	3	14	4	$C_{79}H_{149}N_{21}O_{14}H^{+}_{3}$	-0.09	385973	N_3
572.74948	3	15	4	$C_{84}H_{158}N_{22}O_{15}H^{+}_{3}$	-0.64	543764	N_3
605.77273	3	16	4	$C_{89}H_{167}N_{23}O_{16}H^{+}_{3}$	0.13	583174	N_3
638.7959	3	17	4	$C_{94}H_{176}N_{24}O_{17}H^{+}_{3}$	0.70	679353	N_3
671.81887	3	18	4	$C_{99}H_{185}N_{25}O_{18}H^{+}_{3}$	0.91	334933	N_3
704.84216	3	19	4	$C_{104}H_{194}N_{26}O_{19}H^{+}_{3}$	1.56	126435	N_3
770.88645	3	21	4	$C_{114}H_{212}N_{28}O_{21}H^{+}_{3}$	-0.29	10420	N_3
488.02839	3	11	5	$C_{71}H_{136}N_{20}O_{12}H^{+}_{3}$	-0.90	56846	N_3
521.05133	3	12	5	$C_{76}H_{145}N_{21}O_{13}H^{+}_{3}$	-0.58	109164	N_3
554.07312	3	13	5	$C_{81}H_{154}N_{22}O_{14}H^{+}_{3}$	-2.38	209474	N_3
587.09678	3	14	5	$C_{86}H_{163}N_{23}O_{15}H^{+}_{3}$	-0.79	175804	N_3
620.11944	3	15	5	$C_{91}H_{172}N_{24}O_{16}H^{+}_{3}$	-0.98	117266	N_3
686.16392	3	16	5	$C_{101}H_{190}N_{26}O_{18}H^{+}_{3}$	-2.53	14875	N_3
617.44206	2	10	2	$C_{60}H_{112}N_{16}O_{11}H^{+}_{2}$	-0.07	288410	N_3
666.97659	2	11	2	$C_{65}H_{121}N_{17}O_{12}H^{+}_{2}$	0.42	428372	N_3
716.51093	2	12	2	$C_{70}H_{130}N_{18}O_{13}H^{+}_{2}$	0.58	548131	N_3
766.04432	2	13	2	$C_{75}H_{139}N_{19}O_{14}H^{+}_{2}$	-0.52	464785	N_3
815.5764	2	14	2	$C_{80}H_{148}N_{20}O_{15}H^{+}_{2}$	-3.10	14310	N_3
865.1176	2	15	2	$C_{85}H_{157}N_{21}O_{16}H^{+}_{2}$	5.16	20855	N_3
744.52362	2	13	1	$C_{73}H_{134}N_{18}O_{14}H^{+}_{2}$	0.00	87511	N_3
794.06071	2	14	1	$C_{78}H_{143}N_{19}O_{15}H^{+}_{2}$	3.63	22546	N_3
843.59346	2	15	1	$C_{83}H_{152}N_{20}O_{16}H^{+}_{2}$	1.69	5125	N_3
429.8145	4	15	4	$C_{84}H_{158}N_{22}O_{15}H^{+}_{4}$	0.69	3585	N_3
454.58124	4	16	4	$C_{89}H_{167}N_{23}O_{16}H^{+}_{4}$	-0.14	31645	N_3
479.34822	4	17	4	$C_{94}H_{176}N_{24}O_{17}H^{+}_{4}$	-0.39	72829	N_3
504.11536	4	18	4	$C_{99}H_{185}N_{25}O_{18}H^{+}_{4}$	-0.30	122375	N_3
528.8822	4	19	4	$C_{104}H_{194}N_{26}O_{19}H^{+}_{4}$	-0.79	191464	N_3
578.41665	4	21	4	$C_{114}H_{212}N_{28}O_{21}H^{+}_{4}$	-0.30	261909	N_3
603.18408	4	22	4	$C_{119}H_{221}N_{29}O_{22}H^{+}_{4}$	0.25	195540	N_3
627.9511	4	23	4	$C_{124}H_{230}N_{30}O_{23}H^{+}_{4}$	0.11	91259	N_3
652.71949	4	24	4	$C_{129}H_{239}N_{31}O_{24}H^{+}_{4}$	2.08	25605	N_3
677.48553	4	25	4	$C_{134}H_{248}N_{32}O_{25}H^{+}_{4}$	0.43	4649	N_3
415.80737	4	13	5	$C_{81}H_{154}N_{22}O_{14}H^{+}_{4}$	-0.67	4552	N_3
440.57485	4	14	5	$C_{86}H_{163}N_{23}O_{15}H^{+}_{4}$	0.22	15139	N_3
490.10873	4	16	5	$C_{96}H_{181}N_{25}O_{17}H^{+}_{4}$	-0.47	133165	N_3
514.8761	4	17	5	$C_{101}H_{190}N_{26}O_{18}H^{+}_{4}$	0.07	144570	N_3
539.64306	4	18	5	$C_{106}H_{199}N_{27}O_{19}H^{+}_{4}$	-0.20	250292	N_3
589.17716	4	20	5	$C_{116}H_{217}N_{29}O_{21}H^{+}_{4}$	-0.36	237417	N_3
613.94419	4	21	5	$C_{121}H_{226}N_{30}O_{22}H^{+}_{4}$	-0.47	67214	N_3
638.71223	4	22	5	$C_{126}H_{235}N_{31}O_{23}H^{+}_{4}$	1.02	112646	N_3
426.56839	4	14	6	$C_{83}H_{159}N_{23}O_{14}H^{+}_{4}$	0.45	4224	N_3
451.33495	4	15	6	$C_{88}H_{168}N_{24}O_{15}H^{+}_{4}$	-0.78	2658	N_3
476.1023	4	16	6	$C_{93}H_{177}N_{25}O_{16}H^{+}_{4}$	-0.22	47074	N_3

500.86909	4	17	6	$C_{98}H_{186}N_{26}O_{17}H^{+}_{4}$	-0.84	84751	N_3
525.63622	4	18	6	$C_{103}H_{195}N_{27}O_{18}H^{+}_{4}$	-0.75	81187	N_3
550.40309	4	19	6	$C_{108}H_{204}N_{28}O_{19}H^{+}_{4}$	-1.14	102463	N_3
575.17132	4	20	6	$C_{113}H_{213}N_{29}O_{20}H^{+}_{4}$	0.87	34897	N_3
599.93735	4	21	6	$C_{118}H_{222}N_{30}O_{21}H^{+}_{4}$	-0.95	14584	N_3
535.71897	3	14	2	$C_{80}H_{149}N_{17}O_{16}H^{+}_{3}$	-1.08	10714	OH
568.74198	3	15	2	$C_{85}H_{158}N_{18}O_{17}H^{+}_{3}$	-0.66	18990	OH
601.76466	3	16	2	$C_{90}H_{167}N_{19}O_{18}H^{+}_{3}$	-0.83	58650	OH
634.78816	3	17	2	$C_{95}H_{176}N_{20}O_{19}H^{+}_{3}$	0.31	40551	OH
667.81176	3	18	2	$C_{100}H_{185}N_{21}O_{20}H^{+}_{3}$	1.48	19999	OH
700.83677	3	19	2	$C_{105}H_{194}N_{22}O_{21}H^{+}_{3}$	4.56	7341	OH
450.99815	3	11	3	$C_{67}H_{127}N_{15}O_{13}H^{+}_{3}$	-0.86	5046	OH
484.022	3	12	3	$C_{72}H_{136}N_{16}O_{14}H^{+}_{3}$	1.36	70547	OH
517.0439	3	13	3	$C_{77}H_{145}N_{17}O_{15}H^{+}_{3}$	-0.47	172407	OH
550.06698	3	14	3	$C_{82}H_{154}N_{18}O_{16}H^{+}_{3}$	0.05	397389	OH
583.08977	3	15	3	$C_{87}H_{163}N_{19}O_{17}H^{+}_{3}$	0.03	504750	OH
616.1124	3	16	3	$C_{92}H_{172}N_{20}O_{18}H^{+}_{3}$	-0.26	357253	OH
649.13607	3	17	3	$C_{97}H_{181}N_{21}O_{19}H^{+}_{3}$	1.09	374768	OH
682.15986	3	18	3	$C_{102}H_{190}N_{22}O_{20}H^{+}_{3}$	2.48	242821	OH
715.18192	3	19	3	$C_{107}H_{199}N_{23}O_{21}H^{+}_{3}$	1.32	95735	OH
748.20474	3	20	3	$C_{112}H_{208}N_{24}O_{22}H^{+}_{3}$	1.29	21659	OH
399.30042	3	9	4	$C_{59}H_{114}N_{14}O_{11}H^{+}_{3}$	0.23	1425	OH
432.32416	3	10	4	$C_{64}H_{123}N_{15}O_{12}H^{+}_{3}$	2.38	3653	OH
465.34516	3	11	4	$C_{69}H_{132}N_{16}O_{13}H^{+}_{3}$	-1.67	62034	OH
498.36816	3	12	4	$C_{74}H_{141}N_{17}O_{14}H^{+}_{3}$	-1.16	136416	OH
531.39141	3	13	4	$C_{79}H_{150}N_{18}O_{15}H^{+}_{3}$	-0.25	272054	OH
564.41366	3	14	4	$C_{84}H_{159}N_{19}O_{16}H^{+}_{3}$	-1.22	492699	OH
597.43701	3	15	4	$C_{89}H_{168}N_{20}O_{17}H^{+}_{3}$	-0.24	514379	OH
630.4601	3	16	4	$C_{94}H_{177}N_{21}O_{18}H^{+}_{3}$	0.22	360177	OH
663.48387	3	17	4	$C_{99}H_{186}N_{22}O_{19}H^{+}_{3}$	1.67	224944	OH
696.50752	3	18	4	$C_{104}H_{195}N_{23}O_{20}H^{+}_{3}$	2.80	35353	OH
413.6475	3	11	5	$C_{61}H_{119}N_{15}O_{11}H^{+}_{3}$	-0.55	1874	OH
446.66978	3	12	5	$C_{66}H_{128}N_{16}O_{12}H^{+}_{3}$	-1.68	12121	OH
512.71573	3	13	5	$C_{76}H_{146}N_{18}O_{14}H^{+}_{3}$	-0.80	120136	OH
545.73829	3	14	5	$C_{81}H_{155}N_{19}O_{15}H^{+}_{3}$	-1.20	196729	OH
611.78425	3	16	5	$C_{91}H_{173}N_{21}O_{17}H^{+}_{3}$	-0.50	108919	OH
420.31647	4	14	6	$C_{83}H_{160}N_{20}O_{15}H^{+}_{4}$	-0.26	5148	OH
445.08358	4	15	6	$C_{88}H_{169}N_{21}O_{16}H^{+}_{4}$	-0.23	13283	OH
469.8506	4	16	6	$C_{93}H_{178}N_{22}O_{17}H^{+}_{4}$	-0.39	69522	OH
494.61744	4	17	6	$C_{98}H_{187}N_{23}O_{18}H^{+}_{4}$	-0.91	103646	OH
519.38455	4	18	6	$C_{103}H_{196}N_{24}O_{19}H^{+}_{4}$	-0.85	95344	OH
544.15104	4	19	6	$C_{108}H_{205}N_{25}O_{20}H^{+}_{4}$	-1.94	89390	OH
568.91835	4	20	6	$C_{113}H_{214}N_{26}O_{21}H^{+}_{4}$	-1.49	56700	OH
593.68722	4	21	6	$C_{118}H_{223}N_{27}O_{22}H^{+}_{4}$	1.55	11092	OH
423.56233	4	14	4	$C_{84}H_{159}N_{19}O_{16}H^{+}_{4}$	-0.59	1695	OH
448.32907	4	15	4	$C_{89}H_{168}N_{20}O_{17}H^{+}_{4}$	-1.37	2571	OH

473.09576	4	16	4	$C_{94}H_{177}N_{21}O_{18}H^{+}_{4}$	-2.17	7706	OH
522.63075	4	17	4	$C_{104}H_{195}N_{23}O_{20}H^{+}_{4}$	-0.47	122737	OH
547.39739	4	18	4	$C_{109}H_{204}N_{24}O_{21}H^{+}_{4}$	-1.30	131969	OH
572.16408	4	19	4	$C_{114}H_{213}N_{25}O_{22}H^{+}_{4}$	-1.96	94777	OH
621.69847	4	21	4	$C_{124}H_{231}N_{27}O_{24}H^{+}_{4}$	-1.51	24223	OH
646.46779	4	22	4	$C_{129}H_{240}N_{28}O_{25}H^{+}_{4}$	1.98	8890	OH
409.5562	4	14	5	$C_{81}H_{155}N_{19}O_{15}H^{+}_{4}$	0.42	4316	OH
434.32336	4	15	5	$C_{86}H_{164}N_{20}O_{16}H^{+}_{4}$	0.53	14606	OH
459.09009	4	16	5	$C_{91}H_{173}N_{21}O_{17}H^{+}_{4}$	-0.32	68971	OH
508.62404	4	18	5	$C_{101}H_{191}N_{23}O_{19}H^{+}_{4}$	-0.79	170206	OH
431.07733	4	14	7	$C_{85}H_{165}N_{21}O_{15}H^{+}_{4}$	0.47	5904	OH
455.84413	4	15	7	$C_{90}H_{174}N_{22}O_{16}H^{+}_{4}$	-0.22	16794	OH
480.6112	4	16	7	$C_{95}H_{183}N_{23}O_{17}H^{+}_{4}$	-0.28	27880	OH
505.37743	4	17	7	$C_{100}H_{192}N_{24}O_{18}H^{+}_{4}$	-1.99	24137	OH
530.1443	4	18	7	$C_{105}H_{201}N_{25}O_{19}H^{+}_{4}$	-2.34	18582	OH
554.91243	4	19	7	$C_{110}H_{210}N_{26}O_{20}H^{+}_{4}$	-0.39	18632	OH
579.68164	4	20	7	$C_{115}H_{219}N_{27}O_{21}H^{+}_{4}$	3.26	5054	OH

Absolute Average error (ppm)	1
Standard deviation error (ppm)	1.41
Sum weighted EI N_3	52911795
Sum weighted Ox N_3	276953792
Ratio	19.1%
Sum weighted EI OH	24003444
Sum weighted Ox OH	96024100
Ratio	25%

Table S 5.4: ECD assignment of P(Ox19-co-EI1)-N3 Figure 5.7 in chapter text

m/z	Charge	Chemical assignment	Ox	EI	Fragment assignment	Error
187.1441	1	$C_9H_{18}N_2O_2H^+_1$	2	0	a2 0EI	-0.02
286.21252	1	$C_{14}H_{27}N_3O_3H^+_1$	3	0	a3 0EI	0.01
385.28094	1	$C_{19}H_{36}N_4O_4H^+_1$	4	0	a4 0EI	0.02
484.3493	1	$C_{24}H_{45}N_5O_5H^+_1$	5	0	a5 0EI	-0.10
583.41778	1	$C_{29}H_{54}N_6O_6H^+_1$	6	0	a6 0EI	0.03
682.48614	1	$C_{34}H_{63}N_7O_7H^+_1$	7	0	a7 0EI	-0.05
781.55458	1	$C_{39}H_{72}N_8O_8H^+_1$	8	0	a8 0EI	-0.01
880.62312	1	$C_{44}H_{81}N_9O_9H^+_1$	9	0	a9 0EI	0.13
979.69232	1	$C_{49}H_{90}N_{10}O_{10}H^+_1$	10	0	a10 0EI	0.92
1078.76041	1	$C_{54}H_{99}N_{11}O_{11}H^+_1$	11	0	a11 0EI	0.54
1177.82817	1	$C_{59}H_{108}N_{12}O_{12}H^+_1$	12	0	a12 0EI	-0.06
1276.8962	1	$C_{64}H_{117}N_{13}O_{13}H^+_1$	13	0	a13 0EI	-0.36
1375.96509	1	$C_{69}H_{126}N_{14}O_{14}H^+_1$	14	0	a14 0EI	0.01
1475.03446	1	$C_{74}H_{135}N_{15}O_{15}H^+_1$	15	0	a15 0EI	0.66
1574.10216	1	$C_{79}H_{144}N_{16}O_{16}H^+_1$	16	0	a16 0EI	0.17
1673.16682	1	$C_{84}H_{153}N_{17}O_{17}H^+_1$	17	0	a17 0EI	-2.09
1772.24155	1	$C_{89}H_{162}N_{18}O_{18}H^+_1$	18	0	a18 0EI	1.59
131.11793	1	$C_6H_{14}N_2O_1H^+_1$	1	1	a2 1EI	0.31
230.1863	1	$C_{11}H_{23}N_3O_2H^+_1$	2	1	a3 1EI	-0.02
329.2547	1	$C_{16}H_{32}N_4O_3H^+_1$	3	1	a4 1EI	-0.05
428.3231	1	$C_{21}H_{41}N_5O_4H^+_1$	4	1	a5 1EI	-0.07
527.39163	1	$C_{26}H_{50}N_6O_5H^+_1$	5	1	a6 1EI	0.16
626.46012	1	$C_{31}H_{59}N_7O_6H^+_1$	6	1	a7 1EI	0.26
725.5283	1	$C_{36}H_{68}N_8O_7H^+_1$	7	1	a8 1EI	-0.10
824.59696	1	$C_{41}H_{77}N_9O_8H^+_1$	8	1	a9 1EI	0.21
923.66497	1	$C_{46}H_{86}N_{10}O_9H^+_1$	9	1	a10 1EI	-0.25
1022.73335	1	$C_{51}H_{95}N_{11}O_{10}H^+_1$	10	1	a11 1EI	-0.26
1121.80204	1	$C_{56}H_{104}N_{12}O_{11}H^+_1$	11	1	a12 1EI	0.01
1220.87059	1	$C_{61}H_{113}N_{13}O_{12}H^+_1$	12	1	a13 1EI	0.12
1319.9391	1	$C_{66}H_{122}N_{14}O_{13}H^+_1$	13	1	a14 1EI	0.18
1419.00634	1	$C_{71}H_{131}N_{15}O_{14}H^+_1$	14	1	a15 1EI	-0.66
1518.07587	1	$C_{76}H_{140}N_{16}O_{15}H^+_1$	15	1	a16 1EI	0.12
1617.14498	1	$C_{81}H_{149}N_{17}O_{16}H^+_1$	16	1	a17 1EI	0.55
1716.21369	1	$C_{86}H_{158}N_{18}O_{17}H^+_1$	17	1	a18 1EI	0.69
1815.28096	1	$C_{91}H_{167}N_{19}O_{18}H^+_1$	18	1	a19 1EI	0.02
242.16114	1	$C_{10}H_{19}N_5O_2H^+_1$	2	0	x2 0EI	-0.05
341.2296	1	$C_{15}H_{28}N_6O_3H^+_1$	3	0	x3 0EI	0.10
440.29797	1	$C_{20}H_{37}N_7O_4H^+_1$	4	0	x4 0EI	-0.02
539.36636	1	$C_{25}H_{46}N_8O_5H^+_1$	5	0	x5 0EI	-0.06
638.4349	1	$C_{30}H_{55}N_9O_6H^+_1$	6	0	x6 0EI	0.15
737.50353	1	$C_{35}H_{64}N_{10}O_7H^+_1$	7	0	x7 0EI	0.42
935.63838	1	$C_{45}H_{82}N_{12}O_9H^+_1$	9	0	x9 0EI	-1.78

1034.70804	1	$C_{50}H_{91}N_{13}O_{10}H^{+}_{1}$	10	0	x10 0EI	-0.41
1133.77653	1	$C_{55}H_{100}N_{14}O_{11}H^{+}_{1}$	11	0	x11 0EI	-0.31
1232.84499	1	$C_{60}H_{109}N_{15}O_{12}H^{+}_{1}$	12	0	x12 0EI	-0.24
1331.91245	1	$C_{65}H_{118}N_{16}O_{13}H^{+}_{1}$	13	0	x13 0EI	-0.94
836.5715	2	$C_{40}H_{73}N_{11}O_{8}H^{+}_{1}$	8	0	x8 0EI	-0.16
285.20341	1	$C_{12}H_{24}N_{6}O_{2}H^{+}_{1}$	2	1	x3 1EI	0.21
384.27165	1	$C_{17}H_{33}N_{7}O_{3}H^{+}_{1}$	3	1	x4 1EI	-0.30
483.34007	1	$C_{22}H_{42}N_{8}O_{4}H^{+}_{1}$	4	1	x5 1EI	-0.22
582.40847	1	$C_{27}H_{51}N_{9}O_{5}H^{+}_{1}$	5	1	x6 1EI	-0.21
681.47714	1	$C_{32}H_{60}N_{10}O_{6}H^{+}_{1}$	6	1	x7 1EI	0.20
780.54554	1	$C_{37}H_{69}N_{11}O_{7}H^{+}_{1}$	7	1	x8 1EI	0.15
879.61387	1	$C_{42}H_{78}N_{12}O_{8}H^{+}_{1}$	8	1	x9 1EI	0.04
1077.75097	1	$C_{52}H_{96}N_{14}O_{10}H^{+}_{1}$	10	1	x11 1EI	0.29
1176.81899	1	$C_{57}H_{105}N_{15}O_{11}H^{+}_{1}$	11	1	x12 1EI	-0.07
1275.88623	1	$C_{62}H_{114}N_{16}O_{12}H^{+}_{1}$	12	1	x13 1EI	-0.99
1374.95599	1	$C_{67}H_{123}N_{17}O_{13}H^{+}_{1}$	13	1	x14 1EI	0.06
1474.02457	1	$C_{72}H_{132}N_{18}O_{14}H^{+}_{1}$	14	1	x15 1EI	0.17
1573.09323	1	$C_{77}H_{141}N_{19}O_{15}H^{+}_{1}$	15	1	x16 1EI	0.32
1672.16098	1	$C_{82}H_{150}N_{20}O_{16}H^{+}_{1}$	16	1	x17 1EI	-0.10
1771.23076	1	$C_{87}H_{159}N_{21}O_{17}H^{+}_{1}$	17	1	x18 1EI	0.68
710.00737	2	$C_{71}H_{131}N_{15}O_{14}H^{+}_{2}$	14	1	a15 1EI	0.14
759.54101	2	$C_{76}H_{140}N_{16}O_{15}H^{+}_{2}$	15	1	a16 1EI	-0.62
809.07559	2	$C_{81}H_{149}N_{17}O_{16}H^{+}_{2}$	16	1	a17 1EI	-0.12
858.61006	2	$C_{86}H_{158}N_{18}O_{17}H^{+}_{2}$	17	1	a18 1EI	0.19
908.14461	2	$C_{91}H_{167}N_{19}O_{18}H^{+}_{2}$	18	1	a19 1EI	0.56
957.6784	2	$C_{96}H_{176}N_{20}O_{19}H^{+}_{2}$	19	1	a20 1EI	0.10
787.05132	2	$C_{77}H_{141}N_{19}O_{15}H^{+}_{2}$	0	0	x17 1EI	1.67
836.58383	2	$C_{82}H_{150}N_{20}O_{16}H^{+}_{2}$	0	0	x18 1EI	-0.46
886.1183	2	$C_{87}H_{159}N_{21}O_{17}H^{+}_{2}$	0	0	x19 1EI	-0.13
935.65262	2	$C_{92}H_{168}N_{22}O_{18}H^{+}_{2}$	0	0	x20 1EI	-0.01
964.18223	2	$C_{95}H_{175}N_{23}O_{18}H^{+}_{2}$	0	0	CRS-C3H4O	0.71
978.17886	2	$C_{96}H_{175}N_{23}O_{19}H^{+}_{2}$	0	0	CRS-C2H4	-0.15
983.69313	2	$C_{98}H_{178}N_{23}O_{18}H^{+}_{2}$	0	0	CRS-H2O	-0.16
992.19454	2	$C_{98}H_{179}N_{23}O_{19}H^{+}_{2}$	0	0	CRS-H	-0.12
661.79936	3	$C_{98}H_{179}N_{23}O_{19}H^{+}_{3}$	0	0	Precursor	0.75
			Absolute average error (ppm)			0.31
			Std deviation error (ppm)			0.51

Table S 5.5: ECD assignment of P(Ox19-co-EI1)-OH Figure 5.8 in chapter text

m/z	Charge	Chemical assignment	Ox	EI	Fragment assignment	Error
1845.28943	1	$C_{92}H_{169}N_{19}O_{19}H^{+}_{1}$	18	1	x19 1EI	-1.12
1746.21835	1	$C_{87}H_{160}N_{18}O_{18}H^{+}_{1}$	17	1	x18 1EI	-2.71
1647.15545	1	$C_{82}H_{151}N_{17}O_{17}H^{+}_{1}$	16	1	x17 1EI	0.48
1548.08782	1	$C_{77}H_{142}N_{16}O_{16}H^{+}_{1}$	15	1	x16 1EI	1.01
1449.0189	1	$C_{72}H_{133}N_{15}O_{15}H^{+}_{1}$	14	1	x15 1EI	0.73
1349.94865	1	$C_{67}H_{124}N_{14}O_{14}H^{+}_{1}$	13	1	x14 1EI	-0.57
1250.88033	1	$C_{62}H_{115}N_{13}O_{13}H^{+}_{1}$	12	1	x13 1EI	-0.54
1151.81232	1	$C_{57}H_{106}N_{12}O_{12}H^{+}_{1}$	11	1	x12 1EI	-0.24
1052.74394	1	$C_{52}H_{97}N_{11}O_{11}H^{+}_{1}$	10	1	x11 1EI	-0.23
953.67548	1	$C_{47}H_{88}N_{10}O_{10}H^{+}_{1}$	9	1	x10 1EI	-0.30
854.60759	1	$C_{42}H_{79}N_{9}O_{9}H^{+}_{1}$	8	1	x9 1EI	0.28
755.53899	1	$C_{37}H_{70}N_{8}O_{8}H^{+}_{1}$	7	1	x8 1EI	0.07
656.47038	1	$C_{32}H_{61}N_{7}O_{7}H^{+}_{1}$	6	1	x7 1EI	-0.22
557.40212	1	$C_{27}H_{52}N_{6}O_{6}H^{+}_{1}$	5	1	x6 1EI	0.02
458.3337	1	$C_{22}H_{43}N_{5}O_{5}H^{+}_{1}$	4	1	x5 1EI	0.01
359.26527	1	$C_{17}H_{34}N_{4}O_{4}H^{+}_{1}$	3	1	x4 1EI	-0.03
260.19684	1	$C_{12}H_{25}N_{3}O_{3}H^{+}_{1}$	2	1	x3 1EI	-0.11
161.12848	1	$C_{7}H_{16}N_{2}O_{2}H^{+}_{1}$	1	1	x2 1EI	0.16
1772.24212	1	$C_{89}H_{162}N_{18}O_{18}H^{+}_{1}$	18	0	a18	1.91
1673.17031	1	$C_{84}H_{153}N_{17}O_{17}H^{+}_{1}$	17	0	a17	0.00
1574.1017	1	$C_{79}H_{144}N_{16}O_{16}H^{+}_{1}$	16	0	a16	-0.13
1475.03426	1	$C_{74}H_{135}N_{15}O_{15}H^{+}_{1}$	15	0	a15	0.53
1375.96575	1	$C_{69}H_{126}N_{14}O_{14}H^{+}_{1}$	14	0	a14	0.49
1276.89587	1	$C_{64}H_{117}N_{13}O_{13}H^{+}_{1}$	13	0	a13	-0.62
1177.82882	1	$C_{59}H_{108}N_{12}O_{12}H^{+}_{1}$	12	0	a12	0.49
1078.76026	1	$C_{54}H_{99}N_{11}O_{11}H^{+}_{1}$	11	0	a11	0.40
880.62304	1	$C_{44}H_{81}N_{9}O_{9}H^{+}_{1}$	9	0	a9	0.04
781.55459	1	$C_{39}H_{72}N_{8}O_{8}H^{+}_{1}$	8	0	a8	0.00
682.48622	1	$C_{34}H_{63}N_{7}O_{7}H^{+}_{1}$	7	0	a7	0.07
583.4178	1	$C_{29}H_{54}N_{6}O_{6}H^{+}_{1}$	6	0	a6	0.07
484.34935	1	$C_{24}H_{45}N_{5}O_{5}H^{+}_{1}$	5	0	a5	0.01
385.28093	1	$C_{19}H_{36}N_{4}O_{4}H^{+}_{1}$	4	0	a4	-0.01
286.21249	1	$C_{14}H_{27}N_{3}O_{3}H^{+}_{1}$	3	0	a3	-0.10
187.1441	1	$C_{9}H_{18}N_{2}O_{2}H^{+}_{1}$	2	0	a2	-0.02
1716.21872	1	$C_{86}H_{158}N_{18}O_{17}H^{+}_{1}$	17	1	a18 1EI	3.62
1617.14977	1	$C_{81}H_{149}N_{17}O_{16}H^{+}_{1}$	16	1	a17 1EI	3.51
1518.07829	1	$C_{76}H_{140}N_{16}O_{15}H^{+}_{1}$	15	1	a16 1EI	1.72
1419.00635	1	$C_{71}H_{131}N_{15}O_{14}H^{+}_{1}$	14	1	a15 1EI	-0.65
1319.9405	1	$C_{66}H_{122}N_{14}O_{13}H^{+}_{1}$	13	1	a14 1EI	1.25
1220.87048	1	$C_{61}H_{113}N_{13}O_{12}H^{+}_{1}$	12	1	a13 1EI	0.03
1121.80202	1	$C_{56}H_{104}N_{12}O_{11}H^{+}_{1}$	11	1	a12 1EI	-0.01
1022.7329	1	$C_{51}H_{95}N_{11}O_{10}H^{+}_{1}$	10	1	a11 1EI	-0.70

824.59673	1	$C_{41}H_{77}N_9O_8H^+_1$	8	1	a9 1EI	-0.07
725.52816	1	$C_{36}H_{68}N_8O_7H^+_1$	7	1	a8 1EI	-0.29
626.46009	1	$C_{31}H_{59}N_7O_6H^+_1$	6	1	a7 1EI	0.21
527.39158	1	$C_{26}H_{50}N_6O_5H^+_1$	5	1	a6 1EI	0.07
428.32312	1	$C_{21}H_{41}N_5O_4H^+_1$	4	1	a5 1EI	-0.03
329.25467	1	$C_{16}H_{32}N_4O_3H^+_1$	3	1	a4 1EI	-0.14
230.1863	1	$C_{11}H_{23}N_3O_2H^+_1$	2	1	a3 1EI	-0.02
131.11794	1	$C_6H_{14}N_2O_1H^+_1$	1	1	a2 1EI	0.38
908.14387	2	$C_{91}H_{167}N_{19}O_{18}H^+_2$	0	0	a19 1EI	-0.25
873.61482	2	$C_{87}H_{160}N_{18}O_{18}H^+_2$	0	0	x18 1EI	-0.41
			Absolute average error (ppm)			0.55
			Std deviation error (ppm)			0.95

Table S 5.6: ECD assignment of P(Ox17-co-EI4)-OH Figure 5.12 in chapter text

m/z	Charge	Chemical assignment	Ox	EI	Fragment assignment	Error
854.60736	1	$C_{42}H_{79}N_9O_9H^+_1$	7	1	x8 1EI	0.01
755.53934	1	$C_{37}H_{70}N_8O_8H^+_1$	6	1	x7 1EI	0.53
656.47027	1	$C_{32}H_{61}N_7O_7H^+_1$	5	1	x6 1EI	-0.39
557.40207	1	$C_{27}H_{52}N_6O_6H^+_1$	4	1	x5 1EI	-0.07
359.26525	1	$C_{17}H_{34}N_4O_4H^+_1$	3	1	x4 1EI	-0.09
260.19687	1	$C_{12}H_{25}N_3O_3H^+_1$	2	1	x3 1EI	0.01
161.12847	1	$C_7H_{16}N_2O_2H^+_1$	1	1	x2 1EI	0.10
1194.8543	1	$C_{59}H_{111}N_{13}O_{12}H^+_1$	11	2	x13 2EI	-0.41
1095.78631	1	$C_{54}H_{102}N_{12}O_{11}H^+_1$	10	2	x12 2EI	-0.06
996.71797	1	$C_{49}H_{93}N_{11}O_{10}H^+_1$	9	2	x11 2EI	0.01
897.64943	1	$C_{44}H_{84}N_{10}O_9H^+_1$	8	2	x10 2EI	-0.13
798.58125	1	$C_{39}H_{75}N_9O_8H^+_1$	7	2	x9 2EI	0.14
699.51273	1	$C_{34}H_{66}N_8O_7H^+_1$	6	2	x8 2EI	0.01
600.44422	1	$C_{29}H_{57}N_7O_6H^+_1$	5	2	x7 2EI	-0.15
501.37589	1	$C_{24}H_{48}N_6O_5H^+_1$	4	2	x6 2EI	-0.01
402.3075	1	$C_{19}H_{39}N_5O_4H^+_1$	3	2	x5 2EI	0.05
303.23908	1	$C_{14}H_{30}N_4O_3H^+_1$	2	2	x4 2EI	0.04
204.17065	1	$C_9H_{21}N_3O_2H^+_1$	1	2	x3 2EI	-0.02
105.10229	1	$C_4H_{12}N_2O_1H^+_1$	0	2	x2 2EI	0.48
1535.10141	1	$C_{76}H_{143}N_{17}O_{15}H^+_1$	14	3	x18 3EI	-0.54
1436.03455	1	$C_{71}H_{134}N_{16}O_{14}H^+_1$	13	3	x17 3EI	0.51
1336.96507	1	$C_{66}H_{125}N_{15}O_{13}H^+_1$	12	3	x16 3EI	-0.25
1237.89601	1	$C_{61}H_{116}N_{14}O_{12}H^+_1$	11	3	x15 3EI	-0.79
1138.82879	1	$C_{56}H_{107}N_{13}O_{11}H^+_1$	10	3	x14 3EI	0.19
1039.75999	1	$C_{51}H_{98}N_{12}O_{10}H^+_1$	9	3	x13 3EI	-0.17
940.69162	1	$C_{46}H_{89}N_{11}O_9H^+_1$	8	3	x12 3EI	-0.14
841.6234	1	$C_{41}H_{80}N_{10}O_8H^+_1$	7	3	x11 3EI	0.08
742.55497	1	$C_{36}H_{71}N_9O_7H^+_1$	6	3	x10 3EI	0.06
643.48647	1	$C_{31}H_{62}N_8O_6H^+_1$	5	3	x9 3EI	-0.06

544.41808	1	$C_{26}H_{53}N_7O_5H^+_1$	4	3	x8 3EI	-0.03
445.34971	1	$C_{21}H_{44}N_6O_4H^+_1$	3	3	x7 3EI	0.07
346.28129	1	$C_{16}H_{35}N_5O_3H^+_1$	2	3	x6 3EI	0.07
247.21285	1	$C_{11}H_{26}N_4O_2H^+_1$	1	3	x5 3EI	-0.01
148.14447	1	$C_6H_{17}N_3O_1H^+_1$	0	3	x4 3EI	0.21
1380.00773	1	$C_{68}H_{130}N_{16}O_{13}H^+_1$	11	4	x16 4EI	0.09
1280.94012	1	$C_{63}H_{121}N_{15}O_{12}H^+_1$	10	4	x15 4EI	0.73
1082.80326	1	$C_{53}H_{103}N_{13}O_{10}H^+_1$	9	4	x14 4EI	0.83
983.73418	1	$C_{48}H_{94}N_{12}O_9H^+_1$	8	4	x13 4EI	0.23
884.66587	1	$C_{43}H_{85}N_{11}O_8H^+_1$	7	4	x12 4EI	0.38
785.5971	1	$C_{38}H_{76}N_{10}O_7H^+_1$	6	4	x11 4EI	-0.03
686.52842	1	$C_{33}H_{67}N_9O_6H^+_1$	5	4	x10 4EI	-0.42
587.46061	1	$C_{28}H_{58}N_8O_5H^+_1$	4	4	x9 4EI	0.54
488.39204	1	$C_{23}H_{49}N_7O_4H^+_1$	3	4	x8 4EI	0.33
389.32349	1	$C_{18}H_{40}N_6O_3H^+_1$	2	4	x7 4EI	0.06
290.25501	1	$C_{13}H_{31}N_5O_2H^+_1$	1	4	x6 4EI	-0.14
191.18667	1	$C_8H_{22}N_4O_1H^+_1$	0	4	x5 4EI	0.17
1177.82781	1	$C_{59}H_{108}N_{12}O_{12}H^+_1$	11	0	a11	-0.37
1078.75988	1	$C_{54}H_{99}N_{11}O_{11}H^+_1$	10	0	a10	0.05
979.69141	1	$C_{49}H_{90}N_{10}O_{10}H^+_1$	9	0	a9	-0.01
880.62278	1	$C_{44}H_{81}N_9O_9H^+_1$	8	0	a8	-0.25
682.48614	1	$C_{34}H_{63}N_7O_7H^+_1$	7	0	a7	-0.05
583.41781	1	$C_{29}H_{54}N_6O_6H^+_1$	6	0	a6	0.09
484.34937	1	$C_{24}H_{45}N_5O_5H^+_1$	5	0	a5	0.05
385.28096	1	$C_{19}H_{36}N_4O_4H^+_1$	4	0	a4	0.07
286.21252	1	$C_{14}H_{27}N_3O_3H^+_1$	3	0	a3	0.01
187.1441	1	$C_9H_{18}N_2O_2H^+_1$	2	0	a2	-0.02
1518.07434	1	$C_{76}H_{140}N_{16}O_{15}H^+_1$	15	1	a16 1EI	-0.89
1419.00646	1	$C_{71}H_{131}N_{15}O_{14}H^+_1$	14	1	a15 1EI	-0.57
1319.93756	1	$C_{66}H_{122}N_{14}O_{13}H^+_1$	13	1	a14 1EI	-0.98
1220.8705	1	$C_{61}H_{113}N_{13}O_{12}H^+_1$	12	1	a13 1EI	0.05
1121.80215	1	$C_{56}H_{104}N_{12}O_{11}H^+_1$	11	1	a12 1EI	0.11
1022.7336	1	$C_{51}H_{95}N_{11}O_{10}H^+_1$	10	1	a11 1EI	-0.01
923.6649	1	$C_{46}H_{86}N_{10}O_9H^+_1$	9	1	a10 1EI	-0.33
824.5965	1	$C_{41}H_{77}N_9O_8H^+_1$	8	1	a9 1EI	-0.35
725.52837	1	$C_{36}H_{68}N_8O_7H^+_1$	7	1	a8 1EI	0.00
626.46009	1	$C_{31}H_{59}N_7O_6H^+_1$	6	1	a7 1EI	0.21
527.39156	1	$C_{26}H_{50}N_6O_5H^+_1$	5	1	a6 1EI	0.03
428.32314	1	$C_{21}H_{41}N_5O_4H^+_1$	4	1	a5 1EI	0.02
329.25473	1	$C_{16}H_{32}N_4O_3H^+_1$	3	1	a4 1EI	0.04
230.1863	1	$C_{11}H_{23}N_3O_2H^+_1$	2	1	a3 1EI	-0.02
131.11792	1	$C_6H_{14}N_2O_1H^+_1$	1	1	a2 1EI	0.23
1660.1817	1	$C_{83}H_{154}N_{18}O_{16}H^+_1$	16	2	a18 2EI	-2.77
1561.11682	1	$C_{78}H_{145}N_{17}O_{15}H^+_1$	15	2	a17 2EI	-0.68
1462.04918	1	$C_{73}H_{136}N_{16}O_{14}H^+_1$	14	2	a16 2EI	-0.20
1362.98083	1	$C_{68}H_{127}N_{15}O_{13}H^+_1$	13	2	a15 2EI	-0.17
1263.91245	1	$C_{63}H_{118}N_{14}O_{12}H^+_1$	12	2	a14 2EI	-0.15
1164.84406	1	$C_{58}H_{109}N_{13}O_{11}H^+_1$	11	2	a13 2EI	-0.14
1065.77591	1	$C_{53}H_{100}N_{12}O_{10}H^+_1$	10	2	a12 2EI	0.09
966.70755	1	$C_{48}H_{91}N_{11}O_9H^+_1$	9	2	a11 2EI	0.16
867.63895	1	$C_{43}H_{82}N_{10}O_8H^+_1$	8	2	a10 2EI	-0.04

768.57064	1	$C_{38}H_{73}N_9O_7H^+_1$	7	2	a9 2EI	0.09
669.50216	1	$C_{33}H_{64}N_8O_6H^+_1$	6	2	a8 2EI	0.00
570.43366	1	$C_{28}H_{55}N_7O_5H^+_1$	5	2	a7 2EI	-0.15
471.36529	1	$C_{23}H_{46}N_6O_4H^+_1$	4	2	a6 2EI	-0.09
372.29689	1	$C_{18}H_{37}N_5O_3H^+_1$	3	2	a5 2EI	-0.07
273.22849	1	$C_{13}H_{28}N_4O_2H^+_1$	2	2	a4 2EI	-0.05
174.16009	1	$C_8H_{19}N_3O_1H^+_1$	1	2	a3 2EI	0.01
1604.15787	1	$C_{80}H_{150}N_{18}O_{15}H^+_1$	15	3	a17 3EI	-1.38
1505.09109	1	$C_{75}H_{141}N_{17}O_{14}H^+_1$	14	3	a16 3EI	-0.38
1406.02359	1	$C_{70}H_{132}N_{16}O_{13}H^+_1$	13	3	a15 3EI	0.24
1306.95465	1	$C_{65}H_{123}N_{15}O_{12}H^+_1$	12	3	a14 3EI	-0.15
1207.88792	1	$C_{60}H_{114}N_{14}O_{11}H^+_1$	11	3	a13 3EI	1.24
1108.81863	1	$C_{55}H_{105}N_{13}O_{10}H^+_1$	10	3	a12 3EI	0.56
1009.7498	1	$C_{50}H_{96}N_{12}O_9H^+_1$	9	3	a11 3EI	0.20
811.61275	1	$C_{40}H_{78}N_{10}O_7H^+_1$	7	3	a10 3EI	-0.03
712.54415	1	$C_{35}H_{69}N_9O_6H^+_1$	6	3	a9 3EI	-0.29
613.47593	1	$C_{30}H_{60}N_8O_5H^+_1$	5	3	a8 3EI	-0.02
514.40734	1	$C_{25}H_{51}N_7O_4H^+_1$	4	3	a7 3EI	-0.37
415.33908	1	$C_{20}H_{42}N_6O_3H^+_1$	3	3	a6 3EI	-0.09
316.27076	1	$C_{15}H_{33}N_5O_2H^+_1$	2	3	a5 3EI	0.18
					Absolute average error (ppm)	0.24
					Std deviation error (ppm)	0.37

Table S 5.7: ECD assignment of P(Ox17-co-EI4)-OH Figure 5.12 in chapter text

m/z	Chemical assignment	Pox	PEI	Fragment assignment	Error
1475.03221	$C_{74}H_{135}N_{15}O_{15}S_0H^+_1$	15	0	a15 0EI	-0.86
1375.96378	$C_{69}H_{126}N_{14}O_{14}S_0H^+_1$	14	0	a14 0EI	-0.94
1276.89628	$C_{64}H_{117}N_{13}O_{13}S_0H^+_1$	13	0	a13 0EI	-0.30
1177.82835	$C_{59}H_{108}N_{12}O_{12}S_0H^+_1$	12	0	a12 0EI	0.09
1078.75978	$C_{54}H_{99}N_{11}O_{11}S_0H^+_1$	11	0	a11 0EI	-0.05
979.69139	$C_{49}H_{90}N_{10}O_{10}S_0H^+_1$	10	0	a10 0EI	-0.03
880.62234	$C_{44}H_{81}N_9O_9S_0H^+_1$	9	0	a9 0EI	-0.75
781.5544	$C_{39}H_{72}N_8O_8S_0H^+_1$	8	0	a8 0EI	-0.24
682.48626	$C_{34}H_{63}N_7O_7S_0H^+_1$	7	0	a7 0EI	0.13
583.41778	$C_{29}H_{54}N_6O_6S_0H^+_1$	6	0	a6 0EI	0.03
484.34937	$C_{24}H_{45}N_5O_5S_0H^+_1$	5	0	a5 0EI	0.05
385.28093	$C_{19}H_{36}N_4O_4S_0H^+_1$	4	0	a4 0EI	-0.01
286.21254	$C_{14}H_{27}N_3O_3S_0H^+_1$	3	0	a3 0EI	0.08
187.1441	$C_9H_{18}N_2O_2S_0H^+_1$	2	0	a2 0EI	-0.02
1815.27957	$C_{91}H_{167}N_{19}O_{18}S_0H^+_1$	18	1	a19 1EI	-0.75
1716.21064	$C_{86}H_{158}N_{18}O_{17}S_0H^+_1$	17	1	a18 1EI	-1.09
1617.14335	$C_{81}H_{149}N_{17}O_{16}S_0H^+_1$	16	1	a17 1EI	-0.46
1518.07535	$C_{76}H_{140}N_{16}O_{15}S_0H^+_1$	15	1	a16 1EI	-0.22
1419.00654	$C_{71}H_{131}N_{15}O_{14}S_0H^+_1$	14	1	a15 1EI	-0.51
1319.93867	$C_{66}H_{122}N_{14}O_{13}S_0H^+_1$	13	1	a14 1EI	-0.14

1220.87012	$C_{61}H_{113}N_{13}O_{12}S_0H^+_1$	12	1	a13 1EI	-0.26
1121.80148	$C_{56}H_{104}N_{12}O_{11}S_0H^+_1$	11	1	a12 1EI	-0.49
1022.73343	$C_{51}H_{95}N_{11}O_{10}S_0H^+_1$	10	1	a11 1EI	-0.18
923.66568	$C_{46}H_{86}N_{10}O_9S_0H^+_1$	9	1	a10 1EI	0.52
824.59709	$C_{41}H_{77}N_9O_8S_0H^+_1$	8	1	a9 1EI	0.37
725.52848	$C_{36}H_{68}N_8O_7S_0H^+_1$	7	1	a8 1EI	0.15
626.45991	$C_{31}H_{59}N_7O_6S_0H^+_1$	6	1	a7 1EI	-0.08
527.39164	$C_{26}H_{50}N_6O_5S_0H^+_1$	5	1	a6 1EI	0.18
428.32315	$C_{21}H_{41}N_5O_4S_0H^+_1$	4	1	a5 1EI	0.04
329.2547	$C_{16}H_{32}N_4O_3S_0H^+_1$	3	1	a4 1EI	-0.05
230.18631	$C_{11}H_{23}N_3O_2S_0H^+_1$	2	1	a3 1EI	0.03
131.1179	$C_6H_{14}N_2O_1S_0H^+_1$	1	1	a2 1EI	0.08
1660.18466	$C_{83}H_{154}N_{18}O_{16}S_0H^+_1$	16	2	a18 2EI	-0.99
1561.11916	$C_{78}H_{145}N_{17}O_{15}S_0H^+_1$	15	2	a17 2EI	0.82
1462.04825	$C_{73}H_{136}N_{16}O_{14}S_0H^+_1$	14	2	a16 2EI	-0.83
1362.97958	$C_{68}H_{127}N_{15}O_{13}S_0H^+_1$	13	2	a15 2EI	-1.08
1263.91302	$C_{63}H_{118}N_{14}O_{12}S_0H^+_1$	12	2	a14 2EI	0.30
1164.84385	$C_{58}H_{109}N_{13}O_{11}S_0H^+_1$	11	2	a13 2EI	-0.32
1065.77556	$C_{53}H_{100}N_{12}O_{10}S_0H^+_1$	10	2	a12 2EI	-0.24
966.70717	$C_{48}H_{91}N_{11}O_9S_0H^+_1$	9	2	a11 2EI	-0.24
867.63848	$C_{43}H_{82}N_{10}O_8S_0H^+_1$	8	2	a10 2EI	-0.58
768.56996	$C_{38}H_{73}N_9O_7S_0H^+_1$	7	2	a9 2EI	-0.80
669.50388	$C_{33}H_{64}N_8O_6S_0H^+_1$	6	2	a8 2EI	2.57
570.43371	$C_{28}H_{55}N_7O_5S_0H^+_1$	5	2	a7 2EI	-0.06
471.36517	$C_{23}H_{46}N_6O_4S_0H^+_1$	4	2	a6 2EI	-0.34
372.29678	$C_{18}H_{37}N_5O_3S_0H^+_1$	3	2	a5 2EI	-0.37
836.57157	$C_{40}H_{73}N_{11}O_8S_0H^+_1$	8	0	x8 0EI	-0.08
737.50261	$C_{35}H_{64}N_{10}O_7S_0H^+_1$	7	0	x7 0EI	-0.83
638.43411	$C_{30}H_{55}N_9O_6S_0H^+_1$	6	0	x6 0EI	-1.09
539.36655	$C_{25}H_{46}N_8O_5S_0H^+_1$	5	0	x5 0EI	0.29
440.29788	$C_{20}H_{37}N_7O_4S_0H^+_1$	4	0	x4 0EI	-0.23
341.22963	$C_{15}H_{28}N_6O_3S_0H^+_1$	3	0	x3 0EI	0.19
1176.81829	$C_{57}H_{105}N_{15}O_{11}S_0H^+_1$	11	1	x12 1EI	-0.67
1077.75143	$C_{52}H_{96}N_{14}O_{10}S_0H^+_1$	10	1	x11 1EI	0.71
978.68234	$C_{47}H_{87}N_{13}O_9S_0H^+_1$	9	1	x10 1EI	0.09
879.61465	$C_{42}H_{78}N_{12}O_8S_0H^+_1$	8	1	x9 1EI	0.93
780.54511	$C_{37}H_{69}N_{11}O_7S_0H^+_1$	7	1	x8 1EI	-0.40
681.47731	$C_{32}H_{60}N_{10}O_6S_0H^+_1$	6	1	x7 1EI	0.45
582.40861	$C_{27}H_{51}N_9O_5S_0H^+_1$	5	1	x6 1EI	0.03
483.34008	$C_{22}H_{42}N_8O_4S_0H^+_1$	4	1	x5 1EI	-0.20
384.2717	$C_{17}H_{33}N_7O_3S_0H^+_1$	3	1	x4 1EI	-0.17
285.20334	$C_{12}H_{24}N_6O_2S_0H^+_1$	2	1	x3 1EI	-0.04
643.12371	$C_{95}H_{175}N_{23}O_{18}S_0H^+_3$	0	0	Precursor	0.39
964.18115	$C_{95}H_{175}N_{23}O_{18}S_0H^+_2$	0	0	CRS-H	-0.41
929.66506	$C_{93}H_{172}N_{20}O_{18}S_0H^+_2$	18	0	a20 2EI	-0.15
880.13063	$C_{88}H_{163}N_{19}O_{17}S_0H^+_2$	0	0	a19 2EI	-0.41

830.59674	$C_{83}H_{154}N_{18}O_{16}S_0H^+_2$	0	0	a18 2EI	-0.06
781.06314	$C_{78}H_{145}N_{17}O_{15}S_0H^+_2$	0	0	a17 2EI	0.72
731.52778	$C_{73}H_{136}N_{16}O_{14}S_0H^+_2$	0	0	a16 2EI	-0.81
				Absolute average error (ppm)	0.65
				Std deviation error (ppm)	1

6. Ultraviolet dissociation of biocompatible polymers: polyoxazolines and polyacrylamides

Tomos E. Morgan[1], Alina Theisen[1], Anisha Haris[1], Thomas Floyd[1], Sean Ellacott[1], Christopher A. Wootton[1], Mark P. Barrow[1], Anthony W. T. Bristow[2], Sébastien Perrier[1], Peter B. O'Connor[1]

[1]Department of Chemistry, University of Warwick, Coventry, Midlands, CV4 7AL, UK.

[2]Chemical Development, Pharmaceutical Technology & Development, Operations, AstraZeneca, Macclesfield, UK.

The MS, MS/MS, and analysis presented in this chapter were all carried out by the thesis author. Thomas Floyd, Sean Ellacott, and Andrew Kerr carried out the synthesis, purification, and GPC and NMR analysis of the polymer species. The UV modification for SolariX was carried out by Alina Theisen, Christopher Wootton, and Anisha Haris.

The work presented in this chapter has been prepared for publication in ACS Analytical chemistry by authors Tomos E. Morgan, Alina Theisen, Anisha Haris, Thomas Floyd, Sean Ellacott, Christopher A. Wootton, Mark P. Barrow, Anthony W. T. Bristow, Sébastien Perrier, Peter B. O'Connor.

6.1. Abstract

Understanding and developing further analytical techniques for the analysis of synthetic polymers is key for characterizing increasingly complex modifications and variation within polymeric systems. In this contribution, synthetic polyoxazolines and polyacrylamides were analyzed with the use of ultraviolet photodissociation (UVPD) coupled to Fourier transform ion cyclotron resonance mass spectrometry (FT-ICR MS). The dissociation of synthetic polymers by 193 nm photons was shown to give comparable cleavage coverage to electron capture dissociation (ECD) methods while requiring less tuning and much shorter dissociation times. UVPD was able to effectively characterize homo- and random co- polyoxazolines. 193 nm photons also produced terminal fragments containing the trithiocarbonate RAFT reagent, which has not been previously observed in ECD. UVPD spectra of the polymeric species indicate the dual influence of both directed and non-directed fragmentation pathways. Overall, near complete coverage of both polyoxazoline homopolymers, modified poly(oxazoline-*co*-ethylenimine) copolymers and polyacrylamide homopolymers was achieved.

6.2. Introduction

Biocompatible synthetic polymers are seeing increased attention for their use as pharmaceutical excipients or directly conjugated onto active ingredients for their biological properties.[1-3] Synthetic polyoxazoline and polyacrylamide conjugation as an alternative to PEGylation of bioactives is becoming well established.[4-6] Favorable immunogenic responses by further modification of the polyoxazolines by hydrolysis allows use as a polyplexing agent for the transport of DNA/RNA.[7-10] The use of increasingly complex synthetic polymers allows an tighter control of chemical properties.[11,12] Mass spectrometry is becoming increasingly present as a means to analyse synthetic polymers.[13,14] Conventional mass spectrometry methods allow the analysis of the polymer mass distribution as well as accurate chemical composition but lacks the ability to understand synthetic procedures. Tandem mass spectrometry can elucidate the sequence of a polymer and therefore how polymers have been synthetized and modified.[13-17]

One of the most important aspects of tandem mass spectrometry is the method in which the analyte is fragmented in the first instance. Fragmentation by slow heating methods, such as collision activated/induced dissociation (CAD/CID) and infrared multiphoton dissociation (IRMPD), produces very different fragmentation patterns compared to electron induced methods, ExD.[18-20] Previously sequence analysis of polyoxazolines has been carried out by CAD/CID,[21,22] Sequencing of polyoxazolines has also been carried out in this laboratory by radical based electron capture dissociation (ECD).[23] Polyacrylamides modified with trithiocarbonate species have been shown to undergo a radical cascade mechanism producing fragmentation down the backbone of the polymer species after radical capture at the trithiocarbonate terminus.[paper ref] Although this type of capture allows analysis of most of the backbone of the trithiocarbonate modified species it falls short of completely identifying the trithiocarbonate terminus due to radical capture and loss. Put simply, investigation of further fragmentation techniques for the analysis of polymers has both analytical and instrumentation advantages.

Recently, much interest has been gained in the use of ultraviolet dissociation (UVPD) due to advances in the available instrumentation.[24,25] UVPD has so far demonstrated

promising results in the analysis of numerous biological species such as peptides[26,27], proteins by top down[28-30] and in native top down experiments[31,32], lipids[33-35], oligosaccharides[36], and nucleic acids.[37] Depending on the wavelength used, single laser pulse is sufficient to cause dissociation allowing very rapid fragmentation and analysis.[38] Molecules can be modified further to incorporate a chromophore to induce fragmentation by UVPD.[39-41]

Fragmentation by 193 nm wavelength radiation produces both a/x, c/z, and b/y ions in peptide species through mechanisms that are still not fully understood.[42] The mixture of fragments generated in peptides suggest that multiple fragmentation pathways may be a fundamental attribute of UVPD fragmentation and this general pattern may be present in species other than peptides.

In this study, we carried out fragmentation of two homo-polyoxazolines with differing terminal groups as well as a random copolymer of poly(ethylenimine) and polyoxazoline. A different backbone in a polyacrylamide was also tested to assess the viability of UVPD for the analysis of different polymer structures.

6.3. Methods and experimental

Cationic ring opening polymerisation of 2-ethyl oxazoline was carried out producing a methyl- and hydroxyl- capped poly(2-ethyl-2-oxazoline). The resulting poly(2-ethyl-2-oxazoline) was hydrolysed by microwave reaction into a poly(2-ethyl-2-oxazoline) and polyethyleneimine copolymer. A full synthetic procedure is given in the supporting information. The hydrolysed sample was dissolved into a 99.5% solution of purified water obtained from a Direct-Q3 Ultrapure Water System (Millipore, Lutterworth, United Kingdom) at 20 µM in 0.5% formic acid (Sigma- Aldrich, Dorset, United Kingdom).

All experiments were performed on a 12T solariX Fourier transform ion cyclotron resonance mass spectrometer (Bruker Daltonik, GmbH, Bremen, Germany) using a nanoelectrospray (nESI) ion source in positive ion mode. UVPD dissociation was carried out with a single 6 mJ pulse (measured at laser head) from a 193 nm excimer laser (ExciStar XS, Coherent) in the setup used herein translates to <0.6 mJ at the window of the ICR cell. Transients were acquired with a low mass of 98 Da using 4 mega-word (2^{22}, 22 bit) transients (1.12 s) achieving approximately 250,000 resolving power at *m/z* 400. All mass spectra were calibrated internally using fragments present in UVPD spectra (peaks used for calibration are marked). The peaks used for internal calibration were crosschecked using both the *a* and *x* fragment series. The Bruker SNAP algorithm was used for peak picking with the polyoxazoline monomer used as the repeat unit. SNAP matches a calculated isotope distribution adjusted to a repeat unit with increasing mass. [43-45]

6.4. Results and Discussion

Polyoxazoline fragmentation nomenclature is showing in Scheme 1. Fragmentation of the polyoxazoline by *a/x* fragmentation occurs in ECD.[23] Fragmentation of this bond, α to the carbonyl group, is equivalent to the atom directed *c/z* fragmentation observed in peptides and proteins.[18] Fragmentation of the side chain of the amide bond is equivalent to *b/y* fragmentation seen in proteins.

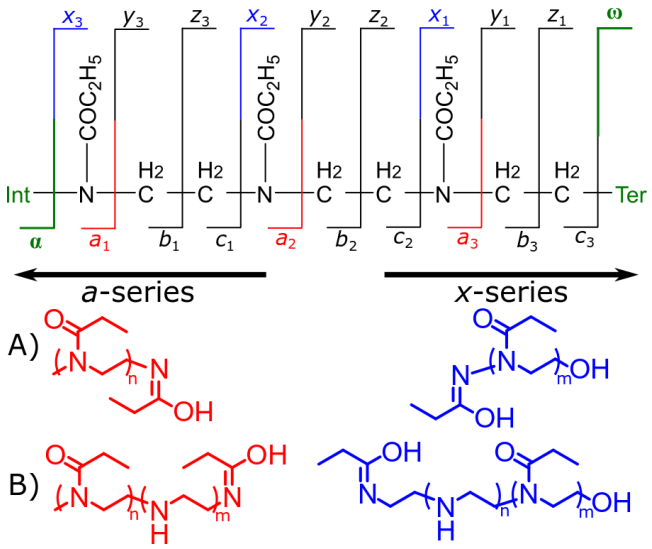

Figure 6.1 Fragmentation diagram of a polyoxazoline previous analysis has shown that *a* and *x* fragmentation can occur through ECD analysis.

nESI of the polyoxazoline produced mainly 2+ and 3+ protonated species of which a triply protonated ion at 672.13754 *m/z* corresponded to the 20 repeat unit hydroxyl terminated polyoxazoline was isolated. Fragmentation of the polyoxazoline species produced fragment 1+, 2+ and 3+ fragment ions. Both *a* and *x* fragments were present containing the terminal end group species. The fragments present were protonated even electron fragments. Singly protonated fragments were present from a_2 (187.14414 *m/z*, 0.11 ppm) to a_{11} (1078.75914 *m/z*, -0.6 ppm); doubly protonated fragments were present from a_9 (440.81544, -0.07 ppm) to a_{18} (936.1577 *m/z*, 0.52 ppm). No triply charged *a* series fragments were observed in the spectrum.

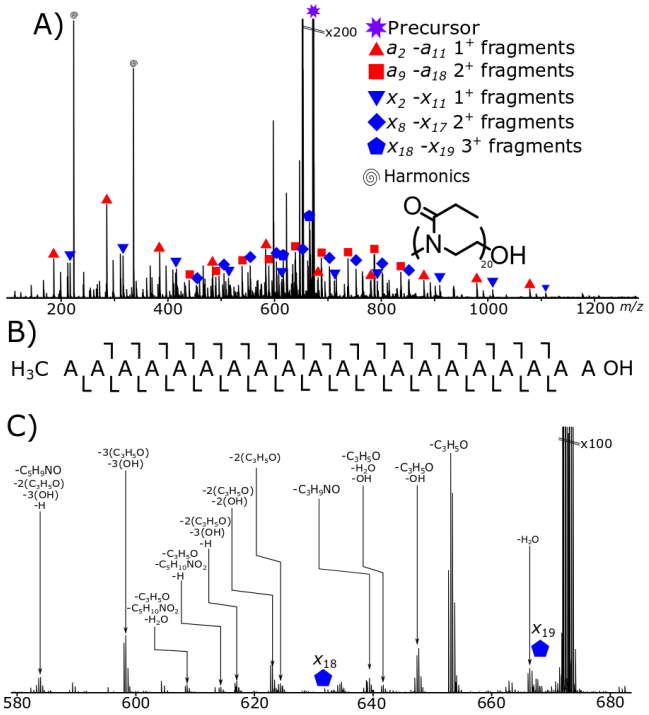

Figure 6.2 A) UVPD fragmentation of a P(Ox)-OH species. Both *a* and *x* fragment series are observed as well a multiple losses from the precursor. B) Fragmentation map showing total coverage. C) triply charged fragments observed showing multiple dissociation events.

OH terminated *x* fragments were observed and 1+, 2+, and 3+ species. Singly charged fragments were observed from 217.15467 *m/z* (x_2, 0.0 ppm) to x_{11} (1108.76819, -2 ppm), doubly charged fragments began at 455.8206 *m/z* (x_8, 0.39 ppm) to x_{17} (901.62878, 0.55 ppm). Two triply charged *x* fragments were observed at 634.4442 and 667.4671, representing the x_{18} and x_{19} fragments respectively. The similar distribution of charge states between the fragment series suggests that charge is evenly distributed across the polymer chain and it unaffected by the fragmentation events occurring.

Overall the fragmentation coverage of the polymer was high with 83% of total possible fragments being observed. The coverage is very similar to the of ECD coverage. The fragmentation efficiency of the UVPD was approximately 4%.

Figure 6.2 shows losses from the precursor that are equivalent to *b/y* fragmentation events. The loss of C_3H_5O produces some an intense triply charged fragment (653.12681 *m/z*, $C_{98}H_{179}O_{20}N_{20}H^+_3$, -0.95 ppm) showing that fragmentation events

equivalent to *b/y* fragmentation in proteins is occurring. In some cases multiple losses are seen with a fragment ion present representing two C_3H_5O losses (634.1165 *m/z*, $C_{95}H_{174}O_{19}N_{20}H^+_3$, 0.66 ppm) suggesting there is excess vibrational energy present allowing further dissociation.

Similar internal fragments to those present in ECD are observed. Internal fragments are not chemically useful as they do not offer terminal information and are very hard to ascertain whether or not the polymer has undergone rearrangement to form the internal fragment species. Common internal fragments are based on alkene formation with side chain loss, internal fragments of this nature are not uncommon in polyoxazoline analysis and doesn't offer a significant insight into the fragmentation mechanism produced by the ultraviolet dissociation.

Table 6.1 Internal fragments caused by the UVPD fragmentation of a p(Ox)-OH

Fragment	Initial fragment mass	Error (ppm)
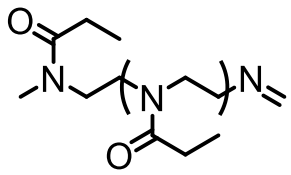	242.186303	0.3
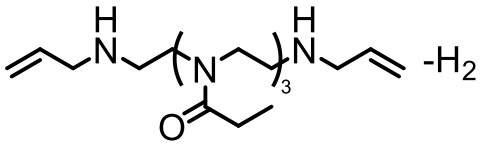	268.201954 (2+)	0.5
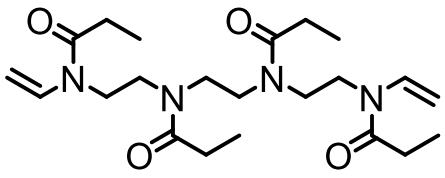	212.151929 (2+)	0.4

Increasing the number of shots of the analysis of the P(Ox) showed that both internal fragmentation and sequence fragmentation increased. Overall, coverage was sufficient with one laser shot so a single laser shot was used for the analysis.

Fragmentation of a P(Ox)-$S_2OC_3H_5$ was carried out by isolation of a 20 monomer unit polymer at 706.461313 *m/z*. Figure 6.3 shows the fragmentation coverage of the polymer showing good fragmentation coverage. Both *a* and *x* fragment series were

observed with singly charged *a* series fragments starting at 187.14414 *m/z* (a_2, 0.19 ppm). Doubly charged fragments were present from a_9 (440.81529 *m/z*, 0.34 ppm) to a_{19} (936.1576 *m/z*, 0.1 ppm); a single triply charged fragment was observed at 624.440565 *m/z* representing an a_{18} fragment (624.44061 *m/z*, 0.1 ppm). The *x* fragment series spanned from x_2 to x_{20} across all three charge states. Singly charged fragments were present from x_2 to x_{11} (321.1302 *m/z*, 0.27ppm, and 1212.74621 *m/z*, 0.31 ppm respectively). Doubly charged fragments start form 507.80831 *m/z* (x_9, 0.32 ppm) and end at 953.61609 *m/z* (x_{18}, 0.1 ppm). Three triply charged fragments are present from x_{18}-x_{20}.

Internal fragmentation from the p(Ox)-$S_2OC_3H_5$ was intense with ring forming or hydrogen loss being the most common fragments. The internal fragment internal oligomer size varied greatly and were seen in multiple charge states.

Table 6.2 Internal fragments caused by the UVPD fragmentation of p(Ox)-$S_2OC_3H_5$

Fragment	Initial fragment mass	Error (ppm)
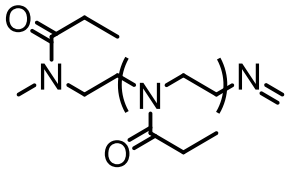	242.186303	0.4
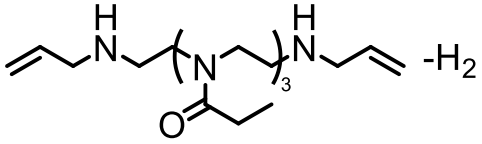	268.201954 (2+)	0.4
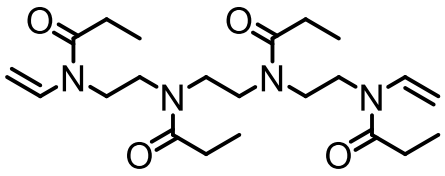	212.151929 (2+)	0.4
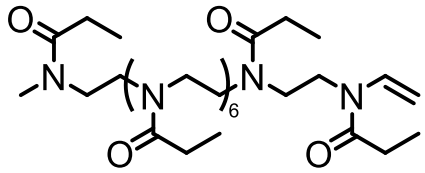	485.795035 (2+)	0.3
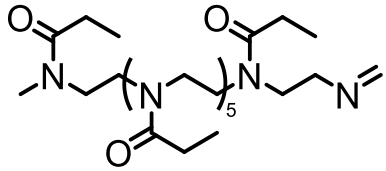	369.267825 (2+)	0.5
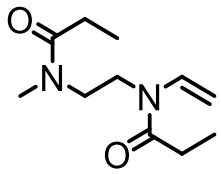	213.15975	0.4
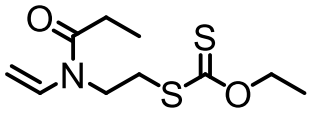	248.077347	0.2

Losses from the precursor showed similar properties to the P(Ox)-OH fragmentation with a large number of fragments being the loss of the C_3H_5O representing *b/y*-like fragmentation across the amide bond. Interestingly, fragmentation across the C-S bond at the ω terminus occurred showing that fragmentation across a C-S occurs

with 193 nm radiation present. Interestingly, no fragmentation is observed at the CO bond present in the $S_2OC_3H_5$ terminus showing that the not all heterogeneous bonds are fragmented directly. Internal fragmentation was similar to that of ECD. All of the internal fragments elucidated contained an unsaturated bond, either between carbons or carbon to nitrogen groups, likely through the loss of a side chain.

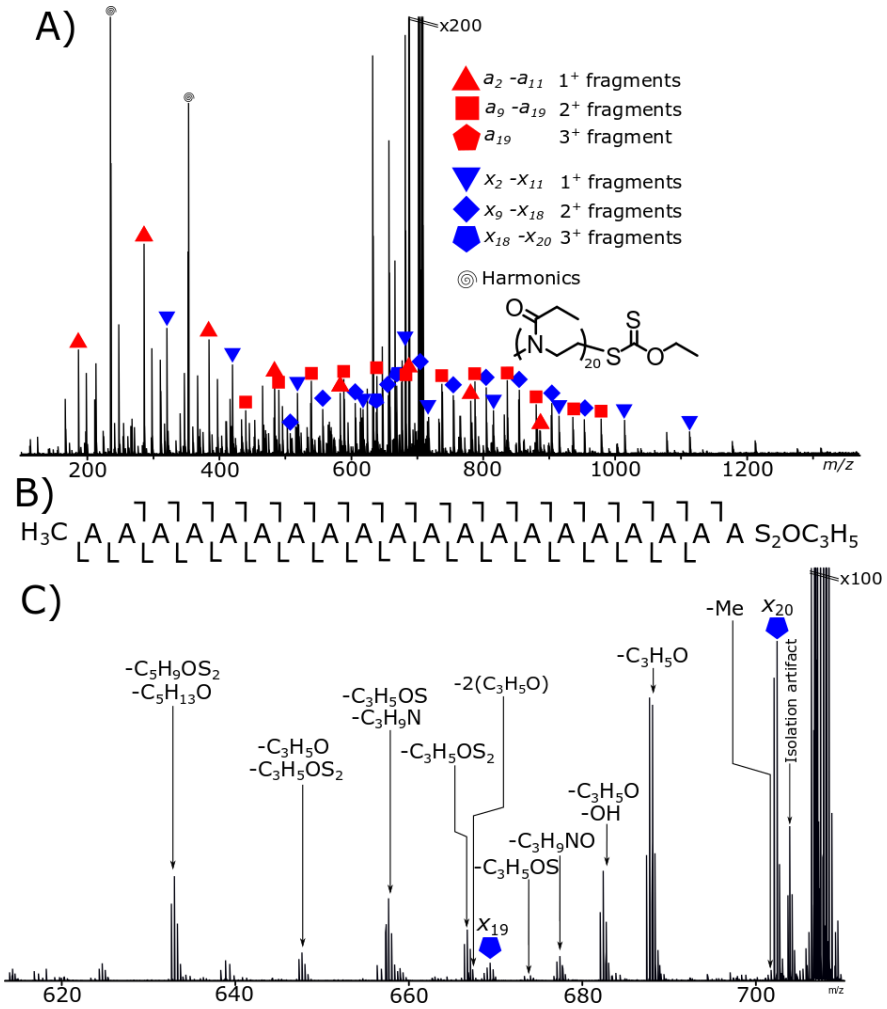

Figure 6.3 A) UVPD fragmentation of a P(Ox)$S_2OC_3H_5$ species. Both *a* and *x* fragment series are observed as well a multiple losses from the precursor. B) Fragmentation map showing total coverage. C) triply charged fragments observed showing multiple dissociation events.

Fragmentation of more complex species was investigated with the analysis of a random P(Ox-*co*-EI) copolymer. The fragmentation of the copolymer produces a much more complex mass spectrum. Fragmentation of P(14Ox-*co*-4EI)-OH produced

good fragmentation coverage of the different levels of PEI across the polymer chain, showing the terminus effect discussed in previous papers.

Fragmentation still occurred at the amide bond, interestingly, there was no observed fragmentation across the C-N bond of the PEI monomer meaning that fragmentation is still localised to the amide bond. The results and coverage were therefore similar to previous ECD analysis. Multiply charged fragment species caused a high density of fragment peaks in *m/z* space making the use of high resolution instrumentation much more important for this type of analysis.

In the analysis the *a*-series fragmentation was observed from 0-EI to 3-EI containing fragment ions. The fragment ions showed similar charge stacking density with doubly charged fragments increasing in intensity once the fragments reached approximately 800 Da. 0-EI containing fragments were observed as singly charged species from a_2 to a_8, only singly charged species were observed as their intensity drops as the oligomer unit grows larger. 1-EI containing species were observed as singly and doubly charged fragments from a_2 to a_{13}, 2-PEI species were observed as singly and doubly charged species from a_5 to a_{15}, 3-EI species were observed as doubly charged fragments from a_9-a_{16}.

The *x*-series had 1-EI containing fragments from x_2-x_4, 2-EI containing singly and doubly charged fragments from x_2-x_{12}. Higher levels of hydrolysis were observed with a high coverage with 3-PEI containing oligomer fragments from x_3 to x_{15}, 4-EI containing species were x_8 to x_{16}.

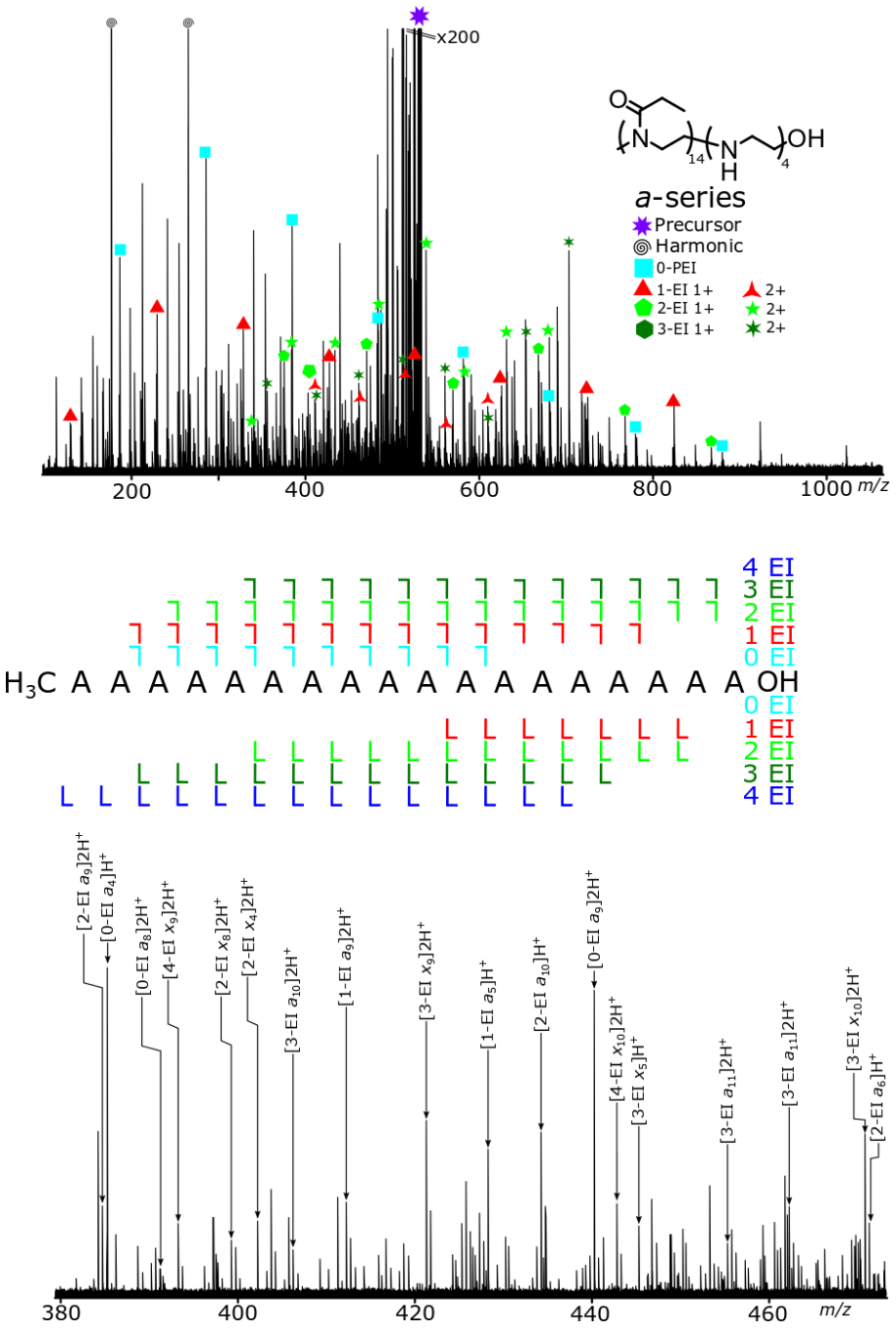

Figure 6.4 A) UVPD fragmentation of a P(14Ox-*co*-4EI)-OH species. Both *a* and *x* fragment series are observed across multiple levels of hydrolysis (EI content). B) Fragmentation maps showing the coverage at each monomer unit showing each hydrolysis level. C) Zoom spectrum showing complexity, unlabelled peaks are internal fragment ions, mostly assigned in the supplementary information.

Investigation of the fragmentation of polyacrylamides was also carried out by the UVPD. The ECD dissociation of butyl-trithiocarbonate terminated polyacrylamides was shown to cause electron capture at the butyl-trithiocarbonate group resulting in dissociation through a radical transfer process. The disadvantage to the use of ECD here is the butyl-trithiocarbonate cannot be confirmed by ECD mass spectrometry apart from its presence as a neutral loss from the charge reduced species. Importantly, only *a*, *b*, and *j*, and *k* fragments were observed in the ECD analysis, Figure 6.5.

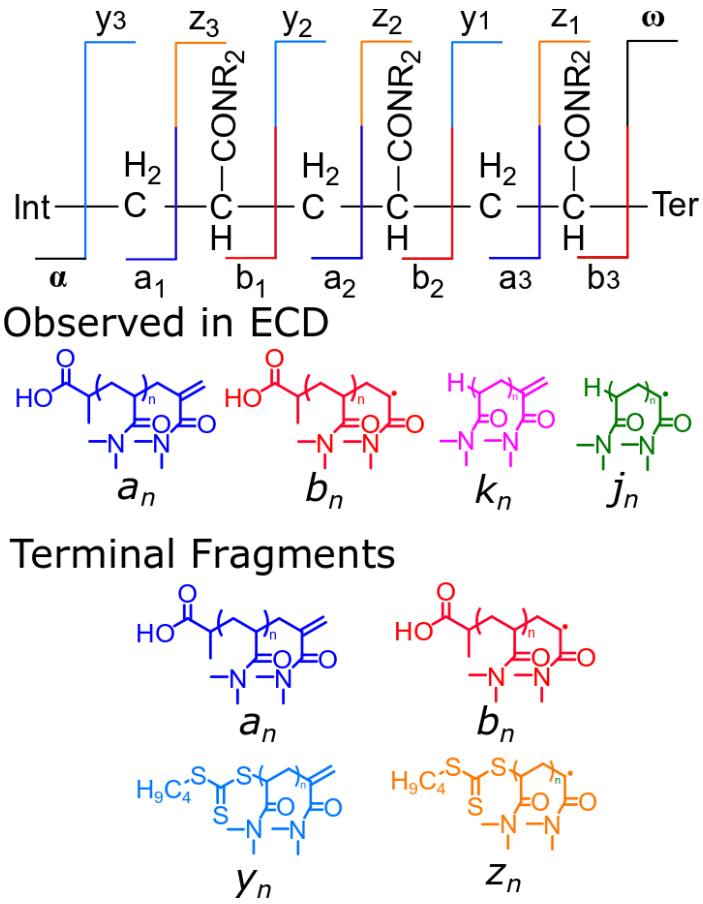

Figure 6.5 Expected fragment series of acrylamides. The fragments observed in the ECD of the molecule consist of the internal fragment *k* and *j* which are not analytically useful. Terminal fragments: *a*, *b*, *y*, and *z* series are the most analytically useful.

Analysis of the butyl-trithiocarbonate terminated P(DMA) was carried out by the same methods described above. Quadrupole isolation of a 20 monomer unit polymer at *m/z* 740.80209 was carried out. Fragmentation of the polymer was shown to

produce *a, b,* and *y* terminal fragments but not *z* fragments. The coverage from the *a* series was also longer than that of the *b* series, coupled with the lack of *z* series fragmentation the observation that less radical containing fragments are formed as part of UVPD of polyacrylamides.

The *a* series fragmentation was present from 285.18079 *m/z* (a_2, -0.32 ppm) to 1275.86502 *m/z* (a_{12}, -1.2 ppm). The *b* series consisted of seven fragments from b_1 to b_7, (173.10467 *m/z*, 0.14 ppm and 767.51608 *m/z*, 1.2 ppm respectively). The *y* fragment series which contains the trithiocarbonate terminus were present from y_2 (363.12274 *m/z*, -0.4 ppm) to y_{11} (1254.73959 *m/z*, 0.75 ppm). The coverage achieved from the *a* and *y* fragment series overlaps meaning complete coverage of the 20 unit polymer chain has been achieved.

High intensity formation of the k_3 and j_2 fragments occurred. The k_3 and j_2 fragments are caused by 5-membered dissociation of a *b* or *z* fragment. The intensity of the fragments suggests there is significant dissociation of the radical containing species forming the fragments.

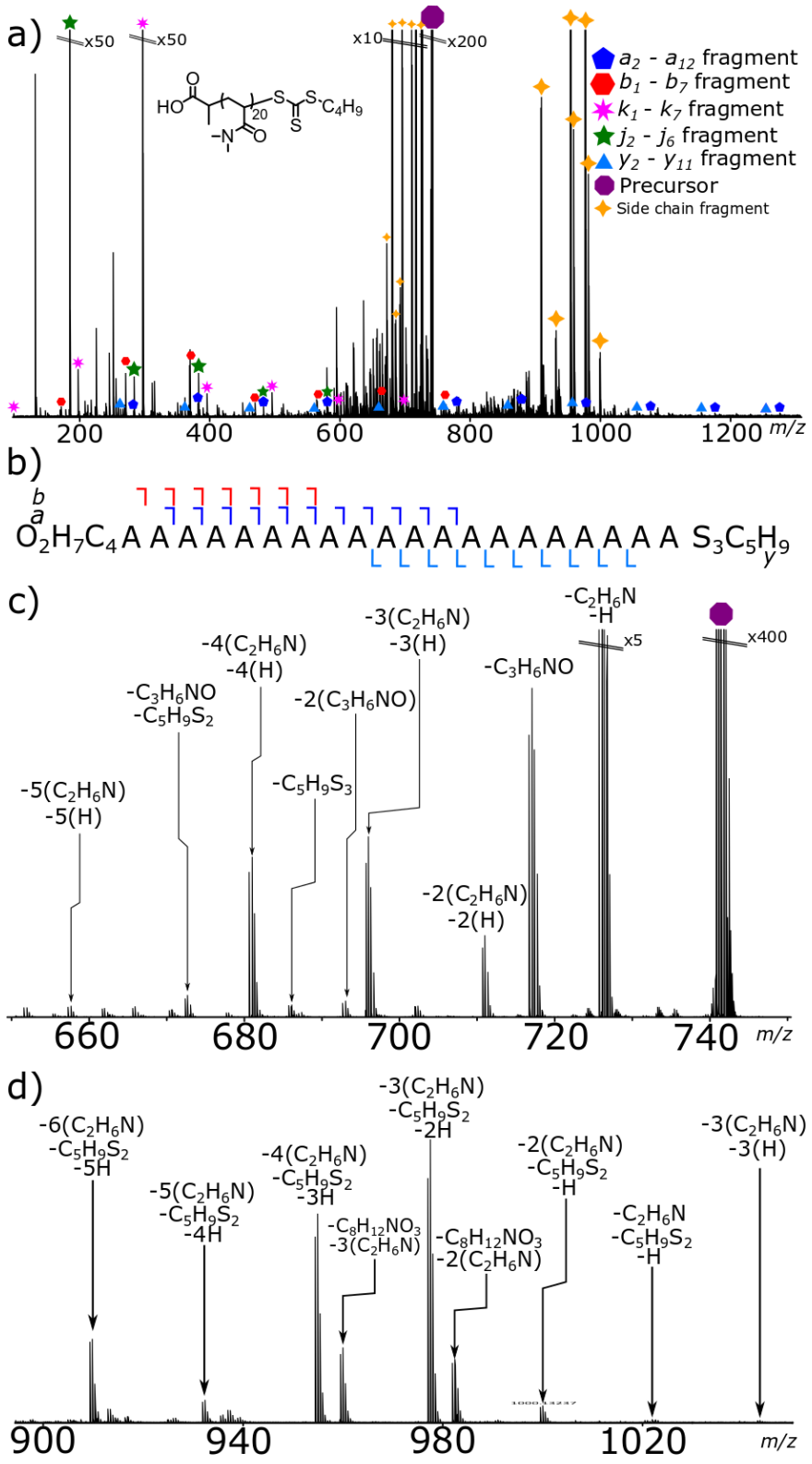

Figure 6.6 A) UVPD fragmentation of P(DMA)$_{20}$ with two laser shots of 6 mJ showing B) overlapping coverage of the *a* and *y* fragment series. C) shows a zoomed region between 660-740 *m/z* showing the 3+ fragments that are side chain losses. D) shows the 900-1040 *m/z* region that shows 2+ side chain losses.

There are numerous side chain losses from the polymer during UVPD. The most common loss observed was that of the loss of C_5H_6N along with a hydrogen which is produced from fragmentation of the amide bond and loss of the dimethylamine group. The loss is also likely to cause the observation of a seeming “charge capture” effect with numerous 2+ fragments. Charge capture is not occurring but more likely the dimethylamine group along the backbone is the significant charge carrier of the polymer therefore with significant losses of dimethylamine groups the likelihood of losing a charge increases. The loss of a hydrogen along with the loss of dimethylamine group suggests that the rearrangement process that a hydrogen is removed from the backbone.

Increasing the number of laser shots from 1 to 9 showed that the intensity of the side chain loss peaks decreased with an increase in the intensity of sequence fragments. There was significant neutral loss fragments from the sequence fragments also with a common loss of C_5H_6N. The relative low intensity of the sequence fragments suggest that the fragmentation pathway to generate them is less favoured than the side chain loss fragmentation.

The other common loss that raised interest is the loss of a $C_5H_9S_2$ bond which represents a breaking of the C-S bond in the trithiocarbonate terminus.

6.5. Conclusions

In conclusion, UVPD gave near complete fragmentation coverage of the polyoxazoline homo- and co-polymer species. Although the fragmentation efficiency was low the total fragmentation coverage of the polymers in one or two shots was effective in the analysis of the polymer species. The polyacrylamide analysis was also effective with overlapping coverage meaning that the polymer chain was completely characterized. UVPD itself offered serval unique advantages, the ability to characterize the trithiocarbonate group as part of the polyacrylamide, as well as sufficient characterization of polyoxazolines in a single shot. The coverage achieved shows that UVPD has a good place in the analysis of synthetic polymer structures.

6.6. References

(1) Viegas, T. X.; Bentley, M. D.; Harris, J. M.; Fang, Z.; Yoon, K.; Dizman, B.; Weimer, R.; Mero, A.; Pasut, G.; Veronese, F. M. Polyoxazoline: chemistry, properties, and applications in drug delivery *Bioconjugate Chem.* **2011**, *22*, 976-986.

(2) Dworak, A.; Trzebicka, B.; Kowalczuk, A.; Tsvetanov, C.; Rangelov, S. Polyoxazolines — mechanism of synthesis and solution properties *Polimery* **2014**, *59*, 88-94.

(3) Bauer, M.; Lautenschlaeger, C.; Kempe, K.; Tauhardt, L.; Schubert, U. S.; Fischer, D. Poly(2-ethyl-2-oxazoline) as alternative for the stealth polymer poly(ethylene glycol): comparison of in vitro cytotoxicity and hemocompatibility *Macromolecular Bioscience* **2012**, *12*, 986 - 998.

(4) Adams, N.; Schubert, U. S. Poly(2-oxazolines) in biological and biomedical application contexts *Advanced Drug Delivery Reviews* **2007**, *59*, 1504-1520.

(5) Liechty, W. B.; Kryscio, D. R.; Slaughter, B. V.; Peppas, N. A. Polymers for drug delivery systems *Annual Review of Chemical and Biomolecular Engineering* **2010**, *1*, 149-173.

(6) Qi, Y.; Chilkoti, A. Protein-polymer conjugation-moving beyond PEGylation *Curr. Opin. Chem. Biol.* **2015**, *28*, 181-193.

(7) Brissault, B.; Kichler, A.; Guis, C.; Leborgne, C.; Danos, O.; Cheradame, H. Synthesis of Linear Polyethylenimine Derivatives for DNA transfection *Bioconjugate Chem.* **2003**, *14*, 581-587.

(8) Tauhardt, L.; Kempe, K.; Knop, K.; Altuntaş, E.; Jäger, M.; Schubert, S.; Fischer, D.; Schubert, U. S. Linear Polyethyleneimine: Optimized Synthesis and Characterization - On the Way to “Pharmagrade” Batches *Macromol. Chem. Phys.* **2011**, 1918-1924.

(9) Yol, A. M.; Janoski, J.; Quirk, R. P.; Wesdemiotis, C. Sequence analysis of styrenic copolymers by tandem mass spectrometry *Anal. Chem.* **2014**, *86*, 9576-9582.

(10) Mees, M. A.; Hoogenboom, R. Full and partial hydrolysis of poly(2-oxazoline)s and the subsequent post-polymerization modification of the resulting polyethylenimine (co)polymers *Polymer Chemistry* **2018**, *9*, 4968-4978.

(11) Obermeyer, A. C.; Olsen, B. D. Synthesis and Application of Protein-Containing Block Copolymers *ACS Macro Letters* **2015**, *4*, 101-110.

(12) Ghosh, S.; Basu, S.; Thayumanavan, S. Simultaneous and Reversible Functionalization of Copolymers for Biological Applications *Macromolecules* **2006**, *39*, 5595-5597.

(13) Altuntaş, E.; Schubert, U. S. "Polymeromics": Mass spectrometry based strategies in polymer science toward complete sequencing approaches: a review *Anal. Chim. Acta* **2014**, *808*, 56-69.

(14) Crotty, S.; Gerislioglu, S.; Endres, K. J.; Wesdemiotis, C.; Schubert, U. S. Polymer architectures via mass spectrometry and hyphenated techniques: A review *Anal. Chim. Acta* **2016**, *932*, 1-21.

(15) Perez Hurtado, P.; Lam, P. Y.; Kilgour, D.; Bristow, A.; McBride, E.; O'Connor, P. B. Use of high resolution mass spectrometry for analysis of polymeric excipients in drug delivery formulations *Anal. Chem.* **2012**, *84*, 8579-8586.

(16) Wei, J.; Bristow, A.; McBride, E.; Kilgour, D.; O'Connor, P. B. D-alpha-tocopheryl polyethylene glycol 1000 succinate: a view from FTICR MS and tandem MS *Anal. Chem.* **2014**, *86*, 1567-1574.

(17) Town, J. S.; Jones, G. R.; Hancox, E.; Shegiwal, A.; Haddleton, D. M. Tandem Mass Spectrometry for Polymeric Structure Analysis: A Comparison of Two Common MALDI-ToF/ToF Techniques *Macromol. Rapid Commun.* **2019**, 1900088-1900094.

(18) Zubarev, R. A.; Kelleher, N. L.; McLafferty, F. W. Electron Capture Dissocaition of Multiply Charged Protein Cations. A nonergodic Process *J. Am. Chem. Soc.* **1998**, *120*, 3265-3266.

(19) Lermyte, F.; Valkenborg, D.; Loo, J. A.; Sobott, F. Radical solutions: Principles and application of electron-based dissociation in mass spectrometry-based analysis of protein structure *Mass Spectrom. Rev.* **2018**, *37*, 750-771.
(20) Qi, Y.; Volmer, D. A. Electron-based fragmentation methods in mass spectrometry: An overview *Mass Spectrom. Rev.* **2017**, *36*, 4-15.
(21) Altuntaş, E.; Weber, C.; Schubert, U. S. Detailed characterization of poly(2-ethyl-2oxazoline)s by energy variable collision-induced dissociation study *Rapid Commun. Mass Spectrom.* **2013**, *27*, 1095-1100.
(22) Baumgaertel, A.; Scheubert, K.; Pietsch, B.; Kempe, K.; Crecelius, A. C.; Bocker, S.; Schubert, U. S. Analysis of different synthetic homopolymers by the use of a new calculation software for tandem mass spectra *Rapid Commun. Mass Spectrom.* **2011**, *25*, 1765-1778.
(23) Morgan, T. E.; Ellacott, S. H.; Wootton, C. A.; Barrow, M. P.; Bristow, A. W. T.; Perrier, S.; O'Connor, P. B. Coupling Electron Capture Dissociation and the Modified Kendrick Mass Defect for Sequencing of a Poly(2-ethyl-2-oxazoline) Polymer *Anal. Chem.* **2018**, *90*, 11710-11715.
(24) Macias, L. A.; Santos, I. C.; Brodbelt, J. S. Ion Activation Methods for Peptides and Proteins *Anal. Chem.* **2019**.
(25) Brodbelt, J. S. Photodissociation mass spectrometry: new tools for characterization of biological molecules *Chem. Soc. Rev.* **2014**, *43*, 2757-2783.
(26) Moon, J. H.; Yoon, S. H.; Kim, M. S. Photodissociation of singly protonated peptides at 193 nm investigated with tandem time-of-flight mass spectrometry *Rapid Commun. Mass Spectrom.* **2005**, *19*, 3248-3252.
(27) Morgan, J. W.; Hettick, J. M.; Russell, D. H. In *Biological Mass Spectrometry*, 2005, pp 186-209.
(28) Shaw, J. B.; Li, W.; Holden, D. D.; Zhang, Y.; Griep-Raming, J.; Fellers, R. T.; Early, B. P.; Thomas, P. M.; Kelleher, N. L.; Brodbelt, J. S. Complete protein characterization using top-down mass spectrometry and ultraviolet photodissociation *J. Am. Chem. Soc.* **2013**, *135*, 12646-12651.
(29) Cannon, J. R.; Kluwe, C.; Ellington, A.; Brodbelt, J. S. Characterization of green fluorescent proteins by 193 nm ultraviolet photodissociation mass spectrometry *Proteomics* **2014**, *14*, 1165-1173.
(30) Mistarz, U. H.; Bellina, B.; Jensen, P. F.; Brown, J. M.; Barran, P. E.; Rand, K. D. UV Photodissociation Mass Spectrometry Accurately Localize Sites of Backbone Deuteration in Peptides *Anal. Chem.* **2018**, *90*, 1077-1080.
(31) Morrison, L. J.; Brodbelt, J. S. 193 nm Ultraviolet Photodissociation Mass Spectrometry of Tetrameric Protein Complexes Provides Insight into Quaternary and Secondary Protein Topology *J. Am. Chem. Soc.* **2016**, *138*, 10849-10859.
(32) Theisen, A.; Black, R.; Corinti, D.; Brown, J. M.; Bellina, B.; Barran, P. E. Initial Protein Unfolding Events in Ubiquitin, Cytochrome c and Myoglobin Are Revealed with the Use of 213 nm UVPD Coupled to IM-MS *J. Am. Soc. Mass. Spectrom.* **2019**, *30*, 24-33.
(33) O'Brien, J. P.; Needham, B. D.; Henderson, J. C.; Nowicki, E. M.; Trent, M. S.; Brodbelt, J. S. 193 nm Ultraviolet Photodissociation Mass Spectrometry for the Structural Elucidation of Lipid A Compounds in Complex Mixtures *Anal. Chem.* **2014**, *86*, 2138-2145.
(34) Morrison, L. J.; Parker, W. R.; Holden, D. D.; Henderson, J. C.; Boll, J. M.; Trent, M. S.; Brodbelt, J. S. UVliPiD: A UVPD-Based Hierarchical Approach for De Novo Characterization of Lipid A Structures *Anal. Chem.* **2016**, *88*, 1812-1820.
(35) Klein, D. R.; Brodbelt, J. S. Structural Characterization of Phosphatidylcholines Using 193 nm Ultraviolet Photodissociation Mass Spectrometry *Anal. Chem.* **2017**, *89*, 1516-1522.
(36) Ko, B. J.; Brodbelt, J. S. 193 nm Ultraviolet Photodissociation of Deprotonated Sialylated Oligosaccharides *Anal. Chem.* **2011**, *83*, 8192-8200.

(37) Smith, S. I.; Brodbelt, J. S. Hybrid activation methods for elucidating nucleic acid modifications *Anal. Chem.* **2010**, *83*, 303-310.
(38) Theisen, A.; Yan, B.; Brown, J. M.; Morris, M.; Bellina, B.; Barran, P. E. Use of Ultraviolet Photodissociation Coupled with Ion Mobility Mass Spectrometry To Determine Structure and Sequence from Drift Time Selected Peptides and Proteins *Anal. Chem.* **2016**, *88*, 9964-9971.
(39) Ly, T.; Julian, R. R. Residue-specific radical-directed dissociation of whole proteins in the gas phase *J. Am. Chem. Soc.* **2008**, *130*, 351-358.
(40) Ly, T.; Julian, R. R. Elucidating the Tertiary Structure of Protein ions in Vacuo with Site Specific Photoinitiated Radical Reactions *J. Am. Chem. Soc.* **2010**, *132*, 8602-8609.
(41) Talbert, L. E.; Julian, R. R. Directed-Backbone Dissociation Following Bond-Specific Carbon-Sulfur UVPD at 213 nm *J. Am. Soc. Mass. Spectrom.* **2018**, *29*, 1760-1767.
(42) Julian, R. R. The Mechanism Behind Top-Down UVPD Experiments: Making Sense of Apparent Contradictions *J. Am. Soc. Mass. Spectrom.* **2017**, *28*, 1823-1826.
(43) Köster, C. United States, US 6188064 B1.2001.Bruker Daltonik GmbH (DE)
(44) Wootton, C. A.; Lam, Y. P. Y.; Willetts, M.; van Agthoven, M. A.; Barrow, M. P.; Sadler, P. J.; PB, O. C. Automatic assignment of metal-containing peptides in proteomic LC-MS and MS/MS data sets *Analyst* **2017**, *142*, 2029-2037.
(45) Kaur, P.; O'Connor, P. B. Algorithms for automatic interpretation of high resolution mass spectra *J. Am. Soc. Mass. Spectrom.* **2006**, *17*, 459-468.

SUPPORTING INFORMATION

to

Ultraviolet dissociation of biocompatible polymers: polyoxazolines and polyacrylamides

by

Tomos E. Morgan[1], Alina Theisen[1], Anisha Haris[1], Thomas Floyd[1], Sean Ellacott[1], Christopher A. Wootton[1], Mark P. Barrow[1], Anthony W. T. Bristow[2], Sébastien Perrier[1], Peter B. O'Connor[1]

[1]Department of Chemistry, University of Warwick, Coventry, Midlands, CV4 7AL, UK.

[2]Chemical Development, Pharmaceutical Technology & Development, Operations, AstraZeneca, Macclesfield, UK.

*Corresponding authors: Peter O'Connor [redacted]

Table S 6.1: MS assignment of p(Ox)-OH Figure 6.2

m/z	charge	chemical formula	error	assignment
1078.75914	1	$C_{54}H_{99}N_{11}O_{11}S_0H^+_1$	-0.64	a_{11}
979.69174	1	$C_{49}H_{90}N_{10}O_{10}S_0H^+_1$	0.33	a_{10}
880.62319	1	$C_{44}H_{81}N_9O_9S_0H^+_1$	0.21	a_9
781.55458	1	$C_{39}H_{72}N_8O_8S_0H^+_1$	-0.01	a_8
682.48642	1	$C_{34}H_{63}N_7O_7S_0H^+_1$	0.36	a_7
484.34939	1	$C_{24}H_{45}N_5O_5S_0H^+_1$	0.09	a_5
385.28085	1	$C_{19}H_{36}N_4O_4S_0H^+_1$	-0.21	a_4
286.21255	1	$C_{14}H_{27}N_3O_3S_0H^+_1$	0.11	a_3
187.14414	1	$C_9H_{18}N_2O_2S_0H^+_1$	0.19	a_2
936.15770	2	$C_{94}H_{171}N_{19}O_{19}S_0H^+_2$	0.52	a_{18}
837.08896	2	$C_{84}H_{153}N_{17}O_{17}S_0H^+_2$	0.20	a_{17}
787.55476	2	$C_{79}H_{144}N_{16}O_{16}S_0H^+_2$	0.22	a_{16}
738.02059	2	$C_{74}H_{135}N_{15}O_{15}S_0H^+_2$	0.28	a_{15}
688.48667	2	$C_{69}H_{126}N_{14}O_{14}S_0H^+_2$	0.72	a_{14}
638.95235	2	$C_{64}H_{117}N_{13}O_{13}S_0H^+_2$	0.60	a_{13}
589.41770	2	$C_{59}H_{108}N_{12}O_{12}S_0H^+_2$	-0.10	a_{12}
539.88373	2	$C_{54}H_{99}N_{11}O_{11}S_0H^+_2$	0.33	a_{11}
490.34955	2	$C_{49}H_{90}N_{10}O_{10}S_0H^+_2$	0.42	a_{10}
440.81544	2	$C_{44}H_{81}N_9O_9S_0H^+_2$	0.68	a_9
1108.76819	1	$C_{55}H_{101}N_{11}O_{12}S_0H^+_1$	-1.99	x_{11}
1009.70254	1	$C_{50}H_{92}N_{10}O_{11}S_0H^+_1$	0.55	x_{10}
910.63358	1	$C_{45}H_{83}N_9O_{10}S_0H^+_1$	0.01	x_9
811.56551	1	$C_{40}H_{74}N_8O_9S_0H^+_1$	0.44	x_8
712.49718	1	$C_{35}H_{65}N_7O_8S_0H^+_1$	0.62	x_7
613.42846	1	$C_{30}H_{56}N_6O_7S_0H^+_1$	0.22	x_6
514.35977	1	$C_{25}H_{47}N_5O_6S_0H^+_1$	-0.27	x_5
415.29147	1	$C_{20}H_{38}N_4O_5S_0H^+_1$	-0.06	x_4
316.22313	1	$C_{15}H_{29}N_3O_4S_0H^+_1$	0.15	x_3
217.15467	1	$C_{10}H_{20}N_2O_3S_0H^+_1$	0.00	x_2
901.62878	2	$C_{90}H_{164}N_{18}O_{19}S_0H^+_2$	0.55	x_{17}
852.09471	2	$C_{85}H_{155}N_{17}O_{18}S_0H^+_2$	0.74	x_{16}
802.56036	2	$C_{80}H_{146}N_{16}O_{17}S_0H^+_2$	0.61	x_{15}
753.02610	2	$C_{75}H_{137}N_{15}O_{16}S_0H^+_2$	0.58	x_{14}
703.49192	2	$C_{70}H_{128}N_{14}O_{15}S_0H^+_2$	0.66	x_{13}
653.95733	2	$C_{65}H_{119}N_{13}O_{14}S_0H^+_2$	0.12	x_{12}
604.42298	2	$C_{60}H_{110}N_{12}O_{13}S_0H^+_2$	-0.10	x_{11}
554.88889	2	$C_{55}H_{101}N_{11}O_{12}S_0H^+_2$	0.10	x_{10}
505.35476	2	$C_{50}H_{92}N_{10}O_{11}S_0H^+_2$	0.26	x_9
455.82060	2	$C_{45}H_{83}N_9O_{10}S_0H^+_2$	0.39	x_8
667.46714	3	$C_{100}H_{182}N_{20}O_{21}S_0H^+_3$	0.37	x_{19}
634.44415	3	$C_{95}H_{173}N_{19}O_{20}S_0H^+_3$	0.10	x_{18}
539.39150	1	$C_{27}H_{50}N_6O_5S_0H^+_1$	-0.08	Internal
440.32310	1	$C_{22}H_{41}N_5O_4S_0H^+_1$	-0.07	Internal

341.25472	1	$C_{17}H_{32}N_4O_3S_0H^+_1$	0.01	Internal
242.18638	1	$C_{12}H_{23}N_3O_2S_0H^+_1$	0.32	Internal
459.82307	2	$C_{47}H_{83}N_9O_9S_0H^+_2$	0.23	Internal
360.75471	2	$C_{37}H_{65}N_7O_7S_0H^+_2$	0.44	Internal
261.68614	2	$C_{27}H_{47}N_5O_5S_0H^+_2$	0.01	Internal
212.15202	2	$C_{22}H_{38}N_4O_4S_0H^+_2$	0.43	Internal
565.40726	2	$C_{58}H_{104}N_{12}O_{10}S_0H^+_2$	0.11	Internal
515.87304	2	$C_{53}H_{95}N_{11}O_9S_0H^+_2$	0.10	Internal
466.33887	2	$C_{48}H_{86}N_{10}O_8S_0H^+_2$	0.19	Internal
416.80464	2	$C_{43}H_{77}N_9O_7S_0H^+_2$	0.16	Internal
367.27043	2	$C_{38}H_{68}N_8O_6S_0H^+_2$	0.17	Internal
317.73629	2	$C_{33}H_{59}N_7O_5S_0H^+_2$	0.41	Internal
268.20209	2	$C_{28}H_{50}N_6O_4S_0H^+_2$	0.51	Internal
666.13561	3	$C_{101}H_{182}N_{20}O_{20}S_0H^+_3$	0.54	Pre-H_2O
653.12681	3	$C_{98}H_{179}N_{20}O_{20}S_0H^+_3$	-0.95	Pre-C_3H_5O
647.45976	3	$C_{98}H_{178}N_{20}O_{19}S_0H^+_3$	-0.14	Pre-C_3H_5O-OH
641.45647	3	$C_{98}H_{176}N_{20}O_{18}S_0H^+_3$	0.22	Pre-C_3H_5O-OH-H_2O
639.11607	3	$C_{96}H_{175}N_{19}O_{20}S_0H^+_3$	0.16	Pre-C_5H_9NO
634.1165	3	$C_{95}H_{174}N_{20}O_{19}S_0H^+_3$	0.66	Pre-2(C_3H_5O)
628.1135	3	$C_{95}H_{172}N_{20}O_{18}S_0H^+_3$	1.50	Pre-2(C_3H_5O)-OH_2
624.10474	3	$C_{94}H_{170}N_{19}O_{19}S_0H^+_3$	0.19	pre-$C_7H_{14}NO_2$
622.78093	3	$C_{95}H_{172}N_{20}O_{17}S_0H^+_3$	0.01	Pre-2(C_3H_5O)-2(OH)
616.77746	3	$C_{95}H_{170}N_{20}O_{16}S_0H^+_3$	0.10	Pre-2(C_3H_5O)-3(OH)-H
614.10145	3	$C_{93}H_{168}N_{19}O_{18}S_0H^+_3$	0.57	Pre-C_3H_5O-$C_5H_{10}NO_2$-H
608.43385	3	$C_{93}H_{167}N_{19}O_{17}S_0H^+_3$	0.54	Pre-C_3H_5O-$C_5H_{10}NO_2$-H_2O
598.10200	3	$C_{92}H_{166}N_{20}O_{15}S_0H^+_3$	0.01	Pre-3(C_3H_5O)-$_3$(OH)
583.75477	3	$C_{90}H_{161}N_{19}O_{15}S_0H^+_3$	0.30	Pre-C_5H_9NO-3(C_3H_5O)-3(OH)-H
672.13754	3	$C_{101}H_{184}N_{20}O_{21}S_0H^+_3$	-1.84	Precursor
		Average	0.22	
		Stadnard deviation	0.35	

Table S 6.2: MS assignment of p(Ox)-$S_2OC_3H_5$ Figure 6.3

m/z	**charge**	**chemical formula**	**error**	**assignment**
1078.76049	1	$C_{54}H_{99}N_{11}O_{11}S_0H^+_1$	0.61	a_{11}
979.69156	1	$C_{49}H_{90}N_{10}O_{10}S_0H^+_1$	0.15	a_{10}
880.62326	1	$C_{44}H_{81}N_9O_9S_0H^+_1$	0.29	a_9
781.55461	1	$C_{39}H_{72}N_8O_8S_0H^+_1$	0.03	a_8
682.48611	1	$C_{34}H_{63}N_7O_7S_0H^+_1$	-0.09	a_7
583.41784	1	$C_{29}H_{54}N_6O_6S_0H^+_1$	0.14	a_6
484.34938	1	$C_{24}H_{45}N_5O_5S_0H^+_1$	0.07	a_5
385.28101	1	$C_{19}H_{36}N_4O_4S_0H^+_1$	0.20	a_4
286.21258	1	$C_{14}H_{27}N_3O_3S_0H^+_1$	0.22	a_3

187.14414	1	$C_9H_{18}N_2O_2S_0H^+_1$	0.19	a_2
936.1573	2	$C_{94}H_{171}N_{19}O_{19}S_0H^+_2$	0.10	a_{19}
886.62555	2	$C_{89}H_{162}N_{18}O_{18}S_0H^+_2$	2.87	a_{18}
837.08859	2	$C_{84}H_{153}N_{17}O_{17}S_0H^+_2$	-0.24	a_{17}
787.55481	2	$C_{79}H_{144}N_{16}O_{16}S_0H^+_2$	0.28	a_{16}
738.02059	2	$C_{74}H_{135}N_{15}O_{15}S_0H^+_2$	0.28	a_{15}
688.48632	2	$C_{69}H_{126}N_{14}O_{14}S_0H^+_2$	0.21	a_{14}
638.95204	2	$C_{64}H_{117}N_{13}O_{13}S_0H^+_2$	0.11	a_{13}
589.41778	2	$C_{59}H_{108}N_{12}O_{12}S_0H^+_2$	0.03	a_{12}
539.88369	2	$C_{54}H_{99}N_{11}O_{11}S_0H^+_2$	0.25	a_{11}
490.34945	2	$C_{49}H_{90}N_{10}O_{10}S_0H^+_2$	0.21	a_{10}
440.81529	2	$C_{44}H_{81}N_9O_9S_0H^+_2$	0.34	a_9
624.44061	3	$C_{94}H_{171}N_{19}O_{19}S_0H^+_3$	0.07	a_{18}
1212.74621	1	$C_{58}H_{105}N_{11}O_{12}S_2H^+_1$	0.31	x_{11}
1113.67801	1	$C_{53}H_{96}N_{10}O_{11}S_2H^+_1$	0.53	x_{10}
1014.6093	1	$C_{48}H_{87}N_9O_{10}S_2H^+_1$	0.29	x_9
915.54081	1	$C_{43}H_{78}N_8O_9S_2H^+_1$	0.24	x_8
816.47195	1	$C_{38}H_{69}N_7O_8S_2H^+_1$	-0.28	x_7
717.40376	1	$C_{33}H_{60}N_6O_7S_2H^+_1$	-0.01	x_6
618.33554	1	$C_{28}H_{51}N_5O_6S_2H^+_1$	0.30	x_5
519.26702	1	$C_{23}H_{42}N_4O_5S_2H^+_1$	0.16	x_4
420.19866	1	$C_{18}H_{33}N_3O_4S_2H^+_1$	0.32	x_3
321.1302	1	$C_{13}H_{24}N_2O_3S_2H^+_1$	0.28	x_2
953.61609	2	$C_{93}H_{168}N_{18}O_{19}S_2H^+_2$	0.09	x_{18}
904.08239	2	$C_{88}H_{159}N_{17}O_{18}S_2H^+_2$	0.65	x_{17}
854.54798	2	$C_{83}H_{150}N_{16}O_{17}S_2H^+_2$	0.46	x_{16}
805.01381	2	$C_{78}H_{141}N_{15}O_{16}S_2H^+_2$	0.53	x_{15}
755.47938	2	$C_{73}H_{132}N_{14}O_{15}S_2H^+_2$	0.27	x_{14}
656.41073	2	$C_{63}H_{114}N_{12}O_{13}S_2H^+_2$	-0.05	x_{12}
606.87663	2	$C_{58}H_{105}N_{11}O_{12}S_2H^+_2$	0.12	x_{11}
557.34243	2	$C_{53}H_{96}N_{10}O_{11}S_2H^+_2$	0.14	x_{10}
507.80831	2	$C_{48}H_{87}N_9O_{10}S_2H^+_2$	0.33	x_9
702.1253	3	$C_{103}H_{186}N_{20}O_{21}S_2H^+_3$	-0.10	x_{20}
669.10259	3	$C_{98}H_{177}N_{19}O_{20}S_2H^+_3$	0.03	x_{19}
636.07973	3	$C_{93}H_{168}N_{18}O_{19}S_2H^+_3$	-0.05	x_{18}
638.4598	1	$C_{32}H_{59}N_7O_6S_0H^+_1$	-0.25	Internal
539.39162	1	$C_{27}H_{50}N_6O_5S_0H^+_1$	0.14	Internal
440.3232	1	$C_{22}H_{41}N_5O_4S_0H^+_1$	0.16	Internal
341.25478	1	$C_{17}H_{32}N_4O_3S_0H^+_1$	0.18	Internal
242.18639	1	$C_{12}H_{23}N_3O_2S_0H^+_1$	0.36	Internal
459.8231	2	$C_{47}H_{83}N_9O_9S_0H^+_2$	0.30	Internal
410.28893	2	$C_{42}H_{74}N_8O_8S_0H^+_2$	0.42	Internal
360.75473	2	$C_{37}H_{65}N_7O_7S_0H^+_2$	0.50	Internal
311.22049	2	$C_{32}H_{56}N_6O_6S_0H^+_2$	0.47	Internal
261.68615	2	$C_{27}H_{47}N_5O_5S_0H^+_2$	0.05	Internal
212.15203	2	$C_{22}H_{38}N_4O_4S_0H^+_2$	0.47	Internal

664.47569	2	$C_{68}H_{122}N_{14}O_{12}S_0H^+_2$	0.12	Internal
565.40725	2	$C_{58}H_{104}N_{12}O_{10}S_0H^+_2$	0.10	Internal
515.87302	2	$C_{53}H_{95}N_{11}O_9S_0H^+_2$	0.06	Internal
466.33891	2	$C_{48}H_{86}N_{10}O_8S_0H^+_2$	0.28	Internal
416.80462	2	$C_{43}H_{77}N_9O_7S_0H^+_2$	0.11	Internal
367.27045	2	$C_{38}H_{68}N_8O_6S_0H^+_2$	0.22	Internal
317.73624	2	$C_{33}H_{59}N_7O_5S_0H^+_2$	0.25	Internal
268.20206	2	$C_{28}H_{50}N_6O_4S_0H^+_2$	0.40	Internal
882.0691	2	$C_{86}H_{155}N_{17}O_{17}S_2H^+_2$	0.46	Internal
832.53467	2	$C_{81}H_{146}N_{16}O_{16}S_2H^+_2$	0.22	Internal
783.00072	2	$C_{76}H_{137}N_{15}O_{15}S_2H^+_2$	0.57	Internal
733.46622	2	$C_{71}H_{128}N_{14}O_{14}S_2H^+_2$	0.20	Internal
683.93217	2	$C_{66}H_{119}N_{13}O_{13}S_2H^+_2$	0.45	Internal
634.39789	2	$C_{61}H_{110}N_{12}O_{12}S_2H^+_2$	0.37	Internal
584.86349	2	$C_{56}H_{101}N_{11}O_{11}S_2H^+_2$	0.07	Internal
535.32931	2	$C_{51}H_{92}N_{10}O_{10}S_2H^+_2$	0.13	Internal
485.7952	2	$C_{46}H_{83}N_9O_9S_2H^+_2$	0.34	Internal
815.07553	2	$C_{82}H_{149}N_{17}O_{16}S_0H^+_2$	-0.19	Internal
765.54134	2	$C_{77}H_{140}N_{16}O_{15}S_0H^+_2$	-0.18	Internal
716.00734	2	$C_{72}H_{131}N_{15}O_{14}S_0H^+_2$	0.09	Internal
616.93889	2	$C_{62}H_{113}N_{13}O_{12}S_0H^+_2$	0.05	Internal
567.4047	2	$C_{57}H_{104}N_{12}O_{11}S_0H^+_2$	0.08	Internal
517.87062	2	$C_{52}H_{95}N_{11}O_{10}S_0H^+_2$	0.34	Internal
468.33639	2	$C_{47}H_{86}N_{10}O_9S_0H^+_2$	0.32	Internal
418.80214	2	$C_{42}H_{77}N_9O_8S_0H^+_2$	0.26	Internal
369.26792	2	$C_{37}H_{68}N_8O_7S_0H^+_2$	0.26	Internal
510.36502	1	$C_{26}H_{47}N_5O_5S_0H^+_1$	0.05	Internal
411.29656	1	$C_{21}H_{38}N_4O_4S_0H^+_1$	-0.05	Internal
312.22828	1	$C_{16}H_{29}N_3O_3S_0H^+_1$	0.36	Internal
213.15985	1	$C_{11}H_{20}N_2O_2S_0H^+_1$	0.45	Internal
793.55463	1	$C_{40}H_{72}N_8O_8S_0H^+_1$	0.05	Internal
595.41759	1	$C_{30}H_{54}N_6O_6S_0H^+_1$	-0.29	Internal
496.34933	1	$C_{25}H_{45}N_5O_5S_0H^+_1$	-0.03	Internal
397.28104	1	$C_{20}H_{36}N_4O_4S_0H^+_1$	0.27	Internal
446.21429	1	$C_{20}H_{35}N_3O_4S_2H^+_1$	0.26	Internal
347.14586	1	$C_{15}H_{26}N_2O_3S_2H^+_1$	0.28	Internal
248.07739	1	$C_{10}H_{17}N_1O_2S_2H^+_1$	0.17	Internal
701.79026	3	$C_{103}H_{185}N_{20}O_{21}S_2H^+_3$	1.18	Pre-Me
687.78493	3	$C_{101}H_{183}N_{20}O_{20}S_2H^+_3$	-1.42	Pre-C_3H_5O
682.11815	3	$C_{101}H_{182}N_{20}O_{19}S_2H^+_3$	-0.26	Pre-C_3H_5O-OH
677.1283	3	$C_{101}H_{183}N_{20}O_{20}S_1H^+_3$	-0.37	Pre-C_3H_5OS
673.77459	3	$C_{99}H_{179}N_{19}O_{20}S_2H^+_3$	0.21	Pre-C_5H_9NO
668.77487	3	$C_{98}H_{178}N_{20}O_{19}S_2H^+_3$	0.46	Pre-$_2$(C_3H_5O)
666.47129	3	$C_{101}H_{183}N_{20}O_{20}S_0H^+_3$	0.14	Pre-$C_5H_5OS_2$
658.76306	3	$C_{97}H_{174}N_{19}O_{19}S_2H^+_3$	-0.07	Pre-$C_7H_{14}NO_2$
658.11781	3	$C_{98}H_{178}N_{20}O_{19}S_1H^+_3$	0.92	Pre-C_3H_5O-C_3H_5OS

657.43923	3	$C_{98}H_{174}N_{19}O_{20}S_1H^+_3$	2.81	Pre-C_3H_5OS-C_3H_9N
647.45989	3	$C_{98}H_{178}N_{20}O_{19}S_0H^+_3$	0.07	Pre-$C_5H_5OS_2$-C_3H_5O
633.11252	3	$C_{96}H_{173}N_{19}O_{19}S_0H^+_3$	0.11	Pre-$C_8H_{14}NO_2S_2$-H
632.7605	3	$C_{94}H_{166}N_{20}O_{20}S_0H^+_3$	0.50	Pre-$C_5H_9OS_2$-C_5H_{13}
		Average	0.4	
		Standard Deviation	0.67	

Table S 6.3: MS assignment of p(Ox-co-EI) Figure 6.4

m/z	charge	chemical formula	error	assignment
187.1441	1	$C_9H_{18}N_2O_2H^+_1$	0.03	0EI a2
286.2125	1	$C_{14}H_{27}N_3O_3H^+_1$	0.08	0EI a3
385.281	1	$C_{19}H_{36}N_4O_4H^+_1$	0.12	0EI a4
484.3494	1	$C_{24}H_{45}N_5O_5H^+_1$	0.15	0EI a5
583.4179	1	$C_{29}H_{54}N_6O_6H^+_1$	0.27	0EI a6
781.5546	1	$C_{39}H_{72}N_8O_8H^+_1$	0.03	0EI a8
880.624	1	$C_{44}H_{81}N_9O_9H^+_1$	1.09	0EI a8
131.1179	1	$C_6H_{14}N_2O_1H^+_1$	0.00	1EI a2
230.1863	1	$C_{11}H_{23}N_3O_2H^+_1$	0.12	1EI a3
329.2547	1	$C_{16}H_{32}N_4O_3H^+_1$	-0.17	1EI a4
428.3232	1	$C_{21}H_{41}N_5O_4H^+_1$	0.18	1EI a5
527.3916	1	$C_{26}H_{50}N_6O_5H^+_1$	0.14	1EI a6
626.4606	1	$C_{31}H_{59}N_7O_6H^+_1$	1.05	1EI a7
725.5282	1	$C_{36}H_{68}N_8O_7H^+_1$	-0.21	1EI a8
824.597	1	$C_{41}H_{77}N_9O_8H^+_1$	0.22	1EI a9
372.2969	1	$C_{18}H_{37}N_5O_3H^+_1$	0.04	2EI a5
471.3654	1	$C_{23}H_{46}N_6O_4H^+_1$	0.04	2EI a6
570.4339	1	$C_{28}H_{55}N_7O_5H^+_1$	0.26	2EI a7
669.5023	1	$C_{33}H_{64}N_8O_6H^+_1$	0.18	2EI a8
768.5708	1	$C_{38}H_{73}N_9O_7H^+_1$	0.23	2EI a9
867.6397	1	$C_{43}H_{82}N_{10}O_8H^+_1$	0.77	2EI a10
412.802	2	$C_{41}H_{77}N_9O_8H^+_2$	0.02	1EI a9
462.3367	2	$C_{46}H_{86}N_{10}O_9H^+_2$	0.89	1EI a10
511.8704	2	$C_{51}H_{95}N_{11}O_{10}H^+_2$	-0.01	1EI a11
561.4048	2	$C_{56}H_{104}N_{12}O_{11}H^+_2$	0.24	1EI a12
610.939	2	$C_{61}H_{113}N_{13}O_{12}H^+_2$	0.21	1EI a13
335.2548	2	$C_{33}H_{64}N_8O_6H^+_2$	0.22	2EI a8
384.789	2	$C_{38}H_{73}N_9O_7H^+_2$	0.27	2EI a9
434.3233	2	$C_{43}H_{82}N_{10}O_8H^+_2$	0.30	2EI a10
483.8574	2	$C_{48}H_{91}N_{11}O_9H^+_2$	0.07	2EI a11
533.3915	2	$C_{53}H_{100}N_{12}O_{10}H^+_2$	-0.07	2EI a12
582.9258	2	$C_{58}H_{109}N_{13}O_{11}H^+_2$	0.15	2EI a13
632.4601	2	$C_{63}H_{118}N_{14}O_{12}H^+_2$	0.16	2EI a14
681.9938	2	$C_{68}H_{127}N_{15}O_{13}H^+_2$	-0.49	2EI a15

356.7759	2	$C_{35}H_{69}N_9O_6H^+_2$	0.12	3EI a9
406.3102	2	$C_{40}H_{78}N_{10}O_7H^+_2$	0.31	3EI a10
455.8444	2	$C_{45}H_{87}N_{11}O_8H^+_2$	0.26	3EI a11
505.3787	2	$C_{50}H_{96}N_{12}O_9H^+_2$	0.42	3EI a12
554.9128	2	$C_{55}H_{105}N_{13}O_{10}H^+_2$	0.33	3EI a13
604.4471	2	$C_{60}H_{114}N_{14}O_{11}H^+_2$	0.43	3EI a14
653.9812	2	$C_{65}H_{123}N_{15}O_{12}H^+_2$	0.23	3EI a15
703.5155	2	$C_{70}H_{132}N_{16}O_{13}H^+_2$	0.33	3EI a16
391.281	2	$C_{39}H_{72}N_8O_8H^+_2$	0.20	0EI a8
440.8152	2	$C_{44}H_{81}N_9O_9H^+_2$	0.12	0EI a9
161.1284	1	$C_7H_{16}N_2O_2H^+_1$	-0.09	1EI x2
260.1969	1	$C_{12}H_{25}N_3O_3H^+_1$	0.05	1EI x3
359.2652	1	$C_{17}H_{34}N_4O_4H^+_1$	-0.12	1EI x4
204.1707	1	$C_9H_{21}N_3O_2H^+_1$	0.03	2EI x2
303.2391	1	$C_{14}H_{30}N_4O_3H^+_1$	0.17	2EI x3
402.3073	1	$C_{19}H_{39}N_5O_4H^+_1$	-0.57	2EI x4
501.375	1	$C_{24}H_{48}N_6O_5H^+_1$	-1.73	2EI x5
600.4444	1	$C_{29}H_{57}N_7O_6H^+_1$	0.12	2EI x6
699.5125	1	$C_{34}H_{66}N_8O_7H^+_1$	-0.33	2EI x7
798.5816	1	$C_{39}H_{75}N_9O_8H^+_1$	0.52	2EI x8
343.7681	2	$C_{33}H_{67}N_9O_6H^+_2$	0.17	4EI x8
393.3024	2	$C_{38}H_{76}N_{10}O_7H^+_2$	0.46	4EI x9
442.8366	2	$C_{43}H_{85}N_{11}O_8H^+_2$	0.46	4EI x10
492.3707	2	$C_{48}H_{94}N_{12}O_9H^+_2$	0.22	4EI x11
541.9049	2	$C_{53}H_{103}N_{13}O_{10}H^+_2$	0.17	4EI x12
591.4391	2	$C_{58}H_{112}N_{14}O_{11}H^+_2$	0.06	4EI x13
640.9733	2	$C_{63}H_{121}N_{15}O_{12}H^+_2$	0.10	4EI x14
690.5076	2	$C_{68}H_{130}N_{16}O_{13}H^+_2$	0.20	4EI x15
740.0417	2	$C_{73}H_{139}N_{17}O_{14}H^+_2$	0.04	4EI x16
272.7127	2	$C_{26}H_{53}N_7O_5H^+_2$	-0.02	3EI x6
322.2469	2	$C_{31}H_{62}N_8O_6H^+_2$	-0.10	3EI x7
371.7811	2	$C_{36}H_{71}N_9O_7H^+_2$	0.11	3EI x8
421.3154	2	$C_{41}H_{80}N_{10}O_8H^+_2$	0.29	3EI x9
470.8495	2	$C_{46}H_{89}N_{11}O_9H^+_2$	-0.07	3EI x10
520.3835	2	$C_{51}H_{98}N_{12}O_{10}H^+_2$	-0.40	3EI x11
569.918	2	$C_{56}H_{107}N_{13}O_{11}H^+_2$	0.09	3EI x12
619.4524	2	$C_{61}H_{116}N_{14}O_{12}H^+_2$	0.35	3EI x13
668.9865	2	$C_{66}H_{125}N_{15}O_{13}H^+_2$	0.18	3EI x14
718.5206	2	$C_{71}H_{134}N_{16}O_{14}H^+_2$	0.10	3EI x15
399.7942	2	$C_{39}H_{75}N_9O_8H^+_2$	0.01	2EI x8
498.8628	2	$C_{49}H_{93}N_{11}O_{10}H^+_2$	0.32	2EI x10
548.3969	2	$C_{54}H_{102}N_{12}O_{11}H^+_2$	0.21	2EI x11
597.9312	2	$C_{59}H_{111}N_{13}O_{12}H^+_2$	0.28	2EI x12
247.2129	1	$C_{11}H_{26}N_4O_2H^+_1$	0.15	3EI x3
346.2813	1	$C_{16}H_{35}N_5O_3H^+_1$	0.15	3EI x4
445.3498	1	$C_{21}H_{44}N_6O_4H^+_1$	0.20	3EI x5

544.4182	1	$C_{26}H_{53}N_7O_5H^+_1$	0.18	3EI x6
643.4862	1	$C_{31}H_{62}N_8O_6H^+_1$	-0.45	3EI x7
742.5549	1	$C_{36}H_{71}N_9O_7H^+_1$	-0.07	3EI x8
483.3575	3	$C_{72}H_{136}N_{17}O_{13}H^+_3$	0.16	4EI a17-1
483.6935	3	$C_{72}H_{137}N_{17}O_{13}H^+_3$	0.36	4EI a17
491.6935	3	$C_{74}H_{137}N_{17}O_{13}H^+_3$	0.42	Pre-$C_5H_{11}NO_2$-$_2$H
492.0294	3	$C_{74}H_{138}N_{17}O_{13}H^+_3$	0.17	Pre-$C_5H_{11}NO_2$-H
492.3658	3	$C_{74}H_{139}N_{17}O_{13}H^+_3$	1.10	Pre-$C_5H_{11}NO_2$
493.3691	3	$C_{73}H_{140}N_{18}O_{13}H^+_3$	0.50	Pre-$_2$(C_3H_5O)
506.0406	3	$C_{76}H_{142}N_{18}O_{13}H^+_3$	-0.31	Pre-(C_3H_5O)-OH_3
506.3767	3	$C_{76}H_{143}N_{18}O_{13}H^+_3$	-0.01	Pre-(C_3H_5O)-OH_2
506.7131	3	$C_{76}H_{144}N_{18}O_{13}H^+_3$	0.91	Pre-(C_3H_5O)-OH
512.3804	3	$C_{76}H_{145}N_{18}O_{14}H^+_3$	0.31	Pre-C_3H_5O
525.3882	3	$C_{79}H_{148}N_{18}O_{14}H^+_3$	0.37	Pre-H_2O
531.3918	3	$C_{79}H_{150}N_{18}O_{15}H^+_3$	0.42	Precursor
169.1335	2	$C_{18}H_{32}N_4O_2H^+_2$	-0.18	Internal
218.6677	2	$C_{23}H_{41}N_5O_3H^+_2$	-0.26	Internal
268.202	2	$C_{28}H_{50}N_6O_4H^+_2$	0.06	Internal
317.7362	2	$C_{33}H_{59}N_7O_5H^+_2$	0.09	Internal
367.2705	2	$C_{38}H_{68}N_8O_6H^+_2$	0.25	Internal
416.8047	2	$C_{43}H_{77}N_9O_7H^+_2$	0.21	Internal
466.3389	2	$C_{48}H_{86}N_{10}O_8H^+_2$	0.25	Internal
205.66	2	$C_{21}H_{39}N_5O_3H^+_2$	0.14	Internal
304.7284	2	$C_{31}H_{57}N_7O_5H^+_2$	0.18	Internal
354.2626	2	$C_{36}H_{66}N_8O_6H^+_2$	0.22	Internal
403.7968	2	$C_{41}H_{75}N_9O_7H^+_2$	0.17	Internal
453.3311	2	$C_{46}H_{84}N_{10}O_8H^+_2$	0.34	Internal
277.2072	2	$C_{28}H_{52}N_6O_5H^+_2$	0.01	Internal 1EI alkene
326.7415	2	$C_{33}H_{61}N_7O_6H^+_2$	0.24	Internal 1EI alkene
376.2758	2	$C_{38}H_{70}N_8O_7H^+_2$	0.29	Internal 1EI alkene
425.81	2	$C_{43}H_{79}N_9O_8H^+_2$	0.29	Internal 1EI alkene
475.3444	2	$C_{48}H_{88}N_{10}O_9H^+_2$	0.64	Internal 1EI alkene
186.1601	1	$C_9H_{19}N_3O_1H^+_1$	0.11	Internal
285.2285	1	$C_{14}H_{28}N_4O_2H^+_1$	0.13	Internal
143.1179	1	$C_7H_{14}N_2O_1H^+_1$	0.14	Internal
242.1863	1	$C_{12}H_{23}N_3O_2H^+_1$	0.15	Internal
		Average	0.26	
		Standard Deviation	0.34	

Table S 6.4: MS assignment of p(Ox-co-EI) Figure 6.4

m/z	charge	chemical formula	error	assignment
100.07569	1	$C_5H_9N_1O_1S_0H^+_1$	0.00	k_1
199.1441	1	$C_{10}H_{18}N_2O_2S_0H^+_1$	-0.02	k_2
298.21248	1	$C_{15}H_{27}N_3O_3S_0H^+_1$	-0.13	k_3
397.28088	1	$C_{20}H_{36}N_4O_4S_0H^+_1$	-0.13	k_4
496.34924	1	$C_{25}H_{45}N_5O_5S_0H^+_1$	-0.21	k_5
595.4174	1	$C_{30}H_{54}N_6O_6S_0H^+_1$	-0.60	k_6
694.48617	1	$C_{35}H_{63}N_7O_7S_0H^+_1$	-0.01	k_7
186.13623	1	$C_9H_{17}N_2O_2S_0H^+_1$	-0.26	j_2
285.20467	1	$C_{14}H_{26}N_3O_3S_0H^+_1$	-0.08	j_3
384.27311	1	$C_{19}H_{35}N_4O_4S_0H^+_1$	0.01	j_4
483.34148	1	$C_{24}H_{44}N_5O_5S_0H^+_1$	-0.08	j_5
582.41016	1	$C_{29}H_{53}N_6O_6S_0H^+_1$	0.39	j_6
285.18079	1	$C_{14}H_{24}N_2O_4S_0H^+_1$	-0.33	a_2
384.24925	1	$C_{19}H_{33}N_3O_5S_0H^+_1$	-0.12	a_3
483.31759	1	$C_{24}H_{42}N_4O_6S_0H^+_1$	-0.25	a_4
582.38604	1	$C_{29}H_{51}N_5O_7S_0H^+_1$	-0.15	a_5
780.52299	1	$C_{39}H_{69}N_7O_9S_0H^+_1$	0.05	a_7
879.59026	1	$C_{44}H_{78}N_8O_{10}S_0H^+_1$	-1.26	a_8
978.66041	1	$C_{49}H_{87}N_9O_{11}S_0H^+_1$	0.64	a_9
1077.72966	1	$C_{54}H_{96}N_{10}O_{12}S_0H^+_1$	1.36	a_{10}
1176.79649	1	$C_{59}H_{105}N_{11}O_{13}S_0H^+_1$	-0.10	a_{11}
1275.86338	1	$C_{64}H_{114}N_{12}O_{14}S_0H^+_1$	-1.29	a_{12}
363.12274	1	$C_{15}H_{26}N_2O_2S_3H^+_1$	-0.49	y_2
462.1916	1	$C_{20}H_{35}N_3O_3S_3H^+_1$	0.58	y_3
561.25948	1	$C_{25}H_{44}N_4O_4S_3H^+_1$	-0.47	y_4
660.3283	1	$C_{30}H_{53}N_5O_5S_3H^+_1$	0.21	y_5
759.39596	1	$C_{35}H_{62}N_6O_6S_3H^+_1$	-0.81	y_6
858.46513	1	$C_{40}H_{71}N_7O_7S_3H^+_1$	0.17	y_7
957.53257	1	$C_{45}H_{80}N_8O_8S_3H^+_1$	-0.87	y_8
1056.60599	1	$C_{50}H_{89}N_9O_9S_3H^+_1$	3.95	y_9
1155.67046	1	$C_{55}H_{98}N_{10}O_{10}S_3H^+_1$	0.20	y_{10}
1254.73959	1	$C_{60}H_{107}N_{11}O_{11}S_3H^+_1$	0.75	y_{11}
173.10467	1	$C_8H_{14}N_1O_3S_0H^+_1$	0.15	b_1
272.17301	1	$C_{13}H_{23}N_2O_4S_0H^+_1$	-0.18	b_2
371.24147	1	$C_{18}H_{32}N_3O_5S_0H^+_1$	-0.01	b_3
470.30989	1	$C_{23}H_{41}N_4O_6S_0H^+_1$	0.01	b_4
569.37789	1	$C_{28}H_{50}N_5O_7S_0H^+_1$	-0.72	b_5
668.44625	1	$C_{33}H_{59}N_6O_8S_0H^+_1$	-0.69	b_6
767.51608	1	$C_{38}H_{68}N_7O_9S_0H^+_1$	1.24	b_7
253.15477	1	$C_{13}H_{20}N_2O_3S_0H^+_1$	0.40	Internal
352.22312	1	$C_{18}H_{29}N_3O_4S_0H^+_1$	0.11	Internal
451.29159	1	$C_{23}H_{38}N_4O_5S_0H^+_1$	0.21	Internal
550.35989	1	$C_{28}H_{47}N_5O_6S_0H^+_1$	-0.04	Internal

649.42865	1	$C_{33}H_{56}N_6O_7S_0H^+_1$	0.50	Internal
214.16758	1	$C_{11}H_{21}N_2O_2S_0H^+_1$	0.00	Internal
313.23613	1	$C_{16}H_{30}N_3O_3S_0H^+_1$	0.44	Internal
214.14373	1	$C_{11}H_{19}N_1O_3S_0H^+_1$	-0.19	Internal
313.21214	1	$C_{16}H_{28}N_2O_4S_0H^+_1$	-0.14	Internal
412.28057	1	$C_{21}H_{37}N_3O_5S_0H^+_1$	-0.07	Internal
511.34885	1	$C_{26}H_{46}N_4O_6S_0H^+_1$	-0.32	Internal
610.41713	1	$C_{31}H_{55}N_5O_7S_0H^+_1$	-0.48	Internal
709.48524	1	$C_{36}H_{64}N_6O_8S_0H^+_1$	-0.84	Internal
808.55406	1	$C_{41}H_{73}N_7O_9S_0H^+_1$	-0.24	Internal
907.62229	1	$C_{46}H_{82}N_8O_{10}S_0H^+_1$	-0.42	Internal
1006.68992	1	$C_{51}H_{91}N_9O_{11}S_0H^+_1$	-1.15	Internal
367.16862	1	$C_{10}H_{22}N_8O_7S_0H^+_1$	0.54	Internal
466.23719	1	$C_{15}H_{31}N_9O_8S_0H^+_1$	0.76	Internal
565.30535	1	$C_{20}H_{40}N_{10}O_9S_0H^+_1$	0.18	Internal
664.37347	1	$C_{25}H_{49}N_{11}O_{10}S_0H^+_1$	-0.29	Internal
763.44193	1	$C_{30}H_{58}N_{12}O_{11}S_0H^+_1$	-0.19	Internal
862.5088	1	$C_{35}H_{67}N_{13}O_{12}S_0H^+_1$	-1.96	Internal
268.15422	1	$C_{14}H_{21}N_1O_4S_0H^+_1$	-0.43	Internal
367.22278	1	$C_{19}H_{30}N_2O_5S_0H^+_1$	0.09	Internal
466.29145	1	$C_{24}H_{39}N_3O_6S_0H^+_1$	0.62	Internal
565.35943	1	$C_{29}H_{48}N_4O_7S_0H^+_1$	-0.26	Internal
664.42776	1	$C_{34}H_{57}N_5O_8S_0H^+_1$	-0.35	Internal
763.49608	1	$C_{39}H_{66}N_6O_9S_0H^+_1$	-0.42	Internal
862.56492	1	$C_{44}H_{75}N_7O_{10}S_0H^+_1$	0.12	Internal
961.63475	1	$C_{49}H_{84}N_8O_{11}S_0H^+_1$	1.58	Internal
1060.7003	1	$C_{54}H_{93}N_9O_{12}S_0H^+_1$	-1.27	Internal
185.12844	1	$C_9H_{16}N_2O_2S_0H^+_1$	-0.08	Internal
284.19695	1	$C_{14}H_{25}N_3O_3S_0H^+_1$	0.29	Internal
383.26531	1	$C_{19}H_{34}N_4O_4S_0H^+_1$	0.07	Internal
581.40221	1	$C_{29}H_{52}N_6O_6S_0H^+_1$	0.17	Internal
322.1648	1	$C_{10}H_{31}N_3O_2S_3H^+_1$	-0.98	Internal
421.23334	1	$C_{15}H_{40}N_4O_3S_3H^+_1$	-0.45	Internal
520.30161	1	$C_{20}H_{49}N_5O_4S_3H^+_1$	-0.64	Internal
619.3701	1	$C_{25}H_{58}N_6O_5S_3H^+_1$	-0.42	Internal
718.43831	1	$C_{30}H_{67}N_7O_6S_3H^+_1$	-0.64	Internal
817.50688	1	$C_{35}H_{76}N_8O_7S_3H^+_1$	-0.37	Internal
916.57697	1	$C_{40}H_{85}N_9O_8S_3H^+_1$	1.49	Internal
1015.64288	1	$C_{45}H_{94}N_{10}O_9S_3H^+_1$	-1.12	Internal
339.19147	1	$C_{17}H_{26}N_2O_5S_0H^+_1$	0.06	Internal
438.25984	1	$C_{22}H_{35}N_3O_6S_0H^+_1$	-0.05	Internal
537.3282	1	$C_{27}H_{44}N_4O_7S_0H^+_1$	-0.14	Internal
636.39663	1	$C_{32}H_{53}N_5O_8S_0H^+_1$	-0.09	Internal
834.53349	1	$C_{42}H_{71}N_7O_{10}S_0H^+_1$	-0.03	Internal
909.52283	2	$C_{91}H_{144}N_{14}O_{22}S_1H^+_2$	0.59	Pre-6(C_2H_6N)-$C_5H_9S_2$-5H
932.05051	2	$C_{93}H_{151}N_{15}O_{22}S_1H^+_2$	-0.76	Pre-5(C_2H_6N)-$C_5H_9S_2$-4H

954.58081	2	$C_{95}H_{158}N_{16}O_{22}S_1H^+_2$	0.70	Pre-4(C_2H_6N)-$C_5H_9S_2$-3H
959.58358	2	$C_{94}H_{164}N_{16}O_{19}S_3H^+_2$	0.27	Pre-($C_8H_{14}NO_3$)-3(C_2H_6N)+3H
977.10975	2	$C_{97}H_{165}N_{17}O_{22}S_1H^+_2$	0.70	Pre-3(C_2H_6N)-$C_5H_9S_2$-2H
982.11252	2	$C_{96}H_{171}N_{17}O_{19}S_3H^+_2$	0.28	Pre-($C_8H_{14}NO_3$)-2(C_2H_6N)+2H
999.63798	2	$C_{99}H_{172}N_{18}O_{22}S_1H^+_2$	-0.01	Pre-2(C_2H_6N)-$C_5H_9S_2$-H
1022.16551	2	$C_{101}H_{179}N_{19}O_{22}S_1H^+_2$	-1.38	Pre-C_2H_6N-$C_5H_9S_2$-H
1043.11344	2	$C_{102}H_{173}N_{17}O_{22}S_3H^+_2$	0.96	Pre-3(C_2H_6N)-2H
651.74206	3	$C_{97}H_{165}N_{17}O_{22}S_1H^+_3$	0.39	Pre-3(C_2H_6N)-$C_5H_9S_2$-3H
661.79128	3	$C_{100}H_{179}N_{19}O_{21}S_0H^+_3$	-0.14	Pre-(C_3H_6NO)-$C_5H_9S_3$
665.7056	3	$C_{98}H_{159}N_{15}O_{22}S_3H^+_3$	0.17	Pre-5(C_2H_6N)-5H
672.44881	3	$C_{100}H_{179}N_{19}O_{21}S_1H^+_3$	0.12	Pre-C_3H_6NO-$C_5H_9S_2$
677.75268	3	$C_{100}H_{175}N_{17}O_{20}S_3H^+_3$	0.03	Pre-(C_2H_6N)-2(C_3H_6NO)-H
680.72499	3	$C_{100}H_{166}N_{16}O_{22}S_3H^+_3$	0.33	Pre-4(C_2H_6N)-4H
685.80659	3	$C_{103}H_{185}N_{20}O_{22}S_0H^+_3$	0.34	Pre-$C_5H_9S_3$
692.77204	3	$C_{102}H_{182}N_{18}O_{20}S_3H^+_3$	0.14	Pre-2(C_3H_6NO)
695.74431	3	$C_{102}H_{173}N_{17}O_{22}S_3H^+_3$	0.37	Pre-3(C_2H_6N)-3H
710.76341	3	$C_{104}H_{180}N_{18}O_{22}S_3H^+_3$	0.11	Pre-2(C_2H_6N)-2H
716.7873	3	$C_{105}H_{188}N_{19}O_{21}S_3H^+_3$	0.53	Pre-C_3H_6NO
725.783	3	$C_{106}H_{187}N_{19}O_{22}S_3H^+_3$	0.53	Pre-C_2H_6N-H
740.80209	3	$C_{108}H_{194}N_{20}O_{22}S_3H^+_3$	0.26	Precursor
		Average	0.46	
		Standard deviation	0.7	

7. Cyclic peptide-polymer conjugate characterization using tandem mass spectrometry techniques

Tomos E. Morgan[1], Alina Theisen[1], Sean Ellacott[1], Anisha Haris[1], Bryan Marzullo[1], Christopher A. Wootton[1], Mark P. Barrow[1], Anthony W. T. Bristow[2], Sebastien Perrier[1], Peter B. O'Connor[1]*

[1]Department of Chemistry, University of Warwick, Coventry, Midlands, CV4 7AL, UK.

[2]Chemical Development, Pharmaceutical Technology & Development, Operations, AstraZeneca, Macclesfield, UK.

The MS, MS/MS, and analysis presented in this chapter were all carried out by the thesis author. Sean Ellacott carried out the synthesis, purification, and GPC and NMR analysis of the cyclic peptide-polymer species. The UV modification for SolariX was carried out by Alina Theisen and Anisha Haris.

The work presented in this chapter has been prepared for publication in ACS Analytical chemistry by authors Tomos E. Morgan, Sean Ellacott, Alina Theisen, Anisha Haris, Christopher A. Wootton, Mark P. Barrow, Anthony W. T. Bristow, Sébastien Perrier, Peter B. O'Connor.

7.1. Abstract

Cyclic peptide-polymer conjugates offer a unique biocompatible system with many advantages but comes at a cost of being analytically complex. Developing further analytical techniques of complex polymer-conjugate systems is key for understanding synthetic and medicinal processes.

In this contribution, a synthetic cyclic peptide-polymer conjugate is analysed using electron capture dissociation (ECD), infrared multiphoton absorption dissociation (IRMPD), and ultraviolet photodissociation (UVPD) on the same mass spectrometry system. IRMPD and UVPD were shown to effectively characterize an unconjugated cyclic peptide specie, ECD was ineffective due to production of multiple sequence scrambling fragments and radical side chain losses.

The polyoxazoline conjugated cyclic peptide species was effectively characterized by combining the ECD and IRMPD fragments due to their complementarity. UVPD effectively characterized both the cyclic peptide and the conjugating polymer in one experiment, being able to produce complete cyclic peptide fragmentation via *b/y* fragment pathways and polymer fragmentation *via a/x* polyoxazoline fragment pathways.

7.2. Introduction

With increasingly potent small molecules being developed for medicinal applications there is a need for increasingly complex drug delivery vectors.[1] The properties of the drug delivery vectors can be tuned to greatly increase the efficacy of the drug by taking advantage of biological phenomena such as the enhanced permeability and retention (EPR) effect.[2,3] Self-assembly nanotubes formed from cyclic peptides produces controlled tubes with specified internal diameters[4] and conjugation of polymers to the cyclic peptide offers a further control of the self-assembly mechanism.[5,6] Variations in the conjugated polymers can produce thermoresponsive,[7] pH responsive,[8-10] redox responsive[11] and even hydrogel forming[12,13] nanotubes for use as drug delivery vectors.[14] The use of alternating D- and L- amino acids offer an amino acid system that can interlink to form nanotube structures though intermolecular bonds; conjugating polymers onto the central cyclic peptide structures produces controllable nanotube lengths.[15]

Both the cyclic peptide central nanotube and the conjugated polymer can be varied;[16] offering a unique analytical challenge. Analysis is often carried out qualitatively by NMR to confirm the presence of the cyclic peptide amongst polymer signals. Analysis of the final nanotube structure is often carried out by light scattering methods.[6]

Protein-polymer conjugate species have been investigated with the use of mass spectrometry analysis[17,18] with peptide-polymer conjugate analysis being carried out by matrix assisted laser desorption ionization (MALDI) and electrospray ionization (ESI) coupled to ion mobility MS.[19] The ability to accurately identify the mass of more complex polymer-conjugate species is incredibly important in confirming that the biological species hasn't been modified during the conjugation process. Assigning complex MS polymer spectra is made more facile with the use of Kendrick[20] mass defect techniques for polymer assignment.[21-23]

Tandem mass spectrometry of various polyoxazoline species have been carried out previously by CAD/CID,[24,25] Sequencing of polyoxazolines has also been carried out in

this laboratory by Ultraviolet photodissociation (UVPD) and radical based electron capture dissociation (ECD).[26-28]

Sequence elucidation of cyclic peptides offers a unique challenge due to the lack of a terminus group.[29,30] All observed cyclic peptide fragment peaks must, therefore, be part of a secondary dissociation event, as a singly dissociation event will break the cyclic peptide but not produce an observable *m/z* change. ECD techniques do not offer an effective characterization of cyclic peptides due to sequence scrambling caused by the free radical cascade.[31] Cyclic peptides have been analyzed by UVPD[32,33] showing high cleavage coverage and effective peptide characterization.

In this contribution a poly(2-oxazoline) conjugated to an alternating D- and L- amino acid cyclic peptides was analyzed by IRMPD, ECD, and UVPD to compare the effectiveness of fragmentation methods in characterizing both the peptide and the conjugating polymer.

7.3. Methods and Experimental

Cationic ring opening polymerisation of 2-ethyl oxazoline was carried out producing a hydroxyl- capped poly(2-ethyl-2-oxazoline). The resulting poly(2-ethyl-2-oxazoline) was then conjugated onto the cyclic peptide. The cyclic peptide polymer conjugate sample was dissolved into a 99.5% solution of purified water obtained from a Direct-Q3 Ultrapure Water System (Millipore, Lutterworth, United Kingdom) at 20 µM in 0.5% formic acid (Sigma- Aldrich, Dorset, United Kingdom).

All experiments were performed on a 12 T solariX Fourier transform ion cyclotron resonance mass spectrometer (Bruker Daltonik, GmbH, Bremen, Germany) using a nanoelectrospray (nESI) ion source in positive ion mode.

UVPD dissociation was carried out with one or two 6 mJ laser pulses (measured at laser head) from a 193 nm excimer laser (ExciStar XS, Coherent) in the setup used herein translates to <0.6 mJ at the window of the ICR cell.

ECD was carried out using the hollow ring cathode, ECD bias voltage was set at 1.2 eV for the analysis of both the cyclic peptide and cyclic peptide-polymer conjugate species. The ECD pulse length was lower for the peptide-conjugate (0.1 s) due to the higher charge compared to the cyclic peptide (0.3 s).

IRMPD analysis of the cyclic peptide was carried out at 45% laser power with a 0.15 second pulse for the cyclic peptide and a 0.25 second pulse for the cyclic peptide-polymer conjugate. Transients were acquired with a low mass of 98 Da using 4 mega-word (2^{22}, 22 bit) transients (1.12 s) achieving approximately 250,000 resolving power at *m/z* 400. All mass spectra were calibrated internally using fragments present in each of the spectra (peaks used for calibration are marked). The peaks used for internal calibration were crosschecked using both the *a* and *x* fragment series to reduce the likelihood of systematic error in calibration. The Bruker SNAP algorithm was used for peak picking with the polyoxazoline monomer used as the repeat unit. SNAP matches a calculated isotope distribution adjusted to a repeat unit with increasing mass. [34-36]

7.4. Results and Discussion

Analysis of a polyoxazoline conjugated cyclic peptide by nESI showed four major distributions of ions. One of the major distributions could be assigned to the cyclic peptide conjugate-polymer conjugate with the adduction of four or five protons. The other distribution was an unreacted hydrogen terminated polyoxazoline species which is a by-product of the polyoxazoline synthesis. The assigned monomer distribution of the cyclic peptide-polymer conjugate observed were from 39 monomer units to 54 monomer units. Monomer assignments for the hydrogen terminated by-product were from 20 monomer units to 63 monomer units. The increased intensity of the by-product could be due to an increased concentration within the mixture analyzed or, that the cyclic peptide-polymer conjugate undergoes self-assembly within the solvent conditions used for analysis, is less available within the solution for ionization by nESI.

The presence of mainly protonated adduct species is expected within the analysis, both the polyoxazoline and conjugating peptide species are hydrophilic and will easily undergo protonation under acidified conditions. Acidified conditions on the short analytical time-scales here showed no evidence of cyclic peptide-polymer conjugate modification or hydrolysis, and analysis was greatly helped from acidification by reducing the number of adducts present.

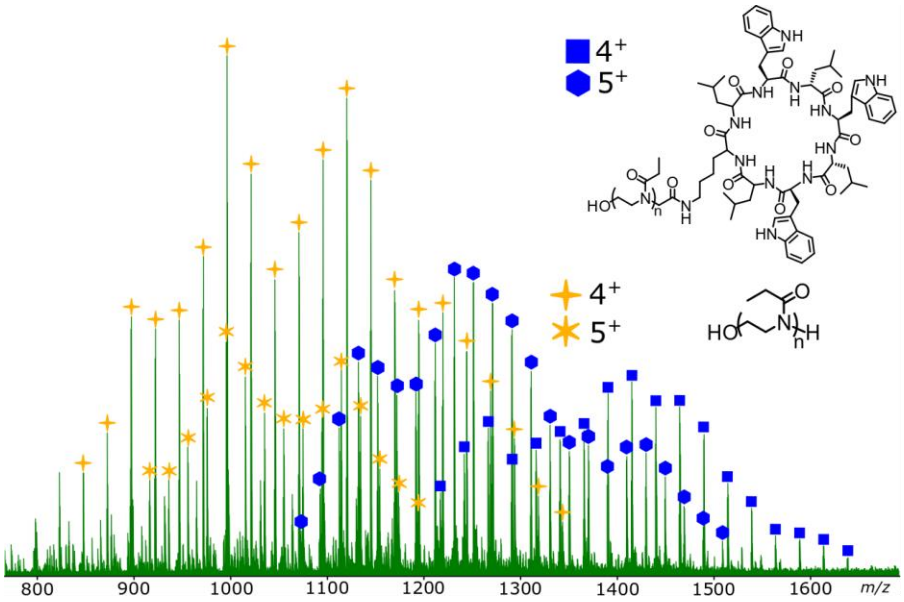

Figure 7.1 nESI analysis of the cyclic peptide-polymer conjugate showing the presence of 4^+ and 5^+ protonated species. The presence of the cyclic peptide-polymer conjugate species and the hydrogen terminated polyoxazoline by-product is assigned.

The mass spectrometry analysis of cyclic peptide before polymer conjugation is included within the supplementary information. The cyclic peptide will often form dimers and higher order peptide structures but freshly solublised and at the low concentrations used in the MS analysis a large peak was observed representing a doubly protonated cyclic peptide species. The doubly charged cyclic peptide species was isolated by quadrupole isolation at *m/z* 570. The isolation of the doubly charged cyclic peptide allowed not only laser induced fragmentation techniques to be used but also electron capture fragmentation techniques.

Tandem mass spectrometry analysis of a cyclic peptide required multiple fragmentation events to occur for fragments to be observed, once to break the cyclic structure and another to actually form the observable fragment. IRMPD analysis of the cyclic peptide produced a fragmentation spectrum, Figure 2A, containing fragment peaks that corresponded to two *b/y* fragmentation events, with both fragment events occurring at the amide bond. The nature of the cyclic peptide means that an obvious sequence is hard to quantitate depending on where the initial

fragmentation event occurred. It is clear though by the fragment coverage that the most intense fragment series follow the expected fragment ladder. Low levels of fragments can be observed that correspond to an incorrect sequence, LL, WW, and WLKW. The scrambled sequence fragments could be due to incorrect synthesis or by secondary rearrangements of the cyclic peptide during the fragmentation event. The intensity of the scrambled fragments compared to the corresponding sequence fragments come to below 10 % of the intensity.

Presence of neutral losses from the fragments was clear with the loss of H_2O being the most prominent loss, marked with a " ' " in the corresponding figures. The intensity of the H_2O loss peak compared to that of the same corresponding fragment before water loss showed a large variation from approximately 10% of the intensity to around 80% intensity. Overall, taking the average intensity of H_2O loss compared to the corresponding fragment the average H_2O loss intensity was 35 %.

Another internal fragment peak that is observed is a loss of CH_3NO, it is likely that in the rearrangement in the secondary fragmentation event to produce the fragments there is a loss of NH_3 and CO, rather than the loss of a CH_3NO unit itself. Although, it is worth noting, there is little evidence of consistent CO or NH_3 loss separately so they may be removed in a concerted process. Taking the $CONH_3$ loss fragment and comparison to the corresponding precursor fragment intensity gives an average intensity of 21 % of $CONH_3$ loss fragments.

The UVPD fragmentation, Figure 7.2B, gave very similar results to the IRMPD, with sequence coverage being achieved through the cyclic peptide. The majority of the fragments observed were that of two *b/y* fragmentation events occurring on the peptide. The production of *b/y* fragments is consistent with UVPD results shown, interestingly there is no evidence of *a/x* fragments observed.

Sequence scrambling fragments were present at lower intensities compared to the IRMPD fragmentation with sequence scrambling fragments coming below 5 % intensity. UVPD analysis also contained the same neutral losses with the loss of H_2O and $CONH_3$. H_2O loss was significantly less for UVPD with a comparitive 11 % of fragments showing H_2O loss compared to the 35 % in IRMPD. A similar result was

seen for $CONH_3$ loss with approximately 10 % of fragments showing $CONH_3$ loss compared to 21 % for IRMPD. Fragmentation efficiency of the UVPD was lower than that of the IRMPD experiment, but the production of lower neutral loss fragments is beneficial to the analysis.

ECD analysis of the cyclic peptide, Figure 7.2C, produced expected results, many of the fragments containing amino acids were scrambled fragments giving no sequence information and there were a large number of side chain losses. Side chain losses that are easily indefinable are the loss of the tryptophan side group which occurs at both carbon positions from the backbone. Other neutral losses consist of carbon and hydrogen loss which is likely due to the presence of multiple leucine groups and radical rearrangement of these groups. Overall, the ECD experiment gave almost no useful analytical information regarding the cyclic peptide species, especially when compared to IRMPD and UVPD methods.

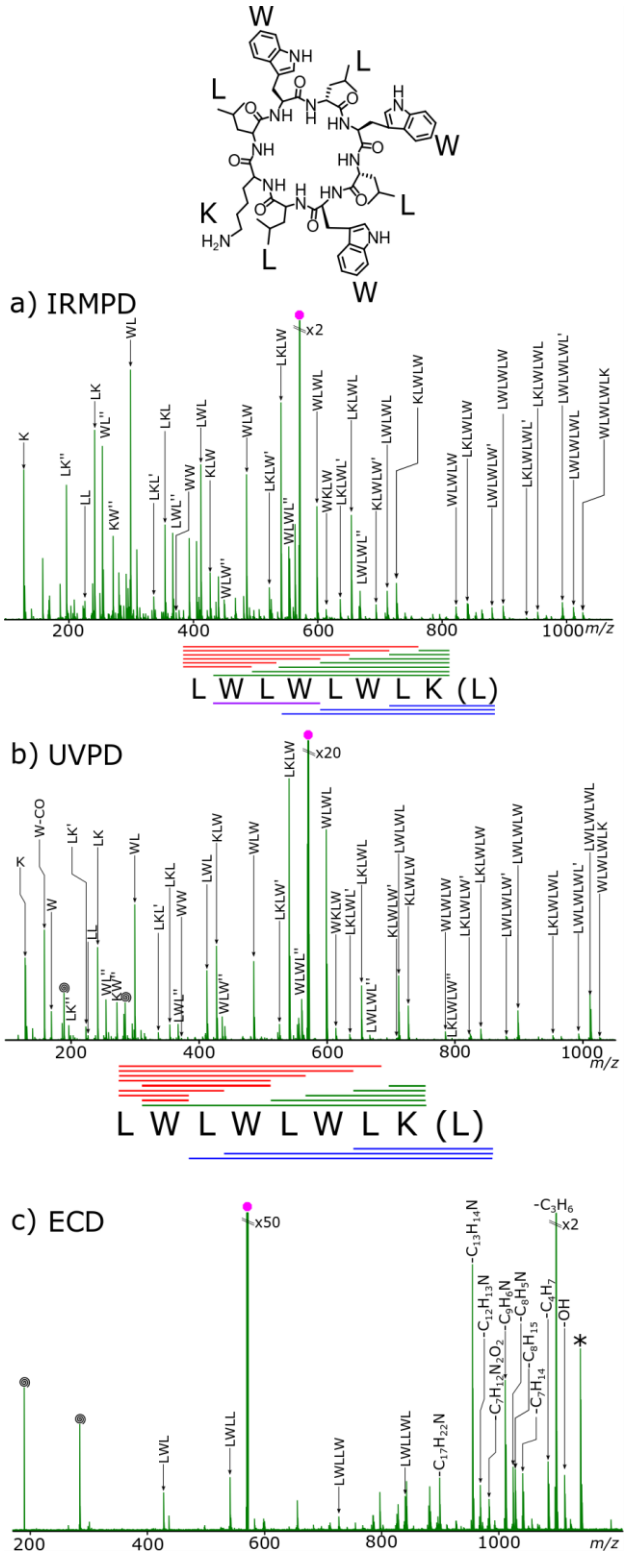

Figure 7.2 Tandem mass spectrometry analysis of a doubly charged cyclic peptide. a) IRMPD, and corresponding fragmentation coverage, b) UVPD and corresponding fragmentation coverage, c) ECD, no fragmentation map is shown as fragmentation coverage is low and primarily of scrambled sequence fragments.

The results from the cyclic peptide studies give an interesting starting point to analysis of the cyclic peptide-polymer conjugate. Previous analysis has shown that ECD and UVPD experiments can be used to sequence polyoxazolines but ECD has just been shown to not accurately sequence a cyclic peptide.

IRMPD fragmentation, Figure 7.3A, of the cyclic peptide-polymer conjugate showed significant fragmentation of the cyclic peptide resulting in complete coverage of the cyclic peptide species. The polymer, though, remains completely uncharacterized. Polymer fragment ions consist of rearranged fragments due to the lack of amide bond in the backbone of the polymer itself. The polymer fragments observed do not contain the terminal fragments, and therefore, do not give useful sequence information.

The ECD spectrum, Figure 7.3B, shows much greater fragment coverage of the conjugating polymer. The *a* series fragments, which contain the terminating OH group span over 4500 Da starting with a a_2 fragment, (singly charged, *m/z* 217.15467, 0.0 ppm) to an a_{46} fragment (doubly charged, *m/z* 2288.58608, 0.8 ppm). Through the two charge states of fragments observed almost complete sequence coverage is observed in the polyoxazoline polymer. The *z* fragment series, which contains the cyclic peptide conjugated to the polymer is present from x_9 (doubly charged, *m/z* 1072.67326, -0.27 ppm) to x_{27} (doubly charged, *m/z* 1964.28928, 0.0 ppm). There is a very low intensity singly charged fragment series present from x_2 to x_{11} (*m/z* 1351.79253, -0.9 ppm, *m/z* 2342.47733, 0.3 ppm respectively). The intensity of the singly charged *z* series was very low, and often overlapped by the charge reduced and neutral loss fragment peaks. The ECD spectrum, complementary to the IRMPD spectrum, doesn't contain any analytically useful cyclic peptide fragments.

Together, the IRMPD and ECD offer complementary fragmentation that results in a high level of characterization of the cyclic peptide-polymer conjugate but across two experiments.

The analysis of the cyclic peptide-polymer conjugate species by UVPD shows that coverage of the cyclic peptide and of the polymer can be achieved within one

fragmentation experiment. The central cyclic peptide is sequenced to much the same extent as the IRMPD fragmentation. UVPD was carried out using 2 6 mJ laser shots.

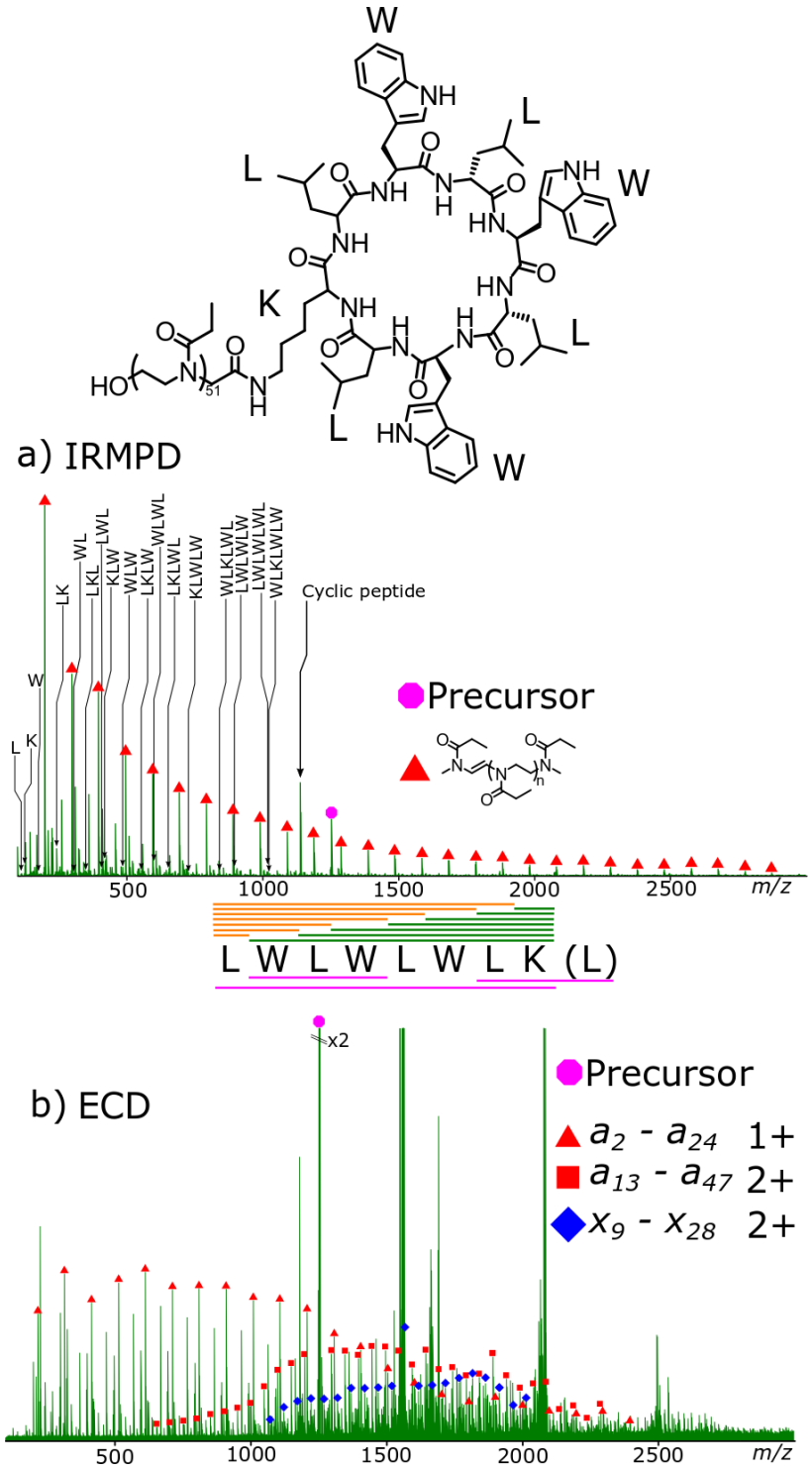

Figure 7.3 Tandem mass spectrum of a cyclic peptide polymer conjugate by a) IRMPD, presents significant cyclic peptide coverage but internal fragmentation of the polymer, b) ECD coverage of *a*, OH terminus containing polymer fragments, and *x*, cyclic peptide containing fragments.

The polymer fragmentation observed is the same *a* and *x* fragmentation seen in the ECD spectrum; but covers the complete range of *a* fragmentation from a_2 (singly charged, *m/z* 217.15469, 0.0 ppm) to a_{51} (quadruply charged, *m/z* 1268.63269, 0.4 ppm). Doubly and triply charge states are also observed for the *a* fragment series producing complete sequence coverage of the polyoxazoline throughout all 51 monomer units covering a mass range of over 5000 Da. The *x* fragment series is, like the ECD, less complete than the *a* fragment series. The cyclic peptide containing *x* series spans from x_{20} (doubly charged, *m/z* 1568.01618, 0.35 ppm) to x_{49} (quadruply charged, *m/z* 1495.00257, -0.2 ppm). Overall, coverage of the polymer series of the cyclic peptide-polymer conjugate is large with the use of UVPD.

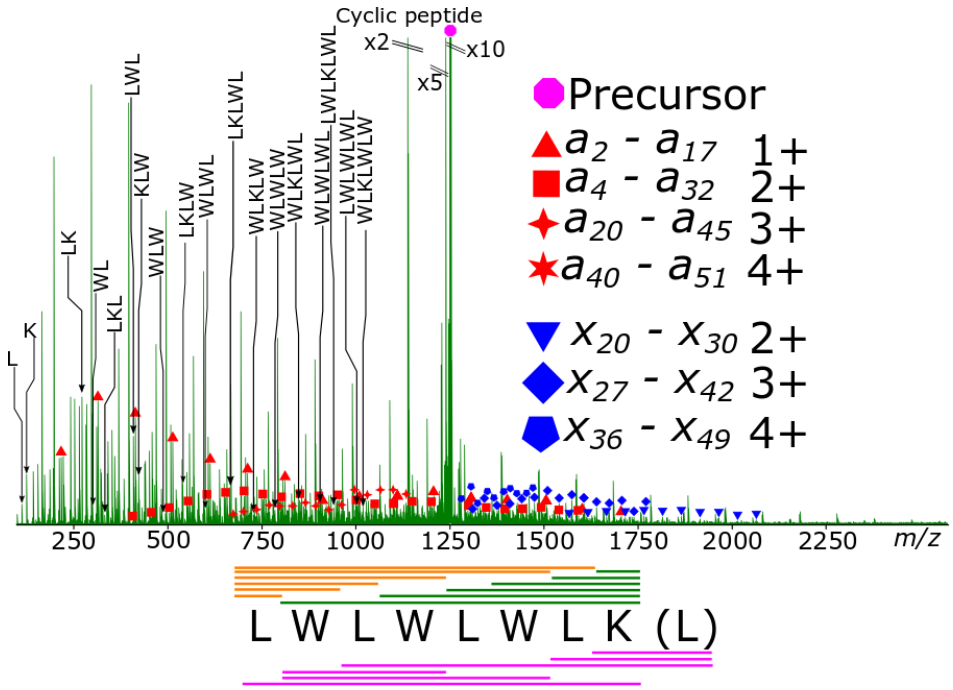

Figure 7.4 Tandem mass spectrum of a cyclic peptide polymer conjugate by UVPD showing the *a* and *x* series fragments as well as coverage of the cyclic peptide conjugate species in one experiment.

IRMPD and UVPD gave complete fragmentation coverage of the cyclic peptide species. Although sequence scrambling was observed, the intensity of the scrambled fragments compared to the sequence fragments was much lower showing scrambling was not the favored pathway in the dissociation. ECD was ineffective at analyzing the cyclic peptide species, with all the fragments observed either being side chain losses or sequence scrambled peptide fragments.

The analysis of the cyclic peptide-polymer conjugate could be carried out effectively with the use of IRMPD and ECD giving complementary fragmentation to one another allowing sequencing of the peptide using IRMPD to then be followed by sequencing of the polymer using ECD. UVPD allowed both the cyclic peptide and the polymer to be sequenced in one experiment.

7.5. References

(1) Petros, R. A.; DeSimone, J. M. Strategies in the design of nanoparticles for therapeutic applications *Nat. Rev. Drug Discov.* **2010**, *9*, 615-627.
(2) Maeda, H.; Wu, J.; Sawa, T.; Matsumura, Y.; Hori, K. Tumor Vascular Permeability and the EPR effect in macromolecular therapeutics: a review *J. Controlled Release* **2000**, *65*, 271-284.
(3) Nicolas, J.; Mura, S.; Brambilla, D.; Mackiewicz, N.; Couvreur, P. Design, functionalization strategies and biomedical applications of targeted biodegradable/biocompatible polymer-based nanocarriers for drug delivery *Chem. Soc. Rev.* **2013**, *42*, 1147-1235.
(4) Khazanovich, N.; Granja, J. R.; McRee, D. E.; Milligan, R. A.; Ghadiri, M. R. Nanoscale Tubular Ensembles with Specified Internal Diameters. Design of a Self-Assembled Nanotube with a 13-A Pore *J. Am. Chem. Soc.* **1994**, *116*, 6011-6012.
(5) Chapman, R.; Danial, M.; Koh, M. L.; Jolliffe, K. A.; Perrier, S. Design and properties of functional nanotubes from the self-assembly of cyclic peptide templates *Chem. Soc. Rev.* **2012**, *41*, 6023-6041.
(6) Danial, M.; Tran, C. M.; Young, P. G.; Perrier, S.; Jolliffe, K. A. Janus cyclic peptide-polymer nanotubes *Nat Commun* **2013**, *4*, 2780.
(7) Chapman, R.; Bouten, P. J.; Hoogenboom, R.; Jolliffe, K. A.; Perrier, S. Thermoresponsive cyclic peptide--poly(2-ethyl-2-oxazoline) conjugate nanotubes *Chem Commun (Camb)* **2013**, *49*, 6522-6524.
(8) Chapman, R.; Warr, G. G.; Perrier, S.; Jolliffe, K. A. Water-soluble and pH-responsive polymeric nanotubes from cyclic peptide templates *Chem. Eur. J.* **2013**, *19*, 1955-1961.
(9) Larnaudie, S. C.; Brendel, J. C.; Jolliffe, K. A.; Perrier, S. pH-Responsive, Amphiphilic Core–Shell Supramolecular Polymer Brushes from Cyclic Peptide–Polymer Conjugates *ACS Macro Letters* **2017**, *6*, 1347-1351.
(10) Méndez-Ardoy, A.; Granja, J. R.; Montenegro, J. pH-Triggered self-assembly and hydrogelation of cyclic peptide nanotubes confined in water micro-droplets *Nanoscale Horizons* **2018**, *3*, 391-396.
(11) Song, Q.; Yang, J.; Hall, S. C. L.; Gurnani, P.; Perrier, S. Pyridyl Disulfide Reaction Chemistry: An Efficient Strategy toward Redox-Responsive Cyclic Peptide–Polymer Conjugates *ACS Macro Letters* **2019**, *8*, 1347-1352.
(12) Shaikh, H.; Rho, J. Y.; Macdougall, L. J.; Gurnani, P.; Lunn, A. M.; Yang, J.; Huband, S.; Mansfield, E. D. H.; Peltier, R.; Perrier, S. Hydrogel and Organogel Formation by Hierarchical Self-Assembly of Cyclic Peptides Nanotubes *Chem. Eur. J.* **2018**, *24*, 19066-19074.
(13) Binfield, J. G.; Brendel, J. C.; Cameron, N. R.; Eissa, A. M.; Perrier, S. Imaging Proton Transport in Giant Vesicles through Cyclic Peptide-Polymer Conjugate Nanotube Transmembrane Ion Channels *Macromol. Rapid Commun.* **2018**, *39*.
(14) Larnaudie, S. C.; Brendel, J. C.; Romero-Canelon, I.; Sanchez-Cano, C.; Catrouillet, S.; Sanchis, J.; Coverdale, J. P. C.; Song, J. I.; Habtemariam, A.; Sadler, P. J.; Jolliffe, K. A.; Perrier, S. Cyclic Peptide-Polymer Nanotubes as Efficient and Highly Potent Drug Delivery Systems for Organometallic Anticancer Complexes *Biomacromolecules* **2018**, *19*, 239-247.
(15) Mansfield, E. D. H.; Hartlieb, M.; Catrouillet, S.; Rho, J. Y.; Larnaudie, S. C.; Rogers, S. E.; Sanchis, J.; Brendel, J. C.; Perrier, S. Systematic study of the structural parameters affecting the self-assembly of cyclic peptide-poly(ethylene glycol) conjugates *Soft Matter* **2018**, *14*, 6320-6326.
(16) Zorzi, A.; Deyle, K.; Heinis, C. Cyclic peptide therapeutics: past, present and future *Curr. Opin. Chem. Biol.* **2017**, *38*, 24-29.

(17) Tao, L.; Kaddis, C. S.; Ogorzalek Loo, R. R.; Grover, G. N.; Loo, J. A.; Maynard, H. D. Synthetic approach to homodimeric protein-polymer conjugates *Chem Commun (Camb)* **2009**, 2148-2150.
(18) Abzalimov, R. R.; Frimpong, A.; Kaltashov, I. A. Structural characterization of protein–polymer conjugates. I. Assessing heterogeneity of a small PEGylated protein and mapping conjugation sites using ion exchange chromatography and top-down tandem mass spectrometry *Int. J. Mass spectrom.* **2012**, *312*, 135-143.
(19) Alalwiat, A.; Grieshaber, S. E.; Paik, B. A.; Kiick, K. L.; Jia, X.; Wesdemiotis, C. Top-down mass spectrometry of hybrid materials with hydrophobic peptide and hydrophilic or hydrophobic polymer blocks *Analyst* **2015**, *140*, 7550-7564.
(20) Kendrick, E. A Mass Scale Based on CH2=: 14.0000 for High Resolution Mass Spectrometry of Organic Compounds *Anal. Chem.* **1963**, *35*, 2146-2154.
(21) Fouquet, T.; Cody, R. B.; Sato, H. Capabilities of the remainders of nominal Kendrick masses and the referenced Kendrick mass defects for copolymer ions *J. Mass Spectrom.* **2017**, *52*, 618-624.
(22) Fouquet, T.; Shimada, H.; Maeno, K.; Ito, K.; Ozeki, Y.; Kitagawa, S.; Ohtani, H.; Sato, H. High-resolution Kendrick Mass Defect Analysis of Poly(ethylene oxide)-based Non-ionic Surfactants and Their Degradation Products *J. Oleo Sci.* **2017**, *66*, 1061-1072.
(23) Fouquet, T. N. J.; Cody, R. B.; Ozeki, Y.; Kitagawa, S.; Ohtani, H.; Sato, H. On the Kendrick Mass Defect Plots of Multiply Charged Polymer Ions: Splits, Misalignments, and How to Correct Them *J. Am. Soc. Mass. Spectrom.* **2018**, *29*, 1611-1626.
(24) Altuntaş, E.; Weber, C.; Schubert, U. S. Detailed characterization of poly(2-ethyl-2oxazoline)s by energy variable collision-induced dissociation study *Rapid Commun. Mass Spectrom.* **2013**, *27*, 1095-1100.
(25) Baumgaertel, A.; Scheubert, K.; Pietsch, B.; Kempe, K.; Crecelius, A. C.; Bocker, S.; Schubert, U. S. Analysis of different synthetic homopolymers by the use of a new calculation software for tandem mass spectra *Rapid Commun. Mass Spectrom.* **2011**, *25*, 1765-1778.
(26) Morgan, T. E.; Ellacott, S. H.; Wootton, C. A.; Barrow, M. P.; Bristow, A. W. T.; Perrier, S.; O'Connor, P. B. Coupling Electron Capture Dissociation and the Modified Kendrick Mass Defect for Sequencing of a Poly(2-ethyl-2-oxazoline) Polymer *Anal. Chem.* **2018**, *90*, 11710-11715.
(27) Zubarev, R. A.; Kelleher, N. L.; McLafferty, F. W. Electron Capture Dissocaition of Multiply Charged Protein Cations. A nonergodic Process *J. Am. Chem. Soc.* **1998**, *120*, 3265-3266.
(28) Zubarev, R. A.; Horn, D. M.; Fridriksson, E. K.; Kelleher, N. L.; Kruger, N. A.; Lewis, M. A.; Carpenter, B. K.; McLafferty, F. W. Electron Capture Dissociation for structural characterization of multiply charged protein cations *Anal. Chem.* **2000**, *72*, 563-573.
(29) Lu, W.-T.; Ng, J.; Meluzzi, D.; Banderia, N.; Gutierrez, M.; Simmons, T. L.; Schultz, A. W.; Linington, R. G.; Moore, B. S.; Gerwick, W. H.; Pevzner, P. A.; Dorrestein, P. C. Interpretation of Tandem Mass Spectra Obtained from Cyclic Nonribosomal Peptides *Anal. Chem.* **2009**, *81*, 4200-4209.
(30) Mohimani, H.; Yang, Y. L.; Liu, W. T.; Hsieh, P. W.; Dorrestein, P. C.; Pevzner, P. A. Sequencing cyclic peptides by multistage mass spectrometry *Proteomics* **2011**, *11*, 3642-3650.
(31) Leymarie, N.; Costello, C. E.; O'Connor, P. B. Electron Capture Dissociation Initiates a Free Radical Reaction Cascade *J. Am. Chem. Soc.* **2003**, *125*, 8949-8958.
(32) Attard, T. J.; Carter, M. D.; Fang, M.; Johnson, R. C.; Reid, G. E. Structural Characterization and Absolute Quantification of Microcystin Peptides Using Collision-Induced and Ultraviolet Photo-Dissociation Tandem Mass Spectrometry *J. Am. Soc. Mass. Spectrom.* **2018**, *29*, 1812-1825.

(33) Crittenden, C. M.; Parker, W. R.; Jenner, Z. B.; Bruns, K. A.; Akin, L. D.; McGee, W. M.; Ciccimaro, E.; Brodbelt, J. S. Exploitation of the Ornithine Effect Enhances Characterization of Stapled and Cyclic Peptides *J. Am. Soc. Mass. Spectrom.* **2016**, *27*, 856-863.
(34) Köster, C. United States, US 6188064 B1.2001.Bruker Daltonik GmbH (DE)
(35) Wootton, C. A.; Lam, Y. P. Y.; Willetts, M.; van Agthoven, M. A.; Barrow, M. P.; Sadler, P. J.; PB, O. C. Automatic assignment of metal-containing peptides in proteomic LC-MS and MS/MS data sets *Analyst* **2017**, *142*, 2029-2037.
(36) Kaur, P.; O'Connor, P. B. Algorithms for automatic interpretation of high resolution mass spectra *J. Am. Soc. Mass. Spectrom.* **2006**, *17*, 459-468.

SUPPORTING INFORMATION

to

Cyclic peptide-polymer conjugate characterisation using tandem mass spectrometry techniques

by

Tomos E. Morgan[1], Alina Theisen[1], Sean Ellacott[1], Anisha Haris[1], Bryan Marzullo[1], Christopher A. Wootton[1], Mark P. Barrow[1], Anthony W. T. Bristow[2], Sebastien Perrier[1], Peter B. O'Connor[1]*

[1]Department of Chemistry, University of Warwick, Coventry, Midlands, CV4 7AL, UK.

[2]Chemical Development, Pharmaceutical Technology & Development, Operations, AstraZeneca, Macclesfield, UK.

*Corresponding authors: Peter O'Connor [redacted]

Table S 7.1: Mass spectrometry assignments of cyclic peptide-polymer conjugate, Figure 7.1 in main text

m/z	charge	Chemical formula	Error (ppm)	Assignment
1414.68783	4	$C_{290}H_{493}N_{57}O_{55}S_0H^+_4$	-5.49	cycpep 4H+
1439.4529	4	$C_{295}H_{502}N_{58}O_{56}S_0H^+_4$	-6.81	cycpep 4H+
1464.22244	4	$C_{300}H_{511}N_{59}O_{57}S_0H^+_4$	-5.03	cycpep 4H+
1538.52342	4	$C_{315}H_{538}N_{62}O_{60}S_0H^+_4$	-5	cycpep 4H+
1563.28744	4	$C_{320}H_{547}N_{63}O_{61}S_0H^+_4$	-6.89	cycpep 4H+
1588.05683	4	$C_{325}H_{556}N_{64}O_{62}S_0H^+_4$	-5.34	cycpep 4H+
1013.07542	5	$C_{260}H_{439}N_{51}O_{49}S_0H^+_5$	-0.41	cycpep 5H+
1032.88715	5	$C_{265}H_{448}N_{52}O_{50}S_0H^+_5$	-2.29	cycpep 5H+
1072.51415	5	$C_{275}H_{466}N_{54}O_{52}S_0H^+_5$	-2.55	cycpep 5H+
1092.33047	5	$C_{280}H_{475}N_{55}O_{53}S_0H^+_5$	-0.09	cycpep 5H+
1112.14362	5	$C_{285}H_{484}N_{56}O_{54}S_0H^+_5$	-0.56	cycpep 5H+
1131.95845	5	$C_{290}H_{493}N_{57}O_{55}S_0H^+_5$	0.46	cycpep 5H+
1151.76931	5	$C_{295}H_{502}N_{58}O_{56}S_0H^+_5$	-2	cycpep 5H+
1171.58213	5	$C_{300}H_{511}N_{59}O_{57}S_0H^+_5$	-2.7	cycpep 5H+
1191.3958	5	$C_{305}H_{520}N_{60}O_{58}S_0H^+_5$	-2.67	cycpep 5H+
1211.21059	5	$C_{310}H_{529}N_{61}O_{59}S_0H^+_5$	-1.71	cycpep 5H+
1250.83863	5	$C_{320}H_{547}N_{63}O_{61}S_0H^+_5$	-1.12	cycpep 5H+
1270.65083	5	$C_{325}H_{556}N_{64}O_{62}S_0H^+_5$	-2.27	cycpep 5H+
1290.46498	5	$C_{330}H_{565}N_{65}O_{63}S_0H^+_5$	-1.87	cycpep 5H+
1310.27935	5	$C_{335}H_{574}N_{66}O_{64}S_0H^+_5$	-1.32	cycpep 5H+
1369.7193	5	$C_{350}H_{601}N_{69}O_{67}S_0H^+_5$	-2.06	cycpep 5H+
1389.53289	5	$C_{355}H_{610}N_{70}O_{68}S_0H^+_5$	-2.1	cycpep 5H+
1409.34737	5	$C_{360}H_{619}N_{71}O_{69}S_0H^+_5$	-1.5	cycpep 5H+
1429.16156	5	$C_{365}H_{628}N_{72}O_{70}S_0H^+_5$	-1.13	cycpep 5H+
1448.97571	5	$C_{370}H_{637}N_{73}O_{71}S_0H^+_5$	-0.79	cycpep 5H+
1468.78819	5	$C_{375}H_{646}N_{74}O_{72}S_0H^+_5$	-1.6	cycpep 5H+
748.5238	4	$C_{150}H_{272}N_{30}O_{31}S_0H^+_4$	1.04	H-terminated 4H+
773.29112	4	$C_{155}H_{281}N_{31}O_{32}S_0H^+_4$	1.29	H-terminated 4H+
798.05744	4	$C_{160}H_{290}N_{32}O_{33}S_0H^+_4$	0.26	H-terminated 4H+
822.82433	4	$C_{165}H_{299}N_{33}O_{34}S_0H^+_4$	0	H-terminated 4H+
847.59173	4	$C_{170}H_{308}N_{34}O_{35}S_0H^+_4$	0.35	H-terminated 4H+
872.3579	4	$C_{175}H_{317}N_{35}O_{36}S_0H^+_4$	-0.73	H-terminated 4H+
897.12555	4	$C_{180}H_{326}N_{36}O_{37}S_0H^+_4$	-0.1	H-terminated 4H+
921.89187	4	$C_{185}H_{335}N_{37}O_{38}S_0H^+_4$	-0.95	H-terminated 4H+
946.65981	4	$C_{190}H_{344}N_{38}O_{39}S_0H^+_4$	-0.04	H-terminated 4H+
971.42593	4	$C_{195}H_{353}N_{39}O_{40}S_0H^+_4$	-1.05	H-terminated 4H+
996.19485	4	$C_{200}H_{362}N_{40}O_{41}S_0H^+_4$	0.8	H-terminated 4H+
1020.95943	4	$C_{205}H_{371}N_{41}O_{42}S_0H^+_4$	-1.69	H-terminated 4H+
1045.72626	4	$C_{210}H_{380}N_{42}O_{43}S_0H^+_4$	-1.92	H-terminated 4H+
1070.49555	4	$C_{215}H_{389}N_{43}O_{44}S_0H^+_4$	0.17	H-terminated 4H+
1095.26043	4	$C_{220}H_{398}N_{44}O_{45}S_0H^+_4$	-1.86	H-terminated 4H+
1120.0289	4	$C_{225}H_{407}N_{45}O_{46}S_0H^+_4$	-0.6	H-terminated 4H+

1144.79449	4	$C_{230}H_{416}N_{46}O_{47}S_0H^+_4$	-1.91	H-terminated 4H+
1169.56270	4	$C_{235}H_{425}N_{47}O_{48}S_0H^+_4$	-0.92	H-terminated 4H+
1194.33023	4	$C_{240}H_{434}N_{48}O_{49}S_0H^+_4$	-0.55	H-terminated 4H+
1243.86529	4	$C_{250}H_{452}N_{50}O_{51}S_0H^+_4$	0.16	H-terminated 4H+
1268.63219	4	$C_{255}H_{461}N_{51}O_{52}S_0H^+_4$	0	H-terminated 4H+
1293.39964	4	$C_{260}H_{470}N_{52}O_{53}S_0H^+_4$	0.26	H-terminated 4H+
700.48991	3	$C_{105}H_{191}N_{21}O_{22}S_0H^+_3$	0.31	H-terminated 3H+
733.51360	3	$C_{110}H_{200}N_{22}O_{23}S_0H^+_3$	1.5	H-terminated 3H+
766.53582	3	$C_{115}H_{209}N_{23}O_{24}S_0H^+_3$	0.67	H-terminated 3H+
799.55900	3	$C_{120}H_{218}N_{24}O_{25}S_0H^+_3$	1.11	H-terminated 3H+
832.58150	3	$C_{125}H_{227}N_{25}O_{26}S_0H^+_3$	0.7	H-terminated 3H+
865.60341	3	$C_{130}H_{236}N_{26}O_{27}S_0H^+_3$	-0.36	H-terminated 3H+
898.62629	3	$C_{135}H_{245}N_{27}O_{28}S_0H^+_3$	-0.26	H-terminated 3H+
931.64967	3	$C_{140}H_{254}N_{28}O_{29}S_0H^+_3$	0.37	H-terminated 3H+
964.67314	3	$C_{145}H_{263}N_{29}O_{30}S_0H^+_3$	1.04	H-terminated 3H+
997.69408	3	$C_{150}H_{272}N_{30}O_{31}S_0H^+_3$	-0.86	H-terminated 3H+
1030.71833	3	$C_{155}H_{281}N_{31}O_{32}S_0H^+_3$	0.57	H-terminated 3H+
1063.74081	3	$C_{160}H_{290}N_{32}O_{33}S_0H^+_3$	0.25	H-terminated 3H+
1096.76361	3	$C_{165}H_{299}N_{33}O_{34}S_0H^+_3$	0.24	H-terminated 3H+
1129.78694	3	$C_{170}H_{308}N_{34}O_{35}S_0H^+_3$	0.69	H-terminated 3H+
1162.80659	3	$C_{175}H_{317}N_{35}O_{36}S_0H^+_3$	-2.04	H-terminated 3H+
1195.83309	3	$C_{180}H_{326}N_{36}O_{37}S_0H^+_3$	1.11	H-terminated 3H+
797.15761	5	$C_{200}H_{362}N_{40}O_{41}S_0H^+_5$	1.14	H-terminated 5H+
816.97043	5	$C_{205}H_{371}N_{41}O_{42}S_0H^+_5$	0.06	H-terminated 5H+
836.78400	5	$C_{210}H_{380}N_{42}O_{43}S_0H^+_5$	-0.08	H-terminated 5H+
856.59747	5	$C_{215}H_{389}N_{43}O_{44}S_0H^+_5$	-0.33	H-terminated 5H+
876.41085	5	$C_{220}H_{398}N_{44}O_{45}S_0H^+_5$	-0.66	H-terminated 5H+
896.22618	5	$C_{225}H_{407}N_{45}O_{46}S_0H^+_5$	1.19	H-terminated 5H+
916.03937	5	$C_{230}H_{416}N_{46}O_{47}S_0H^+_5$	0.63	H-terminated 5H+
935.85247	5	$C_{235}H_{425}N_{47}O_{48}S_0H^+_5$	-0.01	H-terminated 5H+
955.66630	5	$C_{240}H_{434}N_{48}O_{49}S_0H^+_5$	0.14	H-terminated 5H+
975.47982	5	$C_{245}H_{443}N_{49}O_{50}S_0H^+_5$	-0.03	H-terminated 5H+
995.29467	5	$C_{250}H_{452}N_{50}O_{51}S_0H^+_5$	1.15	H-terminated 5H+
1015.10531	5	$C_{255}H_{461}N_{51}O_{52}S_0H^+_5$	-1.87	H-terminated 5H+
1034.92091	5	$C_{260}H_{470}N_{52}O_{53}S_0H^+_5$	0.02	H-terminated 5H+
1054.73506	5	$C_{265}H_{479}N_{53}O_{54}S_0H^+_5$	0.46	H-terminated 5H+
1074.54768	5	$C_{270}H_{488}N_{54}O_{55}S_0H^+_5$	-0.54	H-terminated 5H+
1094.35955	5	$C_{275}H_{497}N_{55}O_{56}S_0H^+_5$	-2.19	H-terminated 5H+
1114.17697	5	$C_{280}H_{506}N_{56}O_{57}S_0H^+_5$	1.21	H-terminated 5H+
1133.98707	5	$C_{285}H_{515}N_{57}O_{58}S_0H^+_5$	-1.97	H-terminated 5H+
1153.80047	5	$C_{290}H_{524}N_{58}O_{59}S_0H^+_5$	-2.18	H-terminated 5H+
1173.61526	5	$C_{295}H_{533}N_{59}O_{60}S_0H^+_5$	-1.2	H-terminated 5H+
1193.42785	5	$C_{300}H_{542}N_{60}O_{61}S_0H^+_5$	-2.1	H-terminated 5H+
1233.05779	5	$C_{310}H_{560}N_{62}O_{63}S_0H^+_5$	0.06	H-terminated 5H+
1252.87239	5	$C_{315}H_{569}N_{63}O_{64}S_0H^+_5$	0.79	H-terminated 5H+
		Average	1.3	
		Standard Deviation	1.7	

Table S 7.2: IRMPD assignments of the cyclic peptide Figure 7.2A in main text

m/z	charge	chemical formula	error	Assignment
129.10227	1	$C_6H_{12}N_2O_1H^+_1$	0.24	K
242.18630	1	$C_{12}H_{23}N_3O_2H^+_1$	-0.01	LK
300.17064	1	$C_{17}H_{21}N_3O_2H^+_1$	-0.04	WL
355.27035	1	$C_{18}H_{34}N_4O_3H^+_1$	-0.05	LKL
413.25470	1	$C_{23}H_{32}N_4O_3H^+_1$	-0.04	LWL
428.26561	1	$C_{23}H_{33}N_5O_3H^+_1$	-0.01	KLW
486.24997	1	$C_{28}H_{31}N_5O_3H^+_1$	0.01	WLW
541.34966	1	$C_{29}H_{44}N_6O_4H^+_1$	-0.04	LKLW
599.33400	1	$C_{34}H_{42}N_6O_4H^+_1$	-0.05	WLWL
654.43376	1	$C_{35}H_{55}N_7O_5H^+_1$	0.02	LKLWL
712.4181	1	$C_{40}H_{53}N_7O_5H^+_1$	0.01	LWLWL
727.42897	1	$C_{40}H_{54}N_8O_5H^+_1$	-0.03	KLWLW
785.41348	1	$C_{45}H_{52}N_8O_5H^+_1$	0.17	WLWLW
840.51292	1	$C_{46}H_{65}N_9O_6H^+_1$	-0.16	LKLWLW
898.49731	1	$C_{51}H_{63}N_9O_6H^+_1$	-0.11	LWLWLW
953.59678	1	$C_{52}H_{76}N_{10}O_7H^+_1$	-0.36	LKLWLWL
1011.58145	1	$C_{57}H_{74}N_{10}O_7H^+_1$	-0.02	LWLWLWL
1026.59187	1	$C_{57}H_{75}N_{11}O_7H^+_1$	-0.49	LWKWLWL
224.17574	1	$C_{12}H_{21}N_3O_1H^+_1$	0.01	LK-H_2O
282.16008	1	$C_{17}H_{19}N_3O_1H^+_1$	-0.03	WL-H_2O
337.25979	1	$C_{18}H_{32}N_4O_2H^+_1$	-0.04	LKL-H_2O
395.24415	1	$C_{23}H_{30}N_4O_2H^+_1$	-0.01	LWL-H_2O
410.25505	1	$C_{23}H_{31}N_5O_2H^+_1$	0.00	KLW-H_2O
468.23945	1	$C_{28}H_{29}N_5O_2H^+_1$	0.10	WLW-H_2O
523.33913	1	$C_{29}H_{42}N_6O_3H^+_1$	0.03	LKLW-H_2O
581.32349	1	$C_{34}H_{40}N_6O_3H^+_1$	0.04	WLWL-H_2O
636.42319	1	$C_{35}H_{53}N_7O_4H^+_1$	0.02	LKLWL-H_2O
694.40751	1	$C_{40}H_{51}N_7O_4H^+_1$	-0.03	LWLWL-H_2O
709.41828	1	$C_{40}H_{52}N_8O_4H^+_1$	-0.21	KLWLW-H_2O
767.40280	1	$C_{45}H_{50}N_8O_4H^+_1$	0.03	WLWLW-H_2O
822.50255	1	$C_{46}H_{63}N_9O_5H^+_1$	0.07	LKLWLW-H_2O
880.48678	1	$C_{51}H_{61}N_9O_5H^+_1$	-0.07	LWLWLW-H_2O
935.58663	1	$C_{52}H_{74}N_{10}O_6H^+_1$	0.08	LKLWLWL-H_2O
993.57041	1	$C_{57}H_{72}N_{10}O_6H^+_1$	-0.50	LWLWLWL-H_2O
197.16484	1	$C_{11}H_{20}N_2O_1H^+_1$	0.00	LK - CO-NH_3
210.12773	1	$C_{15}H_{15}N_1O_0H^+_1$	0.02	WL-$_2$(CO-NH_3)
255.14918	1	$C_{16}H_{18}N_2O_1H^+_1$	-0.04	WL-CO-NH_3
310.24890	1	$C_{17}H_{31}N_3O_2H^+_1$	-0.01	LKL-CO-NH_3
368.23324	1	$C_{22}H_{29}N_3O_2H^+_1$	-0.04	LWL-CO-NH_3
383.24417	1	$C_{22}H_{30}N_4O_2H^+_1$	0.05	KLW-CO-NH_3
441.22850	1	$C_{27}H_{28}N_4O_2H^+_1$	-0.01	WLW-CO-NH_3
496.32833	1	$C_{28}H_{41}N_5O_3H^+_1$	0.23	LKLW-NH_3-CO

554.3126	1	$C_{33}H_{39}N_5O_3H^+_1$	0.06	WLWL-CO-NH_3
667.39661	1	$C_{39}H_{50}N_6O_4H^+_1$	-0.03	LWLWL-CO-NH_3
682.40723	1	$C_{39}H_{51}N_7O_4H^+_1$	-0.44	KLWLW-CO-NH_3
740.39213	1	$C_{44}H_{49}N_7O_4H^+_1$	0.34	WLWLW-CO-NH_3
853.47559	1	$C_{50}H_{60}N_8O_5H^+_1$	-0.41	LWLWLW-CO-NH_3
908.57607	1	$C_{51}H_{73}N_9O_6H^+_1$	0.45	LKLWLWL-CO-NH_3
966.55988	1	$C_{56}H_{71}N_9O_6H^+_1$	-0.13	LWLWLWL-CO-NH_3
227.17540	1	$C_{12}H_{22}N_2O_2H^+_1$	-0.02	LL
272.17573	1	$C_{16}H_{21}N_3O_1H^+_1$	-0.03	KW-CO-NH
373.16589	1	$C_{22}H_{20}N_4O_2H^+_1$	-0.03	WW
596.33421	1	$C_{34}H_{41}N_7O_3H^+_1$	-0.26	WKLW-H_2O
614.34494	1	$C_{34}H_{43}N_7O_4H^+_1$	0.02	WKLW
570.34173	1	$C_{63}H_{86}N_{12}O_8H^+_2$	-0.22	Precursor
		Average	0.11	
		Standard deviation	0.17	

Table S 7.3: UVPD assignments of the cyclic peptide Figure 7.2B in main text

m/z	charge	chemical formula	error	Assignment
129.10235	1	$C_6H_{12}N_2O_1H^+_1$	0.86	K
187.08663	1	$C_{11}H_{10}N_2O_1H^+_1$	0.22	W
242.18630	1	$C_{12}H_{23}N_3O_2H^+_1$	-0.01	LK
300.17063	1	$C_{17}H_{21}N_3O_2H^+_1$	-0.08	WL
355.27033	1	$C_{18}H_{34}N_4O_3H^+_1$	-0.11	LKL
413.25468	1	$C_{23}H_{32}N_4O_3H^+_1$	-0.09	LWL
428.26561	1	$C_{23}H_{33}N_5O_3H^+_1$	-0.01	KLW
486.24996	1	$C_{28}H_{31}N_5O_3H^+_1$	-0.01	WLW
541.34969	1	$C_{29}H_{44}N_6O_4H^+_1$	0.02	LKLW
599.33403	1	$C_{34}H_{42}N_6O_4H^+_1$	0.00	WLWL
654.43381	1	$C_{35}H_{55}N_7O_5H^+_1$	0.10	LKLWL
712.41811	1	$C_{40}H_{53}N_7O_5H^+_1$	0.02	LWLWL
727.42911	1	$C_{40}H_{54}N_8O_5H^+_1$	0.16	KLWLW
785.41381	1	$C_{45}H_{52}N_8O_5H^+_1$	0.59	WLWLW
840.51297	1	$C_{46}H_{65}N_9O_6H^+_1$	-0.10	LKLWLW
898.49751	1	$C_{51}H_{63}N_9O_6H^+_1$	0.11	LWLWLW
953.59574	1	$C_{52}H_{76}N_{10}O_7H^+_1$	-1.45	LKLWLWL
1011.58146	1	$C_{57}H_{74}N_{10}O_7H^+_1$	-0.01	LWLWLWL
1026.59092	1	$C_{57}H_{75}N_{11}O_7H^+_1$	-1.41	WLWLWLK
169.07608	1	$C_{11}H_8N_2O_0H^+_1$	0.33	W-H_2O
224.17575	1	$C_{12}H_{21}N_3O_1H^+_1$	0.05	LK-H_2O
282.16006	1	$C_{17}H_{19}N_3O_1H^+_1$	-0.10	WL-H_2O
337.25974	1	$C_{18}H_{32}N_4O_2H^+_1$	-0.19	LKL-H_2O

395.24409	1	$C_{23}H_{30}N_4O_2H^+_1$	-0.16	LWL-H_2O
410.25504	1	$C_{23}H_{31}N_5O_2H^+_1$	-0.03	KLW-H_2O
468.23927	1	$C_{28}H_{29}N_5O_2H^+_1$	-0.28	WLW-H_2O
523.33918	1	$C_{29}H_{42}N_6O_3H^+_1$	0.12	LKLW-H_2O
581.32355	1	$C_{34}H_{40}N_6O_3H^+_1$	0.15	WLWL-H_2O
636.42314	1	$C_{35}H_{53}N_7O_4H^+_1$	-0.06	LKLWL-H_2O
694.40773	1	$C_{40}H_{51}N_7O_4H^+_1$	0.29	LWLWL-H_2O
709.41887	1	$C_{40}H_{52}N_8O_4H^+_1$	0.62	KLWLW-H_2O
767.40280	1	$C_{45}H_{50}N_8O_4H^+_1$	0.03	WLWLW-H_2O
822.50246	1	$C_{46}H_{63}N_9O_5H^+_1$	-0.04	LKLWLW-H_2O
880.48682	1	$C_{51}H_{61}N_9O_5H^+_1$	-0.03	LWLWLW-H_2O
993.57169	1	$C_{57}H_{72}N_{10}O_6H^+_1$	0.79	LWLWLWL-H_2O
159.09174	1	$C_{10}H_{10}N_2O_0H^+_1$	0.41	W-CO
197.16487	1	$C_{11}H_{20}N_2O_1H^+_1$	0.15	LK - CO-NH_3
210.12774	1	$C_{15}H_{15}N_1O_0H^+_1$	0.07	WL-2(CO-NH_3)
255.14919	1	$C_{16}H_{18}N_2O_1H^+_1$	0.00	WL-CO-NH_3
272.17572	1	$C_{16}H_{21}N_3O_1H^+_1$	-0.07	KW-CO-NH
310.24881	1	$C_{17}H_{31}N_3O_2H^+_1$	-0.30	LKL-NH_3-CO
368.23322	1	$C_{22}H_{29}N_3O_2H^+_1$	-0.09	LWL-CO-NH_3
383.24407	1	$C_{22}H_{30}N_4O_2H^+_1$	-0.22	KLW-CO-NH_3
441.22850	1	$C_{27}H_{28}N_4O_2H^+_1$	-0.01	WLW-CO-NH_3
496.32811	1	$C_{28}H_{41}N_5O_3H^+_1$	-0.21	LKLW-CO-NH_3
554.31258	1	$C_{33}H_{39}N_5O_3H^+_1$	0.02	WLWL-CO_NH_3
667.39649	1	$C_{39}H_{50}N_6O_4H^+_1$	-0.21	LWLWL-CO-NH_3
682.40740	1	$C_{39}H_{51}N_7O_4H^+_1$	-0.19	KLWLW-CO-NH_3
740.39192	1	$C_{44}H_{49}N_7O_4H^+_1$	0.05	WLWLW-CO-NH_3
795.49167	1	$C_{45}H_{62}N_8O_5H^+_1$	0.10	LKLWLW-CO-NH_3
966.55575	1	$C_{56}H_{71}N_9O_6H^+_1$	-4.40	LWLWLWL-CO-NH_3
227.17541	1	$C_{12}H_{22}N_2O_2H^+_1$	0.02	LL
373.16580	1	$C_{22}H_{20}N_4O_2H^+_1$	-0.27	WW
614.34505	1	$C_{34}H_{43}N_7O_4H^+_1$	0.20	WKLW
570.34142	2	$C_{63}H_{86}N_{12}O_8H^+_2$	-0.76	Precursor
		Average	0.30	
		Standard Deviation	0.70	

Table S 7.4: ECD assignments of the cyclic peptide Figure 7.2C in main text

m/z	**charge**	**chemical formula**	**error**	**Assignment**
899.50157	1	$C_{46}H_{64}N_{11}O_8H^+_1$	0.40	CRS-$C_{17}H_{22}N$
955.56391	1	$C_{50}H_{72}N_{11}O_8H^+_1$	0.10	CRS-$C_{13}H_{14}N$
968.57180	1	$C_{51}H_{73}N_{11}O_8H^+_1$	0.17	CRS-$C_{12}H_{13}N$
983.58595	1	$C_{56}H_{74}N_{10}O_6H^+_1$	-0.62	CRS-$C_7H_{12}N_2O_2$
1011.62657	1	$C_{54}H_{80}N_{11}O_8H^+_1$	0.16	CRS-C_9H_6N
1024.63460	1	$C_{55}H_{81}N_{11}O_8H^+_1$	0.36	CRS-C_8H_5N
1028.55891	1	$C_{55}H_{71}N_{12}O_8H^+_1$	-0.14	CRS-C_8H_{15}
1041.56701	1	$C_{56}H_{72}N_{12}O_8H^+_1$	0.12	CRS-C_7H_{14}
1067.59480	1	$C_{59}H_{76}N_{11}O_8H^+_1$	-0.29	CRS-$C_4H_{10}N$
1084.62207	1	$C_{59}H_{79}N_{12}O_8H^+_1$	0.38	CRS-c_4H_7
1097.62928	1	$C_{60}H_{80}N_{12}O_8H^+_1$	-0.19	CRS-C_3H_6
1122.67463	1	$C_{63}H_{85}N_{12}O_7H^+_1$	0.83	Precursor-OH
1139.67645	1	$C_{63}H_{86}N_{12}O_8H^+_1$	0.01	CRS
428.26561	1	$C_{23}H_{33}N_5O_3H^+_1$	-0.01	LWL b/c
541.34969	1	$C_{29}H_{44}N_6O_4H^+_1$	0.02	LLWL b/c
727.42897	1	$C_{40}H_{54}N_8O_5H^+_1$	-0.03	LLWLW b/c
840.51315	1	$C_{46}H_{65}N_9O_6H^+_1$	0.11	LWLLWL b/c
570.34154	2	$C_{63}H_{86}N_{12}O_8H^+_2$	-0.55	Precursor
		Average	0.25	
		Standard Deviation	0.33	

Table S 7.5: IRMPD assignments of the cyclic peptide-polymer conjugate Figure 7.3A in main text

m/z	charge	chemical formula	error	assignment
114.09137	1	$C_6H_{11}N_1O_1H^+_1$	0.26	L
129.10225	1	$C_6H_{12}N_2O_1H^+_1$	0.08	K
187.08662	1	$C_{11}H_{10}N_2O_1H^+_1$	0.16	W
242.18635	1	$C_{12}H_{23}N_3O_2H^+_1$	0.19	LK
300.17071	1	$C_{17}H_{21}N_3O_2H^+_1$	0.19	WL
355.27079	1	$C_{18}H_{34}N_4O_3H^+_1$	1.19	LKL
413.25476	1	$C_{23}H_{32}N_4O_3H^+_1$	0.10	LWL
428.26569	1	$C_{23}H_{33}N_5O_3H^+_1$	0.17	KLW
486.25008	1	$C_{28}H_{31}N_5O_3H^+_1$	0.23	WLW
541.34982	1	$C_{29}H_{44}N_6O_4H^+_1$	0.26	LKLW
599.33429	1	$C_{34}H_{42}N_6O_4H^+_1$	0.43	WLWL
654.43380	1	$C_{35}H_{55}N_7O_5H^+_1$	0.09	LKLWL
712.41823	1	$C_{40}H_{53}N_7O_5H^+_1$	0.19	LWLWL
727.42916	1	$C_{40}H_{54}N_8O_5H^+_1$	0.23	KLWLW
785.41313	1	$C_{45}H_{52}N_8O_5H^+_1$	-0.27	WLWLW
840.51333	1	$C_{46}H_{65}N_9O_6H^+_1$	0.32	WLKLWL
898.49723	1	$C_{51}H_{63}N_9O_6H^+_1$	-0.20	LWLWLW
953.59760	1	$C_{52}H_{76}N_{10}O_7H^+_1$	0.50	LKLWLWL
1011.58238	1	$C_{57}H_{74}N_{10}O_7H^+_1$	0.90	LWLWLWL
1026.59305	1	$C_{57}H_{75}N_{11}O_7H^+_1$	0.66	WLKLWLW
1139.6768	1	$C_{63}H_{86}N_{12}O_8H^+_1$	0.32	cypep
159.09169	1	$C_{10}H_{10}N_2O_0H^+_1$	0.10	W-CO
667.39666	1	$C_{39}H_{50}N_6O_4H^+_1$	0.04	LWLWL-CO-NH_3
740.39257	1	$C_{44}H_{49}N_7O_4H^+_1$	0.93	WLWLW-CO-NH_3
822.50254	1	$C_{46}H_{63}N_9O_5H^+_1$	0.06	LKLWLW-H_2O
853.47564	1	$C_{50}H_{60}N_8O_5H^+_1$	-0.36	LWLWLW-CO-NH_3
880.48694	1	$C_{51}H_{61}N_9O_5H^+_1$	0.11	LWLWLW-H_2O
100.07572	1	$C_5H_9N_1O_1H^+_1$	0.30	Internal
199.14409	1	$C_{10}H_{18}N_2O_2H^+_1$	-0.07	Internal
298.21256	1	$C_{15}H_{27}N_3O_3H^+_1$	0.14	Internal
397.28100	1	$C_{20}H_{36}N_4O_4H^+_1$	0.17	Internal
496.34944	1	$C_{25}H_{45}N_5O_5H^+_1$	0.19	Internal
595.41784	1	$C_{30}H_{54}N_6O_6H^+_1$	0.13	Internal
694.48630	1	$C_{35}H_{63}N_7O_7H^+_1$	0.18	Internal
793.55471	1	$C_{40}H_{72}N_8O_8H^+_1$	0.15	Internal
892.62325	1	$C_{45}H_{81}N_9O_9H^+_1$	0.28	Internal
991.69156	1	$C_{50}H_{90}N_{10}O_{10}H^+_1$	0.15	Internal
1090.76010	1	$C_{55}H_{99}N_{11}O_{11}H^+_1$	0.25	Internal
1189.82837	1	$C_{60}H_{108}N_{12}O_{12}H^+_1$	0.11	Internal
1288.89621	1	$C_{65}H_{117}N_{13}O_{13}H^+_1$	-0.35	Internal
1387.96509	1	$C_{70}H_{126}N_{14}O_{14}H^+_1$	0.01	Internal
1487.03249	1	$C_{75}H_{135}N_{15}O_{15}H^+_1$	-0.67	Internal

1586.1007	1	$C_{80}H_{144}N_{16}O_{16}H^{+}_{1}$	-0.76	Internal
1685.16979	1	$C_{85}H_{153}N_{17}O_{17}H^{+}_{1}$	-0.31	Internal
1784.23723	1	$C_{90}H_{162}N_{18}O_{18}H^{+}_{1}$	-0.84	Internal
1883.30660	1	$C_{95}H_{171}N_{19}O_{19}H^{+}_{1}$	-0.29	Internal
1982.37387	1	$C_{100}H_{180}N_{20}O_{20}H^{+}_{1}$	-0.85	Internal
2081.44084	1	$C_{105}H_{189}N_{21}O_{21}H^{+}_{1}$	-1.50	Internal
2180.51309	1	$C_{110}H_{198}N_{22}O_{22}H^{+}_{1}$	0.32	Internal
2279.58221	1	$C_{115}H_{207}N_{23}O_{23}H^{+}_{1}$	0.62	Internal
2378.64738	1	$C_{120}H_{216}N_{24}O_{24}H^{+}_{1}$	-0.77	Internal
2477.71743	1	$C_{125}H_{225}N_{25}O_{25}H^{+}_{1}$	-0.08	Internal
162.61777	2	$C_{17}H_{29}N_{3}O_{3}H^{+}_{2}$	0.29	Internal
212.15195	2	$C_{22}H_{38}N_{4}O_{4}H^{+}_{2}$	0.10	Internal
261.68618	2	$C_{27}H_{47}N_{5}O_{5}H^{+}_{2}$	0.17	Internal
311.22042	2	$C_{32}H_{56}N_{6}O_{6}H^{+}_{2}$	0.25	Internal
360.75463	2	$C_{37}H_{65}N_{7}O_{7}H^{+}_{2}$	0.22	Internal
410.28883	2	$C_{42}H_{74}N_{8}O_{8}H^{+}_{2}$	0.18	Internal
459.82302	2	$C_{47}H_{83}N_{9}O_{9}H^{+}_{2}$	0.12	Internal
509.35725	2	$C_{52}H_{92}N_{10}O_{10}H^{+}_{2}$	0.15	Internal
558.89145	2	$C_{57}H_{101}N_{11}O_{11}H^{+}_{2}$	0.13	Internal
608.42566	2	$C_{62}H_{110}N_{12}O_{12}H^{+}_{2}$	0.12	Internal
657.95993	2	$C_{67}H_{119}N_{13}O_{13}H^{+}_{2}$	0.21	Internal
707.49401	2	$C_{72}H_{128}N_{14}O_{14}H^{+}_{2}$	0.14	Internal
757.02835	2	$C_{77}H_{137}N_{15}O_{15}H^{+}_{2}$	0.19	Internal
806.56235	2	$C_{82}H_{146}N_{16}O_{16}H^{+}_{2}$	-0.08	Internal
856.09668	2	$C_{87}H_{155}N_{17}O_{17}H^{+}_{2}$	0.07	Internal
		Precursor	0.31	
		Standard deviation	0.41	

Table S 7.6: ECD assignments of the cyclic peptide-polymer conjugate Figure 7.3B in main text

m/z	charge	chemical formula	error	assignment
217.15467	1	C10H20N2O3H+1	0.00	a_2
316.22305	1	C15H29N3O4H+1	-0.10	a_3
415.29142	1	C20H38N4O5H+1	-0.18	a_4
514.35985	1	C25H47N5O6H+1	-0.12	a_5
613.42834	1	C30H56N6O7H+1	0.03	a_6
712.49665	1	C35H65N7O8H+1	-0.12	a_7
811.56518	1	C40H74N8O9H+1	0.03	a_8
910.63372	1	C45H83N9O10H+1	0.17	a_9
1009.70221	1	C50H92N10O11H+1	0.23	a_{10}
1108.77042	1	C55H101N11O12H+1	0.02	a_{11}
1207.83952	1	C60H110N12O13H+1	0.59	a_{12}
1306.90778	1	C65H119N13O14H+1	0.43	a_{13}
1405.97637	1	C70H128N14O15H+1	0.52	a_{14}
1505.04344	1	C75H137N15O16H+1	-0.41	a_{15}
1604.11303	1	C80H146N16O17H+1	0.35	a_{16}
1703.18068	1	C85H155N17O18H+1	-0.12	a_{17}
1802.24818	1	C90H164N18O19H+1	-0.62	a_{18}
1901.31778	1	C95H173N19O20H+1	0.04	a_{19}
2000.38413	1	C100H182N20O21H+1	-0.99	a_{20}
2099.45424	1	C105H191N21O22H+1	-0.14	a_{21}
2198.51471	1	C110H200N22O23H+1	-3.75	a_{22}
2297.59648	1	C115H209N23O24H+1	2.23	a_{23}
2396.65113	1	C120H218N24O25H+1	-3.61	a_{24}
1072.67326	2	C113H174N22O19H+2	-0.28	z_9
1122.20684	2	C118H183N23O20H+2	-0.82	z_{10}
1171.74088	2	C123H192N24O21H+2	-0.93	z_{11}
1221.27591	2	C128H201N25O22H+2	-0.22	z_{12}
1270.80890	2	C133H210N26O23H+2	-1.17	z_{13}
1320.34401	2	C138H219N27O24H+2	-0.44	z_{14}
1369.87803	2	C143H228N28O25H+2	-0.56	z_{15}
1419.41092	2	C148H237N29O26H+2	-1.47	z_{16}
1468.94627	2	C153H246N30O27H+2	-0.64	z_{17}
1518.47992	2	C158H255N31O28H+2	-0.99	z_{18}
1617.54842	2	C168H273N33O30H+2	-0.87	z_{20}
1667.08212	2	C173H282N34O31H+2	-1.15	z_{21}
1716.61699	2	C178H291N35O32H+2	-0.73	z_{22}
1766.15243	2	C183H300N36O33H+2	-0.01	z_{23}
1815.68703	2	C188H309N37O34H+2	0.20	z_{24}
1865.21740	2	C193H318N38O35H+2	-1.86	z_{25}
1914.74772	2	C198H327N39O36H+2	-3.84	z_{26}
1964.28914	2	C203H336N40O37H+2	-0.07	z_{27}
2013.81841	2	C208H345N41O38H+2	-2.52	z_{28}
1351.79130	1	C73H102N14O11H+1	-0.91	z_2

1450.86469	1	C78H111N15O12H+1	2.58	z_3
1648.99588	1	C88H129N17O14H+1	-1.15	z_5
1946.20106	1	C103H156N20O17H+1	-1.00	z_7
2045.27384	1	C108H165N21O18H+1	1.18	z_8
2144.33867	1	C113H174N22O19H+1	-0.54	z_9
2342.47733	1	C123H192N24O21H+1	0.28	z_{11}
653.95716	2	C65H119N13O14H+2	-0.14	a_{13}
703.49161	2	C70H128N14O15H+2	0.22	a_{14}
753.02567	2	C75H137N15O16H+2	0.01	a_{15}
802.55992	2	C80H146N16O17H+2	0.06	a_{16}
852.09448	2	C85H155N17O18H+2	0.47	a_{17}
901.62841	2	C90H164N18O19H+2	0.14	a_{18}
951.16277	2	C95H173N19O20H+2	0.29	a_{19}
1000.69679	2	C100H182N20O21H+2	0.09	a_{20}
1050.23099	2	C105H191N21O22H+2	0.08	a_{21}
1099.76537	2	C110H200N22O23H+2	0.23	a_{22}
1149.29948	2	C115H209N23O24H+2	0.14	a_{23}
1198.83355	2	C120H218N24O25H+2	0.02	a_{24}
1297.90100	2	C130H236N26O27H+2	-0.72	a_{26}
1347.43518	2	C135H245N27O28H+2	-0.72	a_{27}
1396.96947	2	C140H254N28O29H+2	-0.63	a_{28}
1446.50402	2	C145H263N29O30H+2	-0.37	a_{29}
1496.03889	2	C150H272N30O31H+2	0.08	a_{30}
1545.57296	2	C155H281N31O32H+2	-0.01	a_{31}
1595.10537	2	C160H290N32O33H+2	-1.14	a_{32}
1644.64191	2	C165H299N33O34H+2	0.32	a_{33}
1694.17383	2	C170H308N34O35H+2	-1.04	a_{34}
1743.70726	2	C175H317N35O36H+2	-1.46	a_{35}
1793.24110	2	C180H326N36O37H+2	-1.62	a_{36}
1842.77537	2	C185H335N37O38H+2	-1.54	a_{37}
1892.31328	2	C190H344N38O39H+2	0.45	a_{38}
1941.84610	2	C195H353N39O40H+2	-0.27	a_{39}
2040.91835	2	C205H371N41O42H+2	1.62	a_{41}
2090.44512	2	C210H380N42O43H+2	-1.98	a_{42}
2139.98718	2	C215H389N43O44H+2	1.74	a_{43}
2189.51765	2	C220H398N44O45H+2	-0.01	a_{44}
2288.58794	2	C230H416N46O47H+2	0.81	a_{46}
2338.12616	2	C235H425N47O48H+2	2.51	a_{47}
201.15976	1	C10H20N2O2H+1	0.03	Internal
300.22805	1	C15H29N3O3H+1	-0.39	Internal
399.29651	1	C20H38N4O4H+1	-0.18	Internal
498.36491	1	C25H47N5O5H+1	-0.17	Internal
597.43339	1	C30H56N6O6H+1	-0.03	Internal
696.50167	1	C35H65N7O7H+1	-0.22	Internal
795.57018	1	C40H74N8O8H+1	-0.07	Internal
894.63869	1	C45H83N9O9H+1	0.04	Internal

993.70710	1	C50H92N10O10H+1	0.03	Internal
1092.77594	1	C55H101N11O11H+1	0.42	Internal
1389.98154	1	C70H128N14O14H+1	0.59	Internal
1489.04637	1	C75H137N15O15H+1	-1.86	Internal
1588.11559	1	C80H146N16O16H+1	-1.23	Internal
272.19683	1	C13H25N3O3H+1	-0.14	Internal
371.26531	1	C18H34N4O4H+1	0.08	Internal
470.33361	1	C23H43N5O5H+1	-0.18	Internal
569.40200	1	C28H52N6O6H+1	-0.19	Internal
668.47055	1	C33H61N7O7H+1	0.04	Internal
767.53890	1	C38H70N8O8H+1	-0.05	Internal
866.60699	1	C43H79N9O9H+1	-0.42	Internal
965.67582	1	C48H88N10O10H+1	0.06	Internal
1064.74425	1	C53H97N11O11H+1	0.07	Internal
1163.81228	1	C58H106N12O12H+1	-0.27	Internal
1262.88108	1	C63H115N13O13H+1	0.06	Internal
1361.94886	1	C68H124N14O14H+1	-0.41	Internal
1461.01589	1	C73H133N15O15H+1	-1.33	Internal

Table S 7.7: UVPD assignments of the cyclic peptide-polymer conjugate Figure 7.4 in main text

m/z	charge	Chemical formula	error	assignment
114.09140	1	$C_6H_{11}N_1O_1H^+_1$	0.52	L
129.10230	1	$C_6H_{12}N_2O_1H^+_1$	0.47	K
242.18633	1	$C_{12}H_{23}N_3O_2H^+_1$	0.11	LK
300.17070	1	$C_{17}H_{21}N_3O_2H^+_1$	0.16	WL
355.27031	1	$C_{18}H_{34}N_4O_3H^+_1$	-0.16	LKL
413.25472	1	$C_{23}H_{32}N_4O_3H^+_1$	0.01	LWL
428.26574	1	$C_{23}H_{33}N_5O_3H^+_1$	0.29	KLW
486.25007	1	$C_{28}H_{31}N_5O_3H^+_1$	0.21	WLW
541.34968	1	$C_{29}H_{44}N_6O_4H^+_1$	0.00	LKLW
599.33417	1	$C_{34}H_{42}N_6O_4H^+_1$	0.23	WLWL
654.43386	1	$C_{35}H_{55}N_7O_5H^+_1$	0.18	LKLWL
712.41849	1	$C_{40}H_{53}N_7O_5H^+_1$	0.56	LWLWL
727.42984	1	$C_{40}H_{54}N_8O_5H^+_1$	1.16	WLKLW
785.41366	1	$C_{45}H_{52}N_8O_5H^+_1$	0.40	WLWLW
840.51319	1	$C_{46}H_{65}N_9O_6H^+_1$	0.16	WLKLWL
898.49799	1	$C_{51}H_{63}N_9O_6H^+_1$	0.65	WLWLWL
953.59757	1	$C_{52}H_{76}N_{10}O_7H^+_1$	0.47	LWLKLWL
1011.58252	1	$C_{57}H_{74}N_{10}O_7H^+_1$	1.04	LWLWLWL
1026.59239	1	$C_{57}H_{75}N_{11}O_7H^+_1$	0.02	WLKLWLW
1139.67718	1	$C_{63}H_{86}N_{12}O_8H^+_1$	0.65	Cycpep
337.25974	1	$C_{18}H_{32}N_4O_2H^+_1$	-0.19	LKL-H_2O
523.33895	1	$C_{29}H_{42}N_6O_3H^+_1$	-0.32	LKLW-H_2O
255.14918	1	$C_{16}H_{18}N_2O_1H^+_1$	-0.04	WL-CO-NH_3
554.31271	1	$C_{33}H_{39}N_5O_3H^+_1$	0.26	WLWL-CO-NH_3
217.15469	1	$C_{10}H_{20}N_2O_3H^+_1$	0.10	a_2
316.22314	1	$C_{15}H_{29}N_3O_4H^+_1$	0.18	a_3
415.29153	1	$C_{20}H_{38}N_4O_5H^+_1$	0.08	a_8
514.36005	1	$C_{25}H_{47}N_5O_6H^+_1$	0.27	a_5
613.42848	1	$C_{30}H_{56}N_6O_7H^+_1$	0.25	a_6
712.49694	1	$C_{35}H_{65}N_7O_8H^+_1$	0.28	a_7
811.56528	1	$C_{40}H_{74}N_8O_9H^+_1$	0.16	a_8
910.63377	1	$C_{45}H_{83}N_9O_{10}H^+_1$	0.22	a_9
1009.70225	1	$C_{50}H_{92}N_{10}O_{11}H^+_1$	0.27	a_{10}
1108.77104	1	$C_{55}H_{101}N_{11}O_{12}H^+_1$	0.58	a_{11}
1207.83993	1	$C_{60}H_{110}N_{12}O_{13}H^+_1$	0.93	a_{12}
1306.90838	1	$C_{65}H_{119}N_{13}O_{14}H^+_1$	0.89	a_{13}
1405.97682	1	$C_{70}H_{128}N_{14}O_{15}H^+_1$	0.84	a_{14}
1505.04381	1	$C_{75}H_{137}N_{15}O_{16}H^+_1$	-0.16	a_{15}
1604.11281	1	$C_{80}H_{146}N_{16}O_{17}H^+_1$	0.22	a_{16}
1703.17823	1	$C_{85}H_{155}N_{17}O_{18}H^+_1$	-1.55	a_{17}
406.28623	2	$C_{40}H_{74}N_8O_9H^+_2$	0.04	a_4
455.82042	2	$C_{45}H_{83}N_9O_{10}H^+_2$	0.00	a_5

505.35468	2	$C_{50}H_{92}N_{10}O_{11}H^{+}_{2}$	0.10	a_6
554.88890	2	$C_{55}H_{101}N_{11}O_{12}H^{+}_{2}$	0.12	a_7
604.42316	2	$C_{60}H_{110}N_{12}O_{13}H^{+}_{2}$	0.19	a_8
653.95746	2	$C_{65}H_{119}N_{13}O_{14}H^{+}_{2}$	0.32	a_9
703.49178	2	$C_{70}H_{128}N_{14}O_{15}H^{+}_{2}$	0.46	a_{14}
753.02594	2	$C_{75}H_{137}N_{15}O_{16}H^{+}_{2}$	0.37	a_{15}
802.56020	2	$C_{80}H_{146}N_{16}O_{17}H^{+}_{2}$	0.41	a_{16}
852.09452	2	$C_{85}H_{155}N_{17}O_{18}H^{+}_{2}$	0.52	a_{17}
901.62860	2	$C_{90}H_{164}N_{18}O_{19}H^{+}_{2}$	0.35	a_{18}
951.16302	2	$C_{95}H_{173}N_{19}O_{20}H^{+}_{2}$	0.56	a_{19}
1000.69726	2	$C_{100}H_{182}N_{20}O_{21}H^{+}_{2}$	0.56	a_{20}
1050.23124	2	$C_{105}H_{191}N_{21}O_{22}H^{+}_{2}$	0.32	a_{21}
1099.76592	2	$C_{110}H_{200}N_{22}O_{23}H^{+}_{2}$	0.73	a_{22}
1149.29990	2	$C_{115}H_{209}N_{23}O_{24}H^{+}_{2}$	0.51	a_{23}
1198.83358	2	$C_{120}H_{218}N_{24}O_{25}H^{+}_{2}$	0.05	a_{24}
1297.90129	2	$C_{130}H_{236}N_{26}O_{27}H^{+}_{2}$	-0.50	a_{26}
1347.43543	2	$C_{135}H_{245}N_{27}O_{28}H^{+}_{2}$	-0.53	a_{27}
1396.96982	2	$C_{140}H_{254}N_{28}O_{29}H^{+}_{2}$	-0.38	a_{28}
1446.50538	2	$C_{145}H_{263}N_{29}O_{30}H^{+}_{2}$	0.57	a_{29}
1496.04154	2	$C_{150}H_{272}N_{30}O_{31}H^{+}_{2}$	1.85	a_{30}
1545.57474	2	$C_{155}H_{281}N_{31}O_{32}H^{+}_{2}$	1.14	a_{31}
1595.10638	2	$C_{160}H_{290}N_{32}O_{33}H^{+}_{2}$	-0.50	a_{32}
667.46724	3	$C_{100}H_{182}N_{20}O_{21}H^{+}_{3}$	0.52	a_{20}
700.48976	3	$C_{105}H_{191}N_{21}O_{22}H^{+}_{3}$	0.09	a_{21}
766.53573	3	$C_{115}H_{209}N_{23}O_{24}H^{+}_{3}$	0.55	a_{23}
799.55837	3	$C_{120}H_{218}N_{24}O_{25}H^{+}_{3}$	0.33	a_{24}
832.58119	3	$C_{125}H_{227}N_{25}O_{26}H^{+}_{3}$	0.33	a_{25}
898.62633	3	$C_{135}H_{245}N_{27}O_{28}H^{+}_{3}$	-0.22	a_{27}
931.64939	3	$C_{140}H_{254}N_{28}O_{29}H^{+}_{3}$	0.07	a_{28}
997.69468	3	$C_{150}H_{272}N_{30}O_{31}H^{+}_{3}$	-0.26	a_{30}
1030.71759	3	$C_{155}H_{281}N_{31}O_{32}H^{+}_{3}$	-0.15	a_{31}
1096.76311	3	$C_{165}H_{299}N_{33}O_{34}H^{+}_{3}$	-0.22	a_{33}
1129.78621	3	$C_{170}H_{308}N_{34}O_{35}H^{+}_{3}$	0.05	a_{34}
1195.83175	3	$C_{180}H_{326}N_{36}O_{37}H^{+}_{3}$	-0.01	a_{36}
1228.85518	3	$C_{185}H_{335}N_{37}O_{38}H^{+}_{3}$	0.50	a_{37}
1294.90104	3	$C_{195}H_{353}N_{39}O_{40}H^{+}_{3}$	0.66	a_{39}
1327.92278	3	$C_{200}H_{362}N_{40}O_{41}H^{+}_{3}$	-0.15	a_{40}
1393.96908	3	$C_{210}H_{380}N_{42}O_{43}H^{+}_{3}$	0.35	a_{42}
1426.99163	3	$C_{215}H_{389}N_{43}O_{44}H^{+}_{3}$	0.16	a_{43}
1493.03901	3	$C_{225}H_{407}N_{45}O_{46}H^{+}_{3}$	1.34	a_{45}
996.19392	4	$C_{200}H_{362}N_{40}O_{41}H^{+}_{4}$	-0.14	a_{40}
1070.49587	4	$C_{215}H_{389}N_{43}O_{44}H^{+}_{4}$	0.47	a_{43}
1095.26172	4	$C_{220}H_{398}N_{44}O_{45}H^{+}_{4}$	-0.69	a_{44}
1144.79683	4	$C_{230}H_{416}N_{46}O_{47}H^{+}_{4}$	0.13	a_{46}
1169.56357	4	$C_{235}H_{425}N_{47}O_{48}H^{+}_{4}$	-0.18	a_{47}
1194.33003	4	$C_{240}H_{434}N_{48}O_{49}H^{+}_{4}$	-0.72	a_{48}

1268.63269	4	$C_{255}H_{461}N_{51}O_{52}H^{+}_{4}$	0.39	a_{51}
1568.01618	2	$C_{163}H_{264}N_{32}O_{29}H^{+}_{2}$	0.35	x_{20}
1617.54784	2	$C_{168}H_{273}N_{33}O_{30}H^{+}_{2}$	-1.23	x_{21}
1667.08334	2	$C_{173}H_{282}N_{34}O_{31}H^{+}_{2}$	-0.42	x_{22}
1716.61913	2	$C_{178}H_{291}N_{35}O_{32}H^{+}_{2}$	0.51	x_{23}
1766.15317	2	$C_{183}H_{300}N_{36}O_{33}H^{+}_{2}$	0.41	x_{24}
1815.68781	2	$C_{188}H_{309}N_{37}O_{34}H^{+}_{2}$	0.63	x_{25}
1865.21794	2	$C_{193}H_{318}N_{38}O_{35}H^{+}_{2}$	-1.57	x_{26}
1914.75104	2	$C_{198}H_{327}N_{39}O_{36}H^{+}_{2}$	-2.11	x_{27}
1964.29052	2	$C_{203}H_{336}N_{40}O_{37}H^{+}_{2}$	0.63	x_{28}
2013.82005	2	$C_{208}H_{345}N_{41}O_{38}H^{+}_{2}$	-1.71	x_{29}
2063.35857	2	$C_{213}H_{354}N_{42}O_{39}H^{+}_{2}$	0.42	x_{30}
1276.83800	3	$C_{198}H_{327}N_{39}O_{36}H^{+}_{3}$	-0.89	x_{27}
1309.86268	3	$C_{203}H_{336}N_{40}O_{37}H^{+}_{3}$	0.56	x_{28}
1342.88351	3	$C_{208}H_{345}N_{41}O_{38}H^{+}_{3}$	-0.92	x_{29}
1375.90715	3	$C_{213}H_{354}N_{42}O_{39}H^{+}_{3}$	-0.30	x_{30}
1408.93121	3	$C_{218}H_{363}N_{43}O_{40}H^{+}_{3}$	0.60	z_{31}
1474.97611	3	$C_{228}H_{381}N_{45}O_{42}H^{+}_{3}$	0.09	x_{33}
1507.99728	3	$C_{233}H_{390}N_{46}O_{43}H^{+}_{3}$	-0.99	x_{34}
1541.02115	3	$C_{238}H_{399}N_{47}O_{44}H^{+}_{3}$	-0.28	x_{35}
1574.04528	3	$C_{243}H_{408}N_{48}O_{45}H^{+}_{3}$	0.57	x_{36}
1607.06807	3	$C_{248}H_{417}N_{49}O_{46}H^{+}_{3}$	0.55	x_{37}
1640.09151	3	$C_{253}H_{426}N_{50}O_{47}H^{+}_{3}$	0.92	x_{38}
1673.11219	3	$C_{258}H_{435}N_{51}O_{48}H^{+}_{3}$	-0.36	x_{39}
1706.13262	3	$C_{263}H_{444}N_{52}O_{49}H^{+}_{3}$	-1.75	x_{40}
1739.15654	3	$C_{268}H_{453}N_{53}O_{50}H^{+}_{3}$	-1.07	x_{41}
1772.18462	3	$C_{273}H_{462}N_{54}O_{51}H^{+}_{3}$	1.92	x_{42}
1180.78699	4	$C_{243}H_{408}N_{48}O_{45}H^{+}_{4}$	1.59	x_{36}
1205.55168	4	$C_{248}H_{417}N_{49}O_{46}H^{+}_{4}$	-0.44	x_{37}
1279.85335	4	$C_{263}H_{444}N_{52}O_{49}H^{+}_{4}$	-0.13	x_{40}
1304.6199	4	$C_{268}H_{453}N_{53}O_{50}H^{+}_{4}$	-0.56	x_{41}
1329.38647	4	$C_{273}H_{462}N_{54}O_{51}H^{+}_{4}$	-0.95	x_{42}
1354.15504	4	$C_{278}H_{471}N_{55}O_{52}H^{+}_{4}$	0.15	x_{43}
1378.92063	4	$C_{283}H_{480}N_{56}O_{53}H^{+}_{4}$	-0.95	x_{44}
1403.68773	4	$C_{288}H_{489}N_{57}O_{54}H^{+}_{4}$	-0.93	x_{45}
1428.45650	4	$C_{293}H_{498}N_{58}O_{55}H^{+}_{4}$	0.25	x_{46}
1453.22314	4	$C_{298}H_{507}N_{59}O_{56}H^{+}_{4}$	-0.07	x_{47}
1477.98927	4	$C_{303}H_{516}N_{60}O_{57}H^{+}_{4}$	-0.73	x_{48}
1296.86575	4	$C_{267}H_{450}N_{53}O_{49}H^{+}_{4}$	-0.21	x_{41}
1321.63303	4	$C_{272}H_{459}N_{54}O_{50}H^{+}_{4}$	-0.08	x_{42}
1346.39880	4	$C_{277}H_{468}N_{55}O_{51}H^{+}_{4}$	-1.07	x_{43}
1371.16639	4	$C_{282}H_{477}N_{56}O_{52}H^{+}_{4}$	-0.69	x_{44}
1395.93267	4	$C_{287}H_{486}N_{57}O_{53}H^{+}_{4}$	-1.27	x_{45}
1420.69899	4	$C_{292}H_{495}N_{58}O_{54}H^{+}_{4}$	-1.80	x_{46}
1445.46608	4	$C_{297}H_{504}N_{59}O_{55}H^{+}_{4}$	-1.78	x_{47}
1470.23540	4	$C_{302}H_{513}N_{60}O_{56}H^{+}_{4}$	-0.24	x_{48}

1495.00257	4	$C_{307}H_{522}N_{61}O_{57}H^{+}_{4}$	-0.19	x_{49}
1169.77826	4	$C_{241}H_{404}N_{48}O_{44}H^{+}_{4}$	-0.25	x_{36}
1194.54551	4	$C_{246}H_{413}N_{49}O_{45}H^{+}_{4}$	-0.12	x_{37}
1219.31361	4	$C_{251}H_{422}N_{50}O_{46}H^{+}_{4}$	0.70	x_{38}
1268.84649	4	$C_{261}H_{440}N_{52}O_{48}H^{+}_{4}$	-0.38	x_{40}
1293.61410	4	$C_{266}H_{449}N_{53}O_{49}H^{+}_{4}$	0.02	x_{41}
1318.37891	4	$C_{271}H_{458}N_{54}O_{50}H^{+}_{4}$	-1.72	x_{42}
1343.14784	4	$C_{276}H_{467}N_{55}O_{51}H^{+}_{4}$	-0.33	x_{43}
1367.91389	4	$C_{281}H_{476}N_{56}O_{52}H^{+}_{4}$	-1.09	x_{44}
1392.68249	4	$C_{286}H_{485}N_{57}O_{53}H^{+}_{4}$	0.00	x_{45}
1417.44780	4	$C_{291}H_{494}N_{58}O_{54}H^{+}_{4}$	-1.26	x_{46}
1442.21072	4	$C_{296}H_{503}N_{59}O_{55}H^{+}_{4}$	-4.14	x_{47}
1466.98268	4	$C_{301}H_{512}N_{60}O_{56}H^{+}_{4}$	-0.76	x_{48}
341.25478	1	$C_{17}H_{32}N_{4}O_{3}H^{+}_{1}$	0.18	Internal
440.32322	1	$C_{22}H_{41}N_{5}O_{4}H^{+}_{1}$	0.20	Internal
539.39163	1	$C_{27}H_{50}N_{6}O_{5}H^{+}_{1}$	0.16	Internal
638.46009	1	$C_{32}H_{59}N_{7}O_{6}H^{+}_{1}$	0.21	Internal
836.59728	1	$C_{42}H_{77}N_{9}O_{8}H^{+}_{1}$	0.59	Internal
1034.73461	1	$C_{52}H_{95}N_{11}O_{10}H^{+}_{1}$	0.96	Internal
1133.80397	1	$C_{57}H_{104}N_{12}O_{11}H^{+}_{1}$	1.71	Internal
1232.87379	1	$C_{62}H_{113}N_{13}O_{12}H^{+}_{1}$	2.72	Internal
1629.14437	1	$C_{82}H_{149}N_{17}O_{16}H^{+}_{1}$	0.17	Internal
1728.21554	1	$C_{87}H_{158}N_{18}O_{17}H^{+}_{1}$	1.75	Internal
1827.28322	1	$C_{92}H_{167}N_{19}O_{18}H^{+}_{1}$	1.26	Internal
1926.35247	1	$C_{97}H_{176}N_{20}O_{19}H^{+}_{1}$	1.62	Internal
2025.41443	1	$C_{102}H_{185}N_{21}O_{20}H^{+}_{1}$	-1.64	Internal
199.14414	1	$C_{10}H_{18}N_{2}O_{2}H^{+}_{1}$	0.18	is2
298.21252	1	$C_{15}H_{27}N_{3}O_{3}H^{+}_{1}$	0.01	is3
397.28100	1	$C_{20}H_{36}N_{4}O_{4}H^{+}_{1}$	0.17	is4
496.34941	1	$C_{25}H_{45}N_{5}O_{5}H^{+}_{1}$	0.13	is5
595.41788	1	$C_{30}H_{54}N_{6}O_{6}H^{+}_{1}$	0.20	is6
892.62343	1	$C_{45}H_{81}N_{9}O_{9}H^{+}_{1}$	0.48	is9
1090.76060	1	$C_{55}H_{99}N_{11}O_{11}H^{+}_{1}$	0.71	is11
1387.96586	1	$C_{70}H_{126}N_{14}O_{14}H^{+}_{1}$	0.57	is14
1487.03271	1	$C_{75}H_{135}N_{15}O_{15}H^{+}_{1}$	-0.52	is15
1586.10216	1	$C_{80}H_{144}N_{16}O_{16}H^{+}_{1}$	0.16	is16
1982.37456	1	$C_{100}H_{180}N_{20}O_{20}H^{+}_{1}$	-0.50	is20
2081.44294	1	$C_{105}H_{189}N_{21}O_{21}H^{+}_{1}$	-0.49	is21
2180.51554	1	$C_{110}H_{198}N_{22}O_{22}H^{+}_{1}$	1.45	is22
2378.64907	1	$C_{120}H_{216}N_{24}O_{24}H^{+}_{1}$	-0.06	is24
2477.72073	1	$C_{125}H_{225}N_{25}O_{25}H^{+}_{1}$	1.25	is25
324.22818	1	$C_{17}H_{29}N_{3}O_{3}H^{+}_{1}$	0.04	Internal2
423.29666	1	$C_{22}H_{38}N_{4}O_{4}H^{+}_{1}$	0.18	Internal2
522.36515	1	$C_{27}H_{47}N_{5}O_{5}H^{+}_{1}$	0.29	Internal2
621.43360	1	$C_{32}H_{56}N_{6}O_{6}H^{+}_{1}$	0.31	Internal2
212.15200	2	$C_{22}H_{38}N_{4}O_{4}H^{+}_{2}$	0.33	Internal2

261.68619	2	$C_{27}H_{47}N_5O_5H^+_2$	0.21	Internal2
360.75464	2	$C_{37}H_{65}N_7O_7H^+_2$	0.25	Internal2
410.28887	2	$C_{42}H_{74}N_8O_8H^+_2$	0.28	Internal2
459.82306	2	$C_{47}H_{83}N_9O_9H^+_2$	0.21	Internal2
509.35726	2	$C_{52}H_{92}N_{10}O_{10}H^+_2$	0.17	Internal2
558.89154	2	$C_{57}H_{101}N_{11}O_{11}H^+_2$	0.29	Internal2
608.42572	2	$C_{62}H_{110}N_{12}O_{12}H^+_2$	0.22	Internal2
657.95995	2	$C_{67}H_{119}N_{13}O_{13}H^+_2$	0.24	Internal2
707.49425	2	$C_{72}H_{128}N_{14}O_{14}H^+_2$	0.35	Internal2
757.02847	2	$C_{77}H_{137}N_{15}O_{15}H^+_2$	0.35	Internal2
806.56262	2	$C_{82}H_{146}N_{16}O_{16}H^+_2$	0.26	Internal2
856.09693	2	$C_{87}H_{155}N_{17}O_{17}H^+_2$	0.36	Internal2
905.63081	2	$C_{92}H_{164}N_{18}O_{18}H^+_2$	-0.02	Internal2
955.16538	2	$C_{97}H_{173}N_{19}O_{19}H^+_2$	0.36	Internal2
1054.23329	2	$C_{107}H_{191}N_{21}O_{21}H^+_2$	-0.15	Internal2
169.13359	1	$C_9H_{16}N_2O_1H^+_1$	0.30	ip2
268.20198	1	$C_{14}H_{25}N_3O_2H^+_1$	0.10	ip3
367.27039	1	$C_{19}H_{34}N_4O_3H^+_1$	0.06	ip4
466.33888	1	$C_{24}H_{43}N_5O_4H^+_1$	0.21	ip5
565.40730	1	$C_{29}H_{52}N_6O_5H^+_1$	0.19	ip6
664.47588	1	$C_{34}H_{61}N_7O_6H^+_1$	0.41	ip7
763.54368	1	$C_{39}H_{70}N_8O_7H^+_1$	-0.45	ip8
862.61313	1	$C_{44}H_{79}N_9O_8H^+_1$	0.80	ip9
961.68164	1	$C_{49}H_{88}N_{10}O_9H^+_1$	0.82	ip10
233.67305	2	$C_{24}H_{43}N_5O_4H^+_2$	0.09	ip5
283.20726	2	$C_{29}H_{52}N_6O_5H^+_2$	0.09	ip6
332.74147	2	$C_{34}H_{61}N_7O_6H^+_2$	0.08	ip7
382.27572	2	$C_{39}H_{70}N_8O_7H^+_2$	0.18	ip8
431.81000	2	$C_{44}H_{79}N_9O_8H^+_2$	0.33	ip
481.34428	2	$C_{49}H_{88}N_{10}O_9H^+_2$	0.45	ip10
530.87844	2	$C_{54}H_{97}N_{11}O_{10}H^+_2$	0.32	ip11
580.41265	2	$C_{59}H_{106}N_{12}O_{11}H^+_2$	0.30	ip12
629.94689	2	$C_{64}H_{115}N_{13}O_{12}H^+_2$	0.33	ip13
679.48122	2	$C_{69}H_{124}N_{14}O_{13}H^+_2$	0.48	ip14
729.01551	2	$C_{74}H_{133}N_{15}O_{14}H^+_2$	0.56	ip15
828.08369	2	$C_{84}H_{151}N_{17}O_{16}H^+_2$	0.21	ip16
877.61857	2	$C_{89}H_{160}N_{18}O_{17}H^+_2$	0.97	ip17
927.15202	2	$C_{94}H_{169}N_{19}O_{18}H^+_2$	0.10	ip18
173.12852	1	$C_8H_{16}N_2O_2H^+_1$	0.38	iq2
272.19691	1	$C_{13}H_{25}N_3O_3H^+_1$	0.15	iq3
371.26533	1	$C_{18}H_{34}N_4O_4H^+_1$	0.13	iq4
470.33379	1	$C_{23}H_{43}N_5O_5H^+_1$	0.20	iq5
569.40226	1	$C_{28}H_{52}N_6O_6H^+_1$	0.26	iq6
668.47076	1	$C_{33}H_{61}N_7O_7H^+_1$	0.35	iq7
767.53909	1	$C_{38}H_{70}N_8O_8H^+_1$	0.20	iq8
866.60757	1	$C_{43}H_{79}N_9O_9H^+_1$	0.25	iq9

965.67627	1	$C_{48}H_{88}N_{10}O_{10}H^{+}_{1}$	0.52	iq10
1064.74473	1	$C_{53}H_{97}N_{11}O_{11}H^{+}_{1}$	0.52	iq11
532.87586	2	$C_{53}H_{97}N_{11}O_{11}H^{+}_{2}$	0.25	iq11
631.94434	2	$C_{63}H_{115}N_{13}O_{13}H^{+}_{2}$	0.31	iq12
681.47848	2	$C_{68}H_{124}N_{14}O_{14}H^{+}_{2}$	0.19	iq13
731.01289	2	$C_{73}H_{133}N_{15}O_{15}H^{+}_{2}$	0.46	iq14
780.54696	2	$C_{78}H_{142}N_{16}O_{16}H^{+}_{2}$	0.25	iq15
830.08143	2	$C_{83}H_{151}N_{17}O_{17}H^{+}_{2}$	0.55	iq16
879.61534	2	$C_{88}H_{160}N_{18}O_{18}H^{+}_{2}$	0.19	iq17
929.14987	2	$C_{93}H_{169}N_{19}O_{19}H^{+}_{2}$	0.52	iq18
978.68392	2	$C_{98}H_{178}N_{20}O_{20}H^{+}_{2}$	0.34	iq19
1028.21807	2	$C_{103}H_{187}N_{21}O_{21}H^{+}_{2}$	0.27	iq20
1077.75266	2	$C_{108}H_{196}N_{22}O_{22}H^{+}_{2}$	0.61	iq21
1127.28607	2	$C_{113}H_{205}N_{23}O_{23}H^{+}_{2}$	-0.13	iq22
1176.82132	2	$C_{118}H_{214}N_{24}O_{24}H^{+}_{2}$	0.77	iq23
1374.95844	2	$C_{138}H_{250}N_{28}O_{28}H^{+}_{2}$	0.87	iq27
1424.49151	2	$C_{143}H_{259}N_{29}O_{29}H^{+}_{2}$	0.04	iq28
1523.5609	2	$C_{153}H_{277}N_{31}O_{31}H^{+}_{2}$	0.68	iq30
1573.09503	2	$C_{158}H_{286}N_{32}O_{32}H^{+}_{2}$	0.61	iq31
1622.62715	2	$C_{163}H_{295}N_{33}O_{33}H^{+}_{2}$	-0.70	iq32
1672.16126	2	$C_{168}H_{304}N_{34}O_{34}H^{+}_{2}$	-0.73	iq33
1721.69778	2	$C_{173}H_{313}N_{35}O_{35}H^{+}_{2}$	0.63	iq34
1771.23576	2	$C_{178}H_{322}N_{36}O_{36}H^{+}_{2}$	2.74	iq35
619.76899	3	$C_{93}H_{169}N_{19}O_{19}H^{+}_{3}$	0.50	iq18
652.79165	3	$C_{98}H_{178}N_{20}O_{20}H^{+}_{3}$	0.25	iq19
685.81454	3	$C_{103}H_{187}N_{21}O_{21}H^{+}_{3}$	0.36	iq20
718.83742	3	$C_{108}H_{196}N_{22}O_{22}H^{+}_{3}$	0.45	iq21
751.86018	3	$C_{113}H_{205}N_{23}O_{23}H^{+}_{3}$	0.37	iq22
784.88316	3	$C_{118}H_{214}N_{24}O_{24}H^{+}_{3}$	0.58	iq23
817.90572	3	$C_{123}H_{223}N_{25}O_{25}H^{+}_{3}$	0.26	iq24
850.92860	3	$C_{128}H_{232}N_{26}O_{26}H^{+}_{3}$	0.34	iq25
883.95126	3	$C_{133}H_{241}N_{27}O_{27}H^{+}_{3}$	0.16	iq26
916.97421	3	$C_{138}H_{250}N_{28}O_{28}H^{+}_{3}$	0.31	iq27
949.99695	3	$C_{143}H_{259}N_{29}O_{29}H^{+}_{3}$	0.23	iq28
983.01956	3	$C_{148}H_{268}N_{30}O_{30}H^{+}_{3}$	0.03	iq29
1016.04223	3	$C_{153}H_{277}N_{31}O_{31}H^{+}_{3}$	-0.11	iq30
1049.06543	3	$C_{158}H_{286}N_{32}O_{32}H^{+}_{3}$	0.27	iq31
1082.08805	3	$C_{163}H_{295}N_{33}O_{33}H^{+}_{3}$	0.10	iq32
1115.11100	3	$C_{168}H_{304}N_{34}O_{34}H^{+}_{3}$	0.22	iq33
1148.13416	3	$C_{173}H_{313}N_{35}O_{35}H^{+}_{3}$	0.53	iq34
1181.15657	3	$C_{178}H_{322}N_{36}O_{36}H^{+}_{3}$	0.18	iq35
1280.22556	3	$C_{193}H_{349}N_{39}O_{39}H^{+}_{3}$	0.61	iq36
1313.24734	3	$C_{198}H_{358}N_{40}O_{40}H^{+}_{3}$	-0.18	iq37
1346.26874	3	$C_{203}H_{367}N_{41}O_{41}H^{+}_{3}$	-1.22	iq38
1379.29238	3	$C_{208}H_{376}N_{42}O_{42}H^{+}_{3}$	-0.59	iq39
1412.31700	3	$C_{213}H_{385}N_{43}O_{43}H^{+}_{3}$	0.71	iq40

1445.33873	3	$C_{218}H_{394}N_{44}O_{44}H^{+}_{3}$	-0.05	iq41
1478.36196	3	$C_{223}H_{403}N_{45}O_{45}H^{+}_{3}$	0.24	iq42
1544.40792	3	$C_{233}H_{421}N_{47}O_{47}H^{+}_{3}$	0.46	iq44
286.21255	1	$C_{14}H_{27}N_{3}O_{3}H^{+}_{1}$	0.11	Internal
385.28096	1	$C_{19}H_{36}N_{4}O_{4}H^{+}_{1}$	0.07	Internal
484.34946	1	$C_{24}H_{45}N_{5}O_{5}H^{+}_{1}$	0.24	Internal
583.41736	1	$C_{29}H_{54}N_{6}O_{6}H^{+}_{1}$	-0.69	Internal
682.48637	1	$C_{34}H_{63}N_{7}O_{7}H^{+}_{1}$	0.29	Internal
781.55521	1	$C_{39}H_{72}N_{8}O_{8}H^{+}_{1}$	0.80	Internal
880.62417	1	$C_{44}H_{81}N_{9}O_{9}H^{+}_{1}$	1.33	Internal
440.81514	2	$C_{44}H_{81}N_{9}O_{9}H^{+}_{2}$	0.00	Internal
638.95220	2	$C_{64}H_{117}N_{13}O_{13}H^{+}_{2}$	0.36	Internal
688.48676	2	$C_{69}H_{126}N_{14}O_{14}H^{+}_{2}$	0.85	Internal
738.01965	2	$C_{74}H_{135}N_{15}O_{15}H^{+}_{2}$	-0.99	Internal
787.55518	2	$C_{79}H_{144}N_{16}O_{16}H^{+}_{2}$	0.75	Internal
886.62334	2	$C_{89}H_{162}N_{18}O_{18}H^{+}_{2}$	0.38	Internal
936.15274	2	$C_{94}H_{171}N_{19}O_{19}H^{+}_{2}$	-4.77	Internal
381.27382	3	$C_{59}H_{104}N_{12}O_{10}H^{+}_{3}$	-0.18	Internal
414.29626	3	$C_{64}H_{113}N_{13}O_{11}H^{+}_{3}$	-1.05	Internal
447.31983	3	$C_{69}H_{122}N_{14}O_{12}H^{+}_{3}$	0.74	Internal
546.38811	3	$C_{84}H_{149}N_{17}O_{15}H^{+}_{3}$	0.36	Internal
579.41080	3	$C_{89}H_{158}N_{18}O_{16}H^{+}_{3}$	0.14	Internal
612.43300	3	$C_{94}H_{167}N_{19}O_{17}H^{+}_{3}$	-0.85	Internal
645.45689	3	$C_{99}H_{176}N_{20}O_{18}H^{+}_{3}$	0.87	Internal
678.47932	3	$C_{104}H_{185}N_{21}O_{19}H^{+}_{3}$	0.28	Internal
711.50123	3	$C_{109}H_{194}N_{22}O_{20}H^{+}_{3}$	-0.99	Internal
744.52399	3	$C_{114}H_{203}N_{23}O_{21}H^{+}_{3}$	-1.01	Internal
810.56953	3	$C_{124}H_{221}N_{25}O_{23}H^{+}_{3}$	-1.01	Internal
843.59231	3	$C_{129}H_{230}N_{26}O_{24}H^{+}_{3}$	-1.00	Internal
876.61577	3	$C_{134}H_{239}N_{27}O_{25}H^{+}_{3}$	-0.22	Internal
909.63891	3	$C_{139}H_{248}N_{28}O_{26}H^{+}_{3}$	0.16	Internal
942.66016	3	$C_{144}H_{257}N_{29}O_{27}H^{+}_{3}$	-1.49	Internal
975.68437	3	$C_{149}H_{266}N_{30}O_{28}H^{+}_{3}$	0.00	Internal
1008.70532	3	$C_{154}H_{275}N_{31}O_{29}H^{+}_{3}$	-1.84	Internal
1041.72842	3	$C_{159}H_{284}N_{32}O_{30}H^{+}_{3}$	-1.50	Internal
1074.7523	3	$C_{164}H_{293}N_{33}O_{31}H^{+}_{3}$	-0.45	Internal
644.95166	2	$C_{65}H_{117}N_{13}O_{13}H^{+}_{2}$	-0.48	Internal1
694.48643	2	$C_{70}H_{126}N_{14}O_{14}H^{+}_{2}$	0.37	Internal1
793.55484	2	$C_{80}H_{144}N_{16}O_{16}H^{+}_{2}$	0.32	Internal1
843.08937	2	$C_{85}H_{153}N_{17}O_{17}H^{+}_{2}$	0.68	Internal1
942.15772	2	$C_{95}H_{171}N_{19}O_{19}H^{+}_{2}$	0.54	Internal1
991.69191	2	$C_{100}H_{180}N_{20}O_{20}H^{+}_{2}$	0.50	Internal1
1041.22599	2	$C_{105}H_{189}N_{21}O_{21}H^{+}_{2}$	0.35	Internal1
1090.76048	2	$C_{110}H_{198}N_{22}O_{22}H^{+}_{2}$	0.60	Internal1
1140.29463	2	$C_{115}H_{207}N_{23}O_{23}H^{+}_{2}$	0.52	Internal1
1189.82824	2	$C_{120}H_{216}N_{24}O_{24}H^{+}_{2}$	0.00	Internal1

1288.89721	2	$C_{130}H_{234}N_{26}O_{26}H^{+}_{2}$	0.43	Internal1
1338.43102	2	$C_{135}H_{243}N_{27}O_{27}H^{+}_{2}$	0.12	Internal1
1437.49851	2	$C_{145}H_{261}N_{29}O_{29}H^{+}_{2}$	-0.53	Internal1
		Average	0.53	
		Standard deviation	0.76	

8. Two-dimensional mass spectrometry of polymers and future two dimensional methods

Tomos E. Morgan[1], Christopher A. Wootton[1], Maria van Agthoven[1], Alina Theisen[1], Anisha Haris[1], Sean Ellacott[1], Andrew Kerr, Thomas Floyd, Mark P. Barrow[1], Anthony W. T. Bristow[2], Sébastien Perrier[1], Peter B. O'Connor[1]

[1]Department of Chemistry, University of Warwick, Coventry, Midlands, CV4 7AL, UK.

[2]Chemical Development, Pharmaceutical Technology & Development, Operations, AstraZeneca, Macclesfield, UK.

The MS, MS/MS, and analysis presented in this chapter were all carried out by the thesis author. Sean Ellacott and Andrew Kerr carried out the synthesis and purification of the polymer species. The UV modification for SolariX was carried out by Alina Theisen and Anisha Haris.

The work presented in this chapter has been prepared for publication in ACS Analytical chemistry under "advances in 2DMS methods of synthetic polymers" by authors Tomos E. Morgan, Christopher A. Wootton, Maartje van Agthoven, Alina Theisen, Anisha Haris, Sean Ellacott, Andrew Kerr, Mark P. Barrow, Anthony W. T. Bristow, Sébastien Perrier, Peter B. O'Connor

8.1. Abstract

A major drawback of tandem mass spectrometry is the necessity to isolate species using either chromatographic or quadrupolar isolation methods. The complexity produced by the dispersity of polymeric species means their separation by chromatographic methods to singular monomer units is almost impossible. The picture can be complicated further with the presence of variations in terminating end groups, especially conjugating agents.

2DMS offers a methodology in which multiple precursors can be fragmented at the same time without prior separation. 2DMS utilises a pulse program within the mass spectrometer and a spatially resolved fragmentation method to produce a sinusoidal modulation of ion intensities allowing precursors to be matched with their corresponding fragments.

Previous 2DMS studies have shown that ECD can be used as a spatially resolved fragmentation method. ECD was successfully utilised in this chapter for the analysis of polyoxazolines and polyacrylamides. 2DMS showed significant advantages compared with traditional MS/MS and provided the fragmentation patterns of all species within the dispersity, correlated directly with their precursors allowing direct comparisons to be made.

Further experimentation was carried out in the development of UVPD as a possible 2DMS method. Successful tuning of the fragmentation region was carried out and 2DMS analysis of a standard peptide was achieved, the precursors and fragments modulated well to one another allowing the use of UVPD methods for further 2DMS analysis.

8.2. Introduction

As new polymer species are increasingly used as alternatives to poly(ethylene glycol) as conjugating agents there has been an increased focus on the development of analytical methods. Polyoxazolines have produced significant interest as drug delivery agents as they are biologically compatible and have stealth behaviour *in vivo*.[1,2] Polyoxazolines also tend to have a high potential for end group diversity. [3-5] The overall size, and initiating and terminating groups of polyoxazolines are directly related to their chemical properties thus there is a distinct need to understand these aspects of the polyoxazoline directly by mass analysis techniques.[6-8]

Tandem mass spectrometry techniques can be used for the analysis of polymer primary and end group structure[8-13] with examples of collisional-activated dissociation (CID/CAD)[14-16] and the use of electron capture dissociation (ECD) for the characterization of polyoxazoline species. Traditional tandem mass spectrometry techniques require isolation of individual species before fragmentation. To achieve complete tandem MS analysis of a polymer one would therefore require isolation of each individual species present as part of the dispersity perfectly, requiring extremely high isolation resolving power to separate closely m/z spaced species. Different fragmentation methods can show contrasting or complementary fragmentation patterns, for example, ECD often produces different fragments to CID due to it being a radical based fragmentation technique so fragmentation is less affected by weak covalent bonds present in the molecule.[17] The radical nature of the ECD fragmentation process means that there is a significant fragmentation down the back-bone of polyoxazoline polymer species, and fragmentation at the N-C_α bond[18] is much more complete when taking into account fragmentation from both ends of the polymer chain.

Two-dimensional mass spectrometry (2DMS) allows the fragmentation of all species in a sample and correlation of fragments to parent precursor ions in one experiment and without the need for individual species isolation.[19-21] 2DMS relies on the use of a radius dependent fragmentation method, the use of the ring electrode with the infinity cell present in the SolariX allows spatially selectivity via both an infrared laser and the electron cloud formed by a hollow ring cathode.[22] 2DMS has been used to

good effect in the analysis of proteins and peptides.[23-31] Modulation of ions within the fragmentation zone will cause a modulation of precursor and fragment ion intensity, meaning fragments can be directly assigned to precursors as their intensity will modulate at the same cyclotron frequency of the precursor (2nd dimension). Lack of need for separation before fragmentation/detection comes with a significant advantage when considering the dispersity of a polymer population as well as potential by-products that may be produced during the analysis.

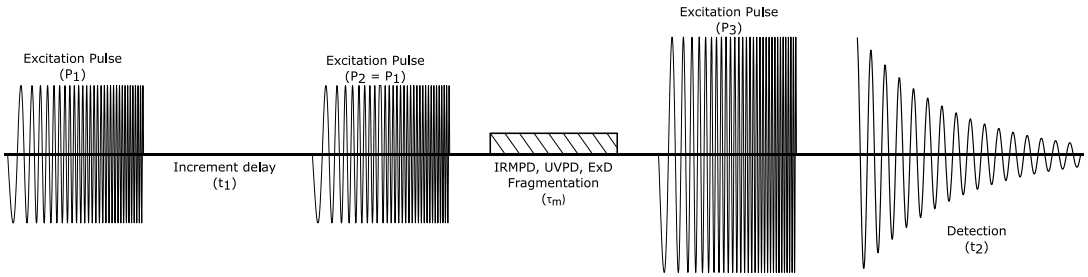

Figure 8.1 Pulse sequence applied within the ICR cell for the analysis of ions by 2DMS to allow for the coupling of fragments and their precursors without isolation.

After processing extraction of data from a 2DMS spectrum can then be treated similarly to multiple regular tandem mass spectra. The use of a modified Kendrick mass defect (MKMD) can also be used on this data. A modification from the much used Kendrick mass defect (KMD)[32,33] the MKMD normalizes the KMD to a homologous series to that of the monomer unit present in the analysed polymer and not that of CH_2.[34-40]

In this study we report the characterization of a methyl initiated polyoxazoline by ECD fragmentation across a section of their dispersity using 2DMS.

8.3. Methods and Experimental

All experiments were performed on a 12 T SolariX Fourier transform ion cyclotron resonance mass spectrometer (Bruker Daltonik, GmbH, Bremen, Germany) using a nanoelectrospray (nESI) ion source in positive ion mode.

ECD was carried out using the hollow ring cathode, ECD bias voltage was set at 1.2 eV for the analysis of both the polyoxazoline and polyacrylamide species. The ECD pulse length was lower for the peptide-conjugate (0.1 s) due to the higher charge compared to the cyclic peptide (0.3 s).

UVPD dissociation was carried out with one or two 6 mJ laser pulses (measured at laser head) from a 193 nm excimer laser (ExciStar XS, Coherent) in the setup used herein translates to <0.6 mJ at the window of the ICR cell.

2DMS methodology of the polyoxazoline and polyacrylamide: 2DMS methodology followed is based on the pulse program in Figure 8.1. The pulse program used had an energy 180 $V_{p\text{-}p}$ for P_1 and P_2. The initial delay and incremented pulse delay was 1.4 µs for the polyoxazoline analysis and 1 µs for the polyacrylamide, corresponding to a low *m/z* for the precursor dimension of *m/z* 420 and *m/z* 328 respectively. Both spectra were acquired using 8192 scans, which represent data points in the *y*-axis, and *x*-axis transients of 1 MW with a low mass cut off of 98 Da.

The data is acquired as a series of scans with corresponding transients, these are converted into one data file as 2D array with each 1D array representing a single scan.

Initial data processing was carried out using a program titled "SPIKE"[41] written by Delsuc and *coworkers*. The SPIKE processing kernel takes batch files of transients (ser files) from an LCMS data set generated from the SolariX instrument during the 2D acquisition process. A multi-hierarchal data format is used for the processing (HDF5 format). After this point the data is separated by each scan, and each scan is Fourier transformed. The data is shifted and demodulated due to SolariX instrumental architecture which involves shifting the timing by a certain number of data points based on the *m/z* used for the highest mass analysed. The data can be denoised with URQRD, a ranked based denoising system based on similar responses within the transients present within the data set. The data can then undergo standard

apodisation and/or zero filling procedures. The corresponding array is then transformed and Fourier transformed again, the equivalent of a Fourier transform in the vertical axis. The corresponding data set contains a 2D array of “hyper complex” numbers, each point contains four coefficients which the modulus can then be taken and the data presented as an magnitude mode spectrum.

The data is then converted to binary file format and processed in an in house t2D program, developed by Wootton, Marzullo, and Morgan. Data can be extracted from T2D into Bruker DataAnalysis files for use with the Bruker suite of programs, or analysed and recalibrated in T2D itself.

8.4. Results and Discussion

8.4.1. Polyoxazoline analysis

nESI-MS of the polyoxazoline acidified solution produced mainly protonated ions in the 3+ and 2+ charge states. The 2DMS, Figure 8.2, showed a rich spectrum with strong autocorrelation, neutral loss, and fragment lines. The mass range in the x-axis is representative of the scanning range of the final excite/detect stage in the FT-ICR analysis, this measures all the fragments and precursors that are present in the FT-ICR cell after the fragmentation has taken place. The second dimension mass axis has a low mass limit based on the pulse delay between initial excitation and de-excitation as part of the 2D process to produce phase differences, and therefore spatial resolution, of the precursor ions, here *m/z* 420. The second-dimension pulse delay is the same as a sampling frequency and therefore the pulse delay must be less than the reciprocal of the Nyquist frequency of the precursor ions as to allow all the precursor ions to be modulated and analysed.

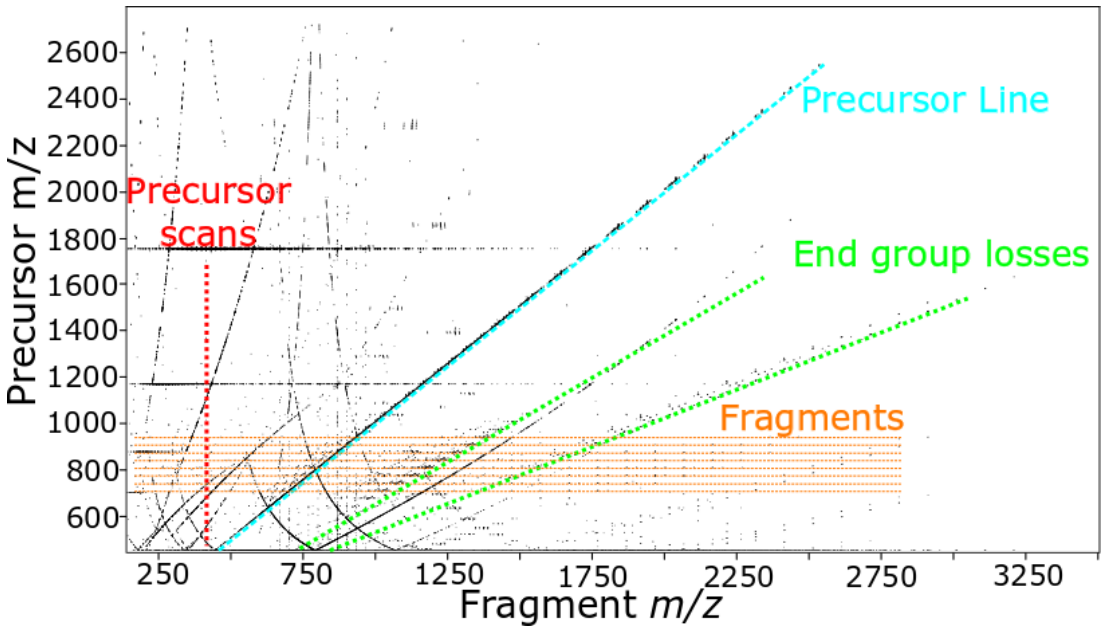

Figure 8.2 2DMS spectrum annotated showing the main features. Fragment *m/z* is present in the *x*-dimension and the related precursor *m/z* in the y-dimension, an un-modified spectrum is contained in the SI.

A series of lines can be extracted from the 2DMS. Each of these lines presents different information corresponding to the 2DMS spectrum. The autocorrelation line

shows the observed precursor ions, this is all the ions observed at the first excitation pulse as part of the analysis. The autocorrelation line is therefore y = x and extraction give a spectrum that looks very similar to a one-dimensional MS without any fragmentation present.

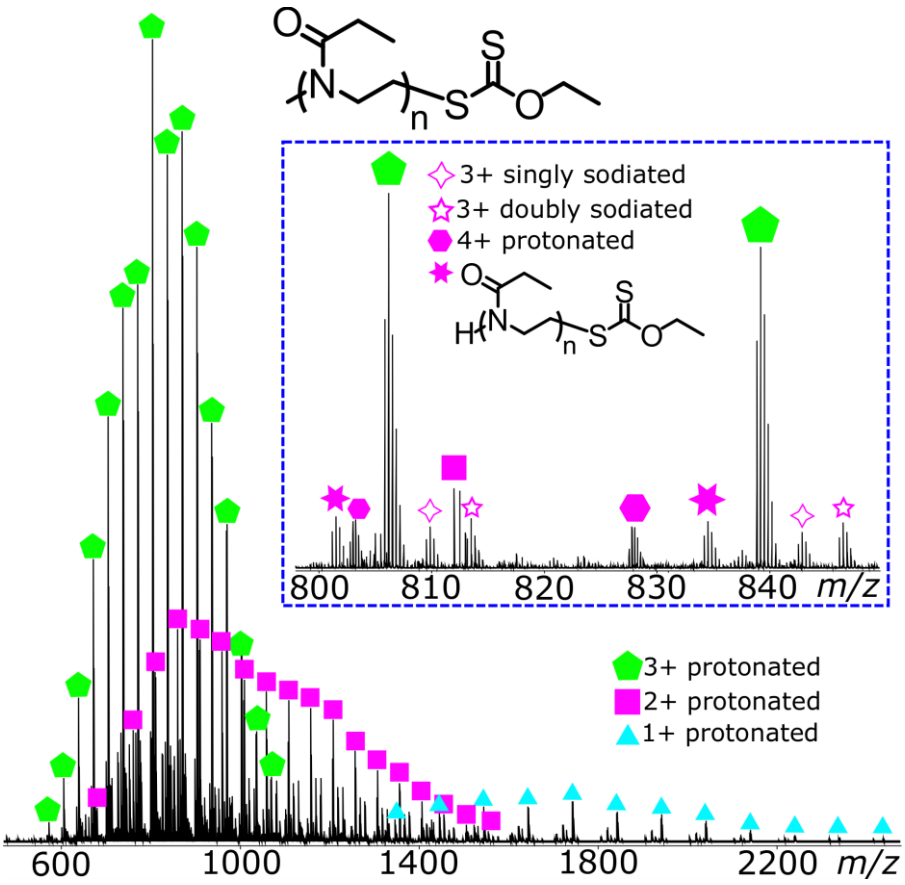

Figure 8.3 Extracted autocorrelation line of 2DMS of polyoxazoline showing the multiply charged species showing the different charge states and dispersity of the precursor.

The autocorrelation line of the 2DMS shows the presence of 3 different protonated ion charge states as well as low levels of sodiation, and a triply protonated ion of the hydrogen-initiated by-product. The autocorrelation line can be handled exactly like a one-dimensional mass spectrum of precursors, over 150 precursor peaks, of predominantly 3+, 2+, and 1+ charge states. For the precursor ion peaks to be observed there must be a modulation in their intensity/response, the modulation is caused by fragmentation, reducing the intensity of the precursor when it is present

in the fragmentation zone and the intensity returning to normal outside of the fragmentation zone.

Examining the precursor signals in 2D space allows a better understanding of the formation of the 2DMS peaks and how they look within the, now three dimensional (precursor *m/z*, fragment *m/z*, and intensity) space. Zooming in on the Precursor present at *m/z* 808 shows the precursor for the polyoxazoline n=23. The precursor is triply charged so the spacing in precursor and fragment *m/z* space is *m/z* 1/3 meaning the gradient of the isotopes is one. Figure 8.4 shows how many peaks were present both as part of the isotopic envelope but also from other precursors present along the autocorrelation line.

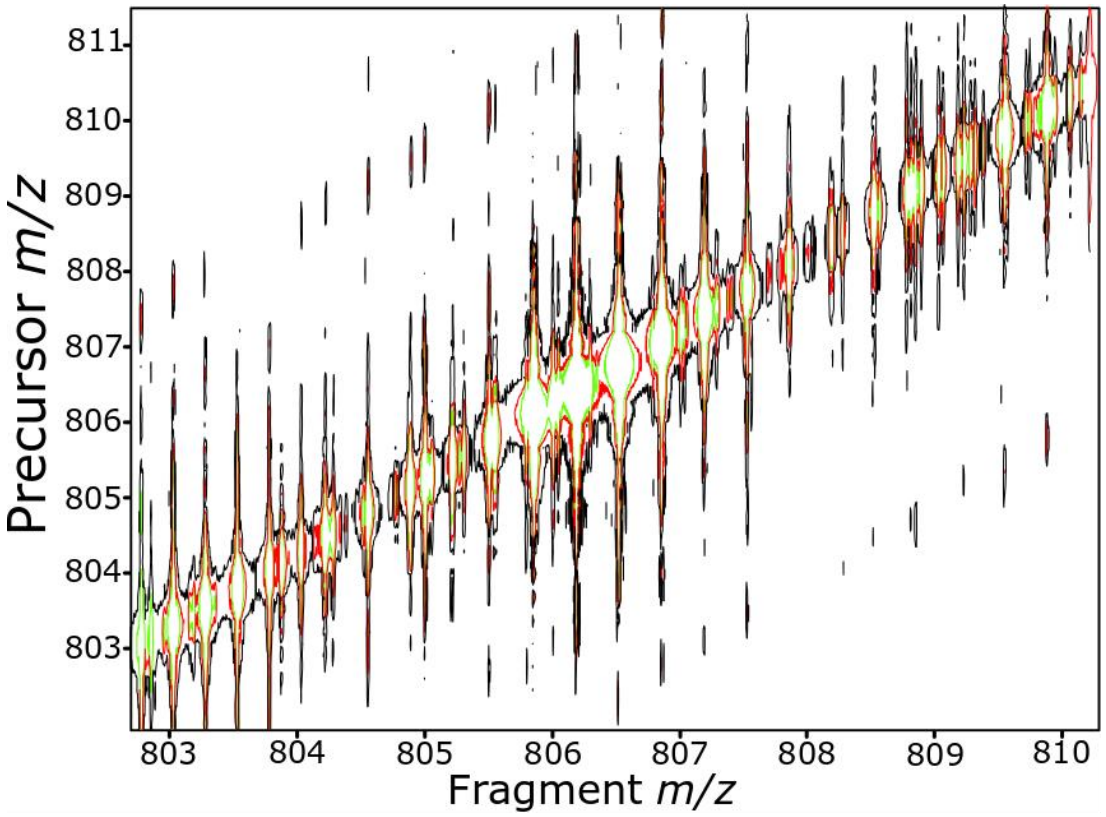

Figure 8.4 Zoom in of the isotopic envelope of the precursor of polyoxazoline n=23 present at 806-808 *m/z*.

Although Figure 8.4 shows the complexity of the spectrum with multiple precursors, visualising the spectrum three dimensionally shows how the precursors of interest are much more intense. Figure 8.5 shows the 3D view from the fragment line, the resolving power in the *x*-dimension is very noticeable here, the spectra were taking

with 0.4 s transients corresponding to approximately 250,000 resolving power at 400 *m/z*.

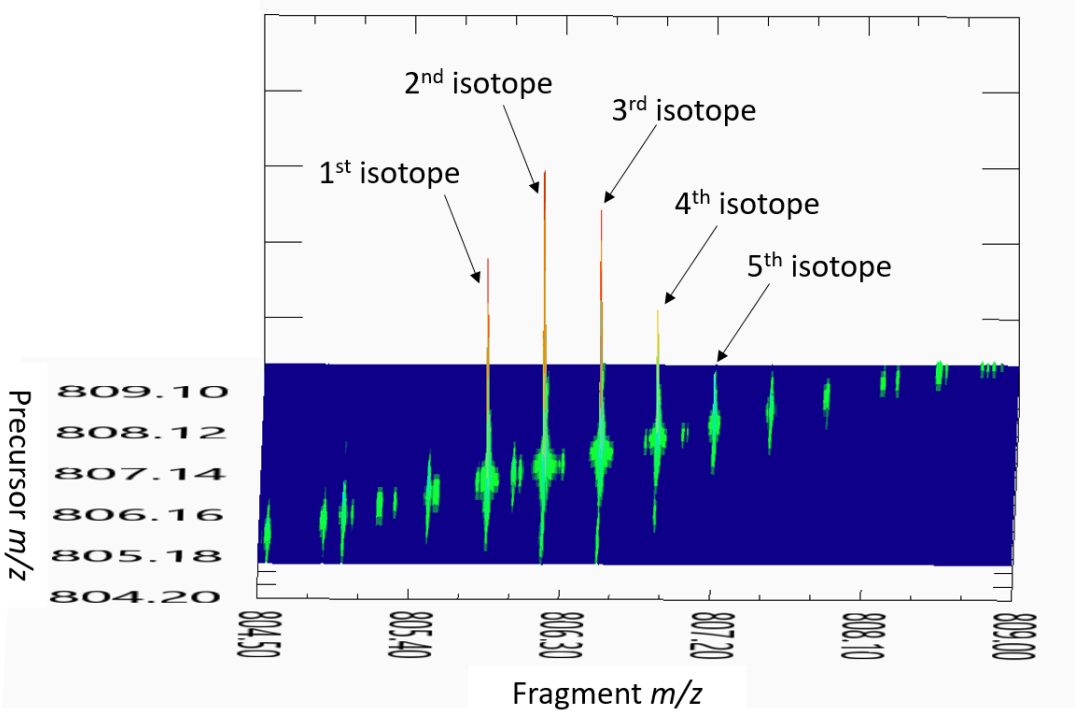

Figure 8.5 3D plot of the isotopic envelope shown in Figure 8.4. The *x*-axis is the Fragment *m/z* which the resolving power is directly linked to the transient length of each scan, thus the ultra-high resolving power of the FT-ICR MS is retained.

The resolution in the *y*-dimension is much lower than that in the *x*-dimension due to the comparatively much shorter transient. The *y*-dimension only contains 8,192 data points, being acquired at an acquisition rate of 1.4 µs, comparable total time 11.5 ms. The width of the peaks is much greater, but importantly, the centres of the peaks do not overlap, allowing distinction between the precursor masses.

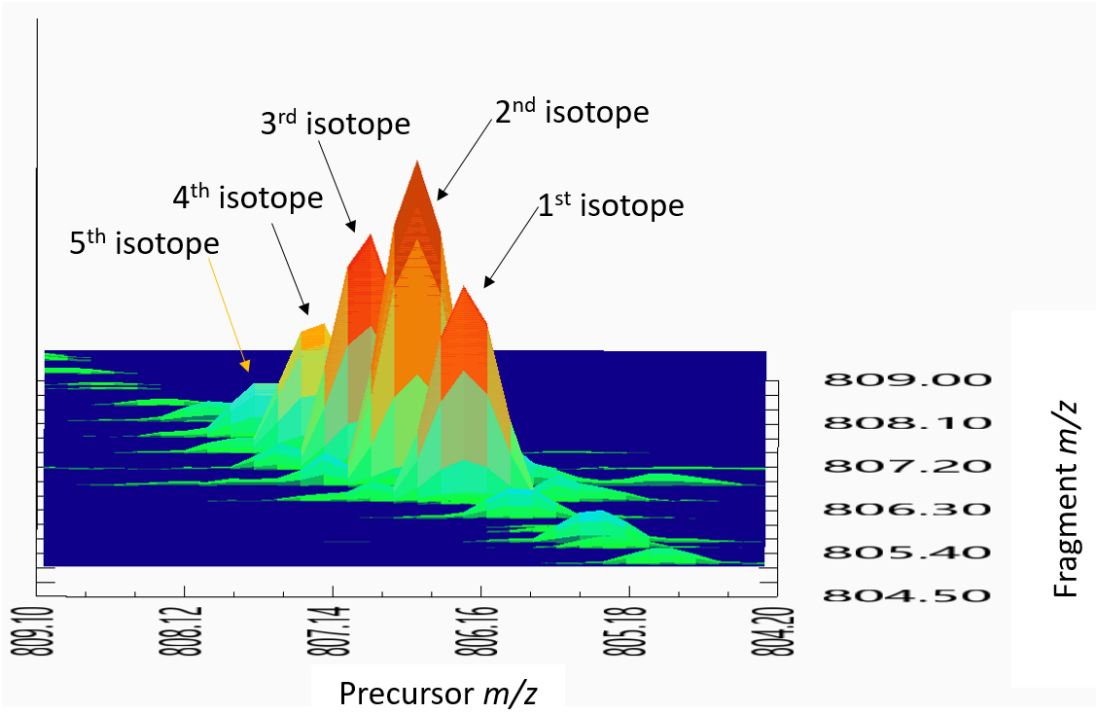

Figure 8.6 3D plot of the isotopic envelope shown in Figure 8.4. The *y*-axis is the precursor *m/z* which the resolving power is proportional to the number of scans taken, the resolution is a lot lower as there are only 8,192 data points taken, compared to the million on the *x*-axis. The peak centres are still obvious and most importantly do not overlap in 3D space.

The isotopic envelope in 3D space along the precursor axis (diagonal) shows the correlation of the isotopes, and that the precursor line has a gradient of one.

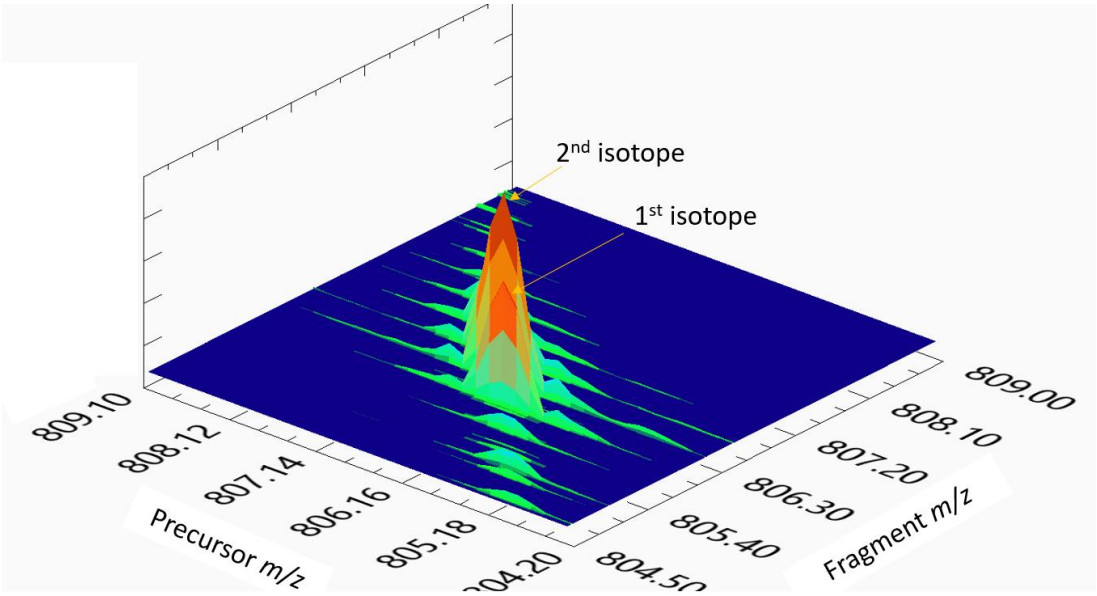

Figure 8.7 3D plot of the isotopic envelope shown in Figure 8.4. The precursor axis has all of the precursor species present, the isotopes visible are the 1st and 2nd as the later isotopes are obscured by the size of the 2nd.

Overall, visualising the 2DMS in 3D space gives an idea of how the peaks overlap and interact with one another and does not threshold smaller peaks from view. Importantly, all data is retained and not reduced for memory efficiency.

The fragmentation of polyoxazolines produces rich sequence coverage as well as significant neutral losses. An important part of the two-dimensional technique is trying to acquire as much information across the polymer dispersity in one experiment, utilizing the resolving power in the second dimension as a way to differentiate fragmentation patterns without the need for prior discrete ion separation by external sources, such as gel permeation chromatography or quadrupole isolation.

The presence of two different species, the methyl initiated polyoxazoline and the hydrogen initiated polyoxazoline makes this a useful sample to test the effectiveness of the ability to analyse two different species contained within a 2DMS. The methyl-initiated species, at its highest intensity gives almost identical sequence and end group fragments to the one dimensional experiment, and maintains full sequence coverage. Figure 8.8A shows the extracted fragment line of the n=23 polyoxazoline, Figure 8.8B shows the line but within 2D space, the peaks are highlighted from one

space to the other. The sequence coverage here starts at *m/z* 286.21252 (a_3, 0.0 ppm) and continues until *m/z* 2168.51932 (a_{22}, 3.2 ppm). The *x* fragment series starts at *m/z* 321.13029 (x_2, 0.2 ppm) and goes through to *m/z* 2203.42893 (x_{21}, *-0.5* ppm).

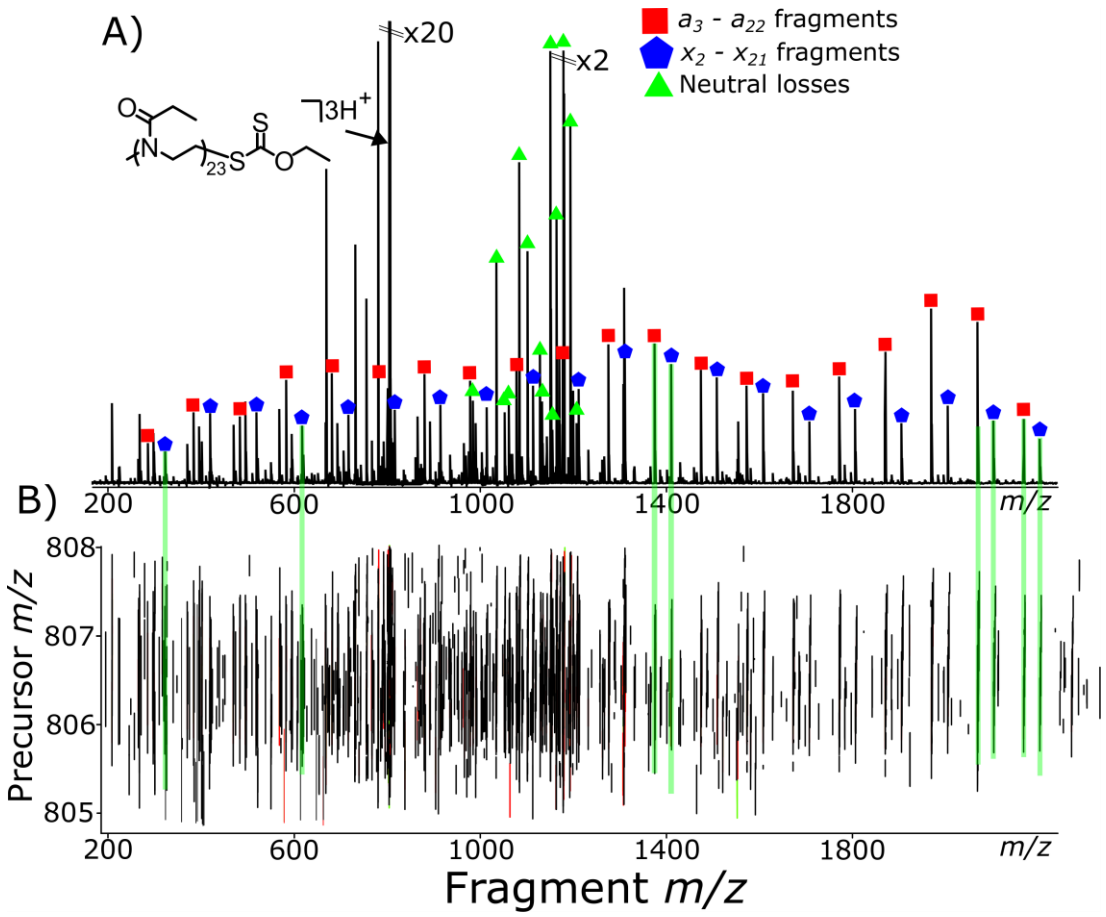

Figure 8.8 A) Fragmentation line spectrum showing coverage of the methyl initiated polyoxazoline, B) 2DMS plot, corresponding to the 2D space the fragment line is extracted from showing a selection of peaks and where they overlap in space.

The end group analysis is almost identical to the fragmentation that is seen in the one-dimensional analysis. Fragmentation from both end groups allows accurate assignment of the initiating and terminating end groups with the fragments at *m/z* 1151.75400 representing the loss of a methyl-initiated end group with a monomer attached. The xanthate species is well characterized by the presence of a peak at *m/z* 1134.29499 and *m/z* 1084.76102 which represent the loss of the ethyl functionalized xanthate and the loss of a xanthate with a monomer unit.

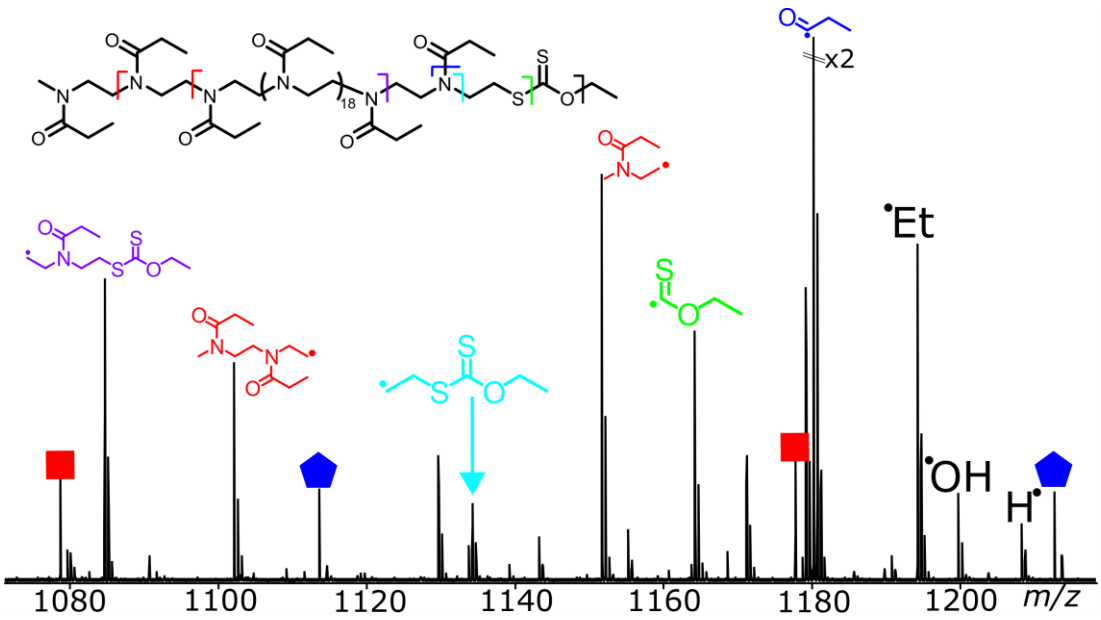

Figure 8.9 End group analysis through the neutral losses from the charge reduced state of the polyoxazoline. The coloured symbols are the *a*- and *x*-fragmentation series shown above.

A key advantage of 2DMS is the ability to ascertain relationships between precursors and fragments based on how each are arranged in space. For example the gradient of a fragment's isotopic envelope is a function of the fragment's charge and the charge of the precursor that produced it. This is an intrinsic advantage of the method where relationships are preserved, unlike quadrupole-functionalised MS/MS where this relationship is inferred from peak picking of the precursor spectrum and estimation therefrom.

A fragments isotopic distribution will be spaced in the fragment (*x*) dimension *m/z* with the spacing expected of the fragment's charge, *i.e m/*z 1, for a singly charged fragment, *m/z* 0.5 for a doubly etc. The spacing in the precursor (*y*) dimension will be based on the spacing of the isotopes of the precursor that will also be spaced by *m/*z 1, for a singly charged precursor, *m/z* 0.5 for a doubly etc. yet the gradient can vary.

A singly charged fragment produced from a triply charged precursor will have an *x*-axis (fragment axis) spacing of *m/z* 1 but a *y-axis* (precursor axis) spacing of *m/z* 1/3. Figure 8.10 shows the a_{21} fragment isotopic envelope. The *m/z* spacing of the isotopes in the *x-axis* is *m/z* 1 and the *y-axis* is *m/z* 1/3. The gradient therefore of the isotopic envelope is 1/3. In the event of overlapping precursors of different charge

states, this method can be used to separate which fragment has come from which precursor.

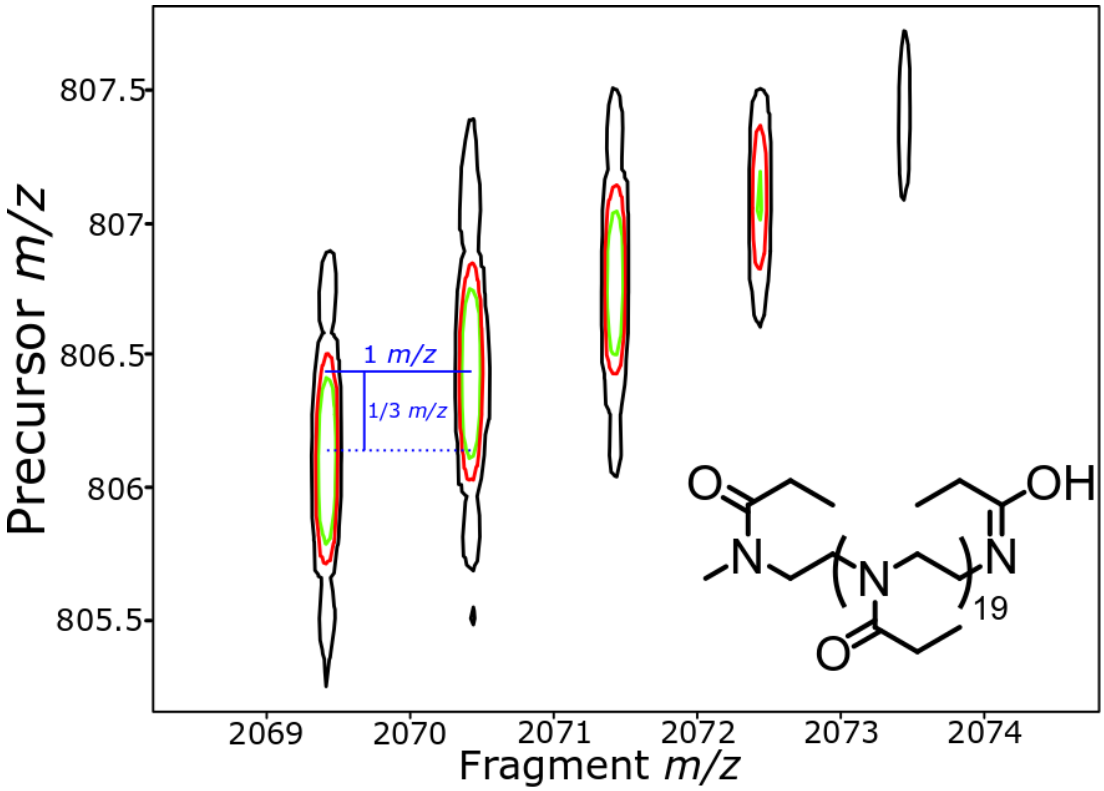

Figure 8.10 Isotopic envelope of the a_{21} fragment showing the relationship between the precursor and fragment isotopes giving a gradient. The 1 m/z x-dimension spacing shows the fragment is a 1+ ion. The 1/3 m/z y dimension spacing shows the fragment came from a 3+ precursor.

So far the focus has been on a single precursor and a single fragment line, a benefit of the 2DMS process is that all precursors in the spectrum are fragmented and all fragmentation patterns are recorded with each scan, so a 2DMS spectrum shows fragment patterns from every precursor observed; a truly DIA process. In the 2DMS approximately 30 individual polymer species are present. Complete fragmentation coverage was achieved for seven polymer precursors. The two fragment spectra presented in Figure 8.11 are from the same 2DMS spectrum. One represents a 20 monomer containing polyoxazoline species and the other a 24 monomer containing polyoxazoline species.

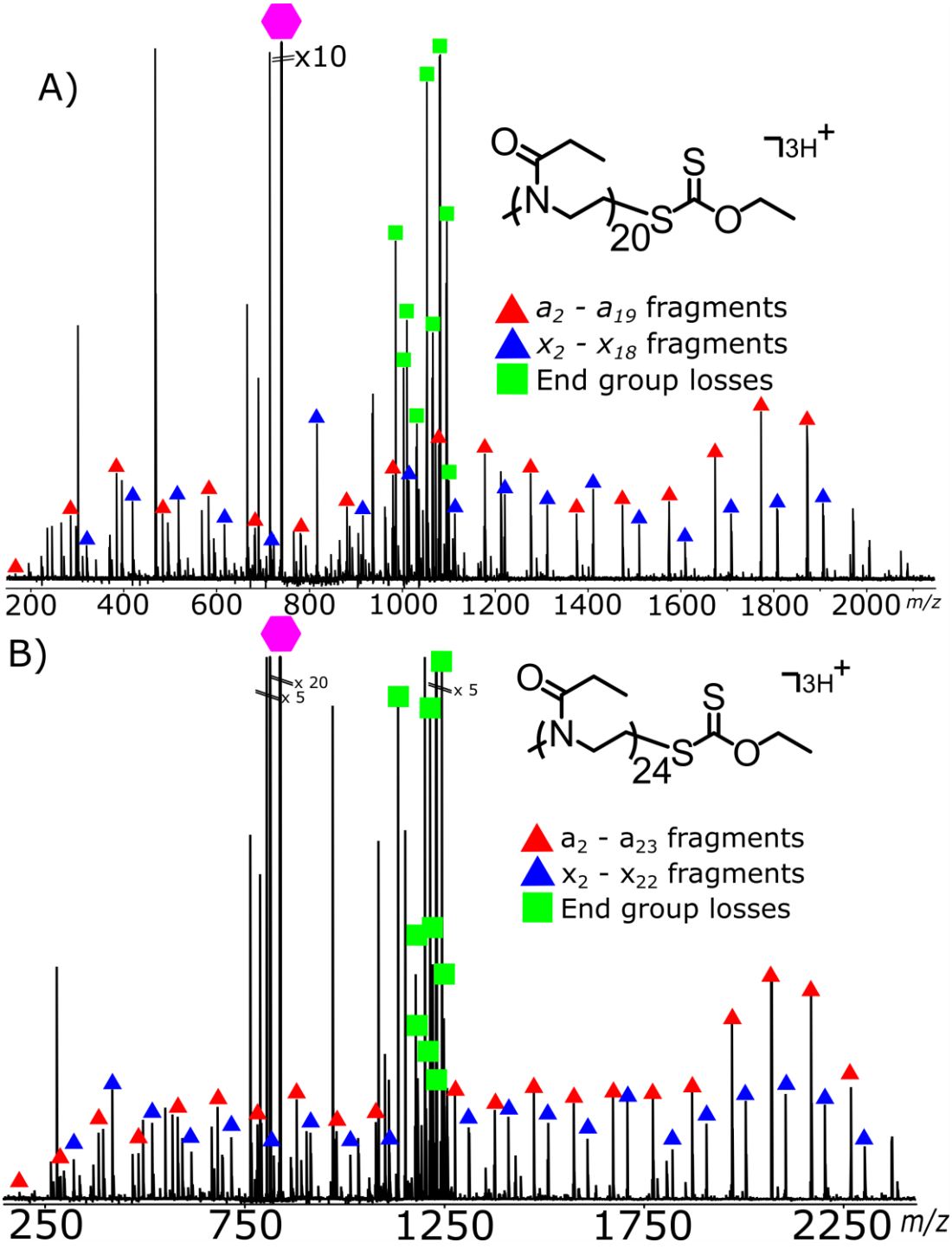

Figure 8.11 Fragment lines of A) a n =20 polyoxazoline and B) a n = 24 polyoxazoline both spectra show complete fragmentation coverage of the polymer equal to the of standard 1D MS techniques.

The hydrogen initiated polyoxazoline was observed at a much lower intensity and so complete sequence coverage by *a* and *x* fragmentation was not present. A number of the high mass *a* fragments were observed, as well as a large number of neutral

losses. Neutral losses contained informative fragments such as the fragment at *m/z* 1127.79022 remaining from the loss of a ethyl xanthate terminal functional group loss. The fragment present at *m/z* 1102.72245 is the result of a fragmentation at the α initiator resulting the loss of two monomer units. Considering the H-functionalised polyoxazoline was approximately ten times less intense than the methyl-functionalised polyoxazoline being able to achieve terminus characterisation is incredibly useful and reveals species specific chemical characterisation of not just the main species, but also chemically similar but distinctly different polymers within the complex mixture.

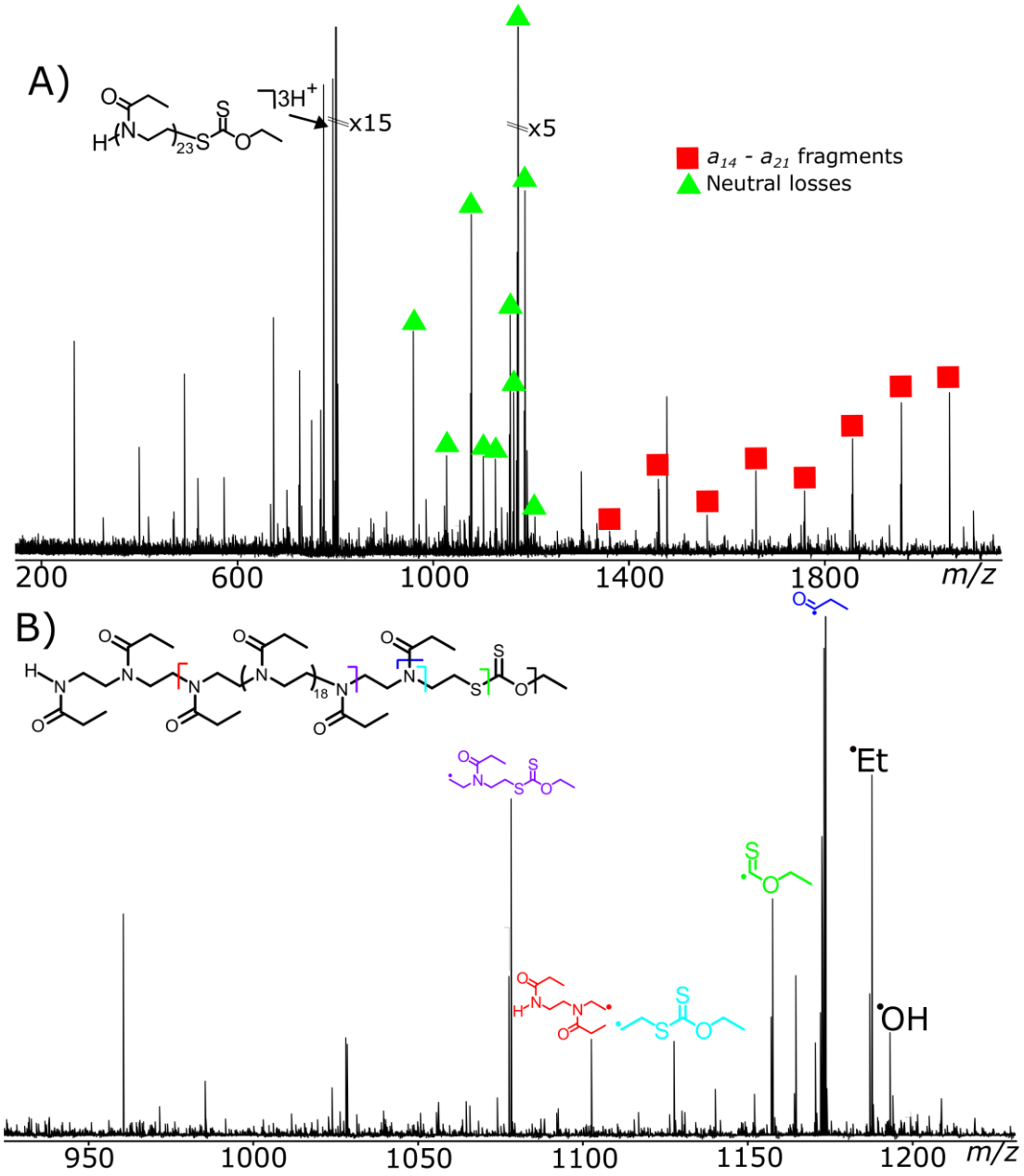

Figure 8.12 A) Fragmentation spectrum showing coverage of the methyl initiated polyoxazoline. B) neutral losses from the charge reduced state showing the presence of a hydrogen initiated fragment loss.

2DMS affords the ability to take vertical lines and reveal which precursors produced a specific fragment ion. Taking the a_3 fragment and the x_3 fragment *m/z* values and then extracting a vertical line gives the ability to immediately view the precursors that produce the corresponding fragment ion. These peaks in the vertical line, called a precursor ion scan, are all equally spaced by the monomer unit divided by three and therefore line up to being present from a triply charged polymeric precursor.

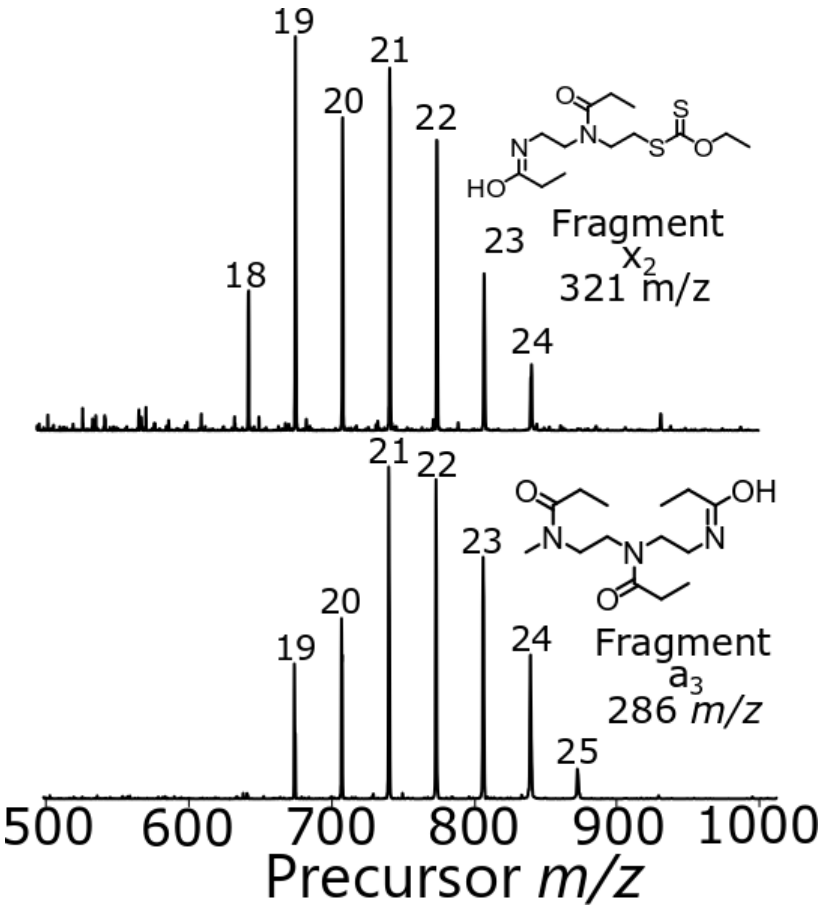

Figure 8.13 Precursor scan line of two different fragments, the x_2 and the a_3 fragments are generated by the precursor *m/z* shown here. The numbers atop the peaks represent the number of monomer units in the corresponding polymer precursor.

8.4.2. Polyacrylamide analysis

2DMS analysis of a terminated butyl-trithiocarbonate species was carried out unsuccessfully. The 2DMS showed no fragments. The reasoning behind lack of corresponding fragment peaks in the 2DMS was likely due to the radical dissociation of the remaining fragments to generate further fragments as discussed in Chapter 4. Although precursors and fragments can be linked through the pulse program, if fragments were rapidly generating further fragments it is understandable that the mutual relationship between precursors and fragments will be greatly diminished and the signal to noise ratio of the corresponding peak after the Fourier transform would also be greatly lowered, even below the noise level and become unobservable.

The full 2DMS of a hydrogen terminated polyacrylamide is shown in Figure 8.14. The scintillation noise (vertical line streaks) are large due to the high intensity of the precursors present and the low threshold for plotting. Intense electron capture lines can be seen moving diagonally to the autocorrelation line.

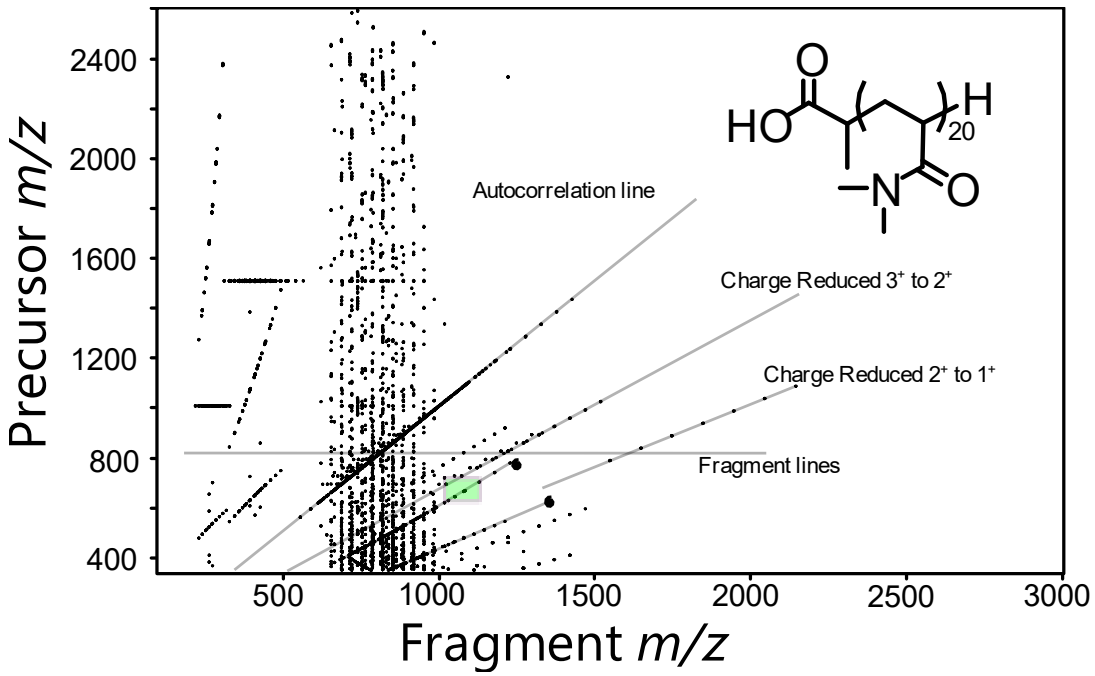

Figure 8.14 Full 2DMS ECD analysis of a hydrogen terminated polyacrylamide species. The autocorrelation line shows all of the precursors present in the sample. Two different charge reduced species lines are shown as well as fragment lines. The highlighted green region shows the region presented in Figure 8.16.

The electron capture lines are not parallel due to the progressively larger absolute difference in mass as the precursor *m/z* mass gets larger compared to the mass of the charge reduced state. The autocorrelation line can be identified moving diagonally through the 2DMS between 600-1400 *m/z*.

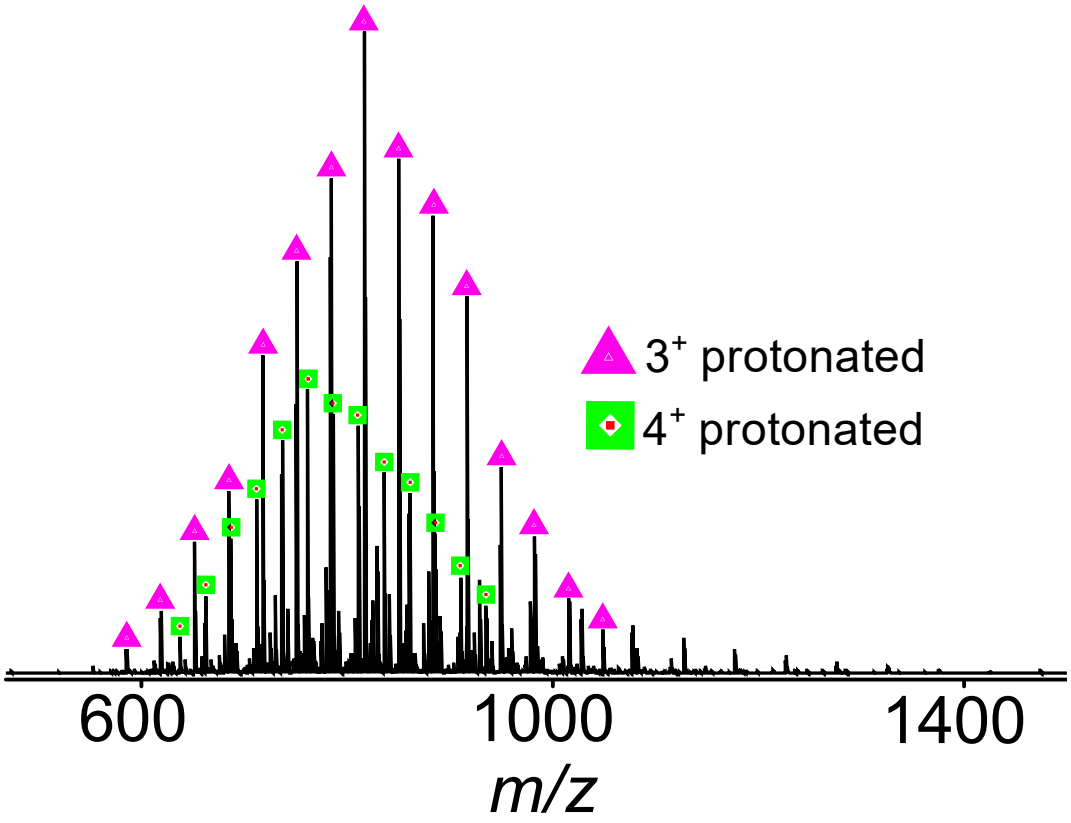

Figure 8.15 Autocorrelation line of the polyacrylamide species.

Although clear horizontal fragment lines are not clear at the observed contour level zooming into a section of the 2DMS it is clear to see fragments that are above the baseline noise level. Figure 8.16 shows clear horizontal and vertical lines present within the 2DMS spectrum. The area chosen for the zoom was predominantly chosen due to the overlapping charge states and the larger fragments having larger isotope envelopes.

In the 2DMS each group of isotopic envelopes directly correspond to a single fragment. The gradient of the isotopes from one another are due to the change in charge and mass. Closer spacing in the *x*- and *y*-axis will be caused by higher charge states.

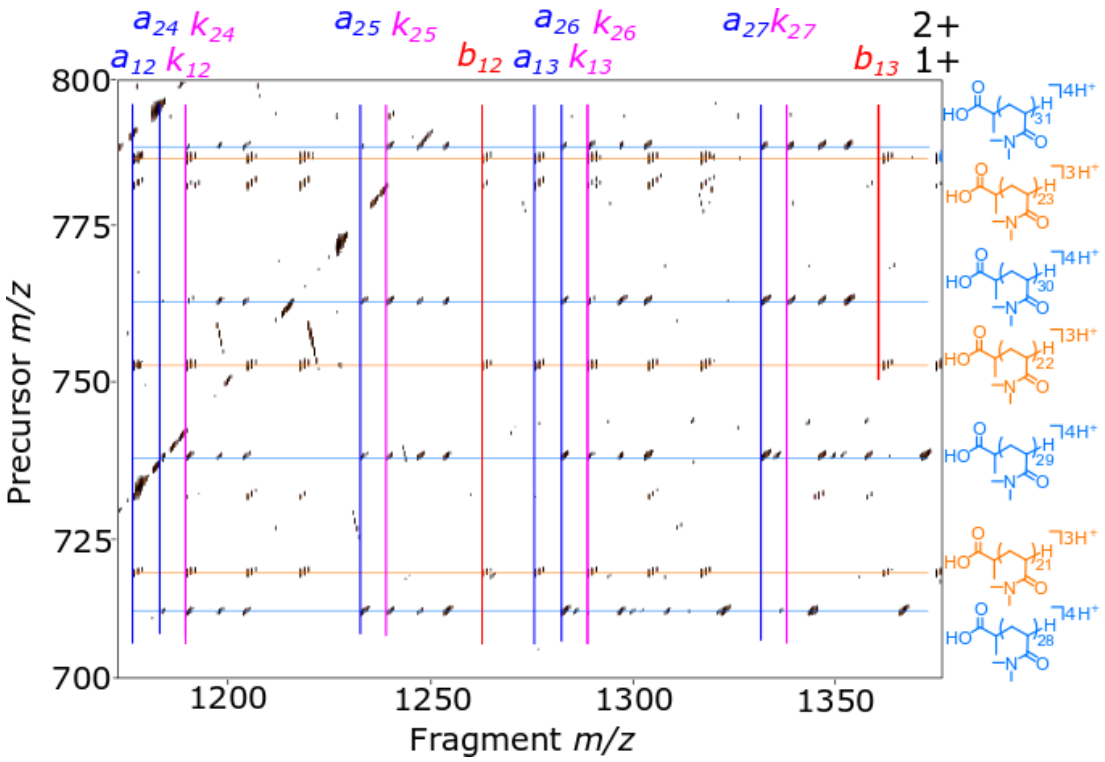

Figure 8.16 zoomed region of 2DMS showing the fragmentation coverage of the 2DMS method. Each vertical line represents shared fragments between precursors and each horizontal line represents shared precursors between fragments.

Figure 8.16 shows the partial fragment lines of seven precursors ranging from triply protonated 21-23 monomer units sized poly(acrylamides) and quadruply protonated precursor ions from 28 to 31 oligomer units. The corresponding fragment ions can be clearly seen as singly and doubly charged fragments moving along the horizontal axis.

Similarly, to the analysis of polyoxazoline previously, horizontal fragment lines can be taken and analysed much like standard tandem mass spectra. Figure 8.17 shows an extracted fragment line at *m/z* 686 of a 20-mer polyacrylamide species. The fragmentation coverage achieved in the 2DMS analysis was similar to that of the tandem mass spectrometry experiment with the analytically useful a_2 and b_2 fragments being produced.

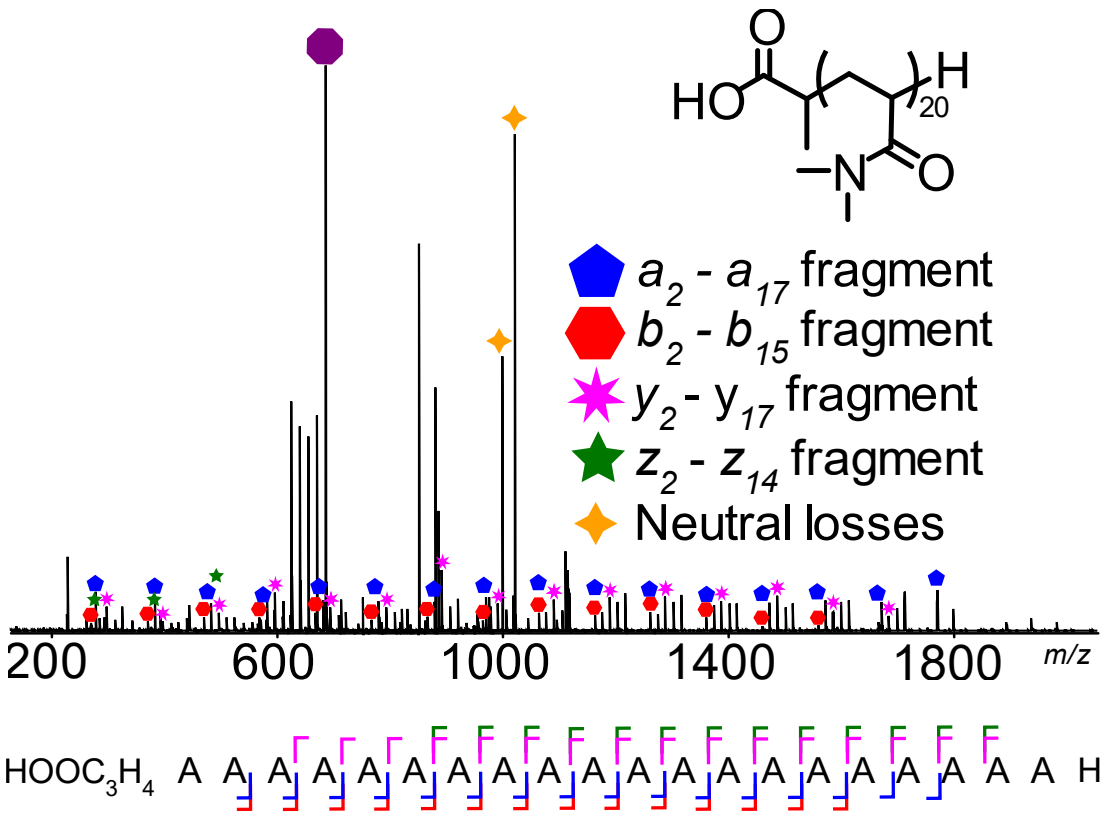

Figure 8.17 Fragment line of a 20-mer hydrogen terminated acrylamide showing almost complete fragmentation coverage, with both end groups being accounted for.

Like the polyoxazoline a comparison of different fragments and their corresponding isotopic distributions can be made. Figure 8.18 shows the isotopic envelope of a singly charged k_{13} fragment. The separation in the *x*-axis is *m/z* 1, and the separation in the *y*-axis is *m/z* 1/3. The gradient of the isotopes therefore are the same as the earlier example of 1/3, revealing a 3+ precursor parent ion.

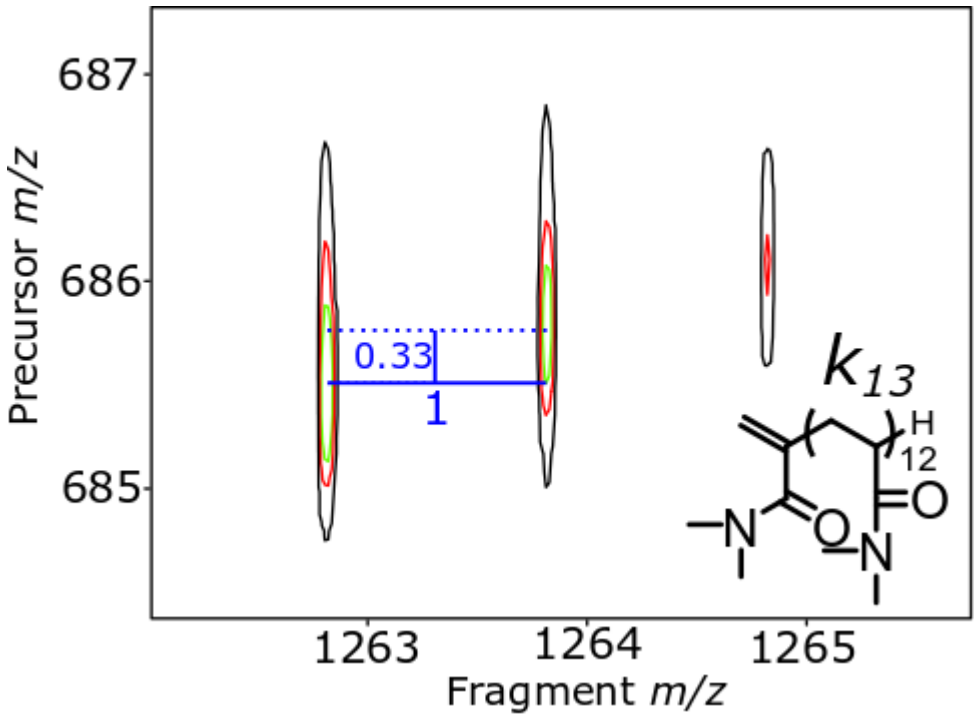

Figure 8.18 k_{12} Fragment isotope envelope. The fragment here can be seen to be a singly charged (*x*-dimension spacing of *m/z* 1) from a triply charged precursor (*y*-dimension spacing of *m/z* 1/3) Giving a gradient of 1/3 for the isotopic envelope.

Another fragment which can be compared is a doubly charged fragment from a quadruply charged precursor. The corresponding gradient between isotopes is 0.5 as the spacing in the *x*-axis is *m/z* 0.5 and the spacing in the *y*-dimension is 0.25. A noticeable effect of the larger fragment ion is the shift in the isotope envelope so higher mass isotopes are more intense.

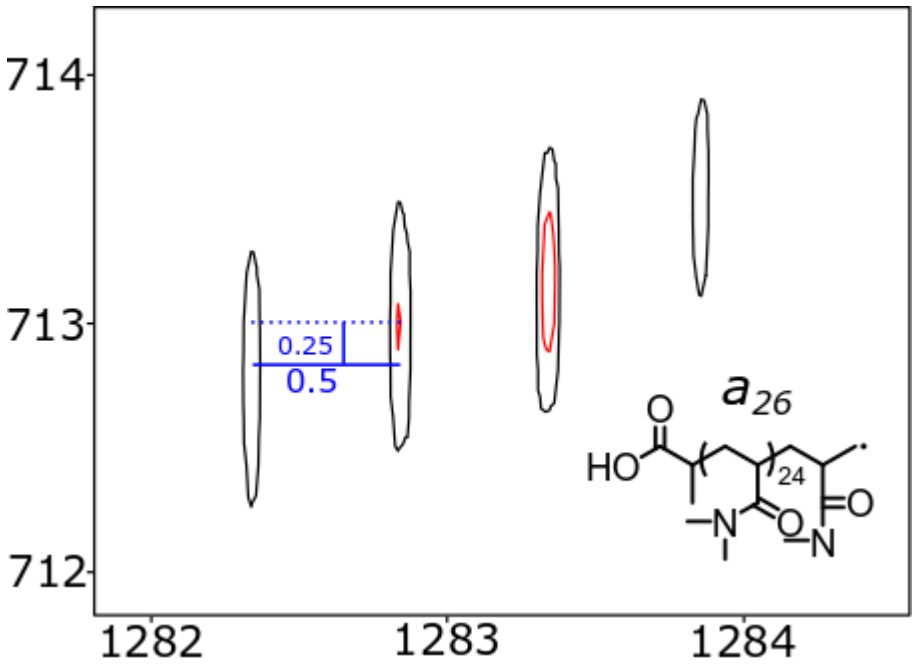

Figure 8.19 a_{26} Fragment isotope envelope. The fragment here can be seen to be doubly charged (*x*-dimension spacing of *m/z* 0.5) from a quadruply charged precursor (*y*-dimension spacing of *m/z* 0.25) Giving a gradient of 0.5 for the isotopic envelope.

Vertical line extraction of the k_3 peak can be carried out and shows the large number of precursors that can be assigned to a fragment. The k_3 fragment line was extracted through a vertical line at *m/z* 298.2125. The corresponding precursors and their relative intensities of generating that fragment can be seen clearly in Figure 8.20 showing precursors present at 19-29 monomer units.

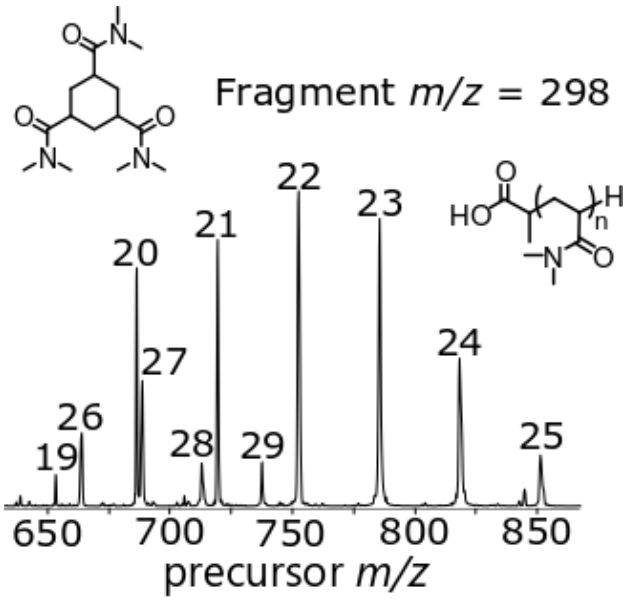

Figure 8.20 Precursor line of the k_3 fragment ion showing coverage from n=19-29 monomer units with the 2DMS experiment. The numbers atop the peaks represent the number of monomer units in that polymeric species.

8.4.3. Further 2D development – UVPD fragmentation

Developing further 2DMS fragmentation methods is important to increase the utility of 2DMS methods. UVPD methods have been shown in this thesis to offer an alternative, and often complementary fragmentation mechanism to ECD.

The development of further fragmentation methods required tuning of the radially resolved pulse program. By adjusting the positioning of the ions within the FT-ICR cell the fragmentation region of the UV laser can be defined. The modulation of the ionic radii should be as close to sinusoidal as possible to maximise the Fourier transform response. The fragmentation also needs to be sinusoidal within the variation of radius of the ion movement.

The UVPD laser produces a well-defined fragmentation zone at the centre of the ICR cell. By exciting the ions out using a low powered chirp pulse followed by the fragmentation event and then the usual excite/detect pulse the radius dependency of the fragmentation can be observed. For the use in 2DMS there is a significant advantage that the radius of the ions after excitation is independent to the *m/z* of the ion being excited. As the *m/z* is independent of the ion radius, the same sinusoidal relationships of the pulse sequence correspond to all the ions within the cell.

$$E(\nu) = E_0 \frac{\sin(2\pi\nu_c T_{excite})}{2\pi\nu_c}$$

Equation 8.1: Relationship between the ion energy (E_v) during a broadband chirp excitation, the final radius of the ion is based on the energy of excitation E_0 and the excitation time T_{excite}.

The pulse sequence used for mapping the fragmentation region is shown in Figure 8.21. With a low amplitude P_1 pulse the ion will stay close to the centre of the cell, at high P_1 energies the ion will be excited out of the fragmentation zone.

Exciting the ion to the point that no fragmentation occurs means the sinusoidal relationship can be diminished between the precursor and fragment generation, leading to flat tpped, or clipped sine waves. Clipped sine waves produce multiple data points where the modulation of the precursor and fragment intensity will not correlate, causing excessive harmonics in the data set.

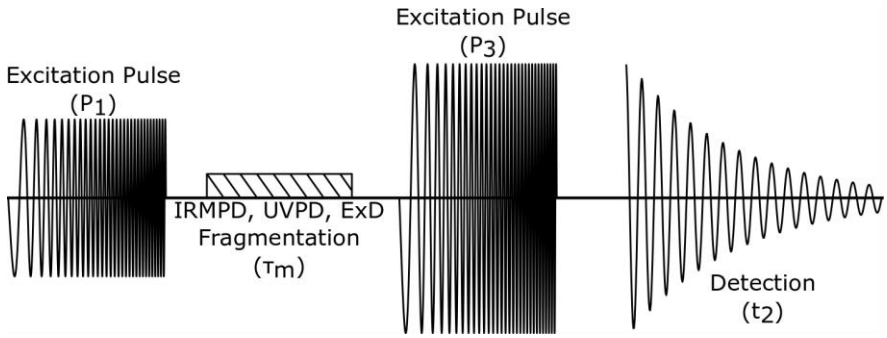

Figure 8.21 Simplified pulse sequence used for the analysis of a fragmentation region. A single pulse is used to excite the ions into a higher radius before fragmentation occurs.

As a precursor ion is excited further out of the fragmentation region it will undergo less fragmentation and therefore have lower intensity fragment ions. Plotting the sweep excitation power against the fragmentation efficiency allows characterisation of the fragmentation region. Figure 8.22 shows the Fragmentation map of the 193 nm Excimer laser. The fragmentation efficiency in the centre of the cell for the peptide LUENK corresponds to approximately 3% fragmentation efficiency, exciting the ion to higher radii causes a drop in fragmentation efficiency until a fragment efficiency of less than 0.1 % by 80 $V_{p\text{-}p}$.

$$V_{p-p} = SP\% \times 5\ V$$

Equation 8.2: The Voltage power is the sweep excitation power (SP) multiplied by five volts on SolariX hardware.

The fragmentation efficiency chosen was that at approximately 0.4% fragment efficiency. Corresponding to 15% of the original fragment intensity, so the ions within a 2DMS experiment would be modulated between 100% and 10% of the maximum possible fragmentation efficiency. The 10% value is chosen to reduce the possibility of harmonic formation as well as maximising the amplitude in the second modulation dimension.

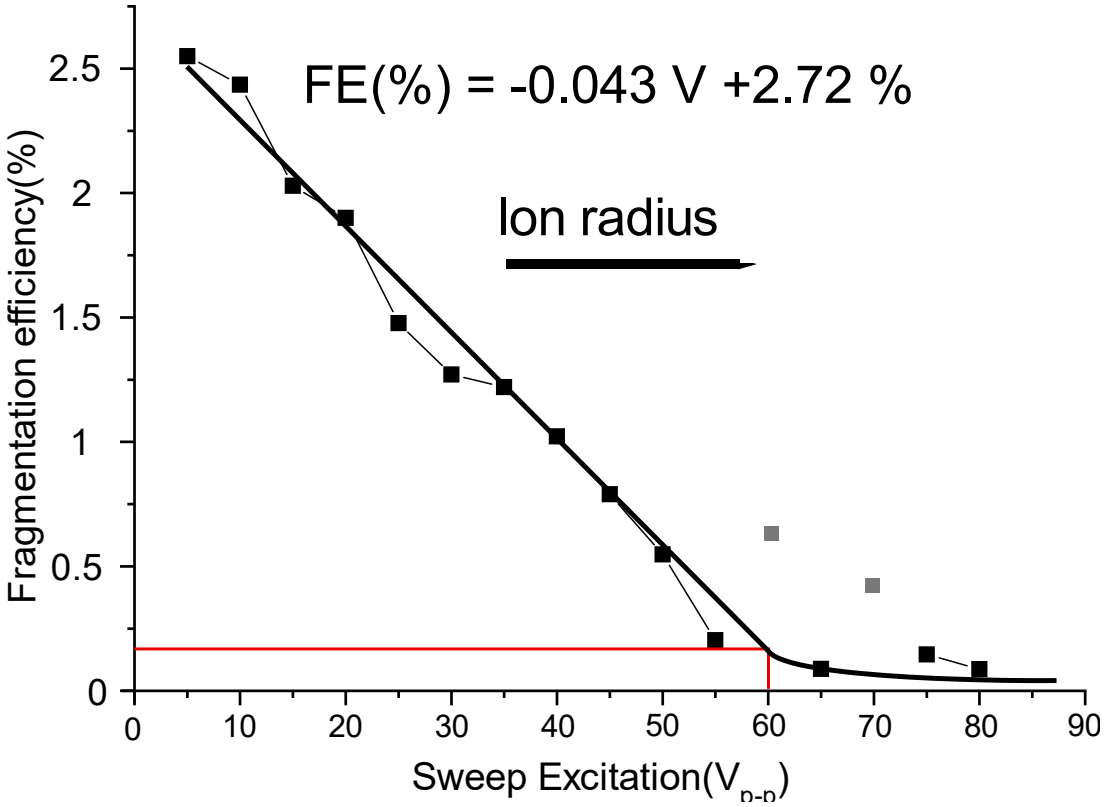

Figure 8.22 Fragmentation map of a 193 nm Excimer laser shot. The sweep excitation power is proportional to the ion radius of the ion. The red line represents 10% fragmentation efficiency and is used as the P_1 and P_2 power level in the 2DMS experiment.

The corresponding V_{p-p} value calculated in the optimisation experiment is based on the radius of the ion after a single excitation pulse. As two excitation pulses are used in the 2DMS experiment to radially separate the ions the experimental V_{p-p} used is half of the value calculated in the optimisation experiment. As the measured value here was 60 V_{p-p} the optimal value for the 2DMS experiment should be 30 V_{p-p}.

The experimental value of 30 V_{p-p} was taken for the following LEUENK 2DMS experiment. The LEUENK ion present at *m/z* 556.2766 can be seen to have multiple fragments at the same precursor *y*-axis the fragments represent sequence fragments as well as some internal fragmentation.

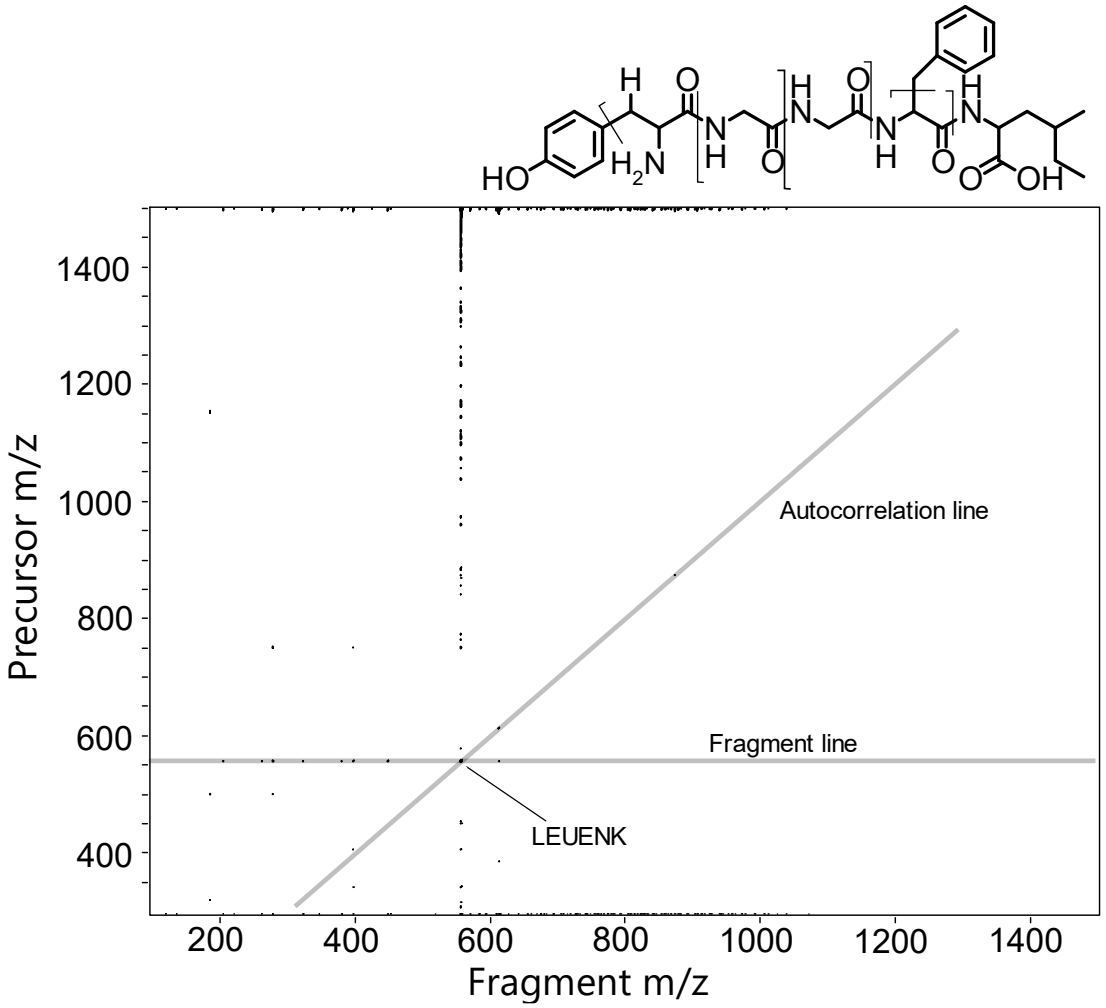

Figure 8.23 2DMS of the LEUENK peptide, showing that UVPD tuned to the previous optimisation setting can successfully produce a 2DMS spectrum with good fragment coverage.

Figure 8.23 shows high scintillation noise, scintillation noise is probably caused by the low fragmentation efficiency of the UVPD method causing a weak intensity change in the *y*-axis, although the intensity change is good enough to produce a good 2DMS spectrum.

Figure 8.23 shows the alignment of the fragments in 2DMS to the extracted fragment spectrum. The loss of a hydrogen atom is common in UVPD analysis as the electron excitation can generate radicals.

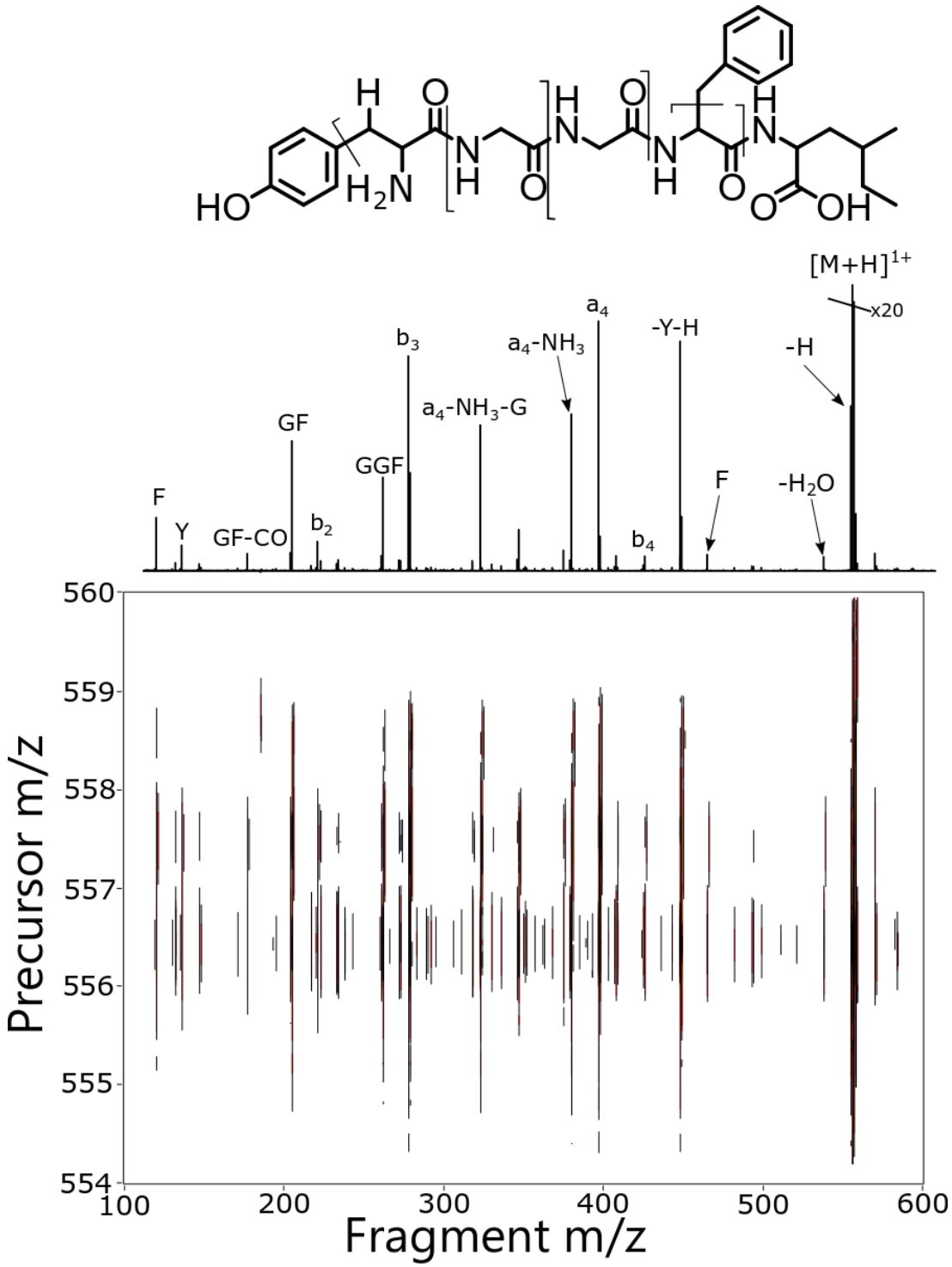

Figure 8.24 2DMS of the LEUENK peptide zoomed onto the fragment region and the corresponding fragment spectrum extracted of the LEUENK peptide precursor ion.

Analysis of LEUENK 2DMS spectrum shows that the use of UVPD as an alternative to ECD for 2DMS analysis is possible and effective. UVPD has been shown in previous chapters to successfully analyse polymers, as well as being extensively used in previous studies for the analysis of biological species. The ability to use UVPD for 2DMS experiments also gives the ability to use 2DMS methods on further mass spectrometry systems as UVPD becomes more ubiquitously used.

The ability to use ECD, UVPD, and IRMPD methods for 2DMS analysis offers a variety of different fragmentation available and therefore many different species that are possible to be analysed by 2DMS methods.

8.5. Conclusions

The analysis of various polymers by ECD 2DMS shows the potential of 2DMS to carry out extremely specific tandem mass spectrometry analysis across the entirety of a polymer dispersity. The ability to carry out analysis across a polymer dispersity offers an advantage of reducing the overall experimentation time compared to traditional quadrupole isolation methods as well as offering a higher resolving power or differentiation of precursor ions from one another, meaning complex polymer blends or copolymers may be analysed on an individual chain length/end group basis.

Introducing further fragmentation methods also offers means in which more species may be analysed by 2DMS methods. UVPD is seeing increased usage for the analysis of a range of biological species so the initial investigation into UVPD 2DMS presented here offers a large increased in 2DMS utility.

The ability to extract precursor lines also gives the ability for diagnostic fragments to be matched to all of their corresponding precursors in one experimental plot. In the future, the use of precursor lines to quickly identify all the polymers with matching end groups could be an incredibly effective tool for the analysis of peptide- and protein- polymer conjugates.

8.6. References

(1) Pelegri-O'Day, E. M.; Lin, E. W.; Maynard, H. D. Therapeutic protein-polymer conjugates: advancing beyond PEGylation *J. Am. Chem. Soc.* **2014**, *136*, 14323-14332.

(2) Qi, Y.; Chilkoti, A. Protein-polymer conjugation-moving beyond PEGylation *Curr. Opin. Chem. Biol.* **2015**, *28*, 181-193.

(3) Hartlieb, M.; Floyd, T.; Cook, A. B.; Sanchez-Cano, C.; Catrouillet, S.; Burns, J. A.; Perrier, S. Well-defined hyperstar copolymers based on a thiol–yne hyperbranched core and a poly(2-oxazoline) shell for biomedical applications *Polymer Chemistry* **2017**, *8*, 2041-2054.

(4) Rudolph, T.; von der Luhe, M.; Hartlieb, M.; Norsic, S.; Schubert, U. S.; Boisson, C.; D'Agosto, F.; Schacher, F. H. Toward Anisotropic Hybrid Materials: Directional Crystallization of Amphiphilic Polyoxazoline-Based Triblock Terpolymers *ACS Nano* **2015**, *9*, 10085-10098.

(5) Dworak, A.; Trzebicka, B.; Kowalczuk, A.; Tsvetanov, C.; Rangelov, S. Polyoxazolines — mechanism of synthesis and solution properties *Polimery* **2014**, *59*, 88-94.

(6) Crotty, S.; Gerislioglu, S.; Endres, K. J.; Wesdemiotis, C.; Schubert, U. S. Polymer architectures via mass spectrometry and hyphenated techniques: A review *Anal. Chim. Acta* **2016**, *932*, 1-21.

(7) Hart-Smith, G. A review of electron-capture and electron-transfer dissociation tandem mass spectrometry in polymer chemistry *Anal. Chim. Acta* **2014**, *808*, 44-55.

(8) Altuntaş, E.; Schubert, U. S. "Polymeromics": Mass spectrometry based strategies in polymer science toward complete sequencing approaches: a review *Anal. Chim. Acta* **2014**, *808*, 56-69.

(9) Altuntaş, E.; Knop, K.; Tauhardt, L.; Kempe, K.; Crecelius, A. C.; Jager, M.; Hager, M. D.; Schubert, U. S. Tandem mass spectrometry of poly(ethylene imine)s by electrospray ionization (ESI) and matrix-assisted laser desorption/ionization (MALDI) *J. Mass Spectrom.* **2012**, *47*, 105-114.

(10) Altuntaş, E.; Krieg, A.; Baumgaertel, A.; Crecelius, A. C.; Schubert, U. S. ESI, APCI, and MALDI tandem mass spectrometry of poly(methyl acrylate)s: A comparison study for the structural characterization of polymers synthesized via CRP techniques and the software application to analyze MS/MS data *J. Polym. Sci., Part A: Polym. Chem.* **2013**, *51*, 1595-1605.

(11) Baumgaertel, A.; Scheubert, K.; Pietsch, B.; Kempe, K.; Crecelius, A. C.; Bocker, S.; Schubert, U. S. Analysis of different synthetic homopolymers by the use of a new calculation software for tandem mass spectra *Rapid Commun. Mass Spectrom.* **2011**, *25*, 1765-1778.

(12) Crecelius, A. C.; Baumgaertel, A.; Schubert, U. S. Tandem mass spectrometry of synthetic polymers *J. Mass Spectrom.* **2009**, *44*, 1277-1286.

(13) Crecelius, A. C.; Vitz, J.; Schubert, U. S. Mass spectrometric imaging of synthetic polymers *Anal. Chim. Acta* **2014**, *808*, 10-17.

(14) Altuntaş, E.; Weber, C.; Kempe, K.; Schubert, U. S. Comparison of ESI, APCI and MALDI for the (tandem) mass analysis of poly(2-ethyl-2-oxazoline)s with various end-groups *Eur. Polym. J.* **2013**, *49*, 2172-2185.

(15) Altuntaş, E.; Weber, C.; Schubert, U. S. Detailed characterization of poly(2-ethyl-2oxazoline)s by energy variable collision-induced dissociation study *Rapid Commun. Mass Spectrom.* **2013**, *27*, 1095-1100.

(16) Baumgaertel, A.; Weber, C.; Knop, K.; Crecelius, A.; Schubert, U. S. Characterization of different poly(2-ethyl-2-oxazoline)s via matrix-assisted laser desorption/ionization time-of-flight tandem mass spectrometry *Rapid Commun. Mass Spectrom.* **2009**, *23*, 756-762.

(17) Tureček, F. N-C alpha Bond Dissociation Energies and Kinetics in Amide and Peptide Radicals. Is the Dissociation a Non-ergodic Process? *J. Am. Chem. Soc.* **2003**, *125*, 5954-5963.
(18) Qi, Y.; Volmer, D. A. Electron-based fragmentation methods in mass spectrometry: An overview *Mass Spectrom. Rev.* **2017**, *36*, 4-15.
(19) Pfandler, P.; Bodenhausen, G.; Rapin, J.; Houriet, R.; Gaumann, T. Two-dimensional Fourier transform ion cyclotron resonance mass spectrometry *Chem. Phys. Lett.* **1987**, *138*, 195-200.
(20) Pfandler, P.; Bodenhausen, G.; Rapin, J.; Walser, M.; Gaumann, T. Broad-Band Two-Dimensional Fourier Transform Ion Cyclotron Resonance *J. Am. Chem. Soc.* **1988**, *110*, 5628-2633.
(21) van Agthoven, M. A.; Delsuc, M. A.; Bodenhausen, G.; Rolando, C. Towards analytically useful two-dimensional Fourier transform ion cyclotron resonance mass spectrometry *Anal. Bioanal. Chem.* **2013**, *405*, 51-61.
(22) Tsybin, Y. O.; Witt, M.; Baykut, G.; Kjeldsen, F.; Hakansson, P. Combined infrared multiphoton dissociation and electron capture dissociation with a hollow electron beam in Fourier transform ion cyclotron resonance mass spectrometry *Rapid Commun. Mass Spectrom.* **2003**, *17*, 1759-1768.
(23) Floris, F.; Chiron, L.; Lynch, A. M.; Barrow, M. P.; Delsuc, M. A.; O'Connor, P. B. Top-Down Deep Sequencing of Ubiquitin Using Two-Dimensional Mass Spectrometry *Anal. Chem.* **2018**, *90*, 7302-7309.
(24) Floris, F.; Chiron, L.; Lynch, A. M.; Barrow, M. P.; Delsuc, M. A.; O'Connor, P. B. Application of Tandem Two-Dimensional Mass Spectrometry for Top-Down Deep Sequencing of Calmodulin *J. Am. Soc. Mass. Spectrom.* **2018**, *29*, 1700-1705.
(25) Floris, F.; Vallotto, C.; Chiron, L.; Lynch, A. M.; Barrow, M. P.; Delsuc, M. A.; O'Connor, P. B. Polymer Analysis in the Second Dimension: Preliminary Studies for the Characterization of Polymers with 2D MS *Anal. Chem.* **2017**, *89*, 9892-9899.
(26) Floris, F.; van Agthoven, M.; Chiron, L.; Soulby, A. J.; Wootton, C. A.; Lam, Y. P.; Barrow, M. P.; Delsuc, M. A.; O'Connor, P. B. 2D FT-ICR MS of Calmodulin: A Top-Down and Bottom-Up Approach *J. Am. Soc. Mass. Spectrom.* **2016**, *27*, 1531-1538.
(27) Floris, F.; van Agthoven, M. A.; Chiron, L.; Wootton, C. A.; Lam, P. Y. Y.; Barrow, M. P.; Delsuc, M. A.; O'Connor, P. B. Bottom-Up Two-Dimensional Electron-Capture Dissociation Mass Spectrometry of Calmodulin *J. Am. Soc. Mass. Spectrom.* **2018**, *29*, 207-210.
(28) Simon, H. J.; van Agthoven, M. A.; Lam, P. Y.; Floris, F.; Chiron, L.; Delsuc, M. A.; Rolando, C.; Barrow, M. P.; O'Connor, P. B. Uncoiling collagen: a multidimensional mass spectrometry study *Analyst* **2016**, *141*, 157-165.
(29) van Agthoven, M. A.; Lynch, A. M.; Morgan, T. E.; Wootton, C. A.; Lam, Y. P. Y.; Chiron, L.; Barrow, M. P.; Delsuc, M. A.; O'Connor, P. B. Can Two-Dimensional IR-ECD Mass Spectrometry Improve Peptide de Novo Sequencing? *Anal. Chem.* **2018**, *90*, 3496-3504.
(30) van Agthoven, M. A.; Chiron, L.; Coutouly, M. A.; Delsuc, M. A.; Rolando, C. Two-dimensional ECD FT-ICR mass spectrometry of peptides and glycopeptides *Anal. Chem.* **2012**, *84*, 5589-5595.
(31) van Agthoven, M. A.; Wootton, C. A.; Chiron, L.; Coutouly, M. A.; Soulby, A.; Wei, J.; Barrow, M. P.; Delsuc, M. A.; Rolando, C.; O'Connor, P. B. Two-Dimensional Mass Spectrometry for Proteomics, a Comparative Study with Cytochrome c *Anal. Chem.* **2016**, *88*, 4409-4417.
(32) Kendrick, E. A Mass Scale Based on CH2=: 14.0000 for High Resolution Mass Spectrometry of Organic Compounds *Anal. Chem.* **1963**, *35*, 2146-2154.
(33) Hsu, C. S.; Qian, K.; Chen, Y. C. An innovative approach to data analysis in hydrocarbon characterization by on-line liquid chromatography-mass spectrometry *Anal. Chim. Acta* **1992**, *264*, 79-89.

(34) Qi, Y.; Hempelmann, R.; Volmer, D. A. Two-dimensional mass defect matrix plots for mapping genealogical links in mixtures of lignin depolymerisation products *Anal. Bioanal. Chem.* **2016**, *408*, 4835-4843.
(35) Fouquet, T.; Sato, H. Extension of the Kendrick Mass Defect Analysis of Homopolymers to Low Resolution and High Mass Range Mass Spectra Using Fractional Base Units *Anal. Chem.* **2017**, *89*, 2682-2686.
(36) Fouquet, T.; Cody, R. B.; Sato, H. Capabilities of the remainders of nominal Kendrick masses and the referenced Kendrick mass defects for copolymer ions *J. Mass Spectrom.* **2017**, *52*, 618-624.
(37) Fouquet, T.; Nakamura, S.; Sato, H. MALDI SpiralTOF high-resolution mass spectrometry and Kendrick mass defect analysis applied to the characterization of poly(ethylene-co-vinyl acetate) copolymers *Rapid Commun. Mass Spectrom.* **2016**, *30*, 973-981.
(38) Fouquet, T.; Shimada, H.; Maeno, K.; Ito, K.; Ozeki, Y.; Kitagawa, S.; Ohtani, H.; Sato, H. High-resolution Kendrick Mass Defect Analysis of Poly(ethylene oxide)-based Non-ionic Surfactants and Their Degradation Products *J. Oleo Sci.* **2017**, *66*, 1061-1072.
(39) Fouquet, T. N. J.; Cody, R. B.; Ozeki, Y.; Kitagawa, S.; Ohtani, H.; Sato, H. On the Kendrick Mass Defect Plots of Multiply Charged Polymer Ions: Splits, Misalignments, and How to Correct Them *J. Am. Soc. Mass. Spectrom.* **2018**, *29*, 1611-1626.
(40) Morgan, T. E.; Ellacott, S. H.; Wootton, C. A.; Barrow, M. P.; Bristow, A. W. T.; Perrier, S.; O'Connor, P. B. Coupling Electron Capture Dissociation and the Modified Kendrick Mass Defect for Sequencing of a Poly(2-ethyl-2-oxazoline) Polymer *Anal. Chem.* **2018**, *90*, 11710-11715.
(41) Chiron, L.; Coutouly, M. A.; Starck, J.-P.; Rolando, C.; Delsuc, M. A. SPIKE a Processing software dedicated to Fourier Spectroscopies *arXiv:1608.06777v1* **2016**, *[physics.comp-ph]*.

SUPPORTING INFORMATION

to

Two-dimensional mass spectrometry analysis of polymers and future two-dimensional methods

by

Tomos E. Morgan[1], Christopher A. Wootton[1], Maria van Agthoven[1], Alina Theisen[1], Anisha Haris[1], Sean Ellacott[1,] Andrew Kerr, Thomas Floyd, Mark P. Barrow[1], Anthony W. T. Bristow[2], Sébastien Perrier[1], Peter B. O'Connor[1]

[1]Department of Chemistry, University of Warwick, Coventry, Midlands, CV4 7AL, UK.

[2]Chemical Development, Pharmaceutical Technology & Development, Operations, AstraZeneca, Macclesfield, UK.

*Corresponding authors: Peter O'Connor [redacted]

Table S 8.1: Mass spectrometry assignments of the p(Ox_{23}) polymer fragment line, Figure 8.8 in main text

m/z	charge	chemical formula	error	*assignment*
286.2125	1	$C_{14}H_{27}N_3O_3H^+_1$	0.01	a_3
385.2809	1	$C_{19}H_{36}N_4O_4H^+_1$	-0.01	a_4
484.3488	1	$C_{24}H_{45}N_5O_5H^+_1$	-1.13	a_5
583.4178	1	$C_{29}H_{54}N_6O_6H^+_1$	0.03	a_6
682.486	1	$C_{34}H_{63}N_7O_7H^+_1$	-0.20	a_7
781.5534	1	$C_{39}H_{72}N_8O_8H^+_1$	-1.57	a_8
880.623	1	$C_{44}H_{81}N_9O_9H^+_1$	0.04	a_9
979.6926	1	$C_{49}H_{90}N_{10}O_{10}H^+_1$	1.21	a_{10}
1078.761	1	$C_{54}H_{99}N_{11}O_{11}H^+_1$	0.81	a_{11}
1177.829	1	$C_{59}H_{108}N_{12}O_{12}H^+_1$	0.68	a_{12}
1276.898	1	$C_{64}H_{117}N_{13}O_{13}H^+_1$	0.66	a_{13}
1375.965	1	$C_{69}H_{126}N_{14}O_{14}H^+_1$	0.07	a_{14}
1475.036	1	$C_{74}H_{135}N_{15}O_{15}H^+_1$	1.46	a_{15}
1574.102	1	$C_{79}H_{144}N_{16}O_{16}H^+_1$	-0.25	a_{16}
1673.172	1	$C_{84}H_{153}N_{17}O_{17}H^+_1$	1.13	a_{17}
1772.239	1	$C_{89}H_{162}N_{18}O_{18}H^+_1$	0.13	a_{18}
1871.308	1	$C_{94}H_{171}N_{19}O_{19}H^+_1$	0.54	a_{19}
1970.377	1	$C_{99}H_{180}N_{20}O_{20}H^+_1$	0.83	a_{20}
2069.444	1	$C_{104}H_{189}N_{21}O_{21}H^+_1$	0.05	a_{21}
2168.519	1	$C_{109}H_{198}N_{22}O_{22}H^+_1$	3.20	a_{22}
321.1303	1	$C_{13}H_{24}N_2O_3S_2H^+_1$	0.56	x_2
420.1986	1	$C_{18}H_{33}N_3O_4S_2H^+_1$	0.08	x_3
519.2669	1	$C_{23}H_{42}N_4O_5S_2H^+_1$	-0.02	x_4
618.3349	1	$C_{28}H_{51}N_5O_6S_2H^+_1$	-0.73	x_5
717.403	1	$C_{33}H_{60}N_6O_7S_2H^+_1$	-1.03	x_6
816.4716	1	$C_{38}H_{69}N_7O_8S_2H^+_1$	-0.75	x_7
915.5417	1	$C_{43}H_{78}N_8O_9S_2H^+_1$	1.21	x_8
1014.608	1	$C_{48}H_{87}N_9O_{10}S_2H^+_1$	-0.66	x_9
1113.68	1	$C_{53}H_{96}N_{10}O_{11}S_2H^+_1$	1.95	x_{10}
1212.749	1	$C_{58}H_{105}N_{11}O_{12}S_2H^+_1$	2.87	x_{11}
1311.815	1	$C_{63}H_{114}N_{12}O_{13}S_2H^+_1$	0.24	x_{12}
1410.884	1	$C_{68}H_{123}N_{13}O_{14}S_2H^+_1$	0.61	x_{13}
1509.952	1	$C_{73}H_{132}N_{14}O_{15}S_2H^+_1$	0.43	x_{14}
1609.02	1	$C_{78}H_{141}N_{15}O_{16}S_2H^+_1$	0.28	x_{15}
1708.088	1	$C_{83}H_{150}N_{16}O_{17}S_2H^+_1$	-0.08	x_{16}
1807.159	1	$C_{88}H_{159}N_{17}O_{18}S_2H^+_1$	1.32	x_{17}
1906.22	1	$C_{93}H_{168}N_{18}O_{19}S_2H^+_1$	-2.64	x_{18}
2005.294	1	$C_{98}H_{177}N_{19}O_{20}S_2H^+_1$	0.21	x_{19}
2104.366	1	$C_{103}H_{186}N_{20}O_{21}S_2H^+_1$	2.00	x_{20}
2203.429	1	$C_{108}H_{195}N_{21}O_{22}S_2H^+_1$	-0.47	x_{21}
		Average	0.80	
		Standard Deviation	1.09	

Table S 8.2: Mass spectrometry assignments of the p(Ox_{23}) polymer fragment line, Figure 8.9 in main text

m/z	charge	ppm error	loss
805.86428	3		
1208.29264	2	-1.61	$H^{\bullet}$
1199.79356	2	0.28	H_2O
1194.28029	2	1.13	$C_2H_5^{\bullet}$
1180.2826	2	0.95	$C_3H_5O^{\bullet}$
1164.29645	2	0.86	$C_6H_{12}NO^{\bullet}$
1151.75383	2	1.10	a_{23}
1134.29483	2	1.10	x_{23}
1102.21948	2	1.02	a_{22}
1084.76089	2	1.23	x_{22}

Table S 8.3: Mass spectrometry assignments of the p(Ox_{20}) polymer fragment line, Figure 8.12 in main text

m/z	charge	chemical formula	error	assignment
286.2125	1	$C_{14}H_{27}N_3O_3S_0H^+_1$	-0.06	a_2
385.28093	1	$C_{19}H_{36}N_4O_4S_0H^+_1$	-0.01	a_3
484.34881	1	$C_{24}H_{45}N_5O_5S_0H^+_1$	-1.11	a_4
583.41778	1	$C_{29}H_{54}N_6O_6S_0H^+_1$	0.03	a_5
682.48604	1	$C_{34}H_{63}N_7O_7S_0H^+_1$	-0.20	a_6
781.55333	1	$C_{39}H_{72}N_8O_8S_0H^+_1$	-1.61	a_7
880.62299	1	$C_{44}H_{81}N_9O_9S_0H^+_1$	-0.01	a_8
979.69252	1	$C_{49}H_{90}N_{10}O_{10}S_0H^+_1$	1.13	a_9
1078.76058	1	$C_{54}H_{99}N_{11}O_{11}S_0H^+_1$	0.70	a_{10}
1177.82887	1	$C_{59}H_{108}N_{12}O_{12}S_0H^+_1$	0.53	a_{11}
1276.89726	1	$C_{64}H_{117}N_{13}O_{13}S_0H^+_1$	0.47	a_{12}
1375.96485	1	$C_{69}H_{126}N_{14}O_{14}S_0H^+_1$	-0.16	a_{13}
1475.03525	1	$C_{74}H_{135}N_{15}O_{15}S_0H^+_1$	1.20	a_{14}
1574.10103	1	$C_{79}H_{144}N_{16}O_{16}S_0H^+_1$	-0.55	a_{15}
1673.17163	1	$C_{84}H_{153}N_{17}O_{17}S_0H^+_1$	0.79	a_{16}
1772.23828	1	$C_{89}H_{162}N_{18}O_{18}S_0H^+_1$	-0.25	a_{17}
1871.30736	1	$C_{94}H_{171}N_{19}O_{19}S_0H^+_1$	0.12	a_{18}
1970.37628	1	$C_{99}H_{180}N_{20}O_{20}S_0H^+_1$	0.37	a_{19}
2069.44302	1	$C_{104}H_{189}N_{21}O_{21}S_0H^+_1$	-0.46	a_{20}
2168.51814	1	$C_{109}H_{198}N_{22}O_{22}S_0H^+_1$	2.66	a_{21}
321.13028	1	$C_{13}H_{24}N_2O_3S_2H^+_1$	0.53	x_2
420.19857	1	$C_{18}H_{33}N_3O_4S_2H^+_1$	0.11	x_3
519.26694	1	$C_{23}H_{42}N_4O_5S_2H^+_1$	0.00	x_4
618.3349	1	$C_{28}H_{51}N_5O_6S_2H^+_1$	-0.73	x_5
717.40302	1	$C_{33}H_{60}N_6O_7S_2H^+_1$	-1.04	x_6
816.47154	1	$C_{38}H_{69}N_7O_8S_2H^+_1$	-0.78	x_7
915.54165	1	$C_{43}H_{78}N_8O_9S_2H^+_1$	1.15	x_8
1014.60824	1	$C_{48}H_{87}N_9O_{10}S_2H^+_1$	-0.76	x_9
1113.67944	1	$C_{53}H_{96}N_{10}O_{11}S_2H^+_1$	1.81	x_{10}
1212.74912	1	$C_{58}H_{105}N_{11}O_{12}S_2H^+_1$	2.71	x_{11}
1311.8143	1	$C_{63}H_{114}N_{12}O_{13}S_2H^+_1$	0.04	x_{12}
1410.88318	1	$C_{68}H_{123}N_{13}O_{14}S_2H^+_1$	0.37	x_{13}
1509.95131	1	$C_{73}H_{132}N_{14}O_{15}S_2H^+_1$	0.15	x_{14}
1609.01944	1	$C_{78}H_{141}N_{15}O_{16}S_2H^+_1$	-0.03	x_{15}
1708.08716	1	$C_{83}H_{150}N_{16}O_{17}S_2H^+_1$	-0.44	x_{16}
1807.15799	1	$C_{88}H_{159}N_{17}O_{18}S_2H^+_1$	0.92	x_{17}
1906.21886	1	$C_{93}H_{168}N_{18}O_{19}S_2H^+_1$	-3.08	x_{18}
2005.29261	1	$C_{98}H_{177}N_{19}O_{20}S_2H^+_1$	-0.27	x_{19}
2104.36468	1	$C_{103}H_{186}N_{20}O_{21}S_2H^+_1$	1.48	x_{20}
2203.4277	1	$C_{108}H_{195}N_{21}O_{22}S_2H^+_1$	-1.03	x_{21}
		Averages	0.75	
		Standard Deviation	1.05	

Table S 8.4: Mass spectrometry assignments of the p(Ox_{25}) polymer fragment line, Figure 8.12B in main text

m/z	charge	chemical formula	error	assignment
187.14386	1	$C_9H_{18}N_2O_2S_0H^+_1$	-1.31	a2
286.21252	1	$C_{14}H_{27}N_3O_3S_0H^+_1$	0.01	a3
385.28038	1	$C_{19}H_{36}N_4O_4S_0H^+_1$	-1.43	a4
484.34917	1	$C_{24}H_{45}N_5O_5S_0H^+_1$	-0.36	a5
583.41928	1	$C_{29}H_{54}N_6O_6S_0H^+_1$	2.61	a6
682.48617	1	$C_{34}H_{63}N_7O_7S_0H^+_1$	-0.01	a7
781.55504	1	$C_{39}H_{72}N_8O_8S_0H^+_1$	0.58	a8
880.62361	1	$C_{44}H_{81}N_9O_9S_0H^+_1$	0.69	a9
979.69234	1	$C_{49}H_{90}N_{10}O_{10}S_0H^+_1$	0.94	a10
1177.82803	1	$C_{59}H_{108}N_{12}O_{12}S_0H^+_1$	-0.18	a11
1276.89627	1	$C_{64}H_{117}N_{13}O_{13}S_0H^+_1$	-0.30	a12
1375.96527	1	$C_{69}H_{126}N_{14}O_{14}S_0H^+_1$	0.14	a13
1475.03364	1	$C_{74}H_{135}N_{15}O_{15}S_0H^+_1$	0.10	a14
1574.10233	1	$C_{79}H_{144}N_{16}O_{16}S_0H^+_1$	0.27	a15
1673.17039	1	$C_{84}H_{153}N_{17}O_{17}S_0H^+_1$	0.05	a16
1772.23646	1	$C_{89}H_{162}N_{18}O_{18}S_0H^+_1$	-1.28	a17
1871.30274	1	$C_{94}H_{171}N_{19}O_{19}S_0H^+_1$	-2.35	a18
1970.37137	1	$C_{99}H_{180}N_{20}O_{20}S_0H^+_1$	-2.12	a19
321.12976	1	$C_{13}H_{24}N_2O_3S_2H^+_1$	-1.09	x2
420.1985	1	$C_{18}H_{33}N_3O_4S_2H^+_1$	-0.06	x3
519.26671	1	$C_{23}H_{42}N_4O_5S_2H^+_1$	-0.44	x4
618.3365	1	$C_{28}H_{51}N_5O_6S_2H^+_1$	1.86	x5
717.40371	1	$C_{33}H_{60}N_6O_7S_2H^+_1$	-0.08	x6
816.4703	1	$C_{38}H_{69}N_7O_8S_2H^+_1$	-2.30	x7
915.54164	1	$C_{43}H_{78}N_8O_9S_2H^+_1$	1.14	x8
1014.61055	1	$C_{48}H_{87}N_9O_{10}S_2H^+_1$	1.52	x9
1113.67892	1	$C_{53}H_{96}N_{10}O_{11}S_2H^+_1$	1.34	x10
1212.74547	1	$C_{58}H_{105}N_{11}O_{12}S_2H^+_1$	-0.30	x11
1311.81184	1	$C_{63}H_{114}N_{12}O_{13}S_2H^+_1$	-1.84	x12
1410.88232	1	$C_{68}H_{123}N_{13}O_{14}S_2H^+_1$	-0.24	x13
1509.95037	1	$C_{73}H_{132}N_{14}O_{15}S_2H^+_1$	-0.47	x14
1609.01601	1	$C_{78}H_{141}N_{15}O_{16}S_2H^+_1$	-2.16	x15
1708.0847	1	$C_{83}H_{150}N_{16}O_{17}S_2H^+_1$	-1.88	x16
1807.15533	1	$C_{88}H_{159}N_{17}O_{18}S_2H^+_1$	-0.55	x17
1906.21815	1	$C_{93}H_{168}N_{18}O_{19}S_2H^+_1$	-3.45	x18
2005.29268	1	$C_{98}H_{177}N_{19}O_{20}S_2H^+_1$	-0.23	x19
		Average	0.99	
		Standard Deviation	1.28	

Table S 8.5: Mass spectrometry assignments of the H-terminated p(Ox) polymer fragment line, Figure 8.14 in main text

m/z	charge	loss	error
801.19347	3		
1193.28683	2	$H^{\bullet}$	-2.08
1187.27058	2	$CH_3^{\bullet}$	-0.45
1173.27314	2	H_2O	-0.44
1157.28703	2	$C_3H_5O^{\bullet}$	-0.51
1127.79022	2	$C_5H_9OS_2$	0.33
1102.72245	2	$C_{10}H_{18}N_2O_2$	0.17
1077.752	2	$C_{10}H_{18}NO_2S_2$	0.25

Table S 8.6: Mass spectrometry assignments of the polyacrylamide species Figure 8.17 in main text

m/z	charge	chemical formula	error	assignment
186.13603	1	$C_9H_{17}N_2O_2H^+_1$	-1.34	j2
285.20459	1	$C_{14}H_{26}N_3O_3H^+_1$	-0.36	j3
384.2731	1	$C_{19}H_{35}N_4O_4H^+_1$	-0.02	j4
483.34156	1	$C_{24}H_{44}N_5O_5H^+_1$	0.08	j5
582.41007	1	$C_{29}H_{53}N_6O_6H^+_1$	0.23	j6
681.47816	1	$C_{34}H_{62}N_7O_7H^+_1$	-0.28	j7
780.54674	1	$C_{39}H_{71}N_8O_8H^+_1$	-0.03	j8
879.61432	1	$C_{44}H_{80}N_9O_9H^+_1$	-0.97	j9
978.68843	1	$C_{49}H_{89}N_{10}O_{10}H^+_1$	4.94	j10
199.1441	1	$C_{10}H_{18}N_2O_2H^+_1$	-0.02	k2
298.21228	1	$C_{15}H_{27}N_3O_3H^+_1$	-0.80	k3
397.28111	1	$C_{20}H_{36}N_4O_4H^+_1$	0.45	k4
496.34935	1	$C_{25}H_{45}N_5O_5H^+_1$	0.01	k5
595.418	1	$C_{30}H_{54}N_6O_6H^+_1$	0.40	k6
694.48636	1	$C_{35}H_{63}N_7O_7H^+_1$	0.27	k7
793.55517	1	$C_{40}H_{72}N_8O_8H^+_1$	0.73	k8
892.62482	1	$C_{45}H_{81}N_9O_9H^+_1$	2.04	k9
1090.7603	1	$C_{55}H_{99}N_{11}O_{11}H^+_1$	0.43	k11
1189.82803	1	$C_{60}H_{108}N_{12}O_{12}H^+_1$	-0.18	k12
1288.89665	1	$C_{65}H_{117}N_{13}O_{13}H^+_1$	-0.01	k13
1387.96489	1	$C_{70}H_{126}N_{14}O_{14}H^+_1$	-0.13	k14
1487.03415	1	$C_{75}H_{135}N_{15}O_{15}H^+_1$	0.45	k15
1586.10609	1	$C_{80}H_{144}N_{16}O_{16}H^+_1$	2.64	k16
1685.17033	1	$C_{85}H_{153}N_{17}O_{17}H^+_1$	0.01	k17
285.18069	1	$C_{14}H_{24}N_2O_4H^+_1$	-0.68	a2
384.24935	1	$C_{19}H_{33}N_3O_5H^+_1$	0.14	a3
483.31772	1	$C_{24}H_{42}N_4O_6H^+_1$	0.02	a4

582.38707	1	$C_{29}H_{51}N_5O_7H^+_1$	1.62	a5
681.45524	1	$C_{34}H_{60}N_6O_8H^+_1$	1.03	a6
780.52254	1	$C_{39}H_{69}N_7O_9H^+_1$	-0.53	a7
879.59037	1	$C_{44}H_{78}N_8O_{10}H^+_1$	-1.13	a8
1474.00461	1	$C_{74}H_{132}N_{14}O_{16}H^+_1$	1.87	a14
1573.07149	1	$C_{79}H_{141}N_{15}O_{17}H^+_1$	0.78	a15
1672.14274	1	$C_{84}H_{150}N_{16}O_{18}H^+_1$	2.43	a16
1771.20696	1	$C_{89}H_{159}N_{17}O_{19}H^+_1$	-0.07	a17
272.17301	1	$C_{13}H_{23}N_2O_4H^+_1$	-0.18	b2
371.24152	1	$C_{18}H_{32}N_3O_5H^+_1$	0.13	b3
470.30993	1	$C_{23}H_{41}N_4O_6H^+_1$	0.09	b4
569.37845	1	$C_{28}H_{50}N_5O_7H^+_1$	0.26	b5
668.44731	1	$C_{33}H_{59}N_6O_8H^+_1$	0.89	b6
767.51671	1	$C_{38}H_{68}N_7O_9H^+_1$	2.06	b7
866.58274	1	$C_{43}H_{77}N_8O_{10}H^+_1$	-0.93	b8
965.64807	1	$C_{48}H_{86}N_9O_{11}H^+_1$	-4.02	b9
1064.72091	1	$C_{53}H_{95}N_{10}O_{12}H^+_1$	0.51	b10
1163.78504	1	$C_{58}H_{104}N_{11}O_{13}H^+_1$	-3.22	b11
1262.85706	1	$C_{63}H_{113}N_{12}O_{14}H^+_1$	-0.11	b12
1361.92267	1	$C_{68}H_{122}N_{13}O_{15}H^+_1$	-2.16	b13
1460.99457	1	$C_{73}H_{131}N_{14}O_{16}H^+_1$	0.37	b14
1560.05948	1	$C_{78}H_{140}N_{15}O_{17}H^+_1$	-1.90	b15
		Average	0.90	
		Standard deviation	1.41	

9. Conclusions and Future work

This thesis contributes to the ability to analyse biocompatible polymers, polyoxazolines, and polyacrylamides and their cyclic-peptide conjugated variants by various mass spectrometry methods.

The ability to simplify complex polymer MS and MS/MS data sets using a modified Kendrick mass defect marries together a petroleomic method into the tandem mass spectrometry space, most often seen for proteomics.

The analysis of polyoxazolines has been carried out extensively, and the ability to use ECD, which is much less end group dependent, over CAD/IRMPD offers a great advantage to the polymer analyst. The possible modifications present in a synthesis method can also be characterised by ECD methods contributing knowledge back into the synthetic process of the biocompatible polymer species. In chapter 5 it is shown how the terminus group can have a direct effect on the hydrolysis of the polyoxazoline. Interestingly, the analysis showed that the hydrolysis events did not show a significant neighbouring effect on the monomers next to a hydrolysed species.

Trithiocarbonate terminated polyacrylamides produced a unique ECD fragmentation mechanism. The ECD fragmentation method was atom directed, rarely seen in an ECD experiment, as well as providing evidence for continued radical dissociation in a linear molecule. The ECD method produced complete coverage of various terminating groups as well as offering a method to characterise block length in block copolymers.

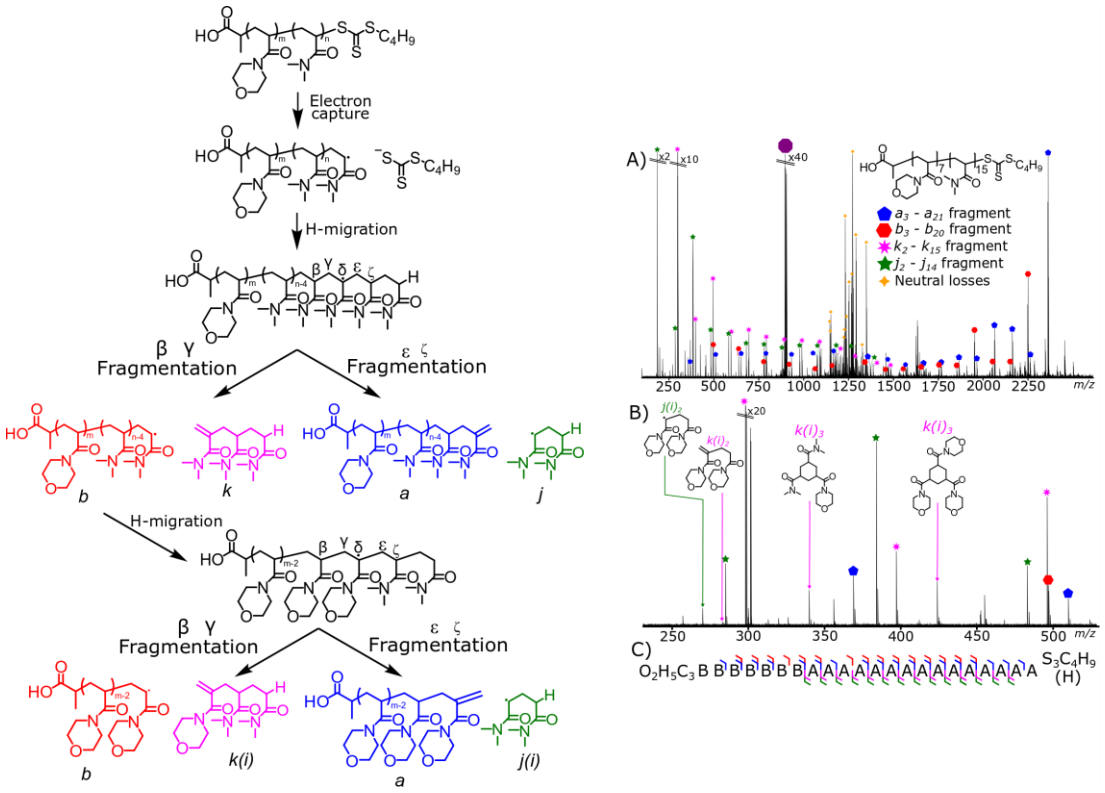

Figure 9.1 Summary figure of Chapter 4 showing the dissociation of a polyacrylamide and the corresponding mechanism via ECD.

The use of UVPD for the analysis of polymers also gives an incredibly useful alternative to the use of ECD. UVPD is becoming much more common in high end mass spectrometry instruments, as it allows many more fragment types to be produced and has offered impressive cleavage coverage of many biological species. Polyoxazolines and polyacrylamides were shown to be fragmented and completely characterised by UVPD methodology.

One of the best examples of the utility of multiple fragmentation methods is the ability to change fragmentation methods to suit the polymer and potentially any other conjugating agents. The cyclic peptide-polymer conjugate analysed shows how both ECD and IRMPD could contribute some analytical information in the analysis of the active species but the use of UVPD allowed the analysis of the both the polymer and the peptide polymer-conjugate within one experiment.

The use of 2DMS also contributes greatly to the utility of mass spectrometry to polymer species. By fragmenting multiple polymers, or polymer blends, in one experiment multiple polymeric species can be characterised at the same time. The

ability to characterise multiple species at the same time, without the use of chromatographic separations which can bias or negatively affect MS analysis, is hugely advantageous to the analysis of polymer species.

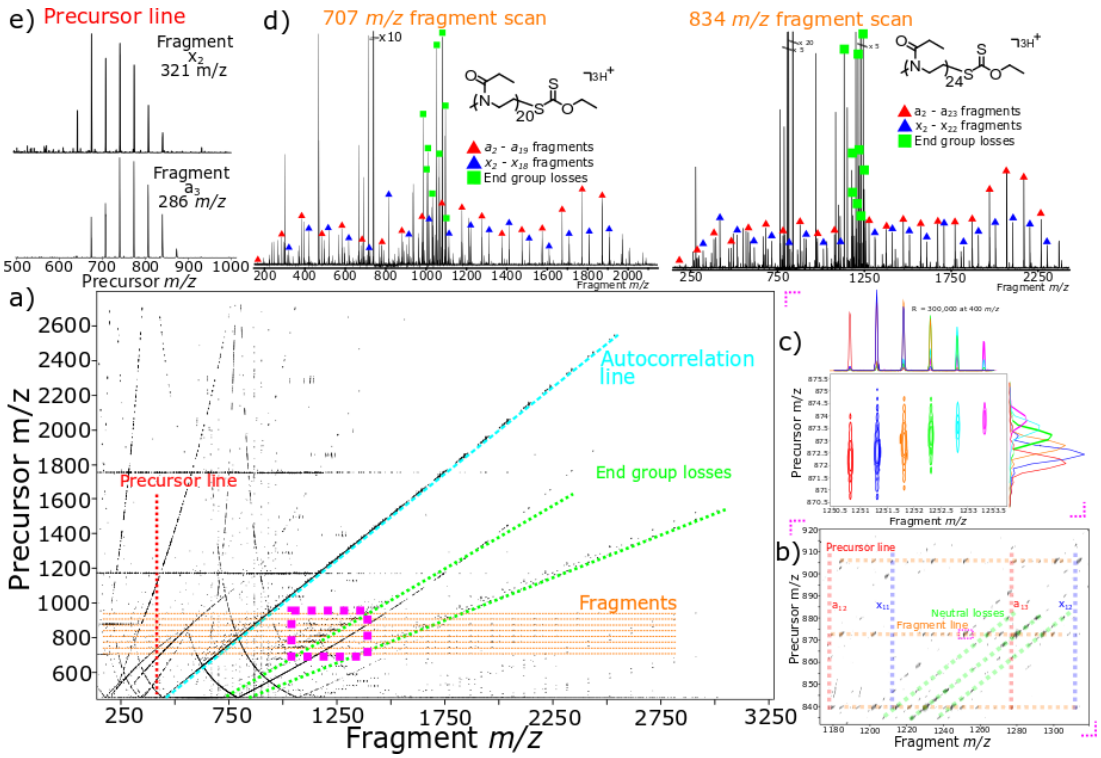

Figure 9.2 Summary figure of Chapter 4 showing the dissociation of a polyacrylamide and the corresponding mechanism via ECD.

Overall, there is still plenty of mass spectrometry advancement possible for the analysis of polymers. As polymers cover such a broad range of chemical reactivities, compositions, variations in back bones, end groups, and conjugating agents need to be considered when analysing any of these species.

The corresponding analysis of biocompatible polymers and cyclic peptide-polymer conjugates by mass spectrometry represented here offers a method of analysis to not only confirm the presence of the expected synthetic material but also insight into the synthesis itself meaning the work here has relevance not just to analytical groups but also the synthetic procedures as a readback on the chemistry occurring for the characterisation and optimisation of the processes used.